UNIVERSITY OF
Southampton

University of Southampton Research Repository
ePrints Soton

Copyright © and Moral Rights for this thesis are retained by the author and/or other copyright owners. A copy can be downloaded for personal non-commercial research or study, without prior permission or charge. This thesis cannot be reproduced or quoted extensively from without first obtaining permission in writing from the copyright holder/s. The content must not be changed in any way or sold commercially in any format or medium without the formal permission of the copyright holders.

When referring to this work, full bibliographic details including the author, title, awarding institution and date of the thesis must be given e.g.

AUTHOR (year of submission) "Full thesis title", University of Southampton, name of the University School or Department, PhD Thesis, pagination

http://eprints.soton.ac.uk

UNIVERSITY OF SOUTHAMPTON

FACULTY OF ENGINEERING, SCIENCE & MATHEMATICS

School of Ocean & Earth Science

High Resolution Palaeoceanography and Palaeoclimatology from Mid and High Latitude Late Cretaceous Laminated Sediments

by

Andrew Davies

Thesis for the degree of Doctor of Philosophy

March 2006

Graduate School of the
National Oceanography Centre, Southampton

This PhD dissertation by

Andrew Davies

has been produced under the supervision of the following persons

Supervisor/s

Prof. Alan E.S. Kemp
Dr John Barron
Dr Jennifer Pike

Chair of Advisory Panel

Prof. Andrew Roberts

Member/s of Advisory Panel

Dr Paul Wilson

UNIVERSITY OF SOUTHAMPTON

ABSTRACT

FACULTY OF ENGINEERING, SCIENCE & MATHEMATICS
SCHOOL OF OCEAN & EARTH SCIENCES
Doctor of Philosophy

HIGH RESOLUTION PALAEOCEANOGRAPHY AND PALAEOCLIMATOLOGY FROM MID AND HIGH LATITUDE LATE CRETACEOUS LAMINATED SEDIMENTS

by Andrew Davies

Late Cretaceous laminated diatomaceous sediments from the Marca Shale (California) and CESAR 6 core (Arctic Ocean) have been analysed using scanning electron microscopy techniques and found to contain marine varves. The varve interpretation is based on the pervasive occurrence of laminae types that can be related to different seasons and placed into robust annual flux cycles. In the Marca Shale this consists of intermittent near-monospecific laminae of *Azpeitiopsis morenoensis* deposited in the late summer, succeeded by a ‘fall dump’ mixed assemblage laminae, dominated by fragmented *Hemiaulus polymorphus, Stephanopyxis* spp. and *Stellarima* spp.. Intermittent near-monospecific *Chaetoceros*-type resting spore laminae, deposited in spring follow and are in turn overlain by terrigenous laminae, reflecting enhanced fluvial runoff during the summer. A mixed floral diatomaceous and terrigenous laminae couplet constitute the annual flux cycle in the majority of varves. Summer terrigenous flux may indicate that the ~43°N palaeolatitude estimate is incorrect, and deposition actually occurred at lower latitudes or alternatively, that the Marca basin was influenced by intense monsoonal summer storms. The CESAR 6 annual flux cycle consists of alternating diatom resting spore and vegetative cell laminae (often dominated by *Hemiaulus*), interpreted to represent spring bloom flux and ‘fall dump’/intermittent summer blooms flux, respectively. Near-monospecific *Rhizosolenia* laminae frequently occur above vegetative laminae, relating to subsequent ‘fall dump’ flux. Common silicoflagellate/setae-rich laminae, often containing diatom hash, occur beneath resting spore laminae, interpreted as the early spring flux of silicoflagellate blooms and grazed diatoms. Seasonally occurring detrital ‘blebs’ and rare detrital laminae are also observed, which may represent ice rafted debris, consistent with Campanian model simulations. Diatom taxa adapted to exploit stratified conditions, sedimented over the summer or in a ‘fall dump’, are important components of both sequences. Spring bloom flux was important in the CESAR 6, but was only a subsidiary component in the Marca Shale. The abundance of *Hemiaulus* spp. at both localities may be evidence for diatom blooms powered by N_2-fixing cyanobacteria. Diatom biostratigraphy indicates a late Late Campanian age for the CESAR 6, although an earliest Maastrichtian age cannot be discounted.

Time-series analysis of laminae thickness data from both sequences and bioturbation index data from the Marca Shale, reveal both sites contain strong quasi-biennial signals (mean periodicities of 27.4 and 30.4 months, respectively), inferred to relate to the Quasi-Biennial Oscillation (QBO). The CESAR 6 contains strong sub-decadal/quasi-decadal peaks interpreted to relate to Northern Hemisphere Annular Mode (NAM) variability. Together with the QBO signals, this suggests NAM variability was robust during the Late Cretaceous. Similar frequency peaks occur in the Marca Shale which, supported by several sedimentological lines of evidence, indicates the presence of an El Niño Southern Oscillation (ENSO)-like oscillation. Theory dictates that a weakening of the ‘Bjerknes’ feedback loop in the equatorial Pacific will lead to a reduction or shutdown of ENSO variability, resulting in a permanent El Niño climate. The Late Cretaceous was witness to a severe weakening of the ‘Bjerknes’ feedback, yet the results of this study demonstrate that there was robust ENSO variability during this greenhouse period, adding to the evidence against permanent ‘El Niño’ climate states. A 10.66 year harmonic peak in the CESAR 6 is taken as evidence for modulation of the NAM by solar variability. Peaks at 10.0, 10.3 and 10.8 years in the Marca Shale are interpreted to relate to the solar modulation of strong ENSO events. Both sites also contain multi-decadal peaks, the frequency of which may also have been modulated by solar variability. Quasi-bidecadal peaks are inferred to relate to the NAM or an oscillation analogous to the Pacific Decadal Oscillation (PDO), possibly influenced by the Hale cycle. A 44 year peak in the Marca Shale is also inferred to relate to the PDO. The CESAR 6 contains a harmonic peak at 78.74 years, interpreted to relate to modulation of the NAM over the Gleissberg solar cycle or alternatively, to modulation of the PDO.

LIST OF CONTENTS

LIST OF FIGURES

LIST OF TABLES

LIST OF PLATES

CHAPTER 1

Introduction

1.1 INTRODUCTION

In this chapter, the rationale and the main objectives for the study are discussed and an outline summary of the thesis are presented.

1.2 BACKGROUND

1.2.1 *Rationale*

Laminated marine sediments are known to contain information on variability in the ocean-atmosphere system on time scales from seasonal to millennial (e.g. Behl & Kennett, 1995; Bull & Kemp, 1995; Pike & Kemp, 1996b; Dean *et al.*, 2001), comparable in quality and resolution to records from ice-cores (Ram & Stolz, 1999), corals (Dunbar *et al.*, 1994), tree rings (Briffa *et al.*, 1992), lacustrine varves (Munoz *et al.*, 2002) and sediment traps (Thunell *et al.*, 1993). The full potential resolution of these important proxy data sets was only realised recently with the use of high resolution backscattered electron imagery (BSEI). Important insights into the nature and persistence of natural climate variability have been gleaned and laminated marine sediments have also been pivotal in exploring the nature of abrupt climate change, such as the Dansgaard-Oeschger interstadials (see Kemp, 2003). High-resolution analysis of sediment fabrics of laminated diatomaceous sediments, in particular, can provide important information on surface and benthic processes. The nature of the diatom assemblage in individual laminae can also help ascertain whether export production resulted from upwelling conditions or from a stratified water column (Kemp *et al.*, 2000). Most of the work on laminated marine sediments has hitherto only been conducted on relatively recent Quaternary material. Laminated marine sediments from greenhouse end-member climate states have the potential to reveal the nature and amplitude of natural climate variability in conditions analogous to those predicted to occur through anthropogenically induced climate change. The small amount of high-resolution material that has been studied from such periods has yielded important data on how the climate system responds to greenhouse conditions (Huber & Caballero, 2003).

Age	**Location**	**Diatom preservation**	**Reference**
Late Maastrichtian	Fresno County, California (Marca Shale member)	Good	Hanna (1927; 1934); Long *et al.* (1946); Barker & Meakin (1946); Hasle and Syvertsen (1985); Sims & Hasle (1987); Sims and Ross (1988); Sims (1989; 1994b; 1994a; 1998; 2000); Fonseca (1997); Nikolaev *et al.* (2001); THIS STUDY
Maastrichtian	Emperor Canyon (off New Jersey coast)	Moderate	Fenner (1982)
Maastrichtian	South Carolina (Peedee Formation)	Pyritised	Abbott (1978)
Maastrichtian	De la Manche Valley, Rougemont, Switzerland	Pyritised	Wiedermann (1964)
Early Maastrichtian	ODP Leg 120, Site 748 (Indian Ocean)	Moderate	Shipboard Scientific Party (1989), Nikolaev and Harwood (2000)
Campanian-Danian	Seymour Island, Antarctic Peninsula	Poor to moderate	Martinez-Machiavello (1987); Harwood (1988)
Late Campanian-early Maastrichtian?	Alpha Ridge, Arctic Ocean	Excellent	Barron (1985b); Kitchell *et al.* (1986); Dell'Agnese and Clark (1994); THIS STUDY
Late Campanian-early Maastrichtian	NW Kanto Mts., Japan (Shoya Formation)	Poor	Takahashi *et al.* (1999)
Campanian-Maastrichtian	Wyoming, Colorado and Kansas (Pierre Shale)	Pyritised	Bergstresser and Krebs (1983)
Campanian-Maastrichtian	Ural Mountains and western Siberian lowland, Russia	Good-Excellent	Jousé (1948; 1949; 1951; 1955); Krotov (1957a; 1957b; 1959); Schibkova (1961); Vekschina (1961); Strelnikova (1964; 1965; 1971; 1974; 1975)
Campanian	Alberta, Canada	Pyritised	Given and Wall (1971); Wall (1975)
Campanian	DSDP Leg 29, Site 275 (SW Pacific)	Excellent	Hajós and Stradner (1975)
Campanian	Tonga Trench	Moderate	Balance *et al.*(1989)
Campanian	ODP Leg 121, Site 758 (Indian Ocean)	Moderate	Fourtanier (1991)
Campanian	DSDP Leg 22, Site 216 (Indian Ocean)	Moderate	Greshan (1986)
Campanian	Central Negev, Israel (Mishash Formations)	Moderate	Moskovitz *et al.* (1983)
Campanian	Westfalia, Germany	Poor	Riegraf (1995)
Campanian	Gdansk, Poland	Good	Schulz (1935)
Early Turonian-Late Campanian	Sergipe Basin, Brazil (Aracaju Member)	Poor	Koutsoukos and Hart (1991)
Turonian	Villers-Sur-Mer, Calvados	Poor	Deflandre (1941)
Turonian	Bohême, Czechoslovakia	Poor	Weisner (1936)
Turonian	Reimerich, Germany	Poor	Müller (1912)
Cenomanian?-Campanian	Arctic Canada	Moderate	Tapia and Harwood (2002)
Albian-early Cenomanian	Ligurian Alps, Italy	Poor	Foulcault *et al.*(1986)

Table 1.1. List of all studied Late Cretaceous diatomaceous deposits. The two localities analysed in this study are indicated by grey shading. Adapted from Tapia and Harwood (2002).

1.2.2 *Upper Cretaceous diatomaceous sediments*

Due to the instability of hydrated amorphous silica (opal-A), the quantity of well preserved Late Cretaceous diatomaceous sediments is relatively low (Table 1.1). Two sites containing some of the best preserved material are analysed in this study; that of the mid-latitude Late Maastrichtian Marca Shale and also from the high-latitude Late Campanian-Early Maastrichtian CESAR 6 core from the Alpha Ridge, Arctic Ocean.

1.2.3 *Marca Shale*

The Marca Shale member of the Moreno Formation, crops out along the Panoche Hills, central California and is characterised by distinct sub-mm scale, alternating laminae composed of diatomaceous and terrigenous material (McGuire, 1988). A modest amount of research has been conducted on this unit (Table 1.1), primarily on diatom taxonomy, with the exception of Fonseca (1997) who made some observations of the nature of the microfabric. The lithology of the Marca Shale is remarkably similar to recent annually laminated marine sediments and consequently the laminations have been interpreted as varves (McGuire, 1988; Fonseca, 1997; Kodama & Ward, 2001).

1.2.4 *CESAR 6*

The CESAR (Canadian Expedition to Study the Alpha Ridge) 6 core contains ~176 cm of biosiliceous sediment comprised of almost pure unconsolidated, superbly preserved diatom ooze (Mudie & Blasco, 1985). The unit exhibits distinct millimetre-scale colour laminations. The CESAR 6 biosiliceous unit is almost identical to a nearby well-laminated Cretaceous diatom ooze (Core Fl-437). However, alternate interpretations of the origin of the laminations in the two cores exist. Laminations in Core Fl-437 have been interpreted to result from the seasonal deposition of diatom vegetative cells and more heavily silicified resting stages (Kitchell *et al.*, 1986), whilst laminations in the CESAR 6 have been interpreted to result from changes in the iron content of the sediment (Stoffyn-Egli, 1987). Contrasting interpretations on the formation of the biosilica in the CESAR 6 also exist. Barron (1985b) interpreted the CESAR 6 diatom ooze to have been deposited rapidly under a highly productive environment, with no evidence for any biostratigraphic changes, further suggesting laminae may be of seasonal origin. Alternatively, Mudie and Blasco (1985) and Mudie *et al*. (1986) suggest the laminations are not seasonal, and interpreted the diatom ooze to have been deposited slowly in a low productivity environment.

1.3 OBJECTIVES OF THE STUDY

- Using high resolution scanning electron microscopy techniques, and in particular BSEI, to study the nature and origins of the laminated microfabrics in the Marca Shale and CESAR 6 and, by virtue of the nature and floral composition of individual laminae, help ascertain if either localities contain marine varves.
- Using the results of high resolution BSEI, resolve any contrasting theories on the formation of the laminated fabrics.
- By analysing the nature of the diatom assemblages within individual laminae types, address the style of marine productivity governing the formation of the biosiliceous sediments.
- To study water column processes and the nature of the benthic palaeoenvironments by identifying and analysing sediment microfabrics such as pellet and aggregate structures and variations in the degree of bioturbation (Anderson *et al.*, 1990; Brodie & Kemp, 1995; Dean *et al.*, 2001).
- If laminations are confirmed as annual, identify any inter and intra-annual variability in any key proxies, which may include the diatom floral composition, diatom productivity, terrigenous flux and benthic oxygen levels.
- To subject long, seasonally resolved data sets from the Marca Shale and CESAR 6 to time-series analysis, in order to determine the presence, nature and vigour of any high-frequency climate variability along the eastern Pacific mid-latitudes, and polar northern latitudes, during an important greenhouse end-member climate state. The origin of any cycles identified will be discussed in the context of the frequency band of modern oscillations including the El Niño Southern Oscillation (ENSO), Quasi-Biennial Oscillation (QBO), Pacific Decadal Oscillation (PDO) and Northern Hemisphere Annular Mode (NAM).
- Using the new Arctic diatom biostratigraphic scheme of Tapia and Harwood (2002), validate claims by Barron (1985b) that no diatom biostratigraphic changes are present within the CESAR 6 and help further constrain the age of the unit.
- In a small NERC grant pilot study of the CESAR 6, Kemp and Pike (unpublished data) identified rare terrigenous laminae, which they interpreted to be ice-rafted detritus. This conclusion will be tested by further study of the terrigenous material.

1.4 STRUCTURE OF THE THESIS

Chapter 2 describes in detail the preparatory and analytical techniques used during this study, with particular emphasis on scanning electron microscopy.

Chapter 3 provides a description of the main diatom taxa encountered in the Marca Shale and the CESAR 6 core, including a discussion of their ecology and palaeoceanographic significance. A comparison of the two floras is made and the main differences summarised. Diatom ecological data discussed in Chapter 3 is used for interpretation of the laminated fabrics in Chapters 4 and 6.

Chapter 4 contains a detailed description of the integrated study of the Marca Shale, with particular attention to the results of BSEI. Various sedimentary fabrics are described and interpreted, including several laminae types, pelletal structures and bioturbation fabrics, along with a number of macroscopic sedimentary structures. Results of clay/bulk mineral and magnetostratigraphic analysis are also presented.

Chapter 5 presents the results of time-series analysis conducted on numerous records of laminae thickness variations and bioturbation index records obtained from the Marca Shale. A discussion of the possible forcing mechanisms and implications of the results on high-frequency climate variability in greenhouse climate states is included. The spectral analysis of the Marca Shale time series were undertaken by Graham Weedon (University of Wales, Swansea), using the Lomb-Scargle algorithm.

In Chapter 6, the results of high-resolution BSEI studies on the CESAR-6 are presented and the numerous laminae types are described and the nature of their origin discussed. Diatom floral changes through the core, analysed using optical microscopic techniques, are presented and discussed. The age of the biosiliceous succession is reviewed in light of a new Late Cretaceous diatom biostratigraphic zonation scheme from the Arctic.

Chapter 7 presents the results of time-series analysis conducted on variations in the total varve thickness, total resting spore varve segment thickness and total vegetative varve segment thickness from two long records obtained from the CESAR 6. The spectral analysis of the CESAR 6 time series were undertaken as an integral part of the study using the SSA-MTM Toolkit, Analyseries and the wavelet analysis software of Torrence and Compo (1998).

The main conclusions of the study are summarised in Chapter 8 and suggestions for further studies made.

Appendix 1 provides a full taxonomic list of the diatom species encountered in the Marca Shale and CESAR 6, including synonyms and rare species not discussed in Chapter 3.

Appendix 2 (CD-ROM) contains all the laminae thickness measurement, diatom strew slide counts, XRD and palaeomagnetic data.

CHAPTER 2

Methodology

2.1 INTRODUCTION

In this chapter, a full description of the methods and analytical techniques used during this study is given.

2.2 METHOD OF MAKING SLIDES FOR BSEI

2.2.1 *Resin embedding lithified (Marca Shale) samples*

Owing to the friable nature of the laminated diatomaceous shale, it was necessary to embed samples in epoxy resin prior to creating polished thin sections. Using a bandsaw, a suitable slice of material was cut from the sample, taking care to include the entirety of the sample, then labelled and orientated. The cut face was then flattened using a belt grinder fitted with 120 grade sandpaper. The cut sample was left to dry on a hot plate at 40°C for 24 hours, after which time it was ready to embed in resin. The resin used is comprised of a mixture of chemicals in the following weight ratio:

Araldite AY105 epoxy resin	40.0 g
Araldite HT972	11.2 g
Methylethylketone	18.8 g
Acetone	3.5g

The HT972 and methylethylketone comprise the hardener and is created by dissolving the HT972 into the methylethylketone. After this mixture has been mixed thoroughly, the AY105 resin is added along with the acetone, which is used to slightly thin the resin. The sample was then placed into a polypropylene tray (which is resistant to resin) and the resin mixture added. The tray (containing the samples) was then placed into a vacuum chamber for 1 hour. After being removed from the vacuum chamber, the sample was transferred from the trays to aluminium foil and placed into an oven at 40°C for 24 hours to cure the resin.

2.2.2 *Resin embedding unconsolidated (CESAR 6) samples*

As with the Marca Shale material, it was necessary to first resin embed the unconsolidated diatom ooze in epoxy resin. However, prior to embedding, the sediment pore fluid must first be removed. This can be achieved by critical point drying (Bouma, 1969), freeze drying (Bouma, 1969), vacuum drying (Kemp, 1990; Patience *et al.*, 1990) and chemical (fluid displacive) drying (Jim, 1985; Pike & Kemp, 1996a). The first three methods cause partial collapse of the sedimentary microfabric as the sediment fluids are removed prior to resin embedding and as such, essential high-resolution textural information is lost. During fluid displacive drying, the sediment is never actually dried and the fabric is supported throughout the procedure, causing no disturbance of the sedimentary microfabrics. Fluid displacive embedding was achieved using the method of Kemp *et al*. (1998), which is a slight modification of the method of Pike and Kemp (1996a) and Jim (1985).

2.2.2.1 *Chemical drying of the sediment*

Sample blocks were subsampled (leaving some sediment for use in topographic stubs) with a scalpel (Fig. 2.1a) and then wrapped in fine-gauge stainless steel/aluminium mesh (Fig. 2.1b), which constrains the sediment whilst still allowing free fluid exchange. The wrapped sediment sample was then transferred to a close-fitting container (polypropylene) onto which the sample number and way-up direction was permanently marked. Next, the sample was completely covered in high-purity acetone, introducing it down the side of the container, so not to disturb the sediment (Fig. 2.1c), within a glass desiccator. It is imperative to ensure the samples are covered and that no desiccation occurs at any stage. Acetone was replaced three times a day for five days.

2.2.2.2 *Resin embedding*

Following the final soaking of acetone, the resin can be added. The resin used was prepared from several chemicals in the following ratio:

vinylcyclohexene dioxide (VCD)	10.0 g
diglycidol ether of polypropyleneglycol (DER 736)	6.0 g
nonenyl succinic anhydride (NSA)	26.2 g
dimethylaminoethanol (DMAE)	0.2 g

DMAE and VCD can have an exothermic reaction and therefore VCD, DER 736 and NSA must be mixed prior to the addition of DMAE. The resin is introduced in fifteen steps, with the initial three additions as an acetone/resin mixture, in a 50:50 proportion, ensuring the sample is completely covered. The subsequent three additions are in the proportion 27:75, followed by three additions in the proportion 10:90. The last six are of pure resin. These replacements were carried out every 12 hours to prevent viscosity increase. After each replacement the sample was gently lifted to ensure fresh resin reached the underside of the sample. Following the final replacement, the sample was left in a desiccator for at least four weeks, ensuring the samples were not exposed to excessive moisture (as this may turn the resin opaque). Samples were then cured for 72 hours at 30°C and 24 hours at 45°C and 60°C, with 24 hours of cooling time between each step.

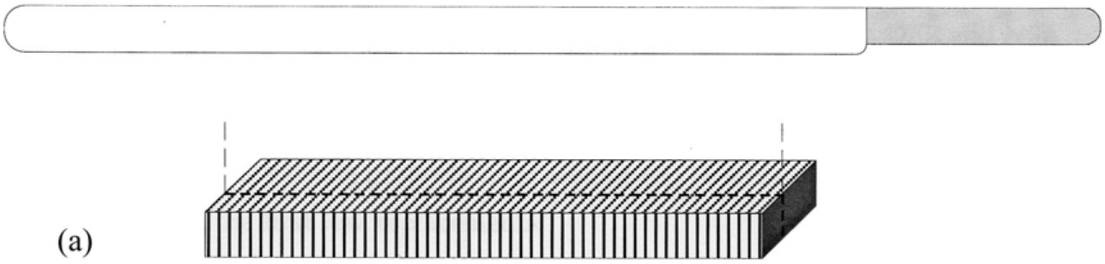

(a)

sub-sample with sharp knife

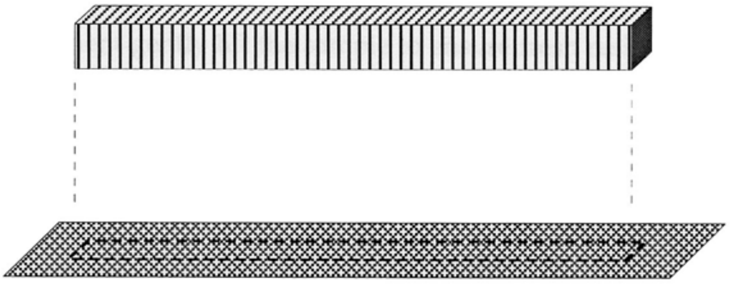

(b)

wrap sample in stainless steel mesh

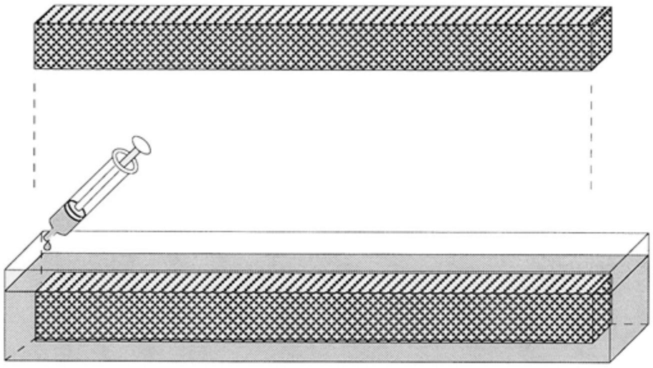

(c)

soak in acetone, followed by epoxy resin mix

Figure 2.1 Fluid displacive drying and resin embedding of unconsolidated, wet sediment, adapted from Dean (2000a).

A quantity of the CESAR 6 material was found to have dried and could not be embedded by the fluid displacive method. Embedding could not be achieved by the method used for the Marca Shale samples as this requires vacuum impregnating and would result in the collapse of the laminated microfabric. Therefore, these sections were wrapped in the fine-gauge stainless steel/aluminium mesh and transferred onto a sheet of aluminium foil, onto which the sample number and way-up direction was permanently marked. Next, a small quantity of the resin used in preparation of the Marca Shale samples was carefully dripped over the surface of the subsampled sediment block. Owing to the highly porous nature of the sediment, the resin was quickly absorbed by the samples. After 30 seconds, more resin was added to the surface of the sediment block and allowed to be absorbed. This process was repeated until the sediment block had become saturated with resin. The samples were then placed into an oven at 40°C for 24 hours.

2.2.3 *Preparation of polished thin sections*

Embedded samples were cut into sufficient sized portions to fit onto the 48mm × 26mm glass slides used for BSEI. Samples were cut at oblique angles so that each slide overlapped and no artificial hiatuses were created. To remove the excess resin and expose the cut face, samples were ground using dry, 320 grade silicon carbide paper. Each sample and corresponding glass slide was cleaned in alcohol before being glued to the slide using Epotek 301 resin. The samples were then placed on a spring mounting jig and left for 12 hours at room temperature. Once the samples had been removed from the jig, they were cut to a thickness of 0.5mm using a Buehler petro-thin machine. Utilizing the same machine, the slides were then ground to a thickness of 250-300 µm. Next the slides were polished with a Buehler petropol polishing system on a Metlap 6 disc with a 9 µm diamond suspension solution for 5 minutes. Slides were then polished with a Texmet cloth, for 30 minutes with a 15 µm diamond suspension solution, 30 minutes with a 9 µm diamond suspension solution and 30 minutes with 3 µm diamond suspension solution. The final polishing was performed for 10 minutes with 1 µm diamond suspension solution. Samples were thoroughly cleaned in alcohol after each session of polishing. The slides were then coated in carbon prior to analysis (Goldstein *et al.*, 1992).

2.3 SCANNING ELECTRON MICROSCOPY (SEM)

Analysis of polished thin sections, topographic stubs (of fractured material and strew slides) and peel slides was performed on a high vacuum LEO 1450VP scanning electron microscope (SEM). Analysis can be carried out in the secondary electron imagery (SEI) or backscattered electron imagery (BSEI) mode. The system is also fitted with a Princeton Gamma-Tech energy dispersive spectrometer (EDS) microanalyser.

2.3.1 *Backscattered electron imagery (BSEI)*

Backscattered electrons result from the elastic collisions between energetic beam electrons and atoms within the specimen (Goldstein *et al.*, 1992). The number of backscattered electrons (the backscatter coefficient, η) relates, primarily, to the average atomic number of the specimen and is recorded in BSEI photographs as image brightness (see Pike & Kemp, 1996a). Mineral grains generally have high atomic numbers (e.g. pyrite, quartz, carbonate, feldspar) and consequently possess high backscatter coefficients, producing bright images in BSEI. Conversely, organic matter and the carbon-based epoxy resin used for embedding, have low atomic numbers, low backscatter coefficients and produce dark images. Consequently, as well as providing compositional data, BSEI photographs also provide porosity information. Diatomaceous laminae are generally highly porous and as such appear dark in BSEI, whilst lithogenic laminae appear bright.

The primary task for each polished thin section was to produce low resolution (66×) photomosaics, which act as basemaps for subsequent high resolution BSEI. This was achieved by taking 10% overlapping images, using an automated imaging program that scans each slide between two user designated points, and merging them into one composite image using the Adobe Photoshop program. Using the same method, high resolution (750× and 1000×) photomosaics were taken of the CESAR 6 slides, as 66× basemaps were found to have insufficient resolution to be able to discern individual lamina fabrics. The off-cut portions of each sample were kept and used to make topographic stubs. Laminae of interest were carefully fractured long the bedding plane and fixed onto SEM stubs using carbon based wax. Samples were originally mounted using sticky carbon pads, but it was found these did not affix the sediment satisfactorily. Stubs were finally coated in gold using a sputter coater.

2.3.2 *Peel slides*

To help better constrain the species make-up of the different laminae types within the CESAR 6 peels were taken of the raw material, using double sided carbon tape. Suitable sized pieces of tape were cut to fit onto standard SEM glass slides. The tape was placed on the surface of the sediment block and gently pressed to ensure contact was made along the entire length of the tape. The tape was then carefully peeled off and affixed onto a glass slide. Two peels were made for each section studied and affixed to the same glass slide. The slides were subsequently coated in gold in preparation for use with the SEM. In this way topographic images of individual fabric types could be taken *in situ*, without causing disturbances to the laminated fabric.

2.3.3 *Secondary electron imagery (SEI)*

Secondary electrons are created by inelastic collisions between high energy beam electrons and the atoms of the specimen (Goldstein *et al.*, 1992). The number of secondary electrons emitted by a sample is affected by its topography and hence the images produced are topographic. SEI can therefore provide better images of topographic stubs and peel slides than BSEI, although charging of the specimens can be a problem. Topographic stubs and peel slides for use with SEI are produced in the same way as those used for BSEI.

2.4 MEASUREMENTS FROM SEM IMAGES

Although measurements of laminae thickness were made manually from the low resolution photomosaics for some of the Marca Shale samples, measurements were primarily conducted using the methods of Francus *et al* (2002). This method involves the use of the Adobe Photoshop program to mark the boundaries between individual laminae on a digitised photo-mosaic of the polished section. The resultant ‘path’ is then exported to Microsoft Excel, where a macro converts the measurements into actual thickness using the known quantities of the number of pixels per centimetre on the image (obtained from Photoshop) and the size of individual pixels (obtained from the SEM). Measurements obtained in this way can be easily revaluated later as a record of the inferred boundaries is produced and they are less prone to errors than measurements created through manual means. Laminae thickness measurements for the CESAR 6 samples were made from the high-resolution (750× and 1000×) photomosaics. Two or three measurements were made per laminae and an average value obtained. Where possible, measurements were made towards the centre of each mosaic, where distortion is minimal.

2.5 DIATOM STREW SLIDE PREPARATION

Diatom strew slides were prepared following an adapted version (Claire S. Allen, British Antarctic Survey, personal communication) of the method of Scherer (1994). Raw diatomaceous material was placed into a 25 ml beaker with 10ml of distilled water. To this 3 ml of dilute (30%) hydrogen peroxide (H_2O_2) and 1ml of hydrochloric acid (HCl) (50%) were added, before the beaker was transferred to a warm hotplate (in a fume cupboard) for 7-8 hours. The reaction was checked periodically, especially at the beginning, and if excess foaming occurred, a few drops of propan-2-ol were added. After oxidisation, the samples were transferred to centrifuging tubes and centrifuged for 2 minutes at 1200 rpm. The supernatant was removed and distilled water was added to the original level before the centrifuging and washing process was repeated. After the washed samples had been transferred back into beakers, 10 ml of dispersing agent (prepared from 2g of sodium hexametaphosphate powder added to 500 ml of distilled water) was added and the samples left to soak for an hour. During this time, two coverslips (per sample) were treated with potato starch, covered and left to air dry (potato starch is a surfactant and allows diatoms to better settle on the coverslips). The coverslips were then glued to glass slides with water-based glue (such as Pritstick) and an SEM topographic stub (one per sample) was prepared by molding a weighted base of blue tack. Next the 1000 ml settling beakers were filled with distilled water and Petri dishes with specially drilled holes added. The pipettes were added, making sure that they entered the hole drilled in the Petri dishes (so that no currents are set up when the beakers are emptied of water), and suction obtained before the clamps were fully closed. Next the treated coverslips and SEM stub were added. Samples were then placed into an ultrasonic bath for 2 seconds to ensure the diatomaceous material was sufficiently disaggregated, before the solution was added to the settling beakers (Fig. 2.2). The beakers were then covered with cling film and left for 4 hours, enabling the diatoms to sediment onto the coverslips and SEM stub. After this time, the valves were slowly opened, until a flow rate of 1 drip/2seconds was obtained, and the beakers were left to drain overnight (see Fig. 2.2). Once the beakers had completely drained, the coverslips were removed from the glass slides and the glue removed. The SEM stub and coverslips were then covered and left to air dry. After drying the coverslips were mounted onto microscope slides using Naphrax and the SEM stub coated in gold. Using this method, 5 samples could be processed simultaneously (creating 10 strew slides and 5 SEM stubs). This method was found to produce an even spread of diatomaceous material over whole coverslips, without bunching of frustules.

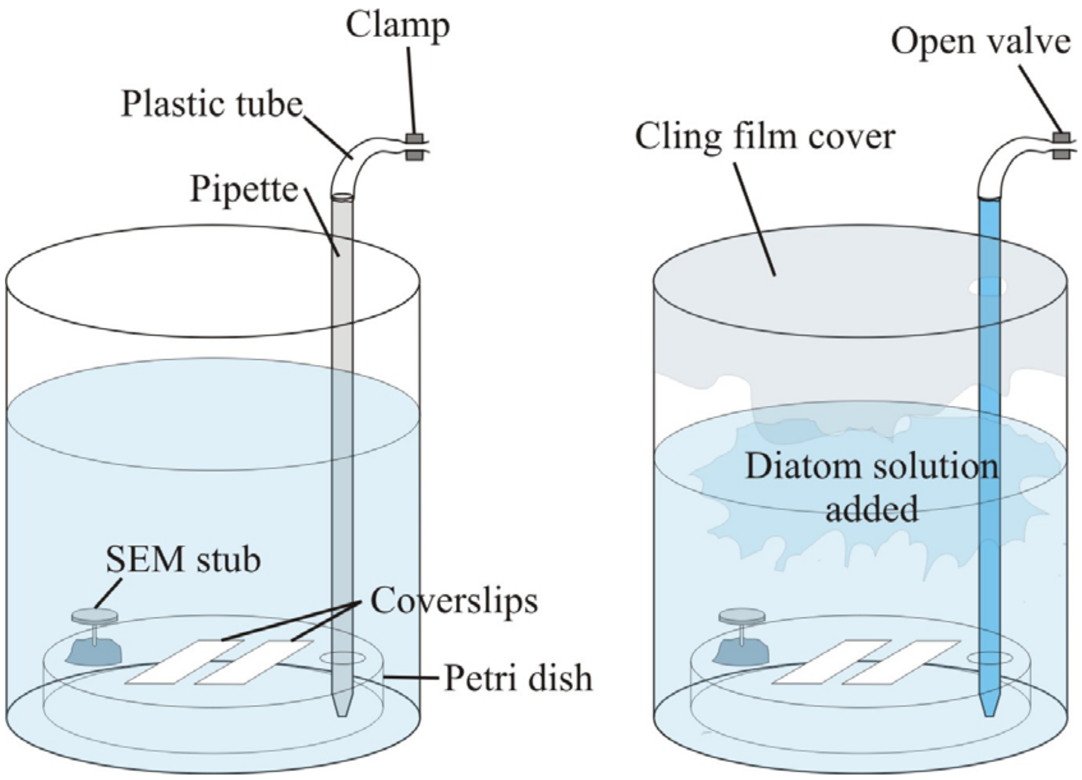

Figure 2.2. Cartoon diagram of the apparatus used to make diatom strew slides.

2.6 X-RAY DIFFRACTION (XRD)

2.6.1 *Bulk mineral analysis*

Sufficient material (~ 20g) for bulk mineral and clay mineral analysis was detached from the sample blocks, avoiding slumps and turbidites. Samples were broken into small chips (1-5 mm) and one third of the material was then ground into a fine powder. The random powder was then pressed into a holder and analysed by XRD in order to characterise the whole rock mineralogy using the method of Schultz (1964), although using peak areas rather than peak heights. Measurements were made at the National Oceanography Centre, Southampton and analysis was carried out by Trevor Clayton.

2.6.2 *Clay mineral analysis*

The remaining two third of the sample material was dispersed in distilled water and carbonates were removed using 10% acetic acid. The samples were then treated with sodium hexametaphosphate to ensure the samples were properly dispersed and the <2 µm clay fraction was separated by settling under gravity (using Stokes Law). The clay fraction was then smeared over glass slides and analysed by XRD on successive air-dried, heated (300ºC and 500ºC respectively) and glycolated samples. The relative abundances of clay minerals were calculated by Trevor Clayton, using the method of Biscaye (1965).

2.7 MAGNETOSTRATIGRAPHIC ANALYSIS

In order to help better constrain the biostratigraphic framework of the Marca Shale, samples were collected for magnetostratigraphic analysis. Samples were orientated in the field, with the horizontal and the direction of north marked on each sample and the dip/strike taken. Measurements of the natural remanent magnetism were made in a magnetically shielded room at the National Oceanographic Centre, Southampton using a 2G-Enterprises cryogenic magnetometer on at least one cube from each sample. Static alternating field demagnetism was conducted using a system in-line with the magnetometer in 5-10 mT steps up to 60 mT. Samples were also subject to thermal demagnetisation (in 40-50 °C steps up to 550 °C) and low-field bulk magnetic susceptibility was measured after each step to monitor thermal alteration. If vector-component diagrams showed samples possessed stable magnetisation the characteristic remanent magnetisation direction was isolated and analysed using principal component analysis (Kirschvink, 1980). Analysis was carried out by Chris Rowan, National Oceanography Centre.

CHAPTER 3

Ecology of the Diatom Flora Preserved in the Late Cretaceous Marca Shale and CESAR 6 Core

3.1 INTRODUCTION

This chapter serves to illustrate the diatom taxa encountered in both the CESAR 6 core and Marca Shale during this study and to highlight the relative abundance of each taxon in the two sections. Where information exists to do so, the ecology of the main diatom genera is discussed, primarily with reference to the two classes of diatom observed; the Coscinodiscophyceae (centric diatoms) and the Fragilariophyceae (araphid pennate diatoms). Diatoms of uncertain systematic position and resting spores of unknown affinity are also discussed. A full taxonomic list is presented in Appendix 1 with a full species list along with any pseudonyms. Interpretations on the origin/nature of laminae presented in Chapters 4 and 6 are based on the ecological information discussed here.

Species	CESAR 6	Marca Shale
Acanthodiscus immaculatus	−	VR
Actinoptychus packii	−	R
A. simbirkianus	R	−
A. taffii	−	R
A. tenuis	R	−
Anaulus sibiricus	A*	−
A. undulatus	−	VR
A. sp 1	R	−
Aulacodiscus archangelskianus	−	VR
Azpeitiopsis morenoensis	−	F*
Urataulina cretacea	−	R
C. sp1	F	−
Chaetoceros-type spore	−	C*
C.-type spore '1'	A*	−
Chasea bicornis	−	R
Coscinodiscus circumspectus	R	?
C. sibiricus	VR	−
C. symbolophorus	VR	−
Euodiella bicornigera	−	VR
Gladiopsis pacificus	R	−
G. speciosa	R	F*
Gloriopthychus callidus	−	VR
Goniothecium odontella	R	−
Helminthopsis wornardti?	VR	VR?
Hemiaulus altus	R	−
H. ambiguus	VR	VR

H. andrewsi	–	VR
H. antiquus	C*	–
H. curvulatus	–	VR
H. danicus	C	–
H. elegans	F	–
H. gleseri	C*	–
H. giganteus?	VR	–
H. hostilis	R	–
H. includens	R	–
H. kittonii	R	–
H. polymorphus	–	A*
H. polymorphus var. *morianus*	VR	–
H. rossicus	R	–
H. tumidicornis	A*	–
H. sp. 1	A*	–
H. sp. 2	R	–
H. sp. 6	R	–
H. sp. G	VR	–
H. sp?	VR	–
H. sp?	VR	–
H. sp?	VR	–
Kentrodiscus aculeatus	–	R
K. blandus	–	R
Medlinia deciusii	–	F
M. mucronata	–	F
Micrampulla parvula	–	F
Odontotropis cristata	VR	–
O. galleonis	–	VR
Paralia crenulata	–	C
Porpeia sp.	–	VR
Proboscia cretacea	F	F
Pseudopyxilla americana	R	–
P. russica	F	R
P. sp Strelnikova	R	–
Pseudostictodiscus picus	–	R
Pterotheca crucifera	VR	VR
P. evermannii	–	F
P. of Strelnikova (1974)	VR	–
Rhizosolenia sp.	C*	–
Sceptroneis dimorpha	F	–
S. grunowii	–	VR
S. praecaducea?	–	VR
S. sp. A	–	VR
S. sp. B	R	–
Sheshukovia excavata	–	VR
Skeletonema subantarctica	F	–
Skeletonemopsis crawfordii	VR	–
S. morenoensis	–	VR
Spore '3'	C	–
Stellarima distincta	–	C *?
S. steinyi	R	A*
S. sp. 1	R*	–
S. sp. 2	R	–
Stephanopyxis appendiculata	–	A*
S. barbadensis	–	R
S. discrepans	–	A*
S. grunowii	–	R
S. turris	R	–
Thalassiosiropsis wittiana	VR	VR
Triceratium indefinitum	R	–
T. planum	R	–
Trinacria acutangulum	R	–

T. aires	–	F
T. insipiens	–	R
T. tessela	R	–
T. tristictia	–	VR
Trochosiropsis polychaeta	A*	–
Xanthiopyxis grantii	–	VR
Unknown	F*	–

Table 3.1. List of the main diatoms encountered in observations of the CESAR 6 and Marca Shale. A = abundant, C = common, F = fair, R = rare, VR = very rare. Taxa observed to form near monospecific laminae marked with *.

All diatoms encountered were identified to at least the generic level using a number of key texts including Hanna (1927), Long *et al.* (1946), Hajós & Stradner (1975), Strelnikova (1975), Barron (1985b), Harwood (1988), Round *et al.* (1990), Dell'Agnese and Clark (1994) and Nikolaev *et al.* (2001). Discussions with P. Sims and R. Jordan also greatly helped identification and interpretations. Table 3.1 shows a list of the main species identified from both the CESAR 6 and Marca Shale. Relative abundances were obtained in two ways. For the CESAR 6, abundances are based on strew slide counts. However, many diatoms in the Marca Shale were found to suffer from extensive fragmentation, making strew slide counts problematic. Estimates for the Marca Shale are therefore based mainly on the frequency that individual specimens were encountered in studies of topographic stubs under the SEM, or in analysis of diatomaceous laminae in polished thin sections using BSEI. The estimates for the Marca Shale take into account the abundance of fragments, which can be more easily ascribed to a specific genus or species using the SEM. Diagenetic nodules taken from the Marca Shale were found to exhibit better preservation of diatom valves and results of the analysis of strew slides processed from these nodules were taken into account when estimating abundances. The ecological preferences of the main diatom species found in the two cores is summarised in Table 3.2.

3.2 Class **COSCINODISCOPHYCEAE** (centric diatoms) Round & Crawford

3.2.1 Genus ***Thalassiosiropsis*** Hasle in Hasle & Syvertsen

Thalassiosiropsis is a fossil genus, known to have an age range of Late Cretaceous (Campanian) to Palaeocene (Hasle & Syvertsen, 1985). Frustules of *Thalassiosiropsis* are discoid, with circular, flat valves (Hasle & Syvertsen, 1985). Cells are solitary, possessing no linking apparatus. *T. wittiana*, the only species of *Thalassiosiropsis* to have been identified to date, has a global distribution, present in both the CESAR 6 and Marca Shale sediments as well as those of Gdansk Bay (Poland), eastern slopes of the Urals and Seymour Island (Antarctica) (Sims, 1994a). On the basis of this cosmopolitan distribution it is likely that *T. wittiana* occupied an open marine planktonic niche, similar to many modern large discoid forms.

3.2.2 Genus ***Gladiopsis*** Gersonde & Harwood

Gladiopsis is a fossil genus that was separated from the genus *Gladius* during a study of some exceptionally well preserved lower Cretaceous diatoms (Gersonde & Harwood, 1990), and is one of the most distinctive Cretaceous diatoms. Frustules of this genus are characteristically long and cylindrical. The forms identified in this study broaden towards the end and are closed by a flat top and possess hexagonal areolae. The ecology of *Gladiopsis* is unknown, although the genus was initially described from a nearshore, shallow marine assemblage (Gersonde & Harwood, 1990). However, individual species of *Gladiopsis* display a cosmopolitan distribution, with *G. speciosus*, for example, known from the CESAR 6, Marca Shale, DSDP Site 275 (Hajós & Stradner, 1975), Seymour Island (Harwood, 1988), the Arctic Canada (Tapia & Harwood, 2002) and Russia (Strelnikova, 1974), suggesting that it may not have been restricted solely to nearshore environments.

3.2.3 Genus ***Stephanopyxis*** (Ehrenberg) Ehrenberg

Stephanopyxis is a fairly common planktonic genus in the present oceans, although fossil deposits contain a larger number of species. *Stephanopyxis turris* is known from both the fossil record (Upper Cretaceous) and the modern oceans. Valves of *Stephanopyxis* are heavily silicified and robust, capable of forming chains of filaments by interlocking processes with sibling valves (Round *et al.*, 1990), commonly seen in both the Marca Shale and CESAR 6 (Fig. 3.1).

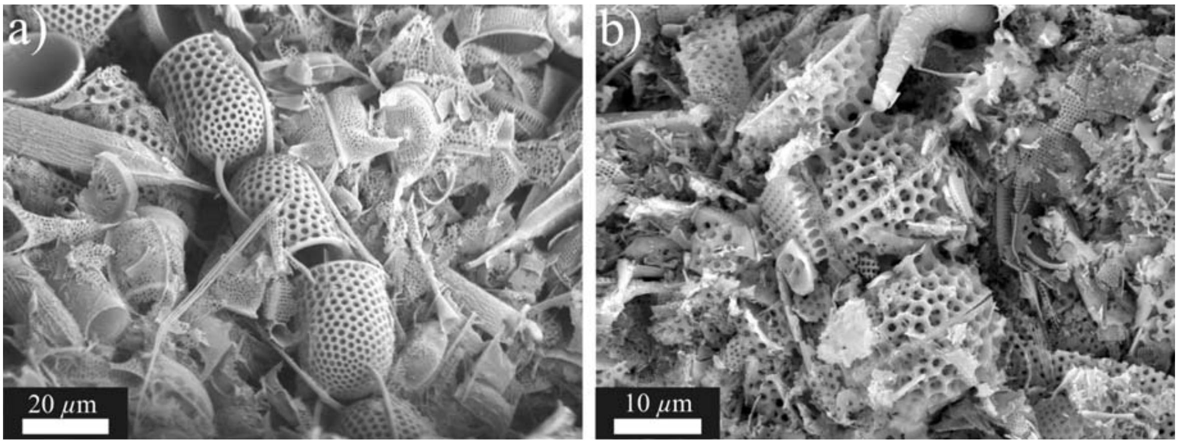

Figure 3.1. Backscattered electron image of a topographic stub, showing a) a small chain of *S. turris* from the CESAR 6 and b) *S. discrepans* from the Marca Shale.

Modern forms of this genus are found in tropical or warm water regions (Round *et al.*, 1990). Long chains of *S. palmeriana* are known to aggregate into large flocculant masses (Goldman, 1993). *S. palmeriana* has been sampled at a depth of 100m in the Sargasso Sea and found to be able to grow in ~2% light levels (Goldman, 1993) with production maintained through the sustained exploitation of nutrients periodically injected by the effects of passing storms, for instance. More recently, the doming of isopycnals under the influence of mesoscale eddies has become regarded as an important mechanism for stimulating blooms and it has been demonstrated that *S. palmeriana* is able to grow fast enough at depths of 100m to 50m (equivalent to 1% light level) to meet the new production estimates resulting from such eddies (Goldman & McGillicuddy, 2003). Valves are preferentially preserved in sediments by virtue of their robust nature, a fact highlighted in studies of the Gulf of California. *S. palmeriana* forms a maximum of 1-2% of the diatom flora in sediment traps although often forms near monospecific laminae in underlying sediments (Pike, 1996). BSEI of these laminated Holocene sediments show the greatest flux of *S. palmeriana* is in the autumn (Pike & Kemp, 1997; Kemp *et al.*, 2000). Sediment trap data from the Santa Barbara Basin show *S. palmeriana* is sedimented during the winter (C.B. Lange, personal observations-see Kemp, 2000). These observations led Kemp *et al.* (2000) to propose a radically different mode of diatomaceous export flux to the spring bloom, that they termed the “fall dump”, where sedimentation occurs *en masse* in response to the breakdown of stratification, in which *Stephanopyxis* is a key player.

3.2.4 Genus ***Triceratium*** Ehrenberg

Triceratium is well represented in the fossil record, with over 400 species recognised by VanLandingham (1978), although many of these have since been transferred to other genera. Round *et al.* (1990) state that the genus has a range from the Eocene to the present, although it has since been established that the genus ranges back into the Cretaceous (e.g. Tapia & Harwood, 2002). Valves are characteristically triangular and shallow, although can also be square. Unlike *Trinacria*, the 3 (or 4) corners of each valve do not possess elongate apices, but instead have elevations ending in ocelli (Round *et al.*, 1990). Although many studies of fossil assemblages group this genera with the holoplankton (e.g. Stickley *et al.*, 2004), modern forms occupy a free-living or attached, coastal marine niche (Round *et al.*, 1990). In a study of large, living epiphytic and epilithic diatoms in southern California, *T. pentacrinus* was found to be one of the most commonly observed marine species, forming long filaments attached to rocks or macroalgae (Tiffany & Lange, 2002).

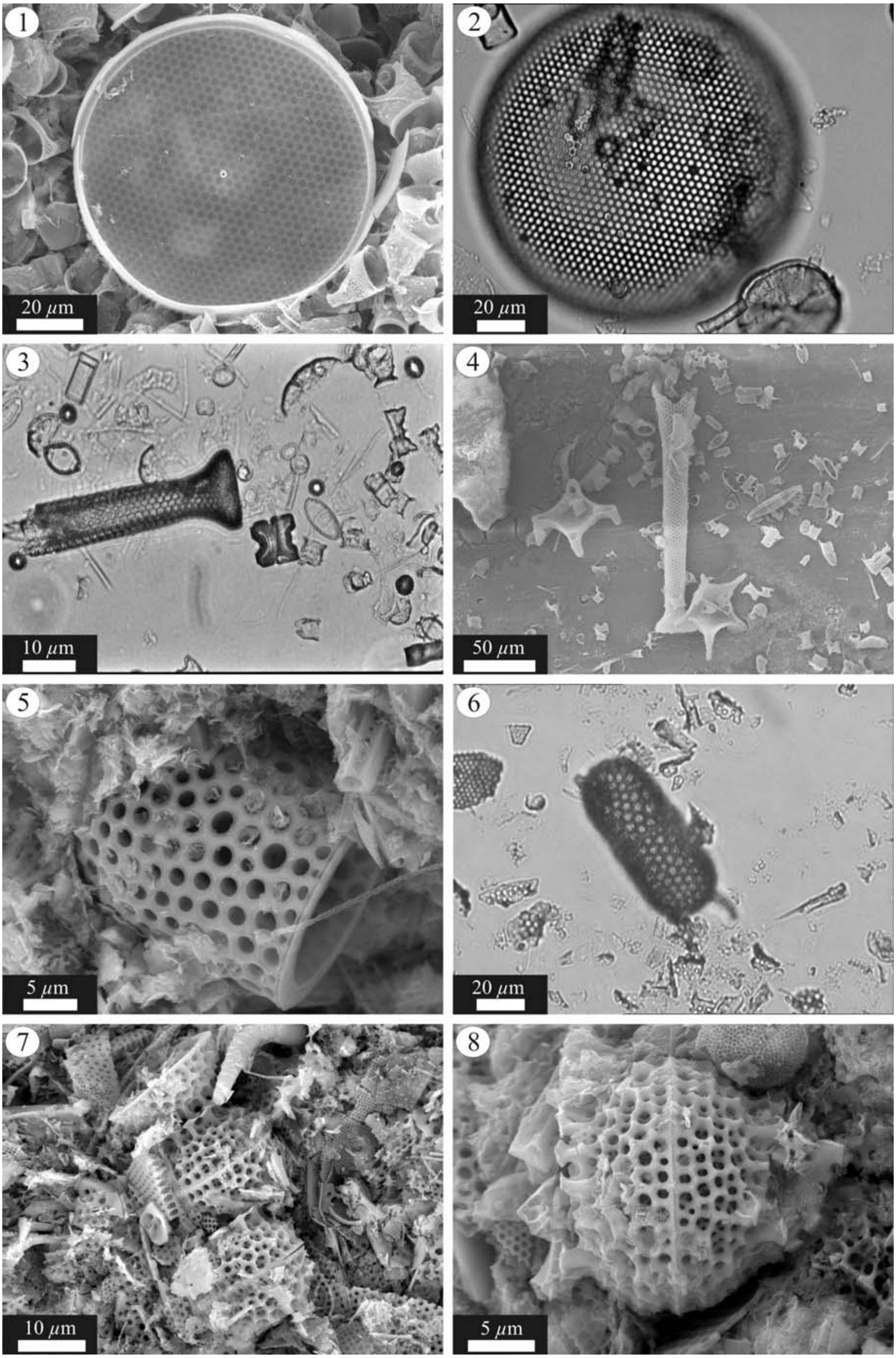

Plate 1. 1-2 *Thalassiosiropsis wittiana*, 3-4 *Gladiopsis speciosa*, 5-6 *Stephanopyxis appendiculata*, 7-8 *S. discrepans.* Images 1-4 are from the CESAR 6 and 5-8 from the Marca Shale.

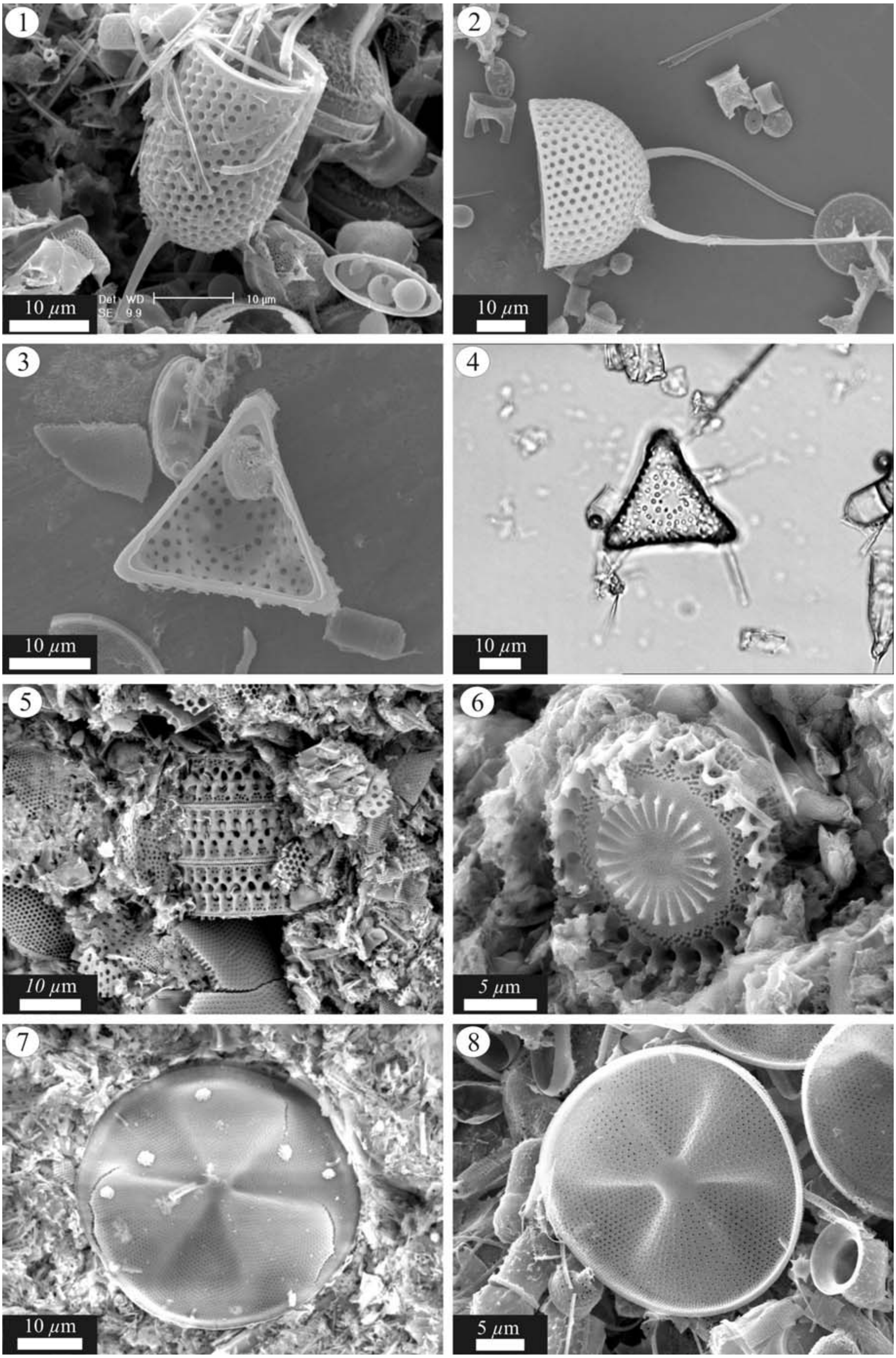

Plate 2. 1-2 *Stephanopyxis turris*, 3-4 *Triceratium indefinitum*, 5-6 *Paralia crenulata*, 7 *Actinoptychus packii*, 8 *A. tenuis*. Images 1-4 and 8 are from the CESAR 6 and 5-7 from the Marca Shale.

3.2.5 Genus ***Paralia*** Heiberg

Paralia represents a small genus in both the modern and fossil realms. Frustules are robust and link to form straight chains that are commonly found in both the plankton and benthos of modern temperate coastal environments (McQuoid & Nordberg, 2003). The extant form *P. sulcata*, remarkably similar in morphology to the fossil species *P. crenulata,* has been associated with a wide variety of environmental factors, including high salinity, low light and strong winds (McQuoid & Nordberg, 2003), although it is most commonly associated with the high primary productivity coastal upwelling zones (e.g. Abrantes, 1991). The species can be found in a range of salinities but is generally thought to be indicative of marine environments. *P. sulcata* does not ordinarily form large blooms, however, but is instead found concentrated in the water column during winter (Hobson & McQuoid, 1997), possibly an advantageous response to the low light conditions or the increased water column mixing. Indeed, primarily growing in the benthos (McQuoid & Hobson, 1998), strong physical mixing (during winter storms for instance) may play a crucial role in transporting cells into the plankton. *P. sulcata* also displays an affinity for arenaceous sediments (Round *et al.*, 1990). Due to its benthic affinity, *Paralia* can be used as an indicator of relative sea level, with lower sea levels characterised by greater numbers of *Paralia* (e.g. Ryua *et al.*, 2005).

3.2.6 Genus ***Actinoptychus*** Ehrenberg

Actinoptychus is an extant neritic genus that possesses characteristic valves that are sectored into alternate elevated and depressed sectors. Species of this genus are very common in neritic collections and there are many fossil examples (Round *et al.*, 1990). In the present oceans, *Actinoptychus* primarily occupies a benthic niche, possessing an epilithic or epiphytic mode of life (Round *et al.*, 1990). Valves are robust and heavily silicified, consistent with an ecological preference to high energy environments, and as such are often preserved in sediments and common in the geological record. In the Gulf of California, Sancetta (1995) regards this genus as a shelf dwelling form that is advected into the pelagic realm during summer storms. After valves have been advected into the plankton, they can be transported hundreds of miles offshore (e.g. Lange & Berger, 1993). Barron *et al*. (2004) have shown that in the Gulf of California, the abundance of *Actinoptychus* drops significantly in post glacial times, which they suggest relates to a decrease in down-slope transport in response to a rising sea level. *Actinoptychus* is therefore useful as a benthic index fossil.

3.2.7 Genus ***Coscinodiscus*** Ehrenberg

Coscinodiscus first appeared in the Late Cretaceous (Harwood & Nikolaev, 1995) and the genus is widespread in the fossil record. Many modern forms are very widespread and cosmopolitan (Round *et al.*, 1990). Cells of this genus are discoid, ranging in morphology from barrel-shaped to almost flat (coin-shaped). Modern representatives of *Coscinodiscus* occupy a free-living, solitary, marine planktonic niche (Round *et al.*, 1990). The Santa Barbara Basin trap experiment (August 1993 to July 1996) demonstrated that several large *Coscinodiscus* spp. (*C. centralis, C. perforatus, C. granii, C. oculus-iridis* and *C. wailesii*) are important components of the early winter and winter flux (Lange *et al.*, 2000b). Similarly, Sancetta (1995) noted high fluxes of *Coscinodiscus* during the late autumn in the Gulf of California. The high flux of large *Coscinodiscus* spp. during the late autumn/early winter has been documented in laminated sediments from the Gulf of California, where they form discrete depositional events in a four part seasonal flux cycle (Pike & Kemp, 1996b; Kemp *et al.*, 2000). *Coscinodiscus* spp., especially larger forms, are key species involved in "fall dump" export flux (Kemp *et al.*, 2000), although some species of *Coscinodiscus* are associated with more mixed conditions. For example, *C. radiatus* is common in the Gulf mixed assemblage laminae, which are related to blooms stimulated by the injection of nutrients into the photic zone in response to winter mixing. El Niño events in the Santa Barbara Basin are characterised by an increase in several large, warm water species (*C crenulatus, C. plicatoides*) (Lange, 1987; Lange *et al.*, 1990).

3.2.8 Genus ***Trochosiropsis*** Gleser

Trochosiropsis is a fossil genus, first appearing in the Campanian (Harwood & Nikolaev, 1995), and known to range into the Tertiary (Harwood, 1988), that possesses cylindrical frustules with valves bordered by a marginal ridge. Robust linking spines occur in the centre of the valves (Sims, 1988), allowing *Trochosiropsis* to form chains, encountered in analysis of topographic stubs (Fig. 3.2). Valves are often observed with broad, fragile girdle bands when attached in chains (Fig. 3.2), although in single valves they are often missing. The relatively robust nature of the *Trochosiropsis* valves in the CESAR 6 sediments has lead some authors to interpret it as a resting spore (e.g. Kitchell *et al.*, 1986; Dell'Agnese & Clark, 1994). However the identification of the long chains of this genus in the CESAR 6 sediments and the presence of girdle bands (see Fig. 3.2 and Plate 3.7-8) is inconsistent with this conclusion (P. Sims, personal communication). The exact ecological preferences of *Trochosiropsis* are unknown, but *T. polychaeta* is geographically widespread, present in the CESAR 6, South Pacific DSDP Site 275 (Hajós & Stradner, 1975), the Ural mountains (Strelnikova, 1971), Arctic Canada (Tapia & Harwood, 2002) and Seymour Island (Antarctica) (Harwood, 1988), suggesting it is likely to have been a planktonic species.

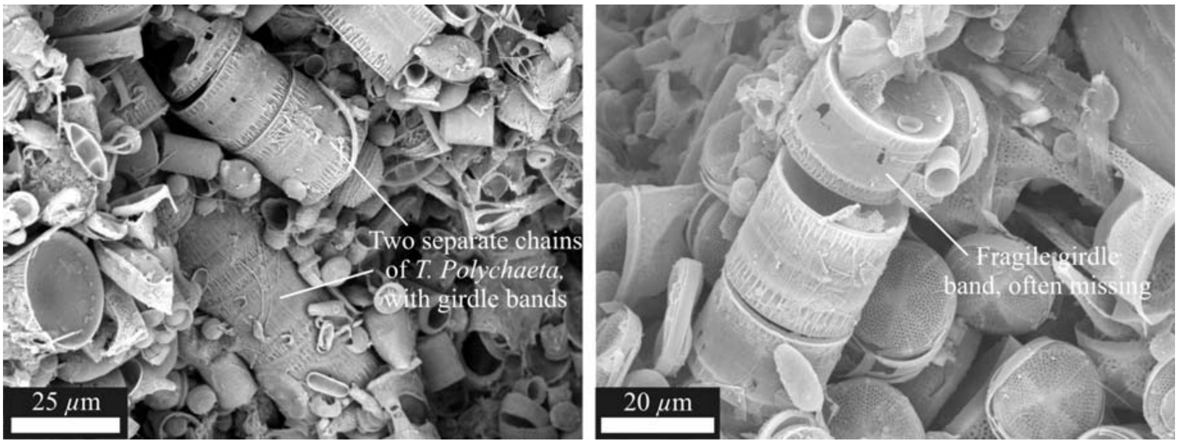

Figure 3.2. BSEI of topographic stubs from the CESAR 6 showing small chains of *T. polychaeta*.

3.2.9 Genus ***Skeletonemopsis*** Sims

Valves of *Skeletonemopsis* are characteristically cylindrical and able to form chains through marginal linking spines. Although this genus is extinct, ranging in age from the Cretaceous to Oligocene (Sims, 1994b), it shares a similar morphology to the extant genus *Skeletonema*, which presently forms an important component of the coastal plankton (Round *et al.*, 1990). *Skeletonema* is associated with well mixed, coastal upwelling regimes and commonly forms spring blooms (Brodie & Kemp, 1994; Dean *et al.*, 2001; Chang *et al.*, 2003). Both genera are characterised by relatively small, lightly silicified cells, capable of forming long chains. However, unlike modern *Skeletonema*, the two species of *Skeletonemopsis* identified in this study appear to have had restricted geographical and/or age distributions. *S. crawfordii* and *S. morenoensis* have only been identified from the CESAR 6 core and Marca Shale, respectively, although other species of *Skeletonemopsis* (e.g. *S. barbadense*, *S. mahoodii*, *S. rugosa*) are known to have cosmopolitan distributions. The restricted distribution of some species may be a taphonomic artefact, related to the small, fragile nature of the valves of this genus, which may also explain why *S. morenoensis* has been omitted from many previous taxonomic studies of the Marca Shale (e.g. Hanna, 1927; Long *et al.*, 1946; Nikolaev *et al.*, 2001).

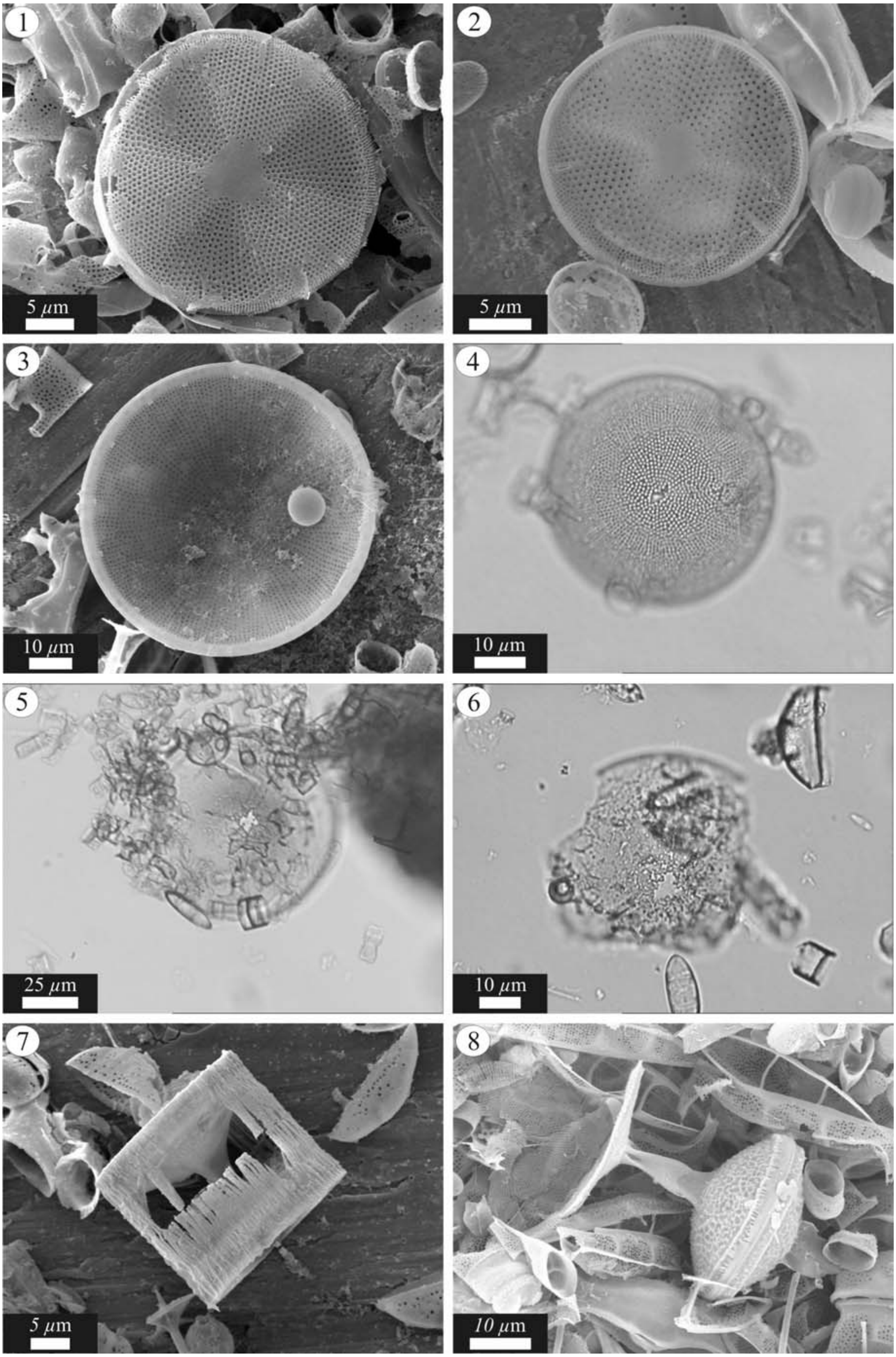

Plate 3. 1-2 *Actinoptychus Simbirkianus*, 3-4 *Coscinodiscus circumspectus*, 5-6 *Coscinodiscus sibiricus*, 7-8 *Trochosiropsis polychaeta*. All images are from the CESAR 6.

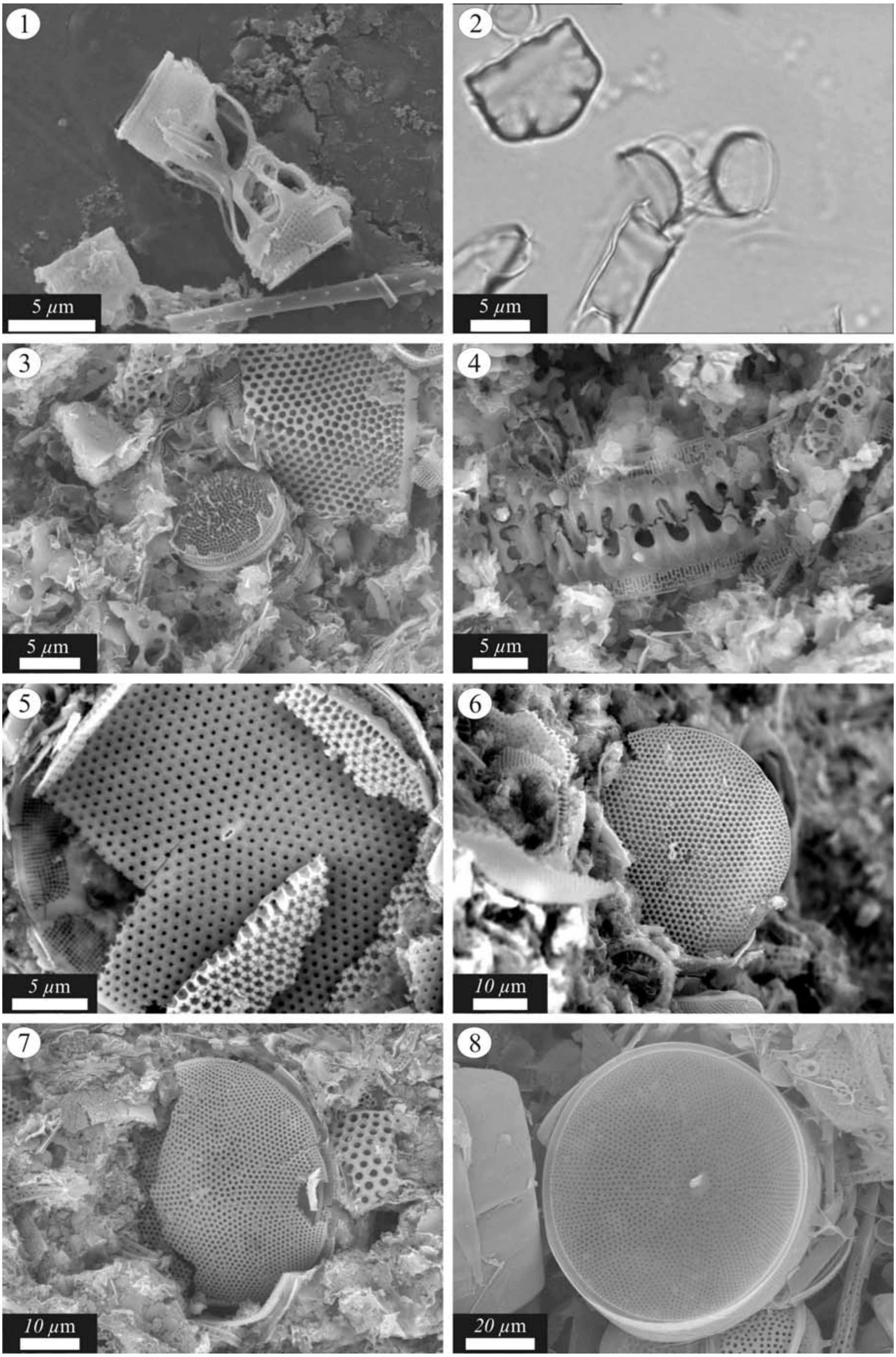

Plate 4. 1-2 *Skeletonemopsis crawfordii*, 3-4 *S. morenoensis*, 5-6 *Stellarima distincta*, 7-8 *S. steinyi*. Images 1, 2, and 8 are from the CESAR 6 and 3-7 are from the Marca Shale.

3.2.10 Genus ***Stellarima*** Hasle & Sims

The genus *Stellarima* is extant and known from sediments of Late Cretaceous-Holocene age (Sims & Hasle, 1987). Formerly placed in the genus *Coscinodiscus*, valves of *Stellarima* are discoid and solitary (Round *et al.*, 1990). The genus is distinct from *Coscinodiscus* in possessing no marginal rimportulae (only central radiate rimportulae) and in having internal closing plates to the areolae (Hasle & Sims, 1986). Modern species of *Stellarima* occupy a solitary, marine, planktonic niche (Abrantes, 1988; Round *et al.*, 1990). Sediment trap studies (by the Baltic Sea Research Institute- http://www.io-warnemuende.de/research/en_galerie.html) have shown that the modern form *S. stellaris*, a warm-temperate water species (Hasle & Syvertsen, 1996), is found concentrated in the water column during the autumn and winter in the Baltic Sea, suggesting it too may be a “fall dump” species. The other well known extant species, *S. microtrias*, is an abundant part of the plankton around Antarctica and is known to form endogenous resting spores, which are similar in morphology to the vegetative cells (Syvertsen, 1985). The distribution of *Stellarima* spp. in the Upper Cretaceous fossil record indicates that at this time the genus was cosmopolitan, consistent with a planktonic mode of life (Sims & Hasle, 1987). For example, *S. steinyi* has been identified in both the CESAR 6 and Marca Shale, as well as in sediments from Seymour Island (Harwood, 1988), Canadian Arctic (Tapia & Harwood, 2002) and western Siberia (Strelnikova, 1974). Sims and Hasle (1987) described both a resting stage and vegetative cell of *S. steinyi* in a study of Late Cretaceous material from Siberia, Arctic Ocean and the Moreno Shale. Both the resting stages and vegetative cells of *S. steinyi*, as described by Sims and Hasle (1987), are present in diatomaceous laminae in the Marca Shale, with the resting stages more abundant. Both the resting stages and the vegetative cells were sedimented concurrently (Fig. 3.3).

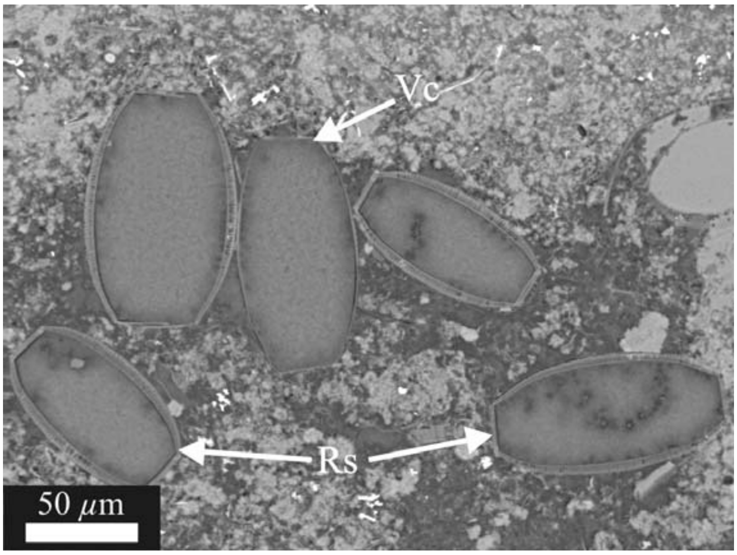

Figure 3.3. Backscattered electron image of a polished thin section prepared from an early diagenetic nodule, depicting both a vegetative cell (Vc) and resting stages (Rs) of *Stellarima steinyi*, demonstrating deposition occurred concomitantly. Note the diatom hash matrix.

3.2.11 Genus ***Azpeitiopsis*** Sims

Valves of the fossil genus *Azpeitiopsis* are large, solitary, discoidal and robustly silicified. The genus was formerly placed in the genus *Coscinodiscus* but separated by virtue of possessing a central tubular opening and rimoportular. *A. morenoensis* is an important biostratigraphical index fossil appearing in the Early Maastrichtian and possesses a global distribution, known from the Marca Shale (Hanna, 1927), Akupa river basin, Russia (Strelnikova, 1975), the Kerguelen Plateau (ODP Leg 120, Site 748) (Shipboard-Scientific-Party, 1989) and both the Tonga Trench and Southern Ocean (Tapia & Harwood, 2002). The closest extant relative of *Azpeitiopsis* is the genus *Azpeitia*, with which *Azpeitiopsis* shares many morphological similarities. A species of *Azpeitia*, *A. nodulifera*, is particularly important in palaeoceanographic studies in the Gulf of California. *A. nodulifera* is generally rare in coastal settings, but is common in subtropical/tropical gyres (Fryxell *et al.*, 1986; Schrader *et al.*, 1993) and its presence in the Gulf of California can be correlated with the warmer, more oceanic conditions of El Niño events (Sancetta, 1995; Barron *et al.*, 2004). Sediment traps deployed at the Namibia upwelling mooring site (central Benguela System) reveal *Azpeitia* spp. has a peak flux in the summer, with a smaller secondary peak in flux in the winter (Romero *et al.*, 2002). Sediment traps off the coast of northern Chile record a peak flux of *Azpeitia* spp. during the late spring, with higher flux over all seasons during El Niño years (Romero *et al.*, 2001). The global distribution of *A. morenoensis* along with its large size and morphological similarities with *Azpeitia*, suggest that this taxa was holoplanktonic and probably oceanic.

3.2.12 Genus ***Hemiaulus*** Ehrenberg

Hemiaulus is common in both the modern and fossil realm, although fossil floras generally have more robust forms than are present today (Round *et al.*, 1990). Cells of this genus are capable of forming long chains by interlocking spines found at the end of protruding polar horns, observed in both the Marca Shale and CESAR 6 (Fig. 3.4). Early studies of Mediterranean floras demonstrated that *Hemiaulus* characteristically dominate the sparse diatom flora after seasonal stratification in warm oligotrophic conditions (Guillard & Kilham, 1977). A recent study has shown that along the eastern Mediterranean coast, highest phytoplankton abundances occur in the summer in response to the abundance of *H. membranaceus*, concurrent with both the lowest phytoplankton diversity and nutrient concentrations (Polat & Isik, 2002). Since the classical studies of *Hemiaulus* in the Mediterranean, it has been shown that cells of *Hemiaulus* (*H. hauckii*) harbour intracellular N_2-fixing cyanobacteria (Villareal, 1991) and as such are capable of inhabiting large areas of the ocean characterised by low ambient nutrients. *H. hauckii* has been recorded dominating summer blooms in the central North Pacific between depths of 45-130m (Brzezinski *et al.*, 1998). A doming of the isopycnals within the nutricline beneath the blooms suggests that, in this study, the bloom was enhanced by eddy pumping. *H. hauckii* has also been observed to grow in, and be exported from the upper mixed-layer (Scharek *et al.*, 1999a). *Hemiaulus* blooms can be spatially extensive. A bloom of *H. hauckii* in the tropical Atlantic was estimated to cover an area of 1.4 to 2.8 × 10^6 km^2 (Carpenter *et al.*, 1999). Nitrogen isotope data also suggests that this bloom had been rather long-lived, on the scale of weeks to months and was related to the outwash plume of the Amazon and Orinoco Rivers. Scharek *et al.* (1999a) proposed that proliferation of *H. hauckii* during the summer may relate to the N_2-fixing capacity of the *H. hauckii* endosymbionts, in conjunction with calm conditions, supported by the increased concentrations of the N_2-fixing cyanobacterium *Trichodesmium* spp. in the water column during summer. The adaptation of *Hemiaulus* to stratified, oligotrophic conditions was highlighted in a study of a Hawaiian mesoscale cyclonic eddy (subtropical Pacific). Distinct differences in the diatom assemblages inside and outside of the eddy were recorded, with *H. hauckii* found to be dominant in the assemblage outside and rare inside of the eddy (Vaillancourt *et al.*, 2003). It was also found that whilst *Hemiaulus* cells outside the eddy possessed endosymbiotic cyanobacteria, those inside the eddy did not, a likely response to the higher nitrate concentrations inside the eddy.

Bottom moored sediment traps situated in the oligotrophic North Pacific gyre show distinct peaks in the flux of *H. hauckii* during the summer. Rarer species of *Hemiaulus* (*H. membranaceus* and *H. sinensis*) displayed similar seasonal flux patterns and shared similar habitats (Scharek *et al.*, 1999b). The flux event was clearly visible at 4000m and followed a documented summer bloom of *H. hauckii* that occurred ~ 3 weeks prior, suggesting sedimentation rates of ca 100 to 200 md^{-1}. Rapid sinking velocities were evidenced by a marked increase in the proportion of cytoplasm containing cells in the sediment traps during these flux events. These rapid sinking velocities cannot be explained by cell aggregation processes (excluding the action of TEP) and thus likely relate to the fact that colonial chains were not disaggregated in the mixed layer and were able to form flocculent masses (Scharek *et al.*, 1999b). Sinking is known to be triggered by physiological responses to depleted macronutrient or iron concentrations (Waite *et al.*, 1992; Muggli *et al.*, 1996) and Scharek *et al.* (1999b) invoked this mechanism to explain their observations. BSEI studies have shown that *H. hauckii* forms near-monospecific sublaminae in Mediterranean sapropels (Pearce *et al.*, 1998) above early winter/spring bloom mixed diatom laminae (Kemp *et al.*, 1999). Kemp *et al.* (2000) initially interpreted these monospecific laminae of *Hemiaulus* as “fall dump” flux, although it now appears that they were deposited in summer in response to the break down of stratification.

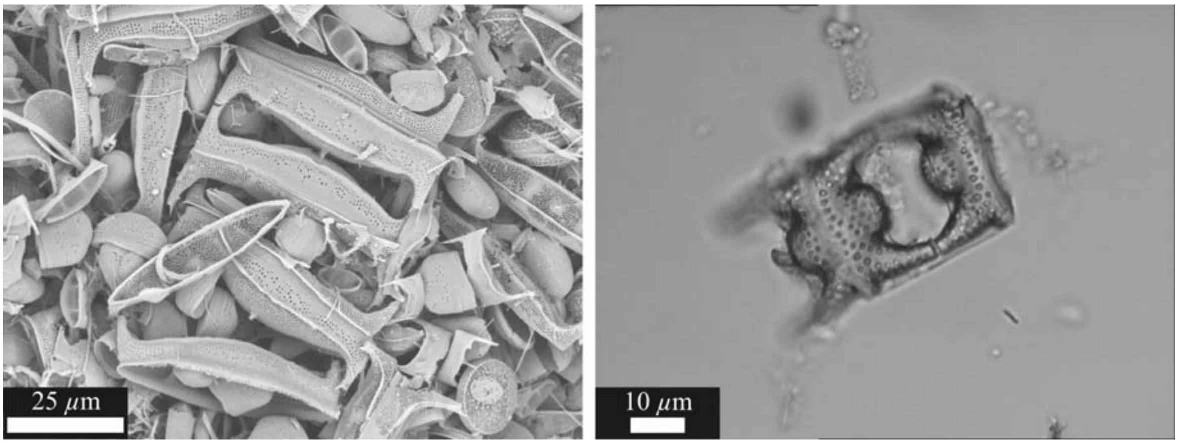

Figure 3.4. Topographic BSEI photograph of a chain of *H. gleseri* from the CESAR 6 and optical photograph of a small chain of *H. polymorphus* valves from the Marca Shale.

3.2.13 Genus ***Cerataulina*** Pergallo

Valves of *Cerataulina* are elongate with a long cylindrical and shorter conical apex, from which numerous long filaments branch. Valves are generally hyaline, although some may possess a finely perforated section near the lower part of the cylindrical part of the valve wall. The lower apex of *Cerataulina*, from which the long filaments emanate, appear to be related to specimens of *Skeletonema subantarctica* (Fig. 3.5), valves of which are often found intertwined with specimens of *Cerataulina* (Plate 10.1-4). It therefore appears that these two diatoms are part of the same valve. Hajós and Stradner (1975) interpreted *C. cretacea* to be a permanent spore from a non-identified planktonic diatom. Specimens of *Cerataulina* have been described from the SW Pacific (Hajós & Stradner, 1975) and the Marca Shale and CESAR 6 (THIS STUDY).

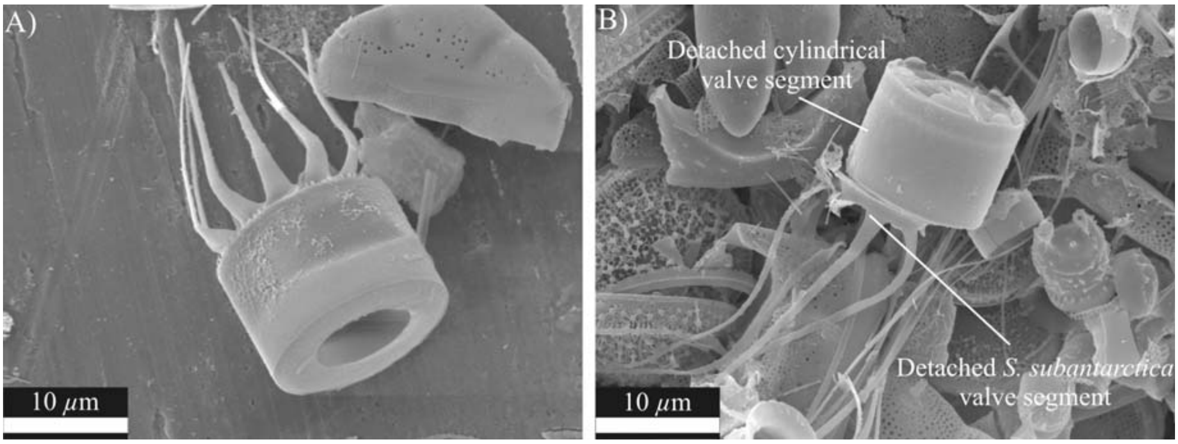

Figure 3.5. Topographic stub BSEI of; A) a complete valve of *Cerataulina* and B) a valve which has separated, forming a detached valve of *S. subantarctica* and a hyaline, cylindrical valve segment.

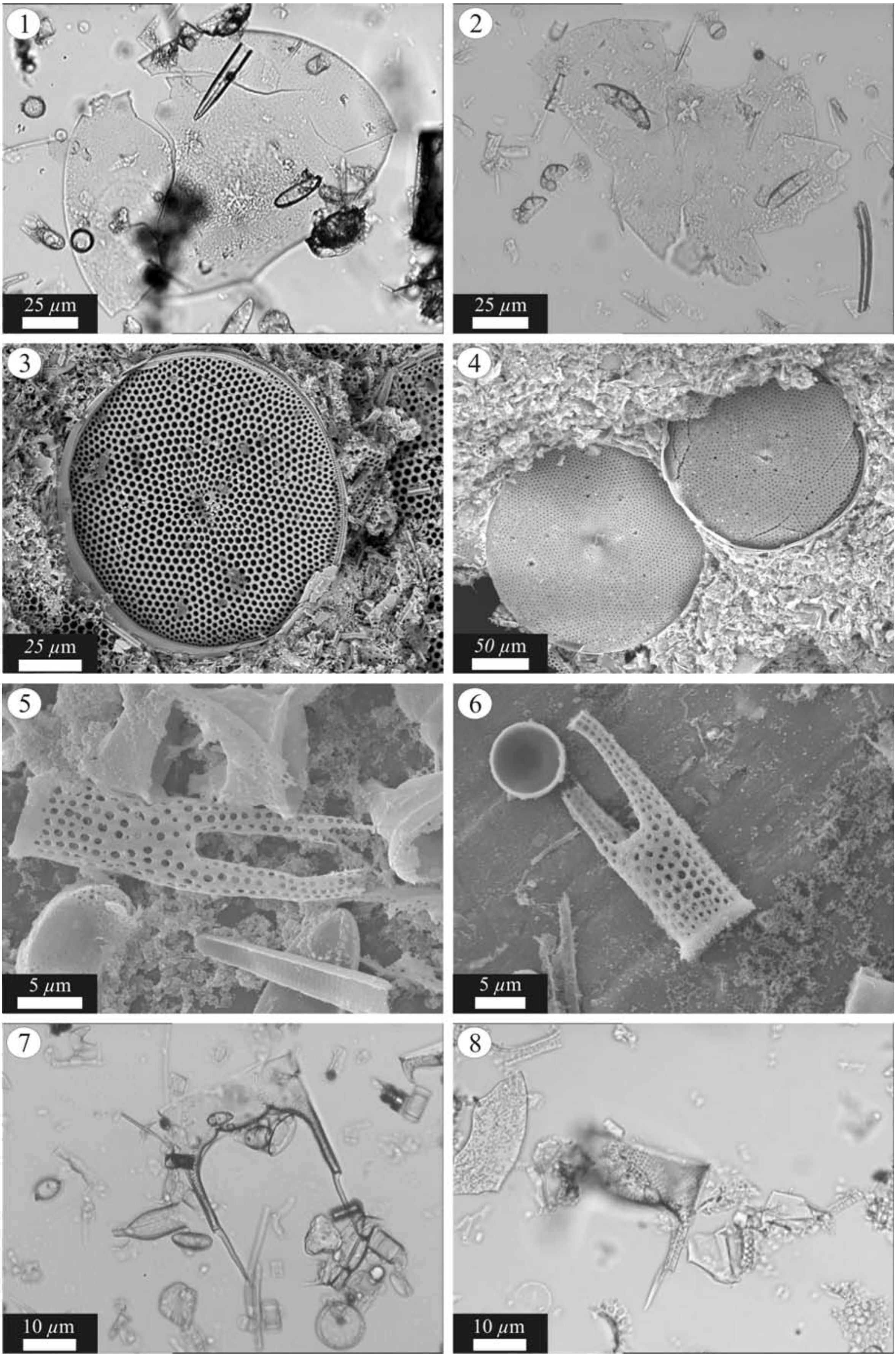

Plate 5. 1-2 *Stellarima* sp.1, 3-4 *Azpeitiopsis morenoensis*, 5-6 *Hemiaulus altus*, 7-8 *H. ambiguus*. Images 1, 2,5,6,7 are from the CESAR 6 and 3, 4, 8 are from the Marca Shale.

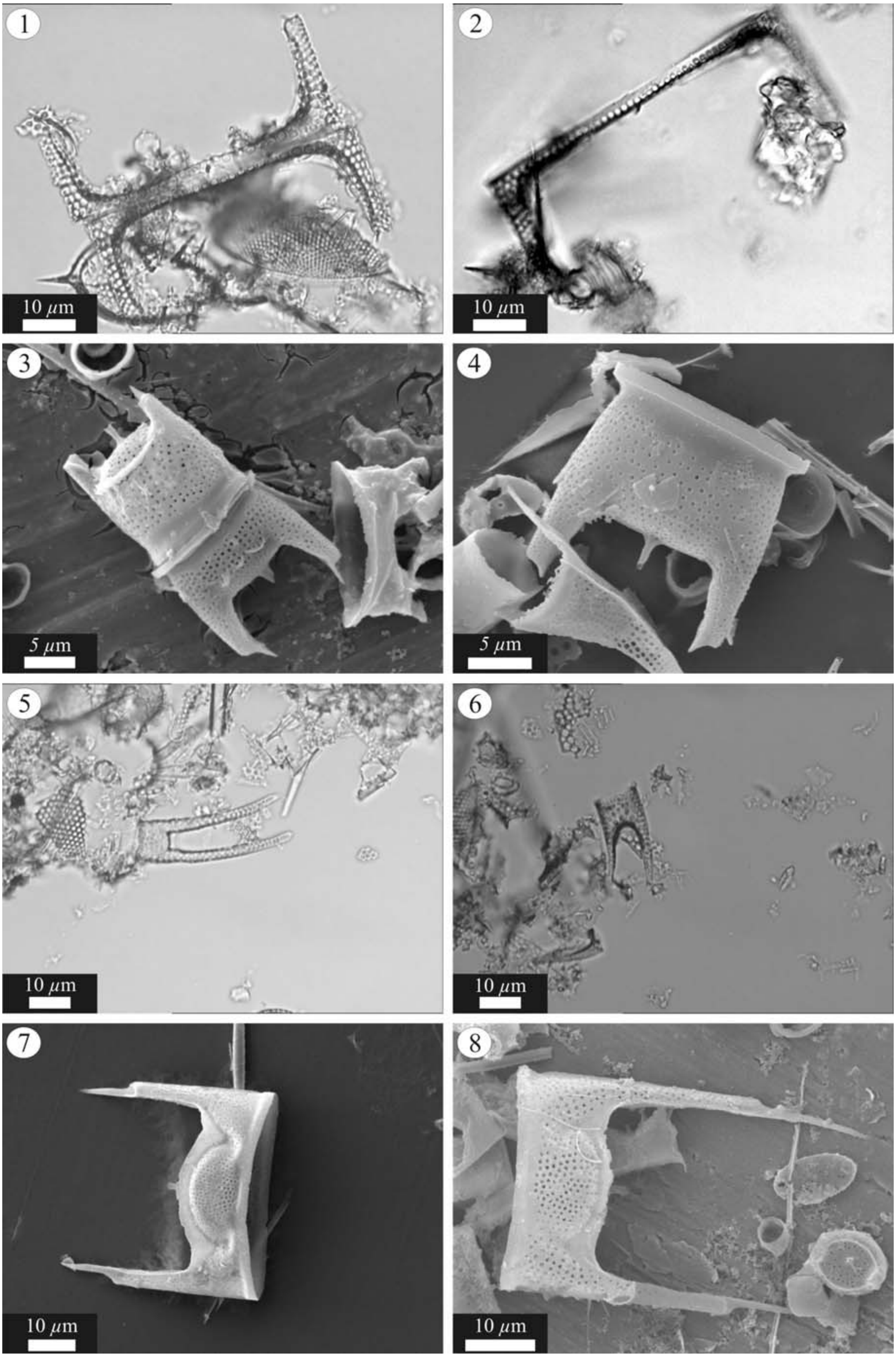

Plate 6. 1-2 *Hemiaulus andrewsi*, 3-4 *H. antiquus*, 5-6 *H. curvulatus*, 7-8 *H. danicus*. Images 1, 3, 4, 7and 8 are from the CESAR 6 and 2 and 5-6 are from the Marca Shale.

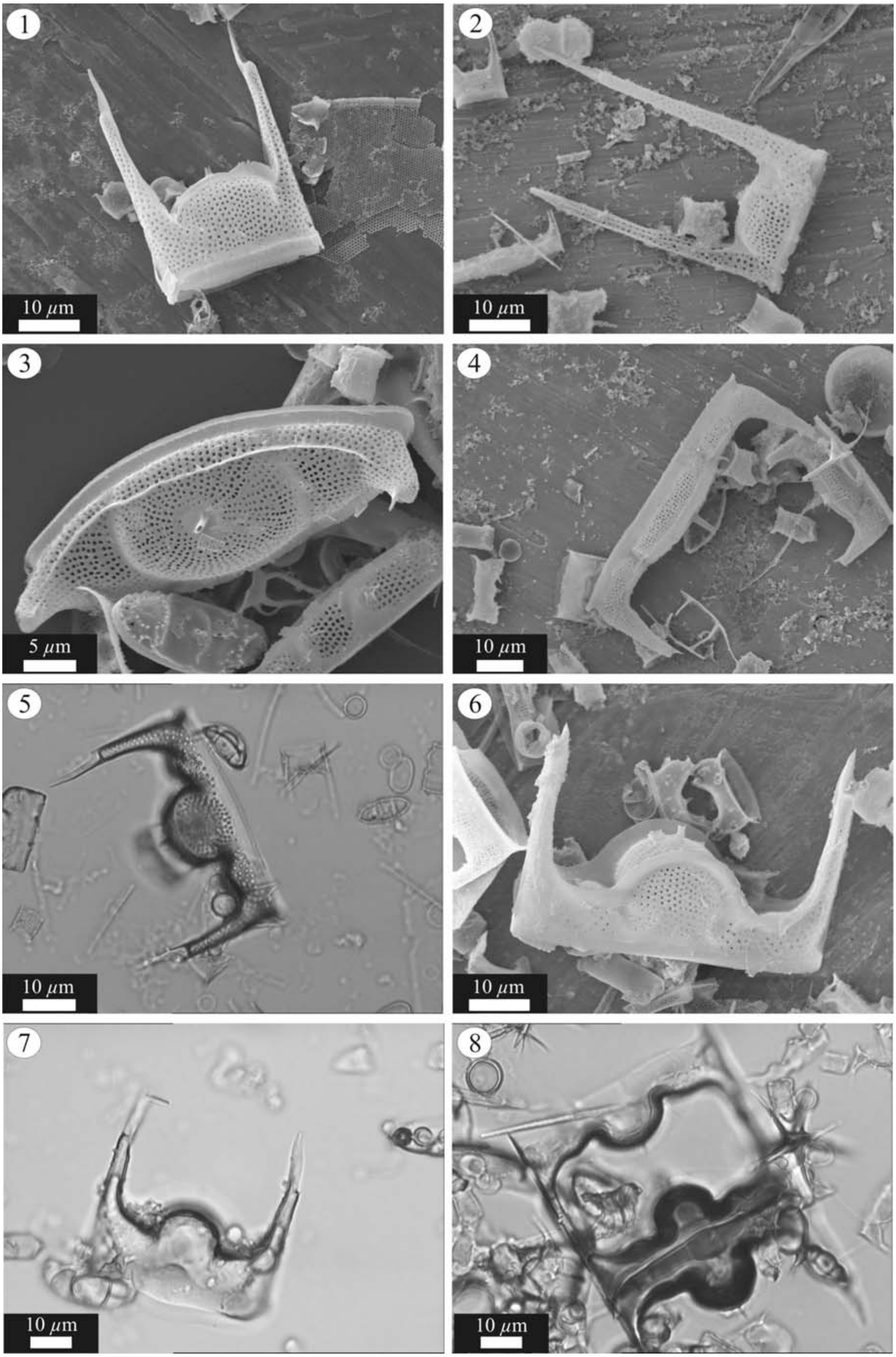

Plate 7. 1-2 *Hemiaulus elegans,* 3-4 *H. gleseri*, 5-6 *H. hostilis*, 7-8 *H. includens*. All images are from the CESAR 6.

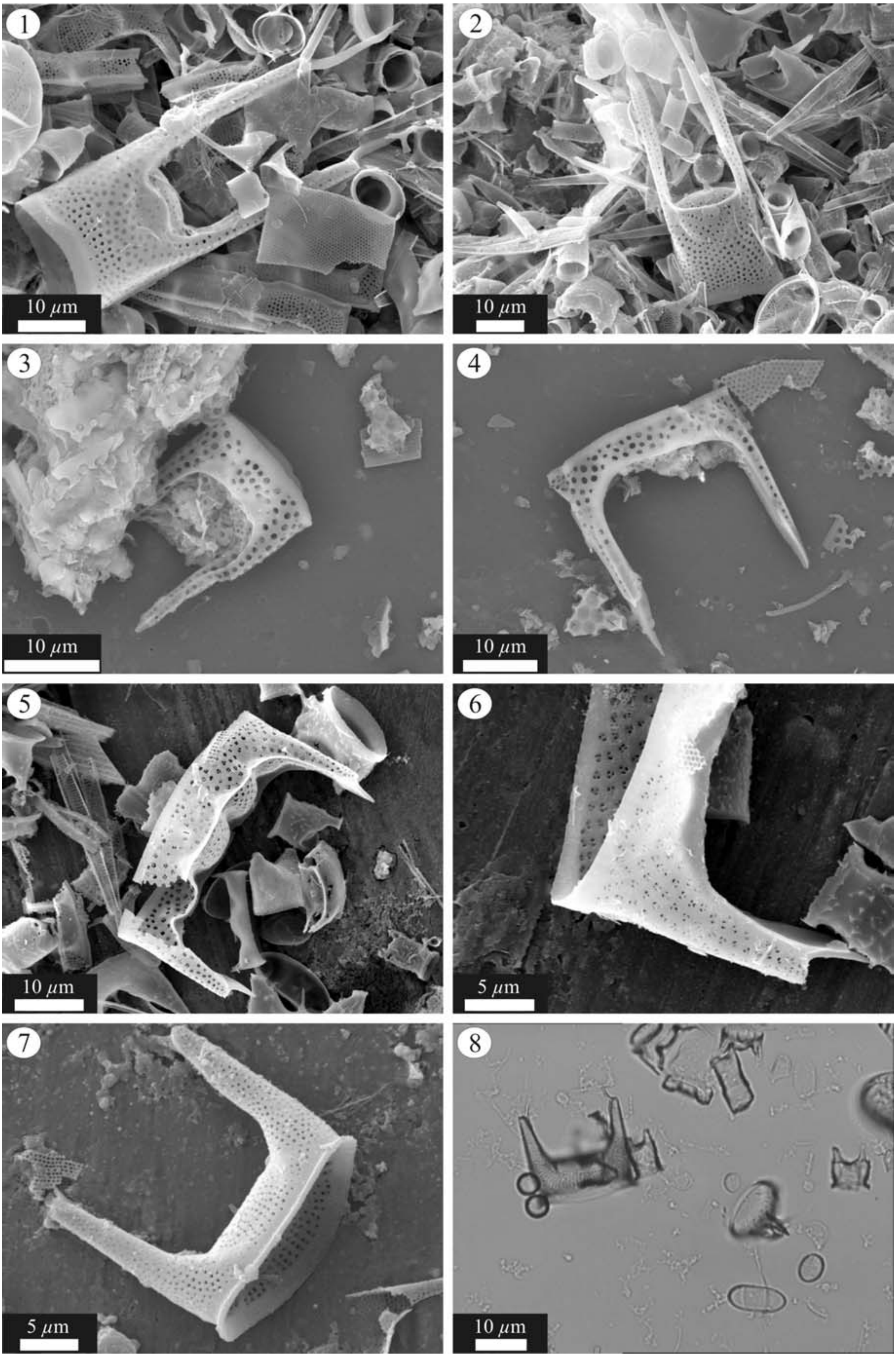

Plate 8. 1-2 *Hemiaulus kittonii*, 3-4 *H. polymorphus*, 5-6 *H. rossicus*, 7-8 *Hemiaulus* 'G'. Images 1-2, 5-8 are from the CESAR 6 and 3-4 are from the Marca Shale.

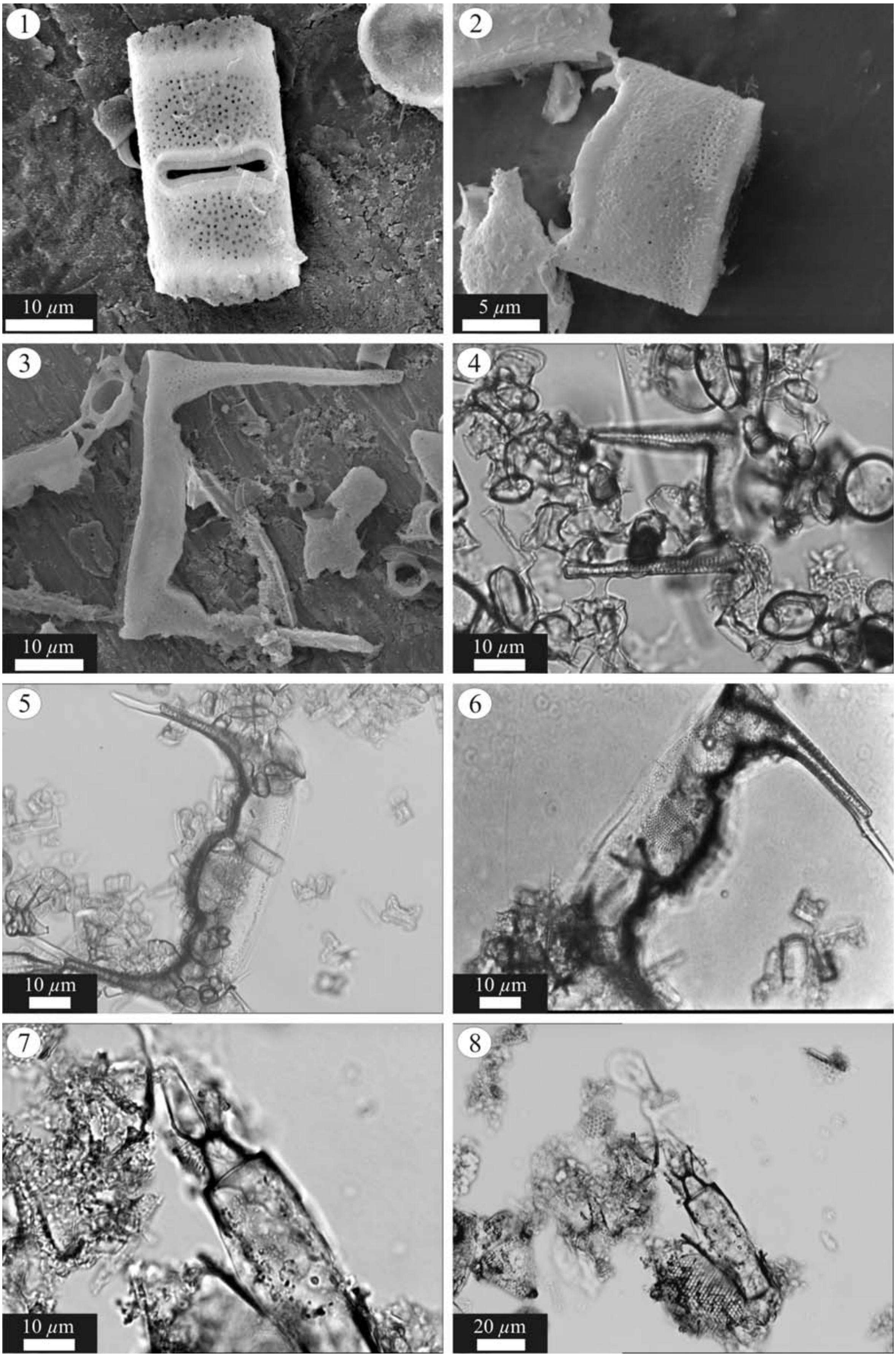

Plate 9. 1-2 *Hemiaulus* '2', 3-4 *Hemiaulus* '6', 5-6 *Hemiaulus* ?, 7-8 *Cerataulina cretacea*. Images 1-5 are from the CESAR 6 and 6-8 are from the Marca Shale.

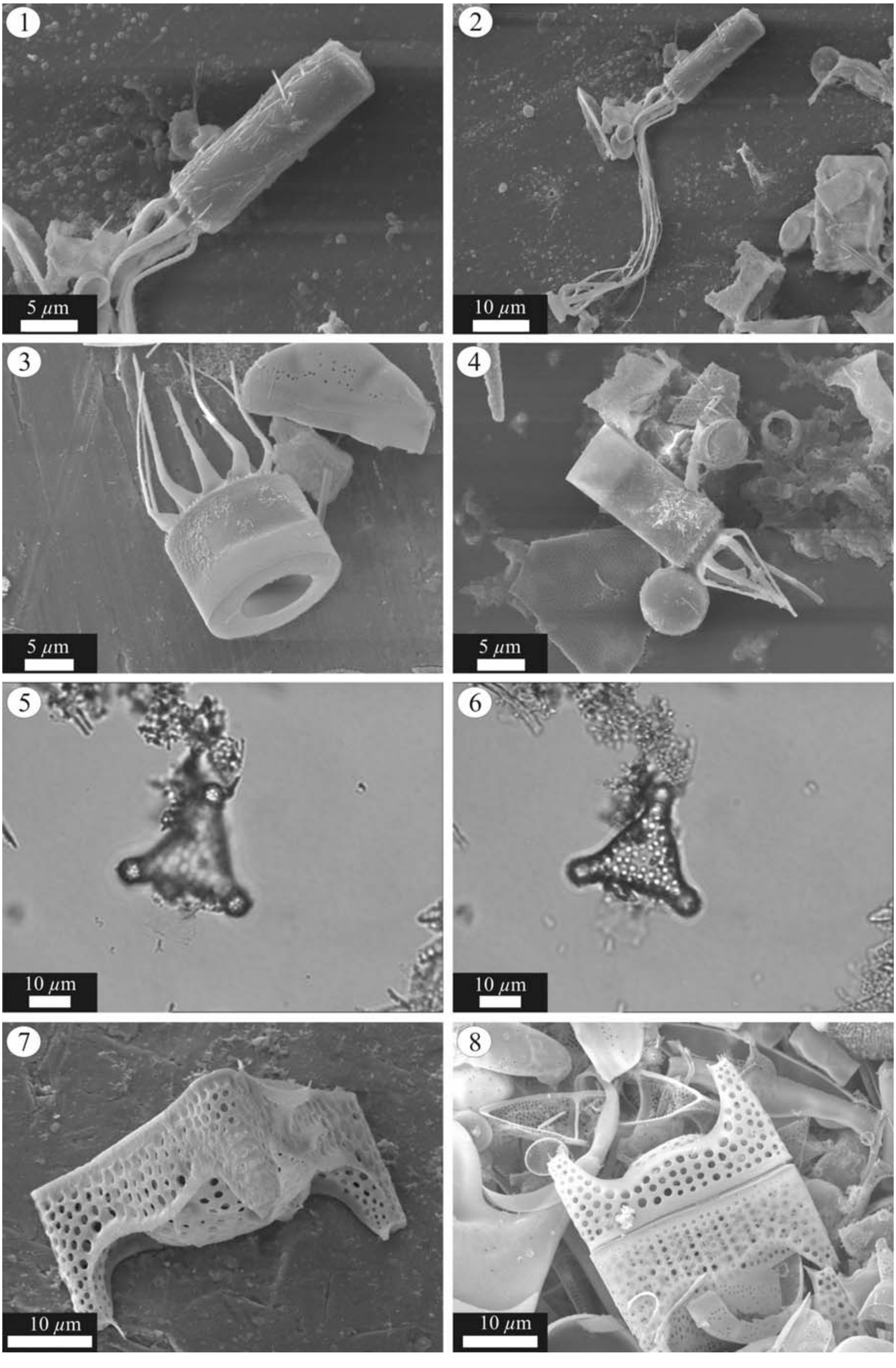

Plate 10. 1-4 *Cerataulina* sp.1, 5-6 *Trinacria aires*, 7-8 *Trinacria acutangulum*. Images 1-4 and 7-8 are from the CESAR 6 and 5-6 are from the Marca Shale.

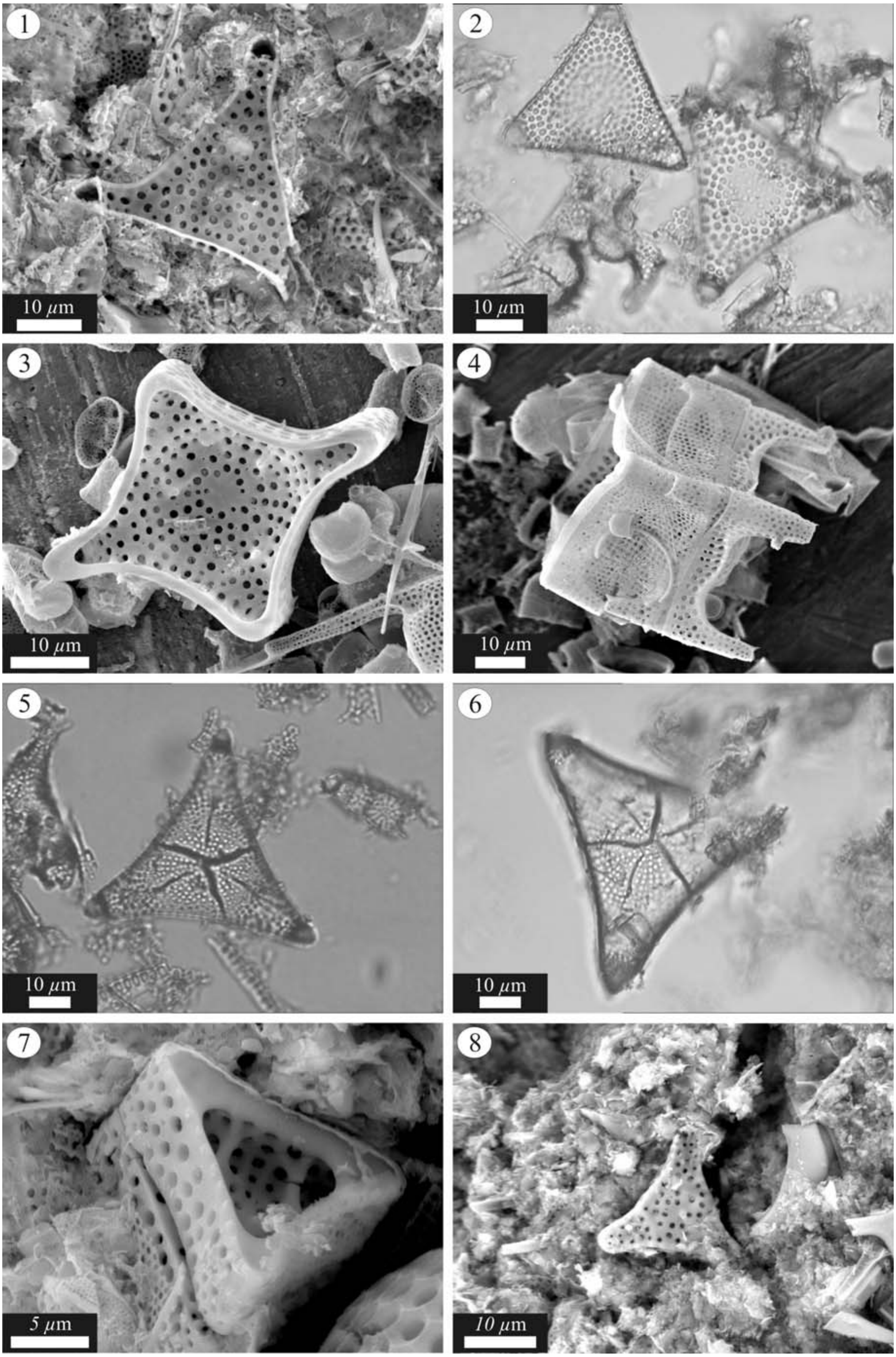

Plate 11. 1-2 *Trinacria insipiens*, 3-4 *Trinacria* tessela, 5-6 *Trinacria tristictia*, 7-8 *Medlinia deciusii*. Images 3-4 are from the CESAR 6 and 1-2 and 5-8 are from the Marca Shale.

3.2.14 Genus ***Trinacria*** Heiberg

Trinacria is an extinct genus that has an age range of Cretaceous-Eocene (Round *et al.*, 1990). Cells are tri-/quadr-angular, forming chains through interlocking extended apices, which are encountered in topographic stubs (Fig. 3.6). *Trinacria* is common in coastal fossil assemblages and is generally considered to be a marine planktonic genus, occupying either a neritic (e.g. Eggar *et al.*, 2003) or offshore niche (e.g. Stickley *et al.*, 2004). Valve morphology places the genus within the Hemiaulaceae, and owing to this, *Trinacria* is often grouped with *Hemiaulus* when analysing the ecology of fossil assemblages (e.g. Harwood, 1988).

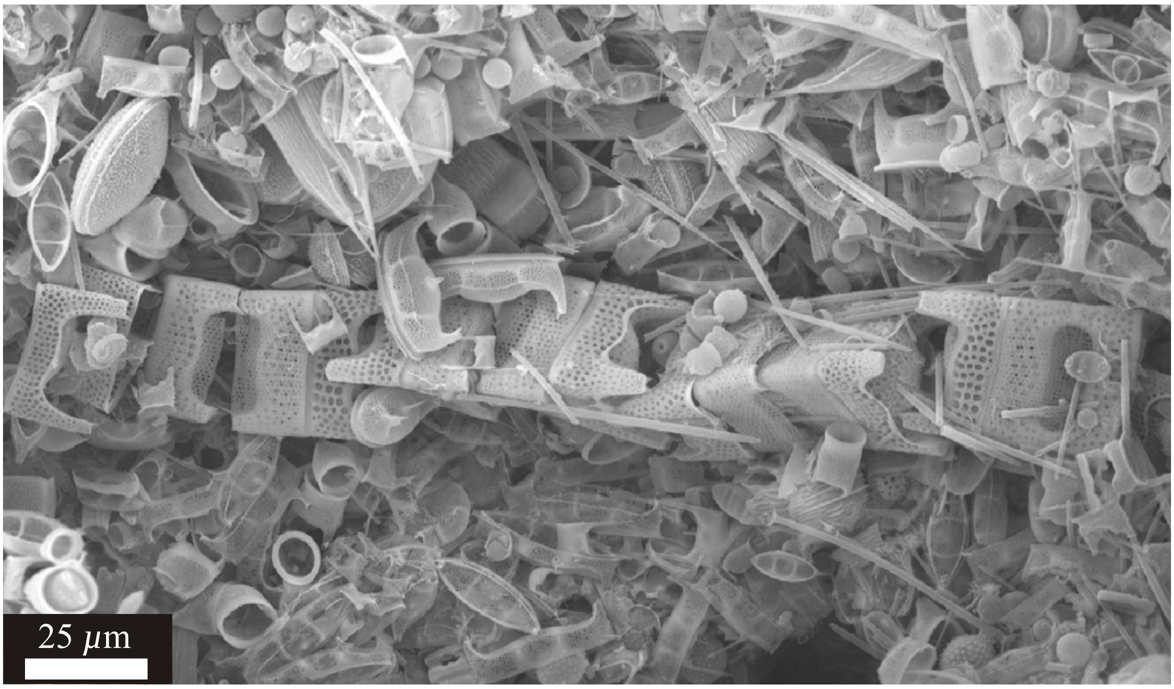

Figure 3.6. BSEI photograph of a topographic stub from the CESAR 6, showing a long chain of *Trinacria acutangulum.*

3.2.15 Genus ***Medlinia*** Sims

Medlinia is only known from the fossil record, with a range from the late Cretaceous (Campanian) to the Oligocene and little ecological information exists for this genus. Valves are tripolar and possess linking mechanisms at the three marginal apices and/or the central area of the valve. Using the linking mechanisms, frustules are capable of forming straight chains with very narrow or no intercellular spaces. The two species discussed in this study possess restricted geographical distributions with *M. deciusii* is only known from the Marca Shale, whilst *M. mucronata* is known from the Marca Shale and Palaeocene of Arkhangelsk, Russia (Schmidt, 1886). In view of the robust nature of the valves of this genus, which are likely to be preserved in the fossil record, the restricted geographical extent suggests that *Medlinia* may have been confined to the near-shore, neritic environment.

3.2.16 Genus ***Anaulus*** Ehrenberg

Valves of the extant genus *Anaulus* possess two conspicuous psuedosepta that cross the valve. The valve surface is areolate, apart from the regions around the psuedosepta, which are hyaline. Cells in all studied samples in this study occur singularly, although modern forms are capable of forming short chains (Round *et al.*, 1990). Based on the dominance of *A. sibiricus* in resting spore laminae and *Hemiaulus elegans* in vegetative laminae in core Fl-437 from the Artic Ocean (Kitchell *et al.*, 1986), Harwood (1988) suggested that *A. sibiricus* is a resting spore of *H. elegans*. However, the presence of areolae, girdle bands and the similarity to extant vegetative *Anaulus* cells, casts doubt on this interpretation.

Many studies of extant species of *Anaulus* show that they have a clear ecological preference for littoral environments and the genus is commonly referred to as a surf-zone diatom (e.g. Talbot & Bate, 1988; e.g. Hewson *et al.*, 2001). *A. australis* commonly forms dense concentrations, visible as dark coloured patches in the surf zone, with up to 12 million cells/ml of seawater along the beaches of southern Australia. However, species of *Anaulus* displays a wide geographical distribution in the fossil record, suggesting that they were not restricted to a littoral niche. For example, *A. sibiricus* is known from sediments deposited in the Arctic (THIS STUDY, Barron, 1985b) and Antarctic (Harwood, 1988). Alternatively, these observations are also consistent with the interpretation that *A. sibiricus* is a resting spore of *Hemiaulus*.

3.2.17 Genus ***Chasea*** Hanna

Harwood (1988) suggested that the genus *Chasea* is probably a resting spore of *Hemiaulus* or *Cerataulina*. The heavily silicified, hyaline valves are consistent with their interpretation as resting spores, yet an apparent inconsistency with this interpretation exists in the absence of *Chasea* in the CESAR 6 sediments. CESAR 6 contains a diverse and abundant assemblage of *Hemiaulus* spp. and *Cerataulina* and if *Chasea* originates from one of these genera then its presence would be expected. Alternatively, *Chasea* could relate to *Hemiaulus polymorphous*, *H. andrewsi*, *H. curvulatus* or *Cerataulina cretacea*, which are not present in the CESAR 6.

3.2.18 **Rhizosolenids** (*Rhizosolenia* and *Proboscia*)

3.2.18.1 Genus ***Rhizosolenia*** Brightwell

The fossil form of *Rhizosolenia* observed in this study has been interpreted as a resting spore, and occurs in two forms; a thin and a thick form, identical in morphology except in respect to the cell diameters (Barron, 1985b; Kitchell *et al.*, 1986). Analysis of both cell morphologies under optical and electron microscopy in this study has revealed for the first time that cells possess a non-ornamented, hyaline cylindrical portion, to which the ribbed conical section, identified as *Rhizosolenia*, is connected by a fine girdle band (Fig. 3.7 and 3.8). In most specimens, the two valve segments have become unconnected. The two valve segments may be connected in a straight line along the central axis of the cylindrical valve section (Fig. 3.7a and 3.8a), or the two valve segments may be joined at an angle (Fig 3.7b and 3.8b). The cylindrical, hyaline portion of the valve has not been associated with the *Rhizosolenia* valve segment until now, and when unconnected resembles valves of *Psuedopyxilla*. Although superficially resembling *Rhizosolenia*, this species differs in a number of important respects. Firstly there appears to be no groove in the valve surface to accommodate the spine of adjacent valves, seen in modern *Rhizosolenia*. The heavily ribbed valves also contrast with modern forms, which also possess numerous scale-like girdle bands, unlike the hyaline valves shown here. The relatively heavily silicified nature of the hyaline valve suggests that the cells are likely to be resting spores, consistent with the conclusions of earlier studies (Kitchell *et al.*, 1986). The morphological similarity between this fossil *Rhizosolenia* and modern forms of *Rhizosolenia*/*Proboscia* suggests it may be a spore of one of these genera. Valves of this species occur above vegetative cell laminae (dominated by *Hemiaulus* spp.) and below resting spore laminae. Alternatively, the Arctic *Rhizosolenia* may be a heavily silicified ‘winter’ stage, by analogy with observations of the modern Antarctic diatom *Eucampia antarctica*. *Eucampia antarctica* is known to form a heavily silicified winter stage, which actively forms chains and undergoes binary cell division when conditions permit growth (Fryxell & Prasad, 1990). This fossil is only known from the Cretaceous/Eocene Arctic cores CESAR 6, Fl-437 and Fl-422 (Barron, 1985b; Dell'Agnese & Clark, 1994) and may therefore have been an endemic Arctic species.

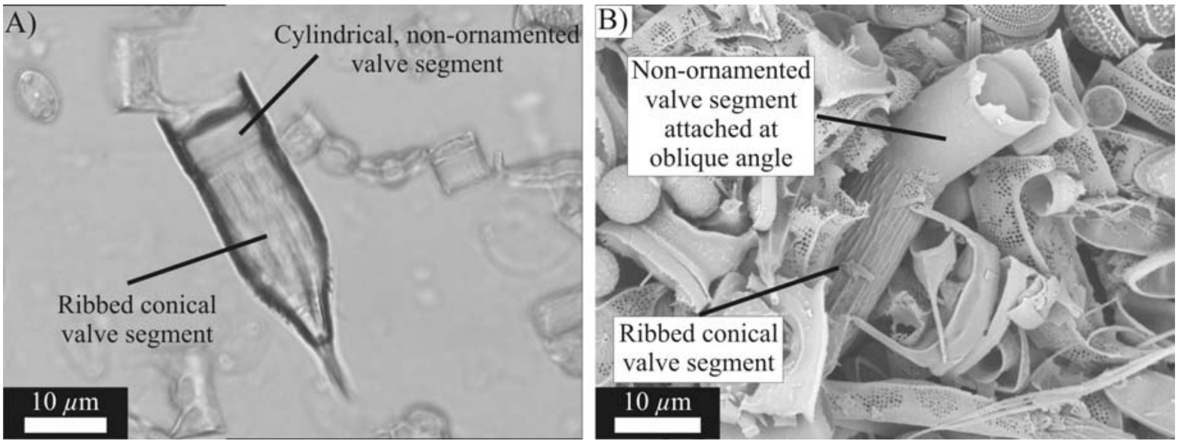

Figure 3.7. Optical and BSEI photographs from the CESAR 6 showing valves of *Rhizosolenia* with; A) the attached cylindrical hyaline valve segment in line with the valve axis and B) offset at an oblique angle.

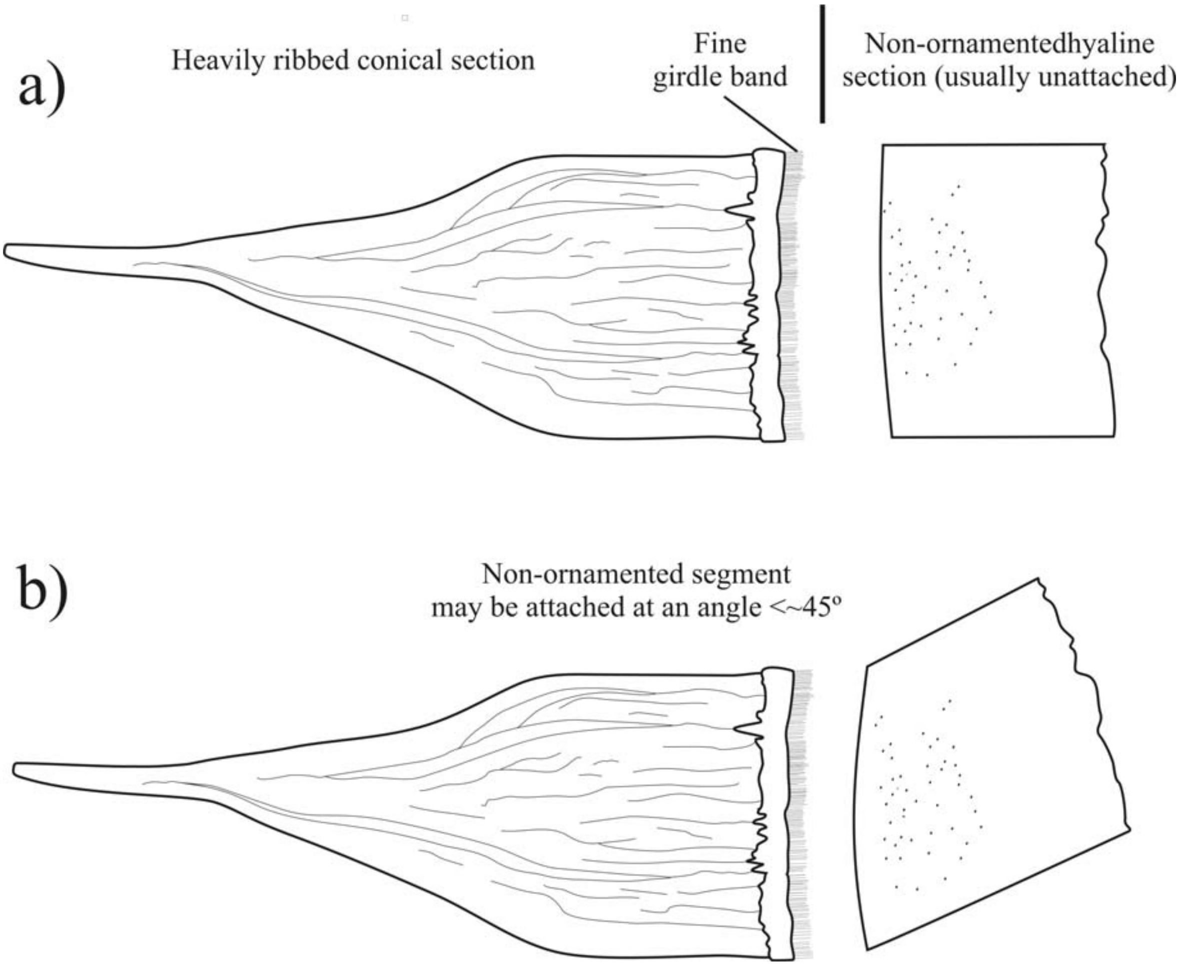

Figure 3.8. Illustration of the different valve components of *Rhizosolenia* observed in the CESAR 6.

3.2.18.2 Genus ***Proboscia*** Sundström

Valves of this fossil species of *Proboscia* are long, curved and tubular, composed of 6 hyaline pillars, separated by sections of perforated valve. The perforations are arranged in strips parallel to the long axis of the valve face, with up to 5 strips of perforations in each section. The species identified in this study, *P. cretacea*, was originally described as *Rhizosolenia* by Hajós & Stradner (1975). However, Jordan and Priddle (1991) demonstrated that the fossil resembles the proboscis of the modern genus *Proboscia*, which only usually occur in the sediment as broken proboscis. Furthermore, it was noted that *P. cretacea* resembles the broken proboscis of modern "winter-form" *Proboscia*. The ecology of this fossil species is unknown, although the basal end of each valve ends in a semilunar grip, which Hajós & Stradner (1975) suggest implies these cells (or cell elements) were connected to another structure. Jordan and Priddle (1991) speculate that chain formation may have involved other structures, analogous to the fossil genus *Pyxilla*. *P. cretacea* is a long ranging (Campanian to Palaeocene), cosmopolitan species, known from both the CESAR 6 and Marca Shale, SW Pacific DSDP Site 275 (Hajós & Stradner, 1975), Seymour Island, Antarctica, (Martinez-Machiavello, 1987), Emperor Canyon (Fenner, 1991) and ODP Site 758, Indian Ocean (Fourtanier, 1991).

Some modern *Rhizosolenia* species form macroscopic mats, which can contain up to seven *Rhizosolenia* species (Villareal & Carpenter, 1989), that are able to regulate their buoyancy in order to move between a deep nutrient source and the photic zone (Villareal *et al.*, 1993; Villareal *et al.*, 1996). Direct evidence of a deep-dwelling habitat come from direct sampling in the Sargasso Sea, where Goldman (1993) obtained samples of *Pseudoguinardia recta* from 100 m water depth and subsequently found that it was able to grow in low-light conditions.

Sediment traps in the Gulf of California (Sancetta, 1995) and off the coast of Oregon (Sancetta *et al.*, 1991; Sancetta, 1992) have shown that large fluxes of *Rhizosolenia* spp. occur in the late autumn/winter, coincident with the breakdown of stratification. A prominent peak flux of *Rhizosolenia setigera* has been recorded in October from Saanich Inlet, British Columbia (Sancetta, 1989b) and the diatom has been found to have a maximum abundance in coastal waters during the autumn (Hobson & McQuoid, 2001). At Station PAPA, northeast Pacific, Takahashi *et al.* (1989) recorded a peak flux of *Proboscia alata* during the autumn over the 1982-1985 period. In the Santa Barbara Basin a large flux of *Rhizosolenia robusta* has been recorded in December (Lange *et al.*, 2000b). However, sediment traps in the North Pacific gyre show peak flux of *Rhizosolenia* cf. *clevei* var. *communis* during the summer (Scharek *et al.*, 1999b), whilst off northwest Africa a single flux event of *P. alata* was recorded in July at 2195 m, accounting for 18% of the total assemblage (Lange *et al.*, 1998).

SEM studies of laminated sediments from the Gulf of California show that Rhizosolenid diatoms are commonly found concentrated along the top of summer terrigenous laminae (Kemp *et al.*, 2000). The assemblage is dominated by *Rhizosolenia bergonii*, but also includes *R. setigera, R. styliformis, R. robusta*, *Proboscia alata* and *Pseudosolenia calcar-avis*. In Mediterranean sapropels, near monospecific laminae of *Pseudosolenia calcar-avis*, with minor quantities of

Rhizosolenia setigera and *R. styliformis*, overlie spring/winter bloom mixed assemblages (Pearce *et al.*, 1998). In conjunction with the sediment trap data, these Rhizosolenid laminae are interpreted to represent "fall dump" export flux, in which Rhizosolenids are regarded as key diatom taxa (Kemp *et al.*, 2000).

3.3 Class **FRAGILARIOPHYCEAE** (araphid pennate diatoms) Round

3.3.1 Genus ***Helminthopsis*** Van Heurck

Helminthopsis is a fossil genus know from Seymour Island (Harwood, 1988), SW Pacific (Hajós & Stradner, 1975) and the CESAR 6 and Marca Shale (THIS STUDY). The ecology of this species is unknown; however, it is possible that it shared a similar ecology to *Sceptroneis*.

3.3.2 Genus ***Sceptroneis*** Ehrenberg

Sceptroneis is an extant genus that was amongst the first representative of the pennate diatoms to appear in the fossil record during the Campanian (Harwood & Nikolaev, 1995). Valves are elongate and generally possess one broad and one tapering end. Although this is an extant genus, relatively little ecological information exists for modern forms. Round *et al.* (1990) suggest that this species occupies a benthic niche and is most likely epiphytic. *Sceptroneis* occurs in coastal/neritic as well as oceanic environments and it has been suggested that the genus shared an ecology similar to that of *Actinoptychus* and *Paralia* (Eggar *et al.*, 2003).

3.4 TAXA OF UNCERTAIN SYSTEMATIC POSITION

3.4.1 Genus ***Pseudopyxilla*** Forti

Psuedopyxilla is a fossil marine genus, ranging in age from the Early Cretaceous − Neogene (Harwood & Nikolaev, 1995). Valves are generally cylindrical and conical at one end and hyaline, although some species do possess some perforations. Its taxonomic position along with its ecology is unknown, although it is generally regarded as a resting spore (e.g. Harwood & Gersonde, 1990).

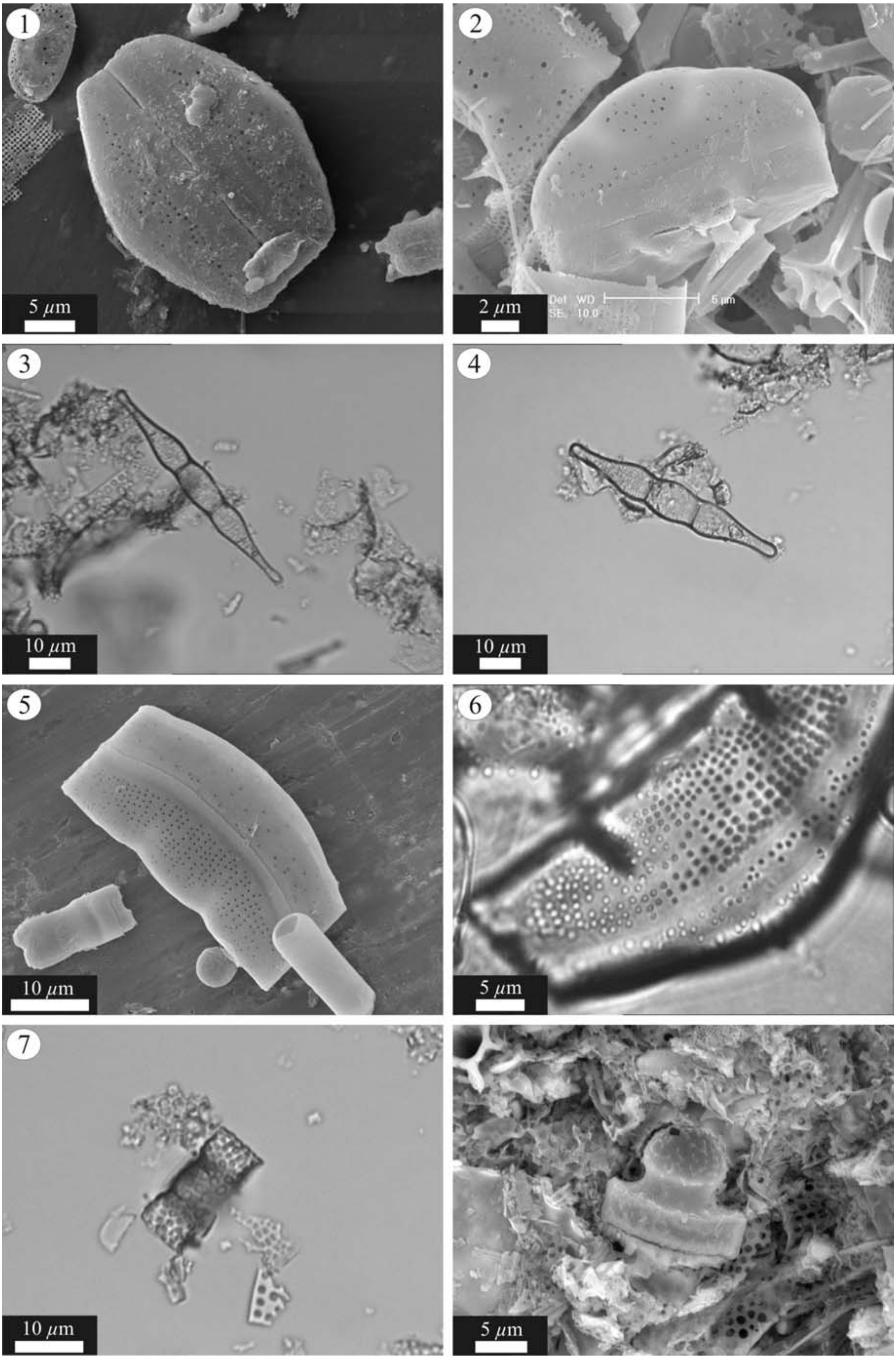

Plate 12. 1-2 *Anaulus sibiricus*, 3-4 *A. undulatus*, 5-6 *Anaulus* sp.1, 7 *Porpeia* sp., 8 *Chasea bicornis*. Images 1-2 and 5-6 are from the CESAR 6 and 3-4 and 5-8 are from the Marca Shale.

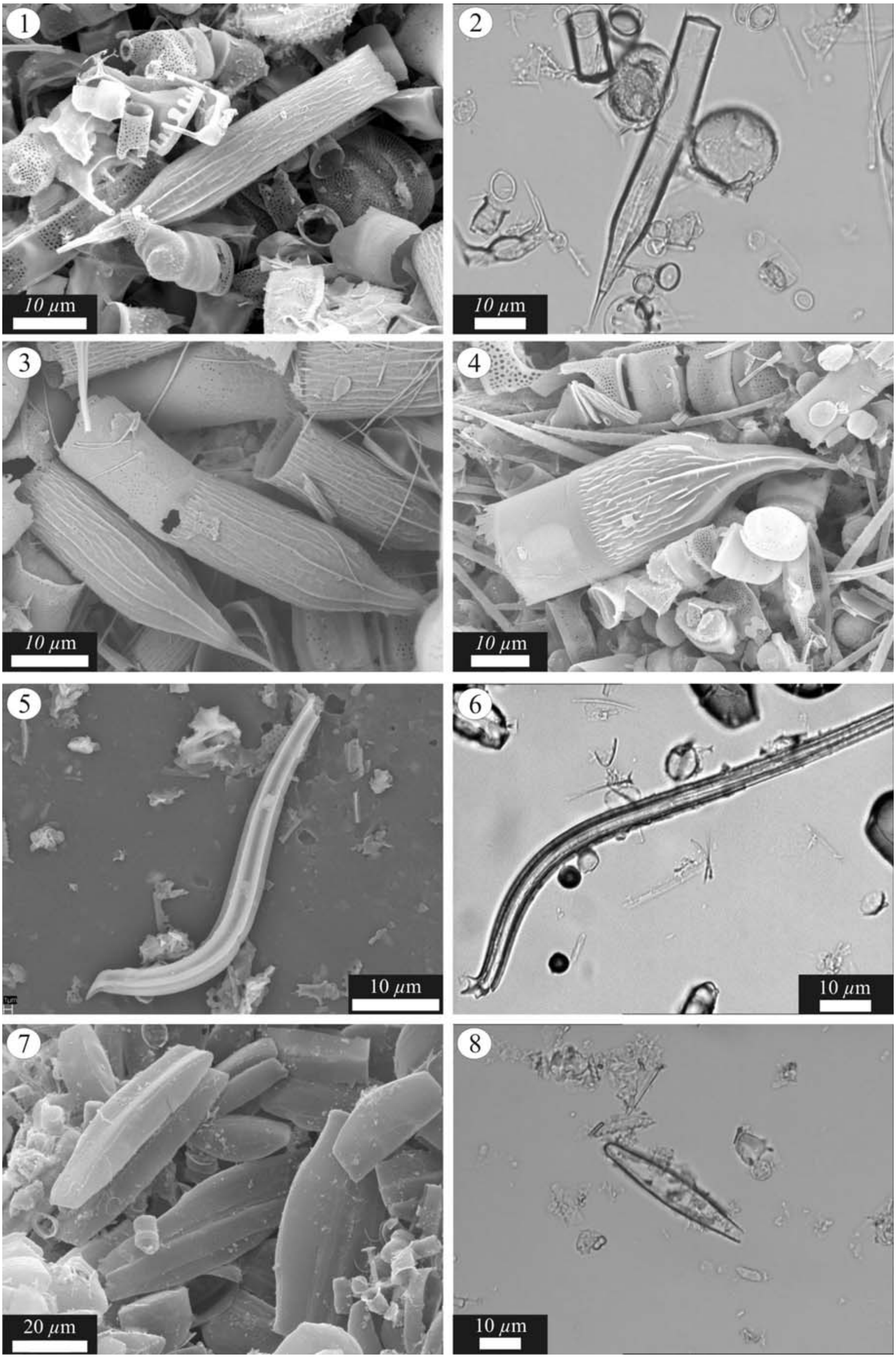

Plate 13. 1-4 *Rhizosolenia* sp., 5-6 *Proboscia cretacea*, 7-8 *Helminthopsis wornardti*. Images 1-4 and 6-7 are from the CESAR 6 and 5 and 8 are from the Marca Shale.

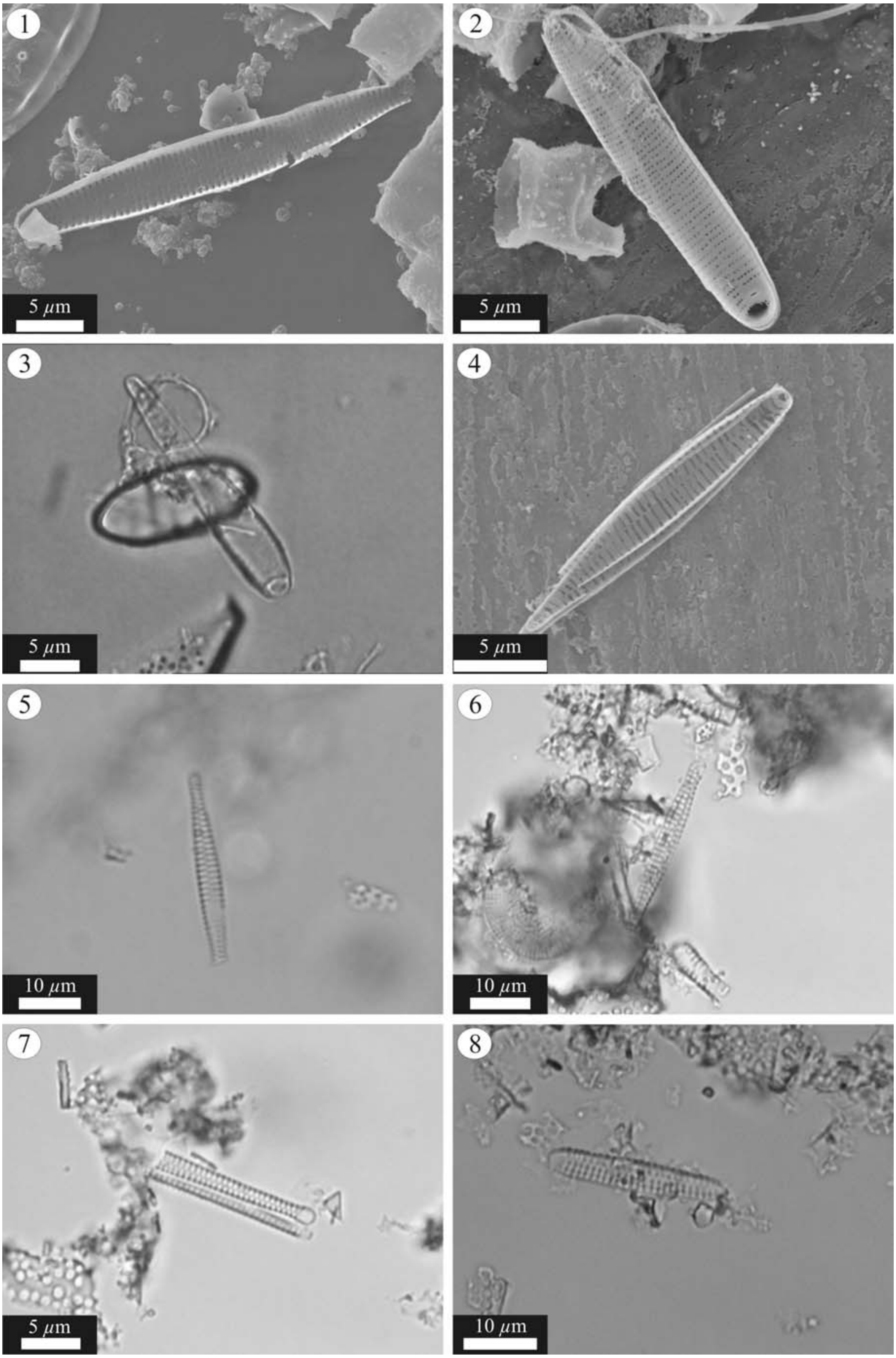

Plate 14. 1-2 *Sceptroneis dimorpha*, 3-4 *Sceptroneis* sp. B, 5-6 *S. grunowii*, 7 *S. praecaducea*?, 8 *Sceptroneis* A. Images 1-4 are from the CESAR 6 and 5-8 are from the Marca Shale.

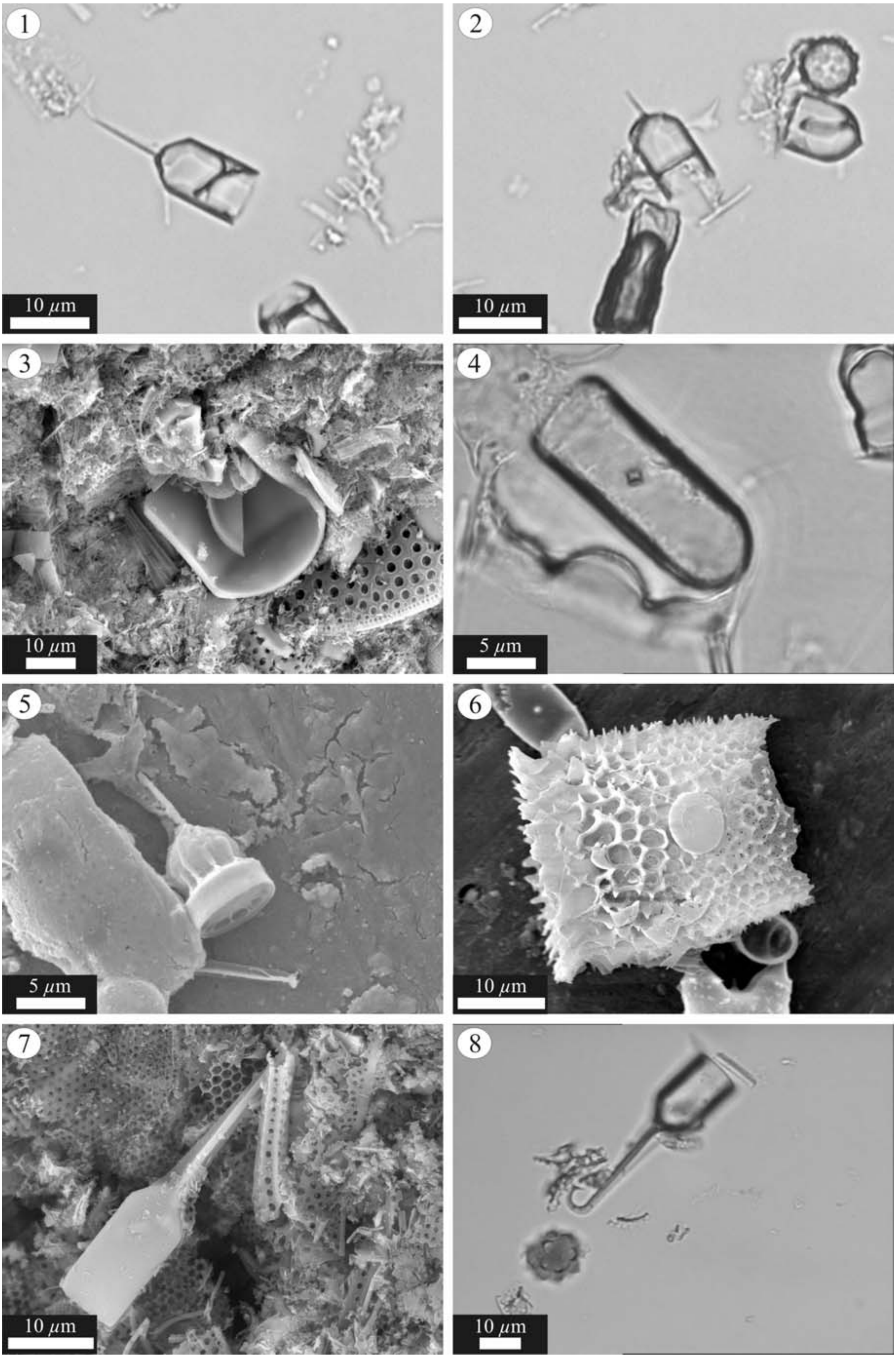

Plate 15. 1-2 *Psuedopyxilla* sp. Strelnikova, 3 *Psuedopyxilla russica,* 4 *Psuedopyxilla americana*, 5 *Pterotheca crucifera*, 6 *Pterotheca* sp. Strelnikova, 7-8 *Pterotheca evermannii*. Images 1-2 and 4-6 are from the CESAR 6 and 3, 7 and 8 are from the Marca Shale.

3.4.2 Genus ***Pterotheca*** Grunow ex Forti

Pterotheca is a fossil (Late Cretaceous-Eocene?) species (Harwood & Nikolaev, 1995). The taxonomic position and ecology of *Pterotheca* is unknown. Individual species can have relatively cosmopolitan distributions. For example *P. crucifera* is known from the Marca Shale (Hanna, 1927), CESAR 6 (this study), SW Pacific (Hajós & Stradner, 1975) and Seymour Island (Harwood, 1988). *Pterotheca* can form a diverse component of fossil assemblages, with for example, 22 species known from Seymour Island. Valves are generally hyaline, cylindrical with thick heavy walls with one end of the valve bearing a large spine projection. In this study, this projection has been noted to form a 'hook' during observations of *P. evermanni* from the Marca Shale flora (Plate 15.8), which could be a possible ecological adaptation. On the basis of the thick, heavily silicified, hyaline nature of the valves, *Pterotheca* is regarded as a resting spore (e.g. Harwood, 1988) and it has been noted that *Pterotheca* resembles the spores of *Rhizosolenia setgera* (Hargraves, 1986).

3.5 RESTING SPORES

Resting spore development is generally associated with unfavourable environmental conditions and sporulation is generally occurs in response to a sudden change in one or more environmental factors (Davis *et al.*, 1980). These include nutrient levels, irradiance, hours of sunshine, pH, temperature and salinity (McQuoid & Hobson, 1996), although nitrogen limitation is commonly found to be the most important factor (e.g. Hargraves & French, 1983). Resting spores mostly occur in species that occupy a coastal niche (Hargraves, 1986). An exception to this is in species that inhabit a "pseudo-benthic" environment at the base of the thermocline in oceanic waters (Bienfang & Szyper, 1981).

3.5.1 ***Chaetoceros* spp.-type spores**

These spores bear a striking resemblance to modern Hyalochaete *Chaetoceros* resting spores, which currently comprise the bulk of biosiliceous sediments underlying zones of coastal upwelling and are indicative of highly productive environments (Bull & Kemp, 1995; Pike & Kemp, 1996b; Thunell, 1998a; Koning *et al.*, 2001). In a multidisciplinary study in the southern Benguela Current system, vegetative cells of *Chaetoceros* spp. were found to dominate the upper water column, whilst resting spores dominated the sediments and water column below the thermocline (Pitcher, 1986). The heavy silicification of the resting spores in contrast to the lightly silicified frustules of the vegetative cells ensures *Chaetoceros* spores are preferentially preserved in the sediments. *Chaetoceros* spores are overwhelmingly deposited following the spring bloom when sporulation occurs in response to the reduction of nutrient levels following weakening of wind-induced upwelling (Kemp, 1995; Sancetta, 1995). Rapid sedimentation is achieved by the expulsion of sticky transparent exopolymer particles (TEP), which allow cells to form flocculating aggregates, which rapidly sink, bypassing the effects of dissolution and grazing in the upper water column (Alldredge *et al.*, 1993; Bull & Kemp, 1995; Grimm *et al.*, 1997). Along the modern Californian margin the abundance of *Chaetoceros* resting spores in the sediments exhibits a strong modulation by ENSO. During non El Niño years *Chaetoceros* spores dominate the assemblage, whilst El Niño years are characterised by a marked drop in their abundance, being replaced by taxa with affinities for warm offshore waters (Lange *et al.*, 1990; Lange *et al.*, 2000a).

3.5.2 *Hemiaulus tumidicornis*

Although previously ascribed to the genus *Hemiaulus*, many authors have suggested that the fossil diatom *H. tumidicornis* is in fact a resting spore (e.g. Kitchell *et al.*, 1986; Dell'Agnese & Clark, 1994). High-resolution BSEI conducted in this study provides clear support for this, showing it to be an endospore of an apparently weakly silicified species of *Hemiaulus* (Plate 16. 5-8). The vegetative stage is seldom preserved in the CESAR 6 sediments, and when it does occur it is only in conjunction with *H. tumidicornis*. Two morphologically distinct types of *H. tumidicornis* are observed; a generally smooth form and a form with numerous spiny projections emanating from near the polar elevations. Both these forms have been grouped as *H. tumidicornis* owing to the fact that they both appear to originate from the same vegetative cell (Plate 16.6,8).

3.5.3 *Hemiaulus* sp. 1

The fossil diatom *Hemiaulus* sp. 1 is morphologically very similar to *Hemiaulus* vegetative cells, being lanceolate, with psuedosepta and two polar elevations with a single labiate process situated near the centre of the valve face, through which extends an external conical tube. The valves are hyaline and exhibit a range of size and morphologies, none of which have been observed to possess a girdle band (see Plate 17. 1-2 and Fig. 3.9). Most specimens have had the tips of the fragile polar horns fractured off, although they are present in a few samples (Fig. 3.9). These specimens show that the polar horns possess a spine, akin to the linking apparatus found on vegetative cells. Despite this, no specimens could be found linked in any of the material studied. These observations may suggest that *Hemiaulus* spore 1 is a resting spore, consistent with earlier conclusions (Barron, 1985b; Kitchell *et al.*, 1986), probably originating from one of the many *Hemiaulus* species described from the CESAR 6. Alternatively, by analogy with observations of the modern Antarctic diatom *Eucampia Antarctica*, *Hemiaulus* sp.1 may be a heavily silicified 'winter' stage (Fryxell & Prasad, 1990).

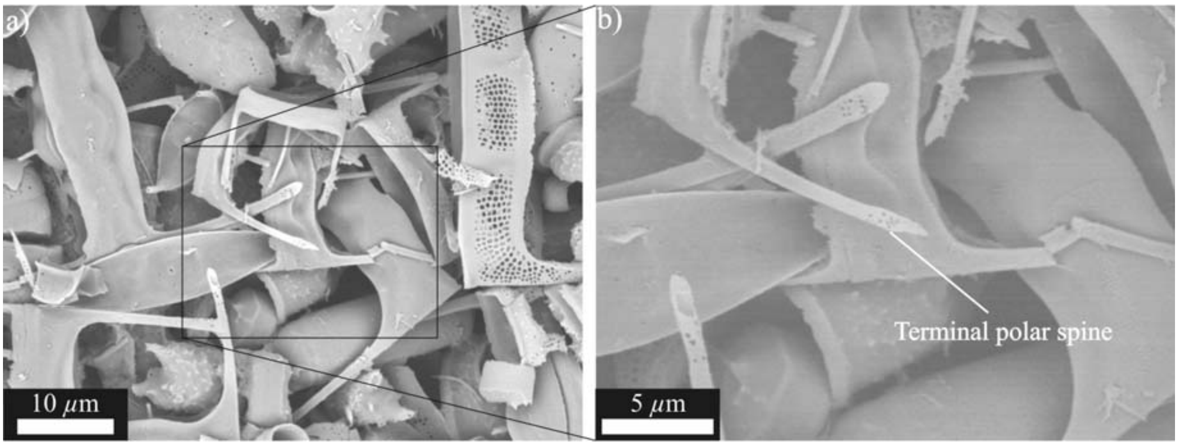

Figure 3.9. Topographic BSEI photographs of *Hemiaulus* sp. 1 illustrating the terminal spine at the end of the polar elevation. In most specimens the tips of the fragile elevations have been fractured off.

3.5.4 *Spore '3'*

Valves of Spore '3' superficially resemble those of *H. tumidicornis*, both of which are small, hyaline, possessing polar elevations, and a single process situated in the centre of the valve face, however, the valves are distinct in several ways. The polar elevations of Spore '3' are much straighter, cylindrical and elongate than those of *H. tumidicornis* and also possess a ring of projections along their apex. The valve face of Spore '3' is also much smoother than that of *H. tumidicornis*, which have crenulated valve face, often with many spiny projections. Based on the similarities of Spore '3' with those of *H. tumidicornis*, Spore '3' is interpreted to be a resting spore of a nonidentified species of *Hemiaulus*.

3.5.5 *Skeletonema subantarctica*

In a study of fossil species of the genus *Skeletonema*, Sims (1994b) examined specimens of both the species *S. subantarctica* and *S. penicillus*. It was noted that both forms possess similar, if not identical, structures, suggesting that the two forms may be conspecific. Girdle bands attached to these valves were found not to be typical of either *Skeletonema* or *Skeletonemopsis*, which along with other valve characteristics (including the fact that the valves are hyaline) led to the conclusion that the specimens were resting spores (Sims, 1994b). This conclusion is further supported in this study with the recognition that valves of "*S. subantarctica*" appear to be associated with valves of *Cerataulina* (see Fig. 3.5).

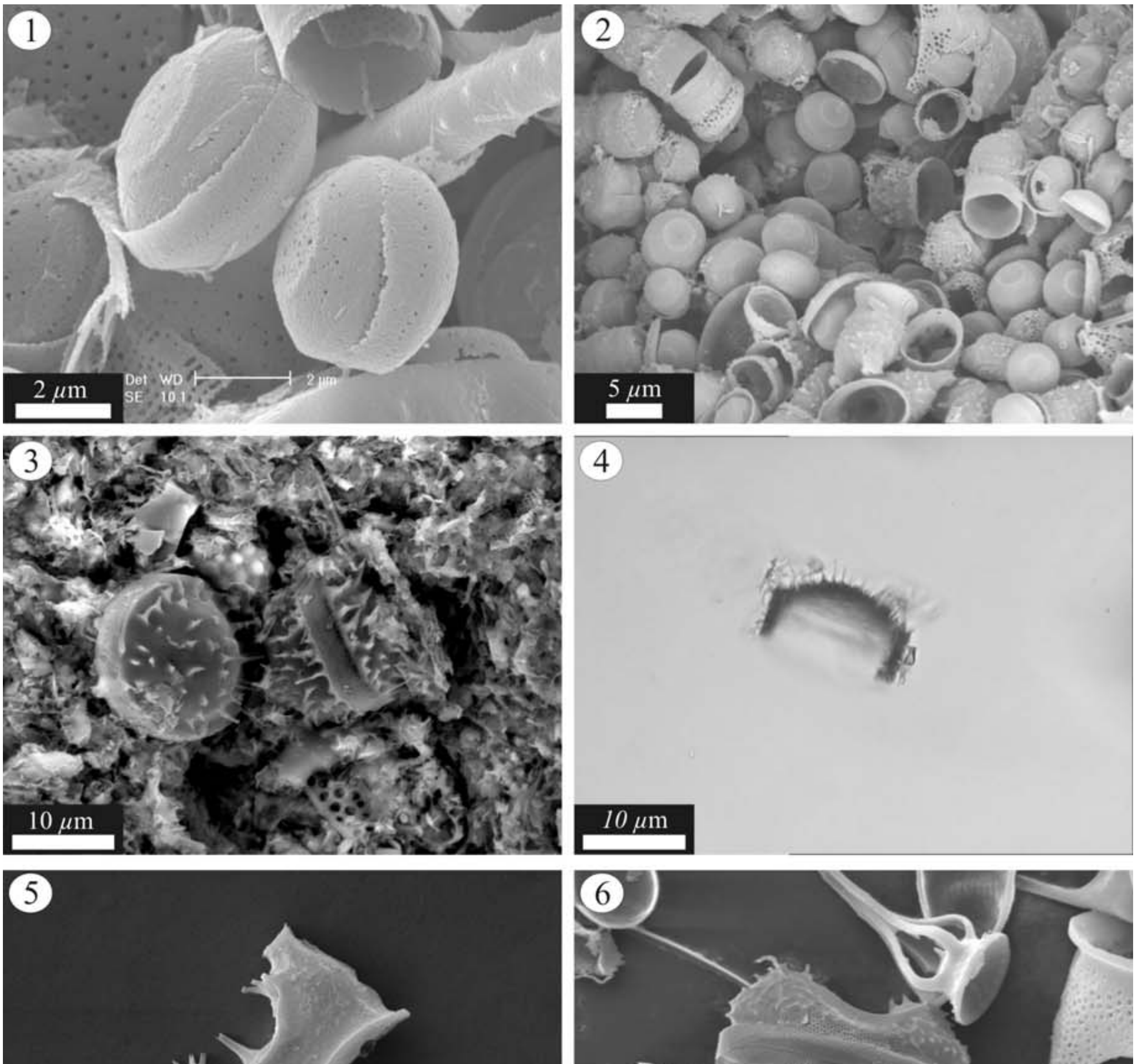

Plate 16. 1-2 *Chaetoceros*-type spores (spore 1, CESAR 6), 3-4 *Chaetoceros* type-spore (Marca Shale), 5-6 *Hemiaulus tumidicornis* (spiny form), 7-8 *H. tumidicornis* (smooth form). Note that in 16.6 and 16.8 it can be seen that *H. tumidicornis* is an endospore, within a rarely preserved vegetative cell. Images 1-2 and 5-8 are from the CESAR 6 and 3-4 are from the Marca Shale.

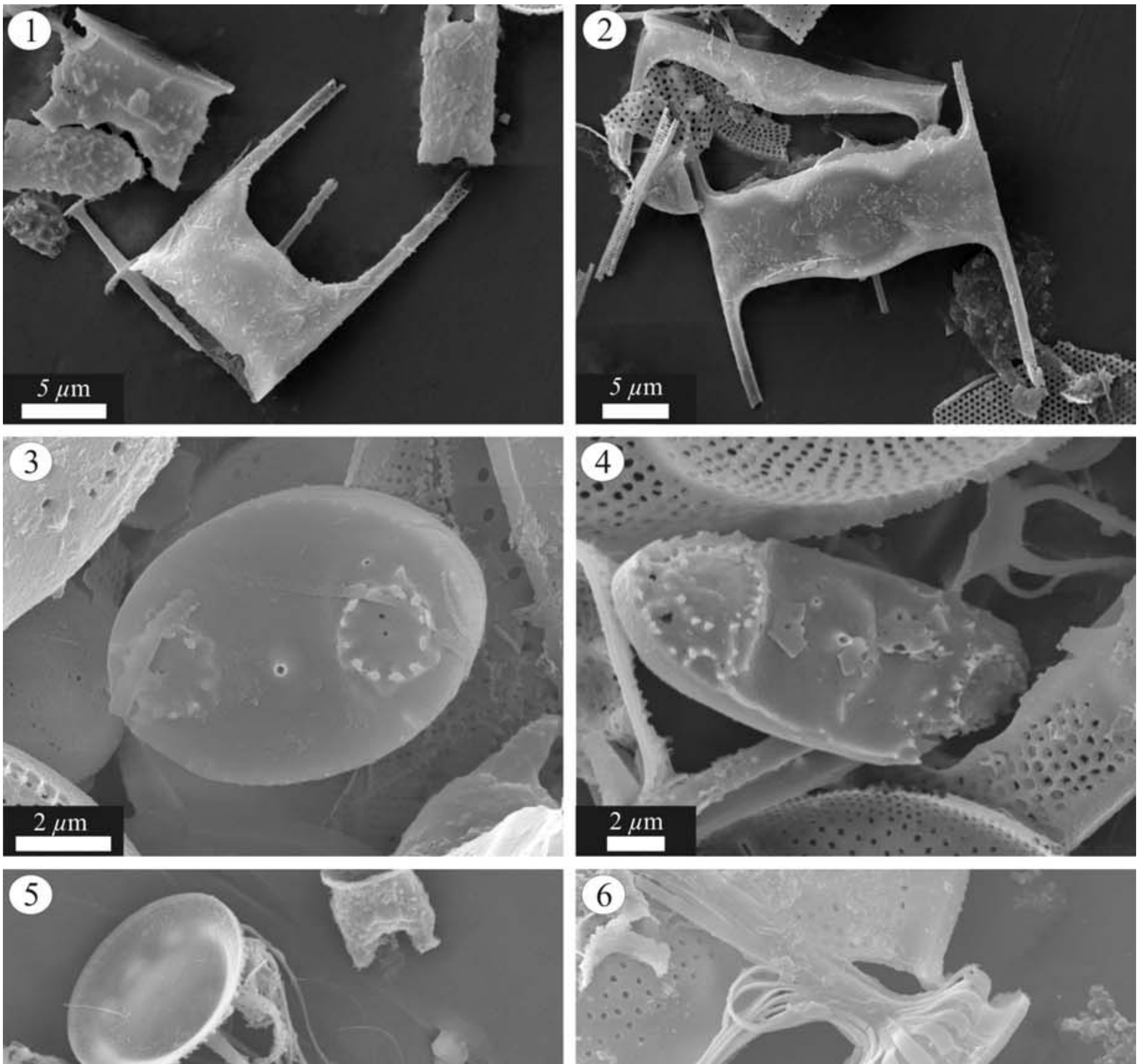

Plate 17. 1-2 *Hemiaulus* sp.1, 3-4 Spore '3', 5-6 *Skeletonema subantarctica*, 7-8 *Goniothecium odontella*. All images are from the CESAR 6.

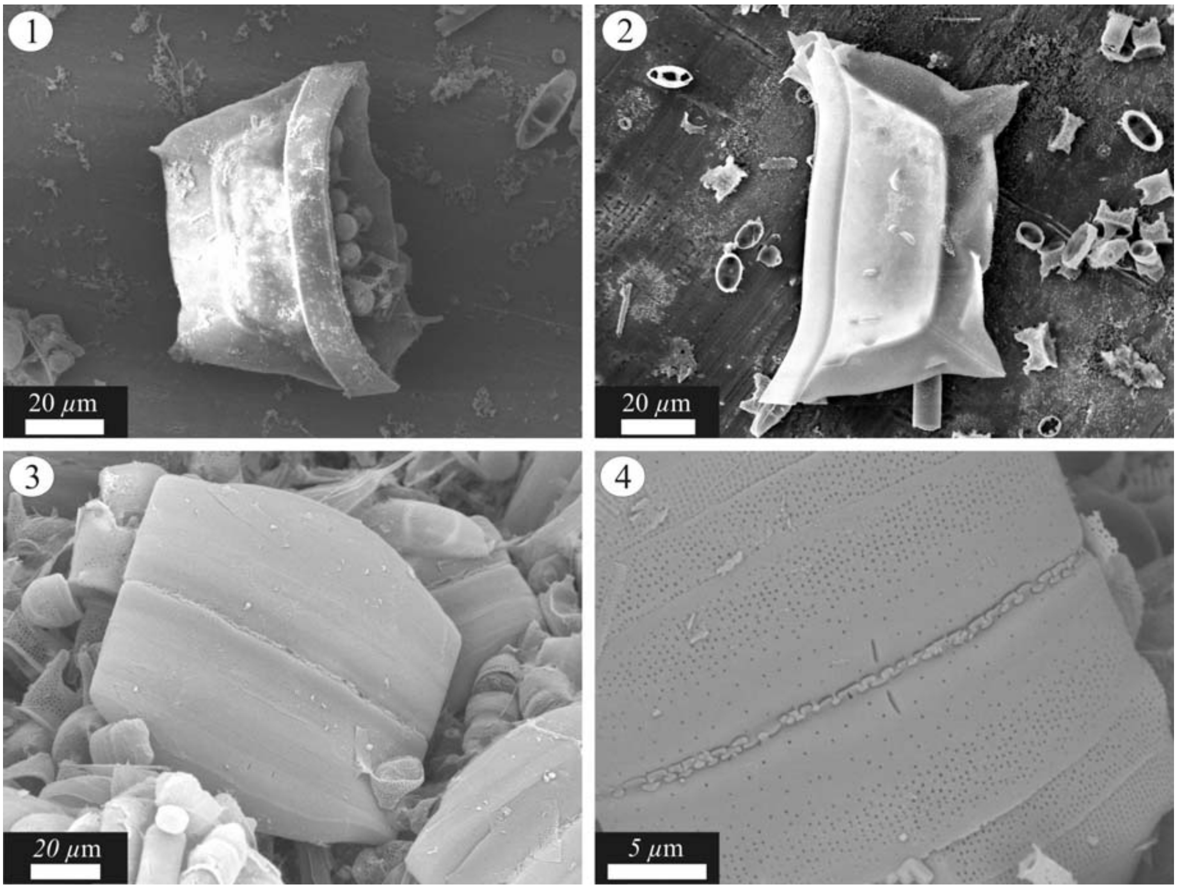

Plate 18. 1-2 *Odontotropis cristata*, 3-4 unknown diatom. All images are from the CESAR 6.

3.5.6 Genus ***Goniothecium*** Ehrenberg

It has been suggested that the fossil genus *Goniothecium* may actually be spores of *Chaetoceros*, wrongly classified as a distinct genera (Ehrenberg, 1844; Hargraves, 1986). The heavily silicified, robust, hyaline valves of *G. odontella* observed in this study are consistent with their interpretation as resting spores. Species of *Goniothecium* can comprise a common component of fossil assemblages and are widespread, with *G. odontella* for example, known from the CESAR 6 (THIS STUDY, Barron, 1985b), Core Fl-437 (Dell'Agnese & Clark, 1994), the Ural Mountains (Jousé, 1951), the SW Pacific (Hajós & Stradner, 1975), and Seymour Island, Antarctica (Harwood, 1988).

3.5.7 Genus ***Odontotropis*** Grunow

Odontotropis is another fossil genera whose ecology and taxonomic position are unknown, although it is regarded as a resting spore (e.g. Hargraves, 1986; e.g. Harwood, 1988) on the basis of the valve thickness, lack of perforations and cingular bands. The genus is cosmopolitan, known from the Marca Shale (Hanna, 1927), Arctic Ocean (THIS STUDY, Dell'Agnese & Clark, 1994), SW Pacific (Hajós & Stradner, 1975), Seymour Island (Harwood, 1988), Canadian Artic (Tapia &

Harwood, 2002), the Ural Mountains (Jousé, 1949) and the Paleocene of the SW Atlantic (Fenner, 1991).

Ecology / Genus	Pelagic	Benthic	Coastal upwelling	Oligotrophic	Chain former	Season of deposition
Stephanopyxis	X			X	X	Autumn/winter
Paralia		X	X		X	Storm induced
Actinoptychus		X				Storm induced
Coscinodiscus	X		X	X		Autumn/winter
Trochosiropsis	X				X	?
Stellarima	X			X		Autumn/winter
Azpeitiopsis	X			X		?
Hemiaulus	X			X	X	Summer
Anaulus	X					?
Rhizosolenia	X			X	X?	Autumn/winter
Proboscia	X			X	X?	Autumn/winter
Chaetoceros-type spores	X		X			(Spring) bloom

Table 3.2. Summary of the ecology/palaeoecology of the main diatom genera in the CESAR 6 and Marca Shale.

3.6 DISCUSSION

3.6.1 *Taphonomic effects on the diatom assemblages*

Due to dissolution in the water column and at the sediment/water interface, along with fragmentation during grazing, only a proportion of diatom valves are incorporated into the sedimentary record (e.g. Nelson *et al.*, 1995). In the modern ocean there are stark differences in the preservation potential between diatom taxa, resulting in a bias towards robust forms in the sediment record (Ryves *et al.*, 2001). At present, this has the effect of removing small and/or weakly silicified forms (Sancetta, 1989a), characteristic of the spring bloom, from the sedimentary record, leading to a possible false impression of seasonal production (Sancetta, 1992). Zooplankton grazing can affect the diatomaceous export flux in several ways. Diatom cells above ~20 µm in diameter suffer fragmentation during maceration (Honjo & Roman, 1978), which may accelerate dissolution (Ferrante & Parker, 1977). However, if the grazed diatom cells are packaged into fecal pellets, they may be protected from dissolution and be efficiently exported to the benthos (Honjo & Roman, 1978). It was long held that fecal pellets were the primary mechanism involved in the export of diatoms to the deep (e.g. Turner & Farrante, 1979), although this view has radically changed (e.g. Turner, 2002).

Through the use of sediment traps (Sancetta, 1989a), SCUBA divers (Alldredge & Goltschalk, 1989) and analysis of diatomaceous sediment (Brodie & Kemp, 1994; Grimm *et al.*, 1997) it was realised that much of the diatomaceous material reaching the sediment was not packaged into fecal pellets, but was rapidly mass sedimented intact. Rapid sedimentation is attributed to the secretion of dissolved polymers, in response to depleted nutrients in surface waters following blooms, which interact with cations in seawater to form transparent exopolymer particles (TEP) that enhance cell aggregation (Alldredge *et al.*, 1993; Passow *et al.*, 1994). Recently, efficient export of intact valves was recognised in another distinct group of diatom species adapted to more stratified conditions and able to exploit deep sources of nutrients. Such species are able to build up significant biomass over the period of stratification and are sedimented *en masse* in the “fall dump” in response to the breakdown of stratification in the autumn (Kemp *et al.*, 2000), forming laminae of intact frustules in underlying sediments (Pike & Kemp, 1997; Pearce *et al.*, 1998; Kemp *et al.*, 2000).

Dissolution at the sediment surface may also significantly modify the assemblage. Using sediment traps in the equatorial Atlantic, Treppke *et al.* (1996) demonstrated that although some dissolution occurred in the water column, considerable modification of the assemblage occurs at the sediment/water interface, resulting in the loss of 98% of biosiliceous material. By comparing the diatom assemblage in surface sediment traps with those in the underlying sediments it was apparent that summer upwelling diatoms and weakly silicified forms characterising the spring bloom were not preserved in the sediment. However, despite the dramatic modification of the assemblage, the assemblage preserved in the sediment was found to reflect the overlying hydrographic conditions and the extent of the upwelling cell (Treppke *et al.*, 1996). Thus even if diatom preservation in sediments is excellent, the assemblage is almost certainly a remnant of the assemblage once present in the water column.

Frustules in diatomaceous deposits of such antiquity as the Marca Shale and CESAR 6 may also be affected by the temporal instability of opal-A and mechanical fragmentation during burial. The amorphous opal comprising diatom frustules is unstable and over time reverts to quartz, passing through a transition phase of Cristobalite-Tridimite. Amorphous opaline tests begin to recrystallise when burial over ~400m (Isaacs, 1981) or heating above ~35 °C (Siever, 1983) occurs. Mechanical fragmentation of diatom valves has been reported in sediments that have been buried to a depth of 300-400m and is usually associated with mild dissolution (Hein *et al.*, 1978).

The state of diatom preservation varies between the two sites studied here. Diatoms in the CESAR 6 are excellently preserved, with little signs of dissolution or fragmentation of the frustules and preservation of fine (<1 μm) setae. Diatoms in the Marca Shale have good preservation, but do suffer from extensive fragmentation and minor dissolution, even within early diagenetic nodules, where preservation is generally better (Fig. 3.3).

3.6.2 *Diatom species not included in previously published floral lists*

3.6.2.1 *Marca Shale*

A number of rare valves have been observed, particularly in optical microscopic investigations of the early diagenetic nodules, not included in recent taxonomic studies of the Marca Shale (Nikolaev *et al.*, 2001). Several different forms of *Hemiaulus* have been observed, including *H. ambiguus*, *H. andrewsi*, and *H. curvatulus*. The occurrence of *Anaulus undalatus*, *Porpeia* spp. and *Trinacria tristictia* have been documented, supporting earlier observations by Long *et al*. (1946). Specimens of *Proboscia cretacea* and *Cerataulina cretacea* have also been confirmed. Valves of *Skeletonemopsis morenoensis* have also been documented, occasionally observed connected in chains. Significantly several early araphid pennate diatoms have been documented, including several species of *Sceptroneis* (S. *grunowii, S. praecaducea? Sceptroneis* sp. A) along with *Helminthopsis wornardti?*. However, this study supports the conclusions of Nikolaev *et al.* (2001) that many species included in descriptions by Long *et al*. (1946) are contaminants from the nearby Eocene Kreyenhagen Formation.

3.6.2.2 *CESAR 6*

Several species have also been added to the CESAR 6 floral list during this investigation. These include a species of *Anaulus* (*Anaulus* sp. 1) a species of *Cerataulina* (*Cerataulina* sp. 1), many species of *Hemiaulus* (*H. altus, H. ambiguus, Hemiaulus* sp. *'G', Hemiaulus* sp. *'2', Hemiaulus* sp. '*6'* and others), an unidentified species of *Sceptroneis* (S. sp. B), *Helminthopsis wornardti*? and two species of *Stellarima* (*Stellarima* sp. 1, *Stellarima* sp. 2).

3.6.3 *Comparisons of the diatom flora of the Marca Shale and CESAR 6*

Of the 46 species in the Marca Shale and 57 in the CESAR 6, only 8 are present in both. The Marca Shale contains a more diverse assemblage, with 30 diatom genera identified in this study, whilst the CESAR 6 contains 22. Although some differences between the two floras may be due to age difference, ecological factors must also be influential. The principal differences between the two floras are summarised in Table 3.3. The CESAR 6 is characterised by a far greater diversity and abundance of *Hemiaulus*, with over 20 morphotypes recognised (although some are spores). The CESAR 6 also has a greater abundance of *Anaulus*, a lower abundance and diversity of *Stephanopyxis*, *Stellarima* and benthic species (*Paralia*, *Medlinia, Actinoptychus*), a greater abundance of *Chaetoceros*-type spores and other resting spores (e.g. Spore '3', *H*. sp.1, *H. tumidicornis*, *Skeletonema subantarctica*) and the presence of *Rhizosolenia* and *Trochosiropsis*.

Genera	**Marca Shale**	**No of species**	**CESAR 6**	**No of species**
Hemiaulus	Common, low diversity	4	Dominant, high diversity	18
Stephanopyxis	Abundant, diverse	4	Rare, low diversity	1
Rhizosolenia	Absent	0	Common	1
Anaulus	Rare	1	Abundant	2
Stellarima	Common	2	Rare	3
Trochosiropsis	Absent	0	Common	1
Chaetoceros-type spores	Common	1	Abundant	1
Other resting spores (e.g. *H. tumidicornis*, Spore '3', *S. subantarctica*)	Rare	6	Common, diverse	12
Neritic species (e.g. *Paralia*, *Actinoptychus* and *Medlinia*)	Common, diverse	5	Rare, lower diversity	4

Table 3.3. Summary of the main differences in the diatom floras of the Marca Shale and CESAR 6.

The lower abundance and diversity of benthic species in the CESAR 6 is an indication that it was deposited in an environment more distal from shore than that of the Marca Shale. A more oceanic setting for the CESAR 6 can be corroborated with the greater diversity and abundance of *Hemiaulus*, which currently dominates blooms in oligotrophic oceanic settings (e.g. central North Pacific and tropical Atlantic). *Stephanopyxis* is currently part of the diatom export flux in coastal settings (e.g. the Gulf of California and Santa Barbara Basin) where it may form monospecific laminae, and the greater abundance and diversity of this genus in the Marca Shale may also relate to deposition in a more coastal setting than the CESAR 6. Alternatively, in the modern oceans *Stephanopyxis* has an affinity for warm/tropical regions (Goldman & McGillicuddy, 2003) and the greater abundance/diversity in the Marca Shale may relate to its lower palaeolatitude. The fossil species of *Rhizosolenia* discussed in this study is only known from Arctic cores, suggesting it may have been an endemic Arctic species. The lack of this form in the Marca Shale may therefore also be an artefact of the differing palaeolatitudes of the two sites. Likewise, although *T. polychaeta* has been identified from numerous sites, all occur at high palaeolatitudes, with DSDP Site 275, at current latitude of 50°26'S, the lowest. This may imply that *T. polychaeta* had an ecological affinity for cooler conditions, providing an explanation for its absence from the Marca Shale.

The greater abundance of *Chaetoceros*-type spores in the CESAR 6 may relate to a greater influence of diatoms with a "bloom and bust" mode of life, indicative of spring bloom assemblages in the modern ocean (Brodie & Kemp, 1994; Bull & Kemp, 1995; Grimm *et al.*, 1996; Lange *et al.*, 1997). Such diatoms are adapted to rapidly exploit available nutrients when conditions are favourable, generally with the onset of stratification and when irradiance levels are sufficient for growth in the spring. The vegetative cells of these diatoms are characteristically lightly silicified (e.g. Treppke *et al.*, 1996) and are rarely preserved in sediments.

Diatoms with different ecologies to the “bloom and bust” forms also produce resting spores. These are the “pseudo-benthic” diatoms (e.g. *Hemiaulus, Rhizosolenids, Stephanopyxis*) that produce resting spores at the base of the upper stratified layer in oceanic waters (Bienfang & Szyper, 1981). As discussed above, resting spore development is generally associated a sudden change in one or more environmental factors, including nutrient levels, irradiance, hours of sunshine, pH, temperature and salinity (McQuoid & Hobson, 1996). Many “pseudo benthic” spores in the CESAR 6 originate, or appear to originate, from *Hemiaulus* further supporting the notion that the spores were formed by “pseudo-benthic” diatoms. *Anaulus* has previously been interpreted as a resting spore of *Hemiaulus*, and its abundance in the CESAR 6 may also relate to “pseudo-benthic” sporulation. The greater abundance and diversity of these resting spores in the CESAR 6 may be an indication of more stressful environmental conditions compared to the Marca Shale. The fact that the CESAR 6 was deposited well within the Arctic Circle suggests that irradiance and hours of sunshine may have been important environmental factors forcing sporulation.

CHAPTER 4

Sedimentology and High-Resolution Analysis of the Marca Shale Microfabric

4.1 INTRODUCTION

Laminated hemipelagic sediments are amongst the highest resolution archives of sedimentary processes and past ocean/climate variability available. The Maastrichtian Marca Shale member, central California, is characterised by pervasive, sub-mm scale couplets of diatomaceous and detrital laminae (McGuire, 1988; Fonseca, 1997; Fonseca, 2000), remarkably similar to recent annually laminated sediments from the Santa Barbara Basin, Gulf of California and Peru shelf. Consequently, Marca Shale lamina couplets have been interpreted as varved couplets (McGuire, 1988; Fonseca, 1997; Kodama & Ward, 2001) without a thorough high-resolution study of the nature of individual laminae. High-resolution backscattered electron imagery (BSEI) studies of more recent laminated sediments have allowed these unique records to be fully utilised, revealing insights into interannual variability, intrannual variability, biological activity, phytoplankton ecology and the nature of rapid climate events (e.g. Brodie & Kemp, 1994; Brodie & Kemp, 1995; Pike & Kemp, 1997; Bull *et al.*, 2000). Although some observations on the nature of individual laminae in the Marca Shale have been made (Fonseca, 1997), the record remains an underutilised high-resolution archive from a dynamic period in earth history.

The purpose of this chapter is to examine the nature of the laminations of the Marca Shale in an integrated high-resolution BSEI study to substantiate whether the laminae couplets were annually sedimented, to identify additional lamina types and make inferences on the probable seasonal sequence of deposition. Once classified, the laminated fabrics are used to infer local and regional palaeoceanographic/ palaeoclimatic changes. The style of marine productivity governing the formation of diatomaceous laminae, previously regarded as being coastal upwelling fuelled spring blooms (McGuire, 1988; Fonseca, 1997; Kodama & Ward, 2001) is addressed in view of the radically different “fall dump” form of export flux proposed by Kemp *et al.* (2000).

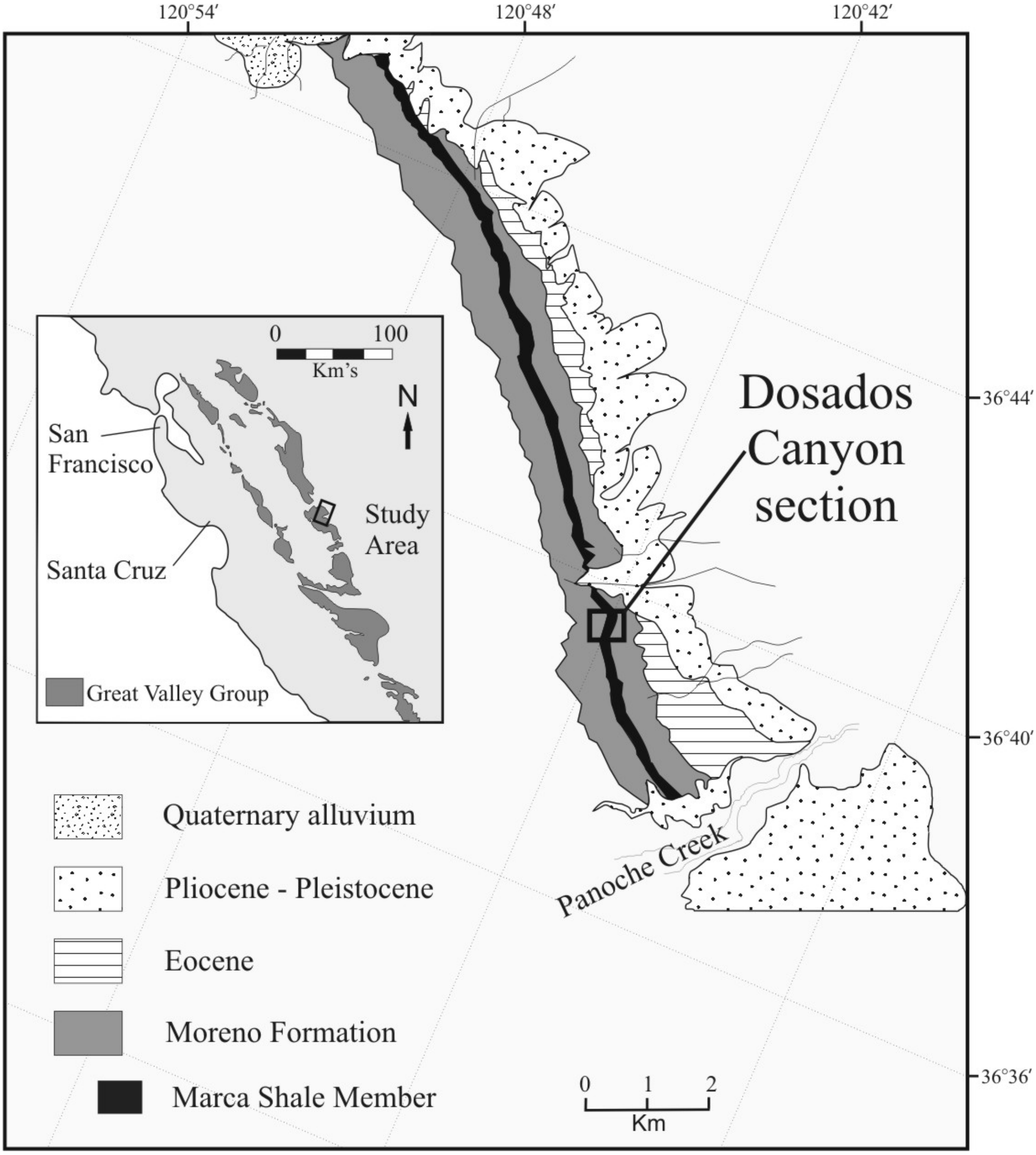

Figure 4.1. Map showing the location of the Marca Shale Member of the Moreno Formation studied in this report. Adapted from Nikolaev *et al*. (2001).

4.1.1 *Locality and stratigraphy*

The Late Cretaceous-Palaeocene Moreno Formation is the youngest of the Great Valley Sequence and crops out along the Panoche Hills on the western flank of the San Joaquin valley, central California (Fig. 4.1). The Moreno Formation is divided into four conformable members; the Dosados Sand, Tierra Loma Shale, Marca Shale and Dos Palos Shale (Fig. 4.2) (Payne, 1951). In the type section at Escarpado Canyon the Moreno Formation averages 800m in thickness and conformably overlies the Panoche Group (Payne, 1951). Biostratigraphic data from foraminifera, diatoms, silicoflagellates, dinoflagellates and radiolarians in the Marca Shale and Dos Palos indicate they represent continuous deposition from late Maastrichtian through early Danian times (Loeblich, 1958; Drugg, 1967; Foreman, 1968; Fonseca, 1997), with the K/T boundary located along the contact of the two members (Fonseca, 1997). By pinning biostratigraphic data with the magnetic polarity chrons of Gradstein *et al*. (1994), Fonseca (1997) estimated that the Marca Shale represents ~1 Ma of sedimentation between 66-65 Ma (Fig. 4.2).

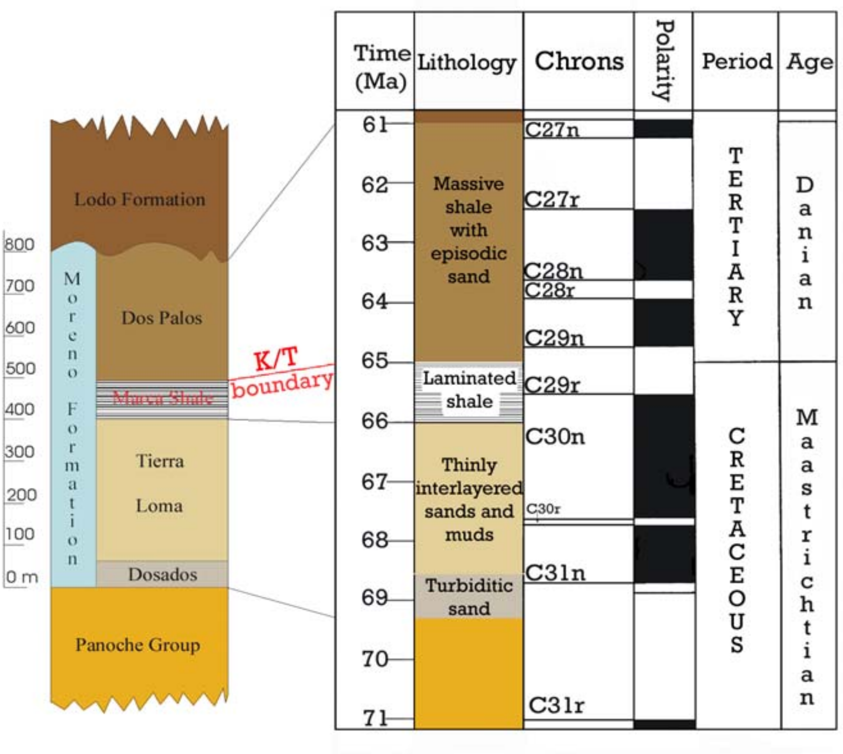

Figure 4.2. Lithostratigraphic column of the Moreno Formation correlated with the magnetic polarity chrons of Gradstein *et al.* (1994). Modified from Fonseca (1997).

A detailed interpretation of the depositional facies of the Moreno Formation is given by McGuire (1988). The Dosados Sand and lower Tierra Loma members are characterised by silty shales incised by arenaceous turbidites deposited on the upper fan/ lower slope of the forearc basin. These grade into the thinly intercalated sands and muds and eventually dark brown phosphatic shales of the upper Tierra Loma member, which were deposited in an oxygen deficient lower/middle slope environment. The thinly laminated diatomaceous shale of the overlying Marca Shale member, characterised by moderate values of organic carbon (2-3%) and hydrogen index (250-330) and the episodic occurrence of phosphatic sediments (Fonseca, 2000) is interpreted to record the intensification of bottom water anoxia and prolonged deposition of biosiliceous sediment in an upper slope/ outer shelf facies (Sliter & Baker, 1972; Williams, 1996). Fonseca (1997) noted large cyclical alterations in colouration through the Marca Shale, with dark chocolate brown intervals juxtaposed against paler buff coloured intervals (Fig. 4.3). The darker intervals reflect a relative increase in detrital input, whilst the paler coloured intervals are more diatomaceous rich. The dark, platy, bioturbated shales and intercalated glauconitic sands of the Dos Palos member deposited in a shelf edge to outer shelf environment record the continued shoaling of the basin into the early Tertiary (McGuire, 1988).

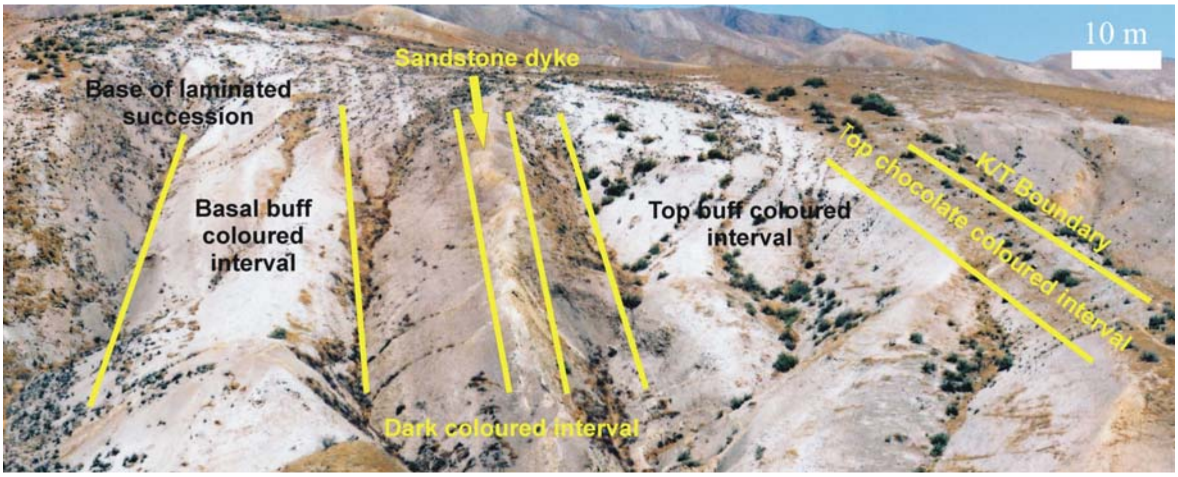

Figure 4.3. Photograph of the Dosados Canyon section, highlighting the alternating pale and darker coloured intervals. The photograph was taken facing north.

4.1.2 *Palaeogeographic setting*

Deposition of the Moreno Formation occurred in an active, silled, forearc basin (Ingersoll, 1978; Bartow & Nilsen, 1990), which was bounded to the east by the Sierra Nevada volcanic arc and to the west by the Franciscan subduction complex (Ingersoll, 1978; Moxon, 1988; Bartow & Nilsen, 1990; Dickinson, 1995). The amalgamating Franciscan subduction complex developed into an outer arc ridge which acted as an effective sill, partly restricted mixing within the basin (Ingersoll, 1978; McGuire, 1988) effectively creating a Gulf of California-like embayment (Fig. 4.4). Arkosic, potassium-rich sediment was supplied to the basin from extensively exposed batholiths (Ingersoll, 1983). Benthic foraminifera and diatom assemblages suggest that the Marca Shale was deposited at palaeo water depths of between 200-500m (Fonseca, 2000), probably within an oxygen minimum zone, which along with the structural sill and high organic content of the sediments, ensured the preservation of the sedimentary microfabric. Fonseca (1997) interpreted the Marca Shale to have been deposited at ~43º N, based on the Late Cretaceous dipoles of Diehl (1991) and Gunderson and Sheriff (1991).

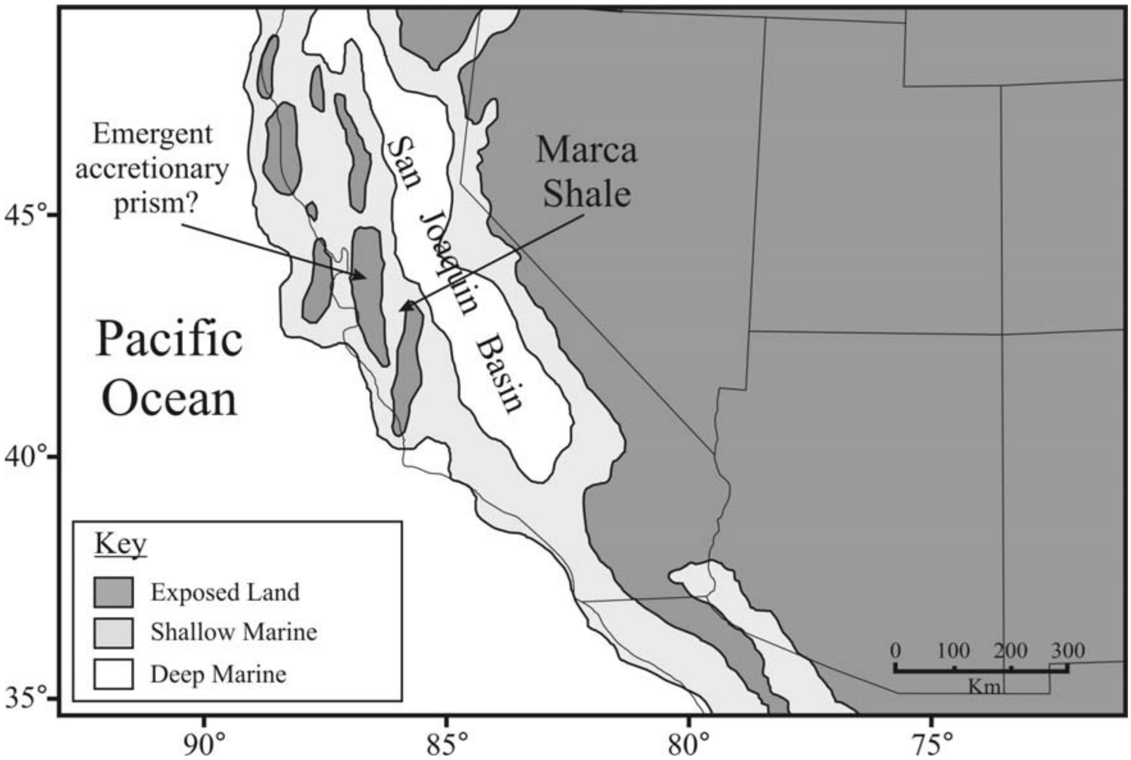

Figure 4.4. Simplified palaeogeographic map of the late Maastrichtian Californian margin, adapted from a palaeogeographic reconstruction by Prof. R.C. Blakey, obtained from the Northern Arizona University at http://jan.ucc.nau.edu/~rcb7/crepaleo.html

4.1.3 *Palaeoclimate*

A compilation of the results of studies into the Maastrichtian climate system is given in Table 4.1. The climate at this time was warmer than that of today, with ρCO_2 estimates ranging from 350-1480 ppmV (Andrews *et al.*, 1995; Ekart *et al.*, 1999; Ghosh *et al.*, 2001; Beerling *et al.*, 2002; Nordt *et al.*, 2002). Many authors identify a rapid rise in ρCO_2 prior to the K/T boundary, attributed to Deccan trap volcanism (e.g. Beerling *et al.*, 2002; e.g. Nordt *et al.*, 2002). High latitudes appear to have been much more equable than at present with high latitude forests occupying extensive areas presently covered by tundra or ice (Wolfe & Upchurch, 1987). Analyses of tree ring records, and vegetational and leaf physiognomy of these Arctic (75-85°N) forests suggest the area experienced a light regime similar to that of the present, although with a mean annual temperature (MAT) of 5 °C (Spicer & Parrish, 1990). Analysis of coeval forests on the Antarctic Peninsula (at 59-62°S) has yielded a similar MAT of ~7 °C, suggesting the South Pole would have experienced a MAT of -2 °C (Francis & Poole, 2002). These studies suggest that seasonal sea ice may have been present in the Arctic and that perennial ice may have existed at altitude at both Poles. However, using TEX_{86} ('tetraether index of 86 carbon atoms') analysis, a new palaeothermometer based on the composition of membrane lipids derived from an abundant and ubiquitous component of marine phytoplankton, Jenkyns *et al.* (2004) obtained an average Maastrichtian sea surface temperature of ~15 °C for the central Arctic Ocean, indicating that plant physiognomy data needs re-evaluating. Indeed, a more recent multi-proxy study of the Antarctic Peninsula material revised the estimate of the MAT to ~ 12 °C at the K/T boundary (Poole *et al.*, 2005).

Author	**Study area**	**Climate information**	**Method used**
Andrews *et al.* (1995)	India	$p\text{CO}_2$ <1300 ppmV	Palaeosols
Ekart *et al.* (1999)	Compilation of data sets	$p\text{CO}_2$ <1000 ppmV	Palaeosols
Ghosh *et al.* (2001)	India	$p\text{CO}_2$ 1480 ppmV	Palaeosols
Nordt *et al.* (2002)	Canada	$p\text{CO}_2$ 780 ppmV, rising to 1440 ppmV ~ 66.5 Ma	Palaeosols
Beerling *et al.* (2002)	USA, Spitsbergen	$p\text{CO}_2$ 350-500 ppmV, rising to 2,300 ppmV 10 ka prior to K/T	Stomatal index of land plant leaves
Goudie (1983)	Montana, USA	Seasonal rainfall	Palaeosols
Retallack (1994)	Montana	Seasonal rainfall of 900-1200 mm/year	Palaeosols
Buck & Mack (1995)	New Mexico	Seasonal rainfall >1000 mm/year	Palaeosols
Falcon-Lang (2003)	Montana, USA	Seasonal, but erratic rainfall	Growth rings in silicified conifer wood
D'Hondt Lindinger (1994)	DSDP Site 528	Large (0.5-1.0 %) fluctuations in δ^{18}O on scales of <100-500 ka over last 4 Ma of Maastrichtian	δ^{18}O of foraminiferal tests
Li & Kellendr (1999)	DSDP & ODP sites 463, 525, 577, 689 & 690	Cooling of IWT by 3-4 °C and SST by 3 °C from 68.5-65.5 Ma. Rapid warming of 3-4 °C between 65.45-65.2 Ma, followed by cooling toward K/T of 2-3 °C	δ^{18}O of foraminiferal tests
Stüben *et al.* (2003)	Tunisia	Three cool periods between 65.7-65.5 Ma, 65.33-65.26 Ma & 62.12-65.04 Ma, and three warm periods between 65.38-65.33 Ma, 65.26-65.12 Ma & 65.04-65.0 Ma.	δ^{18}O δ^{13}C, Sr/Ca, mineralogy and magnetic susceptibility
Clarke & Jenkyns (1999)	Exmouth Plateau, Australia	Maximum palaeotemperature of 12.5 °C at 43°S during Late Maastrichtian, with extrapolated maximum low latitude temperatures ~27-32 °C	δ^{18}O of fine-fraction and bulk sediments
Drugg (1967)	Marca Shale	Warm-temperate to subtropical climate	Palynomorphs
Barrera (1994)	Tropical Pacific DSDP sites	Tropical SST's of 12-20 °C in Maastrichtian	δ^{18}O of foraminifera tests
Wilson & Opdyke (1996)	Western Pacific	Equatorial SST ~27-32 °C at ~69 Ma	δ^{18}O of exceptionally well preserved mollusc shells and cements
Pearson *et al.* (2001)	Tanzania	Tropical SST of ~32 °C at ~67 Ma	δ^{18}O of 'glassy' foraminifera

Steuber *et al.* (2005)	Jamaica	Maastrichtian intrannual variation in SST between 24-31 °C at 8-14° N.	Intra-shell variations in $\delta^{18}O$
Spicer & Parrish (1990)	Northern Alaskan slope	MAT of ~ 5 °C in Maastrichtian at 75-85°N	Vegetational and leaf physiognomy
Francis & Poole (2002)	Antarctic Peninsula	MAT of ~ 7 °C in Maastrichtian at 59-62°S	Dicotyledonous wood anatomy
Poole *et al.* (2005)	Antarctic Peninsula	MAT of ~ 12 °C at K/T boundary at 59-62°S	Leaf physiognomy and wood anatomy
Jenkyns *et al.* (2004)	Core Fl-533, Arctic Ocean	Average SST of 15 °C at ~70 Ma	TEX$_{86}$

Table 4.1. Compilation of the results of different studies on the Maastrichtian climate system.

$\delta^{18}O$ records reveal that the Maastrichtian was characterised by a general cooling trend and also demonstrate that the climate was capable of strong fluctuations (D'Hondt & Lindinger, 1994; Li & Keller, 1998; Li & Keller, 1999; Stüben *et al.*, 2003). Contrary to the high latitudes, many Maastrichtian $\delta^{18}O$ records suggest that tropical waters were much cooler than at present (12-20 °C) (e.g. Barrera, 1994). However, recent data sets produced from exceptionally well-preserved mollusc shells and diagenetic cements (Wilson & Opdyke, 1996), 'glassy' foraminifera tests recovered from impermeable clay-rich sediment (Pearson *et al.*, 2001) and those corrected for the effects of diagenesis (Clarke & Jenkyns, 1999) indicate tropical sea surface temperatures (SST)'s were as least as warm as today (~27-32 °C). Tropical northern latitudes (8-14 °N) were characterised by an annual sea surface temperature range of 24-31 °C (Steuber *et al.*, 2005). Mid-latitudes of North America were influenced by a seasonal climate with a marked, but not severe wet and dry season (Goudie, 1983; Golonka *et al.*, 1994; Retallack, 1994; Buck & Mack, 1995; Falcon-Lang, 2003). Consistent with globally elevated temperatures at this time, palynological data from the Marca Shale suggest the terrestrial vegetation was analogous to that of the present day cloud forests of southern Mexico and mountains of Guatemala (Drugg, 1967).

4.2 MATERIALS AND METHODS

Nineteen sample sets and five early diagenetic nodules were obtained from the Dosados Canyon section, located in the central part of Sec.6, T.15S, R12E at 36°39.5'N, 120°42.0'W (Hanna, 1928; Hanna, 1934), directly from surface outcrops. Seven of these sample sets (Sets H, G, B, B12, N, O and C) were composed of several contiguous sample blocks, yielding long unbroken records, whilst the other samples consisted of either a single sample or several discrete samples. In order to obtain fresh samples it was necessary to remove up to 1m of weathered overburden, partially restricting sampling to gulley sides and resistant outcrops. Samples from the pale coloured intervals are light and friable in hand specimen, whilst samples from darker coloured intervals are denser and more consolidated. The two lowermost samples (sample sets J and F) differ from other samples in being well consolidated, hard and producing a ‘ring’ when struck with a hammer.

Low-resolution (66×) BSEI photomosaic base maps were produced on a LEO 1450VP Scanning Electron Microscope, utilising an automated imaging program. From these base maps sedimentary structures were analysed and laminae thickness measurements made, employing the method of Francus *et al*. (2002). Higher resolution microscopy (1500×) was used to assist in species identification, to identify any sub-layering of lamina and to assess sedimentary microfabrics. Topographic stubs were made to augment diatom identification and to assess sedimentary components. By correlating the embedded off cut counterparts with photomosaic base maps and the original sample blocks, individual laminae of interest were detached from the sample and mounted onto stubs using carbon based wax prior to gold coating. Analysis of the stubs was carried out using secondary electron imagery and BSEI.

Samples were also prepared for optical microscopy using an adaptation of the method of Scherer (1994) (Claire S. Allen, personal communication). In order to help quantify any differences in the degree of fragmentation of diatom valves in early diagenetic nodules and those from the main samples, counts of the relative number of fragments to intact valves were made. Counts were based on the number of fragments and whole valves that passed through the crosshairs during traverses of the coverslip, with a minimum of 300 counts for each slide.

Magnetostratigraphic analysis was carried out by Chris Rowan, National Oceanography Centre, Southampton on 11 specially acquired samples (shown in Table 4.2) in the hope of acquiring two definite datum levels. Current stratigraphic biostratigraphic constraints place the 65.57 Ma C29r reversal within the middle of the laminated sequence. It was hoped that the reversal could be located, allowing any palaeoclimatic/ palaeoceanographic observations to be placed within a well defined stratigraphic framework between this tie point and the K/T boundary at the top of the succession. XRD analysis of both the bulk and clay mineralogy was completed on all samples.

4.3 RESULTS

A total of 470.06 cm of sediment was studied using electron microscopy, amounting to the measurement of 10,319 individual laminations. Of this 427.53 cm (~ 91%) of material was from the pale intervals and 42.53 cm from the darker intervals. Laminations are present in all studied samples and occur ubiquitously as diatomaceous-terrigenous couplets. However, whilst laminations in the pale coloured intervals are pervasive with only infrequent massive intervals, the darker coloured intervals are more massive in nature with laminations occurring in bundles (see Fig. 4.5). Both mean terrigenous and diatomaceous laminae thicknesses are markedly reduced in the dark coloured intervals (see Fig. 4.6 and Table 4.2). Terrigenous laminae comprise a greater proportion of the bulk sediment in these intervals, with mean diatomaceous laminae thickness 68.2% the thickness of mean terrigenous laminae, compared to 85.2% in paler coloured intervals.

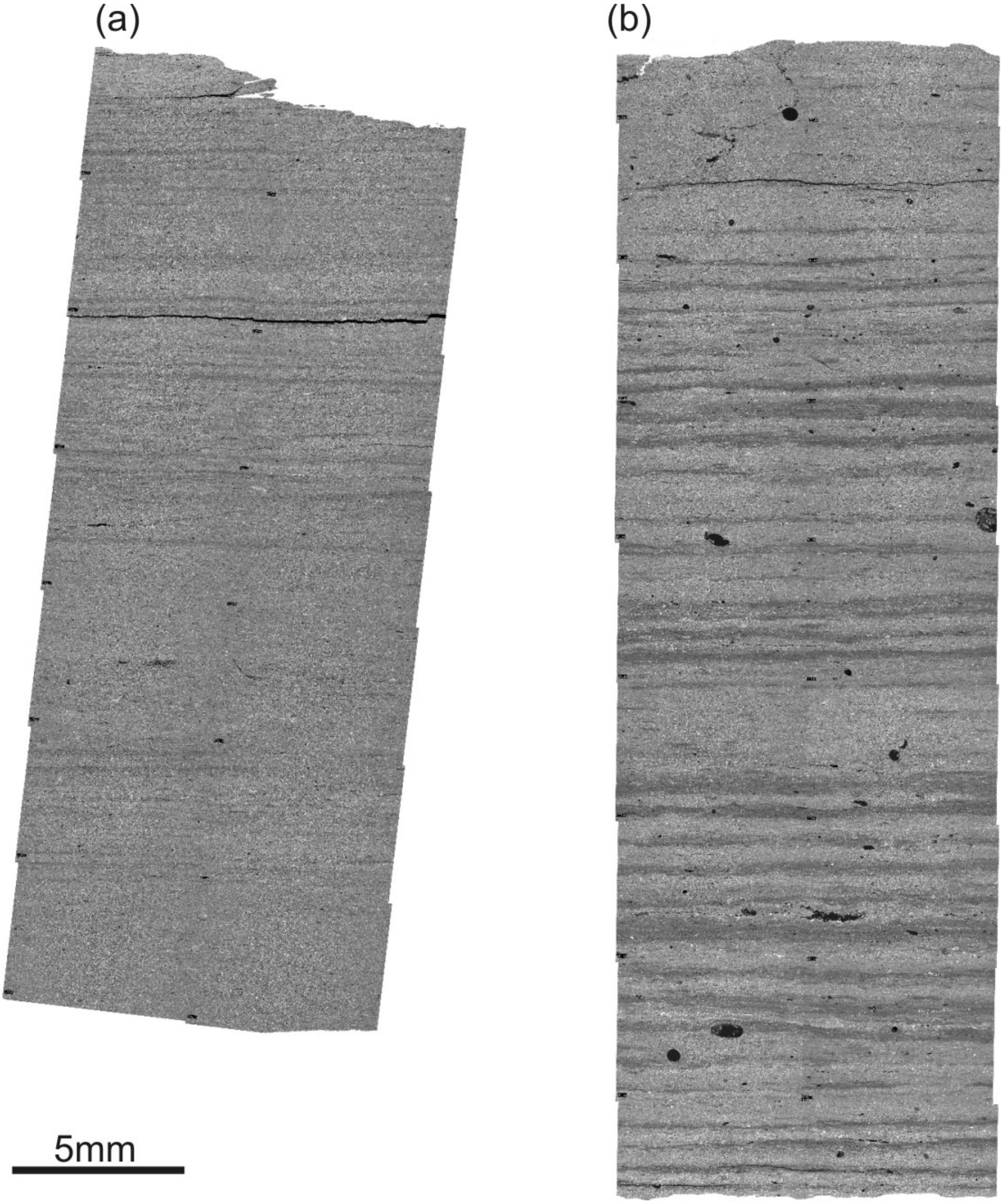

Figure 4.5. BSEI photomosaics to illustrate differences in the laminated fabric between samples from the dark (a) and pale (b) coloured units. Note: contrary to in hand specimens, diatomaceous laminae appear dark in BSEI, whilst terrigenous laminae appear brighter.

Sample set	**Stratigraphic position (m)**	**Lamina type**	**Number of laminae**	**Mean lamina thickness (µm) (s.d.)**	**Mean couplet thickness (µm) (s.d.)**
P	91	D	16	234 (74)	578 (168)
		T	11	335 (188)	
L*	84	D	13	345 (72)	888 (246)
		T	11	586 (259)	
K	80	D	49	191 (48)	510 (163)
		T	41	318 (133)	
C*	68	D	773	231 (109)	540 (207)
		T	737	310 (161)	
O	64	D	541	230 (106)	488 (199)
		T	531	259 (140)	
N	62	D	811	344 (150)	766 (285)
		T	776	424 (218)	
B12	61	D	297	304 (136)	707 (258)
		T	277	401 (211)	
B*	60	D	376	362 (191)	806 (304)
		T	356	446 (259)	
V	56	D	18	156 (38)	308 (73)
		T	14	149 (53)	
A*	53	D	418	115 (52)	314 (124)
		T	401	197 (112)	
E*	39	D	71	139 (53)	300 (107)
		T	65	167 (81)	
Nodules	35.5				
I*	35	D	87	117 (38)	300 (124)
		T	65	186 (100)	
S*	31	D	45	183 (90)	410 (219)
		T	36	223 (147)	
D	28	D	54	95 (22)	235 (69)
		T	38	140 (57)	
G*	19	D	265	325 (153)	664 (309)
		T	251	341 (221)	
H*	17	D	1294	214 (93)	408 (169)
		T	1257	194 (123)	
Q*	10	D	62	174 (63)	335 (92)
		T	57	162 (51)	
F	4	D	71	188 (94)	457 (174)
		T	62	270 (139)	
J*	2	D	39	254 (76)	610 (175)
		T	33	361 (149)	
Total pale coloured		D	4965	253 (140)	
		T	4752	297 (197)	550 (278)
Total dark coloured		D	335	152 (77)	
		T	267	223 (152)	370 (200)

Table 4.2. Mean terrigenous (T) and diatomaceous (D) laminae thickness plus the mean couplet thickness and the number of laminae counted for each sample block (s.d.=standard deviation). Darker coloured intervals are shaded. Note:* denotes samples used for magnetostratigraphic analysis.

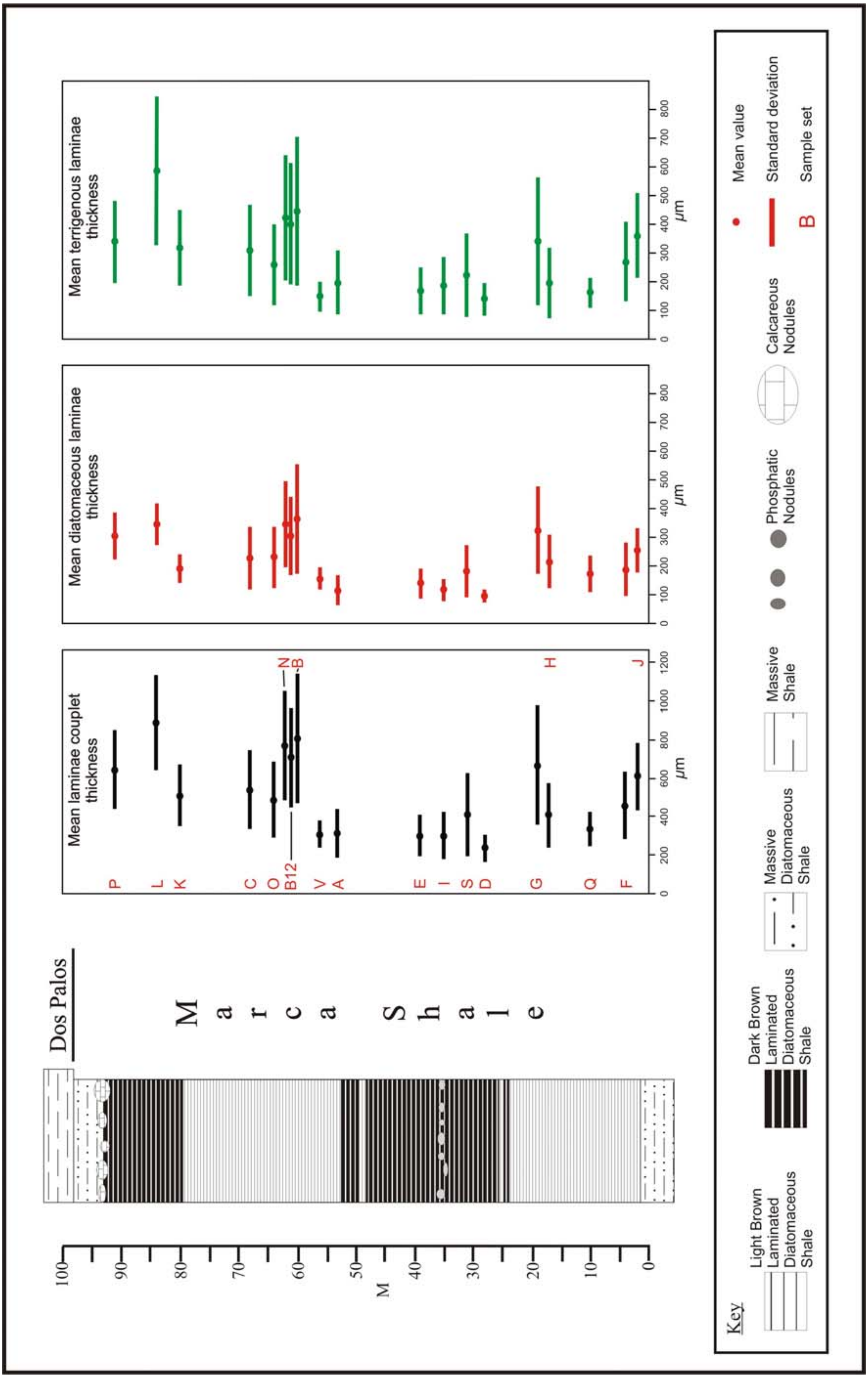

Figure 4.6. Generalised lithostratigraphic column of the studied section, indicating the location of each sample set with the mean couplet and terrigenous and diatomaceous laminae thickness (with the standard deviation) for each sample set.

4.3.1 *Diatomaceous laminae*

Diatomaceous laminae are uniformly composed of >80% diatom frustules, with a minor silt and clay component. Mean laminae thickness of each sample set varies from 95-362 µm, with absolute values ranging between 50-1333 µm. The majority of diatom valves in all samples are moderately to highly fragmented, forming a fine diatomaceous matrix (herein referred to as diatom hash) in which occasional intact valves are present. XRD analysis shows that diatom valves are composed of primary opal-A in all but the two lowermost samples, where some alteration to opal C-T has occurred (Fig. 4.7). Fine-scale structures (e.g. girdle bands, velum) are well-preserved, with little or only minor evidence of dissolution, in both fragments and intact valves. The fragmentary nature of the diatom valves made a traditional quantitative analysis of the floral assemblage problematic, although the floral composition of individual laminae was assessed to at least the generic level using BSEI of polished thin section in conjunction with topographic stubs.

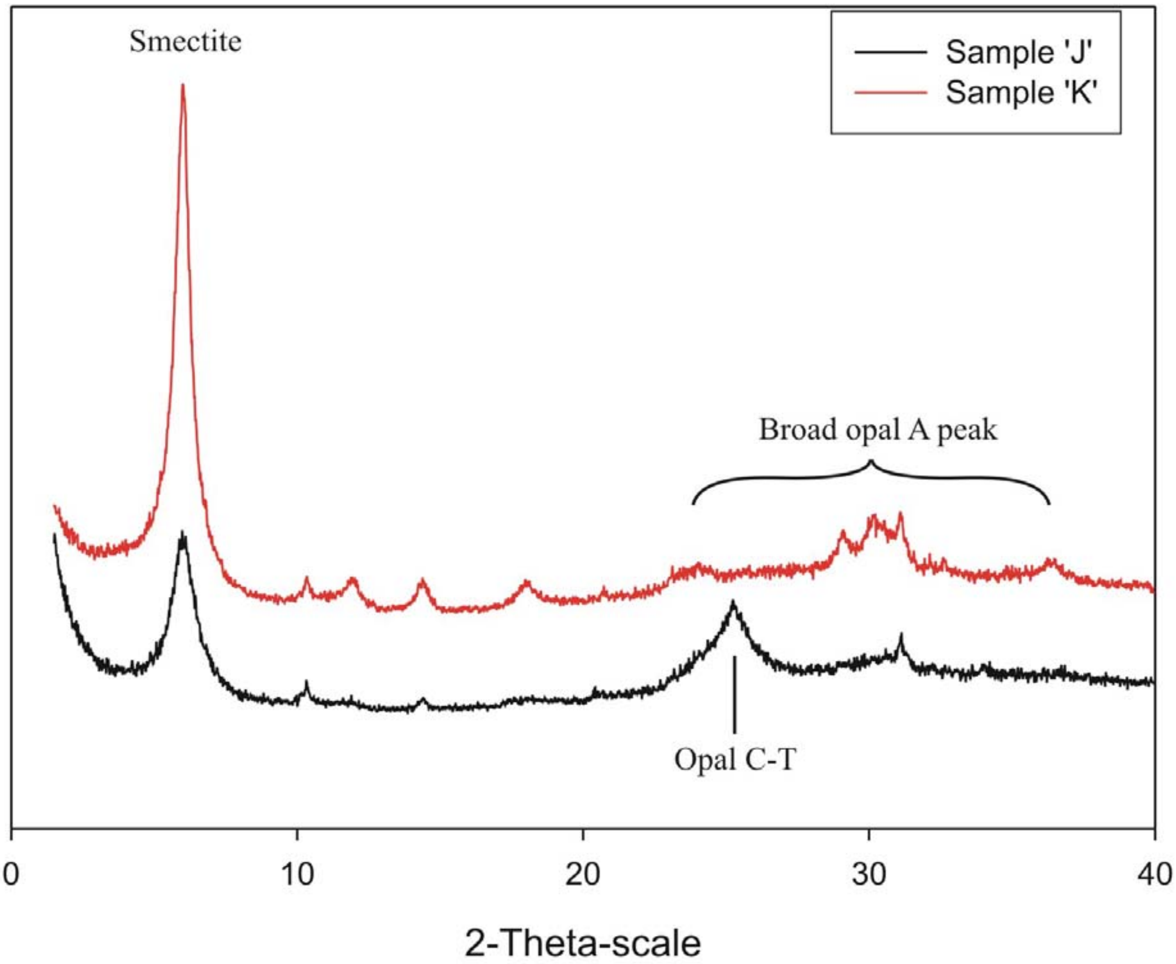

Figure 4.7. Clay mineralogical XRD diffractograms of two samples from the Marca Shale. Sample ‘J’ from near the base of the Marca Shale exhibits a clear opal C-T peak, whilst all other samples show a characteristic broad opal A peak, demonstrating no alteration to opal C-T.

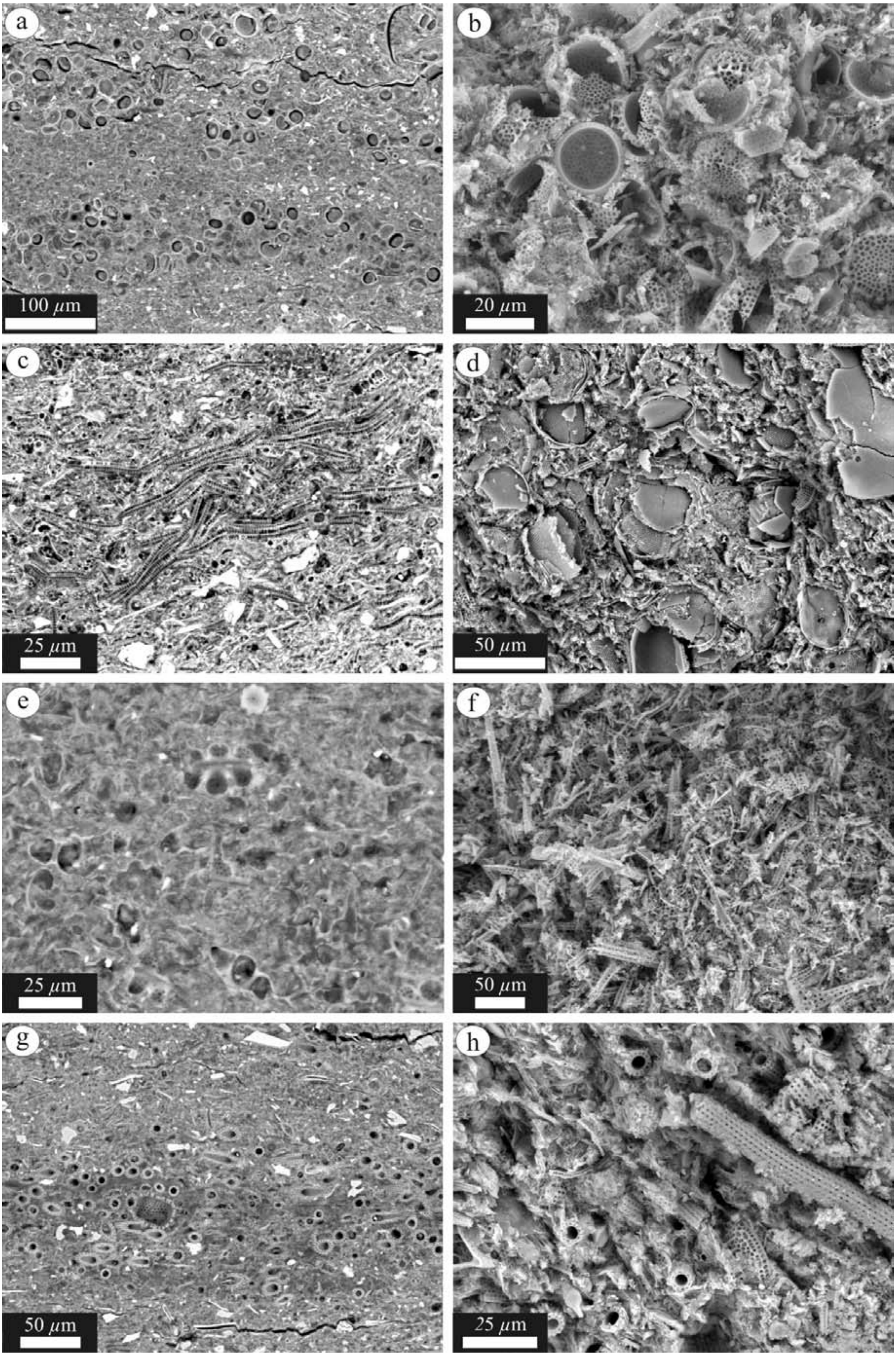

Figure 4.8. BSEI of near monospecific laminae of *Stephanopyxis discrepans* (a-b), *Stellarima steinyi* (c-d), *Hemiaulus polymorphus* (e-f) and *Gladiopsis speciosa*. Images a, c, e and g are of polished thin sections, whilst b, d, f and g are of topographic stubs.

The diatom flora is dominated by the fragments and intact valves of three dominant taxa; *Stephanopyxis* (*S. appendiculata*, *S. barbadensis*, *S.discrepans* and *S. grunowii*), *Hemiaulus polymorphus* and *Stellarima (S. distincta* and *S. steinyi*). Other common forms include the large (>200 *µ*m) *Azpeitiopsis morenoensis*, *Chaetoceros*-type resting spores (remarkably similar to recent forms), *Chasea bicornis*, *Gladiopsis speciosa*, *Kentrodiscus* spp., *Medlinia deciusii, Micrampulla parvula, Paralia crenulata, Pseudopyxilla russica*, *Pterotheca* spp., *Proboscia cretacea* and *Trinacria* spp. (*T. aires and T. insipiens*). Other species are present (Hanna, 1927; Long *et al.*, 1946; Nikolaev *et al.*, 2001) but in low abundance and do not constitute a significant component of diatomaceous laminae (See Chapter 3). Rare near monospecific laminae of *Stephanopyxis* spp. (Fig. 4.8 a-b), *Stellarima* spp. (Fig. 4.8 c-d), *H. polymorphus* (Fig. 4.8 e-f), *A. morenoensis, Chaetoceros*-type resting spores and *Gladiopsis speciosa* occur (Fig. 4.8 g-h).

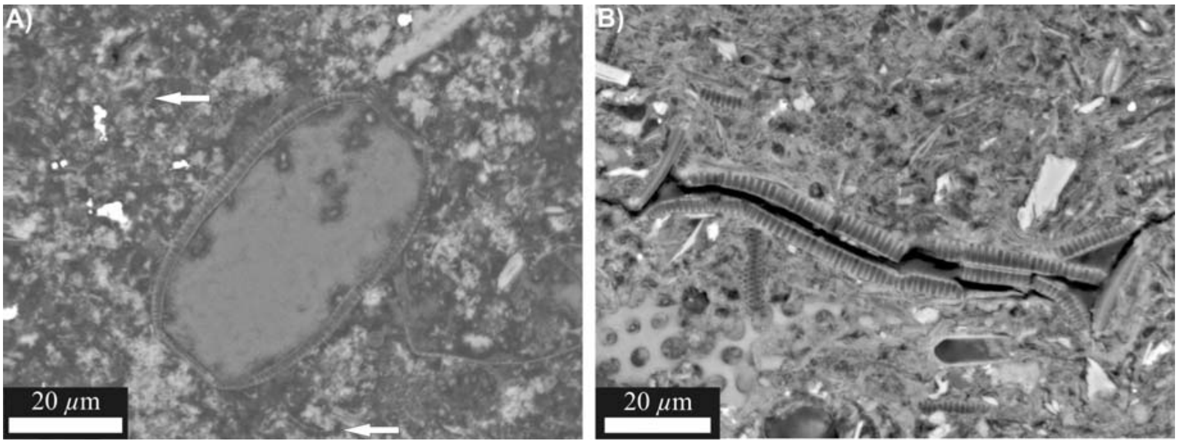

Figure 4.9. BSEI illustrating the difference in the degree of fragmentation in *Stellarima* spp. valves between (a) early diagenetic nodules and the main outcrop (b). Note that the surrounding matrix in the nodule (a) is comprised of diatom fragments (arrows).

4.3.2 *Diatoms in early diagenetic nodules*

BSEI of early diagenetic phosphatic nodules reveal that although larger frustules exhibit a far better degree of preservation, a matrix of diatom hash is present. Most noticeable valves of *Stellarima* spp., exhibit a clear separation of the two valves and in-situ girdle bands in the nodules, whilst in the main samples, the two valves are generally compressed and fractured (Fig. 4.9). Based on counts of the relative number of fragments to whole valves in optical slides, whole valves are an order of magnitude more common in nodules than in the main outcrop samples (Table 4.3). The difference in the degree of fragmentation of the diatom valves is highlighted in Fig. 4.10, which shows a light microscopy image from sample set G (Fig. 4.10a) and from a nodule (Fig. 4.10b). Several representative images of the degree of fragmentation in the main sample sets and that of the nodules are shown in Figs. 4.11 and 4.12.

Material	Percent counts of whole valves with respect to fragments	Mean
Nodules	26.9 - 35.5%	31.6%
Main outcrop	2.1 – 5.1%	3.8%

Table 4.3. Comparison of the percentage of counts of whole valves with respect to fragments between early diagenetic nodules and the main outcrop.

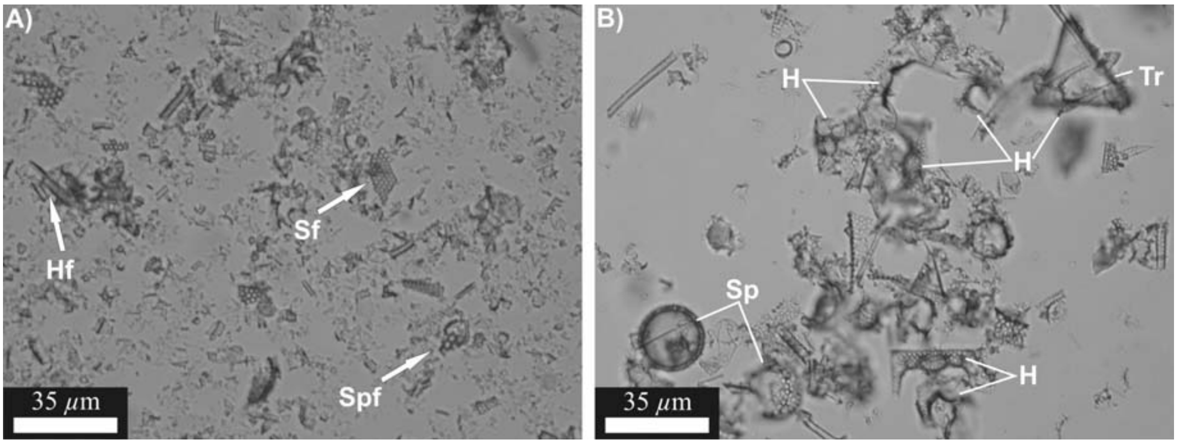

Figure 4.10. Comparison of the degree of fragmentation of diatom valves between; A) the main samples (sample set G) and, B) the nodules. In A) fragments of *Hemiaulus* (Hf), *Stellarima* (Sf) and *Stephanopyxis* (Spf) are highlighted, whilst in B) whole valves of *Trinacria* (Tr), *Hemiaulus* (H) and *Stephanopyxis* (Sp) are shown.

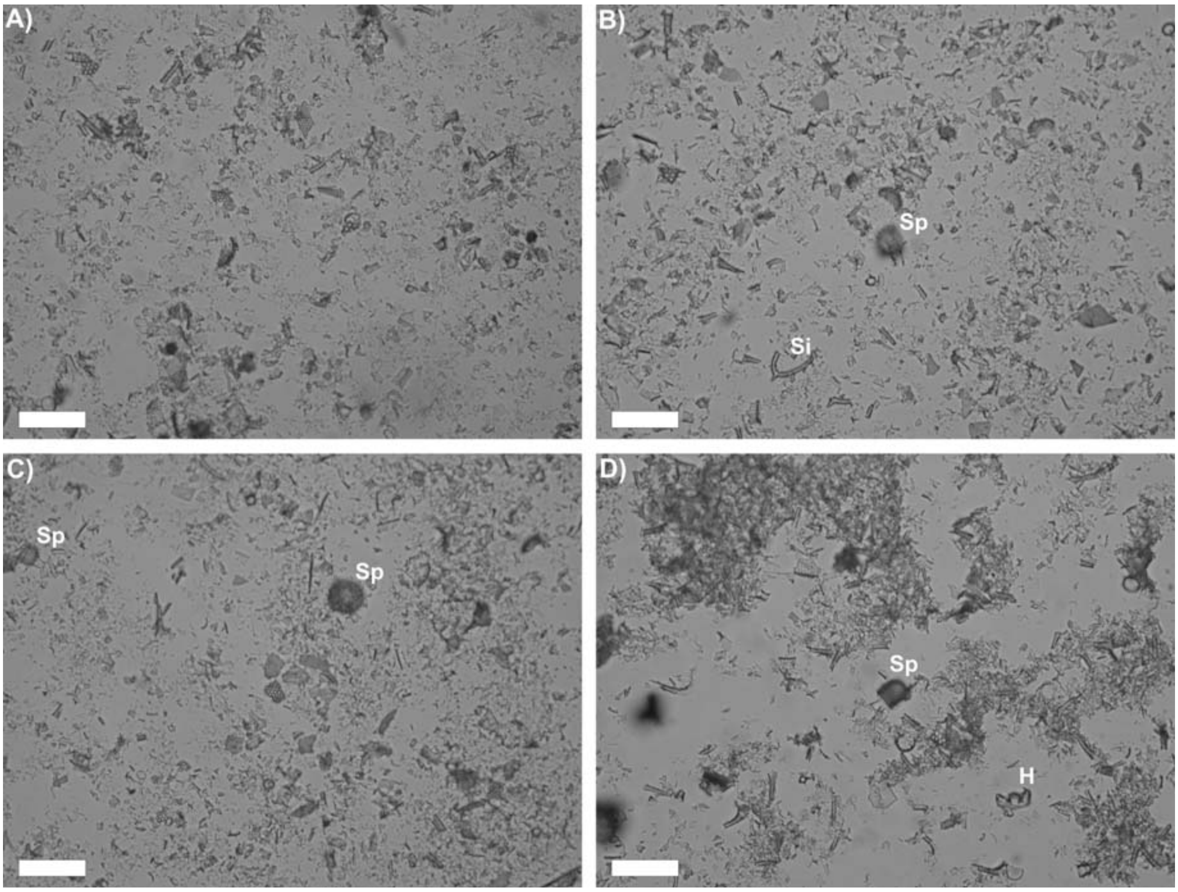

Figure 4.11. (Above) Selection of representative optical microscopy photographs of slides prepared from the main samples (i.e. not the nodules), depicting the level of fragmentation of the diatom valves in the Marca Shale. *Stellarima* and *Stephanopyxis* valve fragments along with disarticulated *Hemiaulus* horns comprise most of the finely fragmented diatomaceous material. Occasional intact valves of *Stephanopyxis* (Sp), *Hemiaulus* (H) are observable along with a large Silicoflagellate fragment (Si). All scale bars = 35 μm.

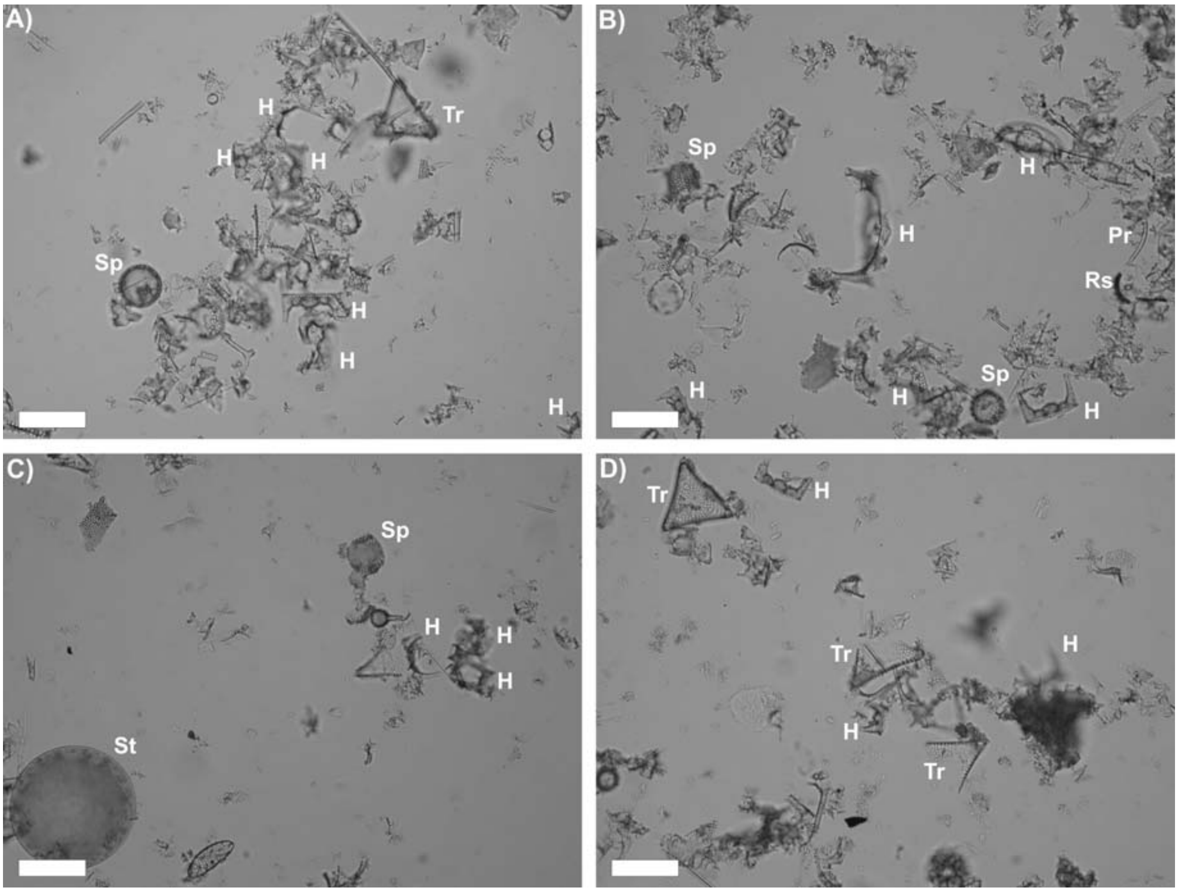

Figure 4.12. Selection of representative optical microscopy photographs of slides prepared from the early diagenetic nodules. Notice the lack of finely fragmented diatomaceous material seen in the main samples (Fig. 4.11), although fragments are visible, and larger numbers of whole valves. These images depict common valve of *Trinacria* (Tr), *Stephanopyxis* (Sp) and *Hemiaulus* (H). In 4.12B a specimen of *Proboscia cretcaea* (Pr) and a *Chaetoceros*-type resting spore (Rs) are present, whilst in 4.12 C, a large intact valve of *Stellarima steinyi* (St) can be seen. All scale bars = 35 μm.

4.3.3 *Terrigenous laminae*

Terrigenous laminae are predominantly composed of arkosic silt to rare fine sand, held in a clay matrix, averaging between 140-586 μm in thickness, with absolute values ranging from 41-1935 μm. Silt content varies from 10% to 80%, estimated from BSEI, with grains moderately/poorly sorted, angular and averaging ~ 10 μm in diameter. Semi quantitative EDS analysis of grains and the results of XRD confirm that the silt is arkosic, comprised mainly of quartz, K feldspar and plagioclase (Fig. 13). Sub-layering and grading is generally absent. Terrigenous laminae also contain a moderate diatomaceous component, comprised mainly of *Stephanopyxis* spp., *H. polymorphus* and *Stellarima* spp., although are concentrated in valves of *P. crenulata* and *Medlinia* *deciusii* with respect to diatomaceous laminae. Frustules in the terrigenous laminae are also highly fragmented, but as with the diatomaceous laminae, intact frustules do occur. In order to quantify the preferences of the main floral components a statistical study of several high-resolution (×1000) photomosaics was undertaken. Each lamina was split into upper and lower halves and the numbers of identifiable valve fragments in each segment counted along the whole width of the photomosaic. The data was then normalised to take into account the differing thickness of laminae, and thickness of section studied allowing direct comparisons to be made across all sample sets and between diatomaceous and terrigenous laminae (Fig. 4.14). The preference of *P. crenulata* for terrigenous laminae is clear although that of *Medlinia deciusii* is masked by *Trinacria* spp. (these two genera are difficult to differentiate in thin-section). Relatively high proportions of *A. morenoensis* are also present (Fig. 4.14a). Terrigenous laminae are also concentrated in sponge spicules (Fig. 4.14b).

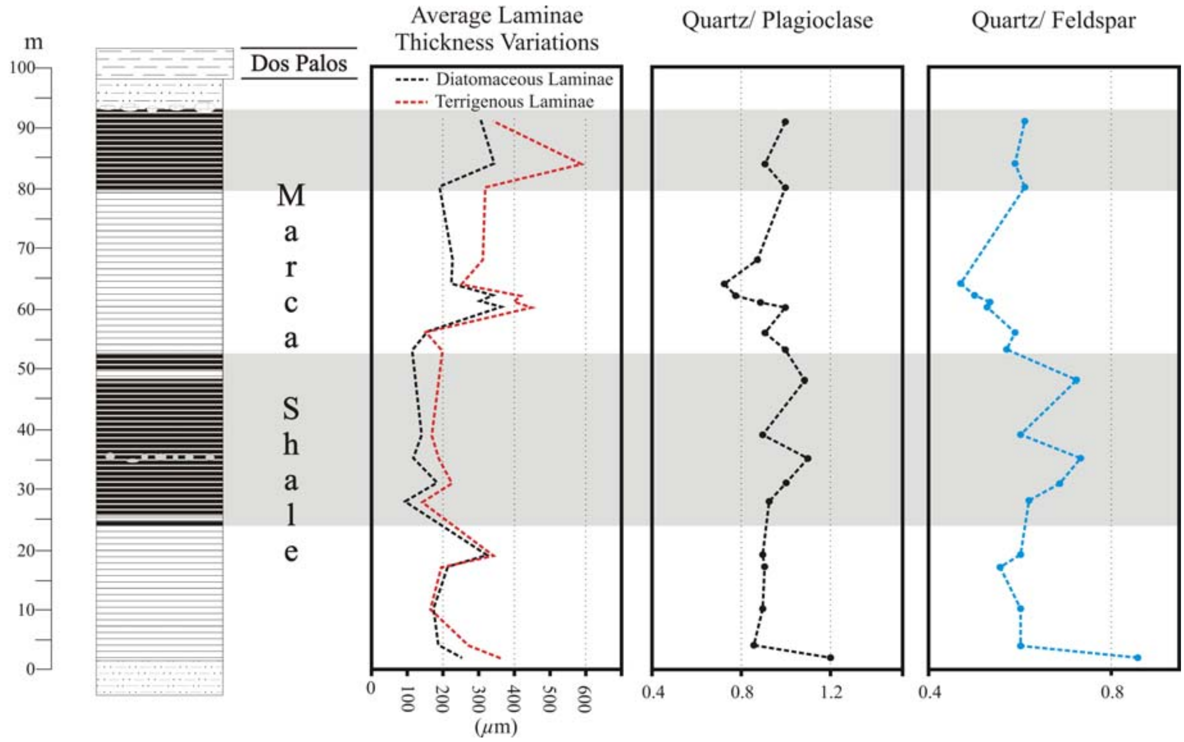

Figure 4.13. Bulk mineralogical composition of the Marca Shale in the Dosados Canyon section. Graphs show the ration of quartz/plagioclase and quartz/total feldspar. Note that the darker coloured interval in the middle of the succession is characterised by increased quartz content relative to feldspar.

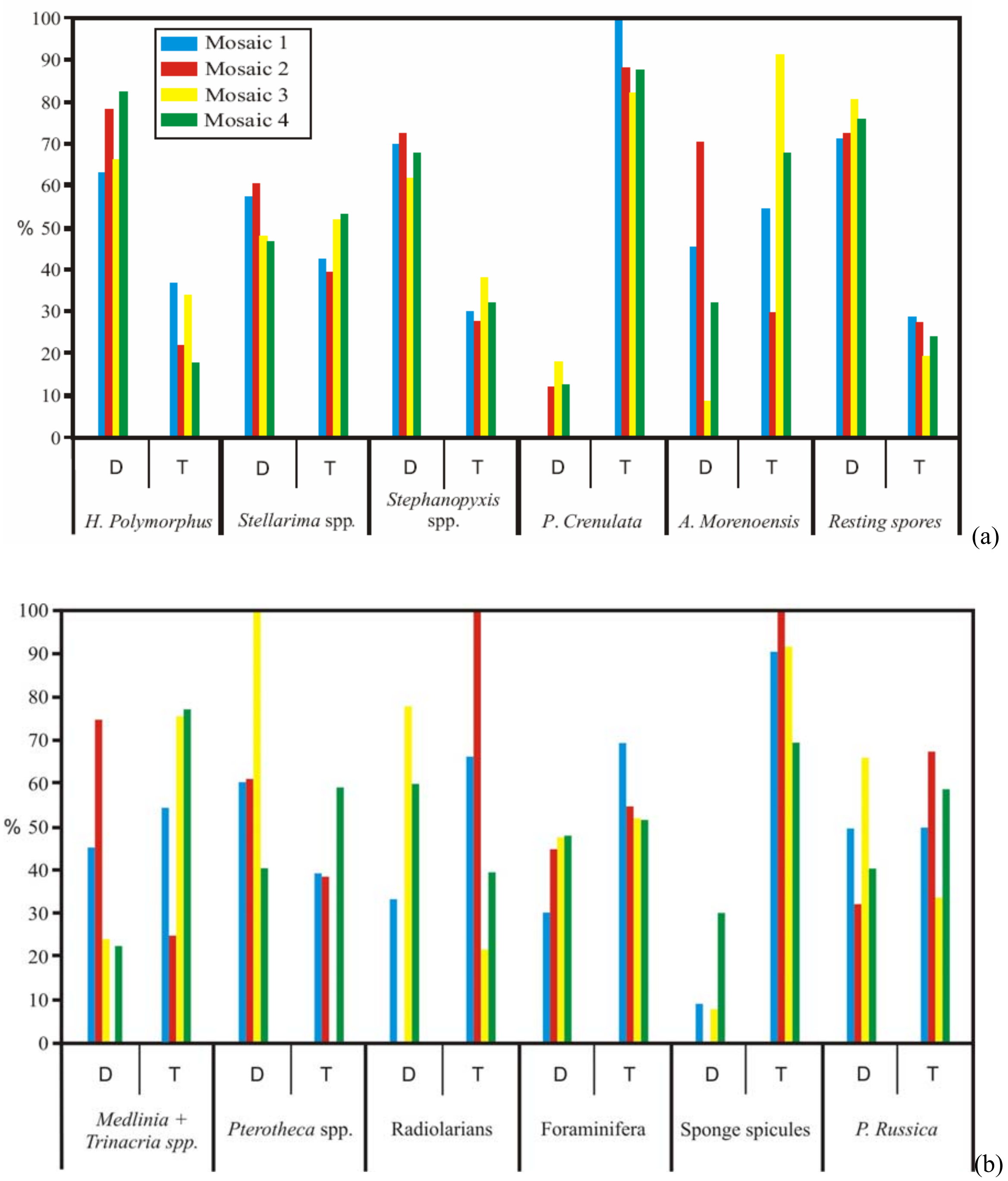

Figure 4.14. A plot of the occurrence of diatom valves in diatomaceous (D) and terrigenous (T) laminae from four high resolution photomosaics. Counts were made on intact valves along with identifiable fragments. Note the relatively high proportion of reworked valves and the dominance of *Paralia crenulata* in terrigenous laminae.

4.3.4 *Higher level of complexity within the laminated fabric*

Occasional near monospecific laminae composed of intact *Chaetoceros*-type resting spores or *A. morenoensis* are observed. *Chaetoceros*-type resting spore laminae consistently occur along the top of diatomaceous laminae, whilst *A. morenoensis* laminae only occur along their base/ top of terrigenous laminae, creating a definite three part diatomaceous succession (Fig. 4.15). Although *A. morenoensis* does form discrete laminae, it more generally forms concentrations along the contact between terrigenous laminae and the main mixed assemblage diatomaceous laminae. High resolution imagery of four sample sets (B, C, N, O) identified 110 laminae of *Chaetoceros*-type spores, of which 80.0% occurred at the top of diatomaceous laminae, 1.8% along the base, 15.5% were scattered throughout the laminae and 2.7% were towards the centre of the laminae. Over the same interval, 101 concentrations of *A. morenoensis* were identified, all of which occurred along the base of diatomaceous laminae. Terrigenous laminae immediately below concentrations of *A. morenoensis* are often observed to contain a coarser silt/ fine sand fraction than adjacent laminae (Fig. 4.16). In order to identify further laminae which may have been masked by the degree of fragmentation, the results of the statistical study of several high-resolution photomosaics were analysed for any species with preferences towards the top/ base of each half of the laminae couplet. This technique revealed that random *Chaetoceros*-type resting spores and *A. morenoensis* fragments concur with the laminae trends, although no further laminae were evident.

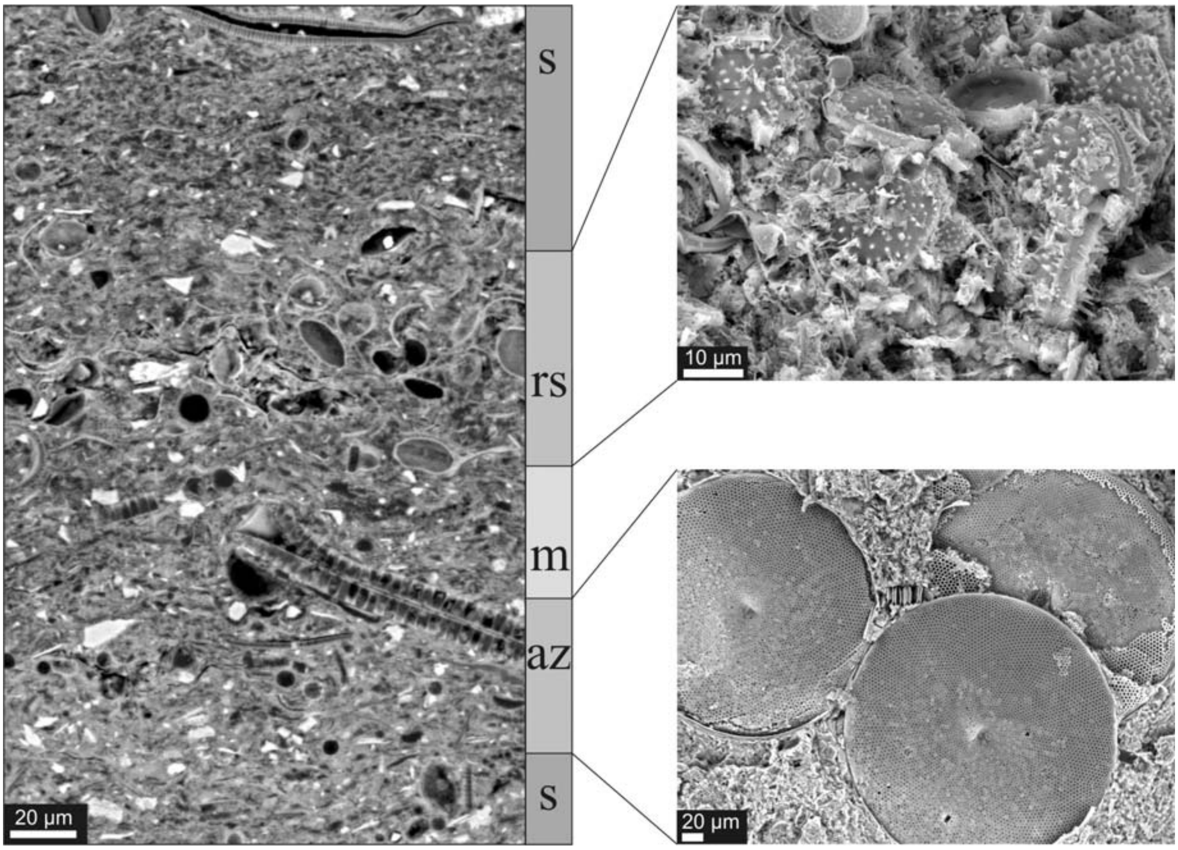

Figure 4.15. BSEI photomosaic depicting the four part flux succession observed in the Marca Shale. Silt and clay laminae (S) are overlain by concentrations of *A. morenoensis*, show in the blow up of topographic stub image. These are overlain by a mixed floral assemblage (m) (*Stellarima, Hemiaulus* and *Stephanopyxis*) which are succeeded by near monospecific laminae of *Chaetoceros*-type resting spores (rs), also shown in a blow up of a topographic stub image.

The number of couplets containing either *Chaetoceros*-type resting spore laminae or concentrations of *A. morenoensis* differs markedly between samples. By using high resolution BSEI in conjunction with low resolution basemaps, the number in each sample was quantified (Fig. 4.17). *Chaetoceros*-type spores show a gradual increase in abundance towards the middle of the outcrop followed by a gradual decrease, before rapidly increasing towards the K/T boundary. *A. morenoensis*, however, shows a much more oscillatory occurrence, although it also increases in abundance towards the K/T boundary.

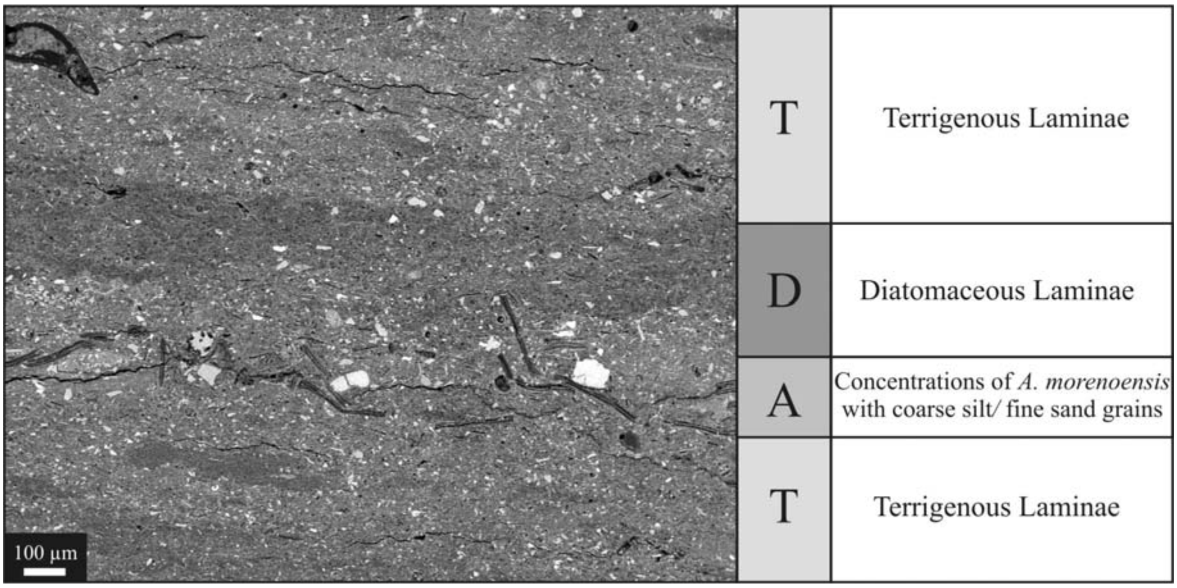

Figure 4.16. BSEI photograph illustrating the coarser silt grains associated with concentrations of *A. morenoensis*.

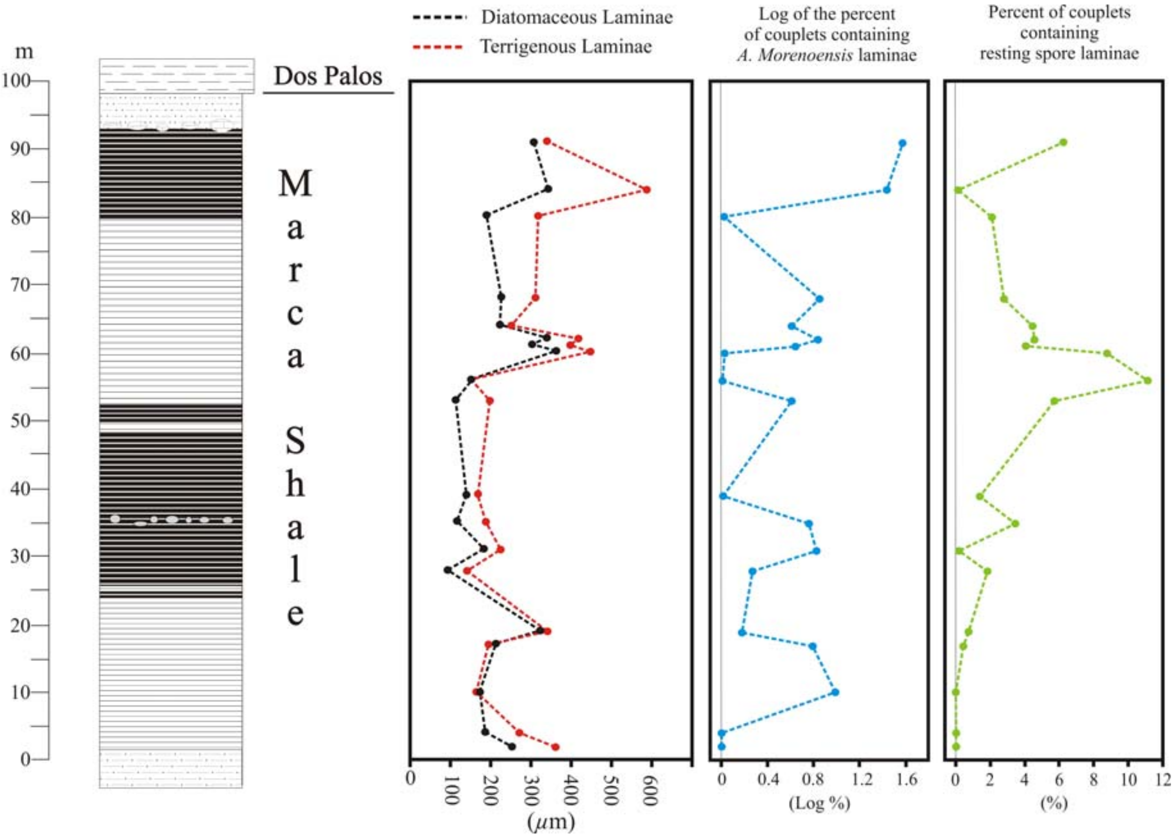

Figure 4.17. Generalised lithostratigraphic column with the mean laminae thickness. Plotted with this is the log of the percent of diatomaceous laminae containing concentrations of *A. morenoensis* for each sample block, along with the percent of laminae couplets with *Chaetoceros*-type resting spore laminae.

4.3.5 *Clay mineralogy*

Clay mineralogy is dominated by Smectite (mean value 91.7%) with minor quantities of Illite (mean value 3.8%) and Kaolinite (mean value 4.5%), whilst Chlorite is absent from all studied samples. Despite the dominance of Smectite, clear variations in the clay mineral assemblages do occur between sample sets, which can be correlated with the variations between pale and darker intervals. The Smectite/Kaolinite (S/K) ratio displays a marked decline towards the onset of the darker coloured intervals. The ratio increases during the dark coloured intervals to reach maximum in the paler coloured intervals (with the exception of the stratigraphically highest sample). Conversely, the Kaolinite/Illite (K/I) ratio displays a clear increase towards the dark-coloured units with minima within the pale-coloured units (Fig. 4.18). Greatest correlation of the clay minerals occurs between the abundance of Smectite and Kaolinite, which exhibit a moderate negative correlation (R^2 =0.8616), a likely reflection of an opposing source/mode of genesis of these minerals. Smectite and Illite exhibit a very weak correlation (R^2 =0.2141), whilst Kaolinite and Illite exhibit no correlation (R^2 =0.0099).

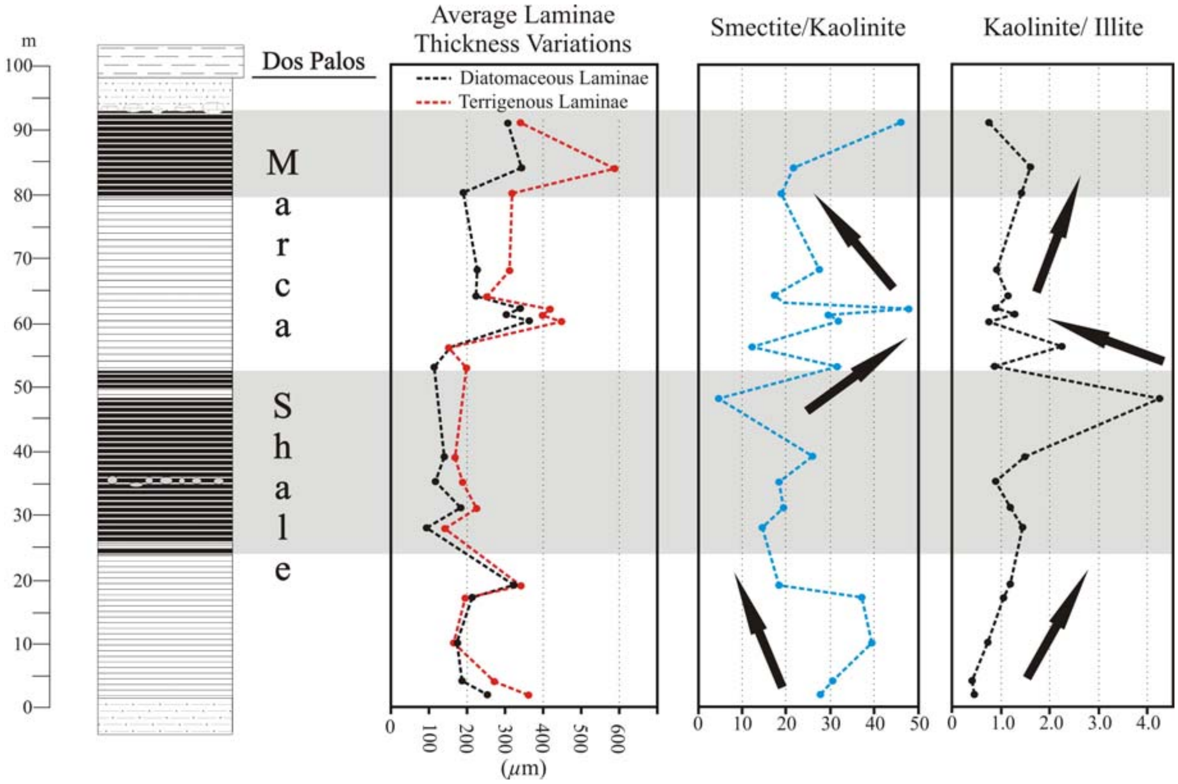

Figure 4.18. Clay mineralogical composition of the Marca Shale in the Dosados Canyon section. Arrows highlight a reduction of the Smectite/Kaolinite ratio and increase in the Kaolinite/Illite ratio prior to the occurrence of the dark-coloured intervals.

4.3.6 *Laminae thickness variations*

The mean terrigenous and diatomaceous laminae thickness of each sample set reveals a strong covariance (R^2 value = 0.7886), although the succession reveals an initial decrease in the relative thickness of terrigenous laminae with respect to diatomaceous laminae, followed by increasing dominance of terrigenous laminae (Fig. 4.19). A moderate correlation (R^2 = 0.4719) exists between Fonseca's (2000) estimate of the basinal water depth, produced using benthic foraminifera data from Sliter and Baker (1972), Lagoe and McDougal (1986) and Williams (1996), and the mean terrigenous laminae thickness for each sample set (Fig. 4.20). No such correlation is evident in the variations in average diatomaceous laminae thickness (R^2 = 0.1916).

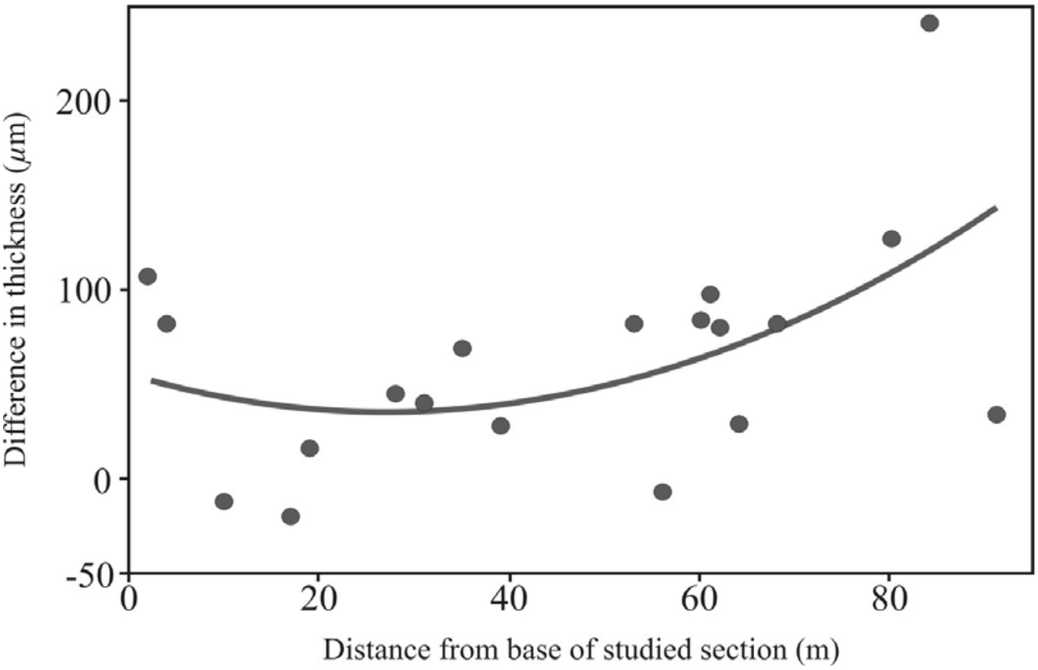

Figure 4.19. Plot of mean terrigenous thickness minus mean diatomaceous laminae thickness for each sample set, with a second order polynomial trend line, highlighting the progressive dominance of terrigenous laminae up-section.

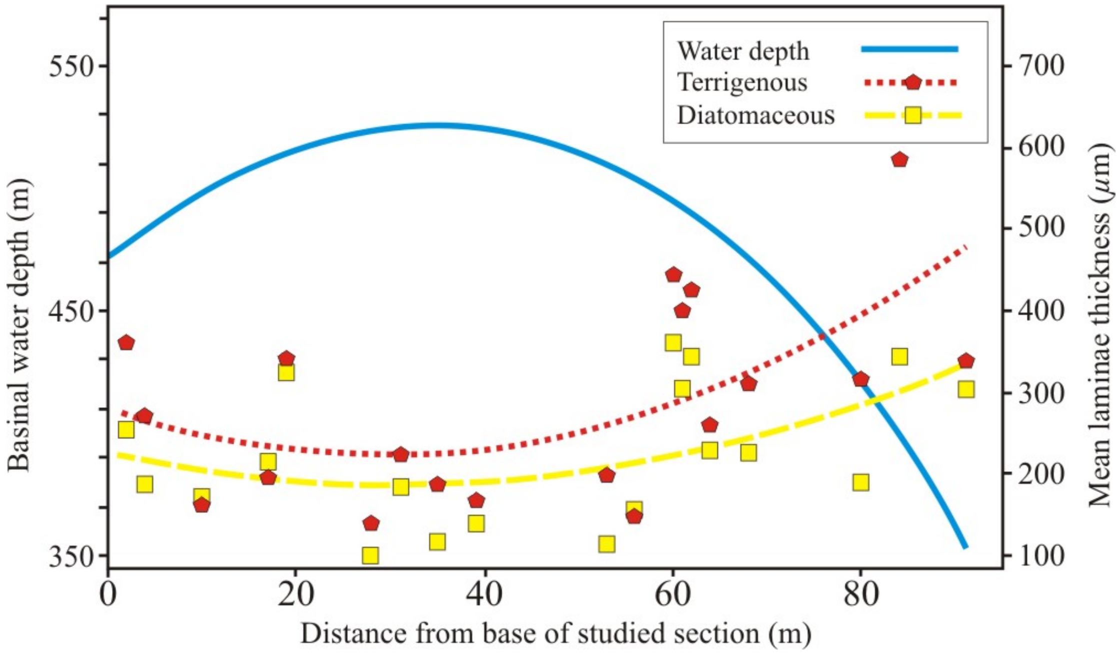

Figure 4.20. Plot of basinal water depth, estimated using benthic foraminiferal data (Fonseca, 1997) with mean terrigenous and diatomaceous laminae thickness for each sample set. A second order polynomial trend line has been plotted to both the mean terrigenous and diatomaceous laminae thickness data.

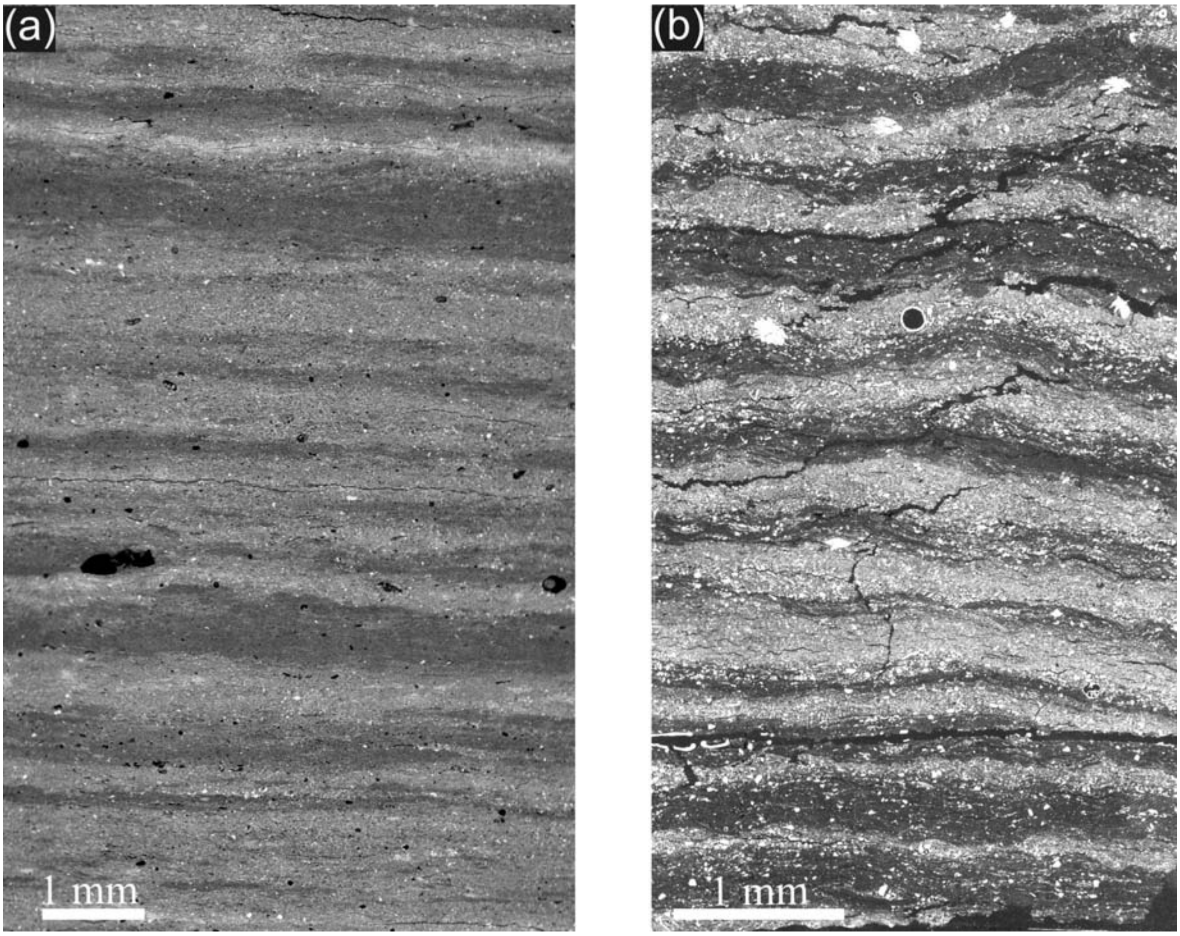

Figure 4.21. BSEI photomosaics showing the comparison between intrannual variability recorded in laminae thickness changes in the Marca Shale (a) and Quaternary sediments from the Santa Barbara Basin (b).

Both diatomaceous and terrigenous laminae also exhibit thickness variations at finer resolutions, ranging on scales of several lamina couplets to hundreds of laminae. In some samples, diatomaceous and terrigenous laminae display an out of phase relationship, whereby thickest terrigenous laminae are juxtaposed against thin diatomaceous laminae and vice versa, similar to ENSO (ENSO is discussed in detail in Chapter 5.4.1.3) induced interannual variability recorded in varved sediments from the Santa Barbara Basin (Bull *et al.*, 2000) (Fig. 4.21). This short-period variability is evident in plots of the standard deviation from the mean laminae thickness averaged over different numbers of laminae (Fig. 4.22). The greatest standard deviation occurs when individual lamina thickness is used, and is greatly reduced when mean values of 5 and 10 couplets are used.

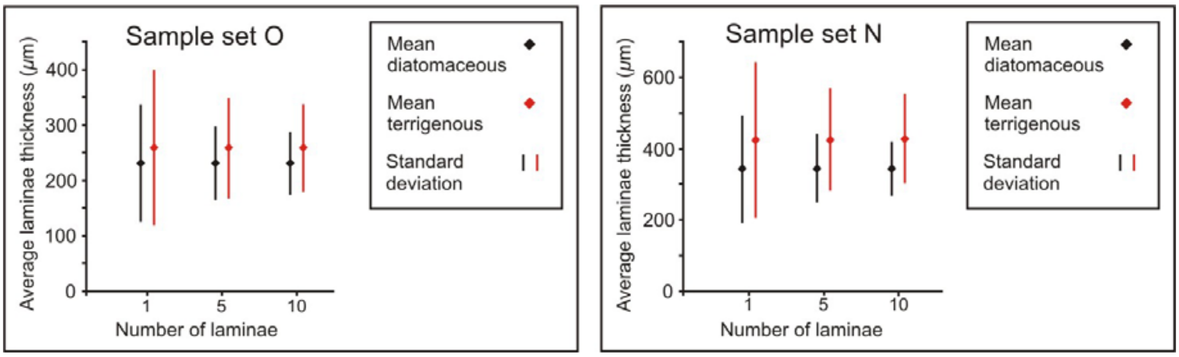

Figure 4.22. Graph of mean diatomaceous and terrigenous laminae thickness, with the standard deviation, taken for each laminae, and averages of 5 and 10 laminae. Both laminae types display decreasing standard deviations when longer time intervals are considered, whilst mean values remain constant.

4.3.7 *Foraminifera*

Mouldic preservation of foraminiferal tests is common, although tests are usually absent through dissolution (Fig. 4.23). Assemblages are dominated by *Praebulimina prolixa* and *Siphogenerinoides whitei* (Fonseca, 2000), both of which are indicators of oxygen deficient environments (Almogi-Labin & Bein, 1993; Ly & Kuhnt, 1994). The remains of benthic agglutinated foraminifera are also common, appearing as pellet shaped silt aggregations, averaging 118 µm in height and 516 µm in length. Pike and Kemp (1996c) identified both remnant tests, characterised by well-sorted silt grains, and discarded "detritic covers", composed of poorly-sorted silt. Remnant tests may preserve the internal structure, although this may be lost due to compaction, whilst the detritic covers never preserve internal structure. Although most of the aggregations in the Marca Shale are structureless, some do exhibit partial structure of the original test morphology. The structured aggregations are not uniformly composed of well sorted grains (Fig. 4.24a) making the distinction between remnant tests and detritic covers problematic. Disruption of the laminated fabric by agglutinated foraminferas is observed (Fig. 4.24d) and their presence suggests that the basin was periodically oxygenated (Bernhard & Reimers, 1991).

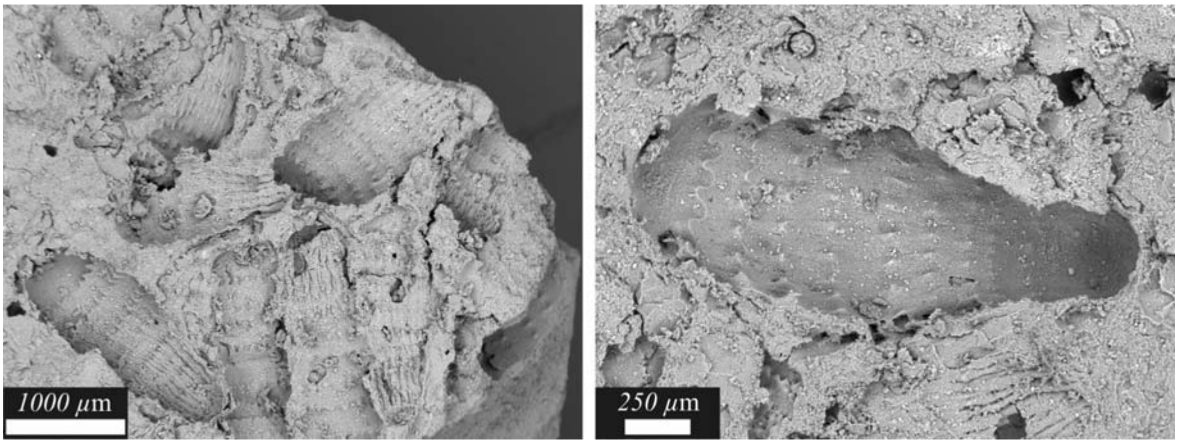

Figure 4.23. Secondary electron SEM images of mouldic casts of *Siphogenerinoides whitei*, taken from topographic stubs. These images were taken of a basal lag section of a turbidite, which are discussed later.

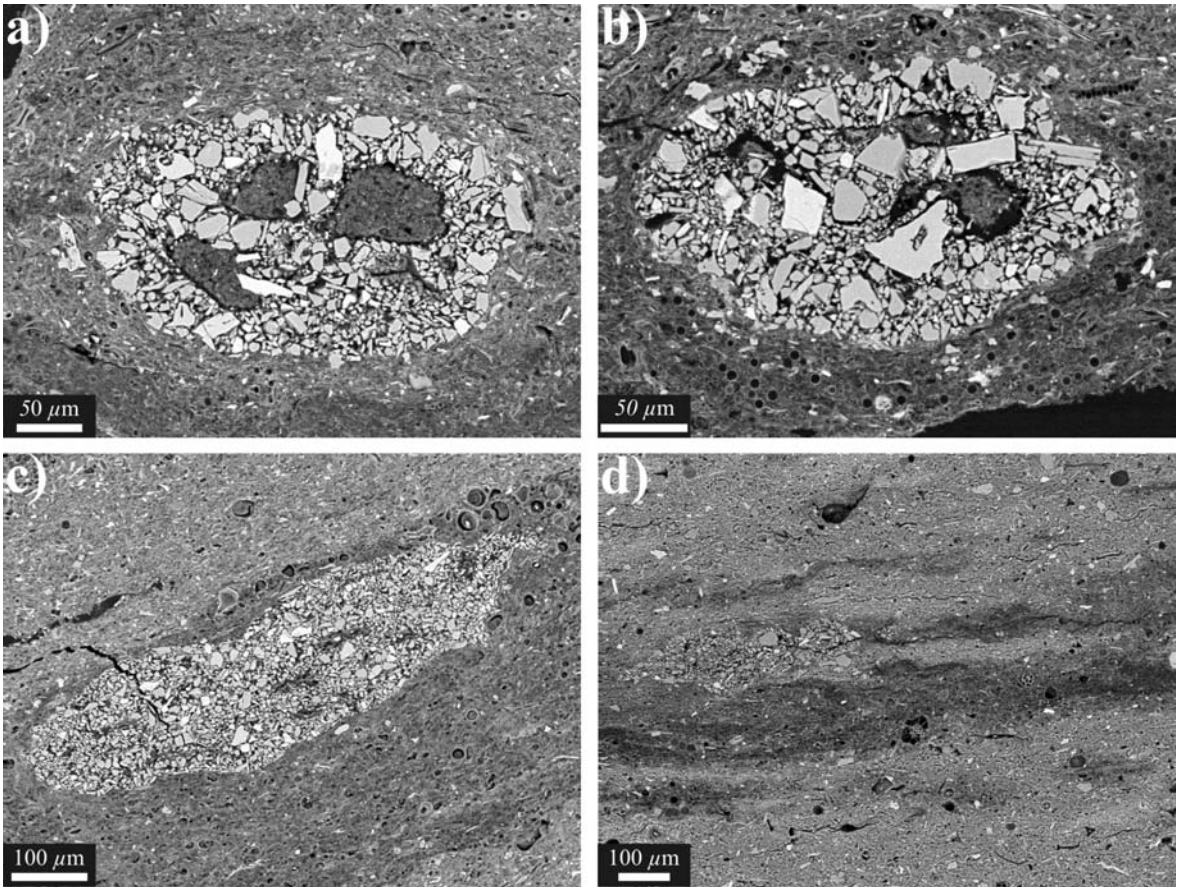

Figure 4.24. BSEI photographs of benthic agglutinated foraminifera. a) Partially structured silt aggregate, composed of poorly sorted grains. b) Moderately sorted silt aggregate exhibiting three discrete internal chambers. c) Moderately sorted aggregation exhibiting no internal chambers, but preserving a definite outline shape. d) Disruption of the laminated fabric by agglutinated foraminifera.

4.3.8 *Pelletal structures*

A number of different pelletal structures are observed, that can be divided into aggregates and pellets after Brodie and Kemp (1995). Aggregates possess diffuse boundaries/irregular boundaries, whilst pellets possess well defined, sharp boundaries. Three types of aggregate structures are observed; intact chrysophytes, intact diatom resting spores and clay/silt-rich aggregates (Fig. 4.25). Chrysophytes and resting spores co-occur so that chrysophyte and resting spore-rich aggregates generally possess both chrysophytes and resting spores, although one of the two is dominant (e.g. Fig. 4.25a and 4.25b). Chrysophyte-rich aggregates occur in both laminae types, although they are on average twice as abundant in diatomaceous laminae. Both chrysophyte and resting spore-rich aggregates are elongate in shape and contain small quantities of crushed or intact vegetative cells. Measured in thin section, the mean height and length of chrysophyte-rich and resting spore-rich aggregates are 89µm by 387µm and 133µm by 822 µm, respectively. Clay/silt rich aggregates are comprised primarily of clay, with up to ~20% silt, and vary in shape between elongate to more circular, with a mean height and length of 95µm and 281µm, respectively. They appear very bright and 'clean' in BSEI, a result of the concentration of clay and lack of diatomaceous material (Fig. 4.25d), and are found to be concentrated in zones where there is disruption of the laminated fabric (Fig. 4.25c).

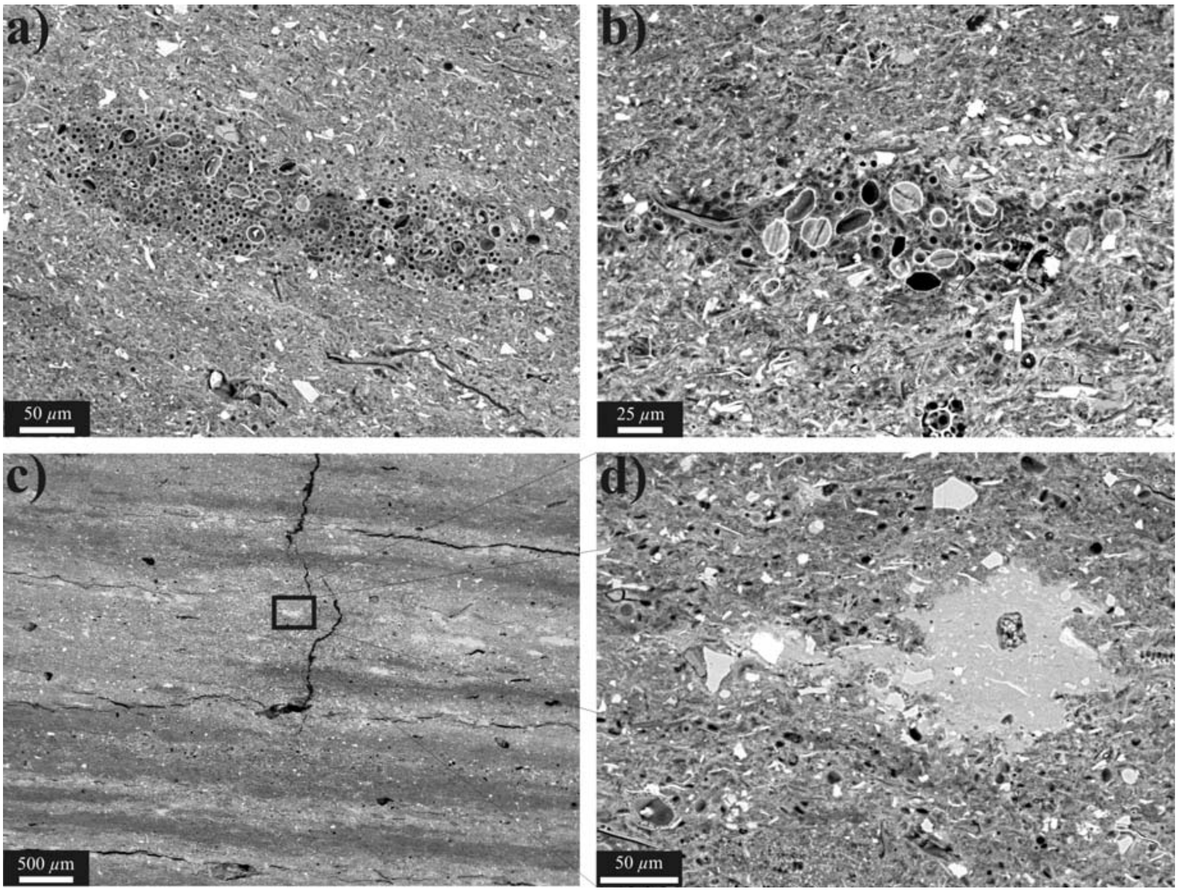

Figure 4.25. BSEI photographs of the different types of aggregates. a) Shows a chrysophyte dominated aggregate, which also contains several resting spores. b) Illustrates a resting spore-rich aggregate, containing several chrysophytes and also two valves of *Stephanopyxis* (arrow). c) The disruption to the laminated fabric associated with clay/silt-rich aggregates. d) Higher resolution image of a clay/silt-rich aggregate displaying an irregular boundary, lack of diatomaceous material and bright, 'clean' appearance.

Pelletal structures can also be divided into three categories based on composition. The most common are silt/clay rich pellets, comprised of densely packed diatom fragments, silts and clays that possess higher silt content than clay/silt-rich aggregates, lack their 'clean' appearance and contain random diatom fragments (Fig. 4.26a and 4.26b). They have a mean height of 86µm and length of 298µm. Relatively rare, elongate (mean height 75µm, mean length 263µm) pellets, primarily comprised of fragmented diatomaceous material, with minor amounts of silt/clay and sponge spicules are also observed (Fig. 4.26c). Diatom fragments are comprised of *Stephanopyxis*, *Stellarima* and the disarticulated horns of *Hemiaulus* and individual pellets are often concentrated in the remains of a single species. Lastly, there occur rare elongate (mean height 57µm, mean length 221µm) pellets composed entirely of sponge spicules, found only within terrigenous laminae (Fig. 4.26d and Fig.4.27).

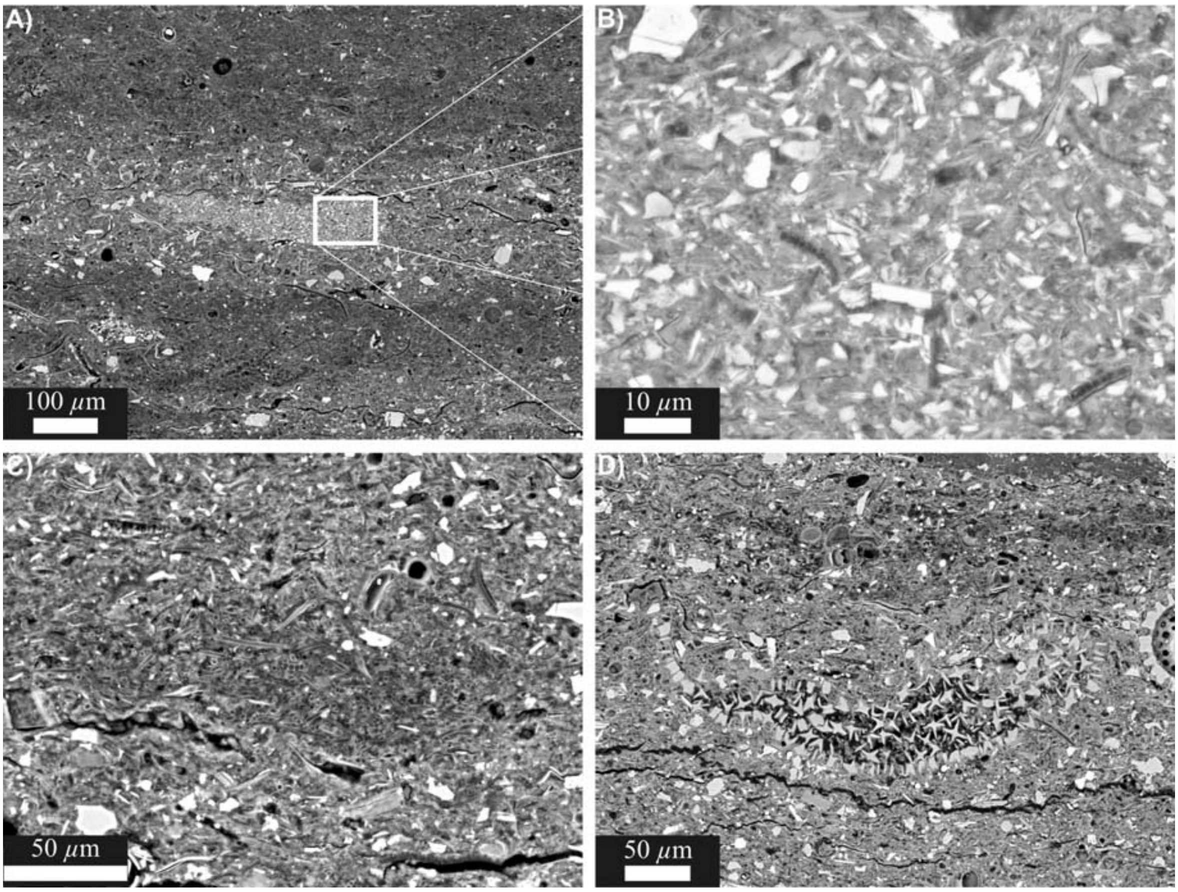

Figure 4.26. BSEI photographs of the different pellets observed in the Marca Shale. a) Clay/silt-rich pellet with well defined boundaries, high silt content and fine diatom fragments, depicted in b). c) Diatom fragment-rich pellet composed primarily of disarticulated *Hemiaulus* horns. d) Sponge spicule pellet, composed entirely of sponge spicules.

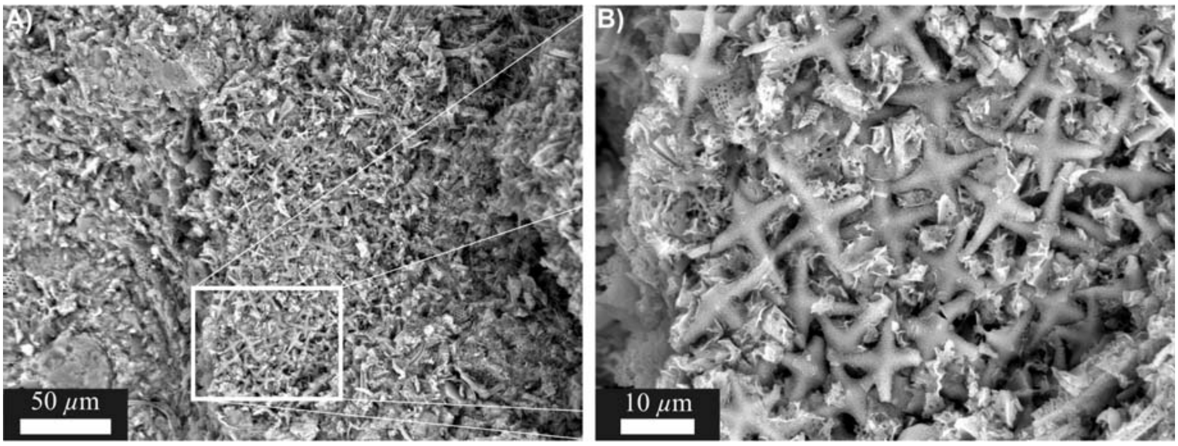

Figure 4.27. Topographic backscattered electron photographs of a sponge spicule-rich pellet.

4.3.9 *Bioturbation*

Although macrobioturbation and large burrows are absent, many laminae have a slightly transitional nature, often containing entrained packets of material from adjacent laminae at their margins. The slight ‘smearing’ of laminae extends through intervals of faint and discontinuous laminae to complete homogenisation of the laminated fabric. Homogenised intervals generally possess gradational upper and lower boundaries and may contain occasional faint discontinuous laminae. Similar disruption has been observed in the laminated fabric of Quaternary sediments from the Peru Shelf due to the activities of benthic organisms in response to elevated benthic oxygen levels (Brodie & Kemp, 1994). Following the scheme of Behl and Kennett (1995), a bioturbation index was established by visual inspection of low resolution (× 66) photomosaics (Fig. 4.28). In order to track more subtle changes in the laminated fabric, the scheme was modified to range from 1-6, where a bioturbation index of 1 represents a well developed laminated fabric, with clear boundaries between diatomaceous and terrigenous laminae, and 6 denotes complete homogenisation. Between these, a bioturbation index of 2 denotes that lamina have ‘smeared’ boundaries, 3 that laminae contain <50% of entrained adjacent material and 4 contain >50%. Faint discontinuous laminae characterise bioturbation index 5. Bioturbation index records provide a proxy for the level of anoxia within the basin, with higher bioturbation indices representing more oxic conditions. Records indicate that levels of benthic oxygenation, which may have been affected by changes in organic export flux, rates of bottom water renewal and levels of oxygenation of communicating waters, were highly variable (e.g. Fig. 4.29).

Plots of average diatomaceous and terrigenous laminae thickness for each bioturbation index indicate that the thickness of both laminae types correlates strongly with benthic oxygen levels (Fig. 4.30). Average terrigenous laminae thickness shows a consistent increase with greater degrees of bioturbation, in contrast to average diatomaceous laminae thickness, which decreases with increasing levels of bioturbation (although the trend is not as clear in some samples).

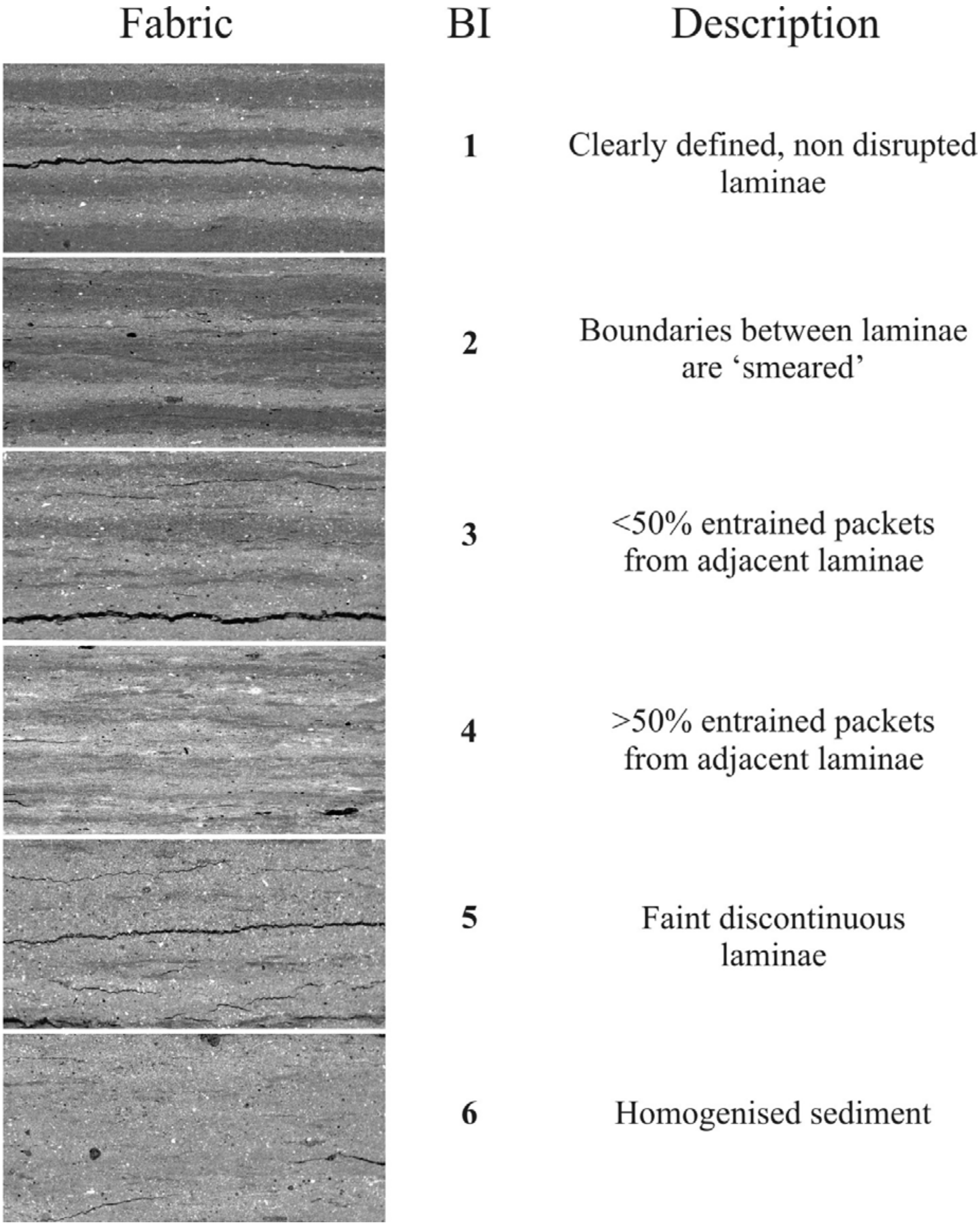

BI	Description
1	Clearly defined, non disrupted laminae
2	Boundaries between laminae are ‘smeared’
3	<50% entrained packets from adjacent laminae
4	>50% entrained packets from adjacent laminae
5	Faint discontinuous laminae
6	Homogenised sediment

Figure 4.28. The bioturbation index (BI) established for the Marca Shale. Backscattered electron images show the level of disruption suffered by the laminated fabric at each bioturbation index.

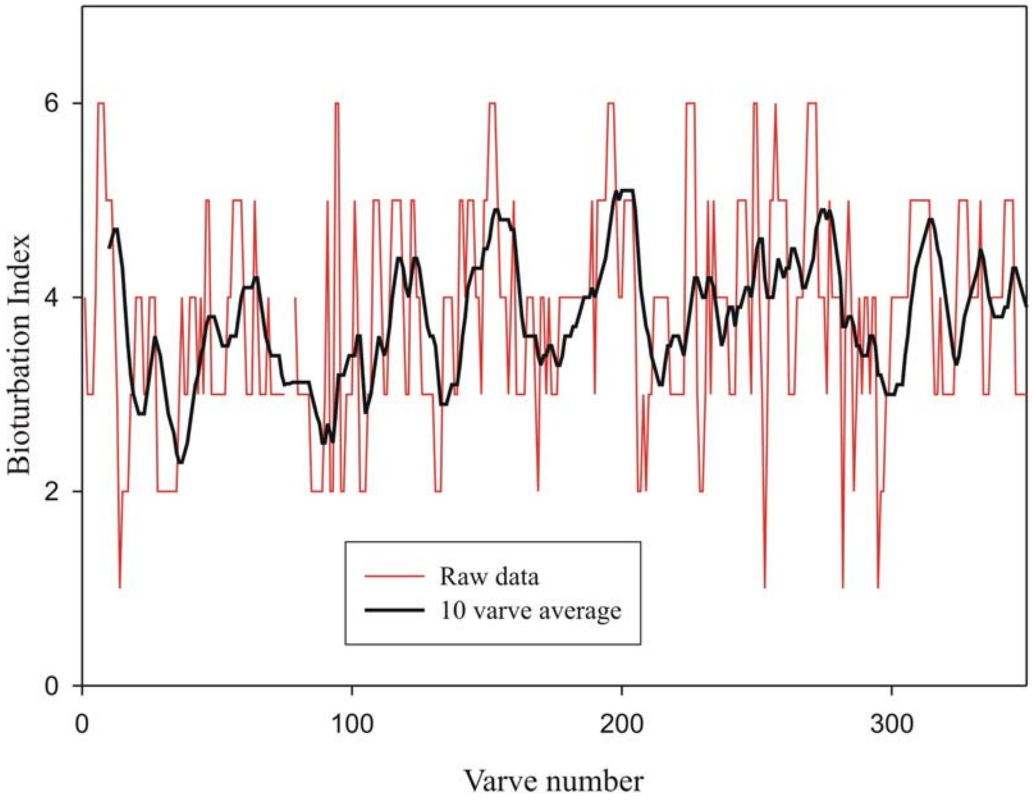

Figure 4.29. Graph showing the fluctuation in the degree of disruption to the laminated fabric over a period of 350 laminae couplets. The black line is a plot of the 10 couplet moving average and helps highlight the oscillatory nature of the degree of disruption.

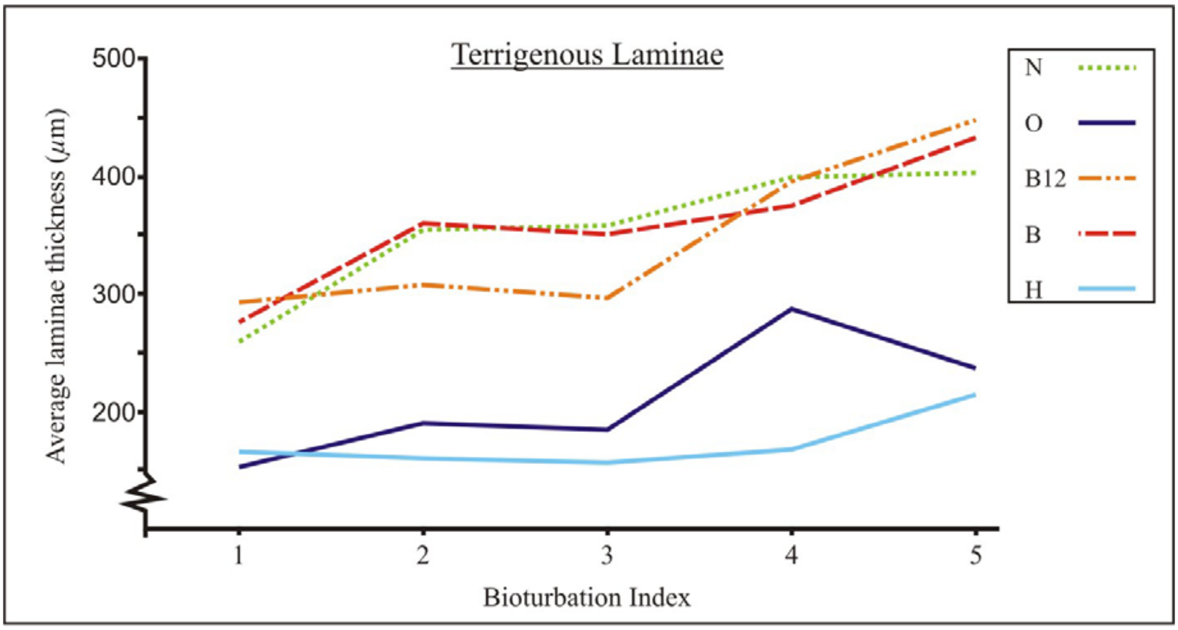

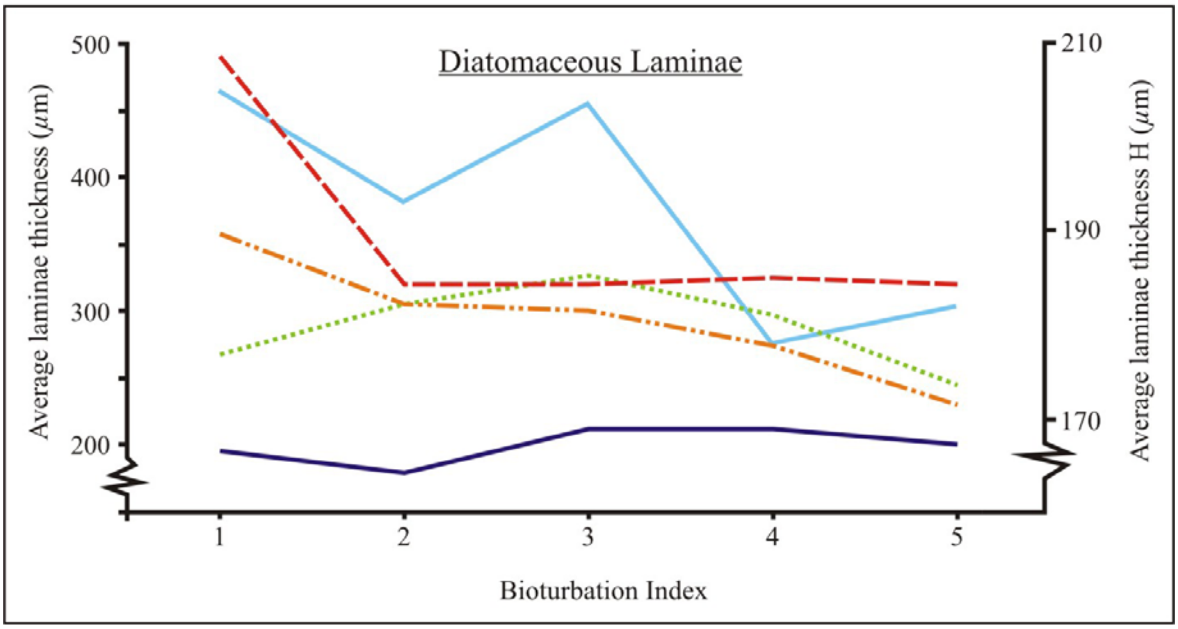

Figure 4.30. Graph showing average terrigenous and diatomaceous laminae thickness at each bioturbation index (excluding bioturbation index 6, where the laminated fabric has been destroyed) for each of the long contiguous records (N, O, B12, B, H). Terrigenous laminae show a clear trend of increasing thickness with a greater degree of bioturbation. Conversely, mean diatomaceous laminae thickness decreases with increasing levels of bioturbation, although the trend is not as clear in some samples.

4.3.10 *'Event beds' and vein structures*

A variety of sedimentary structures are preserved in the studied samples, including low density gravity flows, soft sedimentary slumps, speckled beds, micro-fault veins and "ghost veins" (Fig. 4.31). Of these, the most common are so-called "speckled beds", described by Chang and Grimm (1999), who interpret them to be the instantaneous deposition of slumped blocks of laminated diatomaceous sediment, which evolved through a fluid turbulent flow and into a viscous debris flow. They are distinguished by their sharp bedding-parallel upper and lower contacts and characteristic speckled appearance, imparted by the presence of coherent blebs of diatomaceous material scattered throughout a more terrigenous matrix. The diatomaceous blebs survive due to the frustules creating a strong interlocking framework, which along with the probable presence of biofilms allow them to resist disintegration during transport (Chang & Grimm, 1999). Small laminated intraclasts are occasionally observed along the base of some speckled beds (Fig. 4.31b). The presence of speckled beds attests that during deposition of the interval, laminated diatomaceous sediments existed upslope (at shallower water depths).

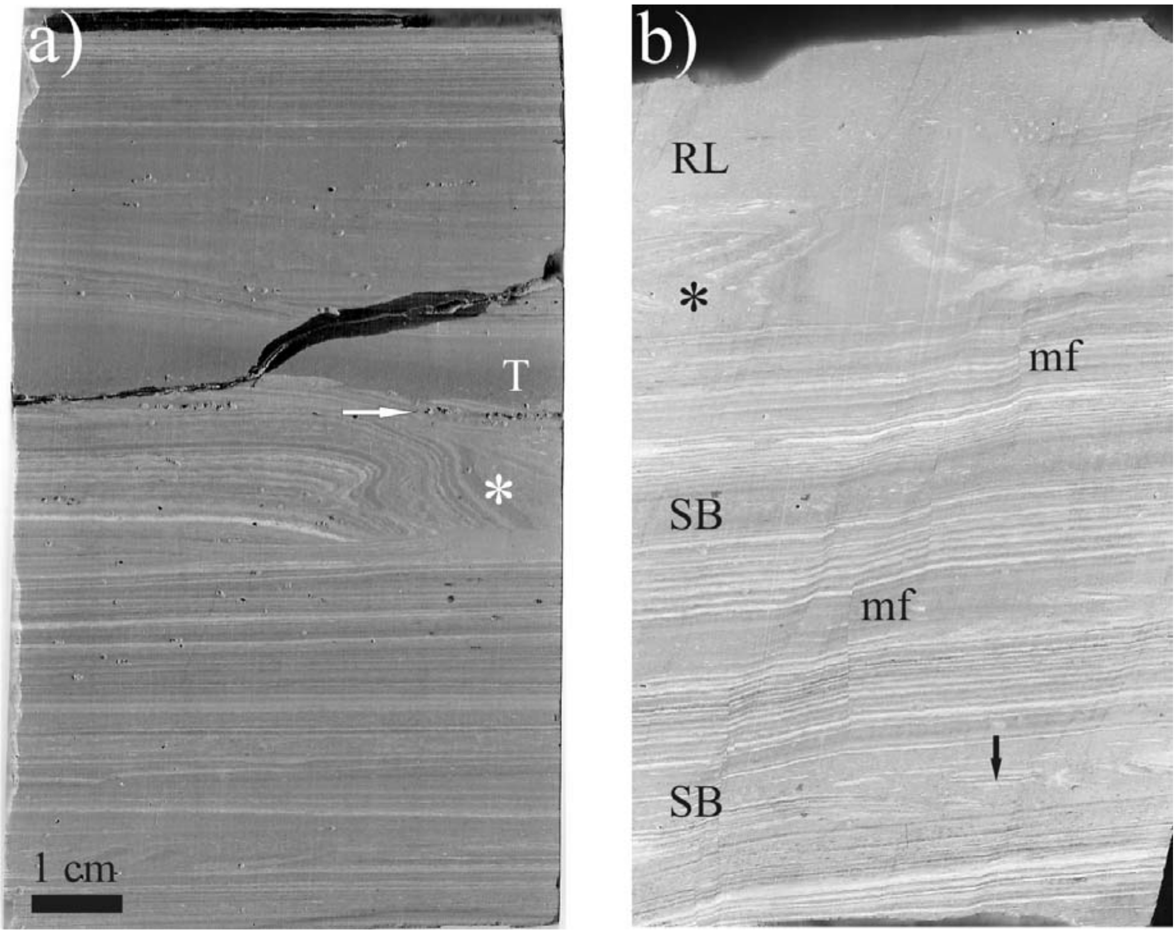

Figure 4.31. a) Slabbed and sanded flatbed scan of sample, showing soft sedimentary slump (*) overlain by a turbidite with a basal concentration of foraminifera (arrow). b) Sample showing multiple speckled beds (SB), with occasional laminated intraclast at the base (arrow). The convoluted laminations of a slumped interval can be observed overlain by a blebby redeposited layer (RL). The sample also exhibits numerous microfaults (mf). Note: contrary to BSEI, flatbed scans depict samples as in hand specimen, so here diatomaceous laminae are bright, whilst terrigenous material appears dark.

Soft sediment slumps are also common features of many sample sets, recognised by the presence of folded and/or convoluted laminae, which may be accompanied by small microfaults and a basal detachment microfault. They are commonly overlain by 'blebby' redeposited layers (Fig. 4.31a) that superficially resemble speckled beds, which, along with the fact that some slumped laminae can be mistaken for inclined laminated intraclasts, means it is possible to confuse some slumps with speckled beds in BSEI. However by closely inspecting the sample block, the geometry of the structure can be quickly ascertained and slumped intervals positively identified.

Low density gravity flows are relatively rare in the studied samples, and often have a similar appearance to terrigenous laminae. They are distinguished by their sharp upper and basal contacts and siltier nature than background detrital laminae. Some thicker flows possess erosional bases, exhibit a gradational upper contact and contain a basal lag of large foraminiferal remains and coarser debris (Fig. 4.31a).

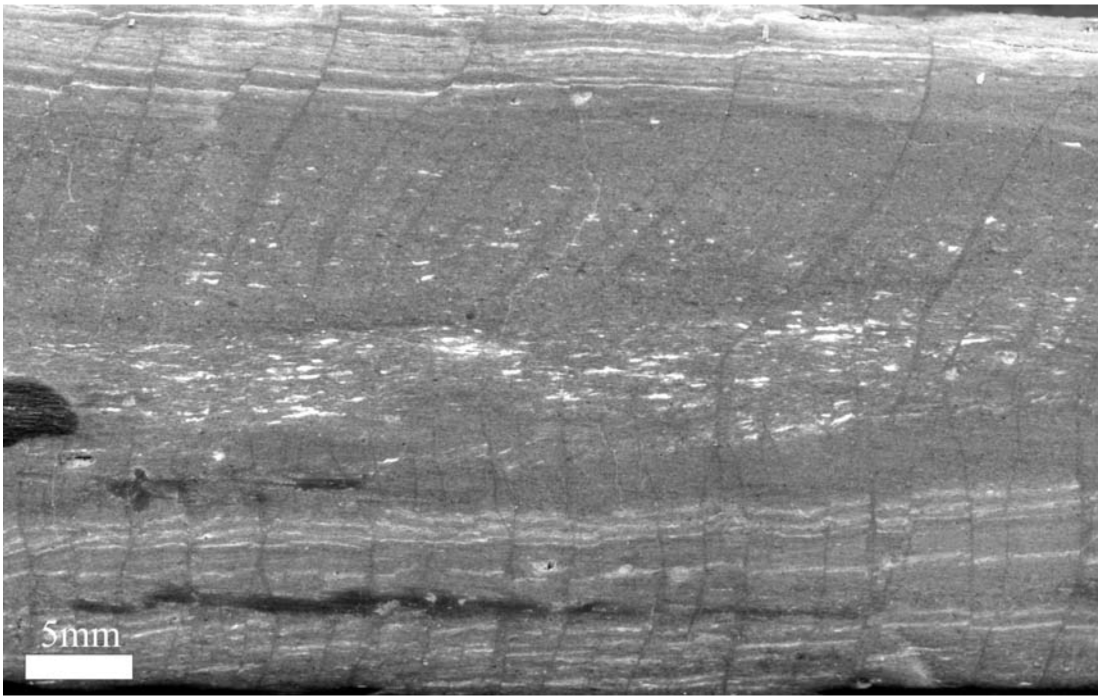

Figure 4.32. Flatbed scan of a slabbed and sanded section of sample P. Note the multiple veins perpendicularly cutting the laminated fabric, creating small micro faults. Note also how the laminated fabric has been completed homogenised in the centre of the image.

The laminated fabric is occasionally disrupted by vein and ghost vein structures, similar to those observed in sediments from the Peru margin, Aleutian margin, Japan trench, Mariana trench and the Lesser Antilles (Lindsley-Griffin *et al.*, 1990), thought to result from the passage of earthquake waves through soft sediments with a strong interlocking framework (Brothers *et al.*, 1996). Sample P, the stratigraphically highest sample studied, collected 7m below the K/T boundary, is unique in that it contains extensive microfaults and veins causing major disruption of the laminated fabric (Fig. 4.32). The scale of disruption signifies either a radical increase in seismicity within the basin (or proximity of the soft sediment to earthquake epicentres) or may relate directly or indirectly (impact related increase in seismicity) to the K/T impact event. Veins and ghost veins, speckled beds, soft sediment slumps, and low density gravity flows all attest to the active seismicity within the basin during the deposition of the Marca Shale.

4.3.11 *Magnetostratigraphy*

Magnetostratigraphic data were found to be heavily overprinted by the current magnetic field and different palaeomagnetic analysis cubes from a particular sample often gave conflicting results making the determination of polarities difficult. A compilation of the palaeomagnetic polarity stratigraphy is shown in Fig. 4.33, demonstrating two intervals of reversed polarity. The specimen with the most conclusive polarity was sample set L, which, based on the existing stratigraphic framework should be within magnetic polarity chron C29r (Fig. 4.2), was found to display normal magnetisation. This may indicate the accepted age of the Marca Shale is incorrect, however, the heavy overprint means there is poor confidence in the polarity of many of the specimens and thus, the data is equivocal for stratigraphic constraints.

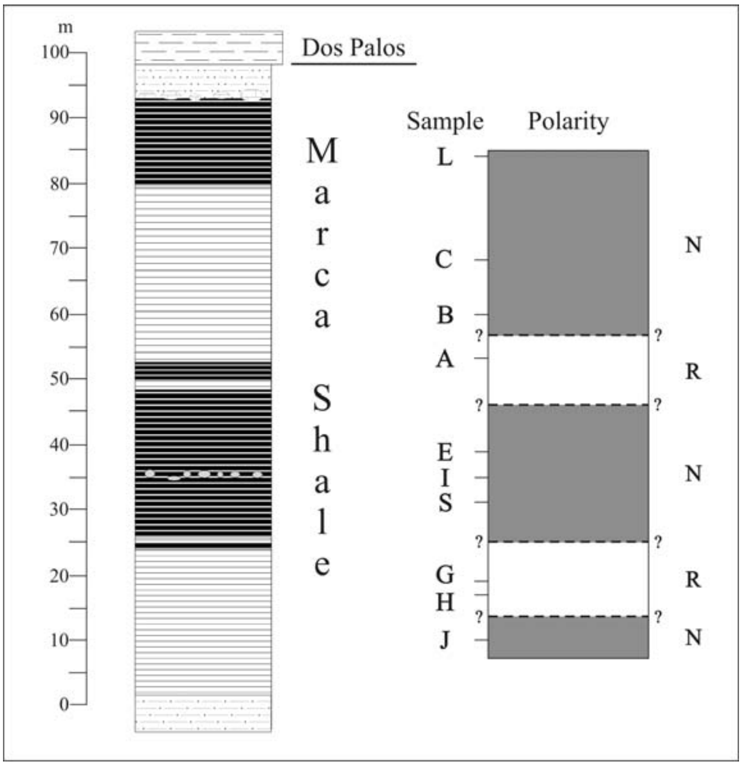

Figure 4.33. Palaeomagnetic reversal stratigraphy for the Marca Shale. N=normal, R= reversed polarity.

4.4 INTERPRETATION AND DISCUSSION

The moderate correlation between mean terrigenous laminae thickness for each sample set and the estimated basinal water depth of Fonseca (2000) (Fig. 4.20) suggests thickness variations between sample sets were largely controlled by relative sea level, with highstands characterised by thinner terrigenous laminae. Inaccuracies in the sea level estimation, perturbations in drainage patterns, terrestrial vegetation cover and precipitation, along with stochastic noise all lessen the robustness of this correlation. It is possible that the increasing dominance could relate to a general increase in detrital input (through increased fluvial runoff for instance). However, when considered in light of the benthic foramifera/diatom data and the correlation of the basinal water depth curve with mean terrigenous laminae, it is more consistent with a fall in relative sea level. The increasing dominance of terrigenous laminae up section (Fig. 4.19) therefore lends support to earlier conclusions of the shoaling of the basin towards the K/T boundary.

4.4.1 *Clay mineralogy and inferences on the cause of the alternating dark/pale coloured units*

Clay minerals are predominantly formed by weathering and as such the nature of clay mineral assemblages is acutely related to climate, drainage patterns and the nature of the source rock. During transportation from their source to marine depocentres, clay minerals may undergo differential deposition. These effects are generally negligible in shallow marine settings however (e.g. Fürsich *et al.*, 2005), such as those characterising the Maastrichtian San Joaquin basin. Evidence for this come from the relative abundance of Smectite, which generally increases more distal from shore because of its high buoyancy (Chamley, 1989; Chamley, 1997). In the Marca Shale, Smectite concentrations fall during greatest basinal water depth (Fig. 4.18). Clay mineral assemblages may also be affected by burial diagenesis (Dunoyer de Segonzac, 1970), although this is unlikely to have influenced assemblages in the Marca Shale as the preservation of fine scale structures and primary opal-A of diatom valves implies burial to only shallow depths. Thus it can be inferred that the preserved clay mineral assemblages are those sourced from the hinterland and may be used for palaeoenvironmental and palaeoclimatological reconstruction.

Smectite is generally a byproduct of intense chemical weathering under warm/hot conditions with strong alternation between wet and arid seasons, but can also reflect volcanic activity (Chamley, 1989). The pervasive alternation of diatomaceous and terrigenous laminae supports a pronounced seasonal climate and the discrete occurrence of terrigenous material relates to strongly seasonal rainfall. The dominance of Smectite may also relate to the weathering of volcanic ash supplied by the Sierra Nevada volcanic arc to the east of the basin. Kaolinite typically forms from intense hydrolytic chemical weathering in perennially warm, tropical, humid conditions (Chamley, 1989). The S/K ratio can therefore be used as a climate proxy that reflects seasonal conditions and may be used as an indicator for the strength of rainfall seasonality (e.g. Adatte *et al.*, 2002). High S/K values are indicative of a climate with alternating arid/wet seasons, whilst lower values indicate warmer, humid and generally wetter conditions, with weaker rainfall seasonality. Chlorite forms in cold, dry or frozen environments and is destroyed by intense chemical weathering (Chamley, 1989). The complete absence of Chlorite from all samples is therefore consistent with the inference of a warm, tropical climate. Illite commonly forms from strong physical weathering in arid and often cool regimes and may therefore be used as a proxy for cooler and/or drier conditions.

The marked decline in the S/K ratio towards the onset of the darker coloured intervals suggests rainfall seasonality was less pronounced during deposition of the dark coloured intervals relative to the paler intervals, which possess the highest S/K values. The simultaneous increase in the K/I ratio towards the dark-coloured units can be interpreted as either an indication of decreasing temperatures or of increasing humidity towards the onset of the occurrence of the dark coloured units. However, changes in the strength of rainfall seasonality, inferred from the clay mineralogy data can be correlated with changes in the laminated fabric. In the darker coloured intervals diatomaceous laminae occur sporadically and terrigenous detritus dominates the fabric (e.g. Fig. 4.5), emphasized in potassium-gamma ray data (Fonseca, 1997). Reduced diatomaceous flux during these times likely results from a reduction in primary productivity in response to reduced seasonality. Basinal water depth appears to have been important in controlling mean terrigenous laminae thickness and it is feasible that increased water depths may have facilitated in greater dissolution of diatom valves, accounting for the apparent reduction in primary productivity in the darker intervals. However this scenario does not account for the dark interval towards the top of the succession when water depth was the lowest for the whole studied sequence (Fonseca, 1997; Fonseca, 2000). Darker coloured intervals are therefore interpreted as representing periods when seasonality was reduced in response to a generally warmer, wetter climate. The high S/K ration in the stratigraphically highest sample may relate to changes in the drainage patterns or source rocks due to the shoaling of the basin. These data validate earlier assumptions by Fonseca (1997), who, through spectral analysis of gamma-ray and total organic carbon data, inferred Milankovitch cyclicity to have forced alterations between wetter (dark coloured) and drier (pale coloured) climatic periods along the Californian margin.

4.4.2 *Origin of pelletal structures*

4.4.2.1 *Resting spore and chrysophyte-rich aggregates*

Both the resting spores and chrysophytes in resting spore and chrysophyte-rich aggregates are below 20µm in diameter, suggesting they would have survived grazing and sedimentation within fecal pellets intact (Honjo & Roman, 1978). However, the inference that they are fecal pellets is inconsistent with their irregular shape and the inclusion of occasional large (100µm) diatom vegetative cells. Some modern diatom species are able to secrete dissolved polymers that interact with cations in seawater to form transparent exopolymer particles (TEP) (Alldredge *et al.*, 1993) that enhance cell aggregation and allow cells to be rapidly exported, effectively bypassing grazing (Bull & Kemp, 1995; Grimm *et al.*, 1997). Due to the non-selective method of export, foreign material may become incorporated within the TEP, providing an explanation for the random vegetative cells and co-occurrence of the chrysophytes and resting spores. The resting spore and chrysophyte-rich aggregates, along with the near monospecific laminae of intact resting spores are thus interpreted to be TEP enhanced flux.

4.4.2.2 *Clay/silt-rich aggregates*

The association of clay/silt-rich aggregates with disruption to the laminated fabric is crucial to understanding their origin. Pike *et al.* (2001) have shown that in the Santa Barbara Basin abundant meiofaunal assemblages are found in severely dysoxic sediments. Using a network of tunnels, ranging in diameter between 18-200μm, meiofauna are able to periodically migrate into aerated zones (Warwick, 1973). In so doing the sediment is redistributed without causing significant disruption of the laminated fabric. Clay-rich aggregates, similar in size and shape to those seen in the Marca Shale have been identified in laminated sediments from the Peru shelf associated with fabric disruption and attributed to the burrowing activity of meiofauna during elevated oxygenation of bottom waters (Brodie & Kemp, 1995) (see Table 4.4). Periodic oxygenation of the basin is supported by the presence of common agglutinated foraminiferal remains and thus the clay/silt-rich aggregates are interpreted as infilled meiofaunal burrows. It is likely that this meiofaunal community is responsible for the pervasive but slight disruption to the laminated fabric characterised by a bioturbation index of 2-4.

4.4.2.3 *Clay/silt-rich pellets*

Although it is feasible that clay/silt-rich pellets could also be infilled meiofaunal burrows, it is difficult to reconcile this with their radically different appearance and shape and account for the occurrence of tightly packed diatom fragments. Clay/silt rich pellets containing diatomaceous fragments have been observed in recent sediments from Saanich Inlet with very similar dimensions to those seen in the Marca Shales (Dean *et al.*, 2001) (see Table 4.5). These were interpreted as pelagic fecal pellets, most probably of zooplankton origin. The high silt/clay content was attributed to feeding in sediment laden waters proximal to a fluvial outwash plume. A similar origin of the clay/silt-rich pellets is inferred here.

4.4.2.4 *Diatom-rich pellets*

The size range of diatom-rich pellets also closely matches those of fecal pellets observed in modern sediments (Honjo & Roman, 1978; Lampitt, 1990; Dean *et al.*, 2001) (Table 4.5). The degree of fragmentation of diatom frustules is consistent with herbivorous grazing (Sancetta, 1989b; Brodie & Kemp, 1995; Dean *et al.*, 2001) and the concentration of single diatom species (e.g. pellets composed entirely of *H. polymorphus* horns) suggests grazing occurred on individual blooms. Diatom-rich pellets are therefore considered to be pelagic fecal pellets, probably of zooplankton origin.

Aggregate	**Composition**	**Length (µm)**	**Height (µm)**	**Reference**
Burrow	Clay	Av 360	Av 95	Brodie & Kemp (1995)
TEP flocculent	Intact diatoms	Few cells-laminae	Few cells-laminae	Dean *et al*. (2001)
Ar	Resting spores	210-2000	50-252	This study
Ac	Chrysophytes	275-560	53-111	This study
Ac/s	Clay/silt	108-743	55-185	This study

Table 4.4. Selection of described aggregates similar to those found in the Marca Shale (Av = mean). Ar = resting spore aggregate, Ac = chrysophyte-rich aggregate and Ac/s = clay/silt-rich aggregate.

Pellet	**Composition**	**Length (µm)**	**Height (µm)**	**Reference**
Copepod		200-600	40-70	Honjo & Roman (1978)
Anchovy		Up to 2000	Up to 1000	Staresinic *et al*. (1980)
Pteropod		Up to 6000	200	Bruland & Silver (1981)
Polychaete worm		120-500	50-200	Cuomo & Rhoads (1987)
Polychaete worm		400-800	100-300	Minoura & Osaka (1991)
Polychaete worm	Diatom fragments	Av 610	Av 251	Brodie & Kemp (1995)
Zooplankton fecal pellet	Clay	Up to 404	28-89	Dean *et al*. (2001)
Zooplankton fecal pellet	Silt	Up to 514	26-93	Dean *et al*. (2001)
Fish fecal pellet	Diatoms/fragments	Up to 3900	400-1400	Dean *et al*. (2001)
Ps	Sponge spicules	192-326	67-83	This study
Pf	Diatom fragments	199-242	50-63	This study
Pc/s	Clay/Silt	187-430	61-128	This study

Table 4.5. Selection of described pellets similar to those found in the Marca Shale (Av = mean). Ps = sponge spicule-rich pellet, Pf = diatom-rich pellet and Pc/s = clay/silt-rich pellet.

4.4.2.5 *Sponge spicule-rich pellets*

Sponge spicule-rich pellets are similar in dimensions to both diatom and clay/silt-rich pellets, suggesting they may also be fecal pellets. However, grazing of sponges primarily occurs by benthic organisms such as starfish and nudibranchs at present and it is unlikely that such organisms would have been present in the dysoxic/anoxic conditions within the basin. The intact, well orientated nature of the individual spicules together with the dimensions of the pellets suggests that they are the remains of individual sponges (Dr O.S. Tendal, personal communication 2005). It is likely that they represent individuals transported off the shelf (most likely during storms) accounting for their occurrence in terrigenous laminae.

4.4.3 *What is the cause of the high degree of fragmentation in the diatom valves?*

The reduced level of fragmentation in the early diagenetic nodules implies that a proportion of the fragmentation is a diagenetic artefact, yet the nodules do contain a significant proportion of diatom hash, in contrast with modern upwelling fuelled diatomaceous deposits (Bull & Kemp, 1995; Pike & Kemp, 1996b; Burke, 2002). It is possible that the diatom hash relates to the temporal instability of opal-A, although XRD analysis, the many intact valves and excellent preservation of delicate girdle bands, fine-scale structures and chrysophyte cysts implies this is not a factor. Current reworking of the valves prior to burial is also unlikely as there are no substantiating sedimentary structures and is inconsistent with the preservation of a finely laminated sediment fabric. The preservation of small, fragile *Sceptroneis* spp. and fine siliceous girdle bands and vela is inconsistent with dissolution as the cause for the fragmentation of heavily silicified, robust diatoms. It can therefore be inferred that the diatom hash relates to either pelagic or benthic grazing. The disruption to the laminated fabric, highlighted by the bioturbation index, implies that benthic grazing may have occurred periodically, possibly causing local fragmentation. The diatom and clay/silt-rich pellets demonstrate that fragmented diatomaceous material was part of the export flux and hence blooms were subjected to pelagic grazing. The scarcity of pelagic fecal pellets probably relates to the fact that many would have disintegrated prior to burial (Turner, 2002). Numerous studies have identified isolated fecal pellets composed of fragmented diatomaceous material (Table 4.6). Chang *et al.* (1998) identified rare individual laminae and sublaminae of fragmented material in the Miocene Monterey Formation, which they attributed to the intensification of grazing, whilst Holocene diatomaceous laminae from Saanich Inlet, exhibits a level of fragmentation attributed to grazing, equal to that seen in the Marca Shale (Dean *et al.*, 2001).

Since grazing, the temporal instability of Opal-A and current reworking have been ruled out, the extra fragmentation of larger frustules documented in the main outcrop must relate to dissolution and/or mechanical fragmentation. Mechanical fragmentation of diatom valves has been reported in sediments buried to a depth of 300-400m, usually associated with mild dissolution (Hein *et al.*, 1978). Mild dissolution is evident in some valves, consistent with this mechanism. In the main outcrop, large diatom valves (in particular *Stellarima* spp.) are observed with both valves compressed and are occasionally fractured into many interlocking pieces (like a jigsaw), suggesting fragmentation occurred in-situ (Fig. 4.9b), whilst in the nodules valves show a clear separation with the girdle band in-situ (Fig. 4.9a). The high degree of fragmentation in the main outcrop samples is therefore primarily attributed to mechanical fragmentation of the larger valves, associated with mild dissolution.

Location and age of sediment	**Depositional Setting**	**Frequency**	**Diatom Taxa Involved**	**Lamina Thickness (µm)**	**Reference**
Gulf of California, Holocene	Restricted, silled, marginal basin	Intermittent	Mixed summer assemblage	Up to 1000	Pike & Kemp (1996b)
Saanich Inlet, Holocene	Silled fjord	Ubiquitous on laminae scale	*Chaetoceros* dominated	150-5000	Dean *et al.* (2001)
Effingham Inlet, Holocene	Silled fjord	Common	Mixed assemblage	Up to 1000	Chang *et al.* (2003)
Santa Barbara Basin, Pleistocene	Silled marginal basin	Absent, apart from in pellets and in some large species	Mixed assemblage	–	Bull & Kemp (1995)
Peru Shelf, L. Quaternary	Open continental shelf	Absent, apart from in pellets	Mixed assemblage	–	Brodie & Kemp (1994; 1995)
Monterey Formation, California, Miocene	Open continental shelf or marginal basin	Sporadic	Diverse assemblage	1000-7000	Chang *et al.* (1998)

Table 4.6. Selected list of the occurrence and degree of fragmentation of diatom valves from studies of laminated marine sediments.

4.4.4 *Inferences on the style of diatom productivity*

Diatom valves were previously inferred to have been deposited by simple settling following upwelling induced blooms (Fonseca, 1997). However, modern relatives of the three dominant diatom genera (*Stephanopyxis, Hemiaulus* and *Stellarima*) are not representative of coastal upwelling fuelled blooms. In the modern oceans, *Stephanopyxis* is known to be able to grow in ~2% light levels (Goldman, 1993) with production maintained through the sustained exploitation of nutrient periodically injected by the effects of passing storms. Doming of isopycnals under the influence of mesoscale eddies is also regarded as an important mechanism for stimulating blooms of *Stephanopyxis* (Goldman & McGillicuddy, 2003). Sediment trap data from the Santa Barbara

Basin show *S. palmeriana* is sedimented during the winter, and BSEI of Gulf of California sediments show the greatest flux of *S. palmeriana* is in the autumn (Pike & Kemp, 1997; Kemp *et al.*, 2000). These observations led Kemp *et al.* (2000) to regard *Stephanopyxis* as one of the key taxa involved in their "fall dump" mode of export flux, which involves several large (>50 μm), robust taxa, built for longevity rather than a bloom and bust mode of life that are able to generate substantial production at depth. Sedimentation occurs *en masse* during the autumn/early winter when the thermocline is broken down (Kemp *et al.*, 2000). Due to the extended length of production and the larger size and durability of the taxa involved, the "fall dump" can be more substantial than that of the spring bloom even though rates of primary production are lower (Kemp *et al.*, 2000; Smetacek, 2000). Although ecological information on warm-temperate species of *Stellarima* is limited, the reports that exist suggest *Stellarima* may be a "fall dump" species.

Modern species of *Hemiaulus* are common in stratified, oligotrophic conditions (Vaillancourt *et al.*, 2003). Cells are known to harbour intracellular N_2-fixing cyanobacteria (Villareal, 1991) and as such are capable of inhabiting large areas characterised by low ambient nutrients, often dominating blooms in the central gyres (Carpenter & Romans, 1992). Blooms may also be stimulated by eddy pumping (Brzezinski *et al.*, 1998) or river plumes (Carpenter *et al.*, 1999). Although initially interpreted as a "fall dump" species, studies in the North Pacific Gyre, sub-tropical Atlantic and Mediterranean have shown that blooms of *Hemiaulus* occur and in the summer (Brzezinski *et al.*, 1998; Scharek *et al.*, 1999a; Scharek *et al.*, 1999b; Polat & Isik, 2002). Cells of *Hemiaulus* have been observed to grow in, and be exported from, the upper mixed-layer during the summer (Scharek *et al.*, 1999a), or may be sedimented response to the break down of stratification (Kemp *et al.*, 2000).

Biosiliceous sediments deposited beneath modern upwelling cells are dominated by *Chaetoceros* resting spores with rare frustules of lightly silicified spring bloom forms (e.g. S*keletonema*, *Chaetoceros*) (Bull & Kemp, 1995; Pike & Kemp, 1996b; Thunell, 1998a; Koning *et al.*, 2001). The near monospecific laminae of *Chaetoceros*-type spores, deposited in TEP mediated flocs, are consistent with upwelling induced export flux. Rare chains of small *Skeletonemopsis morenoensis* valves, morphologically similar to modern bloom forming *Skeletonema* spp., may also represent upwelling fuelled export flux. However, the infrequent occurrence and complete absence of *Chaetoceros*-type spores from some samples contrasts sharply with the majority of upwelling fuelled biosiliceous sediments. A comparable trend in *Chaetoceros* spores is seen in Holocene laminated sediments from Saanich Inlet, British Columbia. Here, a semi-continuous supply of nutrients trigger multiple blooms, resulting in as may as 19 annual laminations (Dean *et al.*, 2001) and as such, the need to sporulate is uncommon. Marca Shale sediments generally exhibit only one diatomaceous depositional event in each diatomaceous/ terrigenous lamina couplet, incompatible with a semi-continuous nutrient supply scenario. The lightly silicified floral assemblage of Saanich Inlet also contrasts with the large, heavily silicified, diatoms of the Marca Shale.

The lack of lightly silicified forms may be a taphonomic artefact (see Chapter 3.6.1), as the preserved floral assemblage has undoubtedly been biased towards robust forms to some degree (Ryves *et al.*, 2001). However, it has been observed that even where the floral composition of the sediments has been modified, *Chaetoceros* spores (being robust and heavily silicified) are well-preserved and can be used as a proxy for upwelling (Abrantes & Moita, 1999). Diatom laminae from the Santa Barbara Basin are dominated by *Chaetoceros* spp., although many laminae are composed of only the vegetative setae (Bull *et al.*, 2000). These setae are rather fine structures, only ~1-2 μm in diameter (Rines & Hargraves, 1988) and it may be that in the Marca Shale such setae were not preserved. Micropalaeontological analysis therefore suggests that the bulk of the preserved export productivity resulted from the prolonged exploitation of nutrients trapped in a stratified water column and was sedimented during the summer/autumn in a “fall dump”. Upwelling-fuelled bloom export flux is a subsidiary component of the preserved flora, although this may be a taphonomic artefact.

A well stratified water column can be corroborated with the high global Maastrichtian SST’s and low meridional temperature gradient, inferred from $\delta^{18}O$ and TEX_{86} analysis (Wilson & Opdyke, 1996; Pearson *et al.*, 2001; Jenkyns *et al.*, 2004). The appearance of many photosynthetic planktonic foraminifera in several warm and cool water sites during the late Maastrichtian is also indicative of oligotrophic conditions associated with increased water column stratification (Abramovich *et al.*, 2003). Eastern boundary currents appear to have been broad, weak features during the Maastrichtian (Bush, 1997) and as such the coastal upwelling of nutrient-rich bottom water would have been less pronounced than present. The apparent paucity of upwelling-fuelled spring bloom flora may also relate to a poleward flowing reverse coastal current. Such a current could be stimulated by the onshore geostrophic flow of marine waters from the Atlantic to the Pacific through an open Isthmus of Panama (Weaver, 1990). A comparable current, the Leeuwin Current, exists today along the western coast of Australia, which carries equatorial waters polewards displacing the north flowing eastern boundary current offshore. Consequently, no coastal upwelling occurs along Western Australia resulting in a warm, wet climate. A warm, saline, poleward flowing current (the Davidson current) also exists during October-February (Hickey, 1979) along the present day Californian margin (Lynn & Simpson, 1987; Strub & James, 2000; Strub & James, 2002) when the equatorial flowing current is weakest. Support for the existence of a poleward flowing coastal current exists in faunal distributions along the Late Cretaceous Californian margin, which require a northward flowing warm current (Anderson, 1958; Gordon, 1973). The Cretaceous Ernédira islands off the northern Baja California Pacific coast exhibit evidence of maximum wave shock from the southeast, resulting from northwest flowing currents/trade winds (Johnson, 2002).

4.4.5 *Nature of terrigenous laminae*

Terrigenous laminae in marginal marine basins relate to one of two mechanisms; increased fluvial runoff or aeolian flux. A key feature of the terrigenous laminae in the Marca Shale is that they commonly contain valves of the benthic diatom *P. crenulata* along with valves of *Medlinia* spp. and sponge spicules. The extant form, *P. sulcata*, has been associated with a wide variety of environmental factors, but is commonly found concentrated in the water column during winter (Hobson & McQuoid, 1997), probably as a result of strong physical mixing. Therefore the concentration of *P. crenulata*, *Medlinia* spp. and sponge spicules in terrigenous laminae indicates that they formed during periods when shelf material was being reworked and transported offshore, consistent with storm activity. The presence of *Actinoptychus* is also consistent with offshore transport during storm activity (Sancetta, 1995). It is difficult to reconcile storm activity and offshore transport with aeolian flux and therefore formation of terrigenous laminae is interpreted to relate to fluvial runoff.

4.4.6 *Laminae succession*

High resolution BSEI has revealed that the diatomaceous-terrigenous laminae couplets are a basis for a more complex flux cycle, containing up to four components (Fig. 4.34). Deposition of intermittent but consistent basal concentrations of intact *A. morenoensis* marks the initiation of diatomaceous deposition, which are succeeded by a mixed assemblage dominated by *H. polymorphus*, *Stephanopyxis* spp. and *Stellarima* spp.. Above this, intermittent laminae of *Chaetoceros*-type resting spores, occasionally associated with chrysophyte cysts, signal the cessation of diatomaceous deposition and are overlain by terrigenous laminae enriched in benthic diatoms (*P. crenulata* and *M. deciusii*) and sponge spicules. This four part succession is similar to the seasonal signal preserved within the Holocene laminated sediments from the Gulf of California (Pike & Kemp, 1996b; Kemp *et al.*, 2000) (Fig. 4.35). Here the breakdown of stratification in the late summer to early winter initiates diatomaceous deposition, forming a basal lamina of large centric diatoms such as *Coscinodiscus* spp., *Stephanopyxis* spp. and Rhizosolenids. The increased wind stress initiates mixing and stimulates a bloom of diverse taxa, which form a mixed floral lamina of *Coscinodiscus* spp. and more lightly silicified species in winter. Succeeding this occur monospecific laminae of *Chaetoceros* spp. resting spores, deposited following spring upwelling, which are overlain by terrigenous laminae deposited in the summer, primarily by aeolian flux from the Sonora Desert and reworking of shelf material during intense monsoonal storms (Baumgartner *et al.*, 1991; Pike & Kemp, 1996b; Thunell, 1998b).

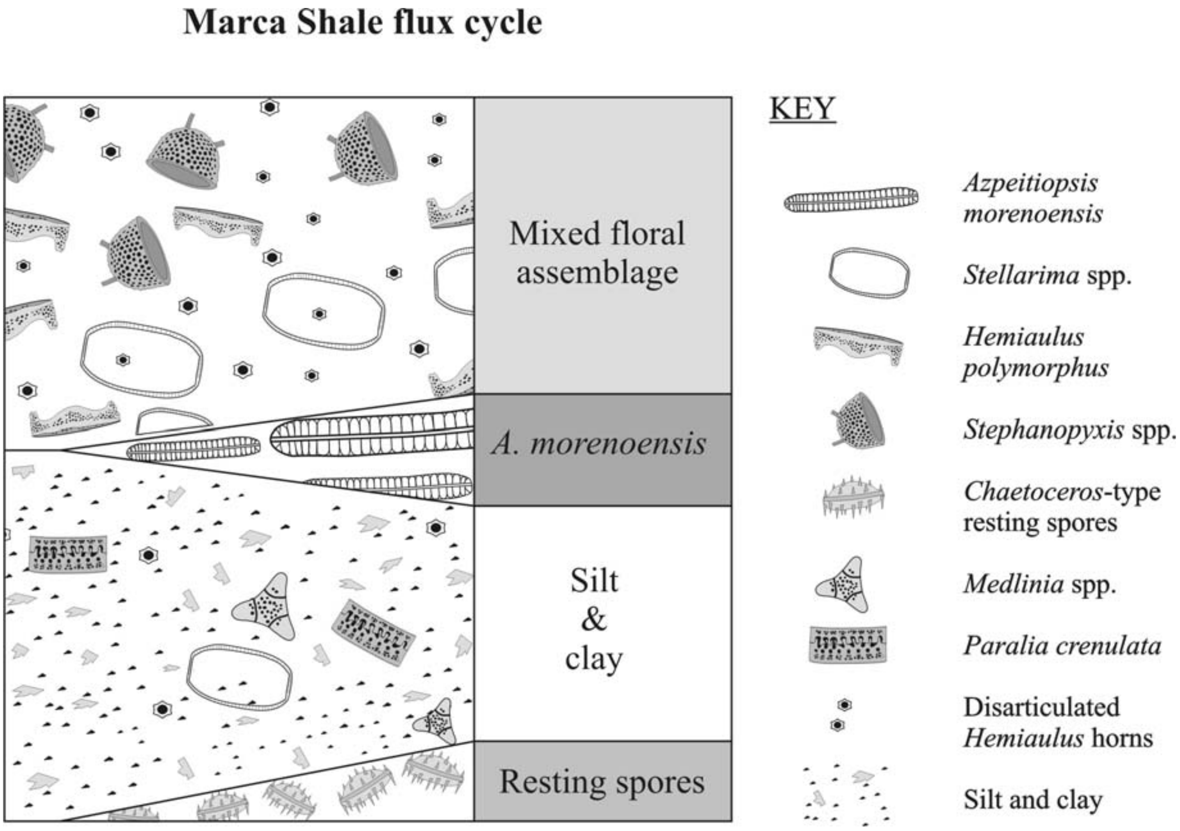

Figure 4.34. Idealised four part flux cycle preserved in the Marca Shale. Intermittent laminae of *Chaetoceros*-type resting spores occur along the base of terrigenous laminae (top the diatomaceous 'varve' segment). Overlying these laminae occur terrigenous laminae, enriched in *P. crenulata*, *Medlinia* spp. and sponge spicules. Terrigenous laminae are succeeded by intermittent concentrations of large *A. morenoensis*, which are overlain by the main mixed assemblage diatomaceous component.

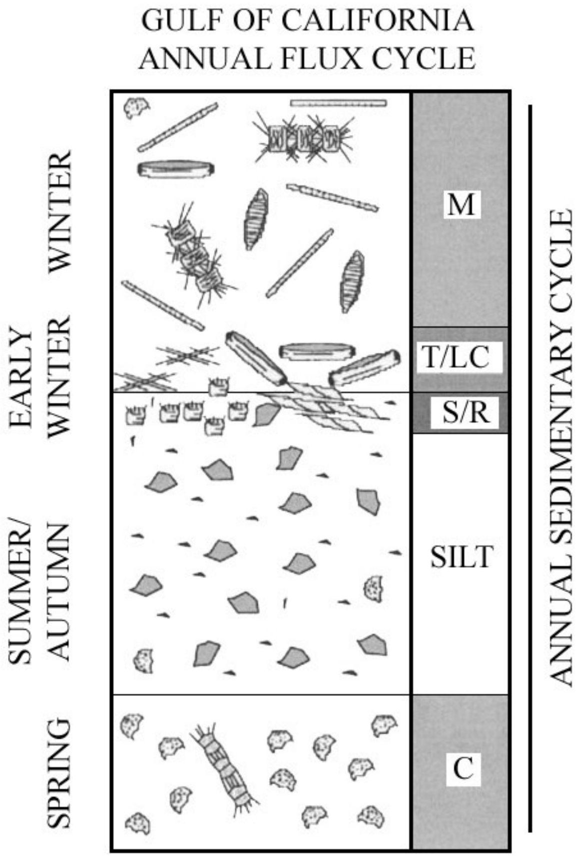

Figure 4.35. Annual flux cycle observed in the Gulf of California, taken from Kemp *et al*. (2000). M=mixed floral assemblage, T =*Thalassiothrix longissima* dominated mats, LC=Large *Coscinodiscus* spp., S=*Stephanopyxis palmeriana*, R=Rhizosolenids and C=*Chaetoceros* spp. vegetative cells and spores.

4.4.7 *Formation of varves and intrannual variability*

Laminae couplets in the Marca Shale have previously been interpreted as varves on the basis of the similarity of the lithology to recent laminated diatomaceous sediments (McGuire, 1988; Fonseca, 1997; Kodama & Ward, 2001). Fonseca (1997) added support to this assumption by performing mass accumulation rates and yielding figures very similar to those of modern coastal varves. The recognition here of a four part flux cycle, similar to that preserved in the Gulf of California, supports the varve interpretation. It is thus feasible to speculate on the seasonal timing of the individual flux events. By analogy with the ecology of modern forms, the mixed floral laminae of *Hemiaulus* spp. and *Stephanopyxis* spp. chains, along with blooms of solitary *Stellarima* spp. are interpreted as late summer/autumn flux. Examination of early diagenetic nodules reveals that many of the valves were deposited intact, although blooms were subject to grazing. Therefore, valves must have been deposited *en masse*, consistent with a “fall dump” type event (Kemp *et al.*, 2000). The near-monospecific laminae of *Chaetoceros*-type spores, interpreted as the self-sedimented aggregations from upwelling-fuelled blooms, are overwhelmingly indicative of spring bloom productivity in modern sediments, although deposition of *Chaetoceros* spp. spores following terminal autumn/winter blooms have been recorded (Pike & Kemp, 1996b; Dean *et al.*, 2001). It is unlikely that a spring bloom or upwelling signal would be completely absent from the sedimentary record and the *Chaetoceros*-type spore laminae are therefore interpreted as a spring upwelling signal. The modern homeophorm of *A. morenoensis*, *Azpeitia* has a peak flux in the summer (Romero *et al.*, 2002). Deposition of the concentrations of *A. morenoensis* during the summer would be consistent with their position below the mixed floral assemblage deposited during the late summer/autumn. The intact nature of the valves implies grazing was bypassed and hence deposition was rapid, likely related to the large size and robustness of the valves.

The season of deposition of terrigenous laminae conveys important climatic information and it is therefore an important aspect to try and resolve. Basins, such as the Santa Barbara basin, which are influenced by a temperate maritime climate, receive the highest terrigenous flux during the winter rainy period. In contrast, the Gulf of California experiences a monsoonal climate, and as such the highest terrigenous flux occurs during the summer through intense convective thunderstorms. Although *P. sulcata* is currently found concentrated in the water column during winter (Hobson & McQuoid, 1997), this is likely related to strong physical mixing and does not help constrain the timing of deposition of terrigenous laminae. However, the interpretations of the season of deposition of the three diatomaceous laminae types confine deposition of the terrigenous laminae to the summer.

This observation is unexpected as peak levels of precipitation at 43°N would conventionally be expected to occur during the winter in response to prevailing surface westerlies. Some of the few climate models for the Maastrichtian suggest that the Californian margin was characterised by wet winters and dry summers (e.g. Barron *et al.*, 1993). One possible explanation is that deposition actually occurred at lower latitudes and the palaeolatitudinal reconstruction of Fonseca (1997) is incorrect. Palynological data suggests the Maastrichtian Californian margin adjacent to the San Joaquin basin had a vegetation cover similar to that of modern day Guatemala and Mexico (Gulbrandsen *et al.*, 1963; Drugg, 1967), which are at present influenced by the ITCZ and characterised by a pronounced monsoonal wet season between May and October. The ~43°N reconstruction of Fonseca (1997) was based on the Late Cretaceous dipoles of Diehl (1991) and Gunderson and Sheriff (1991) from studies in Montana and did not take into consideration the possibility of any strike slip movement. Therefore, if any considerable translation by strike slip faulting occurred during or following emplacement of the terrane, the ~43°N reconstruction would be invalid. Evidence for such strike slip translation is not forthcoming, however. The open communication between the Pacific and Tethys Oceans may have permitted dense, saline, tropical waters from the equatorial current to invade polewards during periods of maximum insolation (Bush & Philander, 1997), which would have been accompanied by intense low pressure systems, promoting the occurrence of intense tropical summer storms. Poleward invasions of tropical waters can be corroborated with evidence of a northwards flowing current along the Californian margin (Anderson, 1958; Gordon, 1973; Johnson, 2002), a reduced meridional temperature gradient (Amiot *et al.*, 2004) and extreme polar warmth (Spicer & Parrish, 1990; Herman & Spicer, 1997; Francis & Poole, 2002; Jenkyns *et al.*, 2004; Poole *et al.*, 2005). Recent analysis of the output of 15 coupled climate models reveals a consistent poleward shift of storm tracks with increased atmospheric ρCO_2, associated with poleward shifts in surface wind stress and precipitation (Yin, 2005). A poleward shift of northern hemispheric tropical precipitation patterns could also account for summer terrigenous deposition.

Maximal fluvial runoff during the summer could therefore indicate that the 43°N palaeolatitude estimate is incorrect. Alternatively, summer terrigenous deposition could have been in response to intense monsoonal storms, resulting from the globally elevated temperatures, shallower meridional temperature gradient and presence of a poleward flowing reverse coastal current along the Late Cretaceous Californian margin and the possible poleward shift of storm tracks. Although such storms are of short duration, they are often associated with very high levels of precipitation and runoff. Valves of *A. morenoensis* often occur within the top of terrigenous laminae, implying that they must have been deposited during the end of the wet season. The analogy of *Azpeitia* with *Azpeitiopsis* is consistent with these observations. *A. nodulifera* is brought into the modern Gulf of California by invading tropical waters which generate the intense summer storms. If *A. morenoensis* was also periodically brought into the basin by invading tropical waters then it would be expected to occur within terrigenous laminae.

4.4.8 *Interannual variability*

Although present, the full seasonal succession is only rarely observed and varves generally possess either a basal concentration of *A. morenoensis* or an upper *Chaetoceros*-type spore lamina. The occurrence of *A. morenoensis* and *Chaetoceros*-type spores is distinctly asynchronous over short time periods, with fluctuations between intervals containing concentrations of *A. morenoensis* and ones with resting spore laminae (Fig. 4.36). Along the modern Californian margin, diatom assemblages exhibit a marked interannual variability in response to ENSO. During El Niño phases, the thermocline and nutricline deepen in response to the eastwards migration of the western Pacific warm pool, causing the upwelling of nutrient-rich waters to be suppressed and diatom assemblages to become enriched in large, oceanic centric diatoms, such as *A. nodulifera* and large *Coscinodiscus* spp.. The situation is reversed during La Niña episodes when the thermocline in the eastern Pacific shallows, the zonal winds strengthen, upwelling of nutrient-rich waters intensifies and resting spores dominate the assemblage (Lange, 1987; Lange *et al.*, 1990; Sancetta, 1995;

Lange *et al.*, 1997; Lange *et al.*, 2000a; Barron *et al.*, 2004). The interannual variability in diatom assemblages in the Marca Shale bears a close resemblance to this ENSO forced variability.

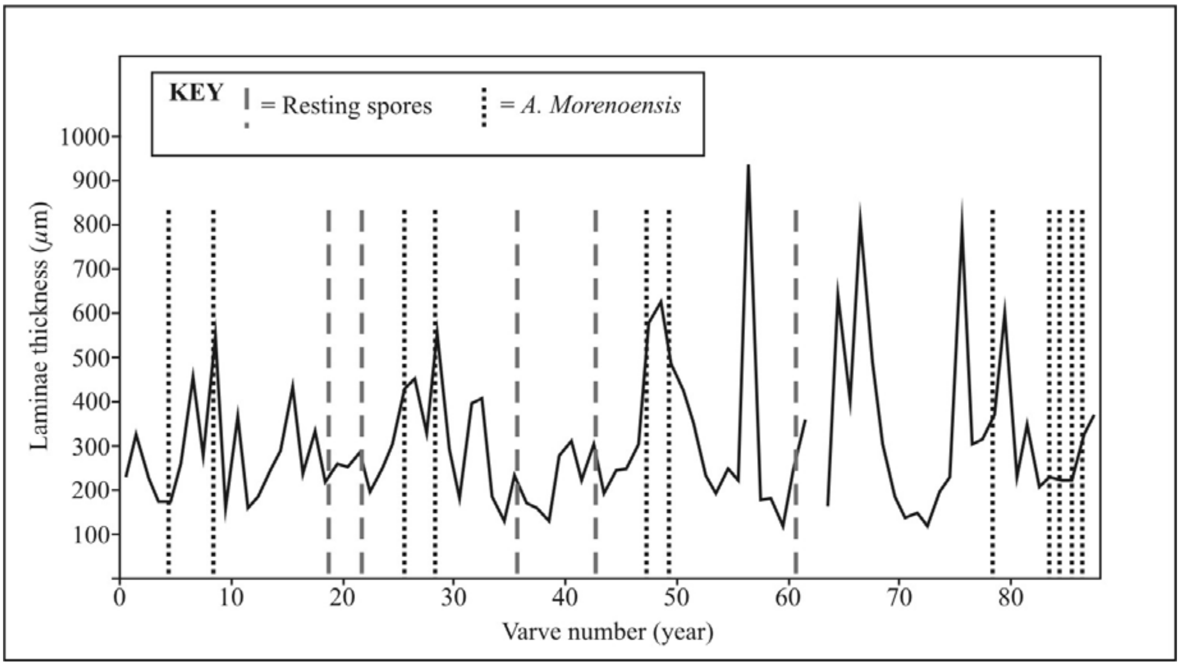

Figure 4.36. Graph showing the short term asynchronous occurrence of *Chaetoceros*-type resting spore laminae and concentrations of *A. morenoensis*, plotted against diatomaceous laminae thickness.

Similar to today, the Pacific Ocean was characterised by an east-west sea surface temperature gradient of ~4ºC (Otto-Bliesner *et al.*, 2002) and as such the main mechanism for ENSO-type dynamics in the ocean-climate system were in place. The asynchronous occurrence of *A. morenoensis* and *Chaetoceros*-type laminae is thus interpreted to relate to an ENSO-like oscillation. Concentrations of *A. morenoensis* are interpreted to have been deposited during El Niño-type events, when the Californian margin was invaded by warm, oceanic waters from the west Pacific warm pool (Fig. 4.37). Consistent with this interpretation is the coarser silt/ fine sand observed in terrigenous laminae below concentrations of *A. morenoensis*, which demonstrates that fluvial runoff/ storm reworking were more energetic at these times. In contrast C*haetoceros*-type resting spore laminae are interpreted to have been deposited during La Niña-type conditions, when the eastern Pacific boundary currents were strengthened and coastal upwelling of nutrient-rich waters was intensified (Fig. 4.37). This may have been accompanied by a weakening of a poleward flowing reverse current (analogous to the Davidson or Leeuwin Current) allowing the displaced eastern boundary current to encroach into coastal areas. A possible shoaling of the thermocline in the eastern Pacific during these times may have allowed subthermocline, nutrient-rich waters to also be upwelled. Climate variability within the ENSO and quasi-decadal bands has been shown to be a robust feature of the Eocene “hothouse” climate (Ripepe *et al.*, 1991; Mingram, 1998; Garric & Huber, 2003; Huber & Caballero, 2003).

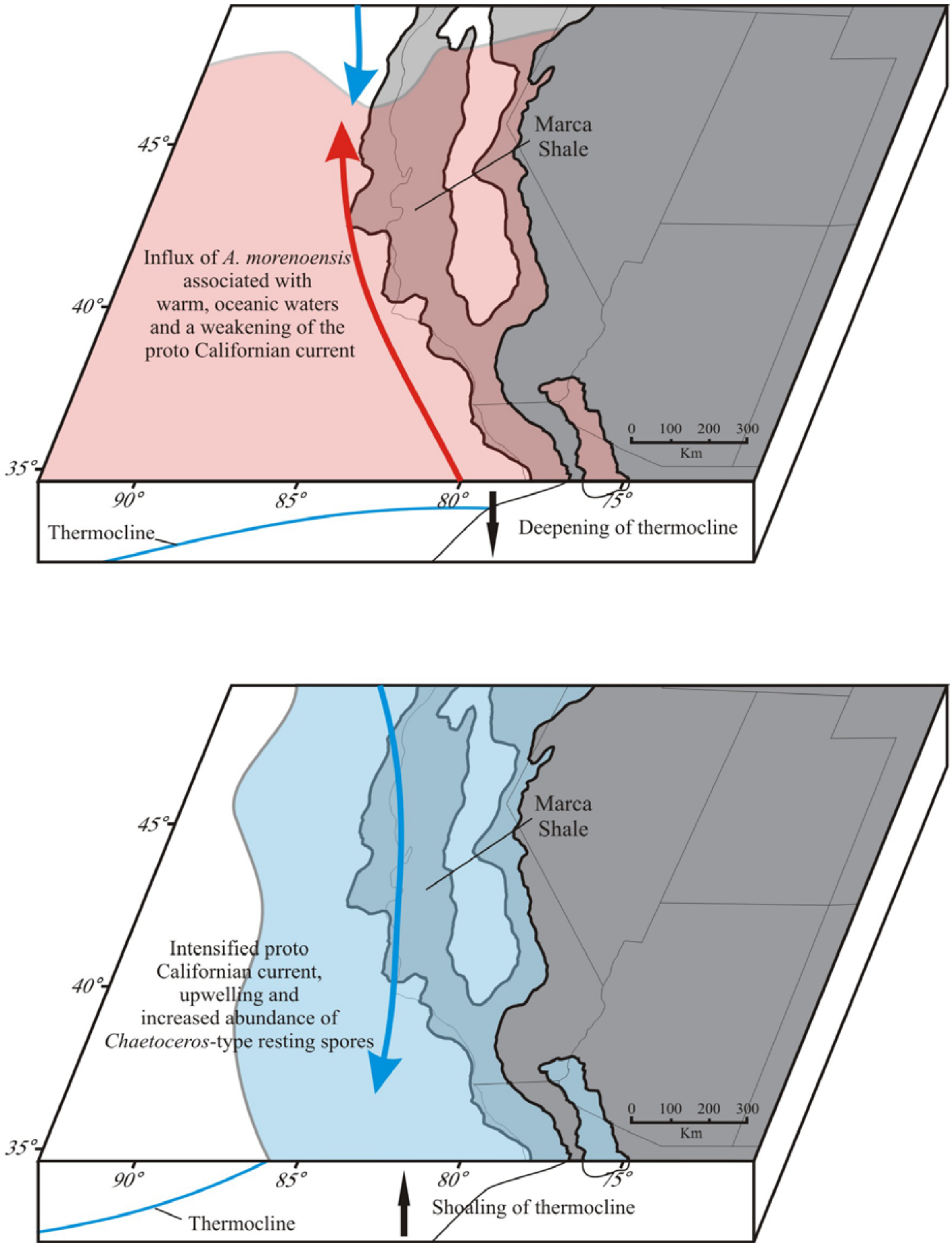

Figure 4.37. Model of the expression of ENSO-type variability along the Maastrichtian Californian margin. During El Niño-type events, warm, tropical water invade the coast, bringing large oceanic diatoms (*A. morenoensis*) and deepening the thermocline. During La Niña-type events the proto California current is intensified, the thermocline shoals allowing subthermocline waters to upwell, resulting in increased abundances and monospecific laminae of *Chaetoceros*-type spores.

Recent work suggests that in a warming climate, El Niño events are liable to be more frequent that La Niña events (Tsonis *et al.*, 2005). Observations lend support to this conclusion. During the period 1976-1998, when the world experienced a marked positive temperature trend, there were several strong El Niño events, but barely any La Niña events. However, the issue of how ENSO manifests itself in a warmer climate system is still open. The relative abundances of *Chaetoceros*-type resting spore laminae and concentrations of *A. morenoensis* in the Marca Shale are consistent with more frequent El Niño events than La Niña events in a warmer climate system. On average 7.2% of lamina (mean value of all the sample blocks) contain concentrations of *A. morenoensis*, whilst only 3.0% contain *Chaetoceros*- type resting spore laminae.

4.4.9 *Interannual variability in the bioturbation index*

Periods of reduced bioturbation, and hence enhanced benthic anoxia, coincide with times of greatest diatomaceous export flux and also with the lowest flux of detrital material. Conversely, more oxic periods, characterised by greater levels of bioturbation correspond with reduced diatomaceous export flux and an increased flux of detrital material. These trends strongly suggest that levels of dissolved oxygen at the sediment water interface were primarily controlled by diatomaceous export flux. Pleistocene varves off California contain alternating zones of varved and bioturbated sediment, spanning several years to millennia, related to ENSO (Anderson *et al.*, 1990). The reduction in upwelling-fuelled productivity and increase in regional precipitation during El Niño events results in higher concentrations of dissolved oxygen at the sediment-water interface, culminating in zones of bioturbation enriched in detrital material (Anderson *et al.*, 1990). La Niña events are characterised by intensified upwelling and a reduction in precipitation, leading to enhanced benthic anoxia, ensuring the preservation of the laminated fabric. Thus, alternations in benthic oxygen levels inferred from the bioturbation index in the Marca Shale are interpreted to have been modulated by ENSO-type variability. Periods of enhanced benthic anoxia reflect La Niña-like conditions, whilst more oxygenated periods reflect El Niño-type conditions. A similar interpretation has been proposed to account for ‘siltier’ more detrital-rich bioturbated intervals in the Miocene Monterey Formation, California (Ozalas *et al.*, 1994)

4.4.10 *Long-term diatom floral changes*

The relative abundance of concentrations of *A. morenoensis* and *Chaetoceros*-type resting spore laminae differs markedly between individual samples sets (Fig. 4.16), reflecting long-term variations in the prevailing climatic/oceanographic conditions. The occurrence of *A. morenoensis* has been interpreted as reflecting El Niño-like conditions analogous to the occurrence of *A.*

nodulifera in the modern Gulf of California. Analysis of diatom assemblages in the Gulf of California over the interval 15.45 ka- 1.33ka, reveals that the relative abundance of *A. nodulifera* changes in a similar fashion to that of *A. morenoensis* in the Marca Shale (Barron *et al.*, 2004). High relative abundances of *A. nodulifera* occur in the Gulf of California during the Bølling–Allerød and from ~6.2 ka to present, when tropical conditions occurred in the Gulf of California and there was robust ENSO variability. Conversely it is virtually absent from samples between 10.6 ka-6.2 ka in response to cooler conditions. A comparative mechanism is inferred to explain the variations in the relative abundance of *A. morenoensis* in the Marca Shale, with high relative abundances characterising warmer, more tropical conditions with robust ENSO variability. There appears to have been a clear oscillation in the occurrence of more tropical conditions in the Marca Shale, reflective of longer term millennial/Milankovitch scale forcing. Without a well constrained chronology however, it is impossible to speculate further on the nature of these cycles.

The relative abundance of *Chaetoceros*-type spores between samples sets in the Marca Shale likely reflects the long term variation in the strength of the proto Californian current/ coastal upwelling relating to more La Niña-like conditions. Unlike the *A. morenoensis* data, the abundance of spores exhibits a clear peak in the middle of the succession when *A. morenoensis* is virtually absent from the record. At this time, incursions of warm oceanic water from the west Pacific warm pool into the San Joaquin Basin were rare, coinciding with a strengthened eastern boundary current and a possible shoaling of the thermocline along with weak ENSO variability. It is known that the Maastrichtian climate was capable of relatively abrupt global temperature fluctuations (Li & Keller, 1999). The inferred strengthening of the eastern boundary current may be explained such a global climate fluctuation intensifying the meridional temperature gradient, causing greater seasonal wind stress and enhanced coastal upwelling.

4.4.11 *Inferences on the age-distribution of the laminated succession*

Having established the Marca Shale to be varved, it is feasible to develop varve-based sedimentation rates. Mean varve thickness of each sample differs markedly and it is therefore not appropriate to use the mean for the whole succession. However, five intervals characterised by samples with similar mean varve thickness are evident (Fig. 4.38) and it is thus possible to use the mean sedimentation rate for each interval to provide an estimate of the period of time over which the Marca Shale was deposited (Table 4.8). Varved-based sedimentation rates suggest the studied 89m laminated succession was deposited over a period of ~210 Ka with a mean sedimentation rate of 42.48 cm/ka, assuming that there are no hiatuses within the succession. It is unlikely that hiatuses are absent from the entire section, especially within the darker coloured intervals, which also contain abundant massive sections where it appears that there was no diatomaceous deposition.

The estimate also fails to take into consideration instantaneous event deposits (e.g. speckled beds and turbidites), causing the total period of deposition to be exaggerated. By extrapolating biostratigraphic zones identified within the Marca Shale and Dos Palos to the magnetic polarity chrons of Gradstein *et al*. (1994), Fonseca (1997) suggested that deposition of the entire (124m) Marca Shale occurred over ~1Ma. Estimates in this study suggest that for the Marca Shale to have been deposited over such an interval would require significant hiatuses to be present or sedimentation rates (most likely in the massive intervals or darker coloured intervals) to have been greatly lower than the varved based estimates. Sedimentation rates are likely to have been relatively high in the upper massive interval due to the shoaling of the basin. The 1Ma period of deposition estimated by Fonseca (1997) therefore is inconsistent with varve based sedimentation rates. Either the Marca Shale was deposited over a shorter period of time than that suggested by Fonseca (1997) or significant hiatuses are present within the laminated succession (possibly within the darker coloured intervals).

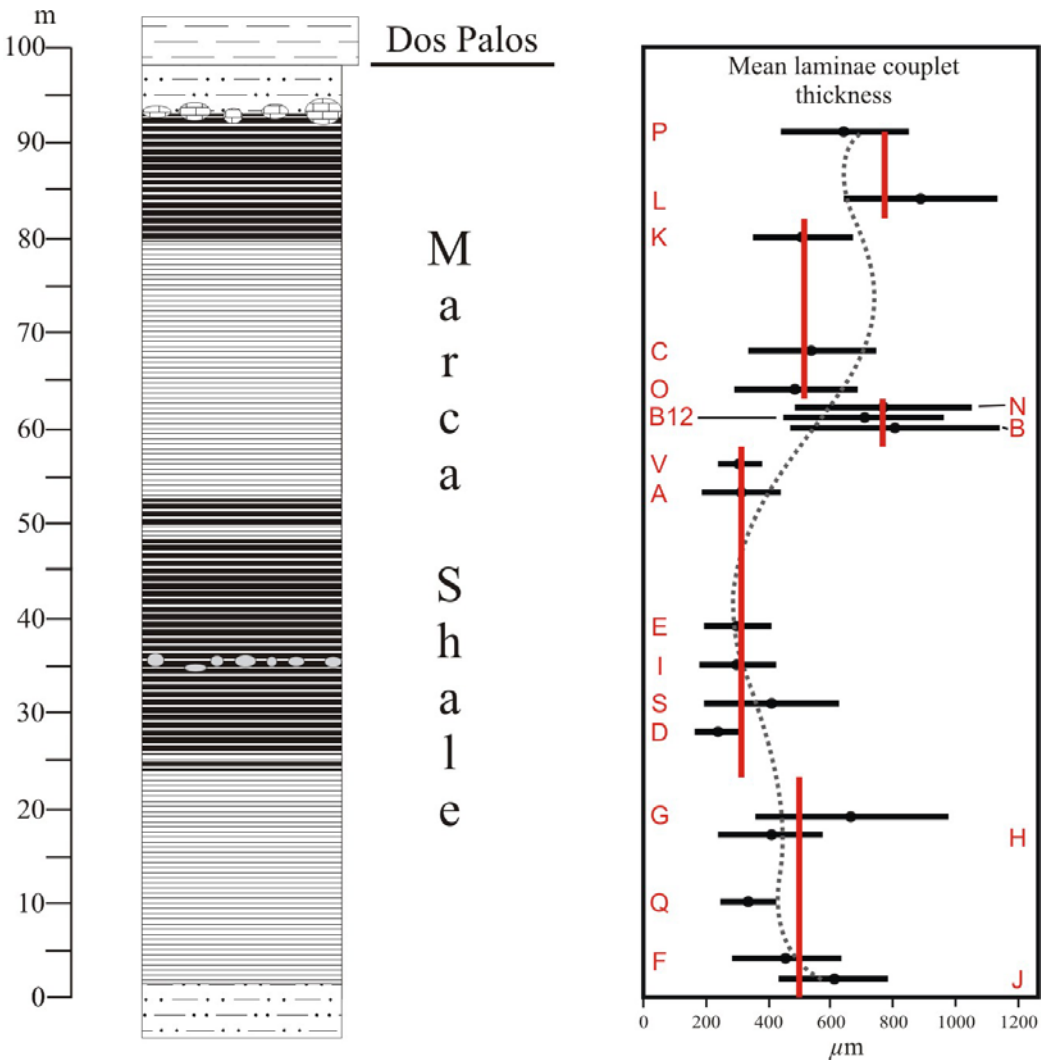

Figure 4.38. Log of the Marca Shale with the five intervals used to calculate the period of deposition of the studied section. The mean varve thickness and the length of each interval are shown by the red lines. The dotted line is a sixth order polynomial plotted for the mean varve thickness of each sample set.

Interval (sample sets)	Length of interval (m)	Mean sedimentation rate (μm/ year)	Period of deposition (years)
1 (J-G)	21.5	494.8	43,452
2 (D-V)	34.5	311.2	110,861
3 (N-B)	5.5	759.7	7,240
4 (O-K)	18.5	510.7	36,225
5 (L-P)	9	766.0	11,749
Total	**89**	**424.8**	**209, 527**

Table 4.7. Varve-based sedimentation rate estimates of the 5 intervals, along with the total period of deposition they represent, used to calculate the mean total sedimentation rate and period of deposition of the whole laminated interval.

4.5 CONCLUSIONS

- Diatomaceous/ terrigenous laminae couplets in the Marca Shale are varves which preserve up to four discrete depositional events each year, similar to the annual flux cycle recorded in Holocene and recent sediments from the Gulf of California.
- Diatom productivity resulted from both the utilisation of nutrients trapped in a stratified water column and from coastal upwelling fuelled blooms. However, export production was dominated by “fall dump” flora (*Stephanopyxis*, *Stellarima* and *Hemiaulus*) with upwelling bloom TEP-enhanced export flux (characterised by *Chaetoceros*-type resting spores) only a subsidiary component.
- Deposition of terrigenous laminae is inferred to relate to enhanced fluvial runoff during the summer, in response to a monsoonal climate system. This finding may suggest that the 43°N palaeolatitude estimate for the Marca Shale is incorrect, and deposition actually occurred in lower latitudes. Alternatively, summer terrigenous deposition could indicate that the Maastrichtian Californian margin was influenced by a monsoonal climate, with intense summer storms, possibly the result of globally elevated temperatures, shallower meridional temperature gradient, the presence of a poleward flowing reverse coastal current or the poleward shift of storm tracks.
- Extensive fragmentation of diatom valves is mainly a result of herbivorous grazing supported by identification of fecal pellets, although analysis of early diagenetic nodules suggests some fragmentation can be attributed to mechanical crushing associated with mild dissolution.
- The asynchronous occurrence of discrete laminae of *Chaetoceros*-like resting spores and concentrations of *A. morenoensis*, along with intrannual variability in diatom productivity (recorded as thickness variations in diatomaceous laminae), suggest an ENSO-like climate cycle was a feature of the Maastrichtian climate system.
- Identification of the remains of agglutinated foraminifera and infilled meiofaunal burrows indicates that the basin was at least periodically oxygenated. Zones where the laminated fabric

is severely disrupted are often concentrated in these meiofaunal burrows. The establishment of a bioturbation index allowed relative changes in benthic oxygen levels to be tracked.

- The bioturbation index records indicate that levels of bottom water anoxia were highly variable and modulated by an ENSO-like phenomenon. Periods of enhanced benthic anoxia were characterised by higher diatom export flux and low detrital flux analogous to modern El Niño conditions along the modern Californian margin. Conversely periods when bottom waters were more oxygenated were characterised by low diatom export flux and enhanced flux of detrital material analogous to La Niña conditions.
- Clay mineralogy suggests that lithological alternations between pale and dark coloured units reflect fluctuations in the strength of the seasonal cycle and in particular of rainfall seasonality. Darker coloured units reflect periods when overall seasonality was reduced and the climate was generally wetter and more humid. In contrast, the paler coloured intervals were deposited in a strongly seasonal climate with a pronounced wet and dry season.
- The moderate correlation between mean terrigenous laminae thickness for each sample set and the basin water depth curve suggests that the variability in mean terrigenous thickness between samples primarily relates to changes in relative sea level.
- Relative thickness changes between the mean terrigenous and diatomaceous laminae thickness for each sample set highlight the increasing dominance of terrigenous laminae up-section at support inferences on the shoaling of the San Joaquin basin towards the K/T boundary.
- Similar to variations in the abundance of *A. nodulifera* in the Pleistocene-recent sediments from the Gulf of California, long term variations in the relative abundance of *A. morenoensis* suggest that incursions of tropical waters along the Californian margin, and hence strength of the ENSO-like cycle, was modulated on longer periods. Determining the exact nature of this modulation is beyond the scope of this investigation but may relate to Milankovitch or millennial-scale cyclicity.
- Long term variations in the abundance of *Chaetoceros*-like resting spores suggest that upwelling fuelled export flux steadily increased to reach a peak near the middle of the Marca Shale unit, before steadily declining. This is likely to have been in response to strengthening of the eastern boundary current in the north Pacific or weakening of a northwards flowing reverse coastal current probably in response to fluctuations in global temperature.

CHAPTER 5

Time-Series Analysis of the Marca Shale: High-Frequency Climate Variability in the Maastrichtian

5.1 INTRODUCTION

Annually laminated marine sediments from, for example, the Santa Barbara Basin, Gulf of California, British Columbia and Peru margin are amongst the highest resolution data sets available for recreating past climate and ocean variability. The application of high-resolution BSEI to these sediments has allowed their full potential as palaeo archives to be realised. In conjunction with time-series analysis, laminated sediments have provided important information on the nature of the high-frequency climate variability, such as the quasi-biennial oscillation (QBO), the El Niño Southern Oscillation (ENSO) and Pacific Decadal Oscillation (PDO) (Pike & Kemp, 1997; Bull *et al.*, 2000; Dean & Kemp, 2004). Time-series analysis of annually laminated sediments from the Arabian Sea and Santa Barbara Basin have also demonstrated possible influence by tidal cycles (Berger & von Rad, 2002; Berger *et al.*, 2004).

The Maastrichtian Marca Shale is characterised by pervasive, sub-millimetre scale detrital and diatomaceous laminae couplets (McGuire, 1988; Fonseca, 1997), remarkably similar in lithology to sediments from the Santa Barbara Basin, Gulf of California and Peruvian margin (Brodie & Kemp, 1994; Bull & Kemp, 1995; Pike & Kemp, 1996b). The contiguous records have average laminae couplet thickness of 408-806 μm, giving lamina-based sedimentation rates of 40.8-80.6 cm/ky (see Table 4.2), which, if compaction is taken into account, closely matches sedimentation rates of recent coastal varves from the Gulf of California (180-260 cm/ky; Thunell et al., 1994), Peruvian margin (100 cm/ky; Kim and Burnett, 1988) and the Arabian Sea (130 cm/ky; Berger and von Rad, 2002). The basic laminae couplet has also been found to contain up to two further diatomaceous laminae that can be related to the sub-seasonal sedimentation of diatom blooms (see Chapter 4.4.6), validating earlier interpretations that the laminations represent annual varves (McGuire, 1988; Fonseca, 1997; Kodama & Ward, 2001).

5.1.1 *Previous high-frequency climate studies of the deep past*

Progress has been made in extracting high-frequency climate data sets from varved sediments from various periods of geological history, including the Proterozoic (Hughes *et al.*, 2003), the Eocene (Ripepe *et al.*, 1991; Mingram, 1998) and the Pliocene (Munoz *et al.*, 2002), although records remain underutilised. Two such studies have independently identified variability within quasi-decadal and ENSO frequencies in middle Eocene records (Ripepe *et al.*, 1991; Mingram, 1998). These findings have been supported by fully coupled climate model simulations, collectively demonstrating that ENSO variability was a robust feature of the ocean/atmosphere system during this "hothouse" climatic period (Garric & Huber, 2003; Huber & Caballero, 2003). These finding contradict theory that indicates such greenhouse climate states would tend to collapse into a permanent El Niño, with reduced, or even devoid of, ENSO variability (Neelin *et al.*, 1998; Fedorov & Philander, 2000).

The modern Californian margin is directly influenced by many ocean/atmospheric oscillations including ENSO, PDO and QBO. As such, the proto Californian margin is an ideal setting to study the nature and dynamics of any high frequency, ocean/climate variability during the Late Cretaceous and in particular for studying the effect of greenhouse conditions along with altered palaeogeography and circulation patterns on ENSO variability. In this study several parameters from the long, continuous annually laminated records, obtained from the Marca Shale are subjected to spectral analysis in order to assess the climate dynamics of a greenhouse climate state. The pervasiveness of any multi-decadal to decadal/ sub-decadal cycles in the Maastrichtian ocean-climate system will be addressed and given the periodicities, speculation on their origin will be made.

5.2 METHODS AND MATERIALS

5.2.1 *Selection of time series for spectral analysis*

In order for time series to be meaningful a number of considerations must be met. Firstly the variable being measured must be an explicit environmental proxy. Secondly, some hypothesis on the origin of the expected spectral peaks is required. Statistically significant spectral peaks may not necessarily relate to a true periodic forcing mechanism and it is necessary to isolate such stochastic noise peaks from real periodic spectral peaks. Thirdly, the record must be of sufficient length to contain variability at the periods of interest. Specific to this study, the variable must also be quantifiable from BSEI analysis. With these factors in mind, time-series analysis was performed on diatomaceous and terrigenous laminae thickness variations and on the bioturbation index records from the seven long contiguous sample sets (sample sets H, G, B, B12, N, O and C). Variations in the thickness of the diatomaceous and terrigenous laminae are taken as proxies for changes in productivity and levels of precipitation (and hence fluvial run off) respectively, whilst the bioturbation index is taken as a proxy for the level of bottom water anoxia. Thickness measurements were acquired using the method of Francus *et al.* (2002) on the 66× BSEI photomosaic basemaps. Three measurements were made for each laminae and the average used. Although the occurrence of *A. morenoensis* and *Chaetoceros*-type resting spore laminae is regarded as palaeoceanographically significant, their infrequent occurrence was not conducive to spectral analysis.

5.2.2 *Data sets*

Two types of data set were analysed. Firstly, due to the fairly regular occurrence of bioturbated intervals, slumps, turbidites or speckled beds, the long records were split into discrete time series devoid of disruptions. However, these data sets were relatively short, with the longest data set containing only 110 varves/years. It was therefore decided to perform spectral analyses on long data sets which included gaps in the varved succession and instantaneous event deposits. Prior to analysis of these data sets, non-erosive event deposits (speckled beds and muddy debris flows) were identified by correlating the photomosaic base maps with the original samples blocks and removed from the varved record. The speckled beds were scrutinised under BSEI for basal intraclasts of laminated sediment, which may have been misidentified as the original laminated fabric. Bioturbated intervals were identified and the number of varves missing calculated using the mean varve thickness for that sample set. The original sample blocks of those containing occasional soft sedimentary slumps were scrutinised to assess the nature of the slump and to try and locate the detachment fault. In some instances the detachment fault could be traced back to the original fault surface (Fig. 5.1) and the whole slumped interval could be simply removed. In most circumstances however this was not possible and the slump was removed from the record by calculating the number of varves missing from the record as for the bioturbated intervals. Slumped intervals were analysed for any repetition of the varved record through faulting and/or folding, which exaggerate the apparent length of the missing time, and any repetition was removed. This procedure allowed data sets consisting of up to 1520 varves/years to be analysed.

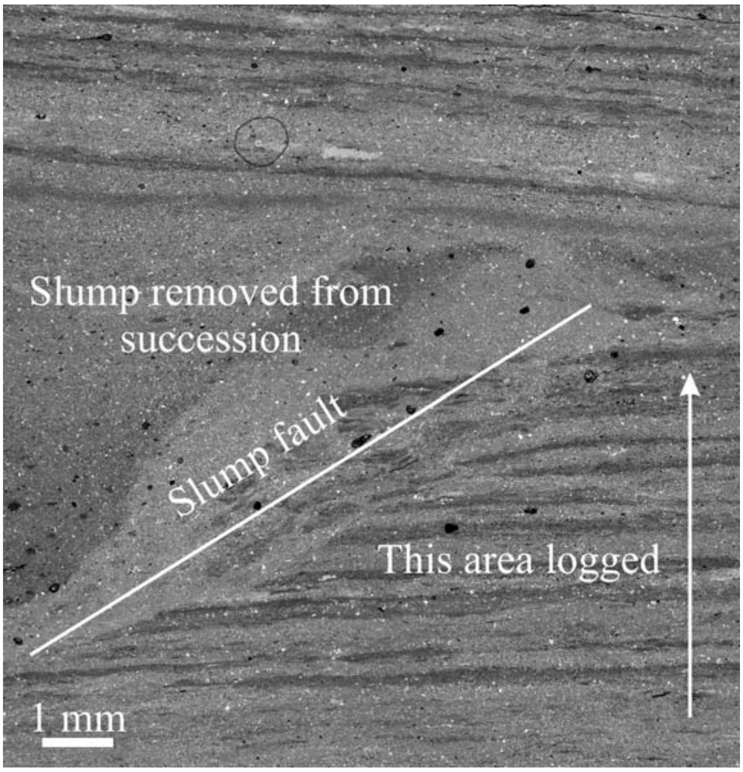

Figure 5.1. BSEI of a slumped interval, where the detachment fault has been located, allowing the slump to be removed from the varved record.

The lack of an underpinning calibrated chronology means that it is feasible that undetected hiatuses exist in the records. Such gaps may cause some periodic cycles to be missed from spectral estimates, introduce noise into the signal causing problems in detecting high frequency cycles and also alter the frequency of any cycles identified (Weedon, 2003). However, the careful inspection of the sedimentary fabrics in the sample blocks in conjunction with high-resolution BSEI analysis of polished thin sections means that this problem has been mitigated as far as possible.

5.2.3 *Time-series analysis*

Prior to spectral analysis, the diatomaceous laminae thickness, terrigenous laminae thickness and bioturbation index data sets were linearly detrended. Analysis was performed by Graham Weedon (University of Wales, Swansea), using the Lomb-Scargle algorithm for irregularly and regularly spaced series to obtain periodogram values. The periodogram was smoothed to acquire spectral estimations with 8 degrees of freedom. Spectral values obtained from the Lomb-Scargle transform may be biased, with spectral amplitudes at the high-frequency end of the spectrum often over estimated (Lomb, 1976; Scargle, 1982). The estimates were consequently corrected using the method of Schulz & Mudelsee (2002). Spectral background noise was modelled as a first-order autoregressive process using the method of Mudelsee (2002) from which the 95% and 99% confidence levels were calculated using the degrees of freedom and assuming a chi-squared distribution of the spectral estimates. By applying the algorithm of Bloomfield (1976) to the bias-corrected sine and cosine terms estimated during generation of the power spectra, coherency and phase spectra were estimated for the diatomaceous and terrigenous laminae thickness data.

5.3 RESULTS

The results of the spectral analyses are summarised in Tables 5.1 and 5.2 and Fig. 5.2. Significant spectral peaks (>95 % confidence level) were recorded in five of the sample sets (H, B, B12, N and O) whilst none were found in sample sets G and C (although only short records were analysed from these sample sets). Bioturbation index records display significant spectral peaks at 10.8, 10.3 and 6.2 years (Fig. 5.3 – 5.4). In the long records, diatomaceous laminae thickness variations show significant spectral peaks at 8.5, 6.7, 5.1, 2.3, 2.2 and 2.1 years, whilst terrigenous laminae spectra have peaks at 44, 5.1, 3.1, 2.5 and 2.3 years (Fig. 5.5-9). In the short uninterrupted data sets, diatomaceous laminae display significant spectral peaks at 26.5, 10.0, 6.1 and 3.8 years and terrigenous laminae at 20.0 and 7.0 years (Fig. 5.10-14). The spectra also exhibit significant peaks that appear to be harmonics of the length of the time series used. For example, in sample set H, the terrigenous lamina spectrum has a significant peak at 40 years, whilst the diatomaceous lamina spectra has peaks at 304 and 80 years (Fig. 5.5), all of which are exact multiples of the length of the time series. All such harmonic peaks have been identified and are omitted from discussions and interpretations.

Only one sample set (set H) was found to contain peaks in the both the terrigenous and diatomaceous laminae with significant coherency (Table 5.1). The spectral peak indicates a periodicity of 2.3 years with significant coherency (> 95%) and a phase relationship of 89.8° (± 25.1°) (diatomaceous laminae leading terrigenous).

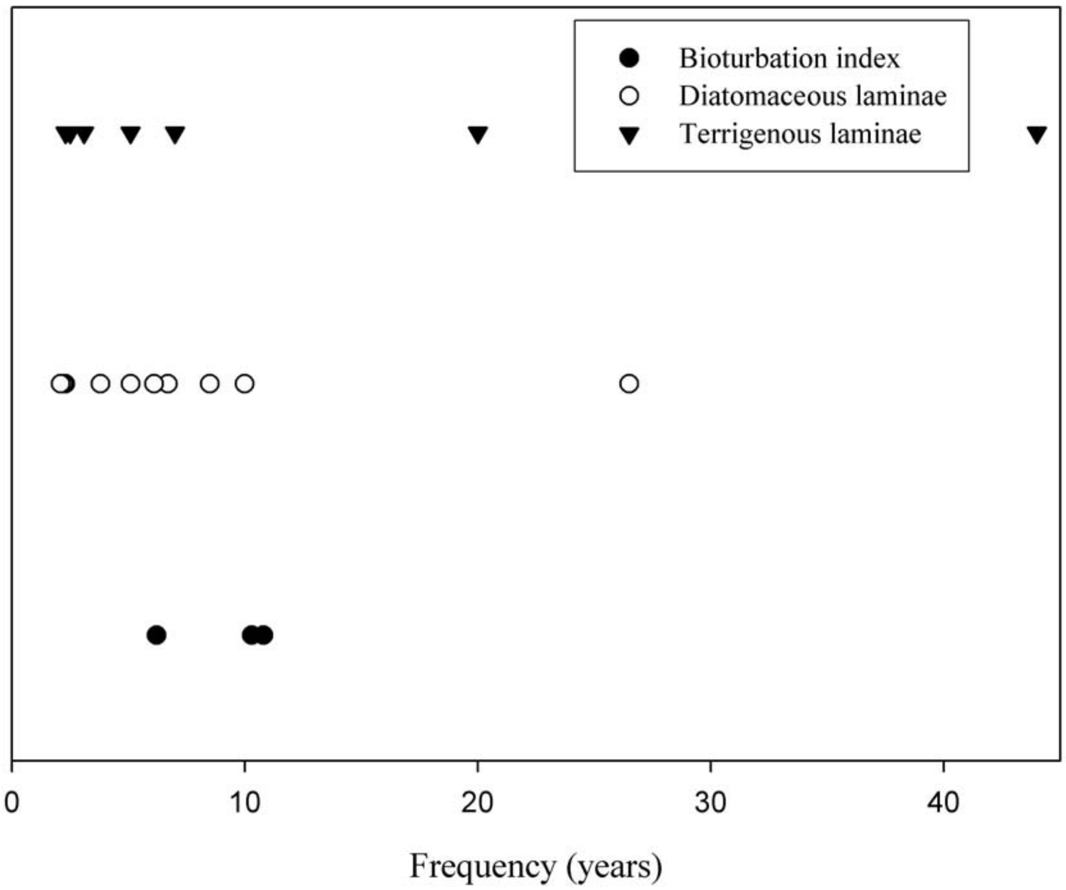

Figure 5.2. Graph showing the significant frequencies identified in spectra from thickness variations in the diatomaceous and terrigenous laminae along with bioturbation index records.

Sample set	Length of series	Confidence level	Parameter analysed	Significant period (yr)	Phase relation (yr)
H	1520	95	TL	**2.3**	-0.56 (±0.16)
		95	DL	8.6 (**8.5**) 8.4	–
		95		**6.7**	–
		95		**2.3**	+0.56 (±0.16)
		95	BI	10.4 (**10.3**) 10.2	–
		95		**6.2**	–
B	544	95	TL	5.2 (**5.1**) 5.0	–
		–	DL	–	–
		–	BI	–	–
B12	400	95	TL	57.5 (**44**) 35.6	–
		95	DL	5.2 (**5.1**) 5.0	–
		–	BI	–	–
N	1170	95	TL	**2.5**	–
		95	DL	**2.2**	–
		–	BI	–	–
O	607	95	TL	**3.1**	–
		95	DL	**2.1**	–
		95	BI	11.2 (**10.8**) 10.5	–

Table 5.1. Summary of the significant spectral peaks for the bandwidth, with the period at maximum power in parenthesis, identified from the long irregularly sampled records. TL=terrigenous laminae, DL=diatomaceous laminae and BI=bioturbation index.

Sample set	**Length of series**	**Confidence level**	**Parameter analysed**	**Significant period (yrs)**	**Phase relation (yrs)**
H	60 (series 9)	95	TL	64.9 (**20.0**) 11.8	–
	49 (series 6)	95		10.0 (**7.0**) 5.4	–
	60 (series 9)	95	DL	15.3 (**10.0**) 7.4	–
	73 (series 7)	95		7.4 (**6.1**) 5.2	–
	110 (series 4)	95		4.1 (**3.8**) 3.5	–
N	–	–	TL	–	–
	106 (n-8)	95	DL	55.6 (**26.5**) 17.4	–

Table 5.2. Summary of the significant spectral peaks for the bandwidth, with the period at maximum power in parenthesis, identified from the short uninterrupted records.

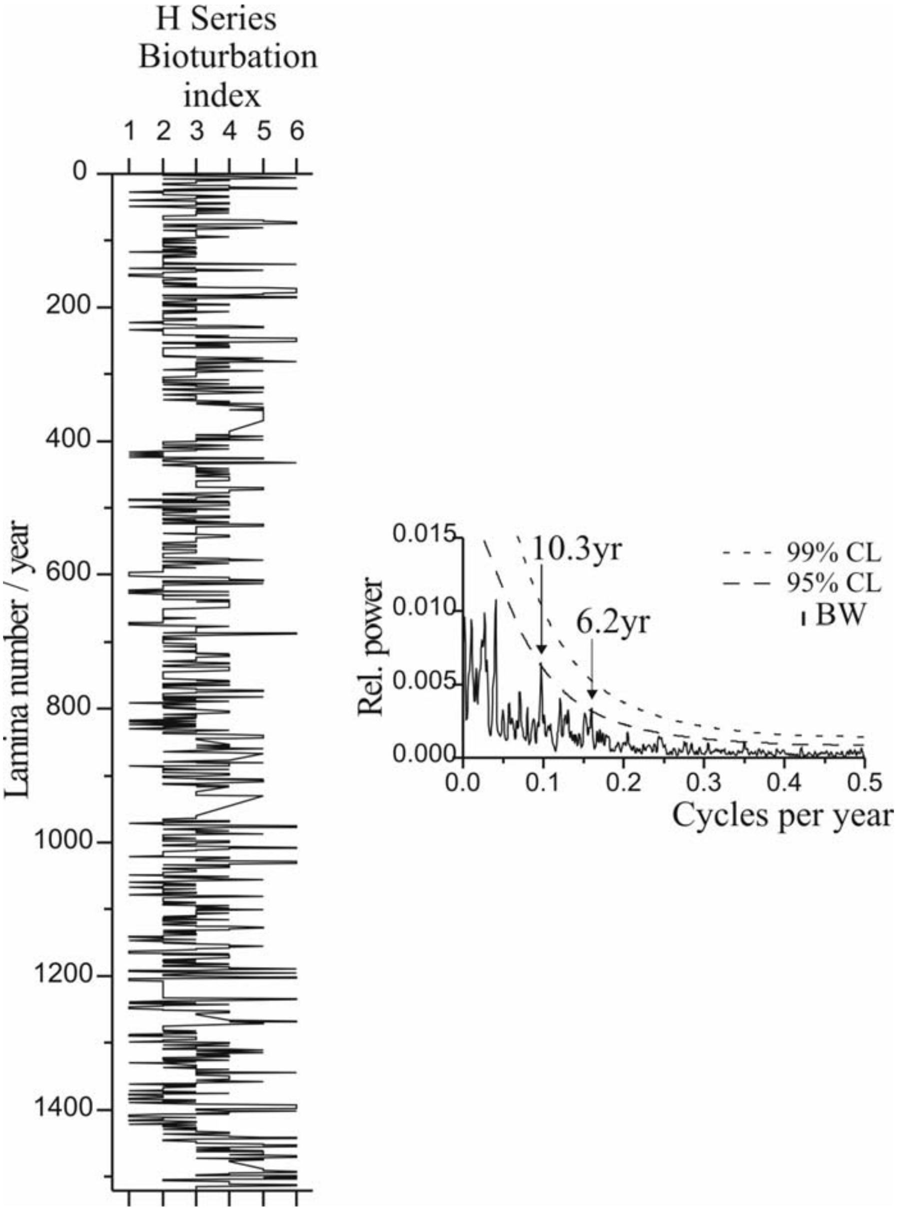

Figure 5.3. Long bioturbation index record and corresponding spectral estimation from sample set 'H'.

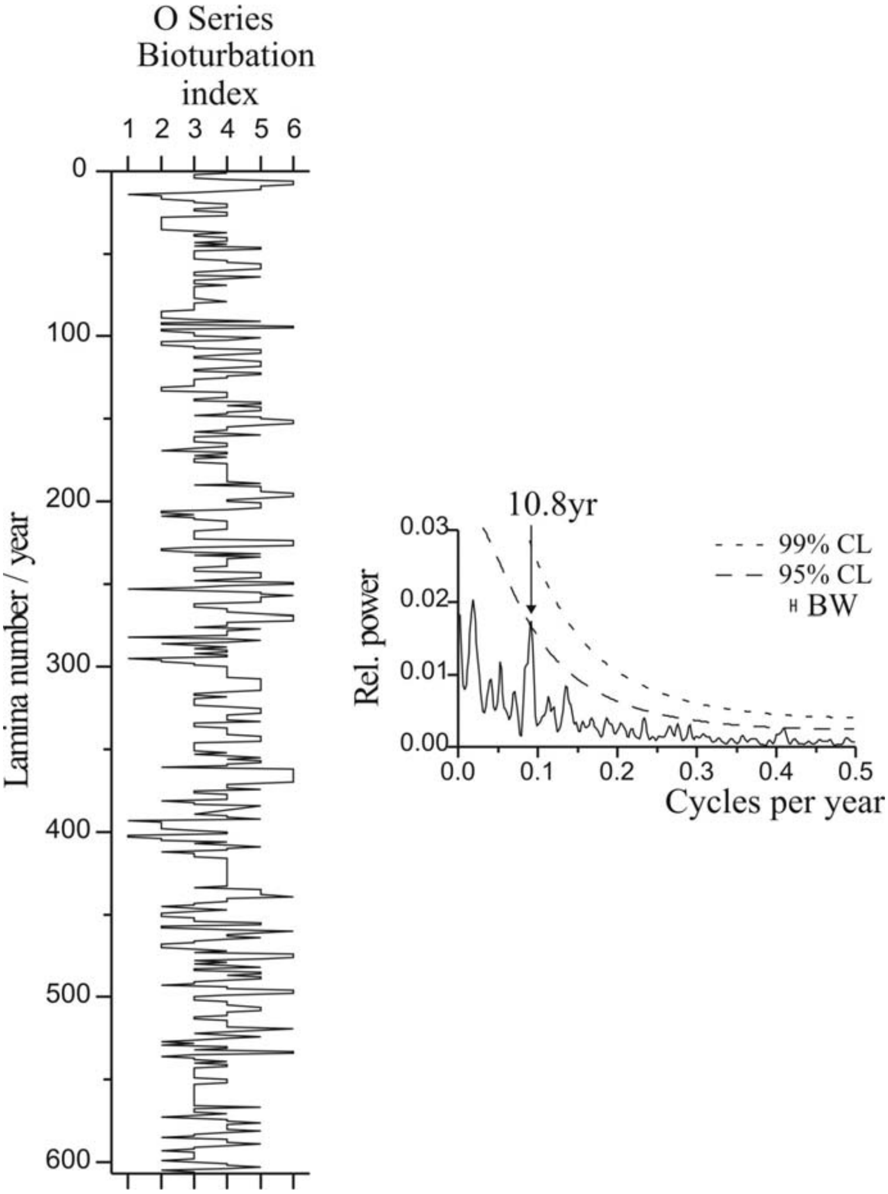

Figure 5.4. Long bioturbation index record and corresponding spectral estimation from sample set 'O'.

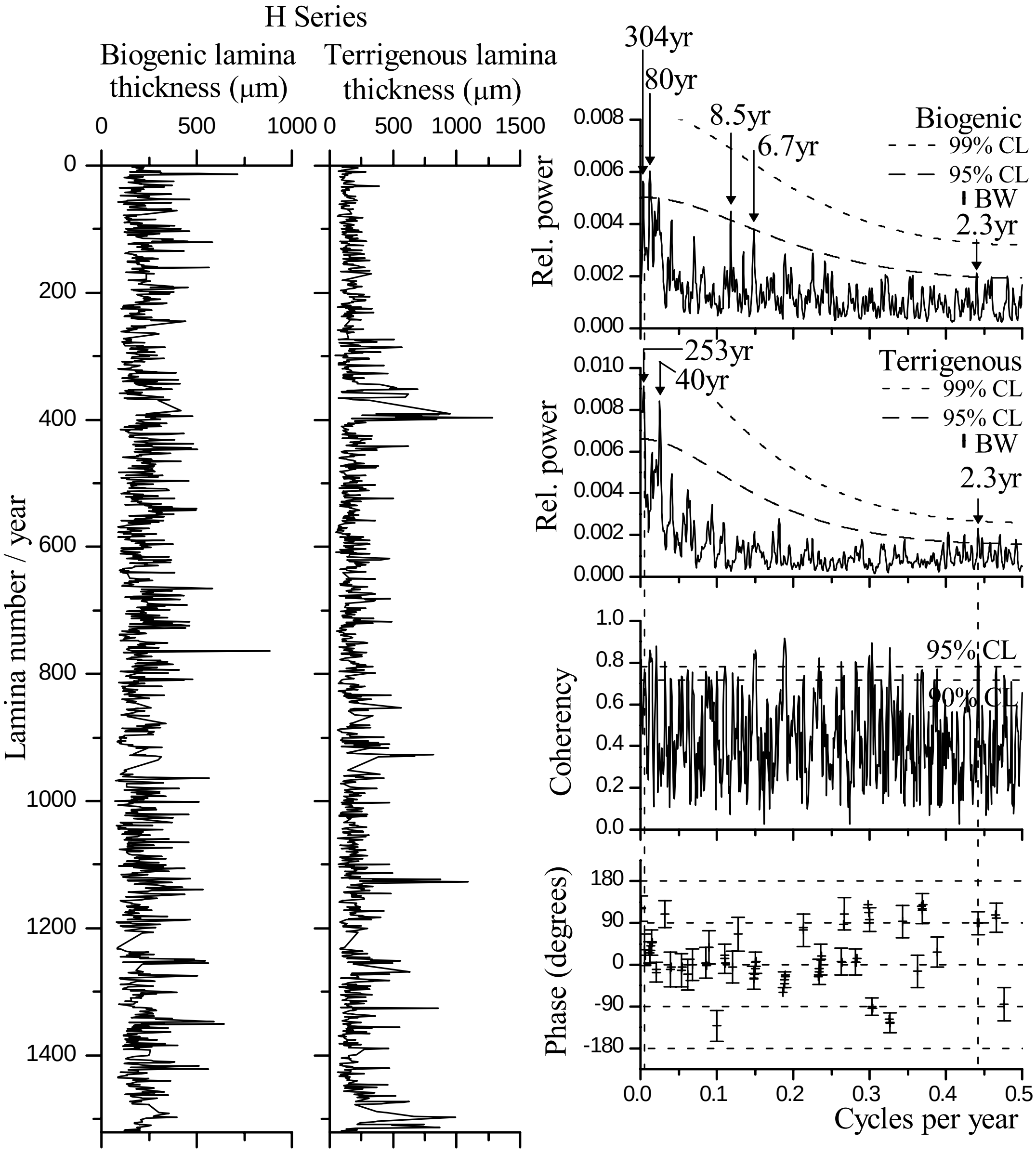

Figure 5.5. Long record of diatomaceous (marked as 'biogenic') and terrigenous laminae thickness variations from sample set 'H', with the corresponding spectral estimates and phase relationships.

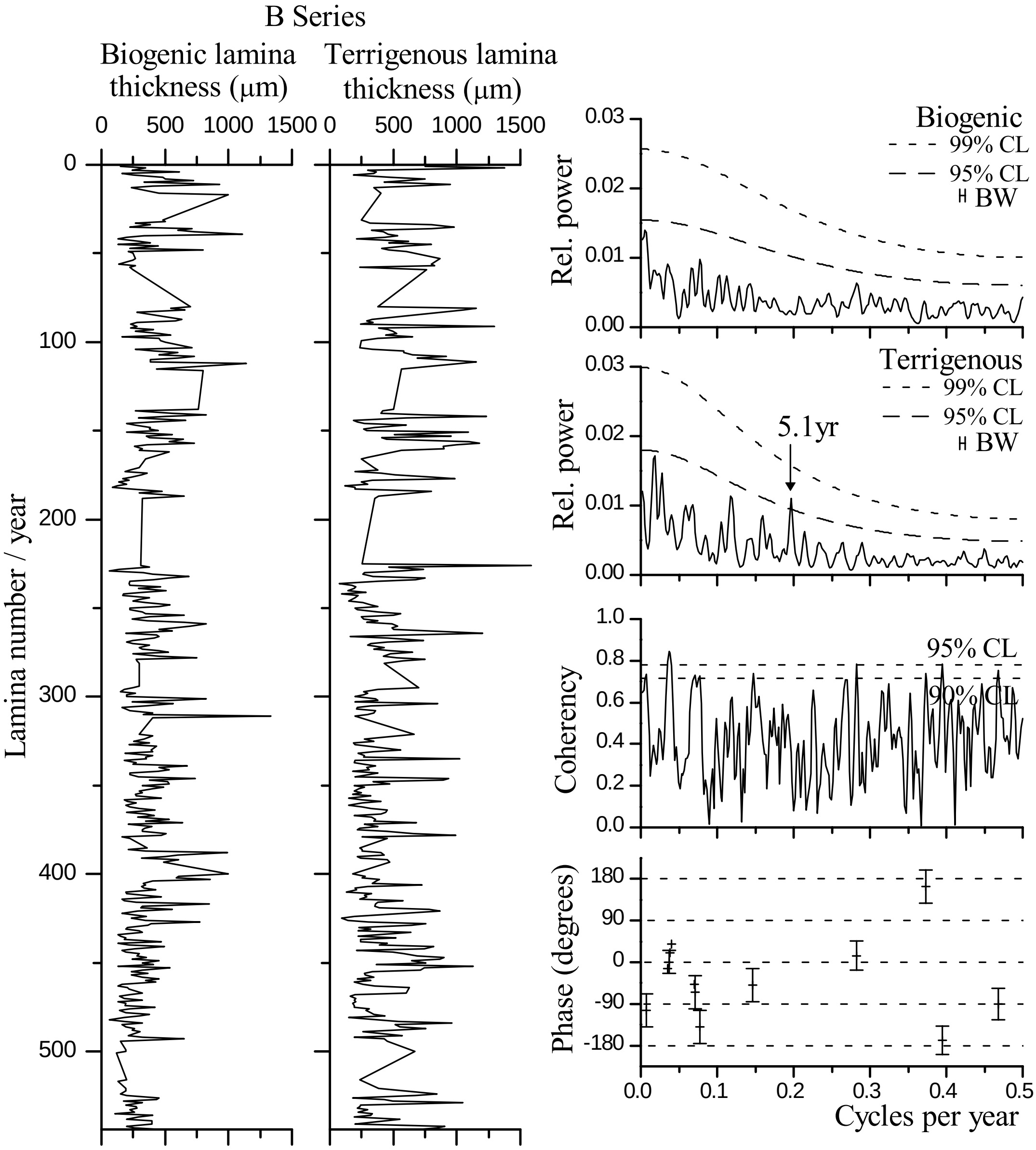

Figure 5.6. Long record of diatomaceous and terrigenous laminae thickness variations from sample set 'B', with the corresponding spectral estimates and phase relationships.

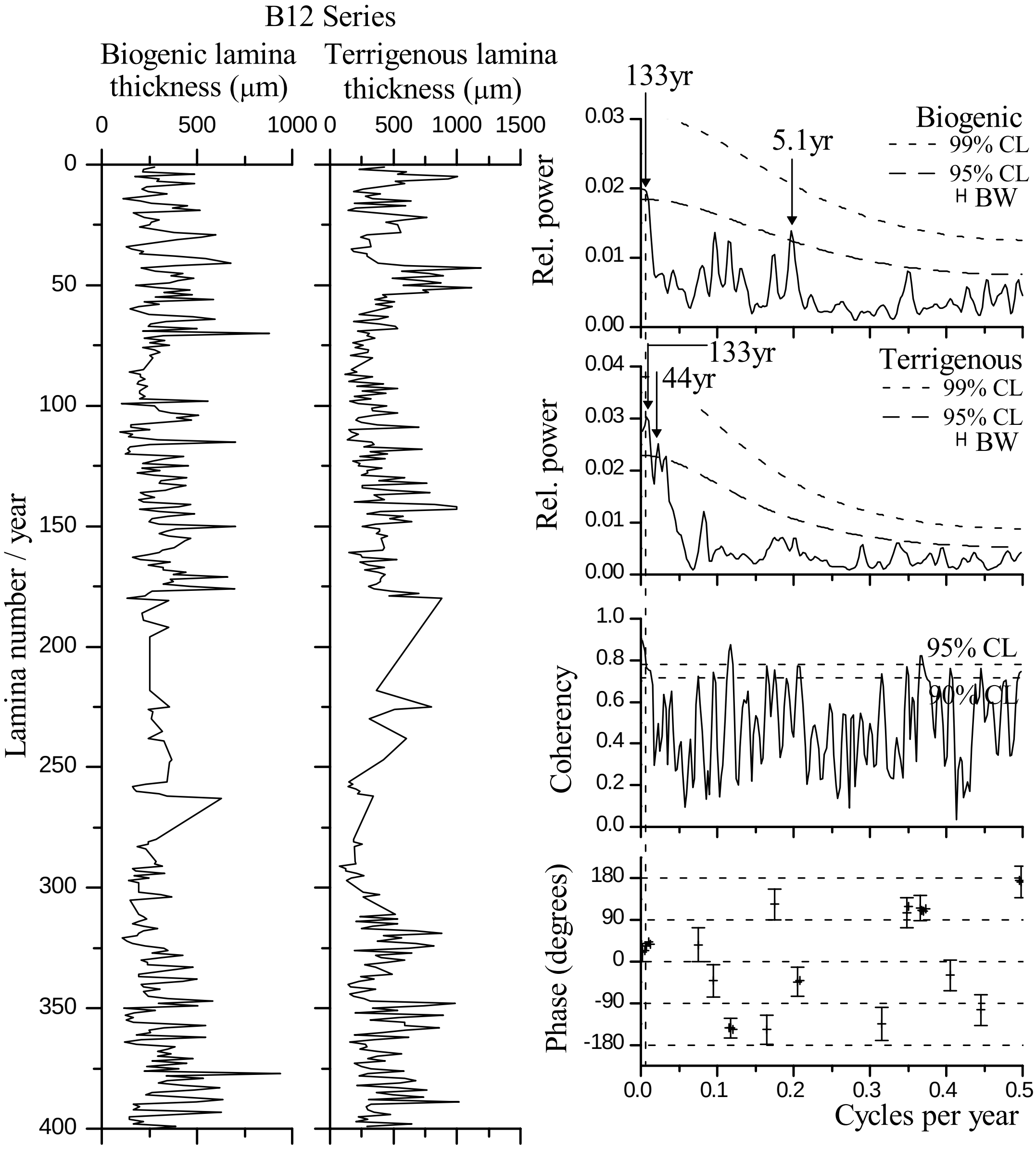

Figure 5.7. Long record of diatomaceous and terrigenous laminae thickness variations from sample set 'B12', with the corresponding spectral estimates and phase relationships.

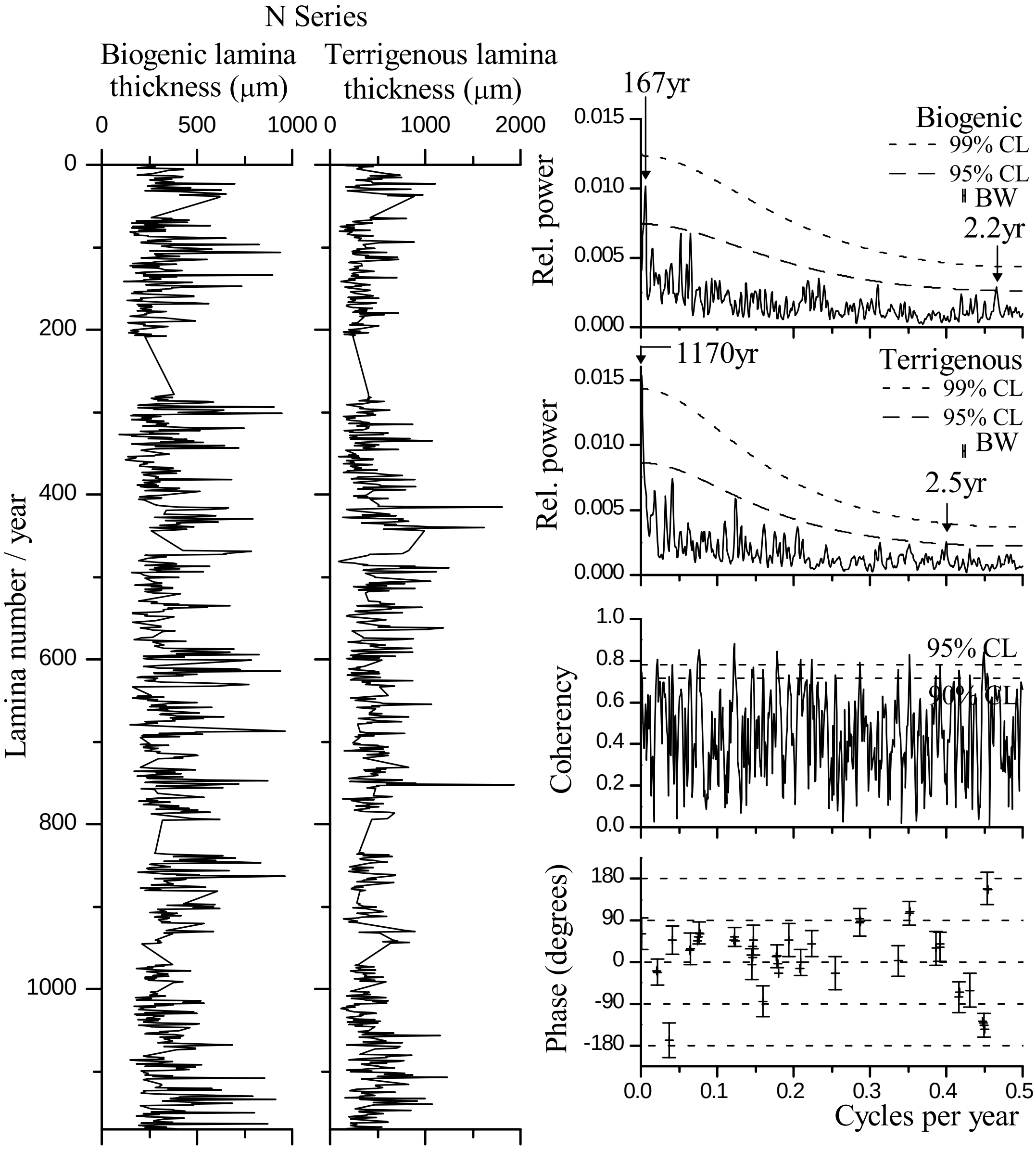

Figure 5.8. Long record of diatomaceous and terrigenous laminae thickness variations from sample set 'N', with the corresponding spectral estimates and phase relationships.

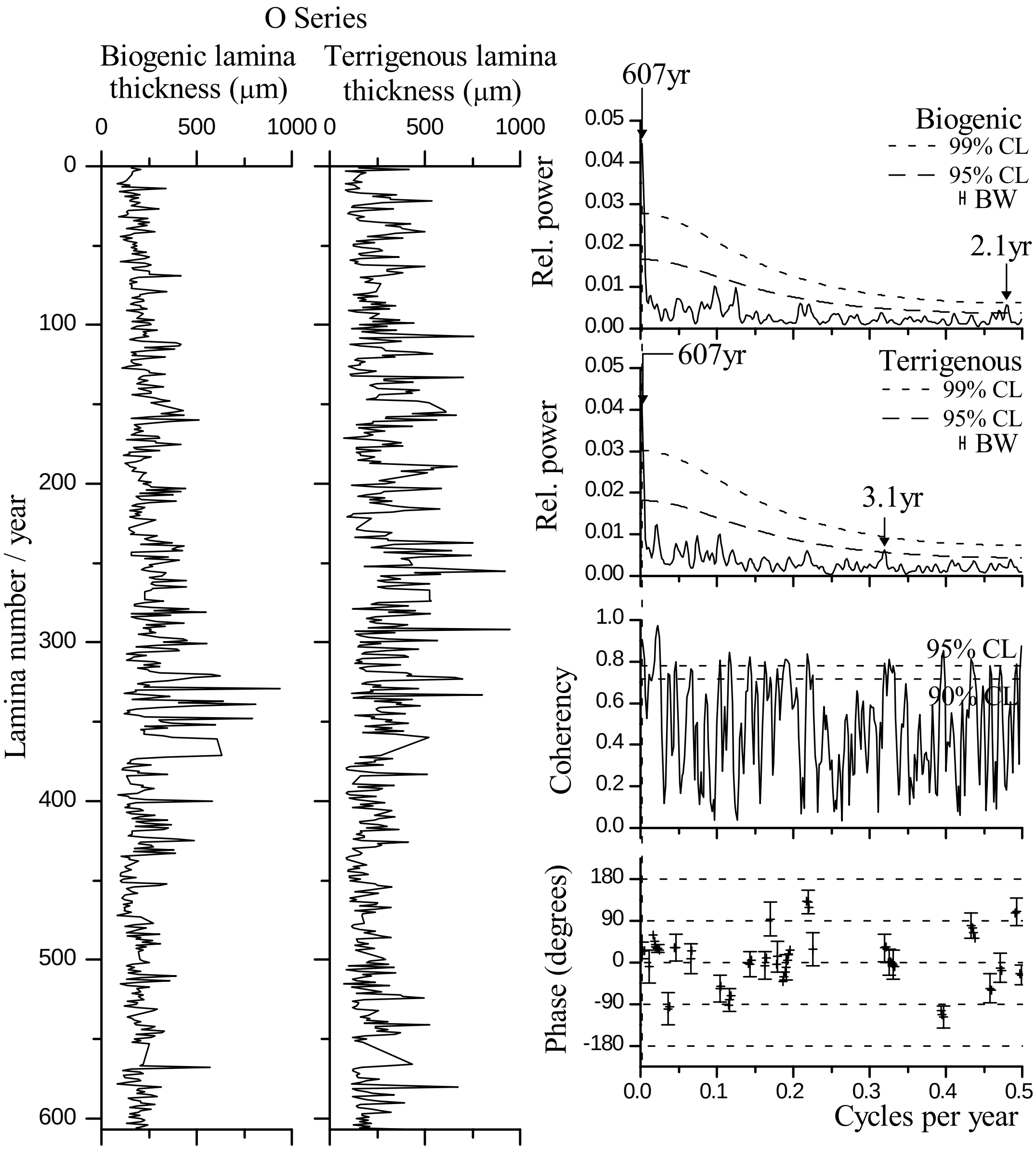

Figure 5.9. Long record of diatomaceous and terrigenous laminae thickness variations from sample set 'O', with the corresponding spectral estimates and phase relationships.

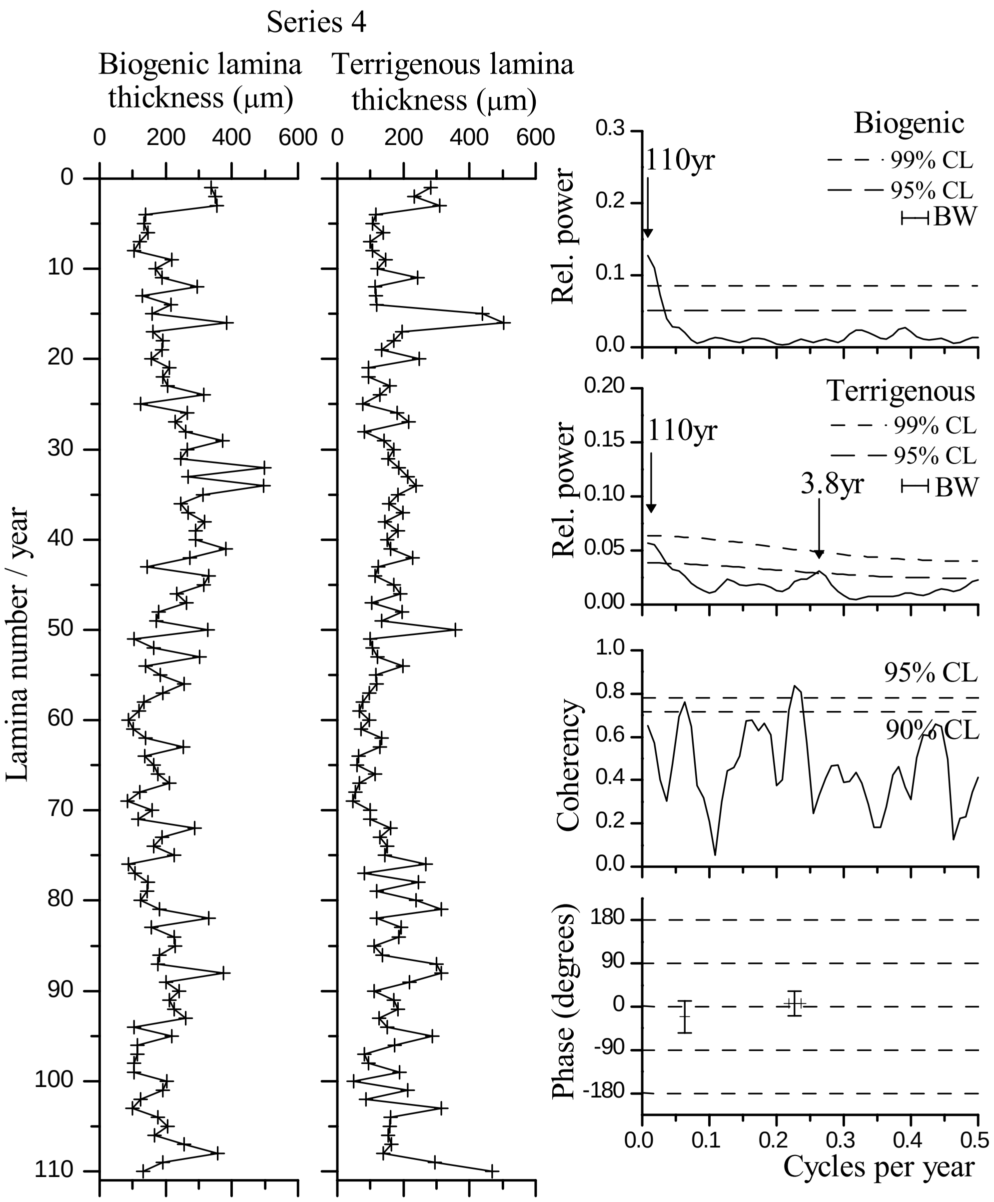

Figure 5.10. Short record of diatomaceous and terrigenous laminae thickness variations from sample set 'H', with the corresponding spectral estimates and phase relationships.

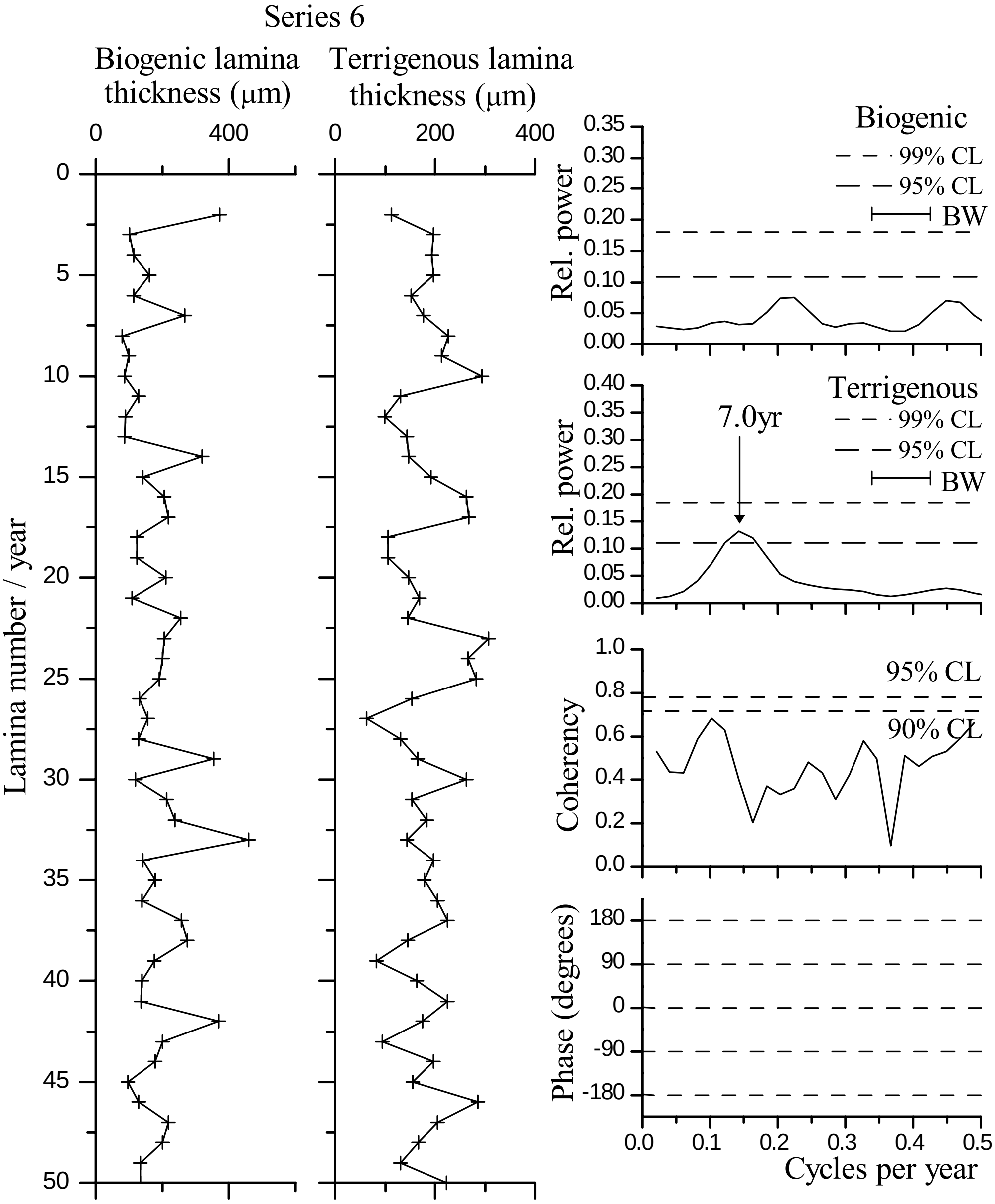

Figure 5.11. Short record of diatomaceous and terrigenous laminae thickness variations from sample set 'H', with the corresponding spectral estimates and phase relationships.

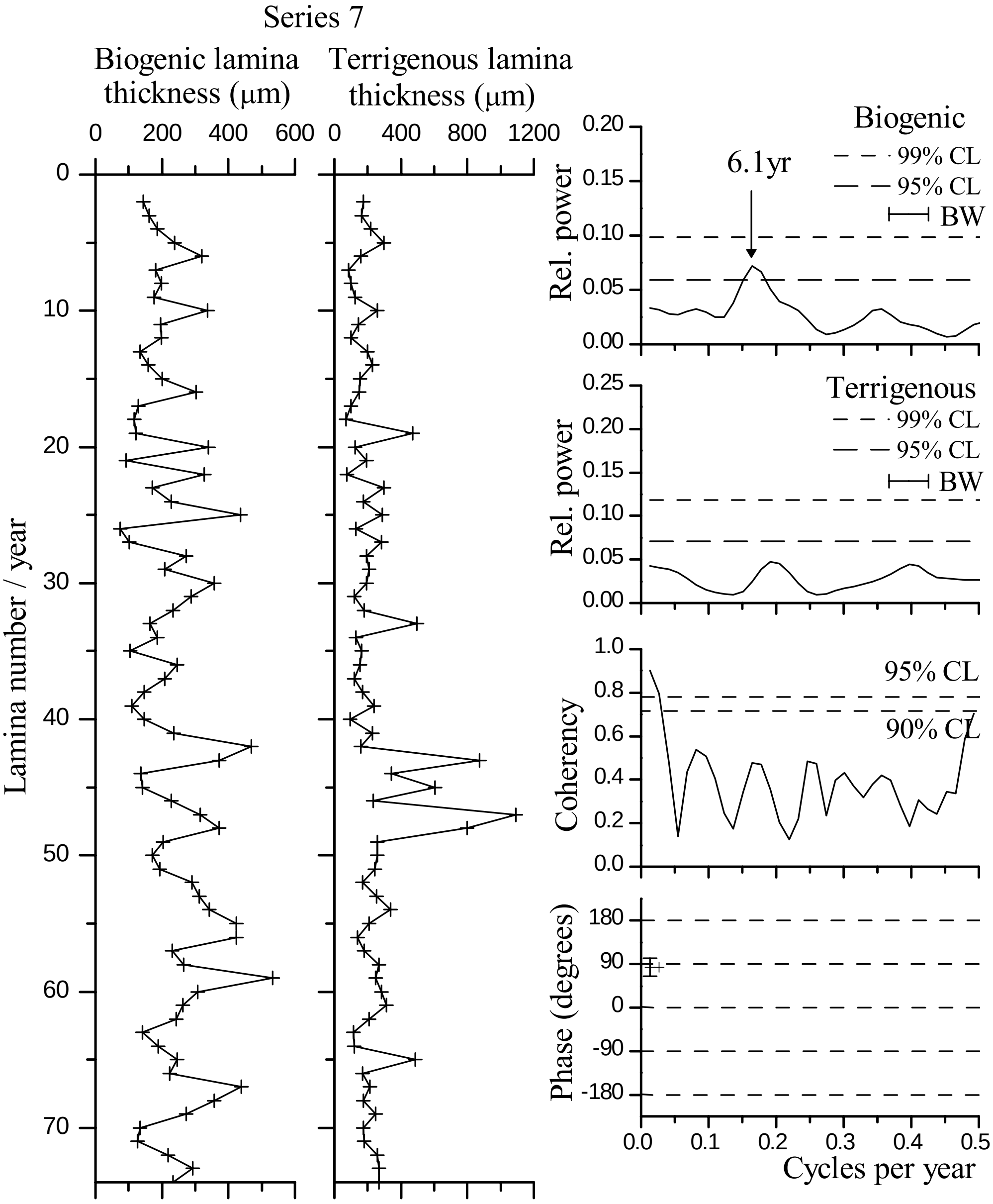

Figure 5.12. Short record of diatomaceous and terrigenous laminae thickness variations from sample set 'H', with the corresponding spectral estimates and phase relationships.

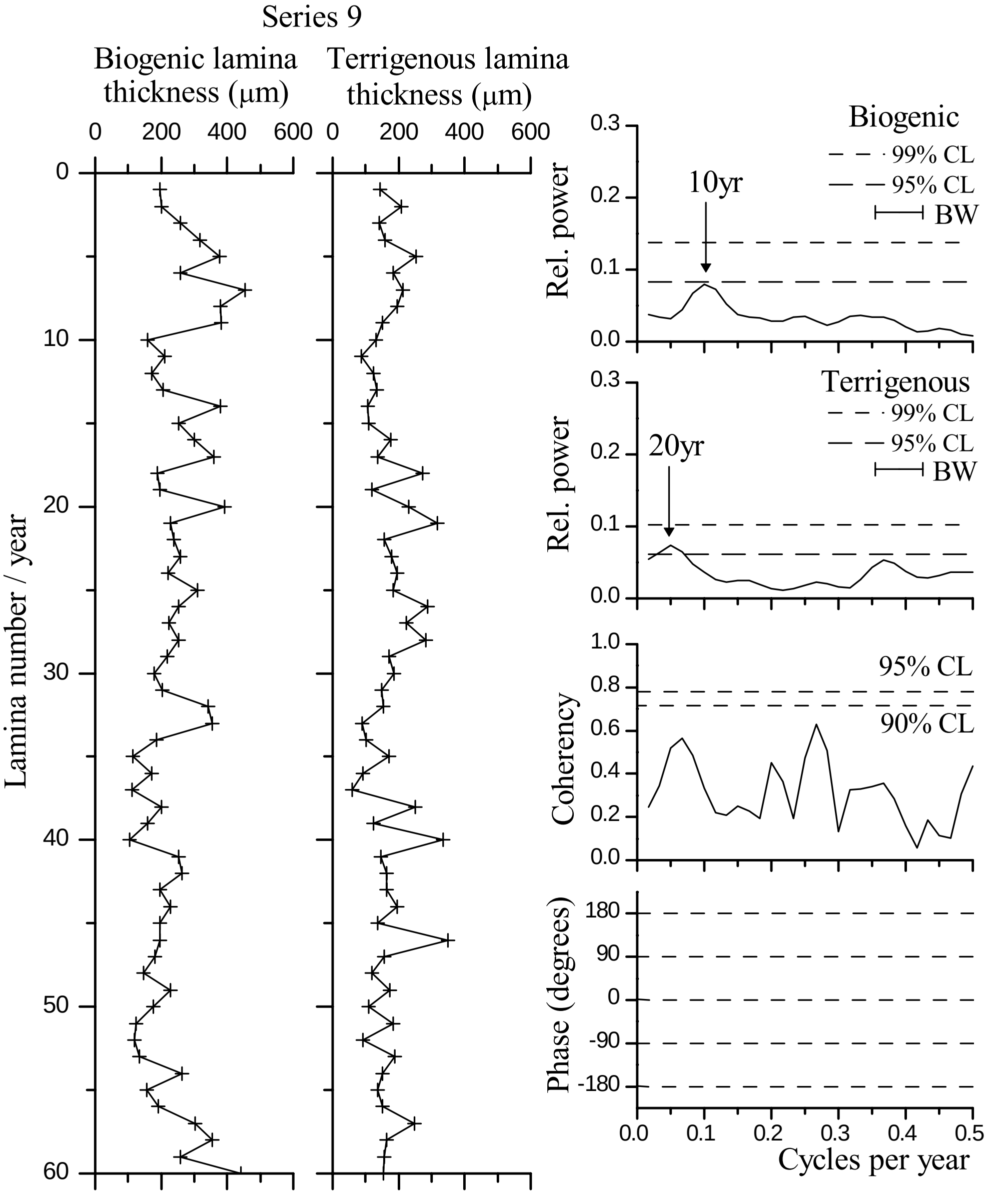

Figure 5.13. Short record of diatomaceous and terrigenous laminae thickness variations from sample set 'H', with the corresponding spectral estimates and phase relationships.

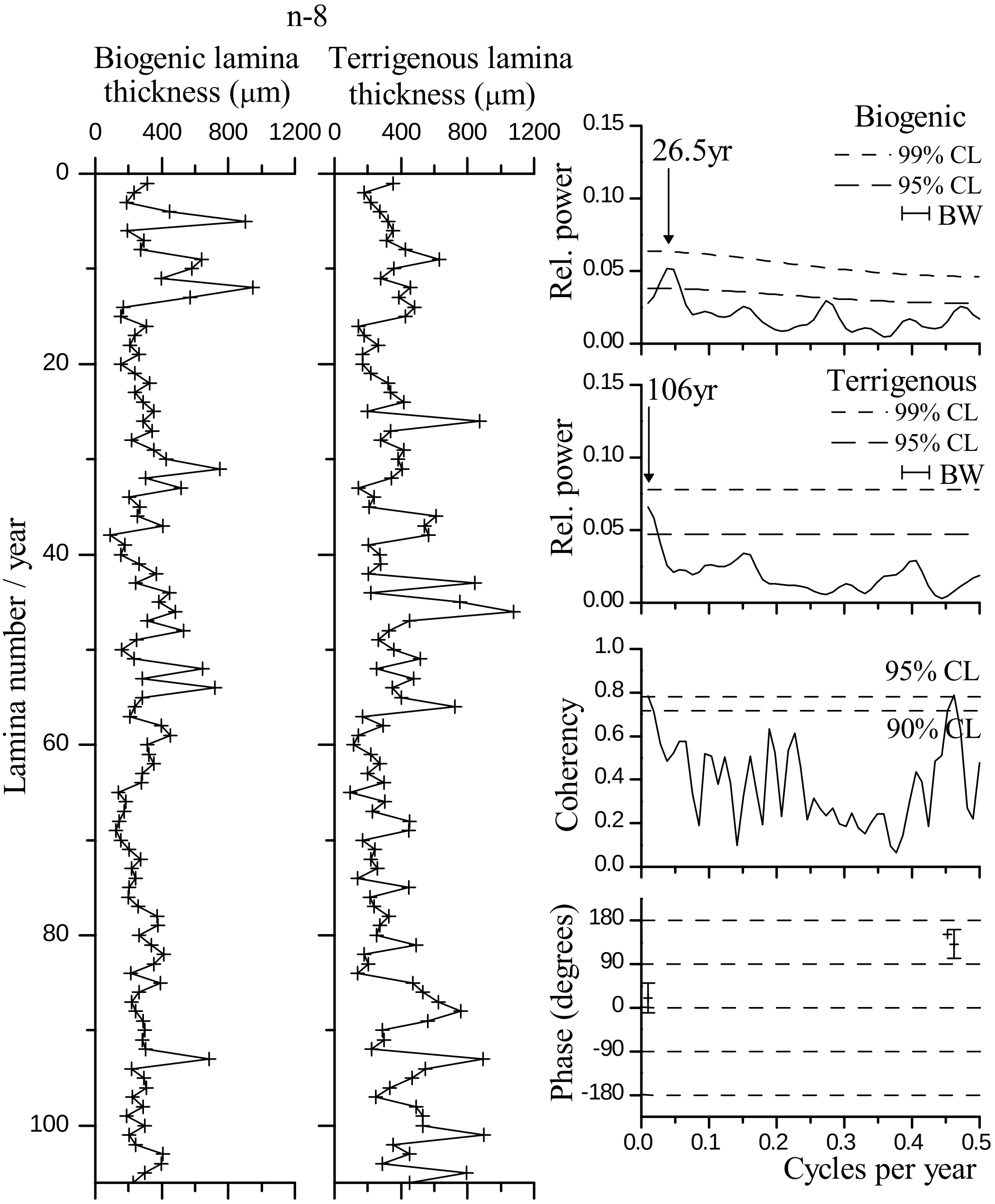

Figure 5.14. Short record of diatomaceous and terrigenous laminae thickness variations from sample set 'N', with the corresponding spectral estimates and phase relationships.

5.4 INTERPRETATION AND DISCUSSION

5.4.1 *Review of the mechanisms capable of producing the observed spectral peaks*

The presence of periodic cycles in the stratigraphic record can be accounted for by a number of different mechanisms, broadly separated into external forcing mechanisms (5.4.1.1 and 5.4.1.2) and internal responses to external forcings (5.4.1.3 - 5.4.1.5). External forcing may arise from variations in solar irradiance and the effect of orbital configurations on tidal forcing. Internal processes relate to climate oscillations in the coupled ocean-atmosphere system, of which the best known is ENSO. A selected list of studies that have identified similar periodicities to those in the Marca Shale is given in Table 5.3, and Fig. 5.15 shows a comparison of the significant spectral peaks with those of modern forcing mechanisms discussed in this section (Chapter 5.4.1).

Author	**Data set**	**Significant periods (years)**
Anderson *et al.* (1990)	Analysis of the occurrence of bioturbation in Pleistocene laminated sediments off coast of northern and central California	~ 20
Ripepe *et al.* (1991)	Image analysis of varved oils shales from an Eocene lake, Wyoming	4.8 5.6 11
Mann & Park (1996)	Sea surface temperature and sea level pressure data for the Northern Hemisphere between 1899-1993	2.1-2.2 3-4 5-7 10-11 16-18
Pike & Kemp (1997)	BSEI of Holocene varved diatomaceous sediment, Gulf of California	11 22-24 50
Conversi & Hameed (1998)	Records of zooplankton biomass, SST and salinity from the Gulf of Alaska	2.4 6 12 24
Mingram (1998)	Optical transmitted light, dark field illumination and fluorescence microscopy of Eocene varved lake sediments, Germany	5.5 8.7
D'Arrigo *et al.* (1999)	Sea surface temperature reconstruction of the North Pacific from tree ring data	3-4 14 25 50
Bull & Kemp (2000)	BSEI of Pleistocene laminated, diatomaceous sediments, Santa Barbara Basin, California	2.0, 2.2 3.1, 3.5 5.6 7.3, 7.6 8.4, 8.8 11 42

Berger & von Rad (2002)	X-radiograph analysis of Holocene laminated sediments, Arabian Sea	12.4 14-15 16.8 18.6 25-26 29-31 39 44
Chavez *et al.* (2003)	Air and ocean temperature, atmospheric CO_2, landings of anchovies and sardines and marine productivity in the Pacific	~ 50
Berger *et al*. (2004)	X-radiography of laminated (Holocene) sediments, Santa Barbara Basin, California	17.7 37.4
Dean & Kemp (2004)	BSEI of Holocene laminated diatomaceous sediments, Saanich Inlet, British Columbia	2.6 3.5 14.8 31.3 42.2
Patterson *et al.* (2004)	Gray scale analysis of Holocene laminated diatomaceous sediments, Effingham Inlet, Vancouver Island	22 27.5 31 45-48

Table 5.3. Selected list of studies that have identified cycles with similar periodicities to those identified in this study.

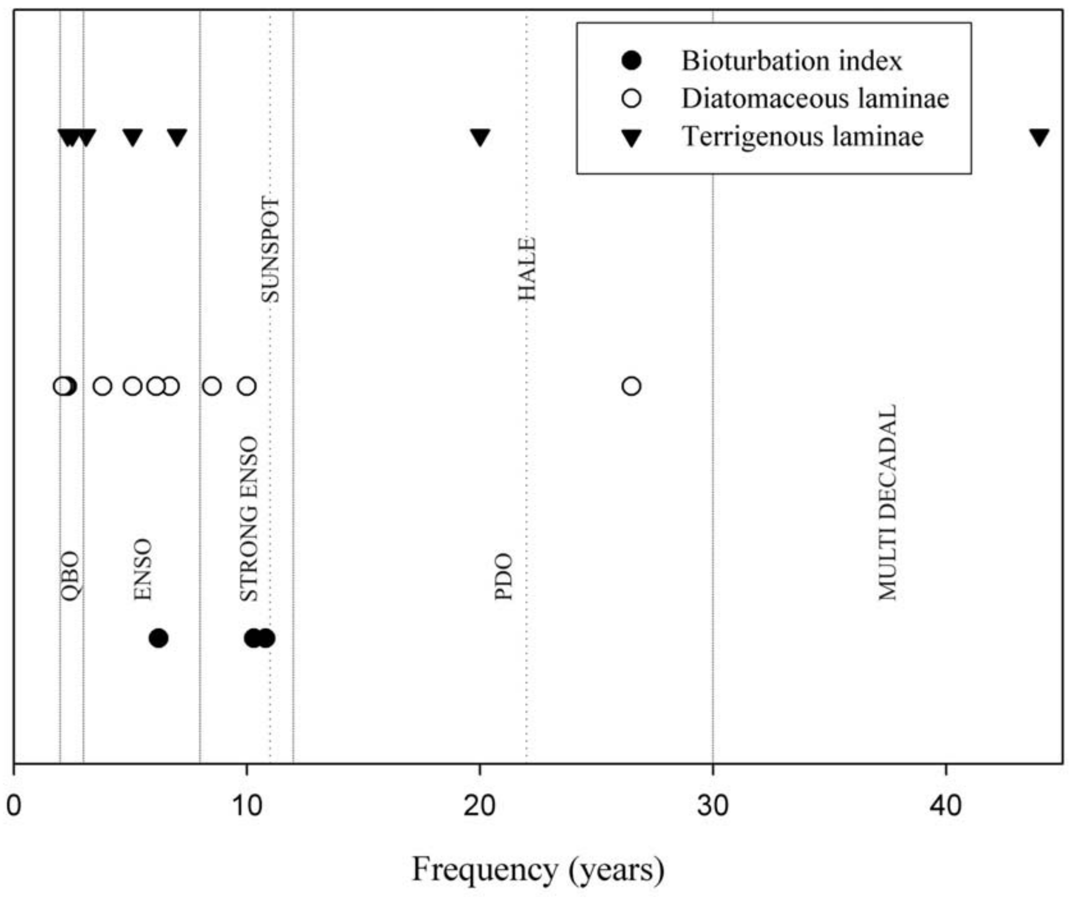

Figure 5.15. Significant frequencies for each parameter analysed along with the modern frequency bands of the major internal and external forcing mechanisms.

5.4.1.1 *Tidal cycles*

The long axis of the Moon's orbit presently rotates with a period of 8.85 years. This results in very high semi-diurnal spring tides every 4.425 years during the March or September equinox, when conjunction/opposition (fortnightly spring-neap tidal cycle) coincide with perigee (the point in the Moon's orbit nearest to the Earth) (Pugh, 1987), creating the perigee cycle. In the present orbital configuration, the Moon's orbit around the Earth is tilted ~5° relative to the equator. The rotation of the Moon's tilted orbit causes the Moon's declination relative to the Earth's orbit to oscillate between a current maximum and minimum of 28.5° and 18.5°, respectively (Weedon, 2003). This cycle is known as the nodal cycle and has a period of 18.6 years at present (Pugh, 1987). Numerous spectral peaks inferred to relate to the perigee or nodal cycles are present in records of varve thickness variations, total organic carbon and abundance of fish scales from the sediments of Santa Barbara Basin (Berger *et al.*, 2004). Similarly, varve thickness variations, the occurrence of turbidites and large excursions in varve thickness in laminated sediments from the Arabian Sea also display spectral peaks that can be associated with tidal cycles (Berger & von Rad, 2002) (Table 5.3). However, it is unclear how such tidal cycles would be manifest during Maastrichtian times when the Moon/ Earth/ Sun configuration was undoubtedly different from that of today.

5.4.1.2 *Solar variability*

The best documented solar cycle is the 11-year sunspot (Schwabe) cycle, over which the number of dark patches (sunspots) varies. Sunspots are areas of cooler photosphere associated with powerful magnetic fields and substantial variation in the number of sunspots occurs over periods of 8-17 years, with a mean period of 11 years (Weedon, 2003). Satellite radiometer measurements have shown that over the 11-year sunspot cycle, solar irradiance varies by 0.1% (Lean et al., 1995), although the variation is not even over all wavelengths. The cycle is connected to large variances (of 6-8%) in the ultra violet part of the spectrum (Chandra & McPeters, 1994). At the end of each Schwabe cycle, the magnetic polarity at the sun's poles and its sunspot groups reverses, resulting in the 22 year magnetic Hale cycle (Dicke, 1979). Alternations in the sun's magnetic field associated with sunspots, affects the solar wind, which deflects cosmic rays (particles originating outside the solar system with energies typically between 100 MeV and 10 GeV) that bombard atmospheric molecules to produce ^{14}C and ^{10}Be. The concentration of ^{14}C and ^{10}Be in the atmosphere is therefore lower during sunspot maxima and higher during sunspot minima. Analysis of ^{10}Be concentrations in ice cores (Beer *et al.*, 1990) and ^{14}C in tree rings (Stuiver & Quay, 1980) indicate that solar activity was reduced in the seventeenth century, a period known as the Maunder Minimum, when there was a prolonged lack/absence of sunspots. The Maunder Minimum corresponds with one of the multiple cold phases of the Little Ice Age, helping consolidate the belief that solar variability and climate change are linked (Eddy, 1976).

Numerous studies have linked cyclicity recorded within varved sediments to the Schwabe and Hale cycles (e.g. Ripepe *et al.*, 1991; Pike & Kemp, 1997; Munoz *et al.*, 2002; Cosentino *et al.*, 2005) (Table 5.3). Inferred sunspot cycles have also been reported from other proxy data sets, including varve/bioturbation cycles (Anderson *et al.*, 1990) (Table 5.3), tree rings (Mori, 1981; Rigozo *et al.*, 2003), ice cores (Beer *et al.*, 1985; Michael & Stolz, 1999; Kang *et al.*, 2005), stalagmites (Paulsen *et al.*, 2003) and foraminiferal $\delta^{18}O$ records (Castagnoli *et al.*, 1999; Black *et al.*, 2004) as well as in historical climate data sets (Thresher, 2002; Lee *et al.*, 2005). Despite these findings, scepticism of the role of solar cycles on climate variability exists due to a lack of a credible mechanism able to transfer the small changes in irradiance to the climate system. Surface records demonstrating a clear 11-year cycle in phase with solar variations are also scarce (Weedon, 2003). It has also been shown that climate oscillations with a period of ~11 years can be produced in general circulation models which exclude external forcing (James & James, 1989; Garric & Huber, 2003). However, Labitzke and van Loon (1990) suggest that the stratospheric QBO (Reed *et al.*, 1961) may be associated with sea level air temperature and pressure variations by modulating the polar night jet (the polar night jet is a high altitude jet stream that develops along the line between sunlight and the wintertime polar night) over the 11-year Schwabe cycle. Fluctuations in the polar stratosphere have been linked to the planetary waves in both the atmosphere and troposphere, which may extend into the tropics (Labitzke & van Loon, 1990). It is known that a much greater proportion of stratospheric perturbations penetrate to the surface during solar maximum rather than solar minimum conditions (Hameed & Lee, 2005). Modelling studies have also demonstrated that a 0.1% variation in solar activity would affect the surface climate through dynamical effects on the stratospheric polar vortex, attributed to an interaction between UV radiation and stratospheric ozone (Balachandran *et al.*, 1999), which in turn result in atmospheric circulation anomalies (Black, 2002). Records exist from the Proterozoic (Hughes *et al.*, 2003), Cretaceous (Masuda & Watanabe, 1979), Eocene (Ripepe *et al.*, 1991) and Pliocene (Munoz *et al.*, 2002) that suggest solar variability was present throughout geological history and that the (11 year) frequency of these solar cycles has changed little.

Evidence exists to suggest that solar variability is able to modulate some of the internal climate oscillations. The periodicity of strong El Niño events occur every ~12 years during periods of strong sunspot activity and ~8 year during periods when solar activity is reduced (Enfield & Cid, 1991). Waple *et al.* (2002) further hypothesised that internal quasi-decadal oscillations can be forced to resonate at an 11 year frequency when the amplitude of solar variability is unusually pronounced.

5.4.1.3 *ENSO*

At present, the El Niño-Southern Oscillation (ENSO) phenomenon is the primary mode of global climate variability at frequencies of 2-7 years. The Southern Oscillation is a fluctuation of sea level air pressure between the east and west Pacific, whilst El Niño refers to periods of intensive warming of the upper ocean in the eastern equatorial Pacific (Fig. 5.16) (Philander, 1990). It is now widely accepted that the cause of the oscillation lies in the mechanisms outlined by Bjerknes (1969). Under "normal" conditions, the equatorial Pacific is 4-10 °C colder in the east than in the west due to the action of easterly trade winds, which create an east-west tilting thermocline and cause cool subthermocline waters to upwell in the eastern Pacific and also cause warm equatorial waters to pool in the western Pacific (Fig. 5.17a). The pronounced SST gradient between the east and west Pacific stimulates an east-west atmospheric overturning circulation, which enhances surface easterly trade winds and creates a positive feedback loop (the "Bjerknes" feedback). This positive feedback loop is strengthened during La Niña events, when the east-west temperature gradient in the Pacific becomes more pronounced (Fig. 5.17c). During El Niño events the positive feedback works in the opposite sense. Warming in the eastern Pacific causes a reduction in the east-west SST temperature gradient, causing the easterly trade winds to weaken or even reverse. Consequently equatorial upwelling in the east Pacific is reduced and the thermocline deepens, further weakening the easterly trade winds (Fig. 5.17b). The "Bjerknes" feedback explains why the system has two favoured modes (El Niño and La Niña), but not why there is an oscillation between them. The instability at the heart of the ENSO is not fully resolved, but is generally thought to relate to instabilities in the tropical Pacific thermocline (Cane, 2005), probably relating to the development of slow moving eastwards (Kelvin) and westwards (Rossby) oceanic waves (e.g. McPhaden & Yu, 1999). Although ENSO originates within the equatorial and tropical Pacific, its influence is transmitted globally through atmospheric "teleconnections", with important impacts on world climate (Philander, 1990).

El Niño events currently occur every 2-7 years (Trenberth, 1997) with an average periodicity of 3-5 years (Weedon, 2003), whilst strong El Niño events occur with a periodicity between ~8 to 12 years (Enfield & Cid, 1991). Evidence exists to suggest that the periodicity of strong El Niño events is modulated by solar variability and the stratospheric QBO (Enfield & Cid, 1991). Analyses of numerous recent records of ENSO variability suggest that the sub-decadal period and strength of the oscillations varies greatly over periods of decades and longer (e.g. Dunbar *et al.*, 1994; Urban *et al.*, 2000). A lake record containing El Niño-related storm deposits appears to show that the modern sub-decadal ENSO variability began around 5000 years ago, and that prior to this time, back to 15,000 years ago, sub-decadal ENSO variability was absent (Rodbell *et al.*, 1999). However, the apparent absence may simply be a reflection of weaker El Niño events (Cane, 2005). Recently Nederbragt and Thurow (2005) presented evidence from varve thickness records from the

Santa Barbara Basin indicating that although the expression of ENSO may have changed, the amplitude of the variability has remained constant over the past 15,000 years. Indeed, other records indicate that modern ENSO variability has been feature of the climate system for at least the last 160,000 years (Bull *et al.*, 2000; Tudhope *et al.*, 2001). Spectral analysis of varved Eocene records suggests that ENSO was even a robust feature of the climate system during greenhouse conditions (Ripepe *et al.*, 1991; Mingram, 1998) (Table 5.3).

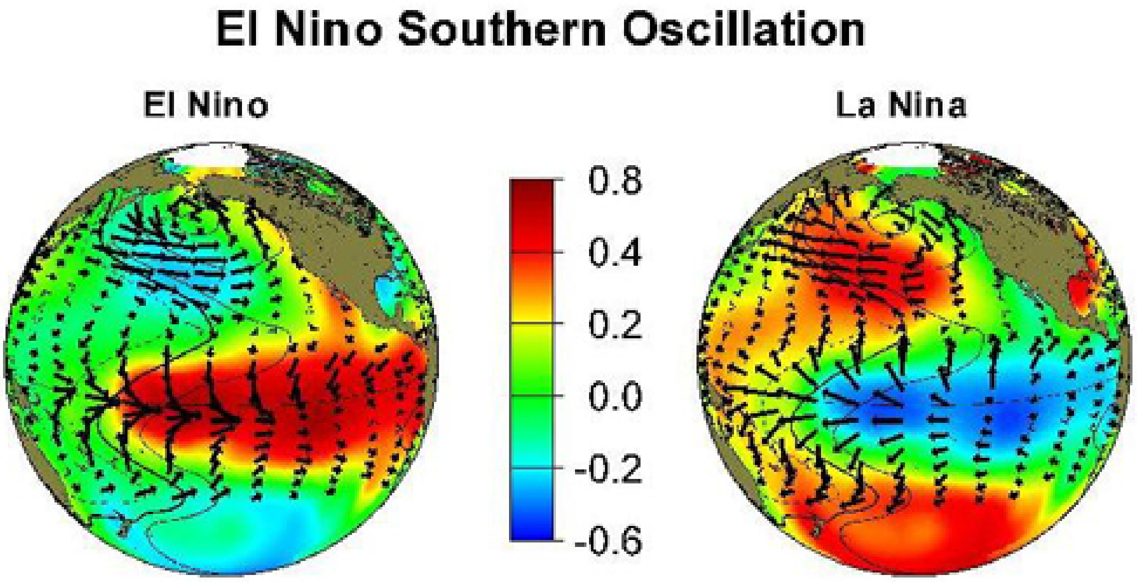

Figure 5.16. Winter sea surface temperature and wind pattern (arrows) anomalies associated with El Niño and La Niña events (courtesy of Nate Mantua, JISAO Univ. of Washington. http://tao.atmos.washington.edu/pdo/graphics.html)

Theory indicates that any factors acting to weaken the “Bjerknes” feedback loop, the mechanism controlling ENSO variability in the tropical Pacific, would tend to cause the climate system to collapse into a permanent El Niño state, with reduced, or even devoid of, ENSO variability (Neelin *et al.*, 1998; Fedorov & Philander, 2000). A permanent El Niño climate state would presumably exhibit features characteristic of a modern El Niño event, such as greater heat transport to high latitudes, elevated global mean temperatures, a weak east-west thermocline tilt and little or no upwelling of cold nutrient-rich water along the eastern Pacific. Molnar and Cane (2002) proposed such a permanent El Niño state to explain characteristics of the warm, equable climate of the pre-Ice Age middle Pliocene (5- ~2.7 Ma). A permanent El Niño would help explain many features of the Maastrichtian climate system, which was characterised by extreme polar warmth, emphasized in recent TEX$_{86}$ palaeotemperature estimates from the Late Cretaceous (70 Ma) Arctic Ocean, indicating SST’s of 15 °C (Jenkyns *et al.*, 2004). Many geological proxies indicate Late Maastrichtian deep water temperatures were significantly warmer than those of today, with global mean temperature estimated as 10.2 °C (D'Hondt & Arthur, 2002). This warmth was manifest in the tropics, although markedly less pronounced with the highest tropical SST’s estimates ranging between 27-32 °C (Wilson & Opdyke, 1996; Pearson *et al.*, 2001; Steuber *et al.*, 2005). Assuming that these observations indicate a deepening of the thermocline and that the temperature difference across it was less than at present, a weakening of the positive feedback system would result, with a consequential reduction in ENSO variability.

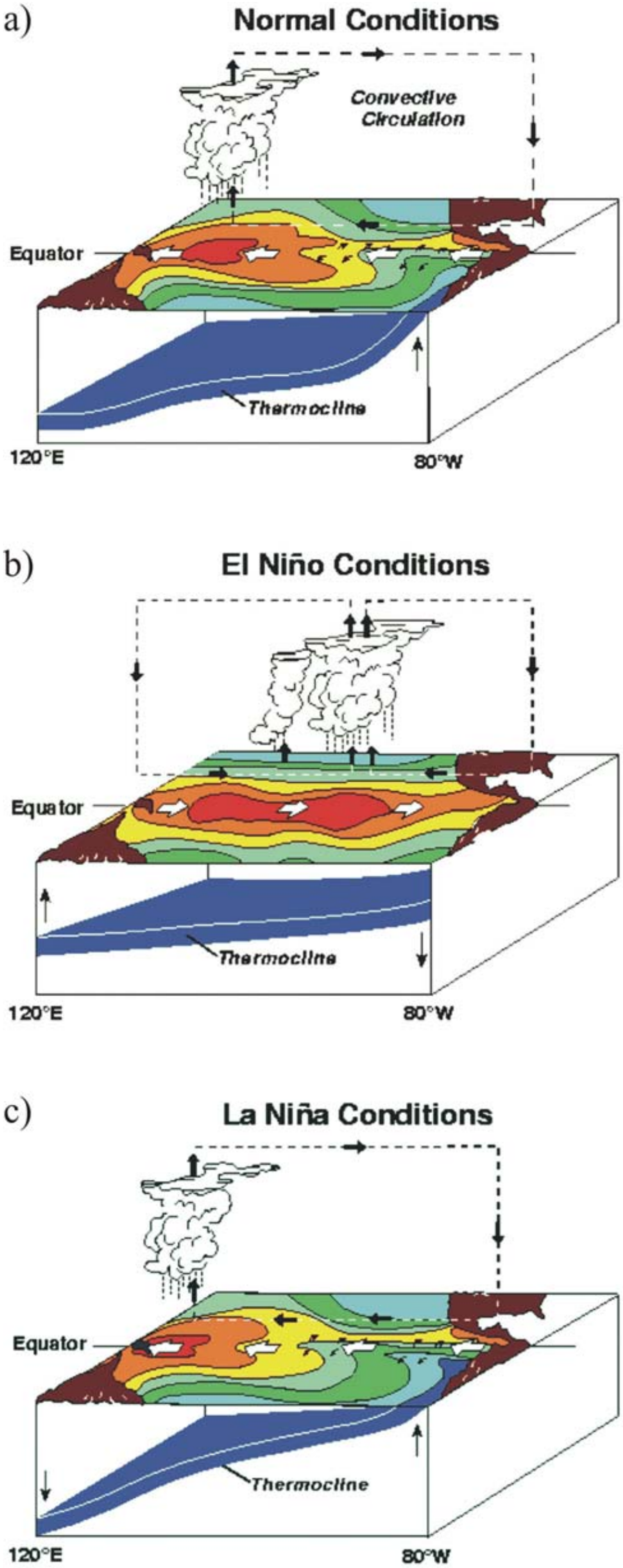

Figure 5.17. Cartoon of the changes in sea surface temperature, atmospheric circulation and structure of the thermocline associated with El Niño and La Niña events in the central Pacific (modified from http://www.pmel.noaa.gov/tao/elnino/nino-home.html#).

It has been argued that the presence of an open Isthmus of Panama would cause the thermocline to deepen in the eastern Pacific (Chaisson & Ravelo, 2000) whilst an unobstructed Indonesian seaway would cause the thermocline to shoal in the west (Cane & Molnar, 2001). Both of these mechanisms would lead to a weakening of the Bjerknes feedback through a reduction in the east-west tilt of the thermocline and during the Maastrichtian, there existed both an open Isthmus of Panama and an unobstructed Indonesian seaway (Hay *et al.*, 1999). Therefore the Maastrichtian global configuration appears to have played host to a severe weakening of the Bjerknes feedback.

5.4.1.4 *Pacific Decadal Oscillation (PDO)*

Recently, a mode of variability with similar spatial climate/oceanographic effects to ENSO, but differing significantly in temporal behaviour, has been recognized and termed the Pacific Decadal Oscillation or Interdecadal Pacific Oscillation. Although patterns of anomalous SST, sea level air pressure and wind stress fields for the PDO and ENSO are very similar (Fig. 5.18), the PDO's climatic fingerprint is most visible in the North Pacific, with secondary signatures in the tropics, opposite to that of ENSO (Zhang *et al.*, 1997). The PDO is also more persistent than ENSO, with each phase of the cycle typically lasting 20-30 years (Mantua *et al.*, 1997; Minobe, 1997), associated with east-west shifts in the position of the Aleutian Low (Miller *et al.*, 1994; Mantua *et al.*, 1997; Biondi *et al.*, 2001) and major biological regime changes in the Pacific (Mantua *et al.*, 1997). Instrumental data indicates that shifts between the warm (positive) and cool (negative) phases of the PDO are rapid and are known to have occurred in 1925, 1947 and 1977 (Minobe, 1997). Proxy data sets obtained from corals (Urban *et al.*, 2000) and tree rings (D'Arrigo *et al.*, 1999) (Table 5.3) have shown the PDO to be a robust feature of North Pacific climate variability, although it does fluctuate in strength (Gedalof *et al.*, 2002).

Air and sea surface temperatures over North America and the North Pacific indicate that the PDO also operates on a longer periodicity of 50-70 years (Minobe, 1997; Biondi *et al.*, 2001; Chavez *et al.*, 2003). The similarity of the ocean/atmosphere perturbations associated with of each phase of the oscillation to those of ENSO, led Chavez *et al.* (2003) to propose the terms El Viejo and La Vieja for the warm and cool phase, respectively. This longer multi-decadal oscillation has also been identified in tree ring data (D'Arrigo *et al.*, 1999), varved sediments (Pike & Kemp, 1997; Bull *et al.*, 2000; Dean & Kemp, 2004; Patterson *et al.*, 2004) and the deposition of sardine/ anchovy scales (Baumgartner *et al.*, 1992) (Table 5.3).

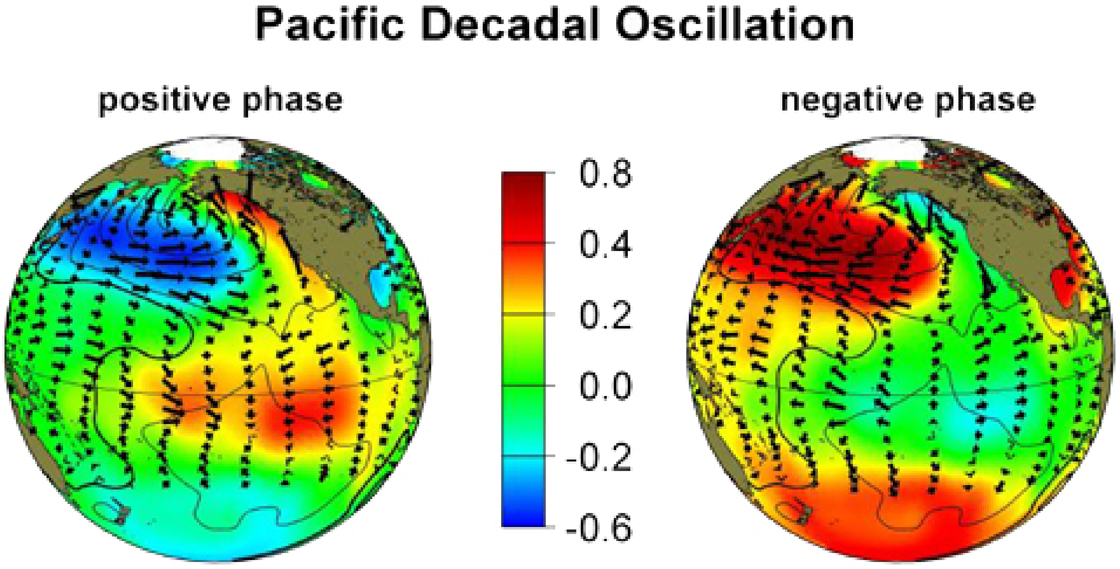

Figure 5.18. Winter sea surface temperature and wind pattern (arrows) anomalies associated with the warm positive phase and cool negative phase of the PDO (courtesy of Nate Mantua, JISAO Univ. of Washington. http://tao.atmos.washington.edu/pdo/).

5.4.1.5 *Quasi-biennial oscillation (QBO)*

The QBO is a downward propagating, east-west reversal in the direction of the zonal flow in the equatorial stratosphere (Reed *et al.*, 1961; Baldwin *et al.*, 2001). The QBO is generally thought to result from equatorially trapped Kelvin waves and Rossby-gravity waves (e.g. Dunkerton, 1997). The period of the present QBO is temporally and spatially variable (Labitzke & van Loon, 1999), although averages ~ 28 months (2.33 years) (Baldwin *et al.*, 2001). It has been shown that the QBO strongly modifies the effect of the 11-year Schwabe sunspot cycle on stratospheric temperatures (Labitzke, 2005). Winter stratospheric temperatures at northern polar latitudes are positively and negatively correlated with the sunspot cycle when the QBO is in a negative and positive phase, respectively. This correlation is opposite at mid-latitudes (Labitzke, 2005). The QBO also impacts the strength and stability of the northern hemisphere wintertime stratospheric polar vortex, with the westerly phase of the QBO favouring a stronger polar vortex (Holton & Tan, 1980; Baldwin *et al.*, 2001).

Signals with similar periodicities to the stratospheric QBO have been identified in various records of sea level pressure, air temperature and sea surface temperature, salinity, zooplankton biomass and laminae thickness variations (relating to productivity and rainfall variations) (Rasmusson *et al.*, 1990; Briffa *et al.*, 1992; Ware, 1995; Mann & Park, 1996; Conversi & Hameed, 1997; Conversi & Hameed, 1998; Bull *et al.*, 2000; Dean & Kemp, 2004) (Table 5.3). The QBO has been invoked as an explanation for the variability in the strength of ENSO (Rasmusson *et al.*, 1990; Kane, 1992) and it has been suggested that the periodicity of strong El Niño events relates to solar variability and the stratospheric QBO (Enfield & Cid, 1991). The precise relationship between the stratospheric QBO (Reed *et al.*, 1961) and the atmospheric/oceanographic QBO remains uncertain. Labitzke and van Loon (1990) suggest that the stratospheric QBO may be associated with sea level pressure and air temperature variations by modulating the polar night jet over the 11-year Schwabe cycle. It has been shown that there exists a robust link between the QBO and the strength of the polar stratospheric vortex, which impacts the Northern Hemisphere Annular Mode (NAM) variability (Baldwin *et al.*, 2001). Fluctuations in the polar stratosphere have been linked to the planetary waves in both the atmosphere and troposphere, which may extend into the tropics (Labitzke & van Loon, 1990). This may result in intensification of the Aleutian Low on biennial scales (Bull, 1998), resulting in biennial variations in rainfall intensity along the present north east Pacific coast (Dean & Kemp, 2004).

5.4.2 *Observed microfabric evidence for high frequency climate cycles in the Marca Shale*

Several sedimentological lines of evidence exist in the Marca Shale suggesting the Late Cretaceous Californian margin was influenced by a high frequency climate cycle with a fingerprint similar to the modern ENSO phenomenon. Firstly, there is the interannual variability in the diatom flora expressed by the periodic occurrence of discrete laminae of *Chaetoceros*-type resting spores and *Azpeitiopsis morenoensis*, the composition and occurrence of which is similar to ENSO forced variability along the modern Californian margin (see Fig 4.36). Secondly, bioturbation index records show that periods of minimal bioturbation (enhanced benthic anoxia) coincide with times of greatest diatomaceous export flux and lowest flux of detrital material. Enhanced benthic anoxia would have been associated with a higher flux of organic carbon associated with the increased diatom flux. Conversely, periods of enhanced bioturbation correspond with reduced diatom export flux and an increased flux of detrital material (see Fig. 4.30), comparable with ENSO forced variations in diatom and detrital export flux and associated benthic oxygenation levels in Pleistocene varves off the Californian margin (Anderson *et al.*, 1990). Finally, there is the strong interannual variability in marine productivity and fluvial runoff, inferred from thickness variations of the diatomaceous and terrigenous laminae respectively. Occasionally the variability in the thickness of each laminae type is observed to be out of phase (see Fig. 4.21), similar to ENSO forced cyclicity in annually laminated Pleistocene sediments from the Santa Barbara Basin (Bull *et al.*, 2000).

5.4.3 *Significance of spectral peaks in the bioturbation index records*

Significant peaks in bioturbation index records lie within the frequency band of modern ENSO and strong ENSO variability. Plots of mean diatomaceous laminae thickness for each of the bioturbation indices reveal a consistent trend of reduced laminae thickness with increasing levels of bioturbation, strongly suggesting levels of dissolved oxygen at the sediment water interface were primarily controlled by diatom and hence organic carbon export flux (see Chapter 4.4.9). Variations in the levels of bottom water anoxia over periods of years to millennia, distinguished by alternating zones of varved and bioturbated sediment, are known from the late Pleistocene upper continental slope off northern and central California and have been used as a proxy for ENSO variability on diatom production (Anderson *et al.*, 1990).

The effect of an ENSO-like phenomenon on terrigenous export flux along the mid-latitude proto Californian margin can be expected to have been analogous to the effects of modern ENSO. Increased SST's in the eastern Pacific during El Niño events would have increased the evaporation of surface waters and in turn increased regional precipitation. This would have caused fluvial runoff to increase, culminating in higher terrigenous flux to the basin, independent of the season of maximum precipitation. Unlike the effects on terrigenous export flux, the effect of an ENSO-like phenomenon on diatom production may not be so straightforward. Diatoms may respond to numerous environmental factors including temperature, salinity, irradiance and water column stability as well as the availability of nutrients. Also, unlike the modern Californian margin, where diatom export flux principally relates to the strength of upwelling, micropalaeontological evidence suggests that diatom export production in the Marca Shale is dominated by taxa adapted to exploit nutrients trapped in a stratified water column. However, the trends shown by average terrigenous and diatomaceous laminae thickness for each bioturbation indice implies that during periods of increased terrigenous flux (inferred to relate to El Niño-like conditions), diatom export flux was reduced. Correspondingly, diatom export flux was elevated during La Niña-like conditions, possibly in response to increased levels of nutrients in the euphotic zone (subsequently trapped below the thermocline) due to enhanced seasonal upwelling.

The significant peaks in bioturbation index records are therefore interpreted to relate to an ENSO-like oscillation, which forced alternations between wet, low productive periods and drier productive periods, analogous to El Niño and La Niña respectively. Although independent proxy estimates of the Maastrichtian SST gradient in the Pacific are unavailable, results from a fully coupled ocean-atmosphere simulation for the Campanian (80 Ma) suggest that similar to today, the Pacific Ocean was characterised by a ~4 ºC east-west sea surface temperature gradient (Otto-Bliesner *et al.*, 2002), and as such, the conditions for an ENSO-type oscillation were in place. The 6.2 year peak is inferred to relate to the effect of moderately strong ENSO variability, whilst the 10.8 and 10.3 year spectral peaks are interpreted to relate to the occurrence of strong ENSO events, which currently occur every 8-12 years (Enfield & Cid, 1991).

Along with lying in the frequency band of modern strong ENSO events, both the 10.8 and 10.3 year spectral peaks lie close to the frequency (11 year) of the modern sunspot cycle (Fig. 5.15). Enfield and Cid (1991) suggested that the frequency of strong ENSO events may be modulated by solar variability and it is hypothesised that internal quasi-decadal oscillations can be forced to resonate at an 11 year frequency when solar variability is unusually pronounced (Waple *et al.*, 2002). The fact that these two spectral peaks lie within this well established frequency band suggests the occurrence of strong ENSO variability may have been modulated by the ~11 year sunspot cycle and provides firm evidence that in these two records at least, the varve chronology is accurate.

5.4.4 *Significance of spectral peaks in laminae thickness variations*

5.4.4.1 *Quasi biennial peaks*

Numerous peaks within the quasi biennial frequency band are present in laminae thickness records from several sample sets in the Marca Shale (Table 5.1 and Fig. 5.15), equally common in diatomaceous and terrigenous laminae records. Such peaks in modern climate records may be related to the biennial component of ENSO variability (Rasmusson *et al.*, 1990). However, in the Marca Shale solitary biennial signals are present without a concurrent ENSO frequency band signal (Fig. 5.8) indicating they must have an independent origin, similar to solitary QBO signals recorded in varved sediments from Saanich Inlet (Dean & Kemp, 2004). The only known biennial periodic forcing mechanism is the QBO and thus significant spectral peaks with quasi-biennial frequencies are interpreted to relate to a QBO-like oscillation. If the stratospheric QBO results from equatorially trapped Kelvin waves and Rossby-gravity waves (Dunkerton, 1997) there is little reason to expect an analogous oscillation to be absent from the Maastrichtian climate. An oscillation similar in nature to the modern QBO is also likely to have been associated with planetary waves in both the atmosphere and troposphere (Labitzke & van Loon, 1990), resulting in intensification of northern high latitude low pressure systems on biennial scales (Bull, 1998), causing biennial variations in rainfall intensity along the proto east Pacific coast. The Holocene varved record from Saanich Inlet shows that the QBO causes consecutive years to be slightly drier/ wetter relative to each other (Dean & Kemp, 2004). Alterations in the intensity of a northern high pressure system are also likely to have influenced water column stability and hence effected biological populations, including diatoms, as evident from Saanich Inlet (Dean & Kemp, 2004). The similarity between the average ~28 month period of the modern QBO and the inferred QBO oscillations in the Marca Shale, which average 2.28 years (27.4 months), is striking. Sample set H displays significant spectral peaks at 2.3 years in both the terrigenous and diatomaceous laminae that display a significant coherency and phase relationship of 89.8° (± 25.1°). Thus, over the 2.3 year cycle, perturbations in the diatomaceous flux were followed by perturbations in terrigenous flux 6.77 (± 1.90) months later. The 6.77 month lag may relate to the seasonal timing of the QBO forced perturbations, with diatom flux responding in autumn (e.g. November) and fluvial runoff during the summer (e.g. June).

5.4.4.2 *Sub-decadal and quasi-decadal peaks*

Sub-decadal peaks are present in four out of the five samples sets and the greatest numbers of peaks are present in this frequency band (Table 5.1 and Fig. 5.15). Variability in the sub-decadal frequency band is dominated by ENSO in the present climate system, although has also been attributed to tidal forcing. However, the ENSO-type oscillation inferred to be responsible for forcing sub-decadal to decadal variations in the level of bottom water anoxia, would also have forced laminae thickness variations on similar frequencies. Based on the frequency bands of modern ENSO (Fig. 5.15), the mean ENSO frequency band in laminae thickness variations is 5.3 years, whilst that of strong ENSO variability is 9.3 years, although is only recorded in diatomaceous laminae.

Although the ~11 year cycle is not well expressed in laminae thickness records there are similarities between the peaks in the bioturbation index and laminae thickness records. The bioturbation index record from sample set H displays significant peaks at 6.2 and 10.3 years. Records of diatomaceous laminae thickness from the same sample set display significant peaks at 6.1, 6.7 and 10.0 years. The 6.1 and 10.0 year peaks are from the short records and therefore have a large bandwidth error. Further to this, although not reaching the 95% significance interval, power is expressed in the ~11 year frequency band in the long record of diatomaceous laminae thickness in sample set O (Fig. 5.9), consistent with the 10.8 year peak in the bioturbation index record from that sample set. These similarities add to the evidence that variations in diatom export flux were responsible for changes in benthic oxygen levels and that diatom export flux and changes in the bioturbation index were forced by the same mechanism.

Variations in the thickness of diatomaceous and terrigenous laminae from the Santa Barbara Basin, forced by ENSO, are distinctly out of phase by ~180° (Bull *et al.*, 2000). Despite analogous out of phase short-term variability identified in the Marca Shale microfabric (see Fig. 4.21) and an antiphasing in the maximal diatom and terrigenous export flux in relation to benthic oxygen levels, no such phase relation was evident in the laminae thickness spectral estimates. The ~180° relation in the spectral estimates from the Santa Barbara Basin reflects a consistent alternation between successive El Niño and La Niña events in these Pleistocene varves. The lack of an ~180° phase relationship may therefore relate to the fact ENSO-type variability in the Maastrichtian did not always result in paired phases of El Niño and La Niña, as defined by Trenberth (1997). Tsonis *et al*. (2005) provide evidence that in a warming climate, El Niño events are liable to be more frequent than La Niña events. Similar, to results from the Marca Shale, spectral analysis from Saanich Inlet found no phase relationship between terrigenous and biogenic varve segment thickness, despite strong ENSO peaks present in both (Dean & Kemp, 2004). Even though ENSO has a profound effect on SST, atmospheric conditions and diatom community structure in the modern Gulf of California, laminae thickness records form the Gulf do not even contain significant spectral peaks in the ENSO band (J. Pike, personal communication). It therefore appears that the sub-decadal ~180° phase relationship seen in the Pleistocene varves from Santa Barbara Basin is an exception and not the rule.

5.4.4.3 *Multi-decadal signals*

Although uncommon, multi-decadal peaks were identified in both diatomaceous (26.5 years) and terrigenous laminae (20.0 years). It is feasible that within the bandwidth error, both peaks relate to the ~22 year Hale magnetic solar cycle, which is commonly inferred to be recorded in proxy climate records (Pike & Kemp, 1997; Ram & Stolz, 1999; Black *et al.*, 2004). Both the 26.5 and 20.0 year peaks lie within the frequency band of the modern PDO (Fig. 5.15) and many proxy climate data sets have identified similar periodicities attributed to the PDO. These include records of terrigenous and diatomaceous laminae thickness from Saanich Inlet (Dean & Kemp, 2004), total varve thickness from Effingham Inlet (Patterson *et al.*, 2004) and summer air temperature (Briffa *et al.*, 1992) and SST (D'Arrigo *et al.*, 1999) reconstructions from tree rings (Table 5.3). A PDO-like oscillation could explain the multi-decadal peaks in both the diatomaceous and terrigenous laminae thickness records in the Marca Shale. Positive phases of a cycle analogous to the PDO would result in anomalously wet conditions, accompanied with reduced upwelling, nutrient availability and hence reduced diatom export production, analogous to El Niño conditions (Fig. 5.18). Negative phases would have been anomalously dry, with increased diatom productivity and export flux, analogous to La Niña conditions. Solar variability, in this case the ~22 year Hale cycle, may have forced the periodicity of the inferred PDO-like phenomenon, as suggested by Enfield and Cid (1991).

Along with the ~20 year spectral peaks, a solitary significant multi-decadal 44 year peak was recorded in terrigenous laminae thickness. Information on analogous oscillations in the modern ocean/atmosphere system is scarce due to the lack of sufficiently long instrumental data sets. However, the modern PDO is known to have a 50-70 year component, identified in air and sea surface temperatures over North America and the North Pacific (Minobe, 1997; Biondi *et al.*, 2001; Chavez *et al.*, 2003), and also in reconstructions of SST's from tree ring data (D'Arrigo *et al.*, 1999). Similar frequency peaks are also present in spectral estimates from varved sediments from the Santa Barbara Basin (Bull *et al.*, 2000), Saanich Inlet (Dean & Kemp, 2004), Arabian Sea (Berger & von Rad, 2002), Effingham Inlet (Patterson *et al.*, 2004) and Gulf of California (Pike & Kemp, 1997) (Table 5.3). Dean and Kemp (2004) interpreted the 42.2 year peak identified in the biogenic varve segment from Saanich Inlet to relate to the occurrence of strong or modulated PDO events. Pike and Kemp (1997) similarly interpreted the 50 year peak recorded in the occurrence of *Thalassiothrix* mats to relate to the 50-70 year PDO oscillation, further surmising that the periodicity may be forced by solar variability. Patterson *et al.* (2004) also interpreted the ~45 year cycle in varve thickness to relate to the PDO, but found it not to relate to solar forcing. The 44 year cycle identified in the occurrence of turbidites in sediments from the Arabian Sea was interpreted by Berger and von Rad (2002) to be a multiple of the tidal Perigee cycle.

An oscillation similar in character and frequency to the modern 50-70 year PDO oscillation could explain the 44 year peak in terrigenous laminae thickness present in the Marca Shale. Alternations between a warm (El Viejo) and cool (La Vieja) phase of such a cycle would result in long term wet and dry episodes along the proto Californian margin similar to the positive and negative phases of the PDO along the modern Californian margin (Fig. 5.18). Alternatively, the 44 year peak may be tidally forced, as proposed by Berger and von Rad (2002), or may be a harmonic of the sunspot or Hale cycle. However, it is difficult to reconcile the presence of a multiple of the Perigee cycle in a spectrum devoid of peaks relating to the Perigee cycle itself (4.425 years) and its other prominent multiples (e.g. 17.7 years). The 44 year peak is therefore interpreted to relate to a PDO-like oscillation similar to that effecting the modern North Pacific and North America (Minobe, 1997; Biondi *et al.*, 2001; Chavez *et al.*, 2003), the frequency of which may have been modulated by solar variability.

5.4.5 *The Bjerknes feedback and a permanent El Niño state*

As discussed in Chapter 5.4.1.3 the Maastrichtian climate state and global configuration should theoretically have played host to a severe weakening of the "Bjerknes" feedback loop and caused a severe decline or cessation of ENSO variability. However, data presented here demonstrates that an oscillation analogous to ENSO was a robust feature of the Maastrichtian climate and consequently the Maastrichtian was not characterised by a permanent El Niño climate state, consistent with a fully coupled ocean-atmosphere simulation for the Campanian (Otto-Bliesner *et al.*, 2002). The concept of a permanent El Niño climate state was recently questioned by Huber and Caballero (2003) in view of two middle Eocene records that display significant variability within ENSO band frequencies (Ripepe *et al.*, 1991; Mingram, 1998) and have been supported by fully coupled climate model simulations, collectively demonstrating that ENSO variability was a robust feature during this “hothouse” climatic period (Garric & Huber, 2003; Huber & Caballero, 2003). This research therefore adds to evidence that warm end-member climate states do not tend to collapse into a permanent El Niño state and that ENSO variability is not only confined to the dynamic climate system of the Quaternary. Although the theory of a permanent El Niño does explain the characteristics of many past climates very satisfactorily, it cannot be used as an explanation for the Maastrichtian climate state.

5.5 CONCLUSIONS

- Spectral analysis of bioturbation index records and thickness variations in diatomaceous and terrigenous laminae reveal numerous significant spectral peaks within well known frequency bands of modern climate cycles.
- All parameters analysed demonstrate strong variance in the ENSO frequency band, which together with other sedimentological evidence indicates that similar to the later greenhouse climate of the Eocene, the latest Maastrichtian climate system was host to robust ENSO-like variability, adding to the body of evidence conflicting with the theory of permanent El Niño climate states.
- Mean ENSO periodicity in laminae thickness variations was 5.3 years and that of strong events 9.3 years (although strong events are only recorded in diatomaceous laminae).
- Bioturbation index records show an ENSO peak at 6.2 years and strong ESNO peaks of 10.3 and 10.8 years. The periodicity of the strong ENSO peaks in bioturbation index may have been modulated by solar variability. Similarities in the bioturbation index and diatomaceous laminae thickness records adds to the evidence that benthic oxygen levels were largely controlled by diatom export flux and that variability at decadal/ sub-decadal periods in the two records were forced by the same mechanism (ENSO).
- Pervasive quasi-biannual peaks are present in laminae thickness records, inferred to be related to a cycle analogous to the QBO. The mean periodicity of quasi-biennial peaks in the Marca Shale (27.4 months) and the modern QBO (28 months) is striking.
- Several multi-decadal peaks were identified in laminae thickness variations at 20.0, 26.5 and 44 years and inferred to relate to an oscillation analogous to the PDO. The 20.0 and 26.5 year peaks relate to the shorter period component of the PDO, whilst the 44 year peak may be a manifestation of the longer period component of the PDO. Both the ~20 year peaks and the longer 44 year peak may have been modulated by solar variability.

CHAPTER 6

High-Resolution Analysis of the CESAR 6 Microfabric, Diatom Floral Analysis and Biostratigraphy

6.1 INTRODUCTION

Unit 4 of core 6 of the 1983 Canadian Expedition to Study the Alpha Ridge (CESAR) comprises almost pure unconsolidated, superbly preserved diatom ooze with very little terrigenous material and exhibits distinct millimetre-scale colour laminations. The ooze is considered to be Late Cretaceous (Campanian-Maastrichtian) in age (Barron, 1985b; Bukry, 1985; Mudie, 1985; Firth & Clark, 1998). Only two other cores containing well-dated Cretaceous sediments have been recovered from the Arctic Ocean; Fletcher's ice island cores Fl-437 and Fl-533 also obtained from the Alpha Ridge. Core Fl-437 comprises a well-laminated diatom ooze, similar in aspect to that of CESAR 6. Laminations in Core Fl-437 and CESAR 6 have been interpreted to result from the alternating deposition of large diatom vegetative cells and smaller diatom resting stages, in response to pronounced seasonality (Kitchell *et al.*, 1986) and from changes in the iron content of the sediment, relating to proximal hydrothermal activity (Stoffyn-Egli, 1987), respectively. In contrast to the two diatom ooze deposits, core Fl-533 consists of a homogenous black, organic-rich mud of mixed terrestrial and marine origin (Clark *et al.*, 1986; Firth & Clark, 1998).

Despite the similarities between the CESAR 6 and Core Fl-437 sediments, there are conflicting interpretations of the origin of the two diatom oozes. Core Fl-437 is interpreted to have been deposited under a highly productive, upwelling cell with laminae forming annually (Kitchell & Clark, 1982; Kitchell *et al.*, 1986; Dell'Agnese & Clark, 1994). Growth of the vegetative cells is inferred to have occurred during the productive upwelling season with resting spore formation in response to environmental stress (Kitchell *et al.*, 1986). Barron (1985b), finding no evidence for any biostratigraphic changes, similarly interpreted the CESAR 6 diatom ooze to have been deposited rapidly under a highly productive environment and suggested laminae may be of seasonal origin. However, Mudie and Blasco (1985) and Mudie *et al*. (1986) were unable to find consistent floral differences between the colour laminations in the CESAR 6 core, from which they inferred that the laminations were not seasonal (unlike laminations in Core Fl-437). They therefore interpreted the diatom ooze to have been deposited slowly in an oxic, low productivity environment. On the basis of the palaeomagnetic data (Asku, 1985) Mudie *et al.* (1986) suggest this to have been over an interval of at least 10 Ma, with sedimentation rates no greater than 0.2 mm/ka. However, Asku (1985) concluded that the palaeomagnetic results were equivocal with respect to determining the sedimentation rate, and further suggested that the oxidisation of magnetite to hematite could have altered the primary remanence, making the pattern of reversals questionable. Recently, Firth and Clark (1998) concluded that the CESAR 6 and cores Fl-437 and Fl-533 all represent high palaeoproductivity, upwelling fuelled biogenic sediments.

In this study, the CESAR 6 diatom ooze is examined using an integrated high-resolution BSEI study to help resolve the nature of the laminae and palaeoenvironmental conditions governing their formation. Laminations are described and the sedimentary fabrics used to infer local and regional palaeoceanographic/palaeoclimatic conditions. The style of marine productivity governing the formation of the diatom ooze will also be addressed. Analysis of the diatom flora is conducted in order to help improve age constraints, by employing the new Arctic biostratigraphy of Tapia and Harwood (2002). The validity of the conclusions by Barron (1985b), that no diatom biostratigraphic changes are present in the diatom flora, will also be substantiated.

6.1.1 *Nature of the Alpha Ridge*

The Alpha Ridge ranges in width from 250-800 km and is roughly symmetrical in bathymetric cross-sections, with greatest elevation at the centre (Jackson *et al.*, 1986). Due to the relative inaccessibility of the Central Arctic Ocean, the nature and origin of the Alpha Ridge has long been a matter of debate. The structure has been variously interpreted as being continental in origin, a former spreading centre, the result of hotspot activity and a former region of subduction or compression (Sweeny *et al.*, 1978; Green *et al.*, 1984; Vogt *et al.*, 1984; Jackson & Johnson, 1985; Jackson *et al.*, 1990; Johnson, 1990; Johnson *et al.*, 1994; Lawver & Mûller, 1994). More recent studies favour the spreading centre or hotspot trail models (Lane, 1997; Jokat, 2003; Gurevich & Merkur'ev, 2005). In contrast to previous ice platform-based expeditions, the 1998 Arctic-98 expedition was the first geoscientific expedition to the Alpha Ridge to use surface ships. Using the powerful Russian nuclear icebreaker ‘Arktika’ in convoy with the German RV ‘Polarstern’, the RV ‘Polarstern’ was able to recover two multichannel seismic profiles along the Alpha Ridge and one parallel with the northern ridge slope. These data indicate that sediments conformably overlie the basement, with some evidence of extensional faulting, and range in thickness from 500-1200m (Jokat, 2003). A strong, broad, seismic reflector divides the sediments into two units, postulated to represent Cenozoic and Cretaceous sedimentation. Several basement samples have been recovered from the ridge escarpment, tentatively identified as alkali basalts, which based on immobile major and trace element contents have been interpreted as of oceanic, within-plate origin (Mûhe & Jokat, 1999). Whole rock Ar^{40}/Ar^{39} dating of the recovered basalt has yielded an age of 82 ± 1 Ma (Jokat, 2003). The velocity structure of the upper crust (which range from 4.3 to 6.7 km s^{-1}) and the seismic characteristics of the basement reflections indicate an oceanic origin of the Alpha Ridge. More recent international projects have provided the most reliable and complete data sets of the anomalous magnetic field in the Central Arctic, yielding three series of sea-floor spreading-type anomalies in the Alpha Ridge area and adjacent parts of the Canada Basin (Gurevich & Merkur'ev, 2005). These data indicate that the source rocks of these anomalies formed near three spreading centres, two in the axial Alpha Ridge and a third confined to its southern slope and adjacent Canada Basin, in the Late Jurassic-earliest Cretaceous. Spreading appears to have terminated by 140 Ma, and was followed by intraplate volcanotectonic activation of the oceanic floor (Gurevich & Merkur'ev, 2005). In combination, these new data provide little doubt as to the oceanic origin of the Alpha Ridge.

6.1.2 *Location and stratigraphy*

During the 1983 CESAR project a total of 16 piston and 14 gravity cores were recovered from a 240 km^2 section of the Alpha Ridge, from a research station installed on drifting sea ice. Core 6, collected from a water depth of 1365m at 85°49.8´N and 109°09.2´W (see Fig. 6.1) was the only core to recover Mesozoic sediment. CESAR 6 was obtained from an erosional surface on top of a fault block to the north of the Alpha Ridge, where a prominent subsurface seismic reflector lies very close to the sea bed (Mudie & Blasco, 1985). A total of 305 cm of sediment was cored, including four lithologically distinct units (Fig. 6.2). Deformation of the sediment was described along the contacts of the four units. Unit 1 (0-99 cm) consists of a brown silty to clayey mud characteristic of Neogene sedimentation in the Arctic Ocean (Mudie & Blasco, 1985). Unit 2 (99-111 cm) is composed of a hard, grey silty clay possessing sharp, irregular contacts with units 1 and 3. Unit 3 (111-134 cm), a reddish silty mud comprised mainly of iron stained feldspar grains, is mineralogically very similar to unit 2. Both units 2 and 3 are interpreted to be volcanic ash deposits, with unit 2 deposited in an oxygen-poor environment and unit 3 in a more oxygen-rich environment (Mudie & Blasco, 1985). Assigning precise ages to units 2 and 3 is difficult due to the scarcity of microfossils and palynomorphs, although both units 2 and 3 contain pollen and dinoflagellates of Eocene to Oligocene age (Mudie, 1985; Mudie *et al.*, 1986).

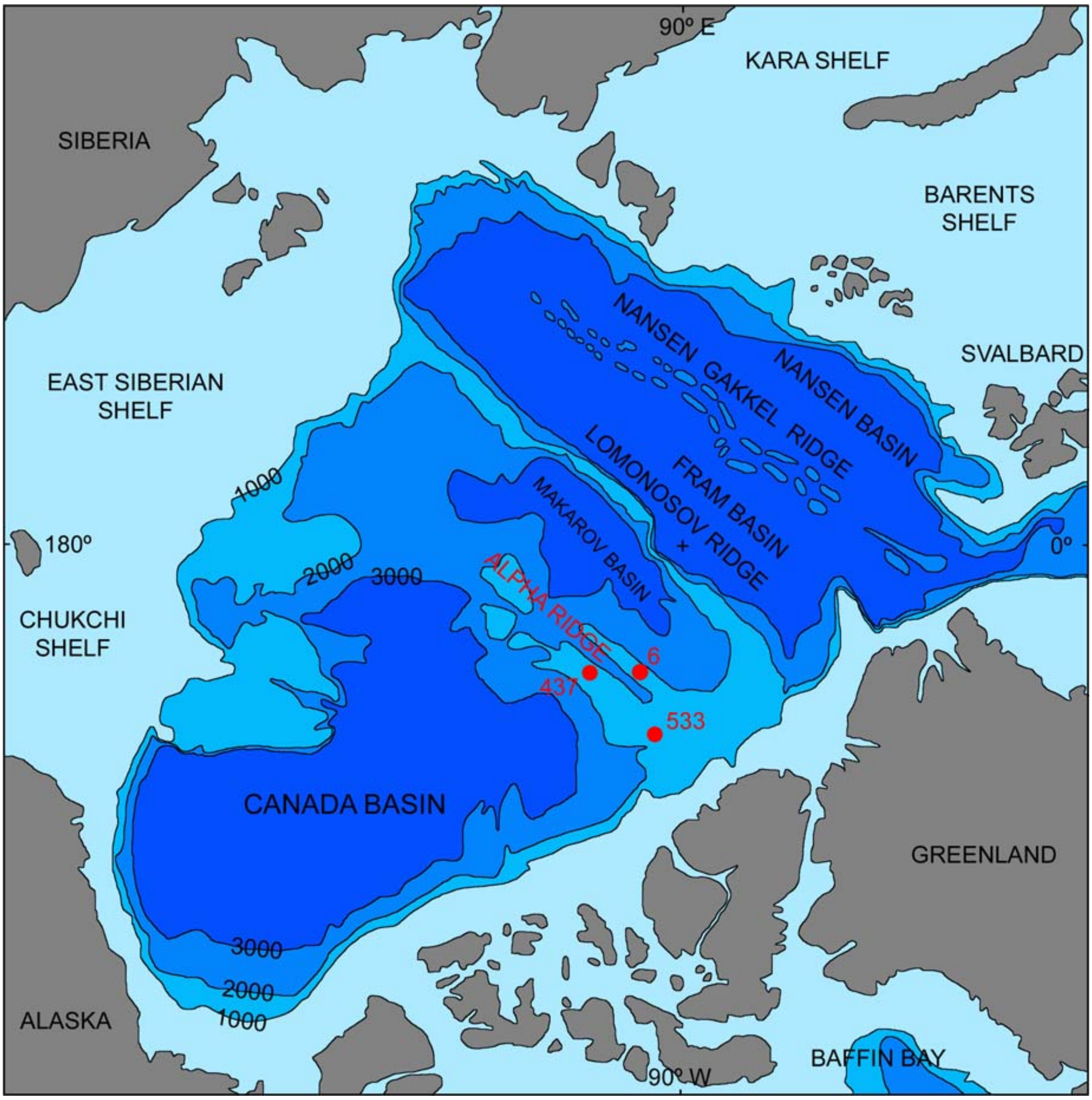

Figure 6.1. Bathymetric map of the Arctic Ocean illustrating the locations of the cores discussed in this chapter; CESAR core 6 and Fletcher Island (Fl) cores 437 and 533. Figure redrawn from Mudie *et al*. (1986). Depths shown are in metres. Cross shows the position of the North Pole.

Underlying volcaniclastic units 2 and 3, unit 4 (134-310 cm) is an uncompacted, laminated diatom ooze, comprised of exceptionally well-preserved diatom valves (Barron, 1985b) with occasional silicoflagellates and chrysophyte cysts. Siliceous valves are composed of primary opal-A (Mudie & Blasco, 1985) implying that the unit has not been subjected to burial greater than 400m (Isaacs, 1981) or heating above ~35 °C (Siever, 1983). Based on the preservation of Fe and Mn oxides, unit 4 was interpreted by Mudie *et al*. (1986) to have been deposited in an oxic environment. The age of the unit is regarded as Late Cretaceous, although encompassing the interval Late Campanian-Maastrichtian depending on whether diatoms (Late Campanian), silicoflagellates (Maastrichtian) or palynomorphs (Maastrichtian) are used as the prime biostratigraphic datum (Barron, 1985b; Bukry, 1985; Mudie, 1985; Firth & Clark, 1998). Distinct colour laminations, ranging from white to dark yellowish brown occur, a few mm or less in thickness are present and result from changes in the iron content of the sediment (Stoffyn-Egli, 1987). The Fe is probably in the form of poorly crystallised iron-oxihydroxides and by virtue of the concentrations of nickel, cobalt and copper with respect to hydrogenous ferromanganese minerals, the iron precipitates are interpreted to be of hydrothermal origin (Stoffyn-Egli, 1987). This interpretation is consistent with a tectonically active Alpha Ridge in the Late Cretaceous and with the recovery of bedrock, which appears hydrothermally altered (Van Wagoner & Robinson, 1985). Elongate black spots aligned parallel to colour laminations ~1 mm in diameter occur throughout the ooze, the result of abundant manganese microconcretions, 1-5 μm in diameter, interpreted to be bacterially-mediated (Stoffyn-Egli, 1987). The basal portion of unit 4 (subunit 4C, 305-296 cm) was noted to differ from the rest of the biosiliceous unit, possessing laminae with a characteristic grey hue, dipping at 30°. Mudie and Blasco (1995) were unable to ascertain whether the sedimentological changes at the top of subunit 4C related to coring or a hiatus.

6.1.3 *Description of the Cretaceous Arctic Ocean cores Fl-437 and Fl-533*

Core Fl-437, collected in 1969, is comprised of a well-laminated diatomaceous ooze with abundant silicoflagellates, chrysophytes and ebridians (Clark, 1974; Kitchell & Clark, 1982). The biosiliceous sediment has also been assigned a Campanian to late Maastrichtian age depending on which group is used as prime biostratigraphic indicator (Ling *et al.*, 1973; Bukry, 1981; Dell'Agnese & Clark, 1994). Diatom and silicoflagellate assemblages of the CESAR 6 and Fl-437 are essentially identical (Bukry, 1985; Dell'Agnese & Clark, 1994).

Core Fl-533, recovered in 1970, consists of a homogenous black, organic-rich mud, with a finely laminated upper 2 cm section, overlain by a yellow, organic-poor clay. The black mud averages 14% organic carbon (by weight) and is comprised of abundant amorphous material; woody fragments, leaf cuticles, spores and pollen along with abundant marine dinoflagellates cysts and is devoid of carbonate (Clark *et al.*, 1986). Hydrogen index and palynological data indicate that the organic matter is of mixed terrestrial and marine origin (Clark *et al.*, 1986; Firth & Clark, 1998). Biomarker analysis confirms a mixed origin of the organic matter and also indicates that diatoms were a significant part of the biota, even though there is no trace of their siliceous frustules (Jenkyns *et al.*, 2004). Initially interpreted to be of late Campanian or late Campanian to Maastrichtian age (Clark *et al.*, 1986; Clark, 1988), subsequent analysis of the acritarchs, prasinophytes and dinoflagellate cysts suggests that these muds are early Maastrichtian in age (Firth & Clark, 1998). The pristine state of the siliceous biota in both the CESAR 6 and Fl-437 cores, the lack of diagenetic alteration of the opal A and thermal immaturity of the marine organic matter (predominance of ββ-homohopane isomers) (Jenkyns *et al.*, 2004) in core F1-533 implies that all three sections have experienced minimal burial diagenesis.

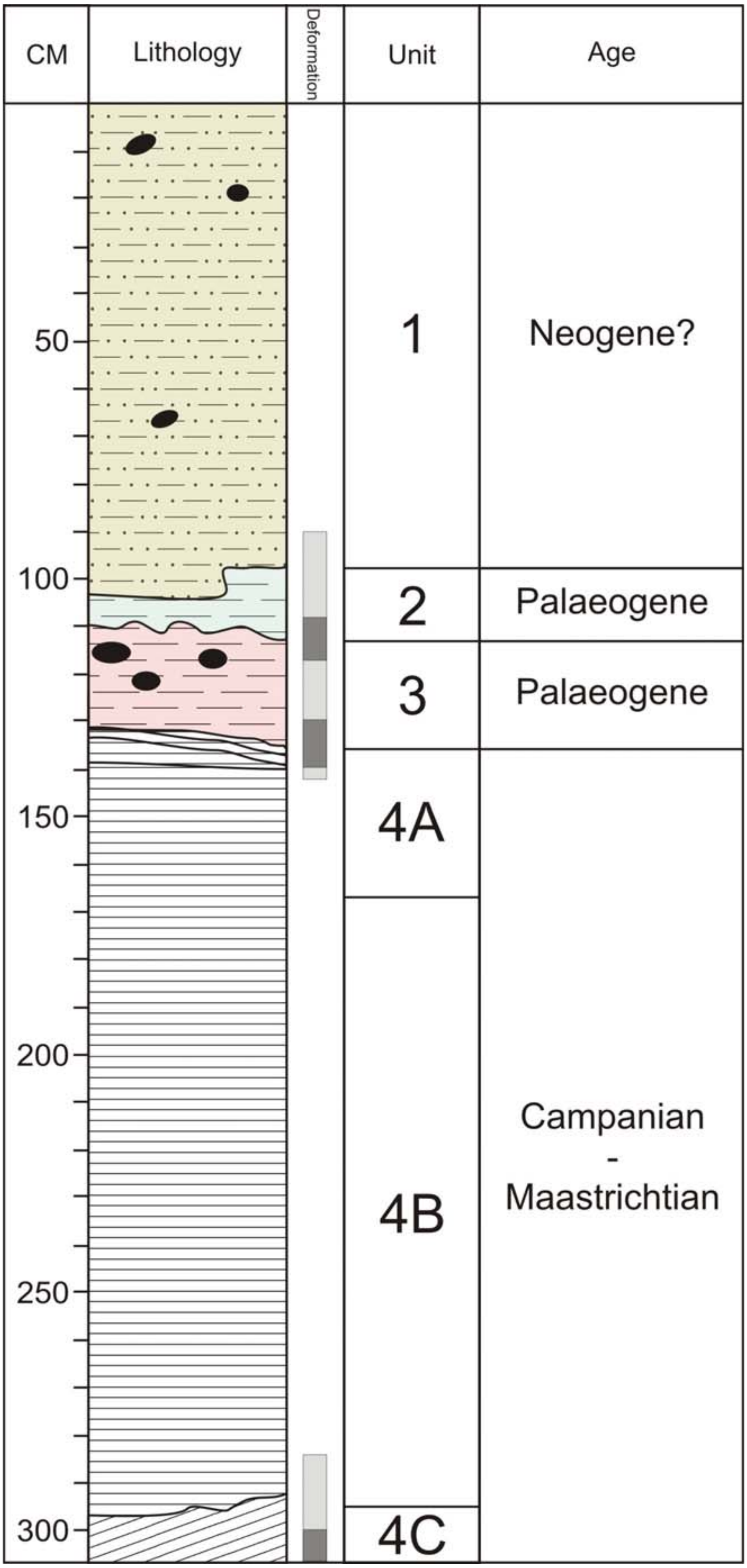

Figure 6.2. Generalised log of CESAR core 6, showing the four lithological units: 1) soft brown silty mud with occasional silt/fine sand laminae, 2) hard grey silty clay, 3) hard red silty clay and 4) laminated diatom ooze. Modified from Mudie and Blasco (1985).

Mudie and Blasco (1985) and Mudie *et al*. (1986) importantly pointed out that the two biosiliceous units lack abundant dinoflagellates and calcareous organisms. If all three Cretaceous cores represent upwelling fuelled sedimentation as Firth and Clark (1998) suggest, what factors influenced the formation of two markedly different lithologies? It has been suggested that the lack of dinoflagellates in the biosiliceous cores relates to prolonged oxidation, whilst the lack of calcareous organisms relates to either an elevated CCD or post depositional dissolution (Mudie & Blasco, 1985; Mudie *et al.*, 1986; Firth & Clark, 1998). Recently, direct evidence for the key role of anoxic conditions on the preservation of organic carbon-rich sediments has been gained from studies of Mediterranean sapropels (Moodley *et al.*, 2005). It is possible that all three cores were deposited in a silled anoxic basin, helping preserve the laminae and organic carbon, although in the biosiliceous cores, the organic carbon was subsequently oxidised. Strongly anoxic or dysaerobic conditions may have been the cause of the post-depositional dissolution of biosilica and carbonate.

6.1.4 *Palaeogeographic/ palaeoceanographic setting*

The abundance of resting spores and lack of shallow water (benthic) diatoms, along with the paucity of terrigenous material, led Barron (1985b) to suggest that deposition of the CESAR 6 diatom ooze occurred near a shelf or bank edge, distal from the shoreline. Dell'Agnese and Clark (1994) interpreted Core Fl-437 to have been deposited in deep water in an off-shelf environment, based on the same observations. Dropstones are absent from all three Cretaceous cores, suggesting an ice-free Arctic ocean at this time. Deposition of all three cores occurred along the eastern margin of the Late Cretaceous Arctic Ocean (Clark *et al.*, 1986) with Greenland and Svalbard the most proximal land masses (Fig. 6.3). However, the lack of a precise age constraint for the cores means that they cannot be unequivocally correlated; they may represent coeval sedimentation or they may alternatively represent successive episodes of pelagic deposition (Fig. 6.4). The two biosiliceous oozes are located 177 km from each other, and the two most distal cores (Fl-437 and Fl-533) are 288 km apart. Thus, if any are coeval it appears as though diatomaceous deposition occurred over a large area of the proto Arctic Ocean.

Figure 6.3. Diagrammatic reconstruction of the Arctic and the palaeo position of the CESAR 6 core (6) in a pre-Eurasian Basin configuration, adapted from Clark *et al.* (1986).

The Late Cretaceous Arctic Ocean does not appear to have possessed any deep-water connections, although transient deep-water connections may have existed with the Pacific during formation of the Canadian Basin (Hay *et al.*, 1999). The Arctic Ocean was also connected to epicontinental seas across Asia and North America (Hay *et al.*, 1999). The Western Interior Seaway is known to have had areas of locally reduced salinity (Cochran *et al.*, 2003) with some of its surface waters originating from the freshwater river systems draining the Sevier Orogenic mountain system (Hay *et al.*, 1993). During the Late Cretaceous, the southern Asian margin was a site of mountain building and much of the runoff from this continent would have been directed north, ensuring a high freshwater input into the Arctic (Hay *et al.*, 1999). It is therefore possible that the Arctic Ocean was less than fully marine at times, and this is supported by a fully coupled ocean-atmosphere Campanian simulation (Otto-Bliesner *et al.*, 2002). As revealed by cores recovered during the recent IODP 32 - ACEX expedition, later in its history, during the middle Eocene, for ~800,000 years the Arctic resembled a giant freshwater pond (Brinkhuis *et al.*, 2005). Simulations of the Campanian ocean suggest that much of the Arctic was characterised by salinities well below 30 ‰, with large areas below 24.7 ‰ (Hay & DeConto, 1999). Given the presence of such low salinity surface waters in the central Arctic Ocean, the formation of bottom waters would have been precluded. Instead the Cretaceous Arctic Ocean may have been characterised by well-stratified surface waters, similar to the Mediterranean during formation of sapropels (Kemp *et al.*, 1999).

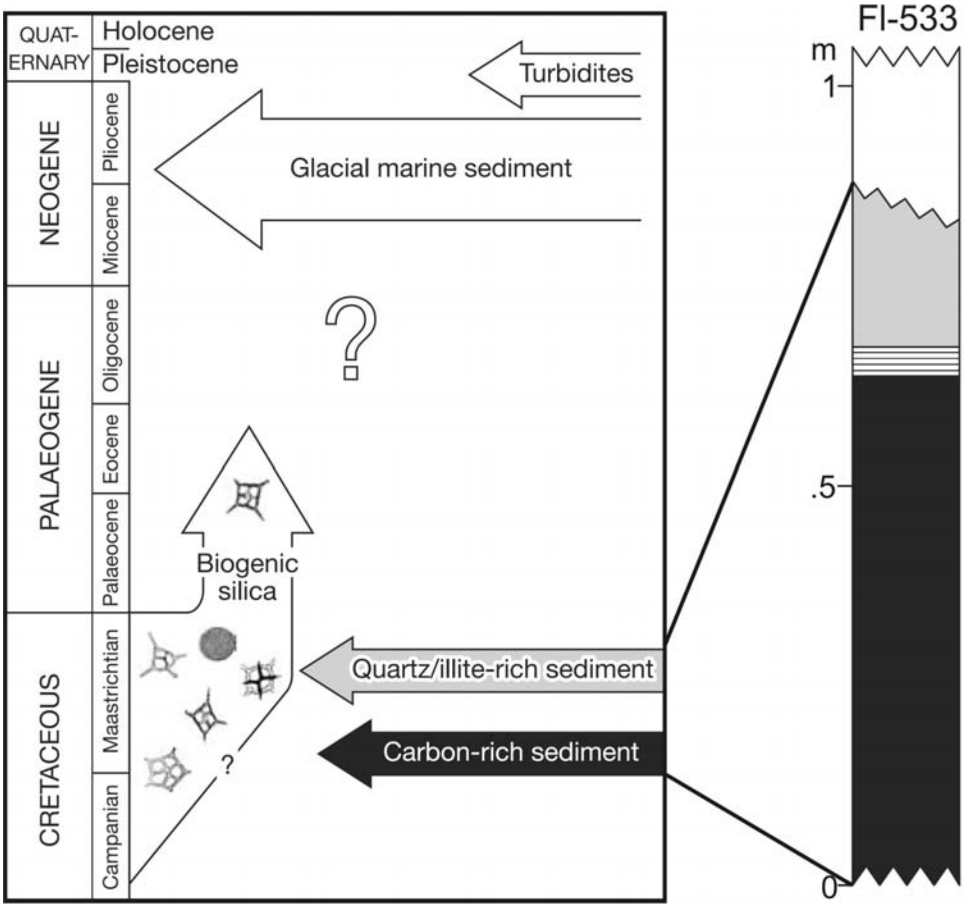

Figure 6.4. Interpreted stratigraphic relationships of the three Late Cretaceous cores obtained from the Alpha Ridge, Arctic Ocean, modified from Jenkyns *et al.* (2004).

It is generally interpreted that all three Cretaceous Arctic cores were deposited under relatively high productivity, upwelling fuelled conditions (Kitchell & Clark, 1982; Barron, 1985b; Kitchell *et al.*, 1986; Dell'Agnese & Clark, 1994; Firth & Clark, 1998). Kitchell and Clark (1982) interpret the biosiliceous ooze as the product of open-ocean upwelling, which they suggest was the consequence of large temperature contrasts between the land and the surface waters of the Arctic Ocean, relating to the different heat storage capacity of the land and the ocean (Fig. 6.5). During the Arctic winter, a cold land surface would have been juxtaposed against relatively warm polar sea surface temperatures, resulting in a pronounced low pressure system with corresponding cyclonic circulation, stimulating divergence and open-ocean upwelling in the central Arctic Ocean (Kitchell & Clark, 1982; Parrish & Curtis, 1982; Barron, 1985a). The situation would have reversed during the summer, when the temperature of the land surface is likely to have exceeded that of the surface of the ocean, causing coastal upwelling. There is no evidence to suggest that the pole of the Earths rotation was significantly different from that of the present. In fact, tree ring records from Campanian/Maastrichtian Arctic forests (75-85°N) indicate the area experienced a light regime similar to that of the present (Spicer & Parrish, 1990). Therefore, within the confines of ordinary Milankovitch parameters, the proto-Arctic Ocean would have experienced prolonged periods of total darkness and sunlight during the winter and summer, respectively, similar to that of today (see Fig. 6.6). Firth and Clark (1998) postulated that the differences in the three Cretaceous Arctic cores may relate to their proximity to the zone of upwelling, suggesting that cores Fl-437 and CESAR 6 may have been situated towards the centre of the upwelling cell, whilst core Fl-533 was more peripheral.

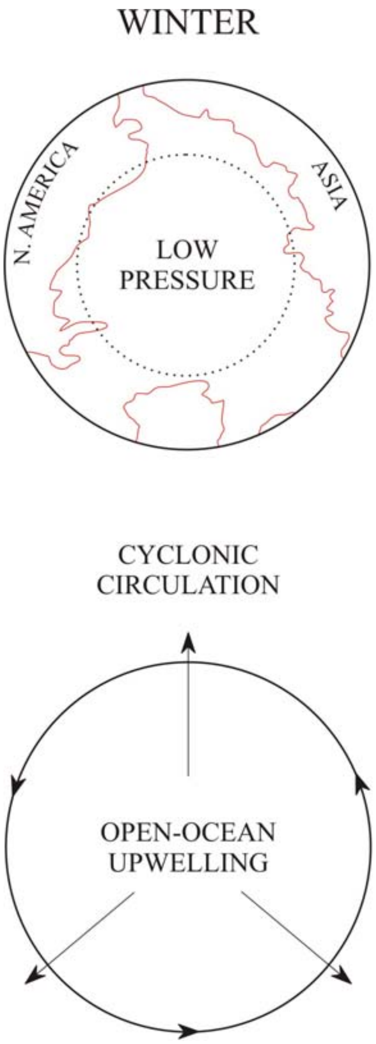

Figure 6.5. Inferred atmospheric conditions, ocean circulation and mode of upwelling for the ice-free late Cretaceous Arctic Ocean during the winter and summer, adapted from Kitchell and Clark (1982).

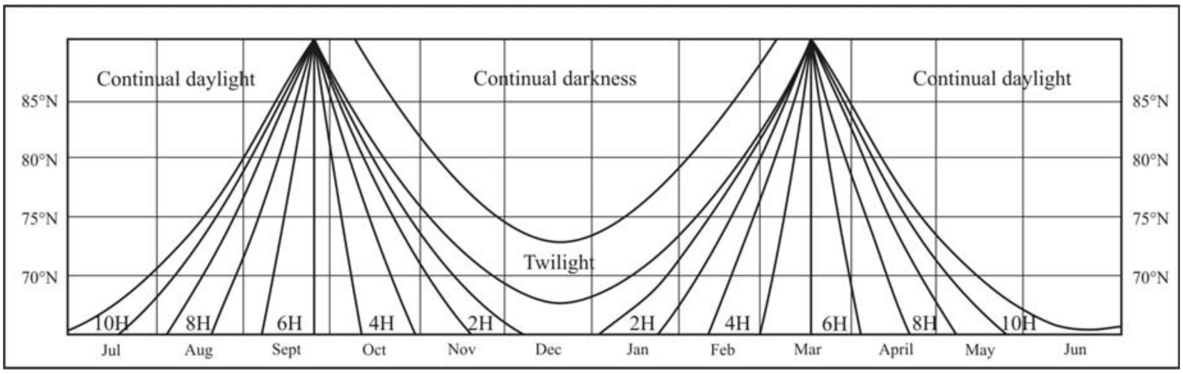

Figure 6.6. Graph illustrating the duration of daylight in the modern Arctic, redrawn from Herman and Spicer (1997).

6.1.5 *Late Campanian-Early Maastrichtian Climate*

Proxy data generally suggest that the climate of the Late Campanian-Early Maastrichtian was warmer than that of the Late Maastrichtian. A summary of the results of different studies into the Campanian-Early Maastrichtian climate system is given in Tables 6.1 and 6.2. Estimates of $p\mathrm{CO}_2$ are higher than those for the Late Maastrichtian, ranging between 2950-1000 ppmV (Ekart *et al.*, 1999; Nordt *et al.*, 2002; Nordt *et al.*, 2003). Mean SST's at low latitudes were higher than present, with estimates ranging between 27-32 °C (Wilson & Opdyke, 1996; Clarke & Jenkyns, 1999). A study of intra-shell δ^{18}O variations from a palaeolatitude of 8-14°N suggests SST's seasonally ranged between 27-35 °C (Steuber *et al.*, 2005). The climate system at this time was also capable of strong fluctuations; δ^{18}O records indicate a 5-6 °C global cooling of intermediate waters between 73-70 Ma, followed by a 2 °C warming between 70-68.5 Ma (Li & Keller, 1999).

As with the Late Maastrichtian, high latitudes were much more equable than at present, with forests extending well into the Arctic Circle. Analysis of leaf and vegetational physiognomy from Campanian/Maastrichtian Arctic forests (75-85°N) indicate the area experienced a MAT of 5 °C (Spicer & Parrish, 1990). As such, the latitudinal temperature gradient was less steep (0.4 ± 0.1 °C/°latitude) than at present (0.6 °C/°latitude) (Amiot *et al.*, 2004). Recently the extent of Late Cretaceous high latitude warmth was highlighted by TEX_{86} data from the organic matter in core Fl-533, interpreted to indicate a mean annual SST of ~15°C (Jenkyns *et al.*, 2004). However, the premise that the TEX_{86} temperature estimates represent a mean annual figure has been questioned. Wuchter *et al.* (2005) demonstrated that the Crenarchaeota responsible for producing the tetraether membrane lipids used in TEX_{86} palaeothermometry are sedimented seasonally. Although tetraether membrane lipids are found in higher amounts below 100m water depths, the signal preserved in the sediment does not correlate with TEX_{86} values from below the photic zone, but rather demonstrates a linear correlation with TEX_{86} values from the upper 100m. Therefore, the membrane lipids reaching the sediment primarily originate from the photic zone, where they are more effectively exported through packaging into fecal pellets and other marine aggregates. Crenarchaeota occur seasonally in surface water, during periods when the majority of phytoplankton are not blooming (Wuchter *et al.*, 2005). It is known that modern marine Crenarchaeota are most abundant in surface waters during the winter-spring (Wuchter *et al.*, 2005) and that in the eastern south Atlantic at least, surface sediments demonstrate the best correlation of TEX_{86} with winter SST's (Schouten *et al.*, 2002). Maintaining a SST of 15 °C during the Arctic winter, a period when there is complete darkness for several months appears highly improbable. However, as the flux of the Crenarchaeotal membrane lipids to the sediments is dependent on the flux of fecal pellets and other marine aggregates, TEX_{86} data may be in fact skewed towards a summer signal (A. Sluijs, personal communication, 2005). Therefore, it is probable that the ~15 °C TEX_{86} SST estimate of Jenkyns *et* *al*. (2004) is in fact a spring-autumn temperature and could possibly relate to peak summer SST's. Support for cooler high latitude temperatures comes from cobbles described from a low-energy, latest Cretaceous, high-palaeo latitude marine deposit in NE Asia (Chukotka) inferred to be ice-rafted dropstones (Ahlberg *et al.*, 2002) along with contemporaneous tree ring records at 75 °N that provide evidence for seasonal frosts (Falcon-Lang *et al.*, 2004). A Campanian fully coupled ocean-atmosphere model simulates the formation of small amounts of thin ice along the northern polar coastlines during the winter (Otto-Bliesner *et al.*, 2002). Jenkyns *et al*. (2004) stated that their TEX_{86} data indicated that the plant physiognomy data of Spicer and Parrish (1990) needed re-evaluating. More recent temperature estimates from Campanian high southern latitude forests suggest MAT's of ~ 15-23 °C (Francis & Poole, 2002; Poole *et al.*, 2005), although these estimates are from much lower palaeolatitudes (59-62°S) than core Fl-533 and the material studied by Spicer and Parrish (1990).

Author	**Study area**	**Climate information**	**Method used**
Ekart *et al.* (1999)	Compilation of data sets	pCO_2 of 2950 ppmV~ 75 Ma	Palaeosols
Nordt *et al.* (2002)	Canada	pCO_2 of 1400-1000 ppmV ~ 77 Ma	Palaeosols
Nordt *et al.* (2003)	Texas	pCO_2 of 1400 ppmV ~ 72 Ma	Palaeosols
Clarke & Jenkyns (1999)	Exmouth Plateau, Australia	Maximum palaeotemperature of 12.4-12.6 °C at 45-47°S during Late Campanian, with extrapolated maximum low latitude temperatures ~27-32 °C	$\delta^{18}O$ of fine-fraction and bulk sediments
Amiot *et al.* (2004)	Worldwide data set	Latitudinal gradient of 0.4 ± 0.1 °C/°latitude during the Late Campanian-Mid Maastrichtian. Polar temperatures ranged between ~ -10 and 0 °C and equatorial temperatures were ~ 30 °C	$\delta^{18}O$ of continental vertebrate apatite
Li & Keller (1999)	DSDP & ODP sites 463, 525, 577, 689 & 690	5-6 °C global cooling of intermediate waters between 73-70 Ma, followed by warming of 2 °C from 70-68.5 Ma.	$\delta^{18}O$ of foraminiferal tests
Steuber *et al.* (2005)	Jamaica and Oman	Mid-Campanian-Maastrichtian intrannual variation in SST between 27-35 °C at 8-14°N.	Intra-shell variations in $\delta^{18}O$
Wilson & Opdyke (1996)	Western Pacific	Equatorial SST of ~27-32 °C at ~69 Ma	$\delta^{18}O$ of exceptionally well preserved mollusc shells and cements

Table 6.1. A compilation of the results of general studies on the Late Campanian-Early Maastrichtian climate system.

Author	Study area	Climate information	Method used
Falcon-lang *et al.* (2004)	Ellesmere Island, Canada	Campanian/Maastrichtian climate at 75°N was temperate, with seasonal frosts and occasional floods	Growth rings in silicified wood
Spicer & Parrish (1990)	Northern Alaskan slope	MAT of ~ 5 °C in Maastrichtian at 75-85°N	Vegetational and leaf physiognomy
Poole *et al.* (2005)	Antarctic Peninsula	MAT of ~15 °C during the Late Campanian at 59-62°S	Leaf physiognomy and wood anatomy
Francis & Poole (2002)	Antarctica Peninsula	MAT of 16-23 °C at 59-62°S in Coniacian to early Campanian, followed by cooling into Maastrichtian	Dicotyledonous wood anatomy
Jenkyns *et al.* (2004)	Core Fl-533, Arctic Ocean	Mean annual SST of 15 °C at ~70 Ma	TEX $_{86}$

Table 6.2. A compilation of the results of studies on the Late Campanian-Early Maastrichtian climate from high latitude sites.

6.2 MATERIAL AND METHODS

6.2.1 *BSEI*

Overlapping polished thin-sections were made for the interval spanning 138 – 305 cm. Several peels were taken from the surface of the raw sediment and imaged using the SEM. Peels slides provided topographic images of the diatoms *in situ* with very little disturbance to the sedimentary microfabric. As microfabrics were analysed primarily from the cross-sectional images obtained from the polished thin sections, the peels greatly facilitated the task of identifying which diatom species occur in different fabric types. The polished thin sections used for BSEI were also imaged with a flatbed scanner at a resolution of 2400 dpi, in order to closely examine the colour laminations which had previously only been examined by visual description. The mineralogy of relatively coarse (< 30 μm) detrital grains was analysed by SEM-EDS, using a count time of 60 s, a spot size of 3 μm and a voltage of 20kV.

6.2.2 *Light microscopy and diatom floral analysis*

Strew slides were prepared from 19 samples of unit 4. To ensure several laminae were included in each slide, each sample was comprised of material homogenised from 1 cm of the core. Samples were taken at intervals of 10 cm, from 138 cm – 298 cm, with additional samples taken at 134 cm and 305 cm. Owing to the unlithified nature of the diatom ooze and lack of carbonate or clay, very little preparation was needed of the raw material, although test samples did react during digestion and it was found that better slides were obtained if organic matter was removed. Therefore, samples were digested and prepared using an adaptation of the method of Scherer (1994) (Claire S.

Allen, personal communication). Quantitative analyses were performed at 500×, with identifications checked at ×1000. Counts were made along several traverses of the cover slips.

6.3 RESULTS

6.3.1 *BSEI analysis of the laminated fabric*

Analysis of the microfabric was completed on polished thin sections from the interval 138 – 305 cm. However, due to problems with resin embedding of some samples, only a total of 58 cm of material from the interval 167.5 – 225.5 cm were able to be used in creating continuous detailed high-resolution BSEI records. The uncompacted, highly porous nature of the diatom ooze means that the carbon-based epoxy resin comprises much of the polished thin sections. The low backscatter coefficient of the resin along with the lack of detrital material results in the sediment having little contrast and being characteristically dark under BSEI. This makes distinguishing different laminae at low magnifications difficult and it was necessary to create high-resolution photomosaic base maps to be able to distinguish the compositional differences between successive laminae.

In contrast to the conclusions of earlier studies, unit 4 of the CESAR 6 core was found to contain a well-preserved, pervasive laminated succession of alternating diatomaceous vegetative cells and smaller, more heavily silicified resting stages (Fig. 6.7). These diatom vegetative/resting spore laminae are an order of magnitude thinner than the colour laminations visible on the core surface and described by earlier workers (Fig. 6.8). The colour laminations are independent of and overprint the compositional laminae (i.e. the diatom vegetative/resting spore laminae). In an examination of the lower ~ 1.6m of the CESAR 6 core, Mudie counted 900 individual colour laminations, yielding an average laminae thickness of ~1778 µm. Analysis of the high resolution flatbed scans of the polished thin sections used in this study (e.g. Fig. 6.8 a) reveal that dark coloured laminations range in thickness from 265-4636 µm (mean 980 µm) whilst pale coloured laminations range from 187-6536 µm (mean 769 µm). Consequently, the mean thickness of a dark-pale coloured laminae couplet is 1749 µm, half the figure obtained by visual inspection. In contrast, the mean thickness of vegetative cell laminae, resting spore laminae and the total couplet is 123.8 µm, 125.5 µm and 250.1 µm respectively (see Table 6.3). Using these figures, each dark-pale lamina couplet therefore contains on average 7 vegetative cell/resting spore laminae couplets. Any study into compositional differences between colour laminations would be unable to detect the alternating vegetative cell/resting spore laminations through too coarse a sampling resolution.

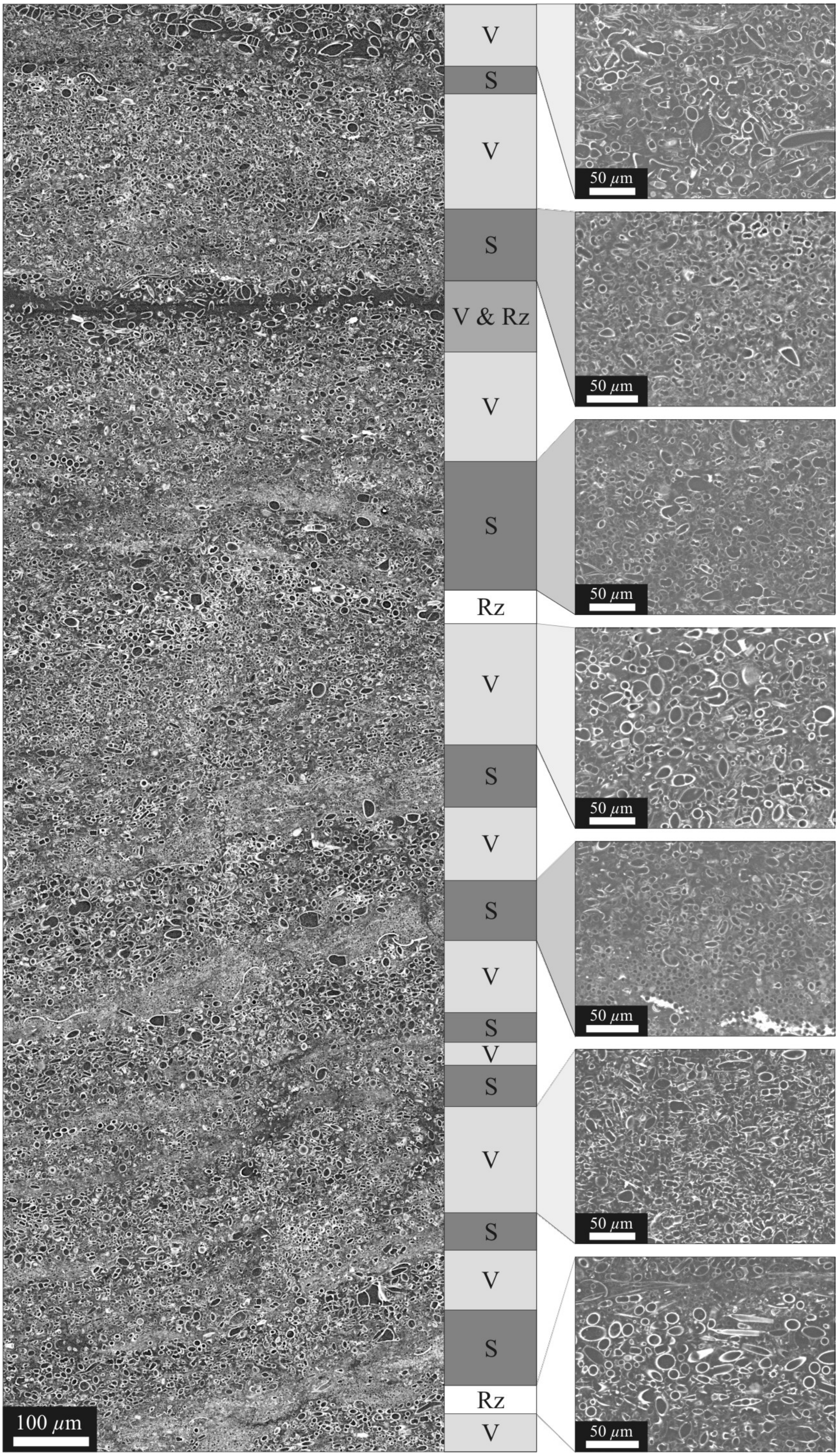
V
S
V
S
V & Rz
V
S
Rz
V
S
V
S
V
S
V
S
V
S
V
S
Rz
V
100 μm
50 μm
50 μm
50 μm
50 μm
50 μm
50 μm
50 μm
50 μm

Figure 6.7. (Above) BSEI photomosaic illustrating the pervasive alternation between diatom resting spore (S) and vegetative cell (V) laminae. Near-monospecific *Rhizosolenia* laminae (Rz) are also present, along with a lamina composed of a mix of large vegetative cells and valves of *Rhizosolenia* (V & Rz). Enlarged images of the laminated fabrics are shown on the left.

Several other lamina types are observed within the basic diatom vegetative cell/resting spore laminae laminated fabric, many of which are shown in Fig. 6.9. These include near-monospecific resting spore laminae, near-monospecific/monogeneric vegetative cell laminae, near-monospecific Rhizosolenia laminae, Silicoflagellate/setae-rich laminae and rare detrital laminae. A list of all the lamina types encountered during the study along with the mean thickness, standard deviation and absolute ranges is given in Table 6.3.

In a SEM EDS study, Stoffyn-Egli (1987) found that the colour differences between laminations are the result of changes in the iron content of the sediment, with diatoms in darker coloured laminae partially coated in very fine iron-rich material, whilst diatoms from paler laminae were mostly uncoated. Although the colour laminations are not generally discernable in BSEI, some of the darkest coloured laminae, where the iron coating is greatest do appear brighter the compositional laminae vegetative-resting spore laminations appear brighter (Fig. 6.10) in response to an increased backscatter coefficient (Goldstein *et al.*, 1992).

6.3.2 *Diatom vegetative cell laminae*

Diatom vegetative cell laminae are mainly comprised of a mixed assemblage, dominated by *Hemiaulus* spp. (mainly *H. antiquus* and *H. gleseri* and to a lesser extent *H. danicus* and *H. elegans*), *Trochosiropsis polychaeta* and *Anaulus sibiricus* (Fig. 6.11a), all of which occasionally form near-monospecific (or monogeneric in the case of *Hemiaulus*) laminae (Fig. 6.11b-d and Fig 6.12). Other less common forms are present, in variable amounts, within the mixed assemblage vegetative laminae, including *Actinoptychus* spp., *Coscinodiscus* spp., *Skeletonemopsis crawfordii, Stellarima* spp., S*tephanopyxis turris, Thalassiosiropsis wittiana, Triceratium* spp., *Trinacria* spp. and representatives of the pennate diatoms (primarily *Sceptroneis* spp.). Preservation of all valves is exceptional, with an almost complete lack of fragmentation or signs of dissolution. Valves often possess intact girdle bands and delicate ornamentation (e.g. the long, fragile processes of *S. turris* and branching marginal spines of *S. crawfordii*). Vegetative cell laminae also contain small quantities of *Rhizosolenia* (thick and thin form), *Hemiaulus* sp 1, *Hemiaulus tumidicornis* and other resting spores.

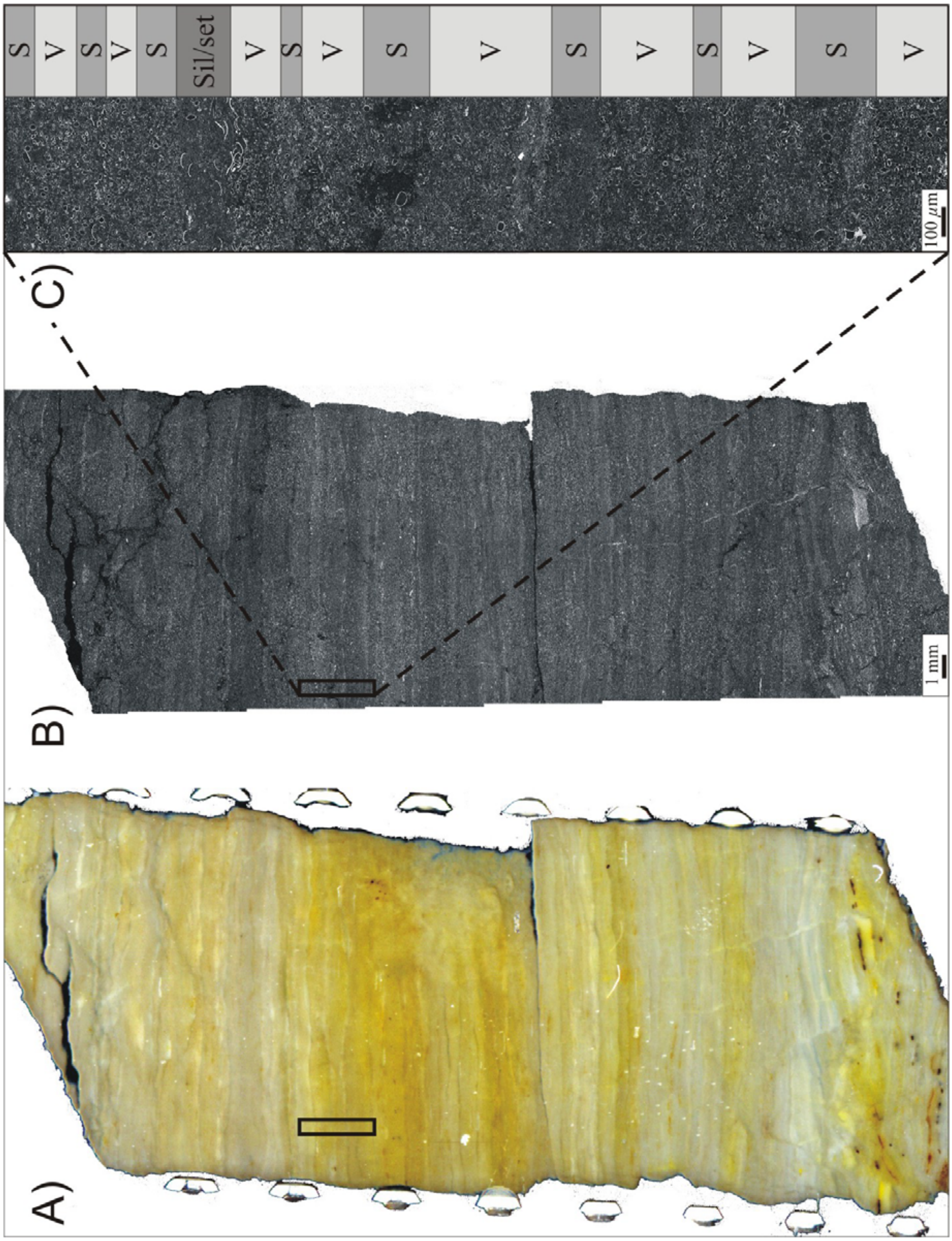

Figure 6.8. Comparison of a flatbed scan (A) and BSEI photomosaic (B) of slide K14. The relatively coarse colour laminations are clearly visible in the flatbed scan, although are not generally discernable in BSEI. However, in the BSEI photomosaic the finer scale resting spore/vegetative laminae can be observed, independent of the coarser colour laminations. To highlight this, an enlarged section of one of the dark coloured laminae is shown in (C) illustrating a succession of 18 individual compositional laminae. Laminations occur mainly as vegetative (V)/resting spore (S) couplets, although a laminae composed of silicoflagellates, setae/hash is also present (Sil/set).

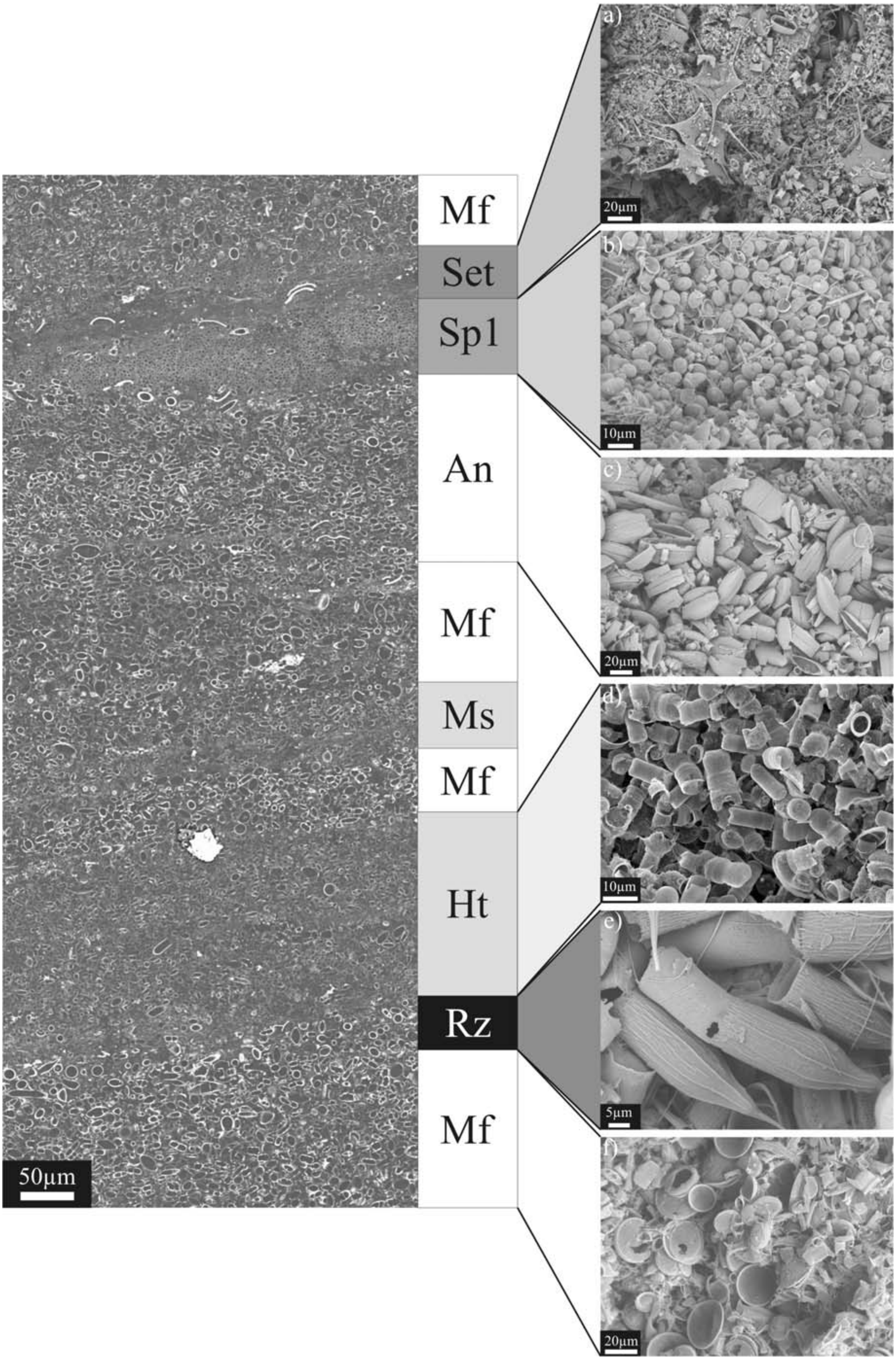

Figure 6.9. High-resolution BSEI photomosaic depicting the main lamina components, which are highlighted in topographic stub images. The two main laminae components are mixed floral diatom vegetative lamina (Mf) and mixed resting spore laminae (Ms). Near-monospecific vegetative laminae occasionally occur; show here by a near-monospecific lamina of *Anaulus sibiricus* (An). Vegetative laminae are commonly overlain by

near-monospecific *Rhizosolenia* laminae (Rz). Resting spore laminae may also occur as near-monospecific; composed of either *H. tumidicornis* (Ht) or Spore '1' (Sp1). Laminae rich in silicoflagellates/setae, diatom hash and containing a minor resting spore component (Set), are also a common component of the laminated fabric, and may occur within or instead of resting spore laminae.

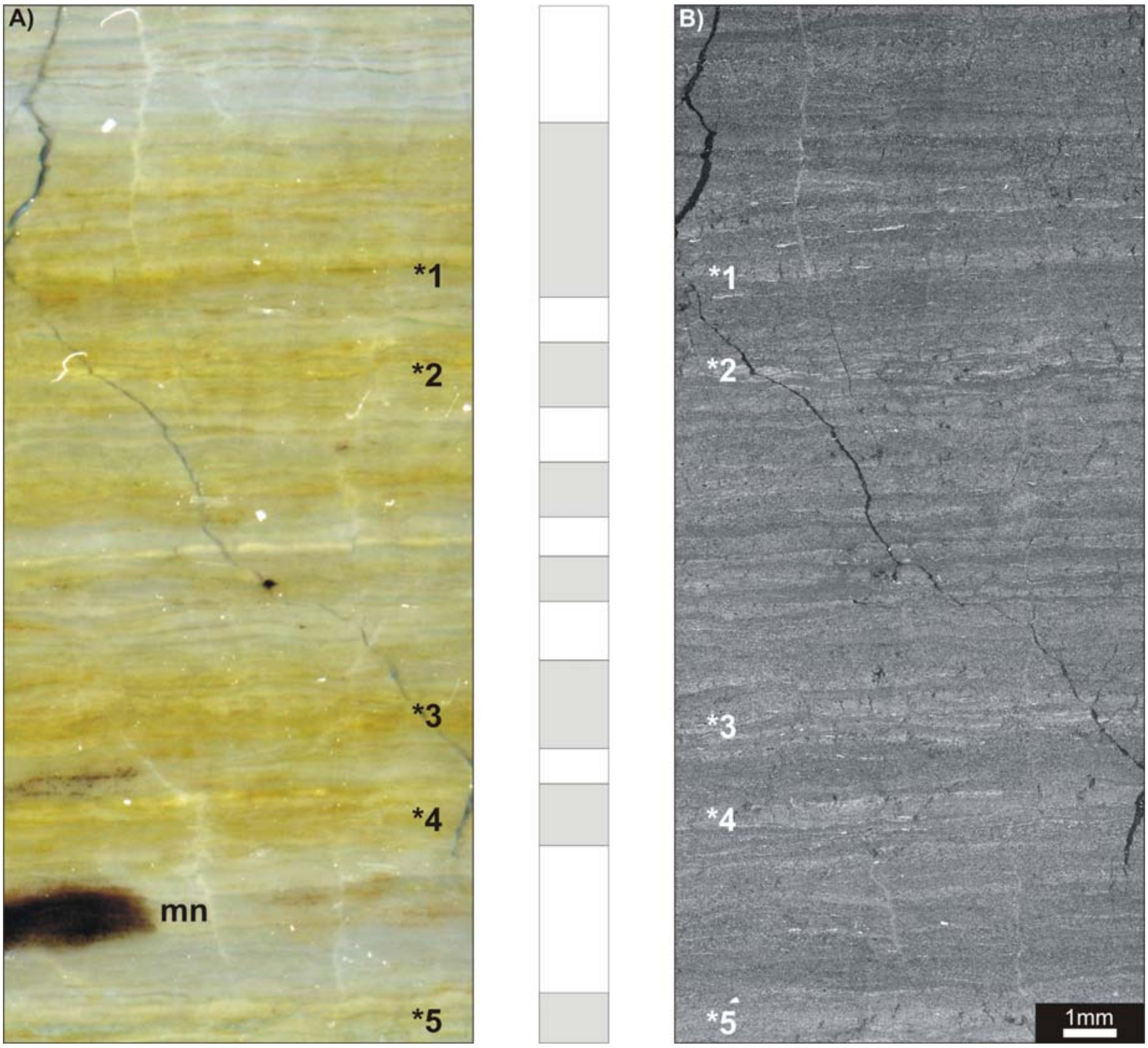

Figure 6.10. Comparison between a flat bed scan (A) and BSEI photomosaic (B) of slide K4 to illustrate the independence of the colour laminations from the compositional laminae. Note how the compositional laminae, seen in the BSEI photomosaic, are pervasive throughout the entire section, regardless of the colour laminations and that the colour laminations are not well represented in BSEI. However it can be seen that compositional laminae in some of the darker coloured laminae (*) have a brighter appearance, reflecting the higher concentrations of iron. Note also how the black spot (mn), relating to high concentrations of manganese microconcretions, is not evident in BSEI.

Laminae component	Mean thickness (µm) (s.d.)	Absolute ranges (µm)	Number of laminae
Mixed floral	124.8 (78.4)	612.4 – 15.3	1259
Monogeneric *Hemiaulus*	91.4 (48.5)	204.1 – 28.6	32
Monospecific *T. polychaeta*	129.7 (76.2)	408.1 – 26.8	73
Monospecific *A. sibiricus*	147.9 (93.6)	610.2 – 30.2	101
Mixed resting spore	140.8 (91.4)	796.7 – 15.0	804
Monospecific *H. tumidicornis*	130.0 (55.6)	264.2 – 39.8	66
Monospecific Spore ‘1’	82.0 (57.6)	518.9 – 14.4	519
Monospecific *Hemiaulus* sp. 1	131.1 (117.9)	697.4 – 24.8	36
Monospecific *Rhizosolenia*	70.6 (37.3)	275.4 – 21.8	81
Silicoflagellate/setae-rich	55.2 (35.3)	288.1 – 9.6	646
Monospecific *Stellarima* sp.1	44.0 (12.1)	57.9 – 36.2	3
Detrital laminae	36.8 (19.6)	50.7–23.0	2
Total vegetative ‘varve’ segment	123.8 (98.6)	1053.1 – 0	1679
Total spore ‘varve’ segment	127.5 (95.0)	852.2 – 0	1701
Total ‘varve’	250.1 (137.0)	1686.1 – 37.4	1693

Table 6.3. Number of each lamina type encountered during high-resolution BSEI, with the mean thickness, standard deviation (s.d.), and absolute ranges.

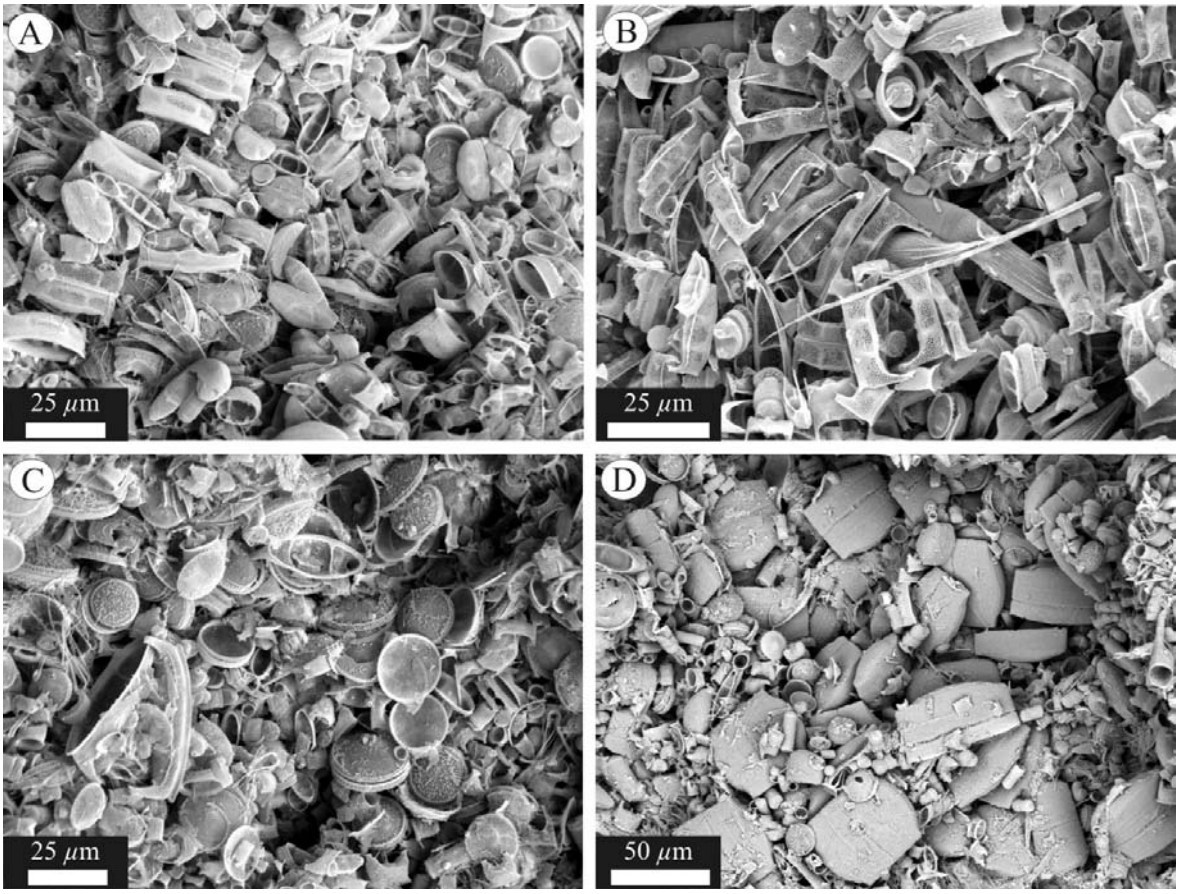

Figure 6.11. Scanning electron photographs of the four main diatom vegetative cell laminae types. A) Image of a mixed floral laminae taken from a peel slide. Near-monogeneric laminae of *Hemiaulus* (B), *Trochosiropsis polychaeta* (C) and *Anaulus sibiricus* (D) taken from topographic stubs.

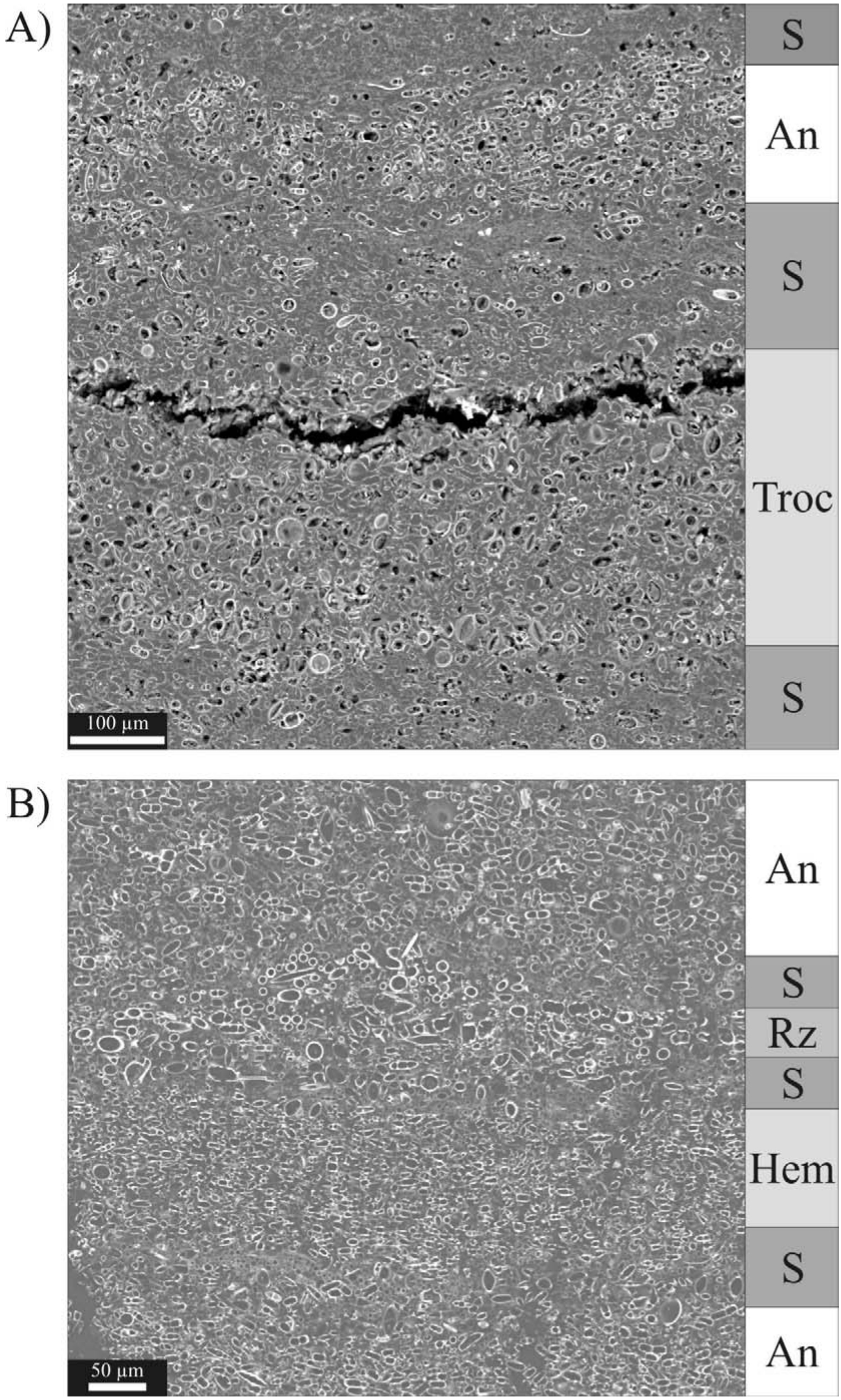

Figure 6.12. BSEI photomosaic depicting numerous laminae components. A) Several resting spore (S) laminae are observed, along with near-monospecific laminae of *Trochosiropsis polychaeta* (Troc) and *Anaulus sibiricus* (An). B) Resting spore laminae alternate with near-monospecific *A. sibiricus* laminae, along with a near-monospecific Rhizosolenia (Rz) and near-monogeneric *Hemiaulus* (Hem) laminae.

The mean thickness of the mixed floral laminae is 124.8 µm, with near-monogeneric/specific laminae of *Hemiaulus* spp., *T. polychaeta* and *A. sibiricus* possessing mean thicknesses of 91.4 µm, 129.7 µm and 147.9 µm respectively (Table 6.3). The appearance of vegetative laminae in BSEI is dependant on the floral compositions. Valves of *T. polychaeta* and *A. sibiricus* are relatively heavily silicified and laminae dominated by these forms have a relatively bright appearance. Valves of *Hemiaulus* tend to be more lightly silicified and hence near-monogeneric *Hemiaulus* laminae generally appear darker.

6.3.3 *Diatom resting spore laminae*

Diatom resting spore laminae can be divided into three primary varieties; mixed assemblage laminae (Fig. 6.13a) and near-monospecific laminae of Spore '1' (Fig. 6.13b) and *Hemiaulus tumidicornis* laminae (Fig. 6.13c). The most common resting spore laminae type are the mixed floral laminae (mean thickness = 140.8 µm), which are composed of a mixture of Spore '1', *H. tumidicornis* and a minor component of Spore '3' and *Skeletonema subantarctica*. Preservation of the valves in resting spore laminae is also exceptional, with delicate ornamentation (e.g. the long filaments branching from valves of *S. subantarctica*) intact. Near-monospecific laminae of Spore '1' (mean thickness of 82.0 µm) occur frequently throughout the studied sections, readily distinguishable through their brighter appearance in BSEI owing to the tight packing of the small spores. The least common of the three primary resting spore laminae are composed of near-monospecific *H. tumidicornis*, which have a mean thickness of 130.0 µm. There also occur rarer laminae composed of near-monospecific *Hemiaulus* sp. 1 (Fig. 6.13d), which possess a mean thickness of 131.1 µm. Chrysophyte cysts are often present within all types of resting spore laminae, although are most common in near-monospecific Spore '1' lamina along with variable amounts of vegetative cells. Very rarely, near-monospecific laminae of the chrysophyte cyst *Acanthosphaeridium reticulatum* are observed. Occasionally, multiple resting spore laminae occur instead of the normal vegetative/resting spore laminae alternation where vegetative laminae are missing from the laminated succession. Multiple resting spore laminae can be recognised by a succession of different resting spore laminae types, often separated by silicoflagellate/setae-rich laminae.

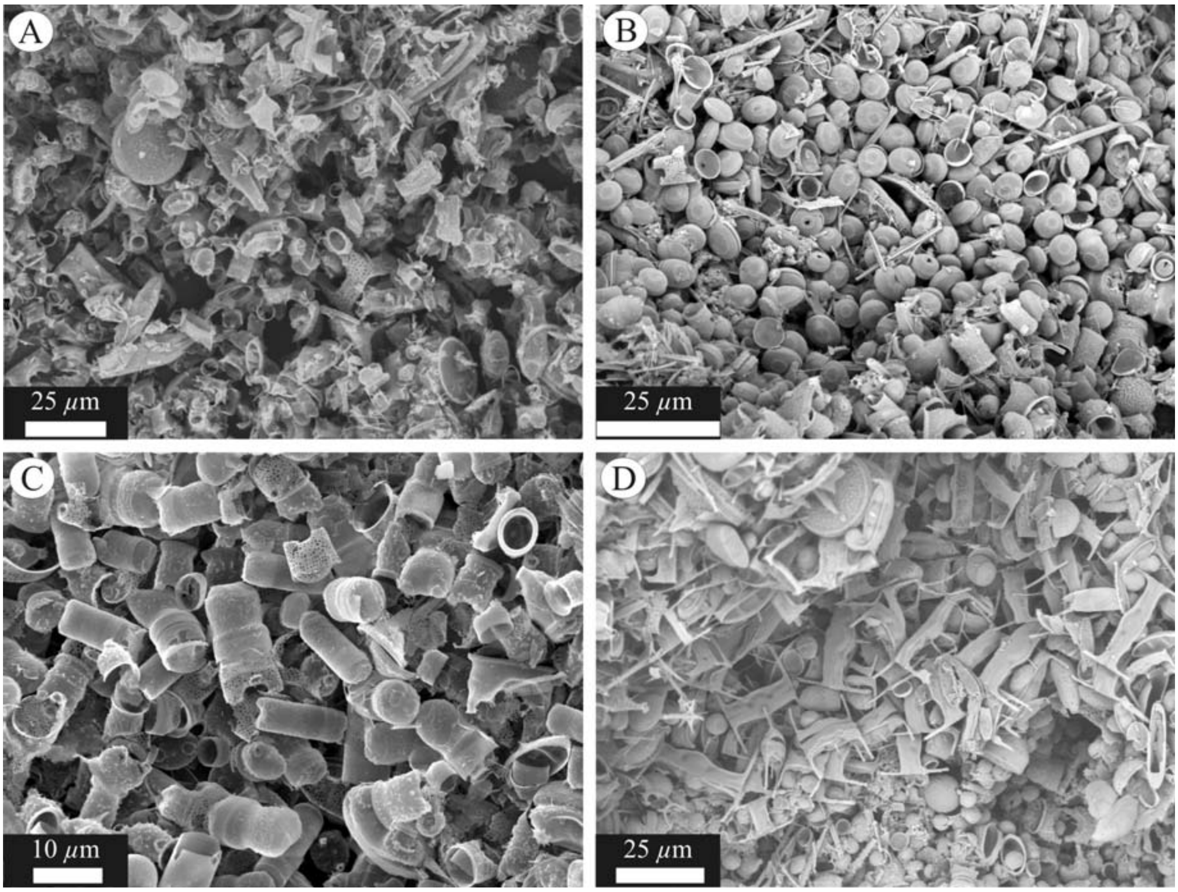

Figure 6.13. Scanning electron photographs of the four main diatom resting spore laminae types. A) Image of a mixed spore laminae taken from a peel slide. Near-monospecific laminae of Spore ‘1’ (B), *Hemiaulus tumidicornis*, showing some of the vegetative cells of this species (C) and *Hemiaulus* sp1, overlying a near-monospecific Spore ‘1’ laminae (D) taken from topographic stubs.

6.3.4 *Silicoflagellate/setae-rich laminae*

Silicoflagellate/setae-rich laminae are distinguished by the abundance of silicoflagellate skeletons and setae of various origins (Fig. 6.14) and constitute the third most common laminae type in the studied sections. They are frequently observed occurring along the top of vegetative cell laminae and base of spore laminae (Fig. 6.15). Silicoflagellate/setae-rich laminae are associated with resting spore laminae (Fig. 6.9 and Fig. 6.15) and contain a significant but variable resting spore component. Unlike all other lamina types, they also contain a component of fragmented diatom valves, which occasionally forms a diatomaceous hash matrix (Fig. 6.14). The diatom hash and fine setae reduce the porosity of this laminae type and as such they are characterised by a comparatively high backscattered coefficient. A small proportion of the setae originate from the detached tips of the silicoflagellate skeletons (Fig 6.16a), which are easily identified by means of their heavily silicified nature, tubular shape and relatively large size. A significant proportion of “setae” are actually comprised of sponge spicules (Fig. 6.16b), of which numerous morphologies occur. Valves of *P. cretacea*, recognised by their hexagonal cross-section, alternate columns of perforations and curved shape, are relatively abundant (Fig. 6.16c). The disarticulated horns of *Hemiaulus* (Fig.

6.16a) and valves of *Gladiopsis* spp. also comprise a small proportion of the setae. There also occur common extremely fine setae (<1 μm in diameter) that tend to form intertwined masses (Fig. 6.16d). Although the origin of these setae is unknown, they bear a striking resemblance to modern *Chaetoceros* spp. setae, which are often found associated with resting spores (e.g. Bull *et al.*, 2000; e.g. Dean, 2000a). Setae are occasionally observed forming pelletal aggregates in topographic stubs with inclusions of fragmented diatoms (Fig. 6.17).

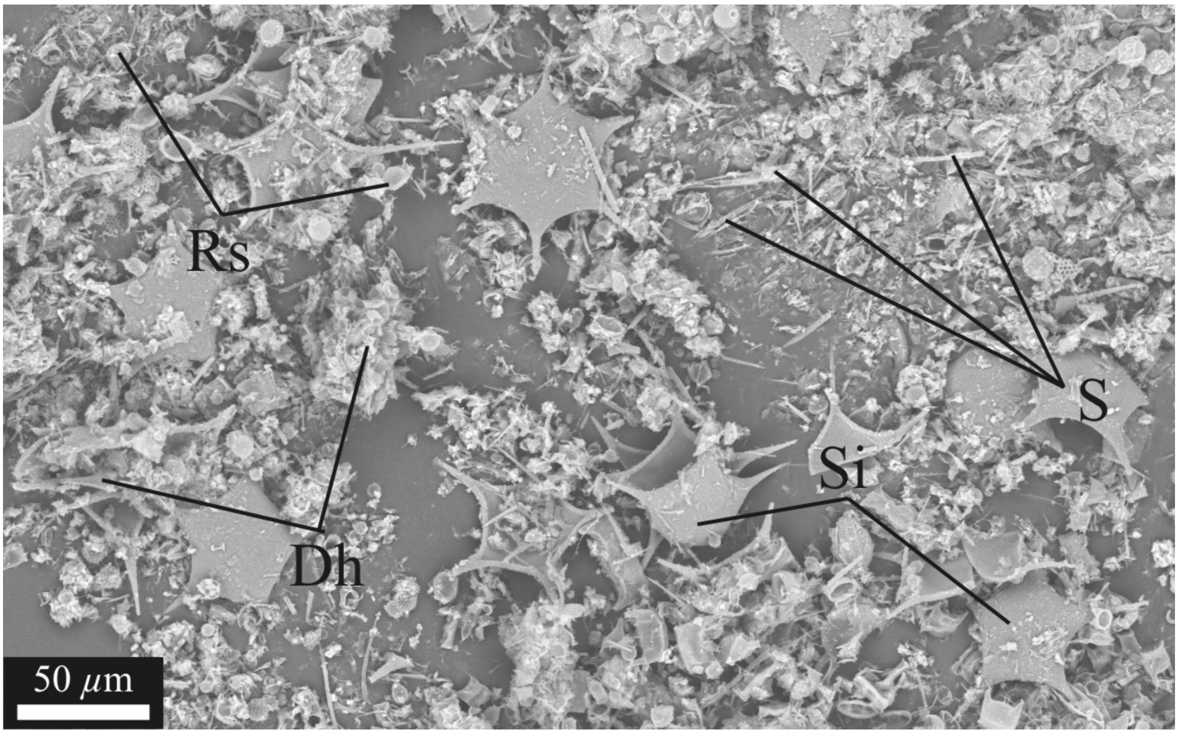

Figure 6.14. Scanning electron photograph of a silicoflagellate/setae-rich laminae from a peel slide depicting numerous silicoflagellate skeletons (Si) and setae (S) along with many diatom resting spores (Rs) and a matrix of diatom hash (Dh).

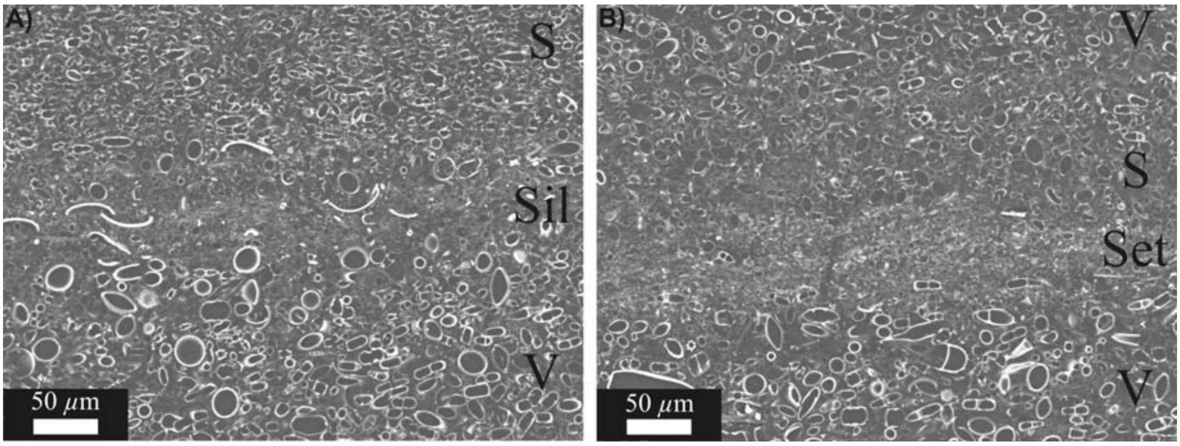

Figure 6.15. BSEI photographs showing that the silicoflagellate (Sil)/setae (Set)-rich laminae occur along the top of the vegetative cell (V) laminae and base of the resting spore (S) laminae.

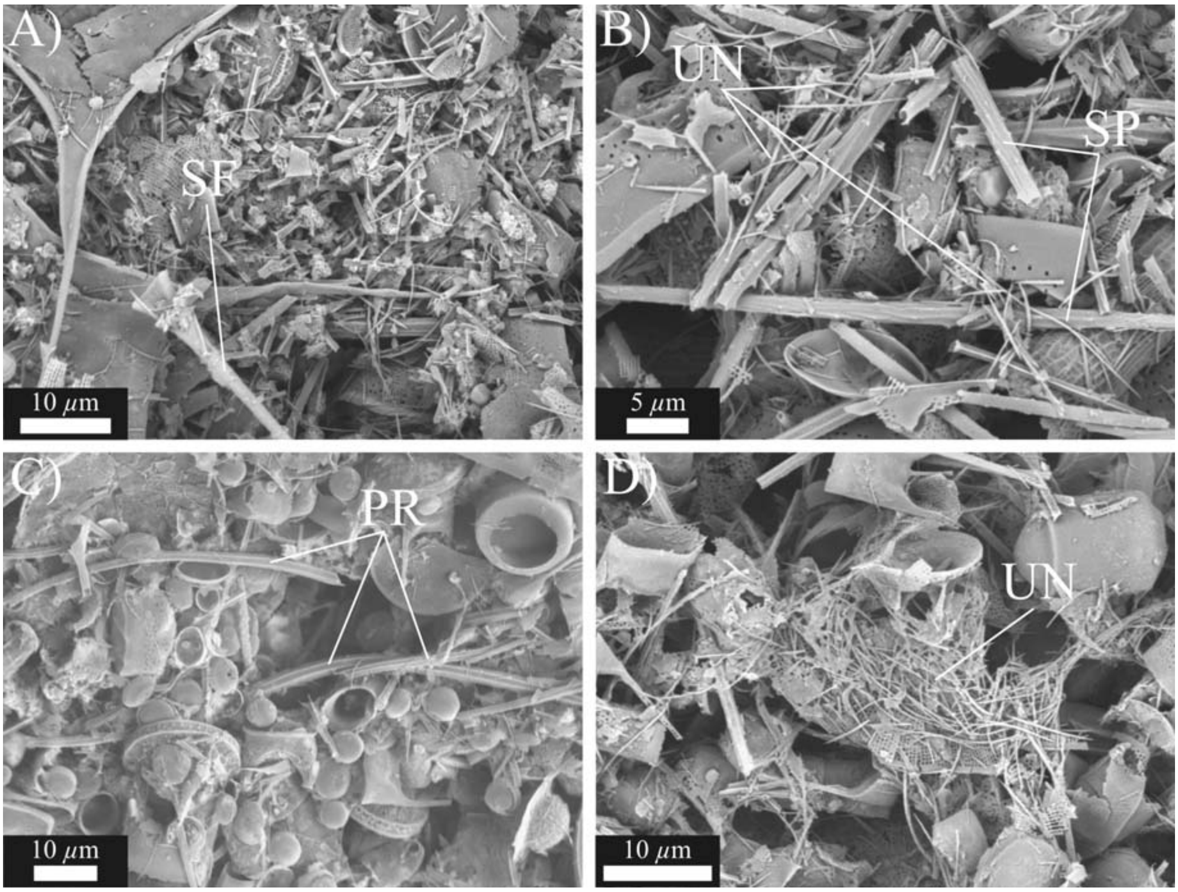

Figure 6.16. High magnification BSEI of the main types of setae within silicoflagellate/setae-rich laminae. A – Large disarticulated silicoflagellate spine (SF) amongst a matrix of other forms of setae and diatom fragments. B – Several large, robust sponge spicules (SP), along with the extremely fine setae of unknown origin (UN). C – Valves of *Proboscia cretacea* (PR) amongst numerous valves of Spore '1'. D – Intertwined mass of the extremely fine setae of unknown origin (UN).

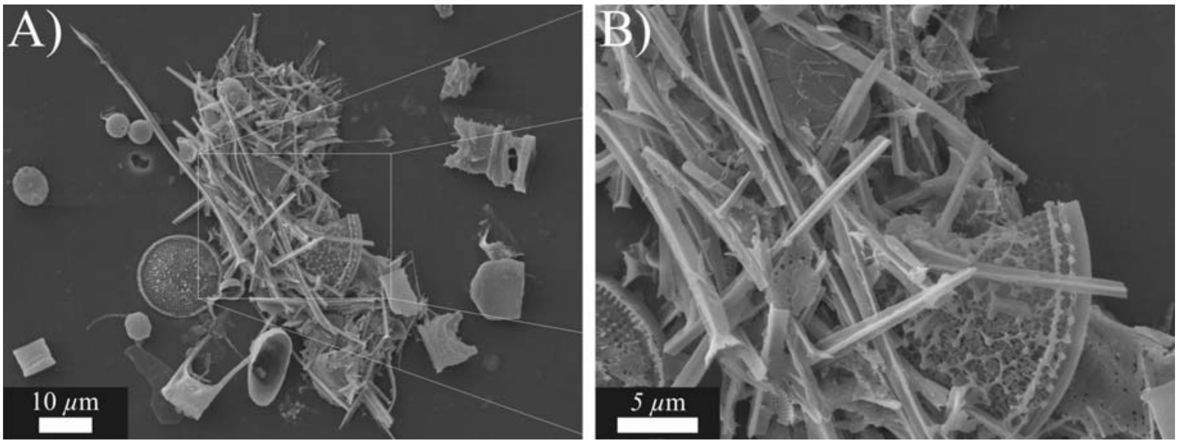

Figure 6.17. A) High magnification BSEI of a pellet shaped concentration of sponge spicules, which was sedimented onto a topographic stub when preparing strew slides. B) Enlarged section of A), depicting the fragment of *T. polychaeta*.

6.3.5 *Near-monospecific Rhizosolenia laminae*

Although vegetative laminae may contain scattered valves of *Rhizosolenia*, valves of *Rhizosolenia* are often observed to form near-monospecific concentrations along the upper margin of vegetative laminae, which are occasionally sufficiently numerous to form discrete laminae (Fig. 6.7, 6.9 and 6.12b). Owing to the thick siliceous frustules of *Rhizosolenia*, these laminae have a characteristically bright appearance in BSEI. Near-monospecific laminae of *Rhizosolenia* are relatively thin, with a mean thickness of 70.6 µm.

6.3.6 *Near-monospecific Stellarima sp. 1 laminae*

Stellarima sp.1 comprises a rare but consistently occurring component of the laminated succession and is rarely observed to form near-monospecific laminae, averaging 44.0 µm in thickness (see Table 6.3). Although only seldom forming near-monospecific laminae, valves of *Stellarima* sp.1 always occur in concentrations within individual laminae. Analysis of which laminae types contain these concentrations reveals that *Stellarima* sp. 1 exhibits a strong preference towards resting spore laminae, with 59.7% of the concentrations within mixed spore, Spore '1' or near monospecific *H. tumidicornis* laminae (Table 6.4). However, silicoflagellate/setae-rich laminae are found associated with resting spores and if included as resting spore laminae, 96.3% of the observed concentrations of *Stellarima* sp.1 occur within the resting spore 'varve' segment of the laminated succession. Valves of *Stellarima* sp.1 are not randomly distributed throughout resting spore laminae however, but are observed to form concentrations either towards the base or top of the lamina (Fig. 6.18).

Percentage of the occurrence of *Stellarima* sp.1 valves in each lamina type

MS	**Spore '1'**	**Sil/set**	***H. tumidicornis***	***Rhizosolenia***	**MF**	***Stellarima* sp. 1**
31.7	27.4	36.6	0.6	0.6	1.8	1.2

Table 6.4. Summary of the occurrence of concentrations of valves of *Stellarima* sp. 1 within the different lamina types. MS = Mixed spore laminae, Sil/set = silicoflagellate/setae-rich laminae, MF = Mixed floral laminae, *Stellarima* sp.1 = near-monospecific laminae of *Stellarima* sp.1. (n=164).

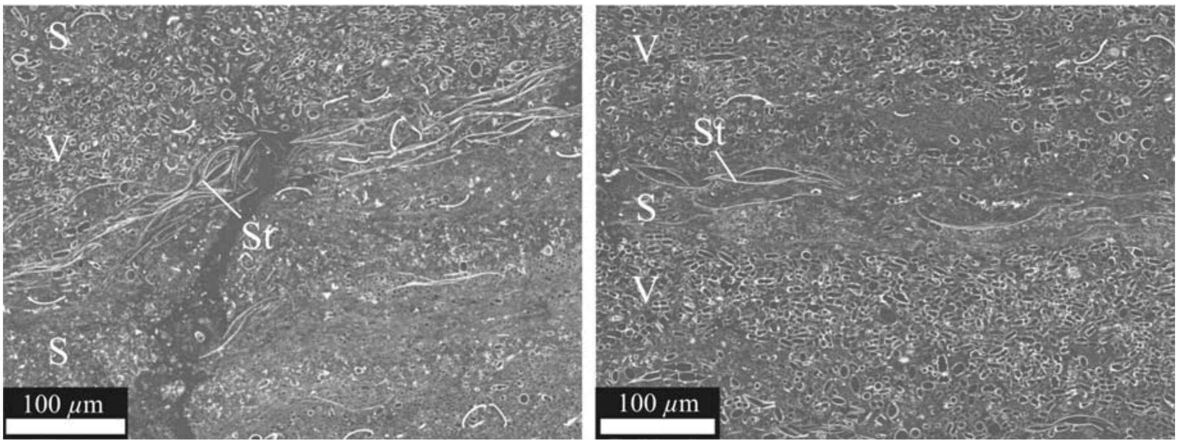

Figure 6.18. BSEI of *Stellarima* sp.1 (St) concentrations in polished thin sections. Diatom vegetative cell (V) and resting spore (S) laminae are highlighted. Note how the concentrations occur exclusively within the resting spore laminae.

6.3.7 *Clay/silt-rich 'blebs' and rare detrital laminae*

Small, elongate 'blebs', composed of clay and silt/fine sand occur commonly throughout the studied sections and range up through discontinuous laminae into rare detrital laminae. Clay blebs (Fig. 6.19a-b) have a mean length and height (measured in cross section) of 132.6 μm and 20.0 μm respectively. SEM-EDS analysis has revealed that the silt/fine sand sized grains are primarily composed of quartz and feldspar supporting earlier work by Mudie *et al*. (1986). Grains are angular, ranging up to 290 μm in diameter with a mean length and height of 87.5 μm and 47.0 μm, respectively. Some grains appear to be volcanic glass shards. These grains are vesicular, although the vesicles are frequently infilled with clay and/or smaller silt grains (Fig. 6.19c). Diatomaceous material is completely absent from all blebs, although valves from the surrounding diatomaceous material are often compressed into their margins (Fig. 6.19b). Rarely, the detrital material form discrete laminae (mean thickness = 36.8 μm) within the succession, primarily comprised of clay and very fine silt with random coarser clasts of feldspar, quartz or volcanic glass interspersed within the finer matrix (Fig. 6.20). It is apparent that the terrigenous material is not evenly distributed amongst the different lamina types, but is clearly concentrated within resting spore laminae (Table 6.5). Resting spore laminae (mixed and near-monospecific *H. tumidicornis* and Spore '1') contain on average 62.8% of the terrigenous material in the studied sections, whilst vegetative laminae (all types) contain only 19.5%. However, if silicoflagellate/setae-rich laminae are included, resting spore laminae contain an average of 77.9% of the terrigenous material.

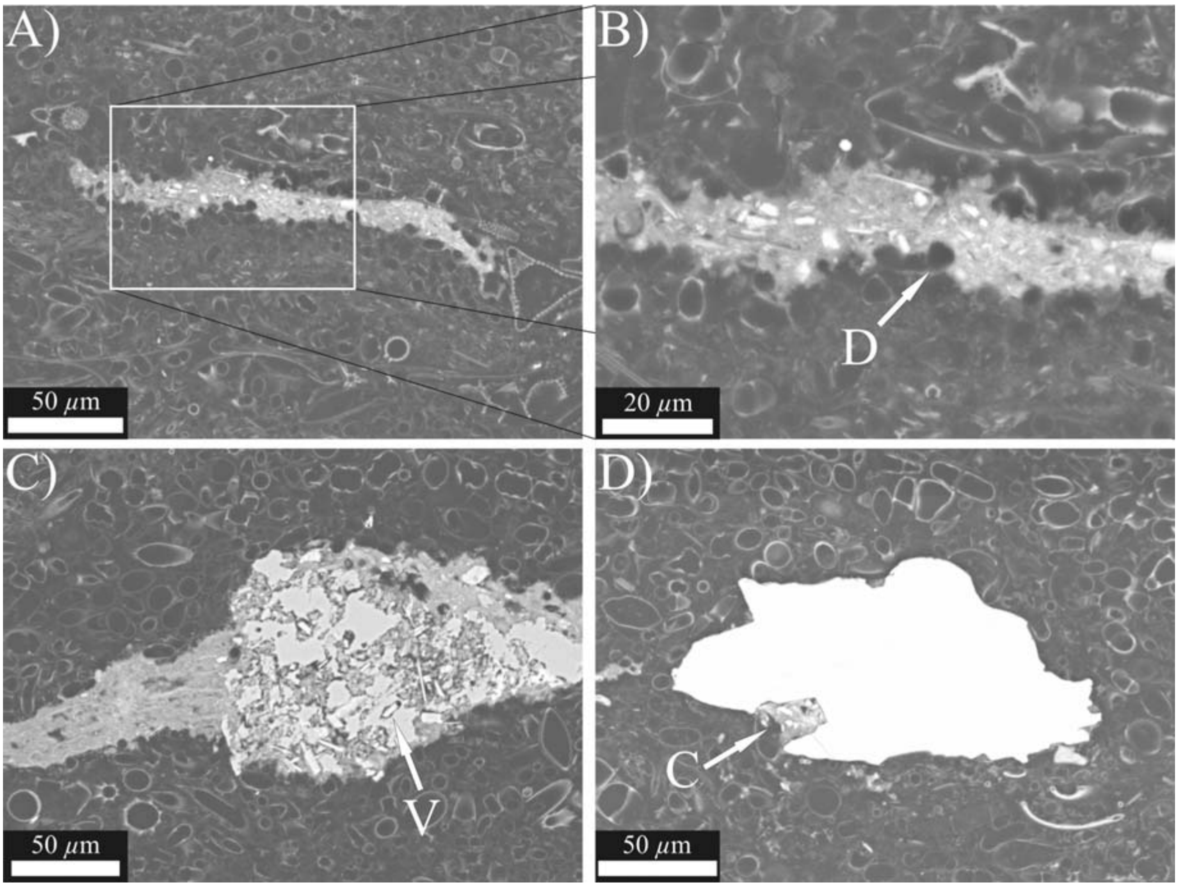

Figure 6.19. BSE images of the non-biogenic components of unit 4 of CESAR 6. A) Elongate clay-rich ‘bleb’ containing fine silt grains and no diatomaceous material, although surrounding valves (D) are characteristically compressed into the margins (B). C) Clay bleb with a core rich in vesicular glass shards (V). D) Relatively coarse detrital grain with a characteristic angular appearance, with cavities filled with clay and fine silt grains (C).

	Percentage of the occurrence of clay ‘blebs’ in each lamina type				
Sample	**Resting spore**	**Silicoflagellate-rich**	***Rhizosolenia***	**Vegetative**	**Total spore**
K1	71.4	8.9	–	19.6	80.4
K2	54.8	14.3	9.5	21.4	69.1
K3	71.4	7.1	5.4	16.1	78.5
K4	54.5	22.7	2.3	20.5	77.2
K5	68.2	22.7	2.3	6.8	90.1
K7	61.3	12	4	22.7	73.3
K8	67.2	14.1	–	18.8	81.3
K9	62.5	16.1	–	21.4	78.6
K11	61.9	14.3	–	23.8	76.2
10a	54.2	20.3	1.7	23.7	74.6
Mean	62.8	15.3	2.5	19.5	77.9

Table 6.5. The occurrence of clay ‘blebs’ within the different laminae types.

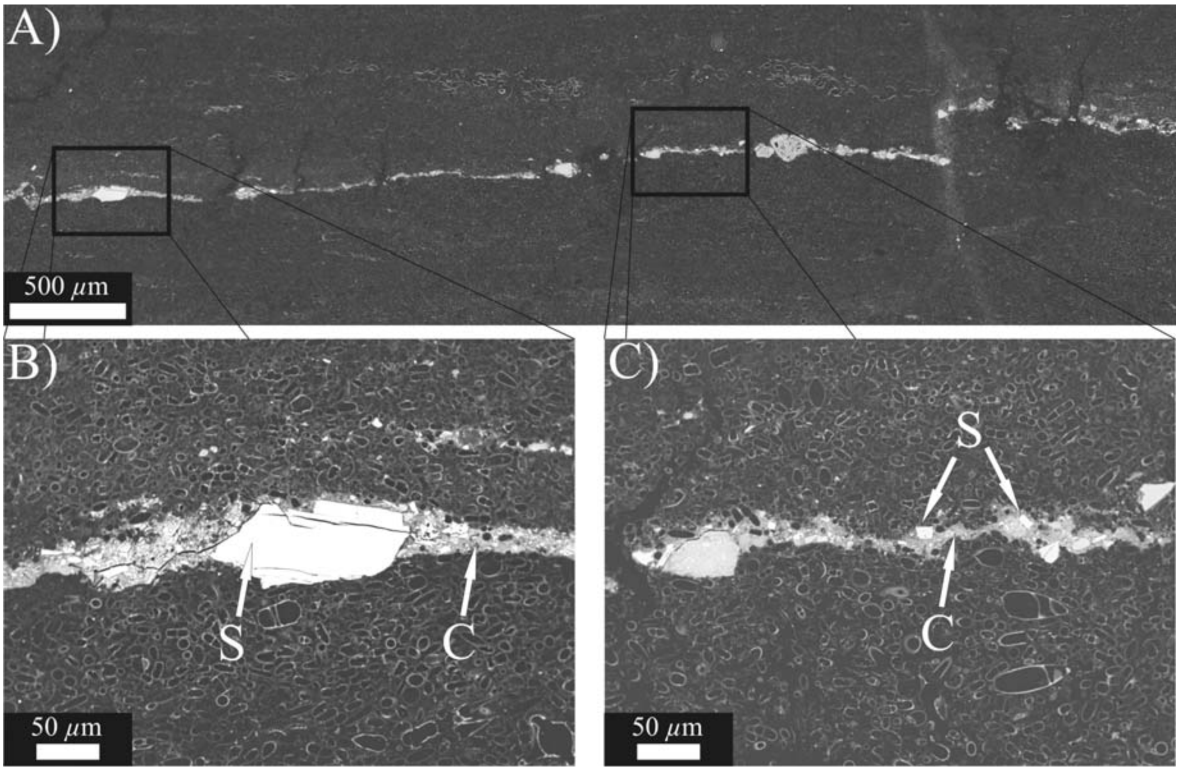

Figure 6.20. A) BSEI of a rare detrital lamina containing terrigenous grains (S) in a clay matrix. Note the poor sorting of the grains, which are mainly in the silt-sized fraction (C) with occasional fine sand sized grains (B).

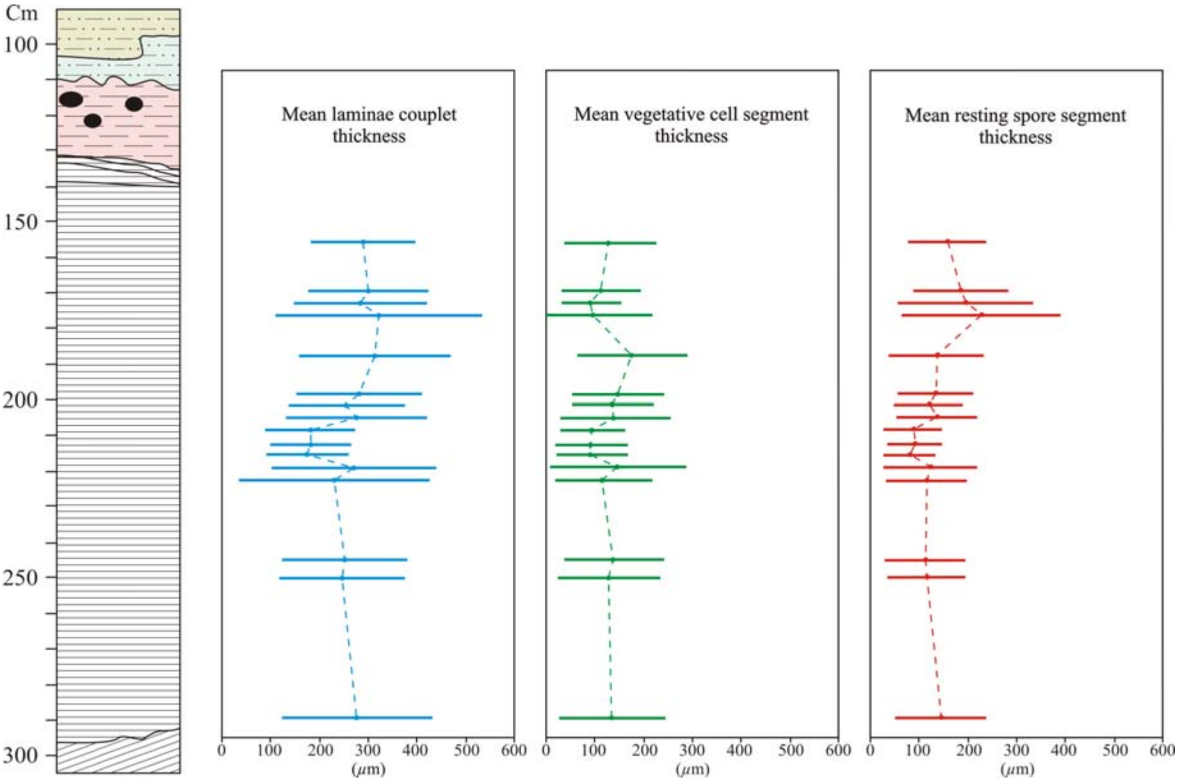

Figure 6.21. Mean thickness variations, with standard deviations, of the vegetative cell lamina segment, resting spore segment and laminae couplet, for each of the studied sections.

6.3.8 *Mean laminae thickness changes along the length of the core*

Mean thickness of the diatom vegetative cell segment, resting spore segment and total couplet thickness remain fairly constant throughout the studied section (Fig. 6.21). When the whole studied section is considered, there is no correlation between the variations in the mean thickness of the vegetative cell and resting spore segment (R^2 = 0.0047). However, a strong covariance in the mean thickness of the vegetative cell and resting spore segment is evident in samples above 196.5 cm (R^2 = 0.7694), whilst samples below 196.5 cm reveal a strong negative covariance (R^2 = 0.8046).

6.3.9 *Diatom floral analysis*

In this study, a total of 54 species from 21 genera were recorded from the 19 samples processed. Strew slides were found to be dominated by chrysophyte cysts and the plain, small, round *Chaetoceros*-type resting spores (Spore ‘1’) (Fig.6.22). Cells of Spore ‘1’ display a peak in abundance in the 227.5-228.5 cm samples, where they comprise 34% of the total counts and then decline in abundance towards the top and base of the unit, with the two lower samples (297.5-288.5 cm and 304-305 cm) almost devoid of Spore ‘1’. Chrysophyte cysts comprise a ubiquitous component of the flora, averaging 17.9% of the total counts, although abundances increase markedly in the two basal samples, where the cysts make up 49% of the total counts.

The diatom flora is dominated by the species described in Chapter 6.3.2 and 6.3.3 (Fig. 6.23 and Fig. 6.24), in agreement with the findings of Barron (1985b). *Hemiaulus* was found to be the most diverse taxa with over 20 species recognised, although some of these are spores. All of the main floral components range throughout the whole of unit 4, with the exception of *Proboscia cretacea* and *Sceptroneis dimorpha* (Fig. 6.25). Barron (1985b) noted that these two forms were missing from his upper two samples (134-136 cm and 150-152 cm). However, in this study, *P. cretacea* was only found to be missing from the section above 137.5-138.5 cm and *S. dimorpha* above 147.5-148.5 cm. Consistent with the findings of Barron (1985b), *T. polychaeta* was found to be rare in the two basal samples, although abundant to common throughout the rest of the core. *H. tumidicornis, H.* sp. 1 and Spore ‘3’ also display a marked decline in abundance towards the base of unit 4. Conversely, *Actinoptychus* spp., *Anaulus sibiricus*, *Goniothecium odontella*, *Odontotropis*, *Pseudopyxilla* sp. (Strelnikova) and *Skeletonemopsis crawfordii* all increase in abundance over the same interval. *Pseudopyxilla* sp. (Strelnikova) was found to be absent from all other samples, although comprising up to 13% of the total counts in the basal sample, whilst *S. crawfordii* although present throughout the core (comprising a mean of 0.09% of the total counts) displays a marked increase in abundance, comprising a peak of 4.7% of the total counts in sample 18 (297.5-298.5 cm).

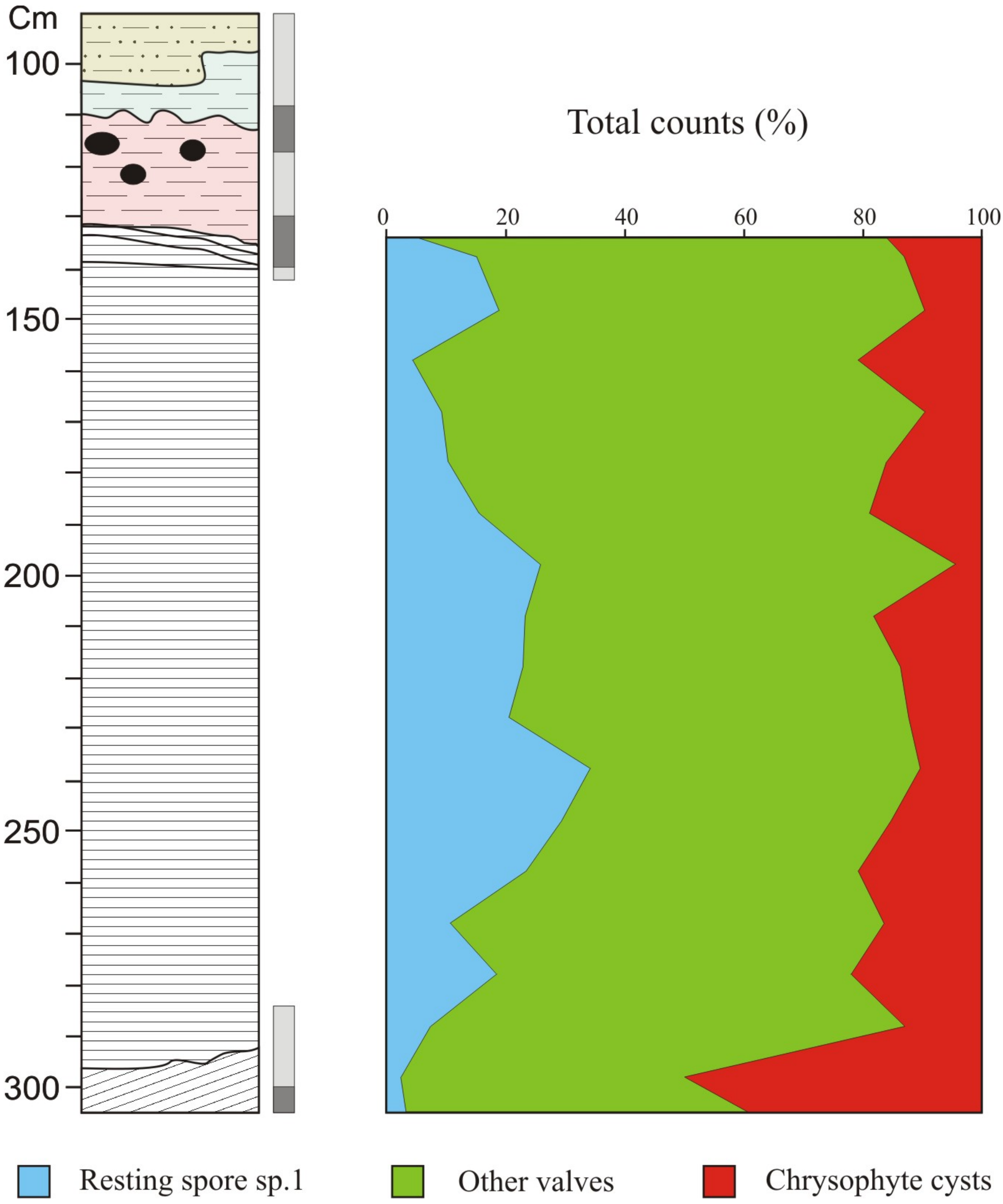

Figure 6.22. Graph showing the relative abundance of *Chaetoceros*-type resting spore (Spore '1'), chrysophyte cysts and all other valves in the 19 samples studied, plotted against the generalised sedimentary log of the CESAR 6.

When the diatoms are split into ecological groups (listed in Table 6.6), the floral composition displays little change with the exception of the lowermost two samples (Fig. 6.26). Here the assemblage displays a pronounced decrease in the abundance of resting spores and increase in the abundance of *Anaulus sibiricus*. Although Harwood (1988) grouped *A. sibiricus* with the resting spores, it is plotted separately here as there is uncertainty of its resting spore status. The same interval is also characterised by an increase in the abundance of benthic diatoms, although the relative contribution of these species to the overall assemblage remains low.

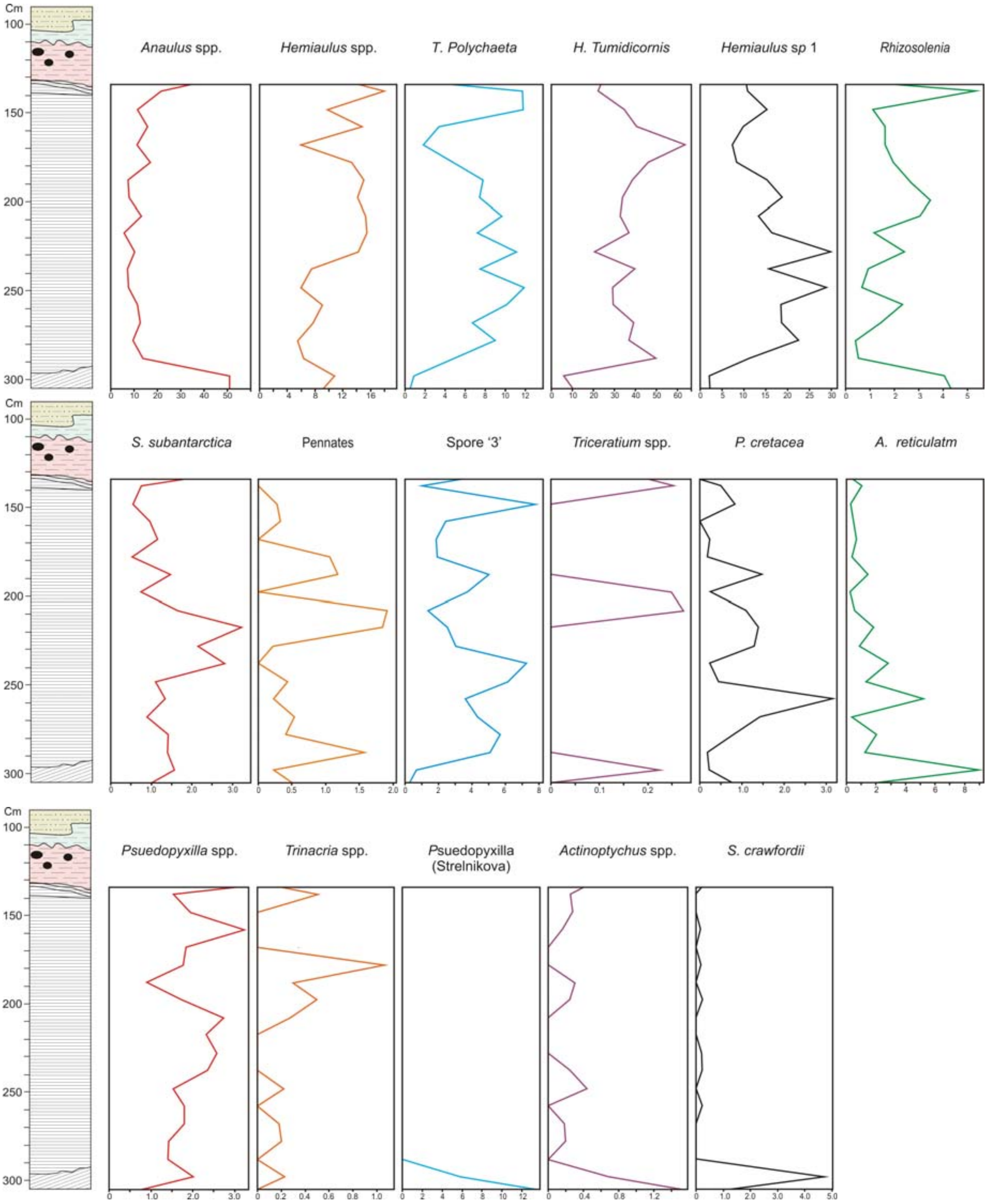

Figure 6.23. Relative abundances of the main diatom species/ taxa, exclusive of Spore '1' and chrysophyte cysts (apart from *A. reticulatum*). Note: the X axis in all graphs is percent of total counts.

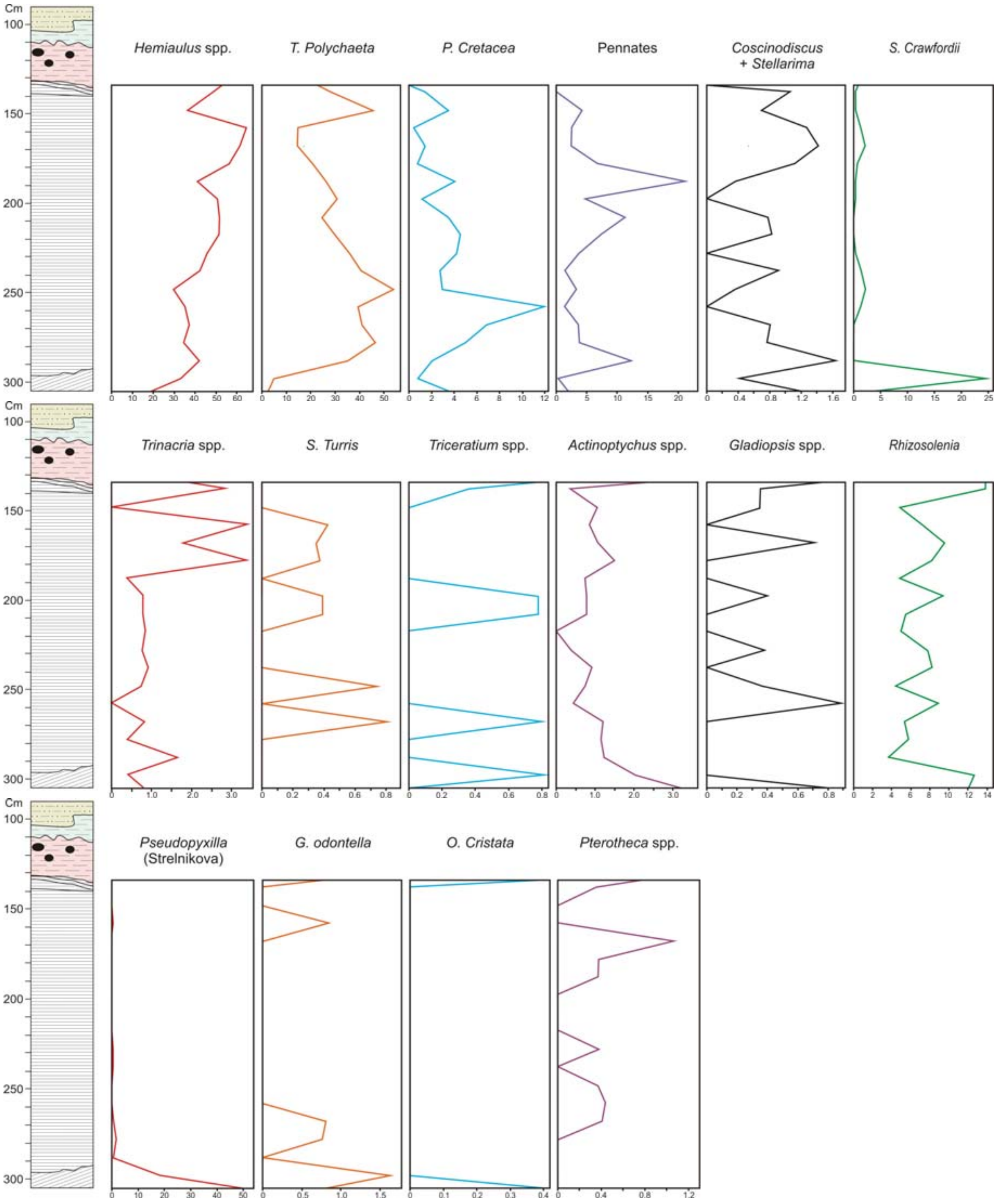

Figure 6.24. Relative abundance of diatom vegetative cells and the rarer resting spores. Counts are exclusive of *Anaulus* spp., *H. tumidicornis*, *Hemiaulus* sp. 1, Spore ‘3’, *S. subantarctica* as well as Spore ‘1’, *A. reticulatum* and other chrysophyte cysts. Note: the X axis in all graphs is percent of total counts.

Figure 6.27 shows a plot of the relative abundances of the vegetative cells and the rarer resting spores and highlights the marked difference in the floral assemblage in the two lowermost samples. Although absolute abundances of each taxon vary along the whole of unit 4, the basal samples are distinct, characterised by high abundances of *S. crawfordii* and *Pseudopyxilla* sp. (Strelnikova), along with low abundances of *Hemiaulus* spp. and *T. polychaeta*. Therefore, although variations in the floral assemblage do occur, this study concurs with the conclusions of Barron (Barron, 1985b), that there is no evidence of any diatom biostratigraphic changes.

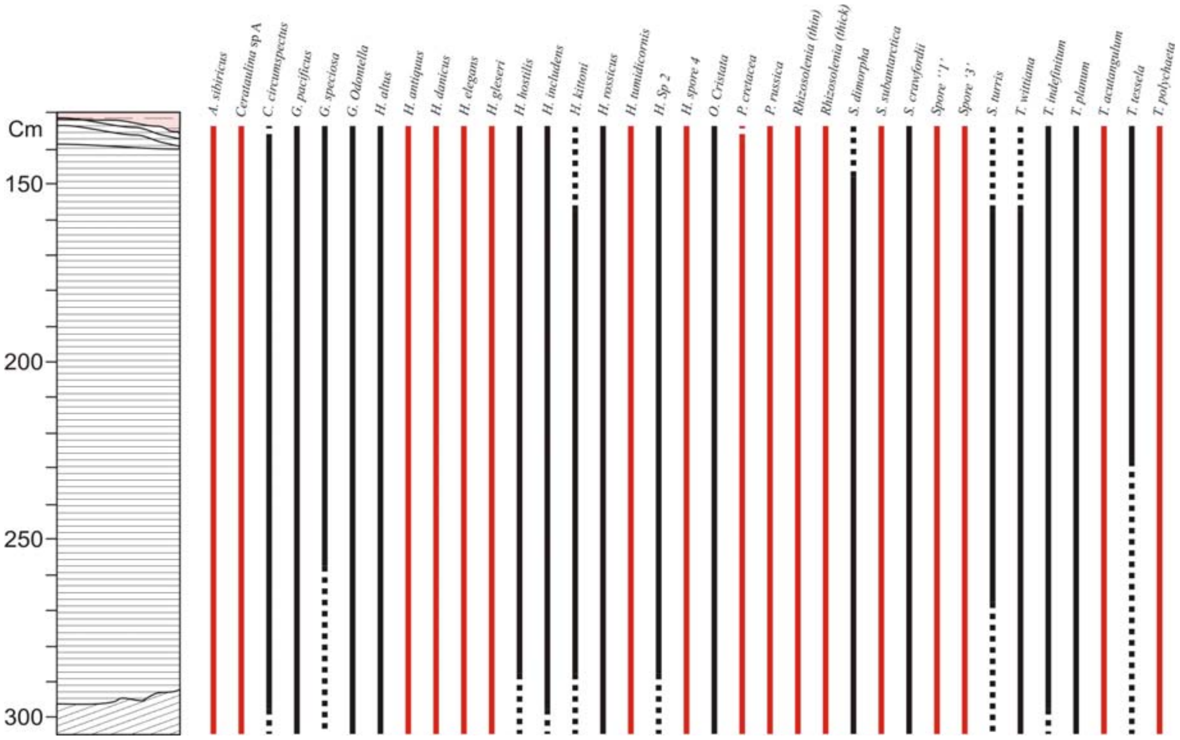

Figure 6.25. Graph illustrating the range of some of the main diatoms throughout the CESAR 6 core. The range of the most abundant species is shown in red. Dashed line indicates species was not identified in that range.

Centrics	**Resting spores**	**Benthics**
Coscinodiscus circumspectus	*Cerataulina* sp1	*Actinoptychus simbirkianus*
C. sibiricus	*Goniothecium odontella*	*A. tenuis*
C. symbolophorus	*Hemiaulus includens*	*Triceratium indefinitum*
Stellarima steinyi	*H. tumidicornis*	*T. planum*
S. sp. 2	*H.* sp. 1	
Thalassiosiropsis wittiana	*Odontotropis cristata*	
	Pseudopyxilla americana	
	P. russica	
	P. sp Strelnikova	
	Pterotheca crucifera	
	P. of Strelnikova (1974)	
	Rhizosolenia sp.	
	S. subantarctica	
	Spore '1'	
	Spore '3'	

Table 6.6. List of the species included in each of the group used in Figure 6.26.

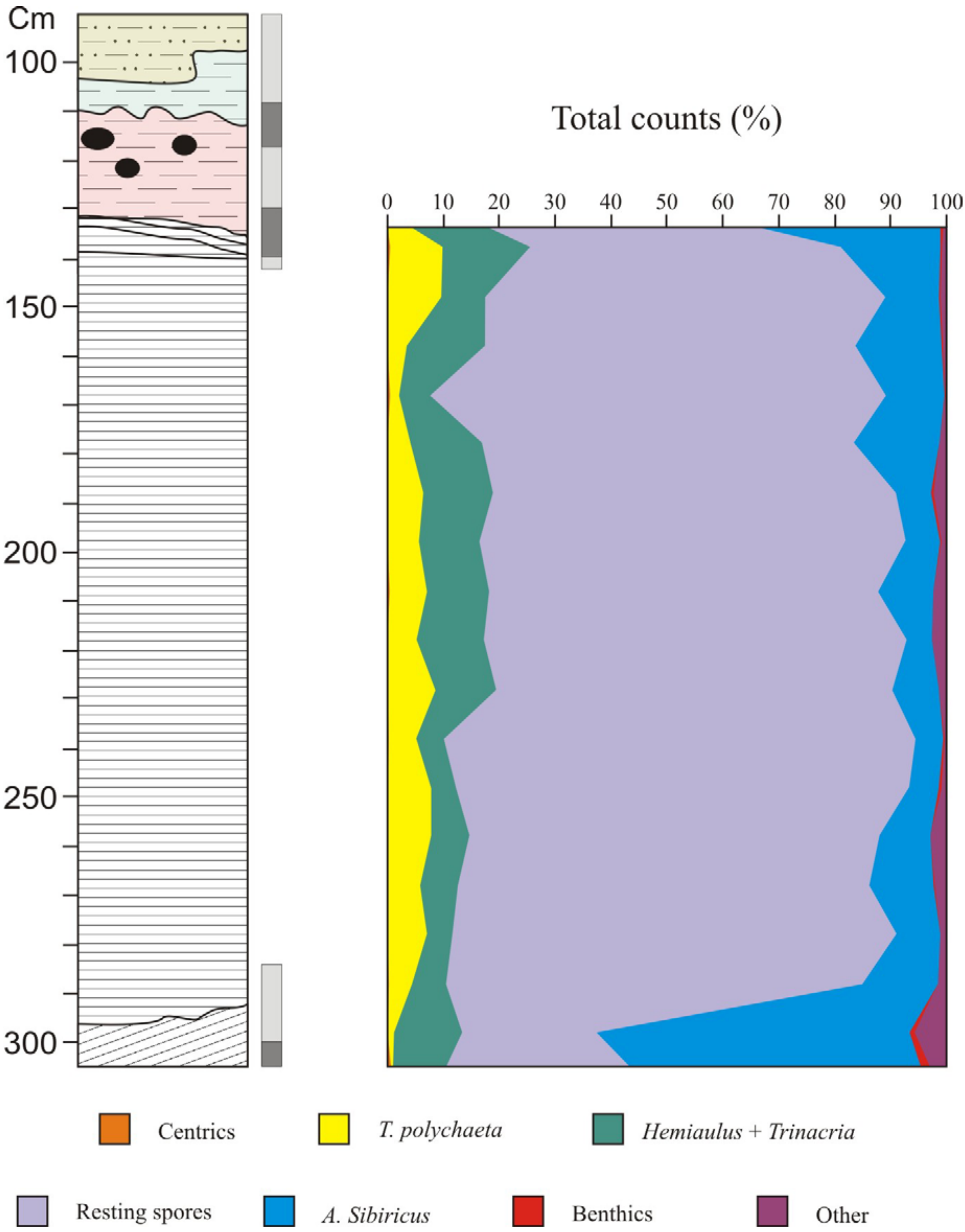

Figure 6.26. Graph of the relative diatom abundance in unit 4 of the Cesar 6 core. Diatom assemblages have been divided into seven groups after Harwood (1988) with *T. polychaeta* and *A. sibiricus* added as separate groups.

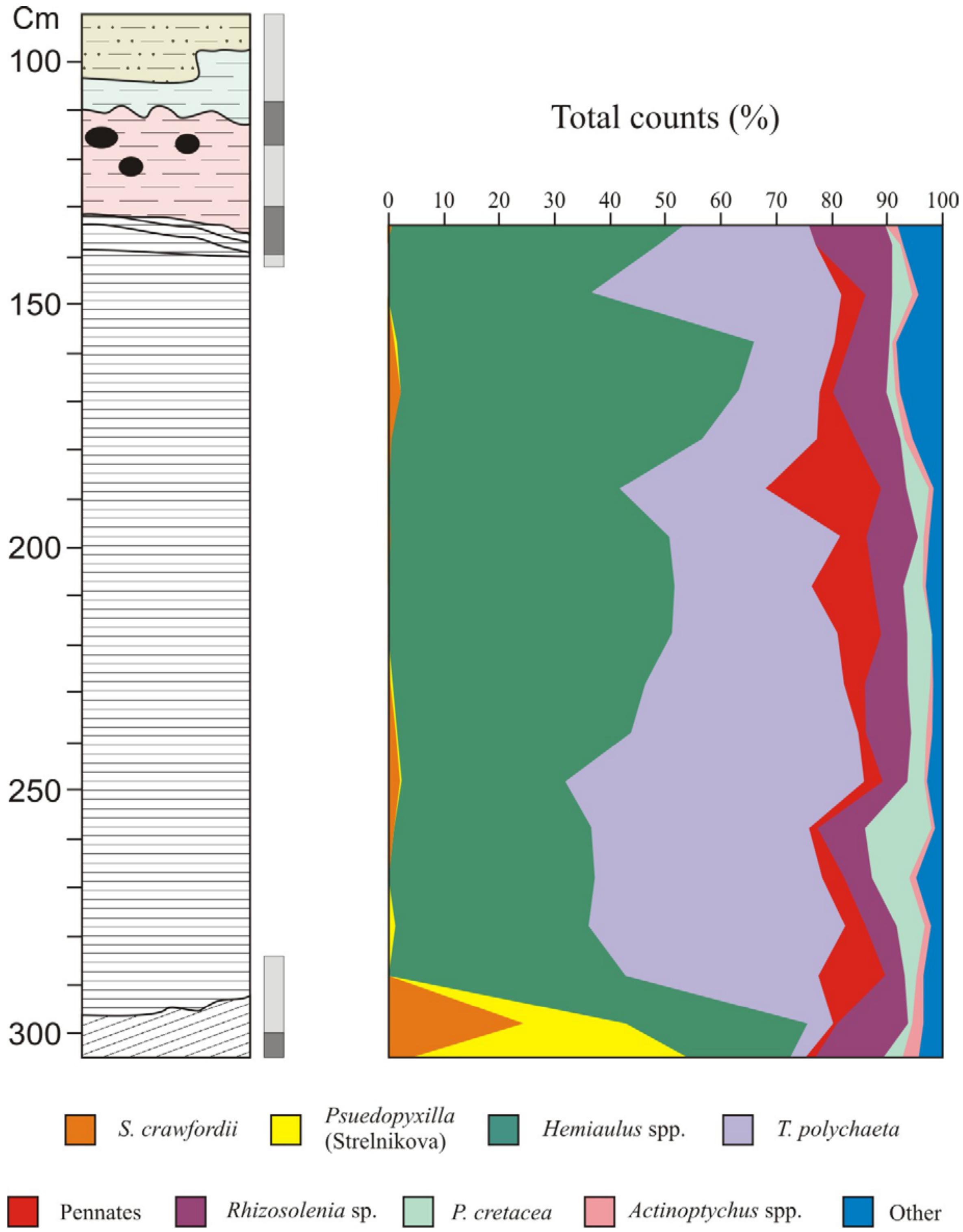

Figure 6.27. Relative abundances of diatom vegetative cells and the rarer resting spores (exclusive of *Anaulus* spp., *H. tumidicornis*, *Hemiaulus* sp. 1, Spore ‘3’, *S. subantarctica* as well as Spore ‘1’, *A. reticulatum* and other chrysophyte cysts).

6.3.10 *Diatom biostratigraphy*

Although the biosiliceous unit of the CESAR 6 core is acknowledged as Late Cretaceous in age, the exact age remains ill constrained. Barron (1985b) assigned a Late Campanian age to the unit based on Strelnikova's (1974; 1975) biostratigraphic divisions of the diatom assemblages of the Ural Mountains, Russia. Comparisons of the CESAR 6 and Marca Shale floras suggested to Barron that the difference between the two was too great to be explained solely by ecology, with only 5 species common to both. In the present study, 8 species were found to be common to both the Marca Shale and CESAR 6 (Table 6.7), all of which are long ranging species. At the time of the initial study by Barron, only one other diatom biostratigraphical scheme existed for the Late Cretaceous; that of the southern high-latitude Campbell Plateau DSDP Site 275 cores (50°26'S, 176°19'E). Hajós & Stradner (1975) tabulated 124 diatom taxa from the two upper Campanian cores recovered from this site. Although many of the key taxa used in the zonation scheme do not occur in the CESAR 6, Barron (1985b) found a moderate correlation between the CESAR 6 assemblages and that of DSDP Site 275, with 21 of the 33 species identified by him common to both deposits. In the present study, only 17 species were found to be common to both the CESAR 6 and DSDP Site 275, and when rather broad species concepts are accepted, this figures stands at 24 (Table 6.7).

Harwood (1988) tabulated 192 species from a ~1400m composite Late Campanian-Danian section on Seymour Island, Antarctica (64°15'S, 56°45'W). Correlations with the undifferentiated assemblages of Seymour Island are also good. The undifferentiated assemblage, containing 28-29 of the diatom species found in the CESAR 6, provides the strongest correlation (Table 6.7). Many of the species common to both the CESAR 6 and Seymour Island assemblages possess long age ranges (e.g. *A. sibiricus, G. odontella, H. ambiguus, H. danicus, H. elegans, H. kittonii, H. rossicus, P. cretacea, S. steinyi, S. turris, T. wittiana, T. indefinitum, T. acutangulum* and *T. polychaeta*). However, several species appear confined to the Upper Campanian – Lower Maastrichtian section of the Seymour Island succession (*H. wornardti, H. gleseri, H. includens* and *P. crucifera*). Although preservation and low abundance of the diatom flora means that true first and last occurrences of some species are not reflected, inferences from the biostratigraphy of Seymour Island tentatively place the CESAR 6 diatom ooze in the Upper Cretaceous – Lower Maastrichtian.

CESAR 6 Species List	**DSDP Site 275 (U. Camp.)**	**Seymour Island (U. Camp. – Danian)**	**Canadian Arctic (Cenoman. – Camp.)**	**Marca Shale (U. Maast.)**
Actinoptychus simbirkianus	–	–	X	–
A. tenuis	–	–	X	–
Anaulus sibiricus	–	X	X	–
A. sp 1	–	cf.	–	–
A. sp?	–	–	–	–
Cerataulina sp1	–	–	–	–
C.-type Spore '1'	–	–	–	–
Coscinodiscus circumspectus	X	–	–	?
C. sibiricus	–	–	–	–
C. symbolophorus	–	–	–	–
Gladiopsis pacificus	X	X	–	–
G. speciosa	X	X	X	X
Goniothecium odontella	X	X	X	–
Helminthopsis wornardti?	X	X	–	X
Hemiaulus altus	X	–	X	–
H. ambiguus	–	X	–	X
H. antiquus	–	–	X	–
H. danicus	X	X	X	–
H. elegans	cf.	X	X	–
H. gleseri	X	X	–	–
H. giganteus	–	–	–	–
H. hostilis	–	X	–	–
H. includens	–	X	–	–
H. kittonii	cf.	X	X	–
H. polymorphus var. *morianus*	–	X	–	–
H. rossicus	X	X	cf.	–
H. tumidicornis	–	–	X	–
H. sp. 1	–	–	–	–
H. sp. 2	–	–	–	–
H. sp. 6	–	–	–	–
H. sp. G	–	X	–	–
Odontotropis cristata	cf.	X	X	cf.
Proboscia cretacea	X	X	X	X
Pseudopyxilla americana	X	X	–	–
P. russica	X	X	X	X
P. sp Strelnikova	–	X	–	–
Pterotheca crucifera	X	X	–	X
P. of Strelnikova (1974)	–	–	–	–
Rhizosolenia sp.	–	–	–	–
Sceptroneis dimorpha	cf.	–	–	cf.
S. sp. B	–	–	–	–
Skeletonema subantarctica	X	X	–	–
Skeletonemopsis crawfordii	–	–	–	–
Spore '3'	–	–	–	–
Stellarima steinyi	cf.	X	X	X
S. sp. 2	–	–	–	–
Stephanopyxis turris	X	X	X	–
Thalassiosiropsis wittiana	X	X	X	X
Triceratium indefinitum	cf.	X	–	–
T. planum	–	–	X	–
Trinacria acutangulum	cf.	X	X	–
T. tessela	–	–	X	–
Trochosiropsis polychaeta	X	X	X	–
Unknown	–	–	–	–

Table 6.7. Occurrence of diatoms from the CESAR 6 in DSDP Site 275 (Hajós & Stradner, 1975), Seymour Island (Harwood, 1988), the Canadian Arctic (Tapia & Harwood, 2002) and the Marca Shale (THIS STUDY, Hanna, 1927; Long *et al.*, 1946; THIS STUDY, Nikolaev *et al.*, 2001). cf = similar species.

The most recent Late Cretaceous diatom biostratigraphic framework has come from the analysis of four Canadian Arctic sections (from 69°27'N, 126°58'W to 79°47'N, 85°22'W), spanning the Upper Cenomanian – Latest Campanian (Tapia & Harwood, 2002). In this work, Tapia and Harwood tabulated 203 diatom taxa from which they propose 4 Upper Cretaceous diatom biostratigraphical zones (Fig. 6.28). Correlation of the CESAR 6 flora with the undifferentiated flora of the Canadian Arctic is good, with 21-22 of the CESAR 6 taxa present (Table 6.7). Comparisons with the flora of each biostratigraphical zones shows that, in general, the CESAR 6 flora bears a close similarity with those of the Early Late Campanian *Trinacria indefinita* and late Late Campanian *Stephanopyxis simonseni* zones, although both *T. indefinita* and *S. simonseni* are absent from the CESAR 6. Numerous CESAR 6 taxa, for example *A. tenuis, G. odontella, H. altus, H. kittonii, P. cretacea, S. steinyi, S. turris, T. wittiana, T. planum*, *T. acutangulum* and *T. polychaeta* are present in both zones. Although *T. polychaeta* does rarely occur in the *Trinacria indefinita* zone, it is more characteristic of the *Stephanopyxis simonseni* zone. *H. tumidicornis* is also only found in the *S. simonseni* zone, and *A. sibiricus* is more abundant in this zone, suggesting the CESAR 6 diatoms have more affinity with the late Late Campanian *Stephanopyxis simonseni* zone.

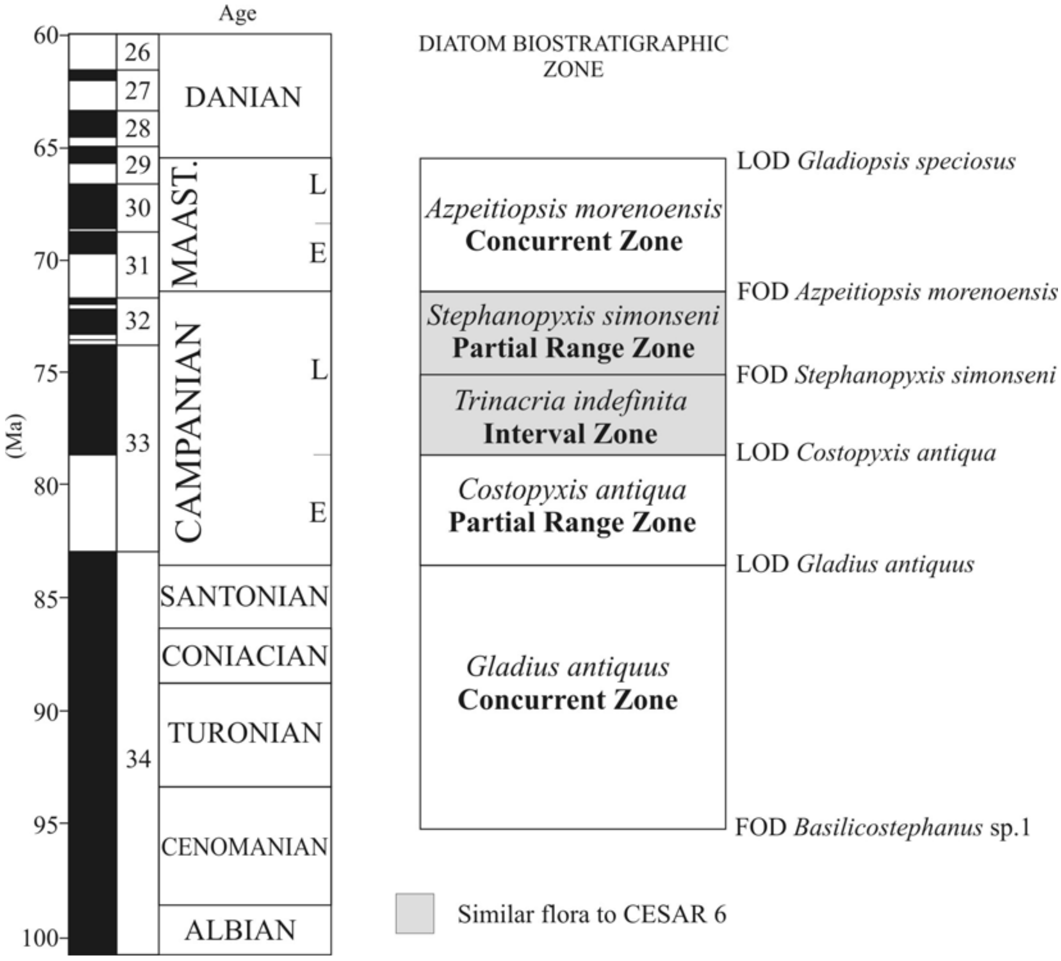

Figure 6.28. Illustration of the new diatom biostratigraphical zones of the Arctic Canada, redrawn from Tapia (2002). The biostratigraphic zones most similar to the CESAR 6 are highlighted in grey.

On the basis of the widespread occurrence of *Azpeitiopsis morenoensis* in Maastrichtian diatomaceous deposits and the fact that *A. morenoensis* is known from Early Maastrichtian sediments of the Kerguelen Plateau (ODP Leg 120, Site 748) but is absent from Campanian deposits, Tapia and Harwood (2002) suggested that an *A. morenoensis* biostratigraphic zone be established. The zone ranges from the first occurrence of *A. morenoensis* at the base of the Maastrichtian to the last occurrence datum of *Gladiopsis speciosus* at the K/T boundary. No specimens of *A. morenoensis* were identified in the CESAR 6 in this or other studies, suggesting that unit 4 of the CESAR 6 core pre-dates the base of the Early Maastrichtian *A. morenoensis* concurrent zone. However, in the Marca Shale, *A. morenoensis* was inferred to be representative of warmer, El Niño-like conditions (Chapter 4.4.8) and as such its absence from the CESAR 6 may relate to ecological constraints.

6.4 INTERPRETATION AND DISCUSSION

The disparity in the thickness of the compositional laminae and the colour laminations explains why no differences in the diatom composition were found between different laminae in some earlier studies (Mudie & Blasco, 1985; Mudie *et al.*, 1986). Any study into compositional differences between colour laminations would be unable to detect the alternating vegetative cell/resting spore laminations due to too coarse a sampling resolution and it is only through the use of high-resolution BSEI that these compositional laminae can be detected and studied. Although Kitchell *et al*. (1986) reported the presence of alternating resting spore and vegetative cell laminae in core Fl-437, their distinction of different laminae was colour based and therefore the results must have had an element of serendipity. Illustrations of the composition of resting spore and vegetative laminae in Kitchell *et al*. (1986) (see Fig.1 in Kitchell *et al*., 1986) also show alternations between *A. sibiricus* plus several *Rhizosolenia* (resting spore laminae) and *Hemiaulus* spp. (vegetative laminae). It has been shown here that *A. sibiricus* and *Rhizosolenia* occur overwhelmingly within the vegetative laminae.

6.4.1 *Origin of colour laminations*

Alternating colour laminations in diatomaceous sediment are well documented from diverse settings, including silled marginal basins and fjords, open continental shelves, marginal seas and lakes (e.g. Kemp, 1996), mostly relating to the alternating seasonal deposition of two sedimentary components (e.g. diatoms, terrigenous material, coccoliths, etc). However, the paucity of detrital matter and the fact that the colour laminations overprint the compositional laminae excludes the formation of colour laminae in the CESAR 6 by the alternating deposition of different sedimentary components. Long-term colour variations have been described in Pleistocene sediments beneath the Benguela Current Upwelling System, related to the concentrations of organic carbon and $CaCO_3$, independent of biogenic opal (Robinson *et al.*, 2002). However this scenario is also inapplicable to the colour laminations in the CESAR 6, which are known to relate to the concentration of Fe, whilst the sediments are organic carbon poor and devoid of $CaCO_3$. The hue of sediments is primarily controlled by the presence of iron oxides and Fe^{2+}/Fe^{3+} changes in clay minerals (Giosan *et al.*, 2002). No observable concentrations of clay blebs or detrital material are present in the darker laminations to account for the increase in Fe concentrations. Therefore, this study concurs with earlier conclusions by Stoffyn-Egli (1987) that the colour laminations likely result from proximal hydrothermal activity. An increase in the Fe content of the sediment in the darker yellow/orange laminae is also consistent with the higher backscatter coefficient of some of the darker laminations.

6.4.2 *Implications for colour banding in other sediments*

Centimetre-scale colour banding, superimposed on submillimetric diatomaceous/terrigenous compositional laminae have been recorded in recent sediments from the Gulf of California (Guaymas Basin, cores JPC56, 96 - 168 cm and JPC44, 430 - 440 cm), the cause or significance of which remains unclear (Pike, 1996). The Gulf and in particular the Guaymas basin are known to be hydrothermally active (e.g. Lonsdale *et al.*, 1980). Using the CESAR 6 as an analogy, it is possible that the centimetre-scale colour banding in some of the Guaymas basin cores relates to proximal hydrothermal activity.

6.4.3 *Origin of the resting spore laminae*

The fact that *H. tumidicornis* and Spore '1' co-occur in mixed spore laminae, along with other spores (e.g. Spore 3 and *S. subantarctica*) indicates that deposition of the main resting spores occurred concurrently. The small size of the spores indicates that sinking velocities of solitary cells would have been low and it is unlikely they would have reached the sediment ungrazed by simple settling. Valves of Spore '1', Spore '3' and many valves of *H. tumidicornis* are below 20 μm in diameter, suggesting they could have been sedimented intact within fecal pellets (Honjo & Roman, 1978). It is unlikely, however, that valves of *H. tumidicornis* within their vegetative cells and the long fragile filaments of *S. subantarctica* often intertwined in pairs (see Plate 10.2), would have survived maceration. Further, no corroborating identifiable fecal pellets have been observed within resting spore laminae. The most consistent interpretation is that cells were able to form aggregations through the mediation of TEP, and attain sufficiently high sinking velocities to sediment intact (Passow *et al.*, 1994; Bull & Kemp, 1995; Grimm *et al.*, 1997).

It has been observed that some resting spores can tolerate darkness, but are unable to tolerate desiccation or burial (Hargraves & French, 1975). Alterations of the light intensity and hours of daylight are known to invoke sporulation and the ~4 months of total darkness during the Arctic winter would have invoked a major environmental stress response. Resting spores are adapted (with respect to vegetative cells) to persist in darkness or low light conditions and are known to survive longer at cold temperatures (Hargraves & French, 1983). Darkness also prolongs the time resting spores can survive. Sporulation could have therefore occurred in response to the reduction of light intensity and day length in the autumn/winter in some species.

Alternatively, the advent of continuous hours of sunlight in the spring (Fig. 6.6), together with the onset of stratification, would have stimulated a bloom of diatoms that were able to rapidly exploit available nutrients in the upper mixed layer of the photic zone. Nutrients may have been made available by winter open-ocean upwelling, as proposed by Kitchell and Clark (1982) or simply through mixing during winter storms. Analogous spring blooms are well documented in the modern ocean (Guillard & Kilham, 1978) and are followed by a large flux of resting spores to the sediment, enhanced by the secretion of TEP (Alldredge *et al.*, 1993) when available nutrients have been exhausted (Brodie & Kemp, 1994; Bull & Kemp, 1995). Modern spring bloom diatoms (e.g. S*keletonema*, *Chaetoceros*) are characteristically lightly silicified and have a low preservation potential (e.g. Treppke *et al.*, 1996) and some vegetative cells are therefore rarely preserved in sediments. Similar diatoms in the proto Arctic Ocean would probably have been dissolved in the water column or at the sediment/water interface. Resting spore laminae are therefore interpreted as the flux of spring bloom diatoms that were able to rapidly exploit nutrients brought into the euphotic zone by winter mixing, analogous to modern *Chaetoceros*. If this interpretation is correct then it appears that *Hemiaulus tumidicornis* was also involved in the spring bloom. As discussed in Chapter 3.5.2, the vegetative cell of *H. tumidicornis* is small and lightly silicified (Plate 16. 6 & 8), in contrast to the relatively large and robust species of *Hemiaulus* in the vegetative laminae. Small, lightly silicified vegetative cells are consistent with adoption to rapidly exploit available nutrients during the spring bloom (Guillard & Kilham, 1978).

It has been regarded that only modern meroplanktonic diatoms form resting spores (e.g. Hargraves, 1986) and thus the presence of resting spores in sediments is evidence of a shelf depth environment (e.g. Barron, 1985b). Yet, *Chaetoceros* spores have been recovered from surface sediments in a water depth of 3600-4700m in the Indian sector of the Southern Ocean (Riaux-Bobin *et al.*, 1997) and in sediments recovered from a depth of 1066m in the Bransfield Strait, Antarctica, where they comprise up to 89.51% of the diatom taxa (Bárcena *et al.*, 2002). It is also known that diatom species inhabiting a “pseudo-benthic” environment at the base of the thermocline in oceanic waters also produce resting spores (Bienfang & Szyper, 1981). Therefore, the occurrence of diatom resting spores cannot be explicitly used as an indication of shelf depth environments.

6.4.4 *Origin of the vegetative laminae*

The excellent preservation of all diatom valves in the CESAR 6 can be attributed to the fact that diatom blooms were able to overwhelm grazing pressures (or grazing was absent) and/or diatom valves were rapidly exported from the water column, effectively bypassing grazing (and/or dissolution) (Alldredge *et al.*, 1993; Bull & Kemp, 1995; Grimm *et al.*, 1996). Rapid export of fresh, ungrazed cells of *Hemiaulus* to the sediment has been observed and interpreted to relate to the fact that the long chains of cells were able to coalesce to form colonies, which lost buoyancy and sank as a physiological response to depleted macronutrient or iron concentrations (Scharek *et al.*, 1999b) (see Chapter 3.2.12). This peak flux consistently occurs during the summer for many modern species of *Hemiaulus* (Scharek *et al.*, 1999b). Modern species of *Hemiaulus* are known to grow in and be exported from the upper mixed-layer (Scharek *et al.*, 1999a), although are able to dominate in oligotrophic conditions through its N_2-fixing endosymbiont. Near-monospecific laminae of *Hemiaulus* have thus far only been described for the modern species *Hemiaulus hauckii* from BSEI studies of the eastern Mediterranean S5 sapropel (Pearce *et al.*, 1998; Kemp *et al.*, 1999). These near-monospecific *H. hauckii* laminae were found situated above early winter/spring bloom mixed diatom laminae (Kemp *et al.*, 1999; Kemp *et al.*, 2000). *Hemiaulus* is therefore regarded as a member of the “fall dump” group of diatoms, sediment following the break down of stratification (Kemp *et al.*, 2000).

Based on these observations, near-monogeneric laminae of *Hemiaulus* in the CESAR 6 are interpreted to represent the “fall dump” (Kemp *et al.*, 2000) style deposition of blooms during the end of the summer or autumn. Intense heating of the surface layer during the summer would have led to a well established seasonal thermocline, which combined with the possible presence of a fresh water cap would have ensured a well stratified surface layer of the proto Arctic Ocean, analogous to the Mediterranean during deposition of *H. hauckii* laminae. The blooms of Hemiaulids in the Cretaceous Arctic may have directly exploited nutrients trapped below a strong thermocline and possibly pycnocline over the stratified period. Alternatively, these Hemiaulid blooms may have been powered by N_2-fixing endosymbionts analogous to *Hemiaulus hauckii*. Blooms of *Hemiaulus* are known to be spatially extensive, with a bloom of *H. hauckii* observed in the tropical Atlantic estimated to have covered an area of 1.4 to 2.8×10^6 km^2 (Carpenter *et al.*, 1999). If the biosiliceous sediment of the CESAR 6 and Fl-437 are indeed contemporaneous, blooms of *Hemiaulus* can be expected to have covered an area large enough to have been deposited at both sites, 177 km apart. The co-occurrence of *T. polychaeta* with *Hemiaulus* spp. implies that it was sedimented concurrently and may therefore have shared a similar ecology to *Hemiaulus*. It has been shown in this study that, analogous to *Hemiaulus*, valves of *T. polychaeta* were able to form chains. The ecology of modern *Anaulus*, a surf zone diatom, differs greatly from that *A. sibiricus* is inferred to have occupied in the CESAR 6. If *A. sibiricus* is indeed a vegetative cell, it must have occupied a radically different ecological niche in the Late Cretaceous. However, although found primarily within diatom vegetative cell laminae, the premise that *A. sibiricus* is a resting spore of *Hemiaulus* cannot be discounted.

6.4.5 *Origin of the Rhizosolenia laminae*

In the modern ocean, Rhizosolenids are known to form macroscopic mats that are able to regulate their buoyancy and move between a deep nutrient (nutricline) source and the euphotic zone (Villareal *et al.*, 1993; Villareal *et al.*, 1996). Sediment trap studies show that they mass sediment during the autumn (see Chapter 3.2.18) and are found forming near-monospecific laminae in the Gulf of California and Mediterranean sapropels (Sancetta *et al.*, 1991; Kemp *et al.*, 1999; Kemp *et al.*, 2000). Rhizosolenids are therefore regarded as key players in the “fall dump” mode of export flux (Kemp *et al.*, 2000). Near-monospecific laminae and concentrations of *Rhizosolenia* sp. frequently occur above/towards the top of vegetative laminae (Fig. 6.7, 6.9 and 6.12b). The occurrence of concentrations and near-monospecific laminae of *Rhizosolenia* in relation to the vegetative laminae, interpreted to represent summer deposition by analogy with modern species of *Hemiaulus*, is therefore consistent with deposition of *Rhizosolenia* during the autumn. The fact that the *Rhizosolenia* in the CESAR 6 are regarded as resting spores or more heavily silicified ‘winter’ stage is still consistent with the conclusion that they were deposited during the autumn following the break down of stratification.

6.4.6 *Origin of the silicoflagellate/setae-rich laminae*

Silicoflagellates are microflagellate phytoplankton that presently dwell in the euphotic zone of the worlds oceans. They possess siliceous skeletons and generally comprise a minor component of microplankton assemblages in the pelagic realm (e.g. Eynaud *et al.*, 1999). A peak flux of silicoflagellates during the autumn/winter appears to be common in the present ocean, observed in sediment trap studies in the central Black Sea (Osawa *et al.*, 2005), the Santa Barbara Basin (Lange *et al.*, 1997), the southeast Pacific (Romero *et al.*, 2001), Jervis Inlet (British Colombia) (Sancetta, 1989b) and the tropical North Atlantic (Boltovoskoy *et al.*, 1996). However, time-series data from sediment traps in the North Pacific reveal that the flux of silicoflagellates is temporally variable, with no obvious seasonal trend at 40° N, and peak fluxes during the winter at 44° N and the spring at 50° N (Onodera & Takahashi, 2005).

Near-monospecific silicoflagellate laminae have previously been observed in sediments from the Santa Barbara Basin (Grimm *et al.*, 1996) and Gulf of California (J. Pike and C.B. Lange, unpublished data, 1995), which Grimm *et al.* (1996) infer to represent the sedimentation of TEP enhanced flocs. Laminated sediments from Effingham Inlet, British Colombia, also preserve near-monospecific blebs and laminae of silicoflagellates (Chang *et al.*, 2003). They occur within either the winter terrigenous laminae or silty diatomaceous laminae, deposited during the autumn, interpreted to reflect intrusions of pelagic water and "fall dump" export flux, respectively (Chang *et al.*, 2003). *Proboscia cretacea* also occurs in the silicoflagellate/setae-rich laminae, and modern forms are known to be involved in the "fall dump" mode of export flux (Chapter 3.2.18). However, the association of the silicoflagellate/setae-rich laminae with resting spore laminae in the CESAR 6 implies that they are not related to a "fall dump" flux event.

The abundant sponge spicules together with a variable diatom hash component could represent reworked material transported offshore. Alternatively, the diatom hash could reflect an intensification of grazing or greater levels of dissolution at this time. Setae are often observed aggregated into pelletal structures in topographic stubs, which often include diatom fragments (Fig. 6.17). The unidentified setae, very similar in appearance to modern *Chaetoceros* vegetative cells (Fig. 6.16d), found within the silicoflagellate/setae-rich laminae may be an important palaeoenvironmental indicator. Vegetative *Chaetoceros* cells are only very rarely preserved in modern sediments, although *Chaetoceros* setae are often found in association with *Chaetoceros* spores (Bull *et al.*, 2000; Dean, 2000a). The *Chaetoceros*-like setae may therefore have originated from a lightly silicified *Chaetoceros*-like spring bloom vegetative cell, which may also have been accountable for the production of the abundant Spore '1' resting spores.

Silicoflagellate/setae-rich laminae are therefore interpreted to represent the deposition from spring blooms. Diatom blooms, forming in the upper mixed layer at this time would have been subject to intense grazing, accounting for the variable diatom hash component. The lightly silicified valves of these species would not have been readily preserved in the sediments, although the setae of such diatoms are commonly preserved, manifest as the *Chaetoceros*-like setae. The association of silicoflagellate/setae-rich laminae with resting spores is consistent with deposition in the early spring, prior to depletion of nutrients in the upper water column and subsequent triggering of sporulation. Silicoflagellates also responded to the increased light intensity and were sedimented *en masse* following nutrient depletion, possibly aided by the secretion of TEP (Grimm *et al.*, 1997). The abundant sponge spicules may represent material that was suspended in the water column during winter mixing that was subsequently deposited with spring flux during calmer conditions.

6.4.7 *Origin of the Stellarima sp.1 laminae*

Although some species of *Coscinodiscus* are characteristic of the "fall dump" (Kemp *et al.*, 2000), others are associated with more mixed conditions. In the Gulf of California, *C. radiatus* is found associated with blooms that are stimulated by the injection of nutrients into the photic zone through mixing. It is feasible that *Stellarima* sp.1 is adapted to more mixed conditions, analogous to some *Coscinodiscus* spp.. Valves of *Stellarima* sp.1 are lightly silicified, in sharp contrast to the other species of *Stellarima* (*S. distincta* and *S. steinyi*) encountered in this study (see Plate 4.5-8), inferred to relate to the "fall dump". The lightly silicified frustules of *Stellarima* sp.1 may be indicative of a spring bloom scenario.

6.4.8 *Speculation on the origin of the clay blebs and rare terrigenous laminae*

Detrital material has previously been described from unit 4 of the CESAR 6 core as "siliceous glass shards of probable volcanic origin" (Stoffyn-Egli, 1987), which Mudie *et al.* (1986) inferred to have been transported offshore by winds. The fact that the detrital material is concentrated in resting spore laminae implies that flux of detrital material was seasonal. It is feasible that deposition from volcanic eruptions occurred seasonally through favourable prevailing winds, most likely during spring/summer (see Fig. 6.5). However, the relatively common temporal occurrence of detrital material requires volcanic activity to have been almost continuous. Many extant explosive volcanoes are characterised by long periods of quiescence between successive eruptions (Cas & Wright, 1987) and as such a direct input from volcanic activity is highly unlikely. Although an aeolian origin of the detrital material is consistent with many of the observations presented here, an inconsistency lies in the occurrence of relatively coarse (fine sand), solitary grains. If winds were capable of transporting grains of fine sand why should there be a lack of finer detrital material? It is therefore prudent to consider other possible modes of origin of the detrital material.

It is feasible that the detrital material could have been transported into the basin through fluvial runoff. It is likely that precipitation in the Late Cretaceous Arctic would have been seasonal and thus the concentration of the detrital material in resting spore laminae could relate to seasonally high precipitation leading to enhanced fluvial runoff. However, this mechanism also fails to explain the low abundance of the detrital material and the occurrence of relatively large solitary grains. Although this might relate to winnowing by bottom currents, the lack of disturbance to the laminated fabric does not support this.

The size, shape and composition of the clay-rich blebs bear a close resemblance to clay/silt-rich pelagic zooplankton fecal pellets (e.g. see Chapter 4.4.2). Seasonal deposition of the pellets would relate to either the zooplankton abundance or to the size of the fluvial outwash plume, relating to regional precipitation. A fecal pellet origin could also account for the rarity of the blebs, with deposition of detrital material by nektonic organisms into an otherwise sediment starved basin. Although some of the detrital-rich blebs may have a fecal pellet origin, this mechanism cannot account for the relatively coarse solitary grains or rare continuous laminae.

Another possibility is that the detrital material represents plant-rafted or ice- rafted debris (IRD), both of which could suitably account for large solitary grains in otherwise detrital poor sediment. The high proportion of terrestrially derived organic matter in core Fl-533 attests that large amounts of terrestrial plant material were transported into the open Cretaceous Arctic Ocean. Driftwood trees are known to occur in the present day Arctic, originating mainly from the rivers of northwest Russia and Siberia (Johansen & Hytteborn, 2001). With the aid of ice rafting, individual specimens may be transported over great distances, having been identified in the North Atlantic and Arctic North America. However, the most common driftwood genera in the present day Artic can remain afloat for a maximum of 10-17 months (Häggblom, 1982) and thus even without the aid of ice rafting, the potential exists for significant offshore transport. Maximal output of driftwood occurs during spring floods and years with enhanced precipitation are characterised by above average driftwood export. Meandering rivers, with constantly eroding banks have the greatest potential to supply driftwood trees. Driftwood trees produced from erosion in this way often have their root system intact, amongst which soil and other detritus may be transported (see Johansen & Hytteborn, 2001).

Numerous studies have documented the large high latitude forests of the Late Cretaceous (e.g. Spicer & Parrish, 1986; Spicer & Parrish, 1990; Herman & Spicer, 1997). Active mountain building at the southern Asian margin would have deflected drainage systems north (Hay *et al.*, 1999) and thus river systems of Eurasia would have transported driftwood trees directly into the Arctic Ocean. Input of driftwood would probably have occurred from the northern margins of North America and from Greenland and Svalbard, the most proximal land masses to the CESAR 6 (Clark *et al.*, 1986). A large hiatus exists in the Late Cretaceous sequence on Svalbard, although lower Tertiary sandstone sequences contain numerous coal seams, confirming the presence of dense vegetation (Parker, 1967). Lignite-rich beds are also known from the Campanian-Maastrichtian of NW Ellesmere Island, Canada (palaeolatitude of 75°N), which are interpreted to have been deposited in a densely forested coastal peat mire (Falcon-Lang *et al.*, 2004). However, it is likely that some fossil evidence would exist in the biosiliceous sediment given the quantity of plant material necessary to transport the detritus offshore, even if benthic conditions were not favourable for preservation of organic carbon.

The term IRD is usually reserved for terrigenous grains coarser than 500 µm (or sometimes 63 µm) found erratically distributed in deep sea sediments (Clark & Hanson, 1983; Elverhøi *et al.*, 1995). However, most of the material transported by sea ice is in fact clay and silt sized material (Pfirman *et al.*, 1989) and sediment trap studies have shown that IRD can be clearly detectable down to a grain size of ~40 µm (Hebbeln, 2000). One potential source of IRD is from icebergs discharged into the proto Arctic Ocean from mountain glaciers. Such icebergs would have been laden with fine sediment, similar to that observed in CESAR 6. The melting/discharge of such icebergs would also have been seasonal, most likely during the spring. Alternatively, IRD could have been supplied from aeolian material accumulated on the surface of seasonal sea ice, or been picked up in sea ice forming in shallow water, which was subsequently transported offshore (Nürnberg *et al.*, 1994). It is difficult to reconcile the presence of ice with the ~15 °C TEX_{86} estimate from core Fl-533 (Jenkyns *et al.*, 2004). However, if as discussed in Chapter 6.1.5, the TEX_{86} values originate seasonally from the upper 100m of the water column (Wuchter *et al.*, 2005), possibly during the summer (A. Sluijs, personal communication, 2005), the 15 °C SST estimate of Jenkyns (2004) could derive from an intensely thermally stratified upper water column, which would have certainly occurred during the summer period of continuous sunlight. Leaf physiognomy analyses of older (Coniacian), high palaeolatitude (~78°N) floras from northeastern Russia demonstrate the marked temperature difference between the warm and cold months in the greenhouse Arctic region. Estimates of the mean warm month temperature for the floras range between 17.1 °C and 18.2 °C, whilst mean cold month temperature estimates range between 0.9 °C and -2.7 °C (Craggs, 2005). Evidence for cooler (possibly winter) latest Cretaceous high-palaeo latitude temperatures comes from inferred ice-rafted dropstones from NE Asia (Ahlberg *et al.*, 2002) and evidence of seasonal frosts from tree ring records from NW Canada (Falcon-Lang *et al.*, 2004), whilst model simulations for the Campanian indicate small amounts of thin ice along the northern polar coastlines during the winter (Otto-Bliesner *et al.*, 2002). Sea ice may therefore have been able to form during the ~ 4 months of total darkness during the winter.

The exact nature of the detrital grains/laminae and clay-rich ‘blebs’ in the laminated diatom ooze of the CESAR 6 remains obscure, but they are not consistent with aeolian flux. It may be that at least some of the clay blebs represent seasonally deposited fecal pellets, although this mechanism cannot account for the relatively coarse detrital grains. The most consistent mechanism for transporting the observed detrital matter into the open ocean depositional setting of unit 4 is through ice (or possibly plant) rafting.

6.4.9 *Model of the annual flux cycle*

Laminations in the CESAR 6 have previously been interpreted as annual in origin. However, these previous interpretations lacked a thorough high-resolution BSEI study capable of describing the full range of microfabrics. In this study it has been shown that numerous laminae types are present within the biosiliceous unit, all of which can be attributed to different seasonal processes. Using these interpretations, a model of the annual flux cycle in the Late Cretaceous Arctic Ocean can be made. Laminations are considered as annual based on the regular alternation between resting spore and vegetative laminae. A transition matrix of the laminae in the CESAR 6, shown in Table 6.8, demonstrates that in general, mixed spore laminae are succeeded by mixed floral laminae. 93.6% of mixed vegetative laminae follow either mixed spore laminae, silicoflagellate/setae-rich laminae or near-monospecific *H. tumidicornis* and Spore '1' laminae, whilst 69.1% of mixed spore laminae follow one of the vegetative cell laminae. Table 6.8 also shows that 71.7% of silicoflagellate/setae-rich laminae occur above diatom vegetative cell laminae. The matrix also shows that near-monospecific *Hemiaulus* sp.1 laminae overwhelmingly occur above resting spore laminae (85.7%) and principally above Spore '1' laminae.

A B	**MV**	**H**	**Tr**	**An**	**MS**	**Tu**	**Sp.1**	**Hsp1**	**Sil**	**Rz**	**Det**
MV	2.4	–	–	3.6	57.1	–	66.3	–	63.7	36.7	100.0
H	–	–	–	–	0.6	–	–	–	–	3.3	–
Tr	1.6	–	–	–	3.4	–	7.0	–	3.2	3.3	–
An	0.4	–	–	–	8	–	7.0	–	4.8	6.7	–
MS	43.4	100.0	35	60.7	0.6	–	8.1	14.3	13.7	30.0	–
Tu	0.4	–	–	–	–	–	–	–	1.6	–	–
Sp.1	23.3	–	35	14.3	4.6	100	–	42.9	2.4	3.3	–
Hsp1	–	–	–	–	1.1	–	4.7	–	0.8	–	–
Sil	26.5	–	30	21.4	17.1	–	2.3	28.6	3.2	16.7	–
Rz	1.6	–	–	–	7.4	–	4.7	14.3	6.5	–	–
Det	0.4	–	–	–	–	–	–	–	–	–	–

Table 6.8. Transition matrix, showing the percentage of laminae A that follow laminae B. MV = mixed vegetative, H = near-monospecific *Hemiaulus* sp., Tr = near-monospecific *T. polychaeta*, An = near-monospecific *A. sibiricus*, MS = mixed spore, Tu = near-monospecific *H. tumidicornis*, Sp.1 = near-monospecific Spore '1', Hsp1 = near-monospecific *H.* sp. 1, Set = silicoflagellate/setae-rich, Rz = near-monospecific *Rhizosolenia* sp., Det = Detrital laminae. (N = 723).

The seasonal flux cycle may therefore be reconstructed by consideration of the ecology of the diatoms comprising the various laminae types. The intact nature of the various resting spores suggests that they were rapidly exported following blooms. These blooms are interpreted to have occurred during the spring, stimulated by the advent of sufficient irradiation and plentiful nutrients in the photic zone following winter mixing. Resting spore laminae are thus interpreted to represent the export flux following from spring blooms, triggered by the depletion of nutrients in surface waters and aided by the secretion of TEP (Fig 6.29).

Resting spore laminae primarily alternate with diatom vegetative cell laminae, often dominated by a diverse assemblage of *Hemiaulus*. The intact nature of the various diatoms in vegetative cell laminae also implies rapid export. The export mechanism for the vegetative cells is interpreted to relate to the “fall dump” mode of flux, based on the abundance and diversity of *Hemiaulus*. *Hemiaulus* dominates summer blooms in oligotrophic areas of the modern ocean (Brzezinski *et al.*, 1998; Scharek *et al.*, 1999b; Polat & Isik, 2002) forming summer flux or may be deposited in response to the break down of stratification (Kemp *et al.*, 2000). Consequently, vegetative cell laminae are interpreted to represent the summer or autumn “fall dump” export flux of diatom blooms adapted to exploit stratified/low ambient nutrient conditions (Fig 6.29).

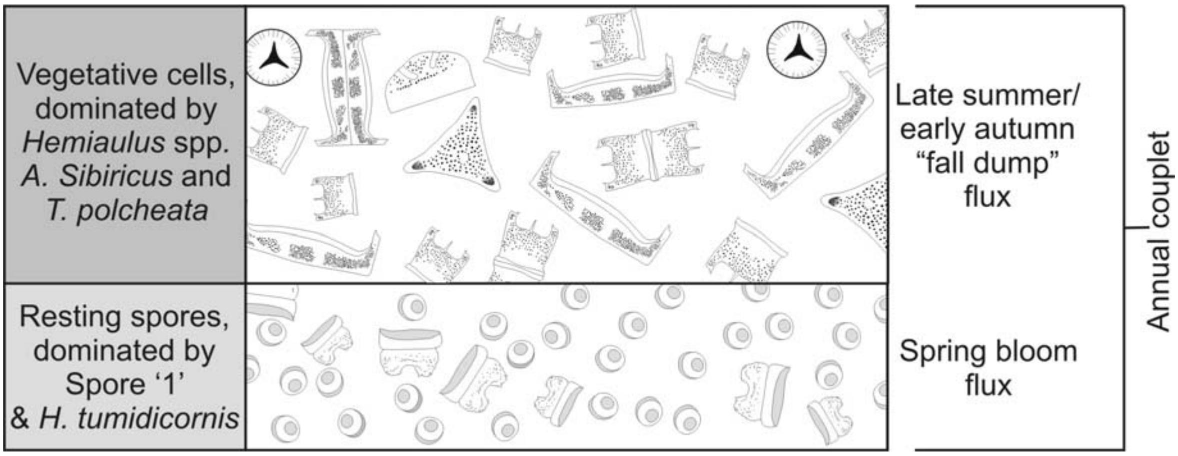

Figure 6.29. Basic two part annual flux cycle recorded in the CESAR 6. Figure shows a schematic representation of the two primary laminae fabrics; 1) resting spore laminae, dominated by Spore ‘1’ valves and *Hemiaulus tumidicornis* and 2) vegetative cell laminae, dominated by a diverse assemblage of *Hemiaulus* species, *Anaulus sibiricus* and *Trochosiropsis polychaeta*. For the key, see Figure 6.30.

The other laminae types also fit into this annual flux cycle. Near-monospecific *Rhizosolenia* laminae are frequently found above the diatom vegetative cell laminae, indicating they were deposited following the summer/autumn flux. Mass sedimentation of modern *Rhizosolenia* spp. occurs in the late autumn/winter, coincident with the breakdown of stratification (Sancetta, 1995). Modern *Rhizosolenid* cells are known to be able to regulate their buoyancy in order to move between a deep nutrient source and the photic zone (Villareal *et al.*, 1993; Villareal *et al.*, 1996) and to be able to grow in low-light conditions (1993). Near-monospecific *Rhizosolenia* laminae are therefore interpreted to be the late autumn/winter “fall dump” flux of deep dwelling diatoms adapted to exploit nutrients in a deep chlorophyll maximum (Fig. 6.30).

Silicoflagellate/setae-rich laminae, often containing a diatom hash component, are also found above diatom vegetative cell laminae, usually as concentrations along the base of resting spore laminae. The diatom hash component and the *Chaetoceros*-like setae within this laminae type are interpreted to represent the flux of spring blooms that were subjected to intense grazing and responsible for producing the abundant resting spores (Fig. 6.30). The flux of silicoflagellates is also interpreted to have been from a spring bloom, possibly aided by the secretion of TEP. The abundant sponge spicules in this laminae type do not seem to fit with the spring flux and may represent material deposited in the spring after being transported offshore and suspended in the water column during winter.

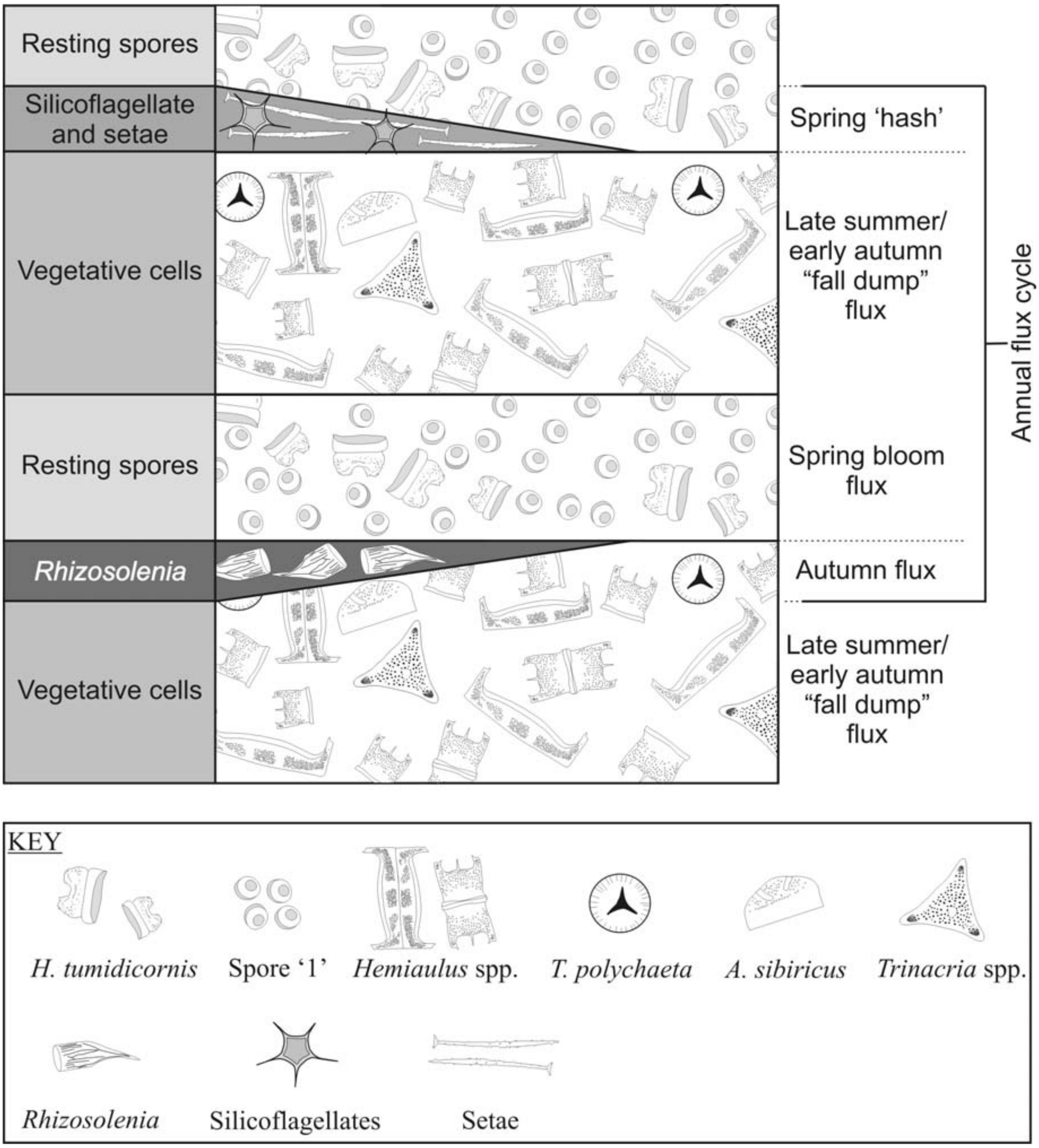

Figure 6.30. Four part annual flux cycle recorded in the CESAR 6. Figure shows a schematic representation of the main laminae fabrics; 1) vegetative cell laminae, which are overlain by 2) sporadic near-monospecific *Rhizosolenia* laminae. 3) Resting spore laminae, which often contain basal silicoflagellate/setae-rich laminae.

On the basis of average laminae thickness (Table 6.3), it is apparent that spring bloom flux and the flux from stratified producers were approximately equally contributors to the accumulation of the biosiliceous sediment.

6.4.10 *Implications of the diatom floral analysis*

Diatom floral analysis demonstrates that there occurs a marked change in the assemblage in the two lowermost samples (297.5-288.5 cm and 304-305 cm). These two samples are devoid of Spore '1' valves, contain only rare *T. polychaeta*, *Hemiaulus* spp., *H. tumidicornis, H.* sp. 1 and Spore '3' and also contain increased abundances of chrysophyte cysts, *Actinoptychus* spp., *A. sibiricus*, *G. odontella*, *Odontotropis*, *Pseudopyxilla* sp. (Strelnikova) and *S. crawfordii*. It does not seem coincidental that these two samples occur in subunit 4C, which is characterised by visual disruption of the laminated fabric. Laminae in subunit 4C dip at ~30°, whilst laminae in subunit 4B are horizontal (Fig. 6.2). The contact between the two subunits at 296 cm may be a hiatus (Mudie & Blasco, 1985). It is probable that the marked change in the floral assemblage between the two lowermost samples does indeed relate to a hiatus at 296 cm.

6.4.11 *Inferences on sedimentation rates and age distribution of unit 4*

Estimates of the sedimentation rate of the biosiliceous unit of the CESAR 6 core range wildly. Using the palaeomagnetic reversal data, Mudie *et al.* (1986) infer a sedimentation rate of no more than 0.02 cm/ka. Conversely, Clark (1988) postulated that the unit could represent as little as ~ 450 years, based on measurements of the colour laminations. In light of the fact that the compositional laminae in the CESAR 6 can be related to an annual flux cycle, it is possible to provide a firm varved based estimate of the sedimentation rate. The average varve thickness for all the laminae studied was found to be 250.1 μm (standard deviation of 137.0 μm), yielding a mean deposition rate of 25.01 cm/ka (11.31 – 38.72 cm/ka). In calculating the total period of deposition of the 176 cm of diatom ooze, it is possible to use the mean varve thickness for the entire core, as the total varve thickness does not vary significantly between samples (Fig. 6.21). Based on these figures, the ooze represents ~ 7037 years of deposition with a maximum and minimum period of deposition of 15564 and 4546 years, respectively. Although these estimates seem a remarkably short period of time, they are consistent with the observation of Barron (1985b) and those presented here, that there no diatom biostratigraphical changes are evident. Sedimentation rates for the CESAR 6 obtained in this study are also consistent with the conclusions of Firth and Clark (1998) and the view of Asku (1985) that palaeomagnetic data were equivocal with respect to determining sedimentation rates. Also a deposition rate of 25.01 cm/ka closely matches those of modern diatomaceous deposits. In the Santa Barbara Basin, diatom ooze is deposited at a rate of ~25-75 cm/ka (Bull & Kemp, 1995), in the Gulf of California at ~103.1 cm/ka (Pike & Kemp, 1996b) and ~185 cm/ka in Effingham Inlet (Chang *et al.*, 2003), whilst in the highly productive Saanich Inlet deposition rates probably average ~350 cm/ka, although are highly variable (ranging from 150 – 1700 cm/ka) (Dean *et al.*, 2001). However, the probable occurrence of a hiatus at the top of subunit

4C indicates that the total period of deposition of the biosiliceous unit is actually longer than that provided by varved based sedimentation rates.

6.4.12 *Implications of the results of BSEI on the benthic palaeoenvironment*

The preservation of submillimetre-scale alternating diatom resting spore/vegetative cell laminae does not fit with the interpretation that unit 4 was deposited in an oxic environment (Mudie & Blasco, 1985; Mudie *et al.*, 1986; Firth & Clark, 1998) but rather requires an anoxic benthic environment to suppress benthic activity. Unlike in the Marca Shale, where diatom valves are highly fragmented, partly as a consequence of mechanical fragmentation due to burial to depths of ~300-400m (Hein *et al.*, 1978), fragmentation of valves in CESAR 6 is virtually absent. This along with the lack of alteration of the primary opal-A suggests that the unit has not been buried to any significant depth and is likely to have been near surface for much of its history. Therefore, the sediment would have been within the influence of the post depositional benthic environment and it is feasible that oxidisation of the Fe and organic carbon within the diatom ooze reflects the influence of post depositional oxygenated pore waters. The volcaniclastic sediment (unit 3) overlying the biosiliceous sediment was interpreted by Mudie and Blasco (1985) to have been deposited in an oxic environment. It is probable that the oxic conditions characterising this later stage of sedimentation were responsible for oxidising the Fe and Mn precipitates and organic carbon in unit 4. Oxidation would have occurred in-situ, preserving the laminated microfabric of the sediment. Therefore, the preservation of the laminated fabric is interpreted to relate to an anoxic/dysaerobic benthic environment, probably relating to the flux of large amounts of organic carbon and presence of a structural sill. Massive intervals within the laminated succession reflect periods of elevated dissolved oxygen concentrations. It is known that in the Mediterranean Sea, diatom valves are only preserved in sediments that are buffered from the silica undersaturated waters in anoxic brine-basins, whose waters contain higher levels of dissolved silica (Kemp *et al.*, 1999). It is possible that some of the lack of biosilica in core Fl-533 relates to a similar mechanism.

6.4.13 *Diatom biostratigraphy and implications for the age of the biosiliceous sediment*

The observations of Barron (1985b) and those presented here, demonstrate that the difference between the Marca Shale and CESAR 6 floras is too great to be explained solely by ecology. Recent work has confined the age of the Marca Shale to 66-65 Ma (Fonseca, 1997) and based on the greater similarity with Late Campanian diatom deposits (Barron, 1985b) (and work presented here) and biostratigraphical constraints from other groups (Mudie & Blasco, 1985), the age of the CESAR 6 diatom ooze can be confidently placed prior to this. Palynomorph and silicoflagellate biostratigraphy place the CESAR 6 in the early Maastrichtian (Bukry, 1985; Firth & Clark, 1998).

Diatom biostratigraphy indicates the unit may be earlier than this, with comparisons with diatom floras from Seymour Island, DSDP Site 275, Ural Mountains and the Canadian Arctic constraining the unit to the late Late Campanian-Maastrichtian. Based on the biozones of Tapia and Harwood (2002), the absence of *A. morenoensis* indicates that the CESAR 6 must pre-date the Campanian-Maastrichtian boundary. However, *A. morenoensis* was interpreted to represent warmer, oceanic (El Niño) conditions in the Marca Shale (Chapter 4.4.8) and its absence may equally relate to an ecological constraint. It has been proposed that the Late Cretaceous central Arctic Ocean was a distinct ecological province (Bukry, 1981; Kitchell & Clark, 1982; Barron, 1985b; Bukry, 1985; Kitchell *et al.*, 1986; Dell'Agnese & Clark, 1994). The dark winters may have prevented many species, more prevalent at lower latitudes from penetrating into the central Arctic. It has also been proposed that there existed significant water-mass differences between the central Arctic Ocean and the sub-Arctic areas during the boreal summer, which may have prevented certain species from entering the Arctic Ocean (Dell'Agnese & Clark, 1994). Diatom biostratigraphy suggests a late Late Campanian age for the biosiliceous sediment of the CESAR 6 core, although an earliest Maastrichtian age cannot be discounted, in agreement with palynomorph and silicoflagellate age constraints.

6.5 CONCLUSIONS

- The biosiliceous unit of the CESAR 6 core contains a well preserved, laminated succession primarily composed of alternating diatomaceous vegetative cell laminae and resting spore laminae. The colour laminae described by Mudie and Blasco (1985) overprint these compositional laminae. The results of BSEI concur with earlier conclusions that the colour laminae relate to variations in the Fe content of the sediment due to proximal hydrothermal activity (Stoffyn-Egli, 1987).
- Resting spore laminae are interpreted to represent the flux from spring bloom diatoms that were able to rapidly exploit nutrients brought into the photic zone during winter mixing with the advent of sufficient incident light levels. Sporulation was triggered when available nutrients had become exhausted, and rapid export flux was mediated by the secretion of TEP.
- Diatom vegetative cell laminae are interpreted to represent the summer/ early fall flux of diatoms adapted to exploit nutrients trapped in a stratified water column or fuelled by N_2-fixing symbionts, based on the abundant and diverse *Hemiaulus* valves.
- The flux from spring bloom and stratified production were approximately equal contributors to the accumulation of the diatomaceous ooze.
- Detrital material concentrated in elongate ‘blebs’ were observed concentrated in resting spore laminae, which on rare occasions was observed to form detrital laminae, composed of clay and silt/fine sand ranging up to 290 μm in diameter. The origin of these detrital blebs and rare

detrital laminae remains enigmatic, although it is hypothesised that they may represent ice-rafted debris.

- On the basis of the regularity of the alternating laminae types and the fact that all fabric components fit into a model of the annual flux cycle, based on modern diatom ecology, the laminae are interpreted to be annual in origin.
- The interpretation of Mudie and Blasco (1985), Mudie *et al.* (1986) and Firth and Clark (1998) that the biosiliceous unit was deposited in an oxidising benthic environment is not compatible with the well-preserved laminated fabric described in this study. It is suggested that the shallow depth of burial of the biosiliceous sediment meant post depositional oxygenated pore waters were able to come in contact with the sediment. This scenario can account for the degradation of organic matter and oxidisation of the Fe precipitates, whilst still precluding benthic activity from disrupting the finely laminated microfabric.
- In agreement with the findings of Barron (1985b), no evidence for diatom biostratigraphic changes was found, consistent with the interpretation that the laminae are annual.
- Varved based sedimentation rates were calculated to be 25.01 cm/ka (± 13.70 cm/ka), indicating that the whole biosiliceous unit may have been deposited over as short a time interval as 7037 years (maximum and minimum of 15564 and 4546 years, respectively). However, the likely presence of a hiatus between subunits 4C and 4B indicate that the actual total period of deposition is likely to be longer than this estimate.
- Diatom biostratigraphic analysis shows that biosiliceous unit is most similar to the late Late Campanian *Stephanopyxis simonseni* zone of Tapia and Harwood (2002). However, in keeping with silicoflagellate and dinoflagellates biostratigraphy (Bukry, 1985; Mudie, 1985; Firth & Clark, 1998), an early Maastrichtian age cannot be ruled out on account of the paucity of early Maastrichtian diatomaceous sediments and the fact that the absence of the Maastrichtian diatom index fossil, *A. morenoensis*, may relate to ecological factors.

CHAPTER 7

Time-Series Analysis of the CESAR 6

7.1 INTRODUCTION

Data presented in Chapter 6 demonstrates that the pervasive, alternating laminae of diatom resting spores and vegetative cells in unit 4 of the CESAR 6 core are annual in nature. Further to this, the lack of any identifiable hiatuses (with the possible exception of the disruption at the top of subunit 4C) and evidence for any diatom evolution suggests that much of unit 4 represents a contiguous annual record of Late Cretaceous polar sedimentation. During the Late Cretaceous, conditions in the Arctic differed vastly from present, with SST's seasonally attaining 15°C (Jenkyns *et al.*, 2004) and forests reaching as far north as 85° (Spicer & Parrish, 1990). Average winter temperatures in the Arctic region have warmed by 3-4°C in the last 50 years, twice the rate of the rest of the globe, inferred to relate to anthropogenic greenhouse warming (Hassol, 2004). Climate model results indicating a further 3.5-6°C temperature increase by 2100 (Hassol, 2004). Parallel with the temperature increase, observed Arctic sea ice decreased by 20% from 1979-2003 and it is projected that the Arctic will lose 50-60% of its ice by 2100, with one model predicting that by 2070, the Artic will be so warm it will be ice-free during the summer (Hassol, 2004). The paucity of high resolution observational data sets meant that the general view amongst scientists prior to the 1990's was that the Artic was a relatively stable environment (Macdonald, 1996). However, in recent years it has become clear that many internal climate oscillations effect conditions in the Arctic region, including the PDO (Bjornsson *et al.*, 1995), ENSO (Jevrejeva *et al.*, 2004), the Arctic Oscillation (AO) (Liu *et al.*, 2004) and the North Atlantic Oscillation (NAO) (Mysak *et al.*, 1996). Although it is unlikely that future anthropogenic greenhouse warming will result in conditions similar to those of the Late Cretaceous, conditions in the Arctic during deposition of unit 4 of the CESAR 6 core do provide a good analogy to the predicted seasonally ice-free Arctic of the near future. It is well established that diatoms are sensitive to changes in oceanic/atmospheric conditions that result from many modern internal oscillations (e.g. ENSO, PDO and the QBO). Therefore, the high-resolution, seasonally resolved data set present within the CESAR 6 core provides a unique opportunity to examine the nature and dynamics of any climate variability within a warm, at least seasonally ice free Arctic Ocean, analogous to that predicted to result from anthropogenic warming.

7.2 MATERIAL AND METHODS

7.2.1 *Data Sets*

Spectral analysis was carried out on two records from subunit 4B. The first record (K4-1) was from the interval 210.5 – 225 cm and the second (K8-5) from the interval 196.5 – 210.5 cm. Even though the two records are contiguous, they could not be merged satisfactorily, due to missing material between K4-1 and K8-5 and thus it was decided to analyse the two records independently. Three parameters were subjected to analysis; total varve thickness, total resting spore varve segment thickness and total vegetative varve segment thickness. Total resting spore thickness is taken as a proxy for the export productivity during the spring bloom, whilst total vegetative cell thickness as a proxy for the export productivity from the period of stratification. Total varve thickness is taken as a proxy for the total annual productivity. The components of the microfabric used in the measurements of total spore thickness are mixed spore laminae, near-monospecific laminae of *Hemiaulus tumidicornis* and Spore ‘1’ along with silicoflagellate/setae-rich laminae. All other microfabric components were used in total vegetative cell thickness, apart from the rare detrital laminae which were removed from the record. K4-1 contains 450 varves (Fig. 7.1), whilst K8-5 is slightly longer at 507 varves (Fig. 7.2). Prior to spectral analysis any outliers, defined in this study as values 5 times greater than the mean, were removed and replaced with this value. Occasional massive intervals within the varved series (representing a maximum of 2.4% of the series) were patched with the average thickness of adjacent laminae, following Berger and von Rad (2002). Due to the fact that the Fourier transform treats the data as though it is repeated infinitely, any trend present in the data set will produce a spectral peak with the same frequency as the length of the time series. Thus, in order to avoid any artificial contamination of the spectrum by power at the lowest frequency, the data set was detrended using a linear function.

7.2.2 *Spectral analysis methods*

Time-series analysis was conducted using the SSA-MTM Toolkit version 4.2 (Dettinger *et al.*, 1995; Ghil *et al.*, 2002) in conjunction with Analyseries 1.2 (see Paillard *et al.*, 1996). Spectral estimations were obtained from three methods; the maximum entropy method (MEM) (Burg, 1975), the Blackman-Tukey method (Blackman & Tukey, 1958) and the multi-taper method (MTM) (Thomson, 1982), in order that the results of each method could be compared and spurious peaks discarded. Estimations from the MEM and Blackman-Tukey method were run using Analyseries 1.2, whilst MTM spectral analyses were run on the SSA-MTM Toolkit. To asses any long term variability in the amplitude and frequency of any significant cycles in the time series, data were also subject to wavelet analysis, using the wavelet transform software of Torrence and Compo (1998) at http://paos.colorado.edu/research/wavelets/.

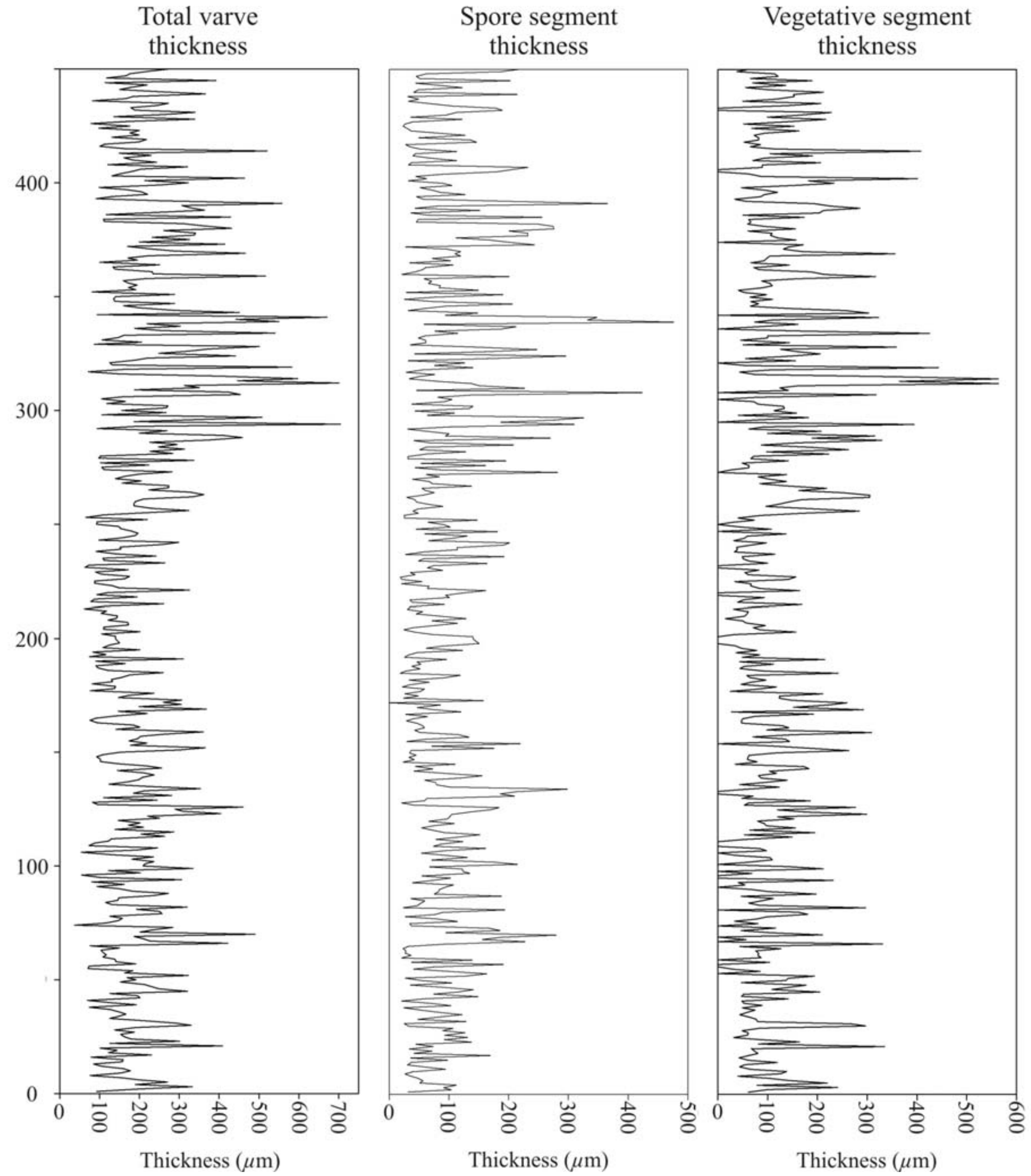

Figure 7.1. Raw total varve, resting spore varve segment and vegetative varve segment thickness time series for the interval K4-1. Data has had outliers removed and gaps have been patched.

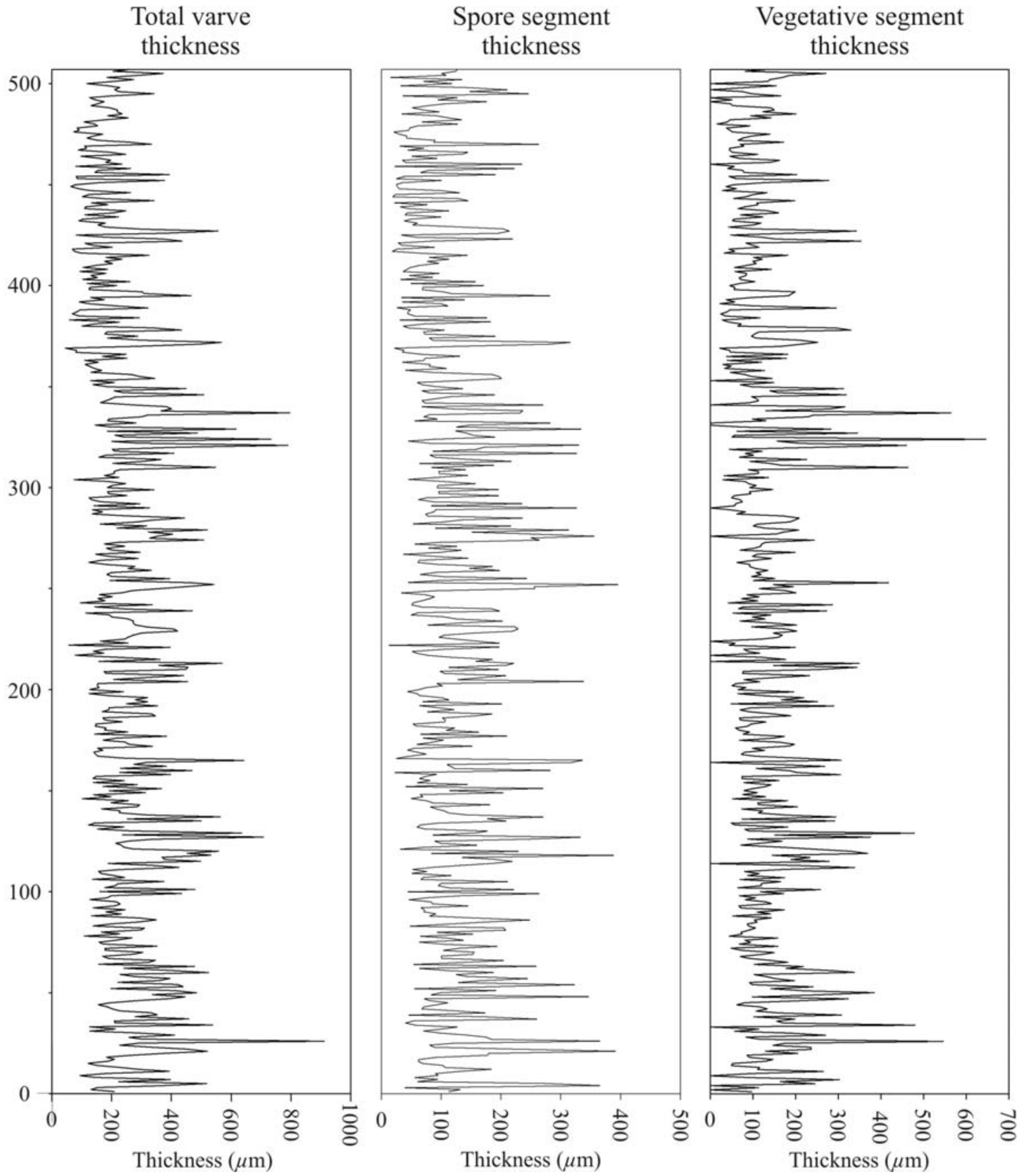

Figure 7.2. Raw total varve, resting spore varve segment and vegetative varve segment thickness time series for the interval K8-5. Gaps in the data have been patched, although no outliers were present.

7.2.2.1 *Maximum entropy method (MEM)*

The MEM is based on the theory that the less regular a time series is, the more information it contains. A time series with only one regular cycle may be entirely described by a single simple equation. In contrast, an irregular series requires a greater number of more complex equations to be explained and therefore ‘contains’ more information. Entropy is a measure of the information per unit time and hence a measure of disorder. The MEM involves initially calculating the autocovariance sequence for the data out to a certain lag or filter length, M. Autocovariance is determined by comparing a time series with itself using different degrees of offset. With the constraint that extrapolated autocovariance functions must agree with those calculated from 0 to M lags, the autocovariance for greater lags is then calculated on the assumption that the time series is as disordered as possible. Therefore the entropy of the time series autocorrelation (the autocorrelation measures the similarity of the times series with the offset counterpart) is maximised (Ulrych & Bishop, 1975; Weedon, 2003). Unlike the other two methods used, the MEM is parametric, equivalent to fitting the data as if they correspond to an autoregressive (red noise) process.

The choice of M (the number of lags or filter length) is critical. Large values of M yield high resolution spectral estimates which are statistically unstable resulting in spurious peaks, whilst lower values produce estimates with greater confidence but with low resolution (Olapido, 1988). M is usually chosen between $N/3$ and $N/20$ (N = the number of data points) (Weedon, 2003). Values of M should not exceed half the length of the time series and values larger than $N/3$ can result in spurious spectral peaks (Press *et al.*, 1992). Therefore in this study, M was set as a compromise between resolution and confidence and then increased incrementally until spectral peaks of interest stabilised. MEM provides spectral estimates with high resolution, although confidence levels can only be determined with great difficulty. MEM is used in this study to help identify spurious spectral peaks and to substantiate the resolution of peaks generated from other methods (e.g. Dean & Kemp, 2004).

7.2.2.2 *Blackman-Tukey method*

Blackman and Tukey (1958) developed the classical method of spectral analysis in which the autocovariance of the data is first computed, before a window (a smoothing function applied to finite observations or their Fourier transforms to minimise spectral “leakage”) is applied and the spectrum is computed. The Blackman-Tukey method is robust and unlikely to produce spurious spectral peaks, although the method does produce considerable smoothing. The Blackman-Tukey method also requires the investigator to select a trade off between confidence and spectral resolution in terms of the length of the autocovariance series. In this study, the length of the autocovariance series is expressed in terms of number of lags as a percentage of the length of the series. Several analyses were performed for each data set with different lengths for the autocovariance series, although a 30% lag was found to provide good estimates for both data sets. A Tukey spectral window was used as the smoothing function in all spectral estimations.

7.2.2.3 *Multi-taper method (MTM)*

In the MTM, time series are tapered using a series (ordinarily up to a maximum of 8) of special orthogonal data windows known as discrete prolate spheroidal sequences, which are constructed to minimise spectral leakage that results from the finite length of the time series. Different parts of the time series are suppressed by each taper and a periodogram is generated after each has been applied to the data. A spectrum is finally produced based on the average of the periodograms generated from each tapered series. The resultant spectral estimate possesses a small bias (well suppressed side-lobes), high frequency resolution and a distribution accommodating to the determination of confidence intervals (Mann & Lees, 1996; Weedon, 2003). The bandwidth can be calculated easily, being the Rayleigh frequency (1/N × sample interval) multiplied by the number of tapers. Owing to these factors, the MTM has been widely applied to atmospheric/ocean data sets (Ghil & Vautard, 1991; Mann & Park, 1993; Mann & Park, 1994; Thomson, 1995; Mann & Park, 1996; Minobe, 1997) and palaeoclimate proxy data (Thomson, 1990; Berger *et al.*, 1991; Mann & Lees, 1996; Olsen & Kent, 1996; Minobe, 1997; D'Arrigo *et al.*, 1999; Rittenour *et al.*, 2000; Tudhope *et al.*, 2001; Andrews *et al.*, 2003; Tiwari & Rao, 2004).

The MTM also suffers from the classical tradeoff between resolution and stability of the spectral estimate (Thomson, 1982). A greater number of tapers produce poor resolution, stable spectral estimates, whilst fewer tapers yield estimates with better resolution that are less stable. The number of tapers (K) used is investigator dependant, although only the first $2p$-1 tapers (where p is the time-frequency bandwidth parameter) are usefully resistant to spectral leakage (Slepian, 1978; Thomson, 1982; Park *et al.*, 1987) and therefore the number of tapers used should not exceed $2p$-1 (e.g. Ghil *et al.*, 2002). For relatively short climate records (of a few hundred data points) it has been suggested that K=3 and p=2 offers a good compromise between the resolution and the degrees of freedom for resolving high frequency (e.g. ENSO and decadal-scale variability) climate signals (Mann & Park, 1993; Mann & Park, 1994). Longer data sets may use a larger number of tapers whilst retaining the desired frequency resolution.

The MTM can provide estimates of both the continuous background component and the line (harmonic) components of the spectral estimate. Harmonic components relate to purely periodic cycles (i.e. cycles with constant frequency and phase). Using the SSA-MTM toolkit, the significance of narrowband signals is measured by their amplitude relative to the estimated noise background, whilst the significance of harmonic signals is measured by the Thomson variance ratio test for periodic signals (F-test). The continuous (narrowband) and harmonic proportions of the spectral estimate are separated by a reshaping procedure. Identified harmonic peaks are reshaped only if they are significant with respect to an estimated noise background. The background continuum spectrum was calculated assuming a robust autoregressive noise model and confidence levels were plotted at 90%, 95% and 99%. However, as spectral estimates from the MTM are often more optimistic than those from other methods, only peaks above or close to the 99% confidence level (and which were also present in the Blackman-Tukey and MEM spectral estimates) are discussed.

7.2.2.4 *Wavelet analysis*

Many climate data time series contain oscillations that are non stationary in terms of the amplitude and frequency. A good example of such an oscillation is ENSO, which has a dominant frequency between 2-7 years (Trenberth, 1997), with strong El Niño events occurring every ~8 to 12 years (Enfield & Cid, 1991). Wavelet analysis is a powerful tool that is able to decompose a time series into time/frequency space simultaneously, so that information on the amplitude of any oscillations is displayed along with how the amplitude of the oscillation varies over the length of the time series (Torrence & Compo, 1998). As such, wavelet analysis has been widely used in studies of atmospheric/ocean data sets (Torrence & Compo, 1998; Minobe & Mantua, 1999; Torrence & Webster, 1999; Chang *et al.*, 2004) and palaeoclimate proxy data sets (Bolton *et al.*, 1995; Patterson *et al.*, 2004; Moberg *et al.*, 2005; Niemitz & Billups, 2005). Linearly detrended time series were analysed with the wavelet transform software of Torrence and Compo (1998) assuming a red noise (autoregressive lag1) spectral background, and the 95% confidence levels were plotted. The data was not zero padded prior to analysis.

7.3 RESULTS

Significant spectral peaks (>99 % confidence level) were recorded in all the parameters analysed from both data sets. There is good agreement between the three spectral estimation methods (e.g. MTM, MEM and Blackman-Tukey method) in all analyses, with nearly identical periods for all significant spectral peaks, suggesting the peaks identified are not spurious. The results of the spectral analyses are summarised in Table 7.1 and Fig. 7.3, using the periods, bandwidth error and confidence levels obtained from the MEM. Total varve thickness records display significant spectral peaks at 5.15, 2.65, 2.80 and 2.26 years and a further peak just below the 99% confidence interval at 3.06 years (Fig. 7.4 and 7.8). Total spore varve segment thickness records display significant peaks at 13.48, 2.89, 2.77, 2.26 and 2.11 years, with further peaks just below the 99% confidence interval at 10.66, 8.68, 4.10 and 3.41 years (Fig. 7.5 and 7.9). Total vegetative varve segment thickness records contain significant peaks at 78.74, 25.58, 3.29, 3.11, 2.72, 2.62 and 2.26, (Fig. 7.6 and 7.10).

Time series	**Length of series (varve/years)**	**Parameter analysed**	**Confidence level (%) (H) = harmonic**	**Significant period (yr)**
K4-1	450	Total Varve	99	5.06 (**5.15**) 5.24
			99	2.24 (**2.26**) 2.28
			95	3.03 (**3.06**) 3.09
		Spore	99	12.90 (**13.48**) 14.11
			99	2.86 (**2.89**) 2.92
			99	2.24 (**2.26**) 2.28
			95 (H)	10.29 (**10.66**) 11.05
			95	3.37 (**3.41**) 3.45
		Vegetative	99	23.57 (**25.58**) 27.96
			99	3.08 (**3.11**) 3.14
			99	2.60 (**2.62**) 2.64
			99	2.24 (**2.26**) 2.28
K8-5	507	Total Varve	99 (H)	2.78 (**2.80**) 2.82
			99 (H)	2.63 (**2.65**) 2.67
		Spore	99 (H)	2.75 (**2.77**) 2.79
			99	2.10 (**2.11**) 2.12
			95 (H)	8.46 (**8.68**) 8.91
			95	4.05 (**4.10**) 4.15
		Vegetative	99 (H)	63.86 (**78.74**) 102.67
			99	3.26 (**3.29**) 3.32
			99	2.70 (**2.72**) 2.74

Table 7.1. Summary of the significant spectral peaks identified in total varve thickness and in the spore and vegetative varve segment thickness for K4-1 and K8-5. The periods shown are those identified using the MTM. Periods are shown for the bandwidth with the period at maximum power in parenthesis. Peaks identified as harmonic signals are indicated by (H).

The results of wavelet analysis further confirm the significant periodicities identified using the other spectral methods, but demonstrate that the power of each cycle varied with time. In K4-1 there is a ~100 year period between varves ~150-250 where all periodic oscillations are absent (Fig. 7.7). In total varve thickness, significant variability (>95% confidence interval) is shown in the 2-4 year frequency band, the power of which is greatly modulated on multi-decadal time scales, with greatest power post varve year 250 (Fig. 7.7a). A similar pattern in the quasi-biennial variability is expressed in total resting spore and vegetative segment thickness. Wavelet analysis also shows that variability with a period of ~5 year in the total varve record is only significant in the interval between varves ~280-350. Total resting spore segment thickness displays significant power in the quasi-decadal frequency band, which is best expressed in the interval between varves ~280-350 (Fig. 7.7b). Total vegetative segment displays strong variability with a ~25 year periodicity between varves ~240-350 (Fig. 7.7c).

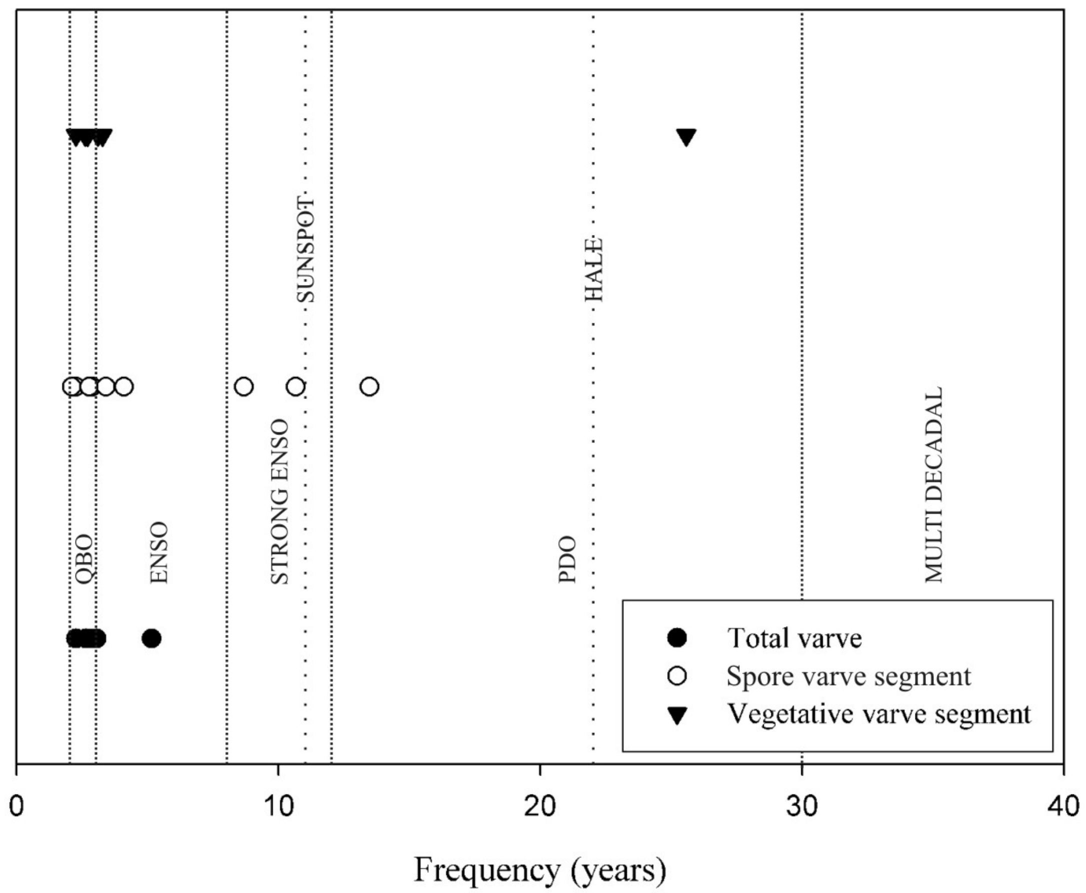

Figure 7.3. Summary of the significant frequencies for each parameter analysed along with the modern frequency bands of the major internal and external forcing mechanisms discussed in Chapter 5.4.1. Note that the 78.74 year peak identified in the vegetative varve segment of K8-5 is not included.

In K8-5 the quasi-biennial variability display modulation on a decadal/ multi-decadal scale, but does not demonstrate a long period of absence seen in K4-1 (Fig. 7.11). Similar periods of strong/ weak quasi-biennial variability are displayed by all three parameters. Total spore varve segment thickness demonstrates significant variability in the sub-decadal (4-8 year) frequency band, and also expresses significant power in the multi-decadal (~20 year) frequency band (Fig. 7.11b). Total vegetative varve segment displays significant power in the ~70-80 year frequency band, identified in the other spectral estimates, through the whole record and also shows power in the quasi-decadal frequency band (Fig. 7.11c).

Figure 7.4. (Below) Results of spectral analysis on total varve thickness from K4-1. A) Multi taper method analysis with background spectrum and 90%, 95%, 99% confidence intervals. Harmonic peaks are also shown. B) Blackman-Tukey spectral estimation with a second order polynomial background spectrum plotted. C) Maximum entropy method spectral estimate.

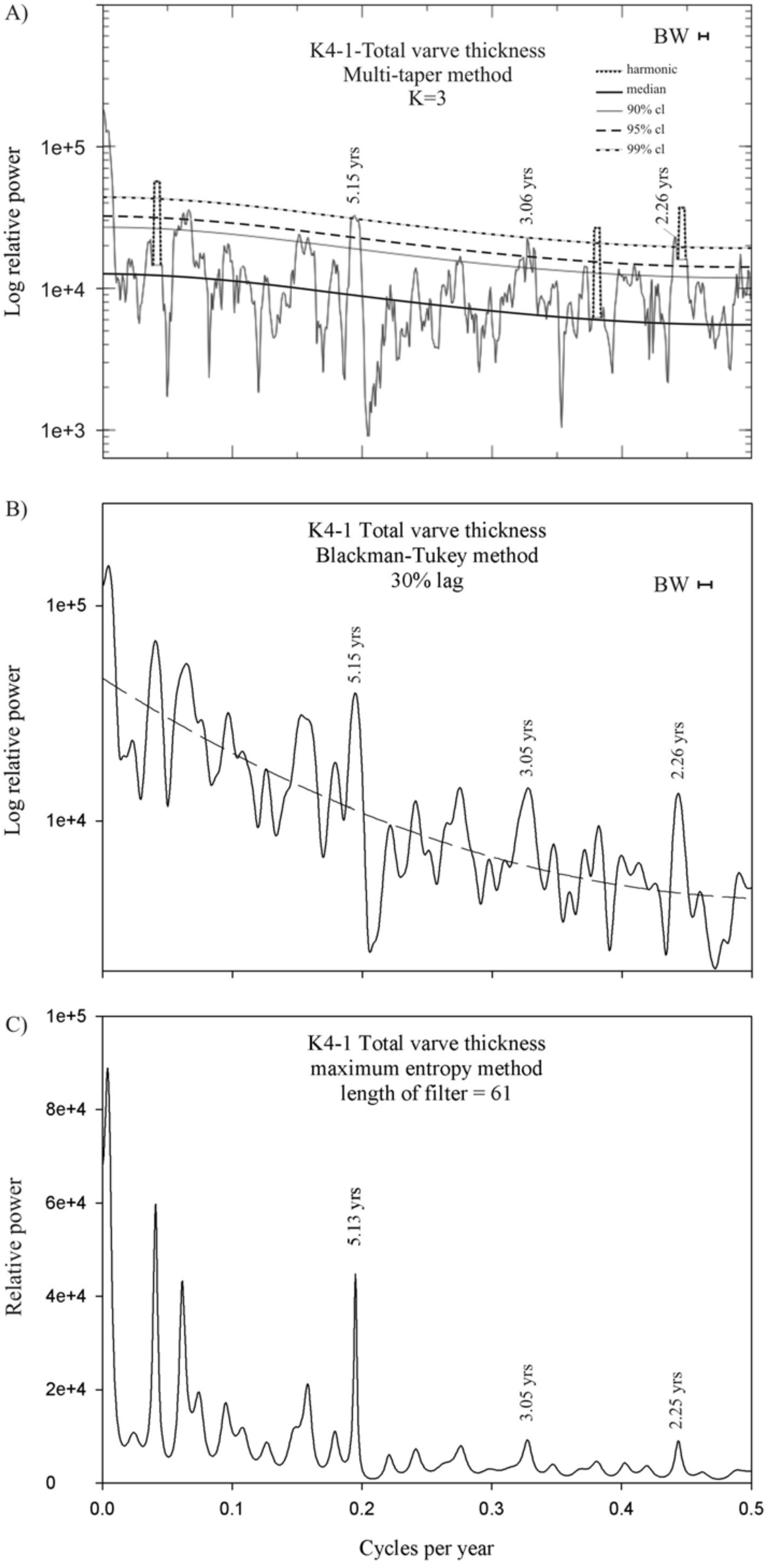
A)
K4-1-Total varve thickness
Multi-taper method
K=3
BW
harmonic
median
90% cl
95% cl
99% cl
5.15 yrs
3.06 yrs
2.26 yrs
Log relative power
1e+5
1e+4
1e+3
B)
K4-1 Total varve thickness
Blackman-Tukey method
30% lag
BW
5.15 yrs
3.05 yrs
2.26 yrs
Log relative power
1e+5
1e+4
C)
K4-1 Total varve thickness
maximum entropy method
length of filter = 61
5.13 yrs
3.05 yrs
2.25 yrs
Relative power
1e+5
8e+4
6e+4
4e+4
2e+4
0
0.0
0.1
0.2
0.3
0.4
0.5
Cycles per year

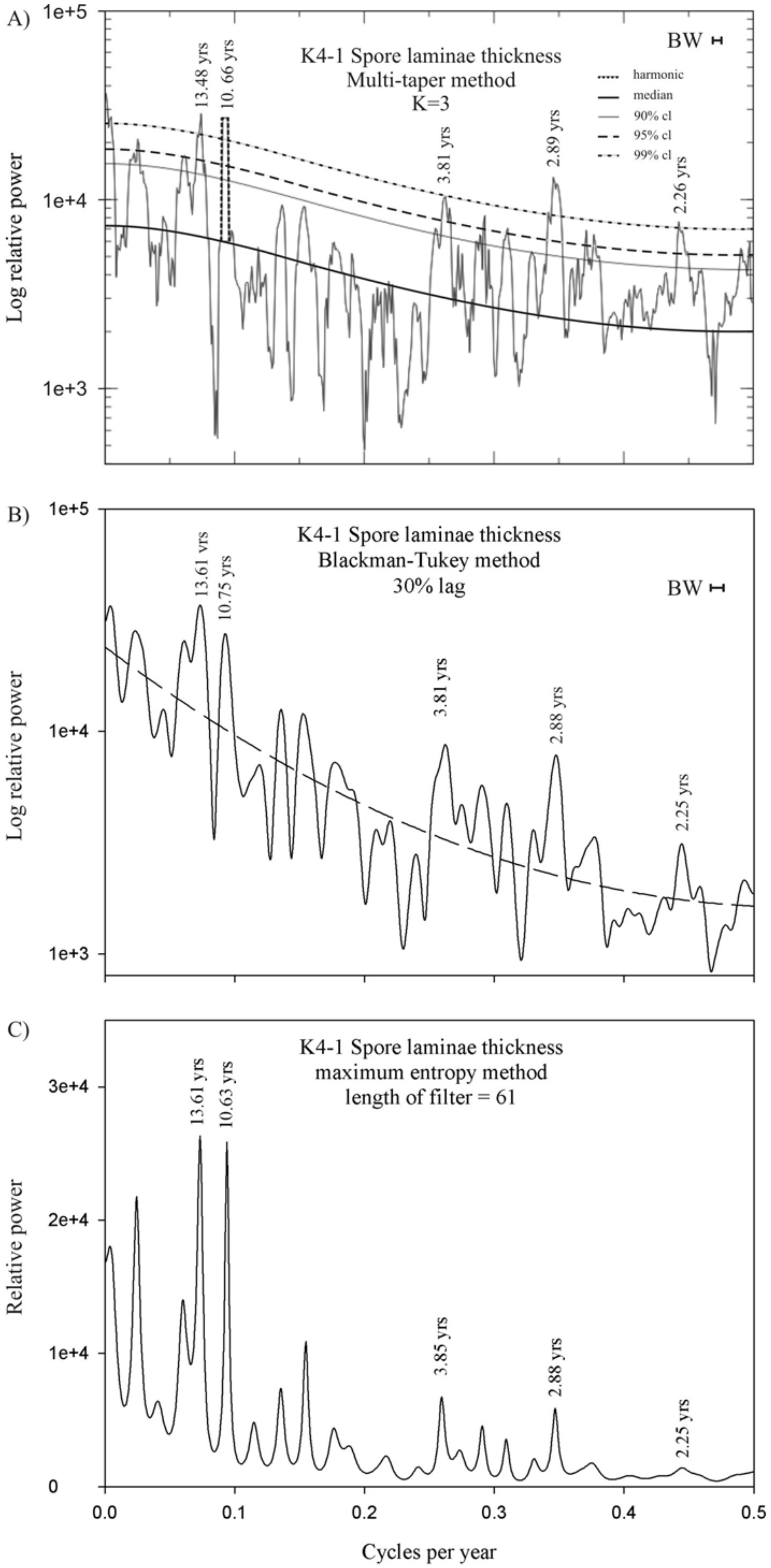

Figure 7.5. Results of spectral analysis on spore laminae thickness from K4-1.

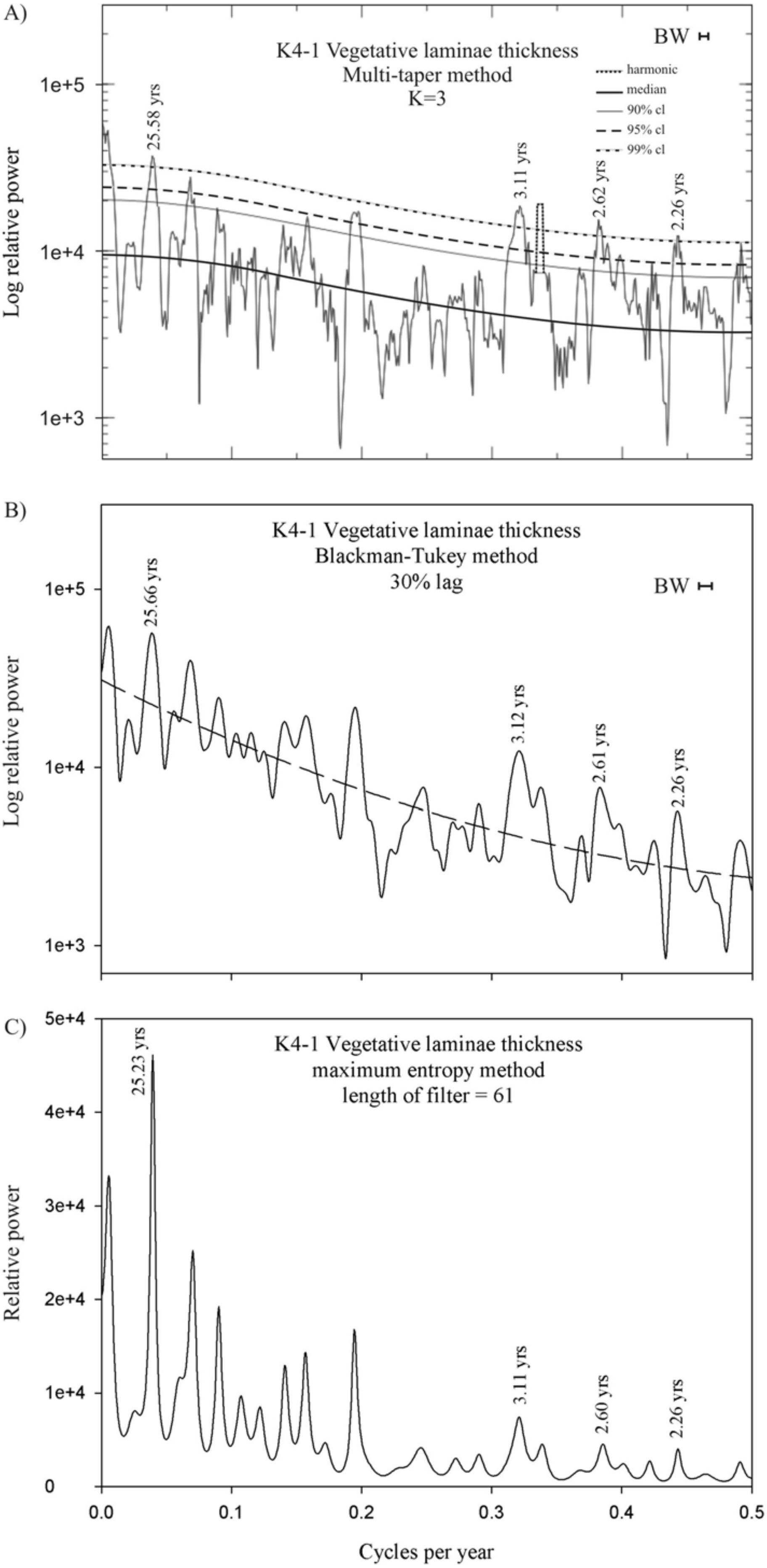

Figure 7.6. Results of spectral analysis on vegetative laminae thickness from K4-1.

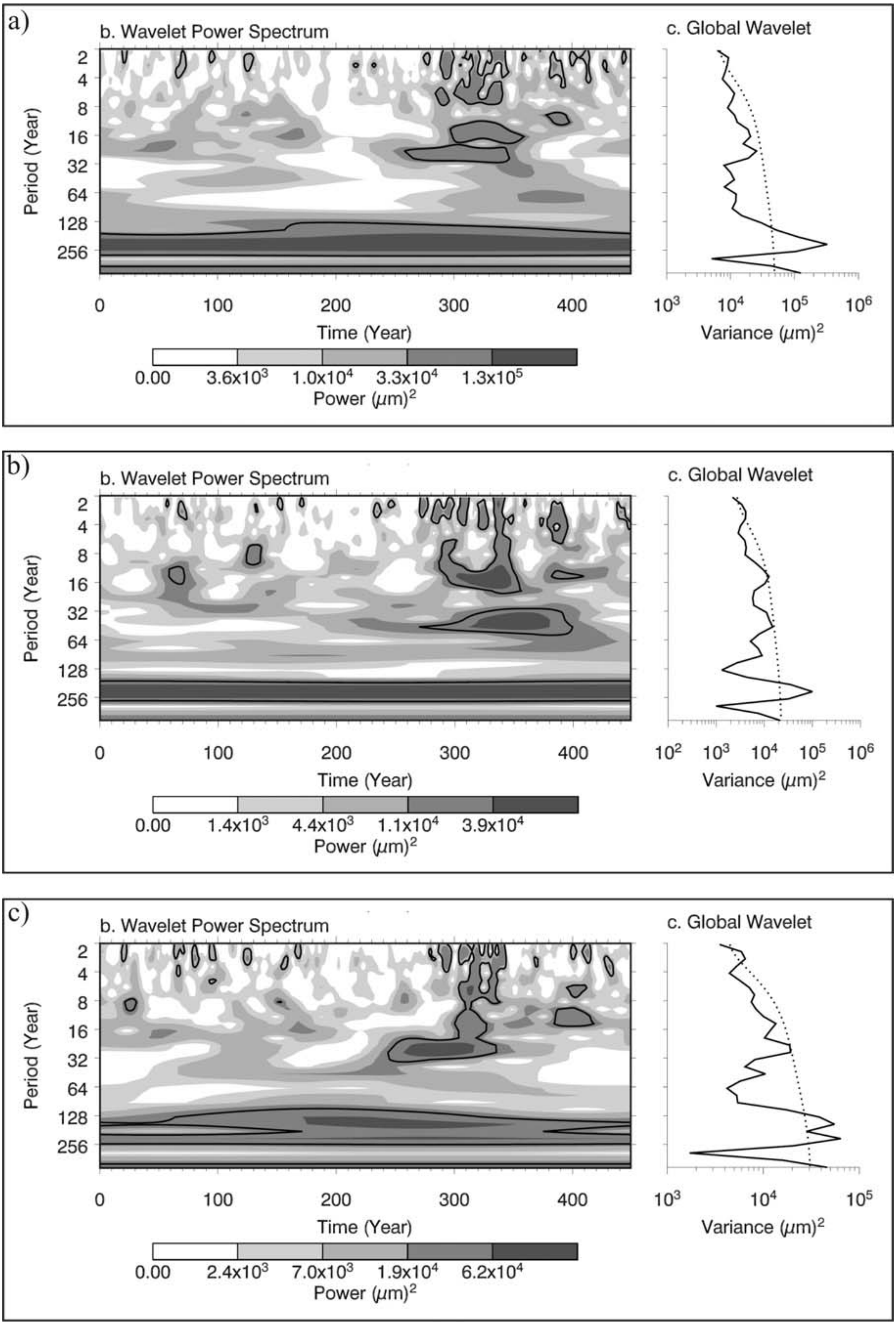

Figure 7.7. Wavelet power spectrum for a) total varve, b) spore laminae and c) vegetative laminae thickness for K4-1. The contour levels are chosen so that 75%, 50%, 25%, and 5% of the wavelet power is above each level, respectively. Black contour is the 5% significance level (95% confidence interval), using a red-noise (autoregressive) background spectrum. The global wavelet power spectrum highlights in which frequencies variability is significant above the 95% significance level (dashed line) for the global wavelet spectrum, using an autoregressive background spectrum.

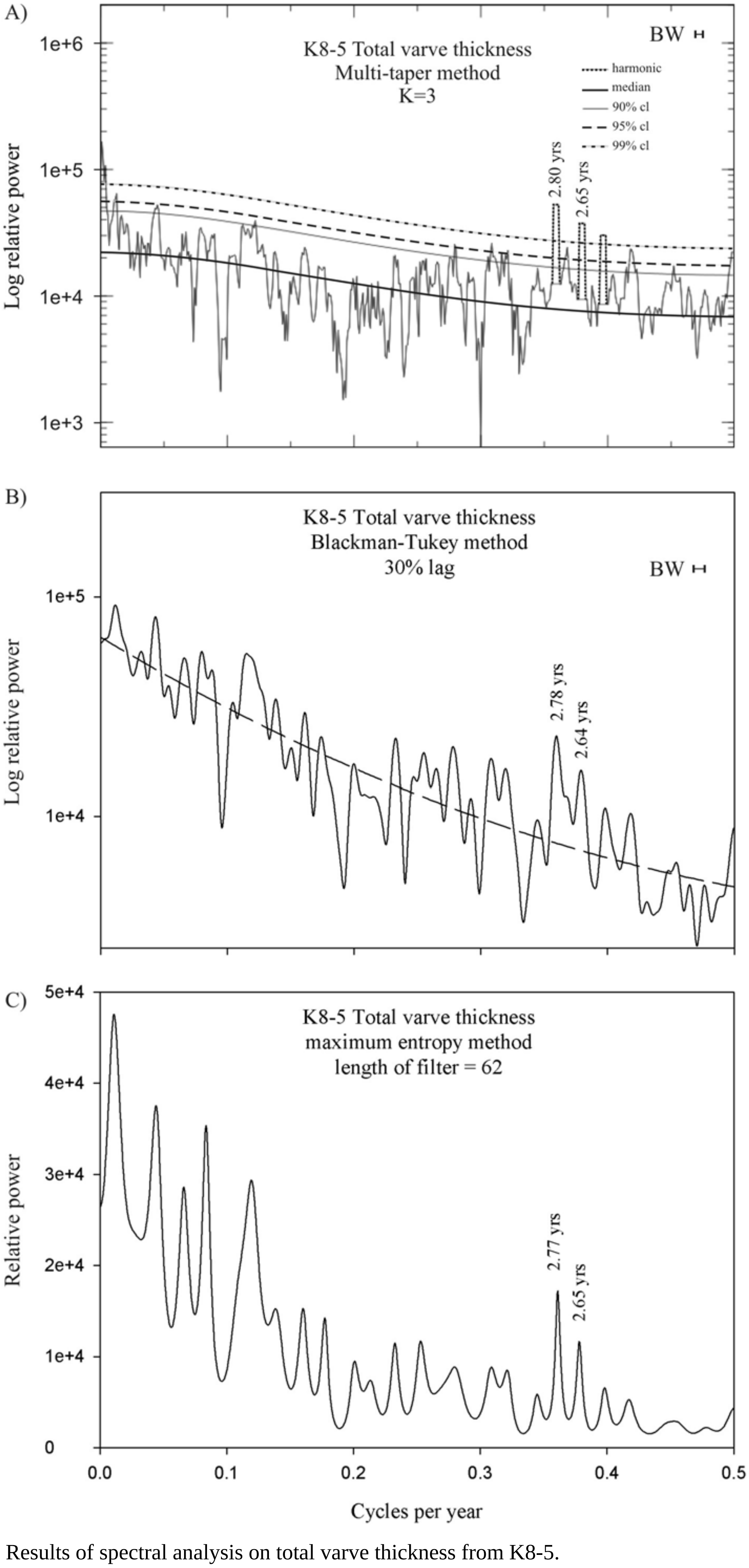

Figure 7.8. Results of spectral analysis on total varve thickness from K8-5.

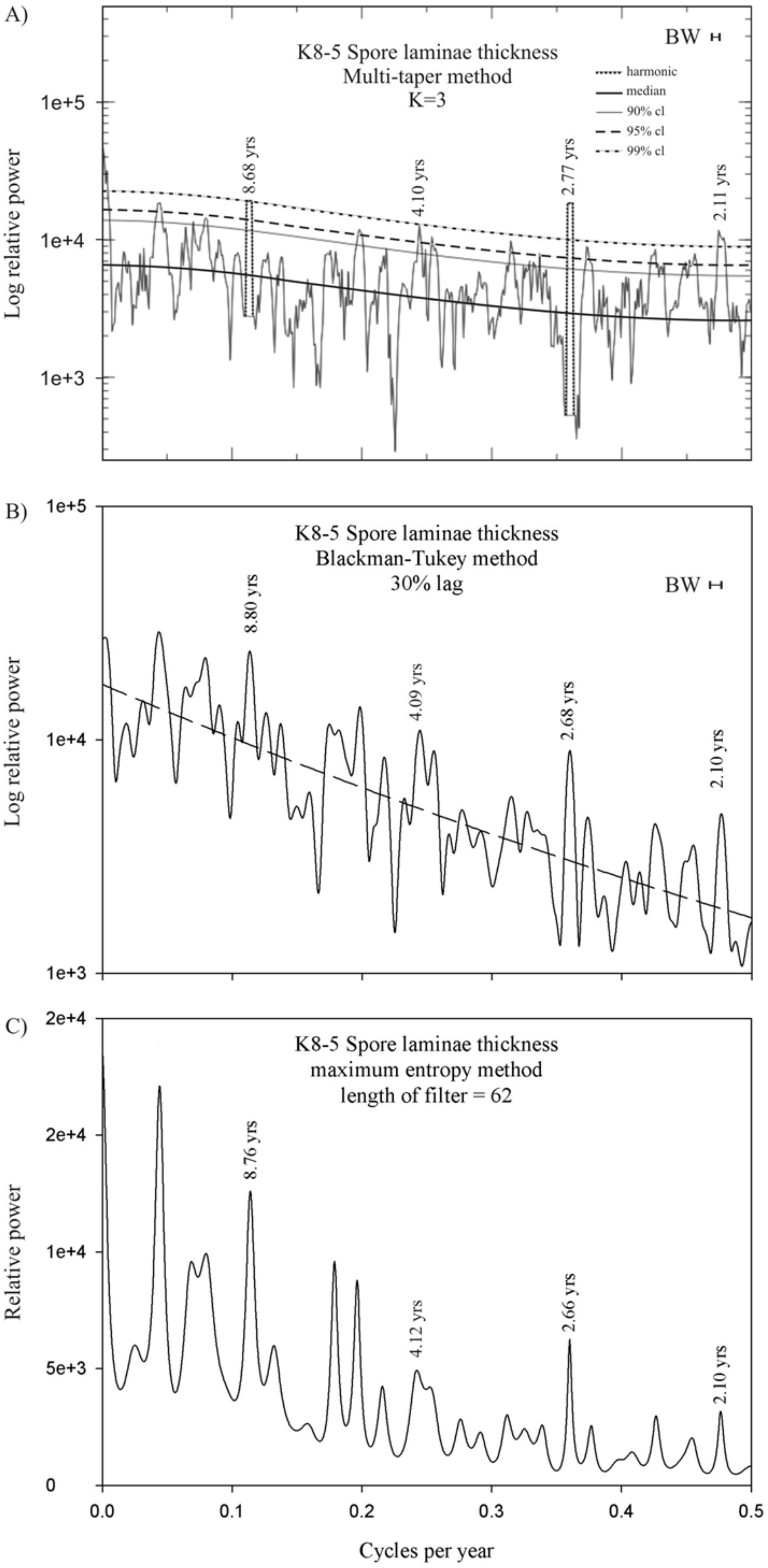

Figure 7.9. Results of spectral analysis on spore laminae thickness from K8-5.

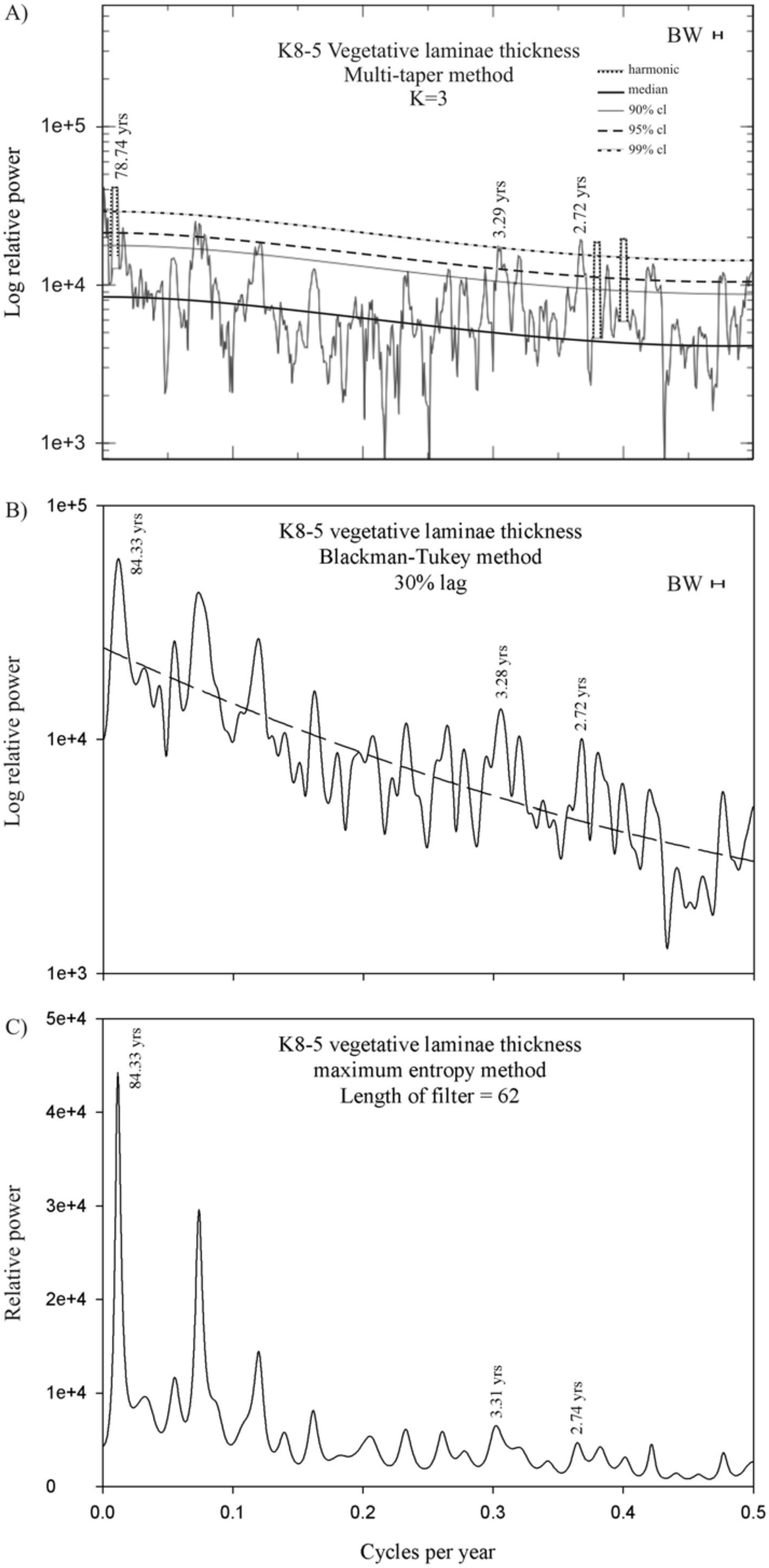

Figure 7.10. Results of spectral analysis on vegetative laminae thickness from K8-5.

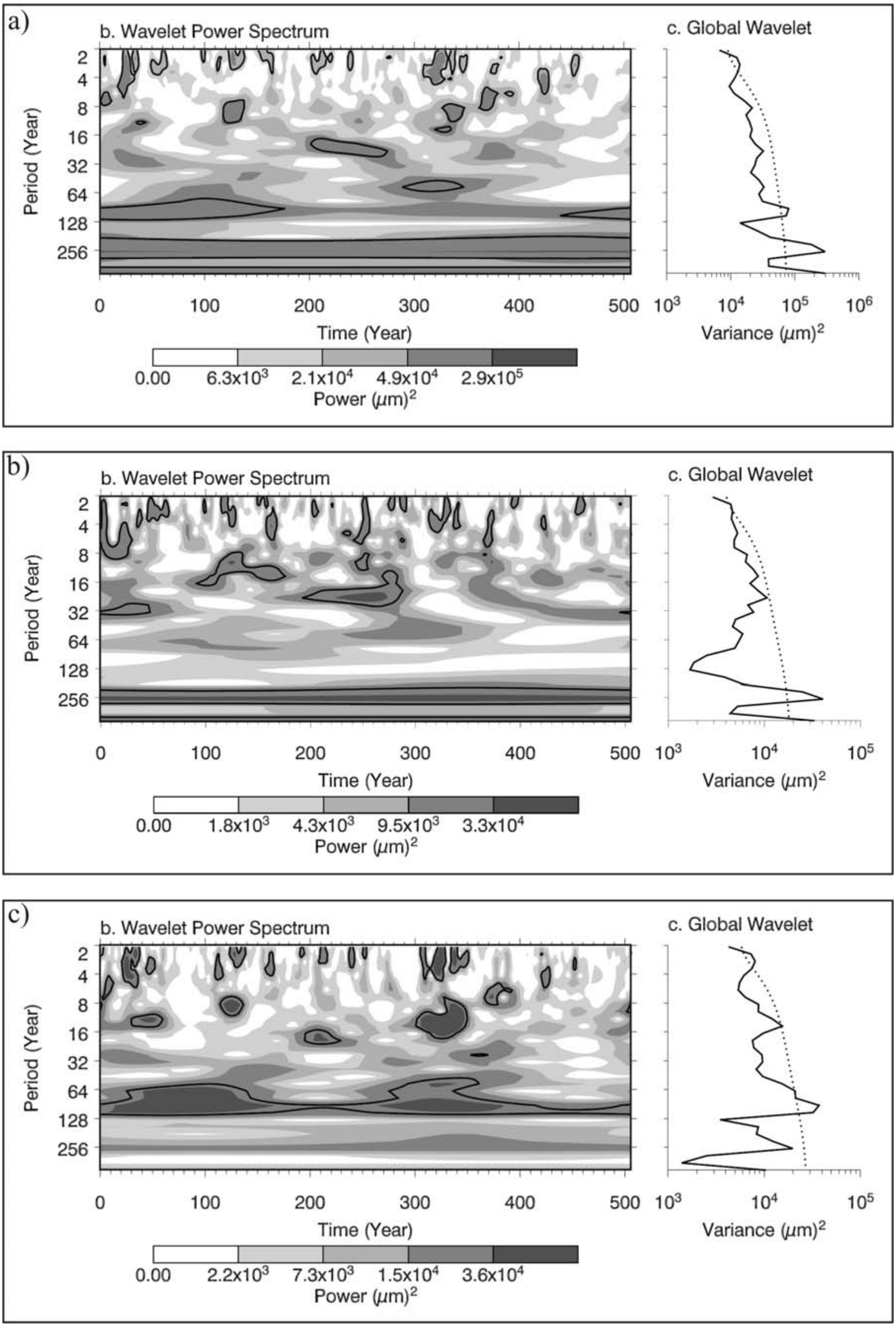

Figure 7.11. Wavelet power spectrum for a) total varve, b) spore laminae and c) vegetative laminae thickness for K5-8. The contour levels are chosen so that 75%, 50%, 25%, and 5% of the wavelet power is above each level, respectively. Black contour is the 95% significance level, using a red-noise (autoregressive) background spectrum. The global wavelet power spectrum highlights in which frequencies variability is significant above the 95% significance level (dashed line) for the global wavelet spectrum, using an autoregressive background spectrum.

7.4 INTERPRETATION AND DISCUSSION

7.4.1 *Review of the possible mechanisms capable of producing the spectral peaks*

Author	**Data set**	**Significant periods (years)**
Rasmusson *et al.* (1990)	Analysis of surface marine wind and SST data from the period 1950–1987, together with sea surface temperature and sea level pressure data from several stations in the north Pacific.	2 – 2.5 4 – 5
Sonett *et al.* (1992)	Laminae thickness changes in Holocene cores from the sub-arctic Swedish Ångermanaälven river valley and estuary.	2.25 – 2.33 3.6 – 3.8 7.6 19.1
Ware (1995)	Analysis of measurements of NE Pacific temperature and wind stress	2 – 3 5 – 7 20 – 25 50 – 75
Mann & Park (1996)	Sea surface temperature and sea level pressure data for the Northern Hemisphere between 1899-1993	2.1 – 2.2 3 – 4 5 – 7 10 – 11 16 – 18
Minobe (1997)	Analysis of air temperatures, sea level pressure and SST in the NE Pacific region	50 – 70
Conversi & Hameed (1998)	Records of zooplankton biomass, SST and salinity from the Gulf of Alaska	2.4 6 12 24
D'Arrigo *et al.* (1999)	Sea surface temperature reconstruction of the Gulf of Alaska from tree ring data	3 – 4 14 25 50
Cook *et al.* (2002)	Analysis of a winter NAO multiproxy reconstruction, spanning the period 1400-1979.	2.7 – 2.04 3.97 7.75
Dean & Kemp (2004)	BSEI of Holocene laminated diatomaceous sediments, Saanich Inlet, British Columbia	2.6 3.5 14.8 31.3 42.2
Jevrejeva *et al.* (2004)	Ice conditions in the Arctic, correlated with the Arctic Oscillation and Southern Oscillation indices, over the period ~1857-2000	2.3 3.5 5.7 13.9
Patterson *et al.* (2004)	Gray scale analysis of Holocene laminated diatomaceous sediments, Effingham Inlet, Vancouver Island	18 – 28 31 – 38 ~75 – 90
Raspopov *et al.* (2004)	Dendrochronological data from the Barents Sea region and northern timberline of Russia coastal, over the last several centuries	11 – 12 23 90

Table 7.2. List of the results of selected studies on material from the high northern latitudes and Arctic region that have identified periodicities similar to those found in the CESAR 6.

In this section, the possible mechanisms capable of producing the observed spectral peaks will be discussed in relation to northern high latitudes. Many of the mechanisms were introduced in Chapter 5.4.1 and will not be discussed in detail again, although some mechanisms specific to the Arctic region will be introduced and discussed in more detail. The results of a selection of studies from northern high latitudes with similar periodicities to those identified in the CESAR 6 are given in Table 7.2.

7.4.1.1 *The Arctic Oscillation (AO) and North Atlantic Oscillation (NAO); the Northern Hemisphere Annular Mode (NAM)*

In the modern climate system, the dominance of two opposing atmospheric pressure systems in northern high and mid latitudes varies with time and has been termed the "Arctic Oscillation" (Brady *et al.*, 1998). The negative (or cool) phase of the AO is characterised by higher than normal pressure over the polar region and lower than normal pressure at midlatitudes (main centre of between 37-45°N), whilst the positive (warm) phase by lower pressure over the pole and higher pressure at midlatitudes. During the positive phase, the intensification in the polar low pressure system (polar vortex) draws greater amounts of warm air from lower latitudes. The AO can therefore be regarded as a robust surface manifestation of the strength of the polar vortex (Brady *et al.*, 1998). The NAO correlates very strongly with the AO and may be regarded as a manifestation of the AO in the Atlantic sector. Collectively, the AO and NAO are known as the Northern Hemisphere Annular Mode (NAM) (e.g. Thompson *et al.*, 2002). Ice core records suggest most of the NAM variability occurs at periods between 13 and 6 years (Appenzeller *et al.*, 1998), whilst a recent multiproxy reconstruction of the NAO contained significant variability at 7.75 years, 3.97 years and QBO frequencies (Tudhope *et al.*, 2001). Over most of the last century the NAM has oscillated between the positive and negative phases, but in ~1988-1989 the NAM entered a strong positive phase. In the Arctic, NAM variability is associated with quasi-decadal oscillation in the extent of sea ice and winter sea level pressure (Mysak & Venegas, 1998; Wang & Ikeda, 2000; Wang *et al.*, 2005). The recent trend of decreasing sea-ice in the Arctic relates to the intensification of the NAM (intensification of the wintertime polar vortex), thought to relate to anthropogenic greenhouse warming and/or longer frequency natural variability (Wang & Ikeda, 2000).

7.4.1.2 *The QBO, ENSO and PDO*

The stratospheric QBO, is known to affect the strength of the polar vortex (Holton & Tan, 1980; Baldwin *et al.*, 2001) and in so doing, to determine the character of the early winter in the Arctic. In December and January, a colder and more stable polar vortex occurs during the west phase of the QBO and a warmer, more disturbed polar vortex during the east phase (Soukharev, 1997). The

QBO therefore, directly impacts the NAM through its influence on the wintertime polar vortex, evidenced by statistically significant coherence on ~27 month timescales in QBO and NAM time series (Coughlin & Tung, 2001) and presence of strong QBO peaks in NAO reconstructions (Tudhope *et al.*, 2001). The QBO is also thought to effect sea level pressure and air temperature through fluctuations in the polar stratosphere, caused by modulations of the polar night jet over the 11-year Schwabe cycle (Labitzke & van Loon, 1990).The importance of the QBO on surface conditions was highlighted by Thompson *et al.* (2002), who found that the signature of the QBO on northern hemisphere winter temperatures is roughly comparable in amplitude to that attributed to ENSO. Through its influence on the polar vortex and consequently the NAM, the QBO is likely to leave a large signature on Arctic time series. QBO signals are known to be present in modern records of ocean biota, SST and salinity from northern high latitudes (Conversi & Hameed, 1997; Conversi & Hameed, 1998; Dean & Kemp, 2004). Sonett *et al.* (1992) also found a strong QBO signal in thickness variations in sedimentary laminae in a core from the sub-arctic Swedish Ångermanaälven river valley. Sea surface temperature and pressure data from the northern hemisphere over the last century also displays strong quasi-biennial variability (Mann & Park, 1996).

Although originating in the equatorial Pacific, the effects of ENSO are known to extend into high northern latitudes (e.g. Dean & Kemp, 2004). However, is it possible that ENSO can have an expression at almost polar northern latitudes? Recent measurements of sea ice distribution in the Arctic have revealed that ENSO signatures are in fact transported to the polar regions (Gloersen, 1995; Jevrejeva *et al.*, 2004; Liu *et al.*, 2004). Jevrejeva *et al.* (2004) found significant peaks in the distribution of sea ice in the Arctic at 2.2, 3.5, 5.7 and 13.9 years, which could be related to similar peaks in the Southern Oscillation Index, AO index and the Niño3 data sets. Phase relationships suggested to the authors that the 2.2, 3.5 and 5.7 year signals detected in ice conditions are generated in the equatorial Pacific and transmitted via stratospheric extra-tropical wave propagation to the Arctic, affecting the breakdown of the wintertime stratospheric polar vortex. The NAM can be thought of as the physical variability associated with the structure of the polar vortex, and therefore the 2.2 – 5.7 year tropical forcing affects high latitude weather patterns by manipulating the NAM. The 13.9 year signal is generated in the western Pacific and is interpreted to relate to the propagation of equatorial coupled waves and fast boundary waves. A similar 13.9 year signal is known from a 2000 year ice core record from Antarctica, inferred to relate to variability in the Antarctic Circumpolar Wave (Fischer *et al.*, 2004), which Park *et al.* (2004) argued related to a teleconnection of ENSO.

In contrast to ENSO, the main climatic fingerprint of the modern PDO is felt in the north Pacific (Chapter 5.4.1.4). As such, the PDO may have a significant influence on conditions in the polar region, although due to a lack of data sets with sufficient temporal extent, this suggestion remains speculative. However, precipitation and runoff in the Mackenzie drainage basin (Canadian Arctic) demonstrates decadal variability (Bjornsson *et al.*, 1995), possibly related to the PDO. Variability attributed to the PDO has also been recorded in tree ring SST reconstruction for the Gulf of Alaska (D'Arrigo *et al.*, 1999), whilst instrumental records of SST and salinity from the Gulf of Alaska show a strong multidecadal signal (Conversi & Hameed, 1998), which may also represent the influence of the PDO.

7.4.2 *Significance of the spectral peaks in total spore varve segment*

7.4.2.1 *Quasi-biennial peaks*

Total spore varve segment thickness records are dominated by quasi-biennial peaks (all of which were above the 99% significance level), occurring at 2.89, 2.77, 2.26 and 2.11 years. In modern climate records, significant spectral peaks in this frequency band may be related to the QBO or to the biennial component of ENSO variability (Rasmusson *et al.*, 1990). The QBO is known to have a significant effect on conditions in the modern Arctic by modulating the polar night jet and the strength of the polar vortex as part of the NAM (Holton & Tan, 1980; Labitzke & van Loon, 1990; Baldwin *et al.*, 2001). It can be expected that a polar night jet would have existed in the Cretaceous Arctic stratosphere and a polar vortex must also have been present during the winter. Modulation of spring bloom export flux probably would have been related to variability in the level of nutrients in the photic zone, analogous to variations in diatom export flux modulated by the strength of upwelling (e.g. Bull *et al.*, 2000). Nutrient availability is interpreted to relate to; 1) the degree of winter mixing, an artefact of the severity of winter storms or alternatively to; 2) winter open-ocean upwelling (Table 7.3), as proposed by Kitchell and Clark (1982), an artefact of the strength of an Arctic low pressure system (i.e. the polar vortex). It is probable that modulation of the polar vortex/polar night jet by the stratospheric QBO would have affected the intensity of winter storms or the development of the winter low pressure system over the Cretaceous Arctic Ocean, causing quasi-biennial fluctuations in the availability of nutrients in the photic zone in the spring. Changes in SST's and salinities also may have been influential in modifying diatom resting spore flux. Although spectral estimates from both total spore varve segment data sets display significant peaks in the sub-decadal ESNO frequency band, these peaks are not as strong as the quasi-biennial peaks, suggesting the two have different origins. It is therefore interpreted that the dominant quasi-biennial spectral peaks in the total resting spore varve segment relate to the influence of a stratospheric QBO on the Cretaceous polar vortex/polar night jet and hence the NAM. The inference of the occurrence of an atmospheric QBO is consistent with quasi-biennial signals, inferred to relate to the QBO, identified in the Marca Shale (Chapter 5.4.4.1). The mean periodicity of the inferred QBO signal in total spore varve segment is 2.51 years (30.1 months), close to the mean periodicity recorded in the modern stratosphere (~28 months) and the inferred QBO oscillations in the Marca Shale (27.4 months).

Factor influencing level of export flux	**Summer/autumn export flux**	**Spring bloom export flux**
Enhanced level of winter mixing	+	+
Enhanced open ocean upwelling during winter	+	+
Enhanced frequency of summer storms	+	×
Longer period of water column stratification	+	-?

Table 7.3. Summary of the effects of the various influences on the export flux from each of the varve segments. Note: + =greater export flux, - = reduced export flux and × = no influence.

7.4.2.2 *Sub-decadal and quasi-decadal peaks*

Several peaks within the sub-decadal/quasi-decadal band are present within the total spore segment thickness records. Most occur just below the 99% confidence interval at 10.66, 8.68, 4.10 and 3.41 years, although one peak at 13.48 years does reach the 99% confidence level. Therefore, although variability in this frequency band is significant, it is not as powerful as that in the quasi-biennial frequency band. Wavelet analysis demonstrates that variability in this frequency band was less persistent than quasi-biennial variability (Fig. 7.7 and 7.11). The modern NAM is known to contain significant variability within this frequency band (Appenzeller *et al.*, 1998; Tudhope *et al.*, 2001). Evidence suggests that ENSO variability can also be expressed in the modern Arctic through stratospheric teleconnections, which affect the breakdown of the wintertime stratospheric polar vortex by modulating the NAM (Jevrejeva *et al.*, 2004). It is therefore suggested that the 3.41 and 4.10 year peaks in the total resting spore varve segment thickness relates directly to the NAM or to the influence of ENSO-like variability on the NAM. This, together with the strong QBO peaks, interpreted to relate to the influence of the stratospheric QBO on the NAM, indicates the importance of the NAM in influencing ocean productivity during the Cretaceous.

The possibility of an ENSO origin of the sub-decadal peaks is consistent with the identification of similar frequency variability in the Marca Shale, interpreted to relate to an ENSO-like oscillation. Conditions during deposition of the CESAR 6 biosiliceous unit were warmer than those during deposition of the Marca Shale (Chapter 6.1.5). It might be expected therefore, that the Bjerknes feedback would have been further weakened with the respect to the Late Maastrichtian, and according to theory (Neelin *et al.*, 1998), the climate more liable to have collapsed into a permanent El Niño. The presence of variability in the Late Cretaceous Arctic of possible ENSO origin provides further support to the conclusions in Chapter 5.4.5, that greenhouse end member climates, such as those during deposition of the CESAR 6, do not necessarily collapse into a permanent El Niño state.

Although the 8.68 year peak lies within the frequency band of the NAM and modern strong ENSO events, the fact that it was found to be harmonic suggests that the peak does not relate to internal variability. Internal oscillations have a notoriously variable periodicity and it is unlikely that any would have produced a spectral peak with a constant frequency. The lunar perigee cycle (Chapter 5.4.1.1) currently causes very high semi-diurnal spring tides every 4.425 years and also modulates tides with a periodicity of 8.85 years, related to the orbital advance of the Moon at perigee. Multiples of the perigee cycle are described in spectral estimates from Arabian Sea (Berger & von Rad, 2002) and Santa Barbara Basin (Berger *et al.*, 2004) data sets. The 8.68 year peak may therefore relate to the periodic variation in the degree of vertical tidal mixing in the Cretaceous Arctic Ocean, perhaps in relation to bathymetric features, relating to the lunar perigee cycle.

The 10.66 year peak is in the frequency range of a well known band of variability within the ocean-climate system, often related to the ~11 year solar cycle. Interestingly, the 10.66 year peak was also found to be harmonic, possessing a constant frequency and phase. Similar period peaks were found in spectral estimates from the Marca Shale at 10.0, 10.3 and 10.8 years and related to the occurrence of strong ENSO events that were modulated by external solar variability (i.e. the 11 year sunspot cycle). The fact that the 10.66 year peak identified here is a harmonic signal suggests an external influence. Raspopov *et al.* (2004) identified similar decadal periodicities in dendrochronology data, spanning the last several hundred years, from the northern coastal region of Russia. The authors inferred the decadal (11-12 year) signals to relate to the influence of the Schwabe solar cycle on internal variability, consistent with the work of Waple *et al.* (2002). It is known that a much greater proportion of stratospheric perturbations penetrate to the surface, changing weather patterns through the NAM, during solar maximum rather than solar minimum conditions (Hameed & Lee, 2005). It is probable that the 10.66 year peak relates to the solar modulation of the NAM, depending on interaction with the QBO phases (Labitzke & van Loon, 1990). The occurrence of a quasi-decadal harmonic peak in the CESAR 6 adds support to the conclusion in Chapter 5 that similar frequency peaks identified in the Marca Shale relate to solar modulation of internal climate variability.

One other quasi-decadal spectral peak in the total spore thickness record, found to be above the 99% confidence interval, was identified at 13.48 years. The frequency of this peak falls within the band of strong recent NAM variability, and thus may also relate to the NAM. However, the frequency of the 13.48 year peak also lies close to the 13.9 year peak identified in modern records of Arctic ice conditions (Jevrejeva *et al.*, 2004) and in an Antarctic ice core (Fischer *et al.*, 2004), interpreted to relate to the propagation of ENSO related equatorial coupled waves, generated in the western Pacific. It is possible that the 13.48 year peak identified in the total spore varve segment thickness record has a similar origin. Alternatively, the 13.48 year peak may relate to an oscillation analogous to the PDO.

7.4.3 *Significance of the spectral peaks in total vegetative varve segment*

7.4.3.1 *Quasi-biennial peaks*

Total vegetative varve segment thickness records are also dominated by numerous quasi-biennial spectral peaks above the 99% confidence interval at 2.72, 2.62 and 2.26 years. Significantly, the 2.26 year peak in total vegetative varve segment comes from the same sample (K4-1) containing a 2.26 year peak in the total spore segment thickness. It is therefore apparent that the quasi-biennial peaks in total vegetative varve segment relate to the same mechanism that produced quasi-biennial in total resting spore varve segment. Further support for this comes from wavelet analysis, which demonstrates that intervals where quasi-biennial variability is most powerful are coincident in the total resting spore varve segment and the total vegetative varve segment records. Changes in the total vegetative varve segment thickness are interpreted to relate to alterations in the export productivity of stratified producers. This may relate to; 1) the stability of the water column (e.g. longer period of stratification allows greater biomass to build up), 2) nutrient availability, including silicic acid concentrations or 3) the severity of summer storms, influencing eddy pumping and mixing (Table 7.3). The quasi-biennial oscillation of a polar low pressure system would have modified surface nutrient levels as well as the stability of the water column (as discussed in 7.4.2.1). The mean periodicity of the QBO signals recorded in total vegetative varve segment is 2.53 years (30.4 months), close to that in the total spore varve segment.

7.4.3.2 *Sub-decadal peaks*

Significant peaks within the sub-decadal frequency band are also present in total vegetative varve segment spectral estimates at 3.29 and 3.11 years, both above the 99% confidence level. Variability within this band is dominated by ENSO in the modern climate system and a 3.5 years ENSO related peak has been identified in the modern Arctic (Jevrejeva *et al.*, 2004). However, the modern NAM also has powerful variability in this frequency band (Tudhope *et al.*, 2001) The quasi-triennial peaks in total varve thickness are therefore inferred to relate to the NAM or to the effects of an ENSO-like oscillation on conditions in the Late Cretaceous Arctic.

7.4.3.3 *Multi-decadal peaks*

Multi-decadal peaks are also present in the total vegetative varve segment thickness records at 25.58 years and a harmonic peak at 78.74 years. The 25.58 year peak lies within a well known frequency band of modern climate variability, with similar frequency peaks observed in NE Pacific temperature and wind stress data (Ware, 1995), SST and salinity records (Conversi & Hameed, 1998) and SST reconstruction (D'Arrigo *et al.*, 1999) for the Gulf of Alaska, laminated sediments from Effingham Inlet (Patterson *et al.*, 2004) and tree ring data from Russia's Arctic coast (Raspopov *et al.*, 2004). Variability in this frequency is generally attributed to the PDO (D'Arrigo *et al.*, 1999) or to modulation of internal climate variability by the Hale solar cycle (Patterson *et al.*, 2004; Raspopov *et al.*, 2004). Solar variability is known to affect the downward propagation of stratospheric perturbations, changing weather patterns through the NAM (Hameed & Lee, 2005). The 25.58 year peak in total vegetative varve segment is therefore inferred to relate to the influence of solar variability on the NAM or a cycle analogous to the PDO, the frequency of which may have been modulated by solar variability. A PDO-like oscillation may have affected SST's, salinity, wind patterns and the levels of precipitation in the Cretaceous Arctic and in turn, influenced water column stability and nutrient availability.

The 78.74 year peak also lies close to the frequency band of the longer period PDO variability of 50-70 years in the modern climate (Minobe, 1997). The fact that the 78.74 year peak is harmonic suggests it was modulated by external forcing. This external influence could originate in solar variability or tidal cycles. Interestingly, the spectral estimates from the B-T method and the MEM show this peak to occur at 84.33 years. A frequency of 84.33 years lies close to the mean frequency of the Gleissberg solar cycle of 88 years (Hoyt & Schatten, 1997). The Gleissberg solar cycle relates to amplitude modulation of the 11-year Schwabe collar cycle (Dean, 2000b) and has a periodicity of ~72-90 years (Gleissberg, 1958; Garcia & Mouradian, 1998). Strong ~90 year signals have been identified in dendrochronological data sets from the Arctic coast of Russia (Raspopov *et al.*, 2004), which were confidently related to the Gleissberg solar cycle, supported by work by Ogurtsov *et al.* (2002), who found similarities between tree-ring data and proxy and measured data on solar variability from a similar site. A ~75-90 year cycle has also been observed in grey-scale and varve thickness records from laminated marine varves in Effingham Inlet, NE Pacific, that correspond very well to the Gleissberg solar cycle (Patterson *et al.*, 2004). The 78.74 year peak is therefore interpreted to relate to the modulation of the polar vortex/night jet (NAM) over the Gleissberg solar cycle or alternatively, to modulation of an internal oscillation analogous to the PDO.

7.4.4 *Significance of the spectral peaks in total varve thickness*

7.4.4.1 *Quasi-biennial peaks*

Variations in the total varve thickness relate to the interplay of factors controlling the export flux of each of the varve segments (Table 7.3). Increased winter mixing and/or open ocean upwelling would have caused an increased flux of spring and summer/autumn producers resulting in relatively thick varves. Increased frequency of summer storms would have increased summer/autumn flux, whilst spring flux would not have been impacted, also resulting in relatively thick varves. Years characterised by a longer period of water column stratification would probably have positively impacted summer/autumn export flux, whilst negatively impacted spring export flux and as such would not impacted total varve thickness. Spectral estimates of total varve thickness are also dominated by quasi-biennial peaks at 2.26, 2.65 and 2.80 years. These quasi-biennial signals are also interpreted to relate to the influence of the QBO on total diatom export production, as in the total resting spore and vegetative varve segment thickness records. Support that they do not relate to a quasi-biennial ENSO component comes from the fact that the K5-8 data set does not contain any peaks in the ENSO frequency band. Wavelet analysis demonstrates that periods of strong quasi-biennial variability in total varve thickness coincide with periods of strong quasi-biennial variability in the two varve segment data sets (Fig. 7.7 and 7.11). The mean QBO frequency recorded in total varve thickness records is 2.57 years (30.84 months).

7.4.4.2 *Sub-decadal peaks*

Two peaks are also present within the sub-decadal frequency band; one at 5.15 years and a weaker peak (95% confidence) at 3.06 years. Wavelet analysis demonstrates that periods of strong sub-decadal variability in the resting spore and vegetative varve segment records coincide with strong sub-decadal variability in total varve thickness (Fig. 7.7 and 7.11), suggesting variability in all three records results from the same mechanism. Both peaks are therefore interpreted to relate either directly to the NAM or to the effects of ENSO-like teleconnections on the NAM, based on earlier discussions.

7.5 CONCLUSIONS

- Records of total varve thickness, total resting spore varve segment thickness and total vegetative varve segment thickness from two data sets demonstrate diatom export flux was influenced by high-frequency climate variability.
- All three parameters analysed showed a strong influence by quasi-biennial variability. This quasi-biennial variability is inferred to relate to the effect of the stratospheric QBO on the NAM, through modulation of the polar vortex/polar night jet. Variations in the strength of the polar vortex/polar night jet would have affected the intensity of winter storms or the development of the winter low pressure system over the Cretaceous Arctic Ocean, causing biennial variations in nutrient availability and water column stability. Wavelet analysis demonstrates that the power and frequency of the QBO peaks are strongly modulated along the length of the time series.

- All three parameters also recorded sub-decadal (and in total spore varve segment thickness, quasi-decadal) variability. Variability in this frequency band was not as powerful or pervasive as the quasi-biennial variability. The modern NAM is known to contain significant variability within this frequency band and would have affected conditions in the Cretaceous Arctic in the same way as the QBO forcing. Together with the pervasive QBO signals, this suggests NAM variability was robust during the Late Cretaceous. It is also known that ENSO signals can be transmitted to the Arctic through teleconnections with the NAM. Some of the sub-decadal/ quasi-decadal peaks may therefore relate to an oscillation analogous to modern ENSO. Wavelet analysis demonstrates that the power and frequency of the sub-decadal/quasi-decadal peaks are also strongly modulated over the length of the time series.
- The presence of sub-decadal peaks in the CESAR 6 of possible ENSO origin provides further evidence to support the conclusions in Chapter 5 of the presence of an ENSO-like cycle in the Late Cretaceous and also further supports the conclusions that greenhouse climate states do not necessarily collapse into a permanent El Niño state.
- A harmonic peak was identified in total resting spore varve segment thickness records, at 8.68 years. It is suggested that this peak may relate to modulation of the degree of vertical mixing within the Cretaceous Arctic Ocean relating to the lunar perigee cycle.
- A further harmonic peak at 10.66 years was identified in total resting spore varve segment thickness records. The fact that the peak is a harmonic and lies close to the frequency of the modern Schwabe sunspot cycle is taken as evidence that the peak relates to solar modulation of the NAM. This is consistent with interpretations of modulation of internal climate variability for similar frequency peaks in the Marca Shale.
- Vegetative varve segment thickness also recorded multi-decadal peaks at 25.58 and 78.74 years. The 25.58 year peak is inferred to relate to the influence of solar variability on the NAM or a cycle analogous to the PDO. The 78.74 year peak was found to be harmonic, providing good evidence that it relates to external solar variability and is therefore interpreted to relate to the modulation of the NAM over the Gleissberg solar cycle or alternatively, to modulation of an internal oscillation analogous to the PDO.

CHAPTER 8

Conclusions and Suggestions for Future Research

8.1 CONCLUSIONS

Laminated, diatomaceous Late Cretaceous sediments from the Marca Shale and CESAR 6 both contain marine varves. This interpretation is based on the pervasive occurrence of different laminae types that could be related to different seasonal influences and could be placed into a robust annual flux cycle, confirming earlier suggestions about the nature of laminae in the Marca Shale (e.g. Fonseca, 1997) and resolving conflicting interpretations on the nature of the laminations in the CESAR 6. Laminations in the CESAR 6, previously identified based on colour differences (Mudie & Blasco, 1985), had been interpreted as either seasonal in origin (Barron, 1985b), or relating to changes in the Fe content of the sediment through proximal hydrothermal activity (Stoffyn-Egli, 1987). However, the colour laminae, described by Mudie and Blasco (1985), were observed to overprint the fine, submillimetre-scale diatom resting spore/vegetative cell laminae, which were only identifiable using BSEI.

The annual flux cycle in the Marca Shale consists of the deposition of intermittent near-monospecific laminae and concentrations of *Azpeitiopsis morenoensis* in the late summer, succeeded by a mixed assemblage dominated by *Hemiaulus polymorphus, Stephanopyxis* spp. and *Stellarima* spp., interpreted as “fall dump” export flux. Intermittent near-monospecific laminae of *Chaetoceros*-type resting spores follow, interpreted as spring bloom flux, and are overlain by terrigenous laminae, enriched in benthic diatoms (*Paralia crenulata* and *Medlinia deciusii*) and sponge spicules, inferred to reflect enhanced fluvial runoff during the summer. Diatoms suffer from extensive fragmentation, relating to zooplankton grazing and post depositional mechanical crushing. A couplet comprised of a mixed floral diatomaceous and terrigenous laminae constitute the annual flux cycle in the majority of varves. The fact that diatom ecological constraints and laminae succession indicate terrigenous flux occurred during the summer is surprising, as peak levels of precipitation at 43°N on a western seaboard would be typically expected during winter. A summer flux of terrigenous material suggests that the Marca basin was influenced by a monsoonal climate at this time, similar to the present Gulf of California. It is therefore possible that the ~43°N palaeolatitude estimate for the Marca Shale by Fonseca (1997) is incorrect, and deposition actually occurred in lower latitudes. Alternatively, summer terrigenous deposition could indicate that the mid latitude Marca basin was influenced by intense summer storms, possibly resulting from the globally elevated temperatures, shallower meridional temperature gradient, the presence of a poleward flowing reverse coastal current or the poleward shift of storm tracks.

In the CESAR 6, the annual flux cycle primarily consists of alternating resting spore and diatom vegetative cell laminae, which are often dominated by a diverse assemblage of *Hemiaulus*. Resting spore laminae are interpreted to represent the export flux from spring blooms, whilst the vegetative cell laminae are interpreted to relate to “fall dump” mode of export flux or intermittent blooms, fuelled by mixing events and/or cyanobacterial symbionts, during the summer. Near-monospecific *Rhizosolenia* laminae frequently occur above vegetative laminae, and are inferred to have been deposited during the autumn in a “fall dump”. Common silicoflagellate/setae-rich laminae, often containing a diatom hash component, are also observed below resting spore laminae, and are interpreted to represent the early spring flux of grazed diatoms and blooms of silicoflagellates. Sponge spicules, often abundant in silicoflagellate/setae-rich laminae may represent material deposited in the spring, after being transported offshore and suspended in the water column during the winter.

A major part of the diatom export flux in both assemblages is comprised of taxa adapted to exploit stratified conditions that were sedimented during the summer or in a “fall dump”. This observation contrasts with the traditional interpretation of the formation of diatom-rich sediments, such as the Marca Shale and CESAR 6, which calls for upwelling-fuelled spring bloom export flux (Kitchell & Clark, 1982; Kitchell *et al.*, 1986; Fonseca, 1997). Spring bloom flux was significant in the CESAR 6, contributing approximately half of the total export flux, whilst in the Marca Shale spring bloom flux was only a subsidiary component. The abundance of *Hemiaulus* spp. at both localities may provide evidence for diatom blooms powered by N_2-fixing cyanobacteria in the Late Cretaceous (cf. Kuypers *et al.*, 2004).

Both localities provide excellent archives of surface processes, recording intra- and interannual variability in the diatom flux. Different pelletal structures were observed in the Marca Shale, including diatom-rich pellets considered to be pelagic zooplankton fecal pellets, clay/silt-rich pellets, interpreted as zooplankton fecal pellets, which were feeding in sediment laden waters and resting spore/chrysophyte-rich aggregates, interpreted as the flux of TEP-enhanced aggregates following blooms. Possible pelagic pellets were also observed in the CESAR 6. Pelletal structures of benthic origin were also observed in the Marca Shale, including common agglutinated foraminiferal remains and clay/silt-rich aggregates, interpreted as infilled meiofaunal burrows. The degree of disruption to the laminated fabric in the Marca Shale also allowed a bioturbation index to be established, demonstrating that benthic oxygen levels were highly variable on interannual timescales.

In the CESAR 6, elongate detrital (clay and silt/fine sand ranging up to 290 µm in diameter) ‘blebs’, found concentrated within resting spore laminae, and rare detrital laminae occur. The origin of the detrital material remains enigmatic, although the most coherent mechanism to explain their origin is ice rafting. The possibility that thin sea ice formed during the ~4 months of total darkness during the Late Cretaceous Arctic winter is supported by Campanian model simulations (Otto-Bliesner *et al.*, 2002), evidence of seasonal frosts from tree ring records from NW Canada (Falcon-Lang *et al.*, 2004) and inferred ice-rafted dropstones from NE Asia (Ahlberg *et al.*, 2002).

Time-series analysis of high-resolution data sets from the Marca Shale and CESAR 6 provide complimentary results. Data sets from both sites contain strong quasi-biennial signals, inferred to relate to the influence of the QBO (Table 8.1). The QBO signals dominate records from the CESAR 6, suggesting the QBO variability was a dominant influence at higher latitudes. This is consistent with the fact that the modern QBO directly impacts the strength and stability of the wintertime polar vortex and hence surface conditions in the Arctic through the NAM. Intensification of northern high latitude low pressure systems on biennial scales is inferred to have caused quasi-biennial variations in rainfall intensity, level of mixing and period of stratification along the proto east Pacific coast. The periodicity of the modern QBO is highly variable (Baldwin *et al.*, 2001), although has a mean of ~ 28 months, close to that of the QBO peaks in the Marca Shale (27.4 months) and CESAR 6 (30.4 months).

Both sites also contain strong sub-decadal/quasi-decadal peaks (Table 8.1). Several sedimentological lines of evidence are present in the Marca Shale to indicate the presence of variability analogous to ENSO. Firstly, the occurrence of *Azpeitiopsis morenoensis* and *Chaetoceros*-type spores displays a distinct interannual variability, similar to ENSO forced variability in the diatom flora along the modern California margin. Secondly, bioturbation index records demonstrate that periods of enhanced benthic anoxia coincided with elevated diatom export flux and lower detrital flux, whilst more oxygenated benthic conditions coincided with reduced diatom export flux and enhanced flux of detrital material, analogous to modern La Niña and El Niño conditions, respectively. Lastly, diatom and terrigenous laminae thickness both demonstrate interannual variability, analogous to ENSO forced variability in Pleistocene sediments from the Santa Barbara Basin. Consequently, the sub-decadal peaks in the Marca Shale are interpreted to relate to an ENSO-like oscillation. The modern NAM is known to contain significant variability in the sub-decadal/quasi-decadal frequency band. The NAM would have affected conditions in the Cretaceous Arctic in the same way as the QBO. In the modern Arctic, sub-decadal/quasi-decadal variability is also known to occur related to ENSO’s teleconnections with the NAM (Jevrejeva *et* *al.*, 2004). Sub-decadal/quasi-decadal peaks in the CESAR 6 spectral estimates are therefore interpreted to relate directly to NAM variability, or alternatively to ENSO's teleconnections. Together with the pervasive QBO signals, this suggests NAM variability was robust during the Late Cretaceous. Sub-decadal/quasi-decadal peaks are not as common or significant in the CESAR 6 as in the Marca Shale. If any of the peaks in the CESAR 6 relate to ENSO-like variability, this is consistent with an equatorial origin of the variability.

The detection of significant and robust spectral peaks related to an oscillation analogous to ENSO in the Marca Shale and possibly the CESAR 6, has important ramifications for our understanding of the ocean-atmosphere system and for studies into the effect of anthropogenic climate change. It has been proposed that a weakening of the "Bjerknes" feedback loop in the equatorial Pacific will lead to a reduction of ENSO variability and even its complete shutdown, resulting in a permanent El Niño state (Neelin *et al.*, 1998; Fedorov & Philander, 2000). The Late Cretaceous had all the mechanisms in place to cause a severe weakening of the Bjerknes feedback loop and shutdown of ENSO variability. However, the ENSO related peaks in the Marca Shale and possibly the CESAR 6 and direct sedimentological evidence in the Marca Shale demonstrate that ENSO variability was a robust feature during this greenhouse period, adding to the evidence against permanent "El Niño" climate states (Ripepe *et al.*, 1991; Mingram, 1998; Huber & Caballero, 2003). It appears that even if the climate plays host to severe anthropogenic, natural climate variability will remain a robust feature and must be integrated into any simulations of future (and past) climate states.

Frequency Band	**Marca Shale**			**CESAR 6**		
	D	T	BI	TV	RVS	VVS
Quasi-biennial	2.1 2.2 2.3	2.3 2.5		2.26 2.65 2.80	2.11 2.26 2.77 2.89	2.26 2.62 2.72
Sub-decadal	3.8 5.1 6.7 6.1 8.5	3.1 5.1 7.0	6.2	3.06 5.15	3.41 4.10 8.68	3.11 3.29
Quasi-decadal	10.0		10.3 10.8		10.66 13.48	
Multi-decadal	26.5	20.0 44				25.58 78.74

Table 8.1. Compilation of all significant spectral peaks identified in the Marca Shale and CESAR 6 time series. D = diatomaceous laminae, T = terrigenous laminae, BI = bioturbation index, TV = total varve, RVS = resting spore varve segment and VVS = vegetative cell varve segment.

The Marca Shale and CESAR 6 also contain spectral peaks close to the well known frequency band of variability often attributed to the 11-year Schwabe sunspot cycle (Table 8.1). The CESAR 6 only contained one peak near this frequency (at 10.66 years), but significantly, it was found to be a harmonic peak with a constant frequency. This suggests the peak relates directly to external variability or to modulation of internal variability by external influences. Peaks at 10.0 (although the bandwidth error for this peak is large) 10.3 and 10.8 in the Marca Shale are interpreted to relate to modulation of strong ENSO events by the sunspot cycle. The fact that the 10.66 year peak is harmonic supports this conclusion and it is suggested that the 10.66 year peak relates to the solar modulation of the NAM, depending on interaction with the QBO phases.

Multi-decadal peaks are also present in spectral estimates from both sites (Table 8.1). Both sites have quasi-bidecadal peaks, which may relate to the shorter period variability of an oscillation analogous to the PDO, the frequency of which may have been modulated by external variability (e.g. the Hale solar cycle) or to the influence of solar variability on the NAM. The Marca Shale also contains a peak at 44 years, which lies close to the frequency band of the longer period component of variability (~50-70 years) of the modern PDO. The 44 year peak is therefore inferred to relate to the longer period component of a PDO-like oscillation, the frequency of which may also have been modulated by solar variability. The CESAR 6 spectral estimates contain a harmonic peak at 78.74 years that falls within the frequency band of the Gleissberg solar cycle (Gleissberg, 1958; Garcia & Mouradian, 1998) and since it is harmonic, is consequently interpreted to relate to modulation of the NAM over the Gleissberg solar cycle or alternatively, to modulation of the longer period component of an oscillation analogous to the PDO.

Diatom biostratigraphic analysis indicates that the biosiliceous sediment of the CESAR 6 core is of late Late Campanian age, based on comparisons with diatom floras from Seymour Island, DSDP Site 275, the Canadian Arctic, Ural Mountains and the new diatom biozonation scheme of Tapia and Harwood (2002), in agreement with the study by Barron (1985b). However, an earliest Maastrichtian age cannot be discounted, as the absence of *A. morenoensis*, the diatom Maastrichtian index fossil, from the CESAR 6 may relate to ecological constraints. An early Maastrichtian age is in agreement with palynomorph and silicoflagellate age constraints (Bukry, 1985; Firth & Clark, 1998). A Maastrichtian age of the Marca Shale is consistent with the work of Tapia and Harwood (2002). However, palaeomagnetic analysis may indicate the accepted age of the Marca Shale is incorrect, although due to a heavy overprint with the current magnetic field, there is poor confidence in the data.

8.2 SUGGESTIONS FOR FUTURE RESEARCH

Having demonstrated that long, seasonally resolved data sets can be recovered from Late Cretaceous sediments, yielding important information on intrannual to multi-decadal climate variability should encourage future research into locating and recovering other high resolution (varved) proxy data sets from Mesozoic sediments. Even though they are relatively rare, these unique archives of past climate variability remain underutilised. The study of these unique archives will help to extend our knowledge of the nature and dynamics of high frequency climate variability in greenhouse climate end-members and how they evolved over time.

The Marca Shale is known to contain moderate values (2-3%) of organic carbon (Fonseca, 2000), and as such is liable to be susceptible to TEX_{86} analysis (Schouten *et al.*, 2002). Not only would this provide important data on SST's from the eastern Pacific, but it may also yield important clues on the palaeolatitude of the Marca Shale. Further, if sampled at a high enough resolution, TEX_{86} results may be able to detect the warming (cooling) signatures of the inferred El Niño (La Niña) events, signified by the occurrence of *Azpeitiopsis morenoensis* and *Chaetoceros*-like resting spores, respectively.

In order to corroborate the conclusion of robust ENSO (and other) variability in the Late Cretaceous, a study to compare the results of spectral analysis from the Marca Shale and CESAR 6 with simulations from a fully coupled climate model is planned. A similar study on the Eocene (Huber & Caballero, 2003) showed that there was good agreement between the model predictions and proxy data, providing firm evidence that sub-decadal spectral peaks in proxy data sets relate to robust ENSO variability. The inference that terrigenous export flux in the Marca Shale occurred during the summer and hence, the Maastrichtian Californian margin was influenced by a monsoonal climate needs further investigation. A fully coupled climate model simulation of the eastern Pacific region may shed light on this interpretation, although, before such a study is implemented it is imperative that the palaeolatitude estimate of the Marca Shale is satisfactorily confirmed. The model simulation may also be able to shed light on the nature of the current systems along the eastern Pacific and in particular, help ascertain the nature and strength of the equatorial flowing eastern boundary current and poleward flowing counter current, and how these current systems were affected by the seasonal cycle. Model simulations may also be able to substantiate the conclusion of the presence of a polar vortex/ polar night jet and to determine whether an oscillation analogous to the NAM did indeed exist during the Late Cretaceous. The suggestion that the detrital material in the CESAR 6 biosiliceous unit may represent IRD may also be clarified by the results of further coupled climate models.

Further elucidation of the dynamics of high frequency climate variability in the Late Cretaceous Arctic could be gained by examining the phase relationships between the resting spore and vegetative varve segment records. QBO signals with coherent frequencies in each of the varve segments were identified in the K4-1 time series. Knowing the phase lag between the signal in the resting spore and vegetative varve segment would help constrain how the QBO affected the spring bloom and "fall dump" flux over the quasi-biennial cycle.

If they could be constructed, analysis of longer time series from the CESAR 6 would help reveal the nature of longer period variability in the Late Cretaceous climate. A hint of the nature of longer period variability was given by the ~80 year peak in total vegetative varve segment thickness records, which also demonstrates that longer period variability was a component of the Late Cretaceous climate system. Although the creation of longer time series from the Marca Shale is also feasible, the fact that a 1520 varve year data set was recovered and analysed in this study without identification of any longer period variability indicates that such a study may prove unsuccessful. Further time-series may also be able to be produced from the CESAR 6 on the occurrence of the detrital material, if an adequate way of expressing the presence/abundance of the terrigenous ‘blebs’ could be produced. A system analogous to the bioturbation index used for the Marca Shale in this study may be sufficient. If the terrigenous material is indeed IRD, then time-series analysis of the occurrence of the IRD may provide information on the variability of sea-ice extent, sea surface temperatures, sea surface currents or mountain glacier discharge.

Recent studies of Cretaceous black shales, deposited during oceanic anoxic events, have shown that they contain abundant 2-methylhopanoid membrane lipids; biomarkers specific to cyanobacteria (Kuypers *et al.*, 2004). The ^{15}N content of the organic matter in the black shales was also found to be typical of newly fixed N_2, which led the authors to suggest cyanobacteria were the dominant plankton. The discovery of near-generic/monospecific *Hemiaulus* laminae in the CESAR 6 indicates an alternative scenario is possible, whereby the intracellular cyanobacterial endosymbionts within Hemiaulid blooms were the source of the 2-methylhopanoid membrane lipids and ^{15}N signatures, whilst the diatoms accounted for the large amounts of organic carbon flux. The feasibility of this scenario is demonstrated by the organic carbon-rich Cretaceous core, Fl-533, which is known to contain diatom biomarkers but no diatom frustules. If Hemiaulid blooms in the Late Cretaceous were fuelled by N_2-fixation, it is possible that 2-methylhopanoid membrane lipids are preserved in near-monospecific *Hemiaulus* and *Hemiaulus*-rich laminae within the CESAR 6. However, the paucity of organic material in the biosiliceous unit means it is doubtful if the membrane lipids are preserved. Therefore, Cretaceous black shales need to be meticulously studied for evidence of diatoms, including *Hemiaulus*.

A more exhaustive study of diatom taxonomy is called for. Although new diatom species were discovered in the CESAR 6 and Marca Shale during the course of this study, a full taxonomic description of these species was beyond the realm of this investigation. Many new species, not described in this study, are also present within the CESAR 6 and await appropriate description.

Diatom Taxonomy

The system of classification used in this chapter is based on that of Nikolaev and Harwood (2000) including the changes made by Nikolaev *et al.* (2001), whilst representatives of the pennate diatoms are classified according to scheme of Round *et al.* (1990).

Class: **COSCINODISCOPHYCEAE** Round & Crawford

Subclass: **Archaegladiopsophycidae** Nikolaev & Harwood
  Order: **Archaegladiopsidales** Nikolaev & Harwood
    Family: **Thalassiosiropsidaceae** Nikolaev
    Genus: ***Thalassiosiropsis*** Hasle in Hasle & Syvertsen
      Species: ***Thalassiosiropsis wittiana*** (Pantocsek) Hasle *in* Hasle and Syversten (1985) fig. 29-36.
      Coscinodiscus wittianus Pantocsek, (1889), p. 119; Gleser *et al.* (1974) pl. 8, fig. 8; Barron (1985b), pl. 10.1, fig. 5.
      Coscinodiscus lineatus sensu Weiss, Strelnikova (1974) pl. 9, fig. 3-12; Hajós and Stradner (1975) pl. 3, fig 1-3; pl. 38, fig. 1.

    Genus: ***Gladiopsis*** Gersonde & Harwood
      Species: ***Gladiopsis pacificus*** (Schulz)
      Gladius pacificus Hajós *in* Hajós and Stradner (1975), pl. 11, fig. 1-2.
      Gladiopsis speciosa (Schulz) Gersonde & Harwood (1990), fig. 43-48.
      Gladius speciosus Schulz (1935) pl. 1, fig. 6.

  Order: **Stephanopyxales** Nikolaev
    Family: **Stephanopyxaceae** Nikolaev ex Round & Crawford
    Genus: ***Stephanopyxis*** (Ehrenberg) Ehrenberg
      Species: ***Stephanopyxis appendiculata*** Ehrenberg (1854) pl. 18, fig. 4; Hanna (1927; 1932) pl. 4, fig. 9.
      Stephanopyxis barbadensis (Greville) Grunow (1884) pl. 39; Long Fuge & Smith (1946) 111.
      Stephanopyxis discrepans Hanna (1927; 1932) pl. 4, figs. 10, 11.
      Stephanopyxis grunowii Grove & Sturt in Schmidt *et al.* (1888) pl. 130, figs. 1, 4; Hanna (1927; 1932) pl. 4, fig. 12; Long, Fuge & Smith (1946) 111.

Stephanopyxis turris (Greville and Arnott) Ralfs. Strelnikova (1974), pl. 8, fig. 1-13.

Family: **Triceratiaceae** (Schűtt) Lemmermann

Genus: ***Triceratium*** Ehrenberg

Species: ***Triceratium indefinitum*** (Jousé) Strelnikova, (1974) pl. 30, fig. 18-22 (only) (see Tapia and Harwood, 2002); Dell'Agnese and Clark (1994): 38, fig. 5.3.

Triceratium planum Strelnikova, (1974) pl. 29, fig. 12-17.

Subclass: **Paraliophycidae** Nikolaev & Harwood

Order: **Paraliales** Crawford

Family: **Paraliaceae** Crawford

Genus: ***Paralia*** Heiberg

Species: ***Paralia crenulata*** (Grunow) Gleser in Gleser *et al.* (1992), pl. 41, figs. 1-8.

Subclass: **Heliopelophycidea** Nikolaev & Harwood

Order: **Heliopeltales** Nikolaev & Harwood

Family: **Heliopeltaceae** H. L. Smith

Genus: ***Actinoptychus*** Ehrenberg

Species: ***Actinoptychus packii*** Hanna (1927), pl. 1, fig. 1-3.

Actinoptychus simbirskianus Schmidt

Actinoptychus taffii Hanna (1927), pl. 1, fig. 4.

Actinoptychus tenuis Strelnikova

Genus: ***Glorioptychus*** Hanna

Species: ***Glorioptychus callidus*** Hanna (1927), pl. 2, fig. 7-8.

Subclass: **Coscinodiscophycidae**

Order: **Coscinodiscales** Round & Crawford

Family: **Coscinodiscaceae** Kützing, emend. Round & Crawford

Genus: ***Coscinodiscus*** Ehrenberg

Species: ***Coscinodiscus circumspectus*** Long. Fuge and Smith, (1946), pl. 15, fig. 12; Hajós and Stradner, (1975), pl. 1, fig. 1.

Coscinodiscus sibiricus Strelnikova (1974), pl. 11, fig. 1-4.

Coscinodiscus symbolophorus Grunow, Strelnikova, (1974), pl. 12, fig. 1-7.

Order: **Melosirales** Gleser

Family: **Trochosiraceae** Gleser

Genus: ***Trochosiropsis*** Gleser

Species: ***Trochosiropsis polychaeta*** (Strelnikova) Tapia and Harwood (2002) pl. 8, figs. 3-4.

Sceletonema polychaetum Strelnikova (1971): 42, Tab. 1, fig. 3-5.

Pyrgodiscus triangulates Hajós and Stradner (1975), fig 11a,b, pl. 18, fig. 5-6.

Trochosira polychaeta (Strelnikova) Sims (1988), fig. 15-21, 29-34.

Genus: ***Skeletonemopsis*** Sims

Species: ***Skeletonemopsis morenoensis*** Sims (1994b), fig. 5-8.

? *Skeletonema punctatum* Schmidt (1892), fig. 34.

Skeletonemopsis crawfordii Sims (1994b), fig. 9-13.

Order: **Aulacodiscales** Nikolaev and Harwood

Family: **Aulacodiscaceae** (Schütt) Lemmermann

Genus: ***Aulacodiscus*** Ehrenberg

Species: ***Aulacodiscus archangelskianus*** Witt (1985), pl. 6, fig. 11-12

Aulacodiscus pugnalus Hanna (1927), pl. 1, fig. 6-7.

Aulacodiscus archangelskianus var. pugnalus Long, Fuge and Smith (1946), pl. 13, fig. 12.

Order: **Stellarimales** Nikolaev & Harwood

Family: **Stellarimaceae** Nikolaev ex Hasle & Sims

Genus: ***Stellarima*** Hasle & Sims

Species: ***Stellarima distincta*** (Long, Fuge & Smith) Sims (1987), fig. 19, 26, 32-33.

Coscinodiscus distinctus Long, Fuge & Smith (1946) pl. 15, fig. 15.

Stellarima steinyi (Hanna) Hasle and Sims (1986), fig. 1-7, 27-28.

Coscinodiscus steinyi Hanna (1927), pl. 2, fig. 5-6.

Stellarima sp. 1

Stellarima sp. 2

Genus: ***Azpeitiopsis*** Sims

Species: ***Azpeitiopsis morenoensis*** (Hanna) Sims (1994a), fig. 21-28, 53.

Coscinodiscus morenoensis Hanna (1927), pl. 2, fig. 3-4.

Subclass: **Biddulphiophycidae** Round & Crawford

Order: **Hemiaulales** Round & Crawford

Family: **Hemiaulaceae** Heiberg

Genus: ***Hemiaulus*** Ehrenberg

Species: ***Hemiaulus altus*** Hajós (1975), pl. 5, fig. 17-19

Hemiaulus ambiguus Grunow (1884), pl. 2, fig. 25-26; Harwood (1988), fig. 15.2,3

Hemiaulus andrewsi Hajós (1975), pl. 7, fig. 8.

Hemiaulus antiquus Jousé, Strelnikova (1974), pl. 46, fig. 1-14.

Hemiaulus curvatulus Strelnikova (1971), Tab. 1, fig. 12-13; Hajós and Stradner (1975), pl. 6, fig. 8.

Hemiaulus danicus Grunow (1884): 65, Tab, II (B), fig. 40-41.

Hemiaulus elegans (Heiberg) Grunow (1884): 14; Strelnikova (1974), pl. 44, fig. 1-17.

Hemiaulus gleseri Hajós *in* Hajós and Stradner (1975) pl. 5, fig. 20; pl. 7, fig. 6-7.

Hemiaulus giganteus?

Hemiaulus hostilis? Heiberg

Hemiaulus* sp. cf. *includens (Ehrenberg) Grunow (1884), pl. 2)B), fig. 36-38; Barron (1985), pl. 10.2, fig. 7.

Hemiaulus kittoni Grunow (1884):61

Hemiaulus polymorphus Grunow (1884):14; Hanna (1927), pl. 2, fig. 9-10; Nikolaev *et al*. (2001), pl. 24, fig. 6; pl. 25, fig. 1-3.

Hemiaulus cf. rossicus Pantocsek (1889): Bd. 2, p. 84; Del'Agnese and Clark (1994), fig. 4.3.

Hemiaulus polycystinorum var. simbrikianus Grunow (1884): 65, Tab. II(B), fig. 44-45.

Hemiaulus polycystinorum Ehrenberg, Hajós and Stradner (1975), pl. 6, fig. 4-7.

Hemiaulus polymorphus var morsianus

Hemiaulus tumidicornis Strelnikova (1974), pl. 47, fig. 17-25.

Hemiaulus sp. **1** Barron (1985b), pl. 10.2, fig. 9.

Hemiaulus sp. G Harwood (1988), fig. 14.6.

Hemiaulus 1

Hemiaulus 2

Hemiaulus 6

Hemiaulus ?

Hemiaulus spore 3

Genus: ***Cerataulina*** Pergallo

Species: ***Cerataulina cretacea*** Hajós (1975), pl. 10, fig. 3-4.

Cerataulina sp A

Genus: ***Trinacria*** Heiberg

Species: ***Trinacria aires*** Schmidt et al. 1886: pl. 96, figs. 14-17; Hanna (1927; 1932), pl. 5, figs. 1-2.

Trinacria acutangulum (Strelnikova) Barron (1985b), pl. 10.3, fig. 6, 8, 9.

Triceratium acutangulum Strelnikova (1974) Tab. 32, fig. 1-10.

Trinacria insipiens Witt (1985):172, pl. 10, fig. 1; pl. 11, fig. 5, 7, 11; pl. 12, fig. 2; Hanna (1927; 1932), pl. 5, figs. 7-9.

Trinacria tessela (Krotov) Tapia & Harwood (2002)

Triceratium tessela Strelnikova, (1974) pl. 29, fig. 8-11.

Trinacria tristictia Hanna (1927), pl. 5, fig. 11,12; Hajós & Stradner (1975), pl. 9, fig. 6,6.

Trinacria interlineata Long, Fuge and Smith (1946), pl. 18, fig. 11.

Family: **Sheshukoviaceae** Gleser

Genus: ***Sheshukovia*** Gleser

Species: ***Sheshukovia excavata*** (Heiberg) Nikolaev & Harwood (2001), pl. 29, fig. 1-5.

Trinacria excavata Heiberg (1863), pl. 4, fig. 9.

Genus: ***Medlinia*** Sims

Species: ***Medlinia deciusii*** (Hanna) Nikolaev & Kociolek (2001), pl. 27, fig. 4-6.

Trinacria deciusii Hanna (1927), pl. 5, fig. 3-5.

Medlinia mucronata (Schmidt) Nikolaev & Barron (2001) pl. 26, fig. 5-6.

Triceratium mucronatum Schmidt *el al.* (1886), pl. 11, fig. 1-2.

Trinacria mucronata Hanna (1927), pl. 5, fig. 10.

Genus: ***Euodiella*** Sims

Species: ***Euodiella bicornigera*** (Hanna) Sims (2000), fig. 1-6.

Triceratium bicornigerum Hanna (1927), pl. 4, fig. 13-14.

Order: **Stictodiscales** Round & Crawford

Family: **Stictodiscaceae** (Schütt) Simonsen

Genus: ***Pseudostictodiscus*** Grunow ex Schmidt

Species: ***Pseudostictodiscus picus*** Hanna (1927), pl. 3, fig. 1-4.

Order: **Anaulales** Round & Crawford

Family: **Anaulaceae** (Schütt) Lemmerman

Genus: ***Anaulus*** Ehrenberg

Species: ***Anaulus sibiricus*** Strelnikova, (1974), pl. 52, fig. 1-5.

Anaulus undalatus Long, Fuge and Smith (1946), pl. 14, fig. 3.

Anaulus sp1

Genus: ***Porpeia*** Bailey

Species: ***Porpeia* sp1** Long, Fuge and Smith (1946), pl. 17, fig. 11.

Order: **Chaetocerotales** Round & Crawford

Family: **Chaetocerotaceae** Ralfs

Genus: ***Chasea*** Hanna

Species: ***Chasea bicornis*** Hanna (1934), pl. 48, fig. 12-16

Subclass: **Rhizosoleniophycidae** Round & Crawford

Order: **Rhizosoleniales** Silva, emend. Round & Crawford

Family: **Rhizosoleniaceae** De Toni

Genus: ***Rhizosolenia*** Brightwell

Species: ***Rhizosolenia* spp.** (thick and thin form) Barron, (1985b), pl. 10.3, fig. 2-3.

Family: **Probosciaceae** Nikolaev & Harwood

Genus: ***Proboscia*** Sundström

Species: ***Proboscia cretacea*** (Hajós and Stradner) Jordan and Priddle (1991): 56, fig. 3-4.

Rhizosolenia cretacea Hajós and Stradner (1975), pl. 7, fig. 1.

Class: **FRAGILARIOPHYCEAE** Round

Subclass: **Fragilariophycidae** Round

Order: **Fragilariales** Silva

Family: **Fragilariaceae** Silva

Genus: ***Helminthopsis*** Van Heurck

Species: ***Helminthopsis wornardti*?** Hajós and Stradner (1975), pl. 13, fig. 24.

Order: **Rhaphoneidales** Round

Family: **Rhaphoneidaceae** Forti

Genus: ***Sceptroneis*** Ehrenberg

Species: ***Sceptroneis dimorpha*** Strelnikova, (1974), pl. 54, fig. 18-30

Sceptroneis grunowii? Anissimova (1938); Hajós and Stradner (1975), pl. 11, fig. 14-15; Harwood (1988), fig. 17.9, 10.

***Sceptroneis* praecaducea?** Hajós and Stradner (1975), pl. 13, fig. 13-14.

Sceptroneis sp. A? Harwood (1988), fig. 17.12.

Sceptroneis sp. B

Genera of Unknown Taxonomic Position

Genus: ***Acanthodiscus*** Pantocsek

Species: ***Acanthodiscus immaculatus*** (Hanna) Nikolaev and Barron (2001), pl. 34, fig. 1-4.

Coscinodiscus immaculatus Hanna (1927), pl. 2, fig. 2.

Genus: ***Kentrodiscus*** Pantocsek

Species: ***Kentrodiscus aculeatus*** Hanna (1927), pl. 3, fig. 6-7.

Kentrodiscus blandus Long, Fuge and Smith (1946), pl. 19, fig. 3-5.

Genus: ***Micrampulla*** Hanna

Species: ***Micrampulla parvula*** Hanna (1927), pl. 3, fig. 15.

Genus: ***Pseudopyxilla*** Forti

Species: ***Pseudopyxilla russica*** (Pantocsek) Forti (1909), pl. 1, fig. 13, Hanna 1927:27, pl. 4, fig. 4.

Pseudopyxilla sp. Strelnikova (1974), pl. 54, fig. 16; Harwood (1988), fig. 17.25.

Genus: ***Pterotheca*** Grunow ex Forti

Species: ***Pterotheca evermannii*** Hanna 1927:31, pl. 4, fig. 6.

Pterotheca crucifera Hanna 1927:30, pl. 4, fig. 5.

Pterotheca. sp. Strelnikova (1974), pl. 57, fig. 33-34; Barron (1985), pl. 10.2, fig. 11.

Genus: ***Xanthiopyxis*** Ehrenberg

Species: ***Xanthiopyxis grantii*** Hanna 1927:31, pl. 5, fig. 13-14.

Resting spores

Genus***: Goniothecium***

Species: ***Goniothecium odontella*** Ehrenberg (1844): 82; Ehrenberg (1854), tab. 18, fig. 94, tab. 33, XIII, fig. 13-14, tab. 33, XV, fig. 16; Hajós and Stradner, (1975), pl. 10, fig. 11-12; Barron (1985b), pl. 10.2; Dell'Agnese and Clark (1994): 38, fig. 3.8.

Genus: ***Odontotropis*** Grunow (1884)

Species: ***Odontotropis cristata*** (Grunow, 1882) Grunow (1884), pl. 5(E), fig. 58.

Odontotropis galleonis Hanna (1927), pl. 4, fog. 1-3.

Genus: **Unknown**

Species: ***Skeletonema subantarctica*** Hajós *in* Hajós and Stradner (1975), pl. 2, fig.1.

Skeletonema penicillus Grunow *in* Van Heurk (1883), pl. 83, fig. 6.

"Chaetoceros-type" spores

Spore '1'

Unknown

REFERENCES

Abramovich, S., Keller, G., Stüben, D. and Berner, Z. 2003. Characterisation of late Campanian and Maastrichtian planktonic foraminiferal depth habitats and vital activities based on stable isotopes. *Palaeogeography, Palaeoclimatology, Palaeoecology*, **202**: 1-29.

Abrantes, F. 1988. Diatom assemblages as upwelling indicators in surface sediments off Portugal. *Marine Geology*, **85**.

Abrantes, F. 1991. Increased upwelling off Portugal during the last Glaciation: diatom evidence. *Marine Micropaleontology*, **17**: 285-310.

Abrantes, F. and Moita, M.T. 1999. Water column and recent sediment data on diatoms and coccolithophorids, off Portugal, confirm sediment record of upwelling events. *Oceanologica Acta*, **22**: 67-84.

Adatte, T., Keller, G. and Stinnesbeck, W. 2002. Late Cretaceous to early Paleocene climate and sea-level fluctuations: the Tunisian record. *Palaeogeography, Palaeoclimatology, Palaeoecology*, **178**: 165-196.

Ahlberg, A., Herman, A.B., Raikevich, M., Rees, A. and Spicer, R.A. 2002. Enigmatic late Cretaceous high palaeo-latitude lonestones in Chukotka, northeasternmost Asia. *GFF*, **124**: 197-199.

Alldredge, A.L. and Goltschalk, C.G. 1989. Direct observations of the mass floculation of diatom blooms: Characteristics, settling velocities and formation of diatom aggregates. *Deep-Sea Research Part I*, **36**: 159-171.

Alldredge, A.L., Passow, U. and Logan, B.E. 1993. The abundance and significance of a class of large, transparent organic particles in the ocean. *Deep Sea Research Part I*, **40**: 1131-1140.

Almogi-Labin, A. and Bein, A. 1993. Late Cretaceous upwelling system along the southern Tethys Margin (Israel): Interrelationship between productivity, bottom water environments and organic matter preservation. *Paleoceanography*, **8**: 671-690.

Amiot, R., Lécuyer, C., Buffetaut, E., Fluteau, F., Legendre, S. and Martineau, F. 2004. Latitudinal temperature gradient during the Cretaceous Upper Campanian - Middle Maastrichtian: δ18O record of continental vertebrates. *Earth and Planetary Science Letters*, **226**: 255-272.

Anderson, F.M. 1958. Upper Cretaceous of the Pacific coast. *Geological Society of America Memoir*, **71**: 378 p.

Anderson, R.Y., Linsley, B.K. and Gardner, J.V. 1990. Expression of seasonal and ENSO forcing in climatic variability at lower than ENSO frequencies: evidence from Pleistocene marine varves off California. *Palaeogeography, Palaeoclimatology, Palaeoecology*, **78**: 287-300.

Andrews, J.E., Tandon, S.K. and Dennis, P.E. 1995. Concentration of carbon dioxide in the Late Cretaceous atmosphere. *J. Geol. Soc. London*, **152**: 1-3.

Andrews, J.T., Hardadottir, J., Stoner, J.S., Mann, M.E., Kristjansdottir, G.B. and Koc, N. 2003. Decadal to millennial-scale periodicities in North Iceland shelf sediments over the last 12 000 cal yr: long-term North Atlantic oceanographic variability and solar forcing. *Earth and Planetary Science Letters*, **210**: 453-465.

Appenzeller, C., Stocker, T.F. and Anklin, M. 1998. North Atlantic oscillation dynamics recorded in Greenland ice cores. *Science*, **282**: 446-449.

Asku, A.E. 1985. Paleomagnetic stratigraphy of the CESAR cores. In: *Initial Geological Report on CESAR - the Canadian Expedition to Study the Alpha Ridge, Arctic Ocean* (Eds H.R. Jackson, P.J. Mudie and S.M. Blasco), pp. 101-114. Geological Survey of Canada, Paper 84-22, report 7.

Balachandran, N.K., Rind, D., Lonergan, P. and Shindell, D.T. 1999. Effects of solar cycle variability on the lower stratosphere and troposphere. *Journal of Geophysical Research*, **104**: 27321-27339.

Baldwin, M.P., Gray, L.J., Dunkerton, T.J., Hamilton, K., Haynes, P.H., Randel, W.J., Holton, J.R., Alexander, M.J., Hirota, I., Horinouchi, T., Jones, D.B.A., Kinnersley, J.S., Marquardt, C., Sato, K. and Takahashi, M. 2001. The Quasi-Biennial Oscillation. *Reviews of Geophysics*, **39**: 179-229.

Ballance, P.F., Barron, J.A., Blome, C.D., Bukry, D., Cawood, P.A., Chaproniere, G.C.H., Frisch, R., Herzer, R.H., Nelson, C.S., Quinterno, P., Ryan, H., Scholl, D.W., Stevenson, A.J., Tappin, D.G. and Vallier, T.L. 1989. Late Cretaceous pelagic sediments, volcanic ash and biotas from near the Louisville hotspot, Pacific Plate, paleolatitude ~42° S. *Palaeogeography, Palaeoclimatology, Palaeoecology,* **71**: 281-299.

Bárcena, M.A., Isla, E., Plaza, A., Flores, J.A., Sierro, F.J., Masqué, P., Sanchez-Cabeza, J.A. and Palanques, A. 2002. Bioaccumulation record and paleoclimatic significance in the Western Bransfield Strait. The last 2000 years. *Deep-Sea Research Part II*, **49**: 935-950.

Barker, J.W. and Meakin, S.H. 1946. New diatoms from the Moreno Shale. *Journal of the Quekett Microscopical Club of London,* **series 4**: 143-144.

Barrera, E. 1994. Global environmental changes preceding the Cretaceous-Tertiary boundary: Early-late Maastrichtian transition. *Geology*, **22**: 877-880.

Barron, E.J. 1985a. Numerical climate modeling, a frontier in petroleum source rock prediction: results based on Cretaceous simulations. *American Association of Petroleum Geologists Bulletin*, **69**: 448-459.

Barron, E.J., Peterson, W.H., Pollard, D. and Thompson, S. 1993. Past climate and the role of ocean heat transport: model simulations for the Cretaceous. *Paleoceanography*, **8**: 785-798.

Barron, J.A. 1985b. Diatom Biostratigraphy of the CESAR 6 Core, Alpha Ridge. In: *Initial Geological Report on CESAR-the Canadian Expedition to Study the Alpha Ridge* (Eds H.R. Jackson, P.J. Mudie and S.M. Blasco), pp. 137-148. Geological Survey of Canada, Paper 84-22, Report 10.

Barron, J.A., Bukry, D. and Bischoff, J.L. 2004. High resolution palaeoceanography of the Guaymas Basin, Gulf of California, during the past 15 000 years. *Marine Micropaleontology*, **50**: 185-207.

Bartow, A.J. and Nilsen, T.H. 1990. Review of the Great Valley Sequence, Eastern Diablo Range and Northern San Joaquin Valley, Central California. In: *Structure, Stratigraphy and Hydrocarbon Occurrences of the San Joaquin Basin, California: Tulsa* (Eds J.G. Kuespert and S.A. Reid), pp. 253-265. Society for Sedimentary Geology (SEPM)-Pacific Section.

Baumgartner, T.R., Ferreira-Bartrina, V. and Moreno-Hertz, P. 1991. Varve formation in the central Gulf of California: a reconsideration of the origin of the dark laminae from the 20th Century varve record. In: *The Gulf Peninsular Province of the Californias* (Eds J.P. Dauphin and B.R.T. Simoneit), **47**, pp. 617-635. American Association of Petroleum Geologists Memoir.

Baumgartner, T.R., Soutar, A. and Ferreira-Bartrina, V. 1992. Reconstruction of the History of Pacific Sardine and Northern Anchovy Populations over the Past Two Millennia from Sediments of the Santa Barbara Basin,California. *CalCOfi rep*, **33**: 24-40.

Beer, J., Blinov, A., Bonani, G., Finkel, R.C., Hofmann, H.J., Lehmann, B., Oeschger, H., Sigg, A., Scwander, J., Staffelbach, T., Stauffer, B., Suter, M. and Wölfli, W. 1990. Use of ^{10}Be in polar ice to trace the 11-year cycle of solar activity. *Nature*, **347**: 164-166.

Beer, J., Oeschger, H., Finkel, R.C., Castagnoli, G., Bonino, G., Attolini, M.R. and Galli, M. 1985. Accelerator measurements of ^{10}Be: the 11 year solar cycle. *Nuclear Instruments and Methods in Physics Research B*, **10**: 415-418.

Beerling, D.J., Lomax, B.H., Royer, D.L., Upchurch, G.R., Jr. and Kump, L.R. 2002. An atmospheric $p\mathrm{CO}_2$ reconstruction across the Cretaceous-Tertiary boundary from leaf megafossils. *Proceedings of the National Academy of Sciences of the United States of America*, **99**: 7836-7840.

Behl, R.J. and Kennett, J.P. 1995. Brief interstadial events in the Santa Barbara Basin, NE Pacific, during the past 60 kyr. *Nature*, **379**: 243-246.

Berger, A., Melice, J.L. and Hinnov, L. 1991. A strategy for frequency spectra of Quaternary climate records. *Climate Dynamics*, **5**: 227-240.

Berger, W.H., Schimmelmann, A. and Lange, C.B. 2004. Tidal cycles in the sediments of Santa Barbara Basin. *Geology*, **32**: 329-332.

Berger, W.H. and von Rad, U. 2002. Decadal to millennial cyclicity in varves and turbidites from the Arabian Sea: hypothesis of tidal origin. *Global and Planetary Change*, **34**: 313-325.

Bergstresser, T.J. and Krebs, W.N. 1983. Late Cretaceous (Campanian-Maastrichtian) diatoms from the Pierre Shale, Wyoming, Colorado and Kansas. *Journal of Paleontology*, **57**: 883-891.

Bernhard, J.M. and Reimers, C.E. 1991. Benthic foraminiferal population fluctuations related to anoxia: Santa Barbara Basin. *Biochemistry*, **15**: 127-149.

Bienfang, P.K. and Szyper, J.P. 1981. Phytoplankton dynamics in the subtropical Pacific Ocean off Hawaii. *Deep Sea Research Part I*, **28**: 981-1000.

Biondi, F., Gershunov, A. and Cayan, D.R. 2001. North Pacific decadal climate variability since 1661. *Journal of Climate,* **14**: 5-10.

Biscaye, P.E. 1965. Mineralogy and sedimentation of recent deep-sea clay in the Atlantic Ocean and adjacent seas and oceans. *Geological Society of America Bulletin*, **76**: 803-832.

Bjerknes, J. 1969. Atmospheric teleconnections from the equatorial Pacific. *Mon. Weather. Rev.*, **97**: 163-172.

Bjornsson, H., Mysak, L.A. and Brown, R.D. 1995. On the Interannual Variability of Precipitation and Runoff in the Mackenzie Drainage Basin. *Climate Dynamics* **12**: 67-76.

Black, D.E., Thunell, R.C., Kaplan, A., Peterson, L.C. and Tappa, E.J. 2004. A 2000-year record of Caribbean and tropical North Atlantic hydrographic variability. *Paleoceanography,* **19**: PA2022 1-11.

Black, X.R. 2002. Stratospheric forcing of surface climate in the Arctic oscillation. *Journal of Climate*, **15**: 268-277.

Blackman, R.B. and Tukey, J.W. 1958. *The Measurement of Power Spectra From the Point of View of Communication Engineering*. Dover publications, New York, 190 pp.

Bloomfield, P. 1976. *Fourier Analysis of Time Series: an Introduction*. Wiley, London.

Bolton, E.W., Maasch, K.A. and Lilly, J.M. 1995. A wavelet analysis of Plio-Pleistocene climate indicators: a new view of periodicity evolution. *Geophysical Research Letters*, **22**: 2753-2756.

Boltovoskoy, D., Uliana, E. and Wefer, G. 1996. Seasonal variation in the flux of microplankton and radiolarian assemblage composition in the northeastern tropical Atlantic at 2195m. *Limnology and Oceanography*, **41**: 615-635.

Bouma, A.G. 1969. *Methods for the Study of Sedimentary Structures*. Wiley, New York.

Brady, E.C., DeConto, R.M. and Thompson, S.L. 1998. Deep Water Formation and Poleward Ocean Heat Transport in the Warm Climate Extreme of the Cretaceous (80 Ma). *Geophysical Research Letters,* **25**: 4205-4208.

Briffa, K.R., Jones, P.D. and Schweingruber, F.H. 1992. Tree-ring density reconstructions of summer temperature patterns across western North America since 1600. *American Meteorological Society*, **5**: 735-754.

Brinkhuis, H., Schouten, S., Collinson, M.E., Sluijs, A., Sinninghe Damsté, J.S., Dickens, G.R., Huber, M., Cronin, T.M., Bujak, J.P., Stein, R., Eldrett, J.S., Harding, I.C. and Sangiorgi, F. 2005. A Giant Arctic Freshwater Pond at the end of the Early Eocene; Implications for Ocean Heat Transport and Carbon Cycling. In: *AGU Fall Meeting*, pp. PP51C-0617, San Francisco.

Brodie, I. and Kemp, A.E.S. 1994. Variation in biogenic and detrital fluxes and formation of laminae in late Quaternary sediments from the Peruvian coastal upwelling zone. *Marine Geology*, **116**: 385-398.

Brodie, I. and Kemp, A.E.S. 1995. Pelletal structures in Peruvian upwelling sediments. *J. Geol. Soc. London*, **152**: 141-150.

Brothers, R.J., Kemp, A.E.S. and Maltman, A.J. 1996. Mechanical development of vein structures due to the passage of earthquake waves through poorly-consolidated sediments. *Tectonophysics*, **260**: 227-244.

Brzezinski, M.A., Villareal, T.A. and Lipschultz, F. 1998. Silica production and the contribution of diatoms to new and primary production in the central North Pacific. *Marine Ecology Progress Series*, **167**: 89-104.

Buck, B.J. and Mack, G.H. 1995. Latest Cretaceous (Maastrichtian) aridity indicated by palaeosols in the McRae Formation, south-central New Mexico. *Cretaceous Research*, **16**: 559-572.

Bukry, D. 1981. Cretaceous Arctic silicoflagellates. *Geo-Marine Letters*, **1**: 57-63.

Bukry, D. 1985. Correlation of Late Cretaceous silicoflagellates from Alpha Ridge. In: *Initial Geological Report on CESAR - the Canadian Expedition to Study the Alpha Ridge, Arctic Ocean* (Eds H.R. Jackson, P.J. Mudie and S.M. Blasco), pp. 125-135. Geological Survey of Canada, Paper 84-22, Report 9.

Bull, D. 1998. *High resolution palaeoceanography and palaeoclimatology from late Quaternary laminated sediments from Santa Barbara Basin, California Margin*, University of Southampton.

Bull, D. and Kemp, A.E.S. 1995. Composition and origins of laminae in late Quaternary and Holocene sediments from the Santa Barbara Basin. In: *Proceedings of the Ocean Drilling Program, Scientific Results. Leg146 (Pt. 2)* (Eds J.P. Kennett, J.G. Baldauf and M. Lyle), pp. 77-87. College Station, TX (Ocean Drilling Program).

Bull, D., Kemp, A.E.S. and Weedon, G.P. 2000. A 160-k.y.-old record of El Niño-Southern Oscillation in marine production and coastal runoff from Santa Barbara Basin, California, USA. *Geology*, **28**: 1007-1010.

Burg, J.P. 1975. *Maximum Entropy Spectral Analysis*, Stanford University.

Burke, I.T. 2002. Microfabric study of diatomaceous and lithogenic deposition in laminated sediments from the Gotland Deep, Baltic Sea. *Marine Geology*, **183**: 89-105.

Bush, A.B.G. 1997. Numerical simulation of the Cretaceous Tethys circumglobal current. *Science*, **275**: 807-810.

Bush, A.B.G. and Philander, S.G.H. 1997. The Late Cretaceous: simulation with a coupled atmosphere-ocean general circulation model. *Paleoceanography*, **12**: 495-516.

Cane, M.A. 2005. The evolution of El Niño, past and future. *Earth and Planetary Science Letters*, **230**: 227-240.

Cane, M.A. and Molnar, P. 2001. Closing of the Indonesian seaway as a precursor to east African aridification around 3-4 million years ago. *Science*, **411**: 157-162.

Carpenter, E.J., Montoya, J.P., Burns, J., Mulholland, M., Subramaniam, A. and Capone, D.G. 1999. Extensive bloom of a N_2 fixing symbiotic association in the tropical Atlantic Ocean. *Marine Ecology Progress Series*, **185**: 273-283.

Carpenter, E.J. and Romans, K. 1992. Major role of the cyanobacterium Trichodesmium in nutrient cycling in the North-Atlantic Ocean. *Science*, **254**: 1356-1358.

Cas, R.A.F. and Wright, J.V. 1987. *Volcanic Successions: Modern and Ancient*. Unwin-Hyam, London, 528 pp.

Castagnoli, G., Bernasconi, S.M., Bonino, G., Della Monica, P. and Taricco, C. 1999. 700 year record of the 11 year solar cycle by planktonic foraminifera of a shallow water Mediterranean core. *Advances in Space Research*, **24**: 233-236.

Chaisson, W.P. and Ravelo, A.C. 2000. Pliocene development of the east-west hydrographic gradient in the equatorial Pacific. *Paleoceanography*, **15**: 497-505.

Chamley, H. 1989. *Clay sedimentology*. Springer-Verlag, New York, 623 pp.

Chamley, H. 1997. Clay mineral sedimentation in the ocean. In: *Soils and Sediments Mineralogy and Geochemistry* (Eds H. Paquet and N. Clauer), pp. 269-302. Springer.

Chandra, S. and McPeters, R.D. 1994. The solar cycle variation of ozone in the stratosphere inferred from Nimbus 7 and NOAA 11 satellites. *Journal of Geophysical Research*, **99**: 20665-20671.

Chang, A.S. and Grimm, K.A. 1999. Speckled beds: distinctive gravity-flow deposits in finely laminated diatomaceous sediments, Miocene Monterey Formation, California. *Journal of Sedimentary Research*, **69**: 122-134.

Chang, A.S., Grimm, K.A. and White, L.D. 1998. Diatomaceous Sediments from the Miocene Monterey Formation, California: A Lamina-Scale Investigation of Biological, Ecological and Sedimentary Processes. *Palaios*, **13**: 439-458.

Chang, A.S., Patterson, T.R. and McNelly, R. 2003. Seasonal sediment and diatom record from Late Holocene sediments, Effingham Inlet, British Columbia, Canada. *Palaios*, **18**: 477-494.

Chang, Y.-S., Jeon, D., Lee, H., An, H.S., Seo, J.-W. and Youn, Y.-H. 2004. Interannual variability and lagged correlation during strong El Niño events in the Pacific Ocean. *Climate Research*, **27**: 51-58.

Chavez, F.P., Ryan, J., Lluch-Cota, S.E. and Ñiquen, M. 2003. From Anchovies to Sardines and Back: Multidecadal Change in the Pacific Ocean. *Science*, **299**: 217-221.

Clark, D.L. 1974. Late Mesozoic and early Cenozoic sediment cores from the Arctic Ocean. *Geology*, **2**: 41-44.

Clark, D.L. 1988. Early history of the Arctic Ocean. *Paleoceanography*, **3**: 539-550.

Clark, D.L., Byers, C.W. and Pratt, L.M. 1986. Cretaceous black mud from the central Arctic Ocean. *Paleoceanography*, **1**: 265-271.

Clark, D.L. and Hanson, A. 1983. Central Arctic Ocean sediment texture: a key to ice transport mechanisms. In: *Glacial-Marine Sedimentation* (Ed B.F. Molnia), pp. 301-330. Plenum, New York.

Clarke, L.J. and Jenkyns, H.C. 1999. New oxygen isotope evidence for long-term Cretaceous climatic change in the Southern Hemisphere. *Geology*, **27**: 699-702.

Cochran, J.K., Landman, N.H., Turekian, K.K., Michard, A. and Schrag, D.P. 2003. Paleoceanography of the Late Cretaceous (Maastrichtian) Western Interior Seaway of North America: evidence from Sr and O isotopes. *Palaeogeography, Palaeoclimatology, Palaeoecology*, **191**: 45-64.

Conversi, A. and Hameed, S. 1997. Evidence of quasi-biennial oscillation in zooplankton biomass in the Subarctic Pacific. *Journal of Geophysical Research*, **102**: 15659-15665.

Conversi, A. and Hameed, S. 1998. Common signals between physical and atmospheric variables and zooplankton biomass in the Subarctic Pacific. *Journal of Marine Science*, **55**: 739-747.

Cook, E.R., D'Arrigo, R.D. and Mann, M.E. 2002. A Well-Verified, Multiproxy Reconstruction of the Winter North Atlantic Oscillation Index since A.D. 1400*. *Journal of Climate*, **15**: 1754-1764.

Cook, E.R., D'Arrigo, R.D. and Mann, M.E. 2002. A Well-Verified, Multiproxy Reconstruction of the Winter North Atlantic Oscillation Index since A.D. 1400*. *Journal of Climate*, **15**: 1754-1764.

Cosentino, D., Cipollari, P., Lo Mastro, S. and Giampaolo, C. 2005. High-frequency cyclicity in the latest Messinian Adriatic foreland basin: Insight into palaeoclimate and palaeoenvironments of the Mediterranean Lago-Mare episode. *Sedimentary Geology*, **178**: 31-53.

Coughlin, K. and Tung, K.-K. 2001. QBO Signal found as the Extratropical Surface through Northern Annular Modes. *Geophysical Research Letters*, **28**: 4563-4566.

Craggs, H.J. 2005. Late Cretaceous climate signal of the Northern Pekulney Range Flora of northeastern Russia. *Palaeogeography, Palaeoclimatology, Palaeoecology*, **217**: 25-46

D'Arrigo, R., Wiles, G., Jacoby, G. and Villabla, R. 1999. North Pacific sea surface temperatures: past variations inferred from tree rings. *Geophysical Research Letters*, **26**: 2757-2760.

D'Hondt, S. and Arthur, M.A. 2002. Deep water in the late Maastrichtian ocean. *Paleoceanography*, **17**: 10.1029/1999PA000486.

D'Hondt, S. and Lindinger, M. 1994. A stable isotopic record of the Maastrichtian ocean-climate system: South Atlantic DSDP Site 528. *Palaeogeography, Palaeoclimatology, Palaeoecology*, **112**: 363-378.

Davis, C.O., Hollibaugh, J.T., Seibert, D.L.R., Thomas, W.H. and Harrison, P.J. 1980. Formation of resting spores by *Leptocylindricus danicus* (Bacillariophyceae) in a controlled experimental ecosystem. *Journal of Phycology*, **16**: 296-302.

Dean, J.M. 2000a. *High resolution palaeoceanography and palaeoclimatology from late Holocene laminated sediments, Saanich Inlet, British Columbia*, University of Southampton, Southampton, 228 pp.

Dean, J.M. and Kemp, A.E.S. 2004. A 2100 year BP record of the Pacific Decadal Oscillation, El Niño Southern Oscillation and Quasi-Biennial Oscillation in marine production and fluvial input from Saanich Inlet, British Columbia. *Palaeogeography, Palaeoclimatology, Palaeoecology,* **213**: 207-229.

Dean, J.M., Kemp, A.E.S. and Pearce, R.B. 2001. Paleo-flux records from electron microscope studies of Holocene laminated sediments, Saanich Inlet, British Columbia. *Marine Geology*, **174**: 139-158.

Dean, W.E. 2000b. The Sun and Climate, **USGS Fact Sheet FS-095-00**. U.S. Geological Survey.

Deflandre, G. 1941. Sur la présence de diatomés dans certains silex creux Turoniens et sur un nouveau mode de fossilisations de ces organismes. *comptes Rendus de l'Académiedes Sciences de Paris,* **213**: 878-880.

Dell'Agnese, D.J. and Clark, D.L. 1994. Siliceous microfossils from the warm Late Cretaceous and Early Cenozoic Arctic Ocean. *Journal of Paleontology*, **68**: 31-47.

Dettinger, M.D., Ghil, M., Strong, C.M., Weibel, W. and Yiou, P. 1995. Software expedites singular-spectrum analysis of noisy time series. *Eos, Trans. American Geophysical Union*, **76**: 12,14,21.

Dicke, R.H. 1979. Solar luminosity and the sunspot cycle. *Nature,* **276**: 676-680.

Dickinson, W.R. 1995. Forearc Basins. In: *Tectonics of Sedimentary Basins* (Eds C.J. Busby and R.V. Ingersoll), pp. 221-262. Blackwell Science.

Diehl, J.F. 1991. The Elkhorn Mountains revisited: New data for the Cretaceous-early Tertiary north-central Montana alkalic province. *Journal of Geophysical Research*, **96**: 9887-9894.

Drugg, W.S. 1967. Palynology of the Upper Moreno Formation (Late Cretaceous-Paleogene) Escarpado Canyon, California. *Palaeontographica Abt. B.*, **120**: 1-71.

Dunbar, R.B., Wellington, G.M., Colgan, M.W. and Glynn, P.W. 1994. Eastern Pacific sea surface temperature since 1600AD: the d^{18}O record of climatic variability in Galápagos corals. *Paleoceanography*, **9**: 291-315.

Dunkerton, T.J. 1997. The role of gravity waves in the quasi-biennial oscillation. *Journal of Geophysical Research D: Atmospheres*, **102**: 26053-26076.

Dunoyer de Segonzac, G. 1970. The transformation of clay minerals during diagenesis and low grade metamorphism: a review. *Sedimentology*, **15**: 282-346.

Eddy, J.A. 1976. The Maunder Minimum. *Science*, **192**: 1189-1202.

Eggar, H., Fenner, J.M., Heilmann-Clausen, C., Rögl, F., Sachsenhofer, R.F. and Scmitz, B. 2003. Paleoproductivity of the northern Tethyan margin (Anthering Section, Austria) across the Paleocene-Eocene transition. In: *Causes and Consequences if Globally Warm Climates in the Early Paleogene* (Eds S.L. Wing, P.D. Gingerich, B. Schmitz and E. Thomas), pp. 133-146. Geological Society of America Special Paper 369, Boulder, Colorado.

Ehrenberg, C.G. 1844. Eine Mitteilung uber 2 neue Lager on Geibirgsmassen aus Infusorien als Meers-Absatz in Amerika und eine Vergleichung derselben mit den organischen Kreide-Gebilden in Europa und Afrika. *Berichte der Berliner Akademie*57-97.

Ehrenberg, C.G. 1854. Das Erden und felsen schaffende Wirken des unsichtbar kleinen selbstständigen Lebens auf der Erde. Atlas. Leopold Voss, Leipzig. *Mikrogeologie*, **40 pls**.

Ekart, D.D., Cerling, T.E., Montanez, I.P. and Tabor, N.J. 1999. A 400 million year carbon isotope record of pedogenic carbonate: implications for paleoatmospheric carbon dioxide. *American Journal of Science*, **299**: 805-827.

Elverhøi, A., Andersen, E.S., Dokken, T., Hebbelm, D., Spielhagen, R., Svendsen, J.I., Sørflaten, M., Rørnes, A., Hald, M. and Forsberg, C.F. 1995. The growth and decay of the Late Weichselian ice sheet in western Svalbard and adjacent areas based on provenance studies of marine sediments. *Quaternary Research,* **44**: 303-316.

Enfield, D.B. and Cid, L.S. 1991. Low-frequency changes in El Niño-Southern Oscillation. *Journal of Climate,* **4**: 1137-1146.

Eynaud, F., Giraudeau, J., Pichon, J.J. and Pudsey, C.J. 1999. Sea-surface distribution of coccolithophores, diatoms, silicoflagellates and dinoflagellates in the South Atlantic Ocean during the late austral summer 1995. *Deep Sea Research Part I*, **46**: 451-482.

Falcon-Lang, H.J. 2003. Growth interruptions in silicified conifer woods from the Upper Cretaceous Two Medicine Formation, Montana, USA: implications for palaeoclimate and dinosaur palaeoecology. *Palaeogeography, Palaeoclimatology, Palaeoecology*, **199**: 299-314.

Falcon-Lang, H.J., MacRae, R.A. and Csank, A.Z. 2004. Palaeoecology of Late Cretaceous polar vegetation preserved in the Hansen Point Volcanics, NW Ellesmere Island, Canada. *Palaeogeography, Palaeoclimatology, Palaeoecology,* **212**: 45-64.

Fedorov, A.V. and Philander, S.G. 2000. Is El Niño changing? *Science,* **288**: 1997-2002.

Fenner, J.M. 1982. Cretaceous diatoms off New Jersey. In: *7th Int. Symp. Living and Fossil Diatoms*, Philadelphia (Abstracts).

Fenner, J.M. 1991. Taxonomy, stratigraphy and paleoceanographic implications of Paleocene diatoms. *Proceedings of the Ocean Drilling Program, Scientific Results,* **114**: 123-154.

Ferrante, J.G. and Parker, J.I. 1977. Transport of diatom frustules by copepod fecal pellets to the sediments of Lake Michigan. *Limnology and Oceanography*, **22**: 92-98.

Firth, J.V. and Clark, D.L. 1998. An early Maastrichtian organic-walled phytoplankton cyst assemblage from an organic-rich black mud in Core Fl-533, Alpha Ridge: evidence for upwelling conditions in the Cretaceous Arctic Ocean. *Marine Micropaleontology,* **34**: 1-27.

Fischer, H., Traufetter, F., Oerter, H., Weller, R. and Miller, H. 2004. Prevalence of the Antarctic Circumpolar Wave over the last two millennia recorded in Dronning Maud Land ice. *Geophysical Research Letters*, **31**: L08202, doi:10.1029/2003GL019186.

Fonseca, C. 1997. *Late Cretaceous-Early Tertiary paleoceanography and cyclic sedimentation along the Californian Margin: Evidence from the Moreno Formation,* Stanford University, 449 pp.

Fonseca, C. 2000. Upwelling, sedimentation and anoxia control on deposition of phosphates in the Late Cretaceous California margin. In: *Marine Authigenesis: From Global to Microbial* (Ed L.P. C.R. Glenn), **Special Publication No. 66**, pp. 455-480. SEPM.

Foreman, H.P. 1968. Upper Maestrichtian radiolaria of California. In: *The Paleontological Association, Special Papers in Palaeontology*, pp. 82, London.

Forti, A. 1909. Studi per una Monografia del genere Pyxilla (Diatomee) e dei generi affini. *Nuova Notarisia*, **24**: 19-34.

Foulcault, A., Servant-Vildary, S., Fang, N. and Powichrowski, L. 1986. Un des plus anciens gisements de diatomées découvert dans l'Albien-Cenomanien inférieur des Alpes ligures (Italie): remarque sur l'apparation de ces algues. *Comptes Rendus de l'Académiedes Sciences de Paris, Série II*, **303**: 397-402.

Fourtanier, E. 1991. Diatom biostratigraphy of Equatorial Indian Ocean Site 758. *Proceedings of the Ocean Drilling Program, Scientific Results*, **121**: 189-208.

Francis, J.E. and Poole, I. 2002. Cretaceous and early Tertiary climates of Antarctica: evidence from fossil wood. *Palaeogeography, Palaeoclimatology, Palaeoecology*, **182**: 47-64.

Francus, P., Keimig, F. and Besonen, M. 2002. An algorithm to aid varve counting and measurement from thin-sections. *Journal of Paleolimnology*, **28**: 283-286.

Fryxell, G.A. and Prasad, A.K.S.K. 1990. Eucampia antarctica var. recta (Mangin) stat. nov. (Biddulphiaceae, Bacillarophyceae): life stages at the Weddell Sea ice edge. *Phycologia*, **29**: 27-38.

Fryxell, G.A., Sims, P.A. and Watkins, T.P. 1986. Azpeitia (Bacillariophyceae): Related genera and promorphology. *Systematic Botany Monographs*, **13**.

Fürsich, F.T., Singh, I.B., Joachimski, M., Krumm, S., Schlirf, M. and Schlirf, S. 2005. Palaeoclimate reconstructions of the Middle Jurassic of Kachchh (western India): an integrated approach based on palaeoecological, oxygen isotopic, and clay mineralogical data. *Palaeogeography, Palaeoclimatology, Palaeoecology*, **217**: 289-309.

Garcia, A. and Mouradian, Z. 1998. The Gleissberg cycle of minima. *Solar Physics*, **180**: 495-498.

Garric, G. and Huber, M. 2003. Quasi-decadal variability in paleoclimate records: Sunspot cycles or intrinsic oscillations? *Paleoceanography*, **18**: 1068, doi:10.1029/2002PA000869.

Gedalof, Z., Mantua, N.J. and Peterson, D.L. 2002. A multi-century perspective of variability in the Pacific Decadal Oscillation: new insights from tree rings and coral. *Geophysical Research Letters*, **29**: 2204, doi:10.1029/2002GL015824.

Gersonde, R. and Harwood, D.M. 1990. Lower Cretaceous diatoms from ODP Leg 113 Site 693 (Weddell Sea). Part 1: Vegetative cells. In: *Proceedings of the Ocean Drilling Program, Scientific Results*, **113**, pp. 365-402. Ocean Drilling Program, College Station, Texas.

Ghil, M., Allen, R.M., Dettinger, M.D., Ide, K., Kondrashov, D., Mann, M.E., Robertson, A.H.F., Saunders, A., Tian, Y., Varadi, F. and Yiou, P. 2002. Advanced spectral methods for climatic time series. *Reviews of Geophysics*, **40**: 3.1-3.41, 10.1029/2000GR000092.

Ghil, M. and Vautard, R. 1991. Interdecadal oscillations and the warming trend in global temperature time series. *Nature*, **350**: 324-327.

Ghosh, P., Ghosh, P. and Bhattacharya, S.K. 2001. CO_2 levels in the Late Palaeozoic and Mesozoic atmosphere fro soil carbonate and organic matter, Saptura basin, Central India. *Palaeogeography, Palaeoclimatology, Palaeoecology*, **170**: 219-236.

Giosan, L., Flood, R.D. and Aller, R.C. 2002. Paleoceanographic significance of sediment color on western North Atlantic drifts: I. Origin of color. *Marine Geology*, **189**: 25-41.

Given, M.N. and Wall, J.H. 1971. Microfauna from the Upper Cretaceous Bearpaw Formation of south-central Alberta. *Canadian Petroleum Geology, Bulletin*, **19**: 502-544.

Gleissberg, W. 1958. The eighty-year sunspot cycle. *Journal of the British Astronomical Association*, **68**: 1148-1152.

Gleser, Z.I., Jousé, A.J. and Makarova, I.V. 1974. *Diatoms of the U.S.S.R., fossil and Recent*, **1**, Nauka, Leningrad, 403 pp.

Gleser, Z.I., Makarova, I.V., Moisseeva, A.I. and Nikolaev, V.A. 1992. *The Diatoms of the USSR Fossil and Recent, 2 (2).* St. Petersburg "Nauka" St.-Petersburg branch, St. Petersburg.

Gloersen, P. 1995. Modulation of hemispheric sea-ice cover by ENSO events. *Nature*, **373**: 503-506.

Goldman, J.C. 1993. Potential role of large oceanic diatoms in new primary production. *Deep-Sea Research Part I*, **40**: 159-168.

Goldman, J.C. and McGillicuddy, D.J. 2003. Effect of large marine diatoms growing at low light on episodic new production. *Limnology and Oceanography*, **48**: 1176-1182.

Goldstein, J.I., Newbury, D.E., Echlin, P., Joy Jr., D.C., Lyman, A.D.R., Fiori, C.E. and Lifshin, E. 1992. *Scanning Electron Microscopy and X-ray Microanalysis. 2nd ed.* Plenum, New York, 820 pp.

Golonka, J., Ross, M.I. and Scotese, C.R. 1994. Phanerozoic paleogeographic and paleoclimate modelling maps. In: *Pangea: Global environments and resources.* (Eds A.F. Embry, B. Beauchamp and D.J. Glass), **17**, pp. 1-47. Canadian Society of Petroleum Geologists Memoir.

Gordon, W.A. 1973. Marine life and ocean surface currents in the Cretaceous. *Journal of Geology*, **81**: 269-284.

Goudie, A.S. 1983. Calcrete. In: *Chemical Sediments and Geomorphology* (Eds A.S. Goudie and K. Pye), pp. 93-131. Academic Press, London.

Gradstein, F.M., Agterberg, F.P., Ogg, J.G., Hardenbol, J., Veen, P., Thierry, J. and Huang, Z. 1994. A Mesozoic timescale. *Journal of Geophysical Research*, **99**: 24051-24074.

Green, A.R., Kaplan, A.A. and Vierbuchen, R.C. 1984. Circum-Arctic petroleum potential. In: *W.E. Pratt Memorial Conference*, pp. 44. AAPG, EXXON Production Research, Houston, Tech. Report.

Greshan, C.W. 1986. Cretaceous and Paleogene siliceous phytoplankton assemblages from DSDP Sites 216, 214 and 208 in the Pacific and Indian Oceans. In: *North-Central Sect. Meeting, Geological Society of America*, **18**, pp. 290. GSA Abstracts with Programs, Kent, Ohio.

Grimm, K.A., Lange, C.B. and Gill, A.S. 1996. Biological forcing of hemipelagic sedimentary laminae: evidence from ODP Site 893, Santa Barbara Basin, California. *Journal of Sedimentary Research*, **66**: 613-624.

Grimm, K.A., Lange, C.B. and Gill, A.S. 1997. Self-sedimentation of phytoplankton blooms in the geologic record. *Sedimentary Geology*, **110**: 151-161.

Grunow, A. 1882. Beiträge zur Kenntnis der Fossilen Diatomeen Osterreich-Ungarns. In: *Beiträge zur Paleontologie Osterreich-Ungarns und des Orients* (Eds E. von Mojsisovids and M. Neumayer), **2**, pp. 136-159.

Grunow, A. 1884. Die Diatomeen von Franz Josefs-Land. *Denkschriften der mathematisch-naturwissenschafrlichen Classe oder kaiserlichen Akademie der Wissenschaften, Wien*, **48**: 53-122, 5 pls.

Guillard, R.R.L. and Kilham, P. 1977. The Ecology of Planktonic Diatoms. In: *The Biology of Diatoms* (Ed D. Werner), pp. 372-470. Blackwell Scientific Publications.

Guillard, R.R.L. and Kilham, P. 1978. The ecology of marine planktonic diatoms. In: *The Biology of Diatoms. Botanical Monographs* (Ed D. Werner), **13**, pp. 372-469. University of California Press, Berkeley.

Gulbrandsen, R.A., Jones, D.L., Tagg, K.M. and Reeser, D.W. 1963. Apatitized wood and leucophosphite in nodules in the Moreno Formation, California. *Geological Survey Professional Paper*, **475-C**: C100-C104.

Gunderson, J.A. and Sheriff, S.D. 1991. A new Late Cretaceous paleomagnetic pole from the Adel Mountains, west-central Montana. *Journal of Geophysical Research*, **96**: 317-326.

Gurevich, N.I. and Merkur'ev, S.A. 2005. Evolution of the Alpha Ridge (Arctic Ocean) Inferred from Magnetometric Data. *Doklady Earth Sciences*, **401**: 280-284.

Häggblom, A. 1982. Driftwood in Svalbard as an indicator of sea ice conditions: a preliminary report. *Geografiska Annaler*, **64A**: 81-94.

Hajós, M. and Stradner, H. 1975. Late Cretaceous Archaemonadaceae, Diatomaceae and Silicoflagellatae from the South Pacific Ocean, Deep Sea Drilling Project, Leg 29, Site 275. In: *Initial Reports of the Deep Sea Drilling Project*, **29**, pp. 913-1009, Washington D.C.

Hameed, S. and Lee, J.N. 2005. A mechanism for sun-climate connection. *Geophysical Research Letters*, **32**: L23817, doi:10.1029/2005GL024393.

Hanna, G.D. 1927. Cretaceous diatoms from California. *Occasional Papers of the California Academy of Sciences*, **13**: 5-49, 5 pls.

Hanna, G.D. 1928. Silicoflagellata from the Cretaceous of California. *Journal of Paleontology*, **1**: 259-263.

Hanna, G.D. 1932. The diatoms of Sharktooth Hill, Kern Country, California. *Proceedings of the California Academy of Sciences.*, **20**: 161-263, pls. 2-8.

Hanna, G.D. 1934. Additional notes on diatoms from the Cretaceous of California. *Journal of Paleontology*, **8**: 352-355, pl. 48.

Hargraves, P.E. 1986. The relationship of some fossil diatom genera to resting spores. In: *Proceedings of the 8th International Diatom Symposium* (Ed M. Ricard), pp. 67-80, Koenigstein: O. Koeltz.

Hargraves, P.E. and French, F.W. 1975. Observations on the survival of diatom resting spores. *Beih Nova Hedwigia*, **53**: 229-238.

Hargraves, P.E. and French, F.W. 1983. Diatom resting spores: significances and strategies. In: *Survival Strategies of the Algae* (Ed G.A. Fryxell), pp. 49-68. Cambridge University Press, Cambridge.

Harwood, D.M. 1988. Upper Cretaceous and lower Paleocene diatom and silicoflagellate biostratigraphy of Seymour Island, eastern Antarctic Peninsula. In: *Geology and Paleontology of Seymour Island, Antarctic Peninsula.* (Eds M.R. Feldmann and M.E. Woodburne), **169**, pp. 55-129. Geological Society of America Memoir, Boulder.

Harwood, D.M. and Gersonde, R. 1990. Lower Cretaceous diatoms from ODP Leg 113 Site 693 (Weddell Sea). Part 2: resting spores, chrysophycean cysts, an endoskeletal dinoflagellate, and notes on the origins of diatoms. In: *Proceedings of the Ocean Drilling Program, Scientific Results* (Eds P.F. Barker and J.P. Kennett), **113**, pp. 403-425. Ocean Drilling Programme, College Station, Texas.

Harwood, D.M. and Nikolaev, V.A. 1995. Cretaceous diatoms: morphology, taxonomy, biostratigraphy. In: *Siliceous Microfossils* (Ed C.D. Blome, et al (convenors)), *Paleontological Society Short Courses in Paleontology*, **8**, pp. 81-106, pls 1-4.

Hasle, G.R. and Sims, P.A. 1986. The diatom genera *Stellarima* and *Symbolophora* with comments on the genus *Actinoptychus*. *British Phycological Journal*, **21**: 97-114.

Hasle, G.R. and Syvertsen, E.E. 1985. *Thalassiosiropsis*, a new genus from the fossil records. *Micropaleontology*, **31**: 82-91.

Hasle, G.R. and Syvertsen, E.E. 1996. Marine diatoms. In: *Identifying Marine Diatoms and Dinoflagellates* (Ed C.R. Tomas), pp. 5-386. New York (Academic Press).

Hassol, S.J. 2004. Impacts of a Warming Arctic: Arctic Climate Impact Assessment, Cambridge University Press.

Hay, W.W. and DeConto, R.M. 1999. Comparison of modern and Late Cretaceous meridional energy transport and oceanology. In: *Evolution of the Cretaceous Ocean-Climate System* (Eds E. Barrera and C.C. Johnson), **332**, pp. 283-300. Geological Society of America Special Paper, Boulder, Colorado.

Hay, W.W., DeConto, R.M., Wold, C.N., Wilson, K.M., Voigt, S., Schulz, M., Wold-Rossby, A., Dullo, W.-C., Ronov, A.B., Balukhovsky, A.N. and Sóding, E. 1999. Alternative global Cretaceous paleogeography. In: *Evolution of the Cretaceous Ocean-Climate System* (Eds E. Barrera and C.C. Johnson), pp. 1-47. Geological Society of America Special Paper 332, Boulder, CO.

Hay, W.W., Eicher, D.L. and Diner, R. 1993. Physical oceanography and water masses in the Cretaceous Western Interior Seaway. In: *Evolution of the Western Interior Basin* (Eds W.G.E. Caldwell and E.G. Kauffman), **39**, pp. 297-318. Geological Association of Canada Special Paper.

Hebbeln, D. 2000. Flux of ice-rafted detritus from sea ice in the Fram Strait. *Deep Sea Research Part II*, **47**: 1773-1790.

Heiberg, P.A. 1863. *Conspectus criticus Diatomacearum Danicarum*. Wilhelm Priors Forlag, Kjøbenhavn, 135 pp.

Hein, J.R., Scholl, D.W., Barron, J.A., Jones, M.G. and Miller, J. 1978. Diagenesis of late Cenozoic diatomaceous deposits and formation of the bottom simulating reflector in the southern Bering Sea. *Sedimentology*, **25**: 155-181.

Herman, A.B. and Spicer, R.A. 1997. New quantitative palaeoclimate data for the Late Cretaceous Arctic: evidence for a warm polar ocean. *Palaeogeography, Palaeoclimatology, Palaeoecology*, **128**.

Hewson, I., O'Neil, J.M. and Abal, E. 2001. A low-latitude bloom, of the surf-zone diatom, *Anaulus australis* (Centrales, Bacillariophyta) on the coast of Southern Queensland (Australia). *Journal of Plankton Research*, **23**: 1233-1236.

Hickey, B.M. 1979. The California Current System-hypotheses and facts. *Progress in Oceanography*, **8**: 191-279.

Hobson, L.A. and McQuoid, M.R. 1997. Temporal variations among planktonic diatom assemblages in a turbulent environment of the southern Strait of Georgia, British Columbia, Canada. *Marine Ecology-Progress Series*, **150**: 263-274.

Hobson, L.A. and McQuoid, M.R. 2001. Pelagic diatom assemblages are good indicators of mixed water intrusions into Saanich Inlet, a stratified fjord in Vancouver Island. *Marine Geology*, **174**: 125-138.

Holton, J.R. and Tan, H.-C. 1980. The influence of the equatorial quasi-biennial oscillation on the global circulation at 50 mb. *Journal of Atmospheric Science*, **37**: 2200-2208.

Honjo, S. and Roman, M.R. 1978. Marine copepod faecal pellets: production, preservation and sedimentation. *Journal of Marine Research*, **36**: 45-57.

Hoyt, D.V. and Schatten, K.H. 1997. *The role of the Sun in Climate Change*. Oxford University Press, Oxford, 279 pp.

Huber, M. and Caballero, R. 2003. Eocene El Niño: Evidence for Robust Tropical Dynamics in the "Hothouse". *Science*, **299**: 877-881.

Hughes, G.B., Giegengack, R. and Kritikos, H.N. 2003. Modern spectral climate patterns in rhythmically deposited argillites of the Gowganda Formation (Early Proterozoic), southern Ontario, Canada. *Earth and Planetary Science Letters*, **207**: 13-22.

Ingersoll, R.V. 1978. Paleogeography and paleotectonics of the Late Mesozoic forearc basin of northern and central California. In: *Mesozoic Palaeogeography of the Western United States:*

Tusla. (Eds D.G. Howell and K.A. McDougall), **2**, pp. 471-482. Society of Sedimentary Geology (SEPM)-Pacific Coast Paleogeography Symposium.

Ingersoll, R.V. 1983. Petrofacies and provenance of Late Mesozoic forearc basin, northern and central California. *American Association of Petroleum Geologists Bulletin*, **67**: 1125-1142.

Isaacs, C.M. 1981. Porosity reduction during diagenesis of the Monterey Formation, Santa Barbara coastal area, California. In: *The Monterey Formation and Related Siliceous Rocks of California.* (Eds R.E. Garrison, R.B. Douglass, K.E. Pisciotto, C.M. Issacs and J.C. Ingle), *Special Paper of the Society of Economic Paleontologists and Mineralogists.*, pp. 257-271.

Jackson, H.R., Forsyth, D.A., Hall, J.K. and Overton, A. 1990. Seismic reflection and refraction. In: *The Geology of North America, The Arctic Region* (Eds A. Grantz, G.L. Johnson and W.J. Sweeny), **L**, pp. 153-170. Geological Society of America, Boulder.

Jackson, H.R., Forsyth, D.A. and Johnson, G.L. 1986. Oceanic affinities of the Alpha Ridge, Arctic Ocean. *Marine Geology*, **73**: 237-261.

Jackson, H.R. and Johnson, G.L. 1985. Summary of Arctic geophysics. *Journal of Geodynamics*, **6**: 245-262.

James, I.N. and James, P.M. 1989. Ultra-low-frequency variability in a simple atmospheric circulation model. *Nature*, **342**: 53-55.

Jenkyns, H.C., Forster, A., Schouten, S. and Sinninghe Damsté, J.S. 2004. High temperatures in the Late Cretaceous Arctic Ocean. *Nature*, **432**: 888-892.

Jevrejeva, S., Moore, J.C. and Grinsted, A. 2004. Oceanic and atmospheric transport of multiyear El Niño-Southern Oscillation (ENSO) signatures to the polar regions. *Geophysical Research Letters*, **31**: L24210, doi:10.1029/2004GL020871.

Jim, C.Y. 1985. Impregnation of moist and dry unconsolidated clay samples using Spurr resin for microstructural studies. *Journal of Sedimentary Petrology*, **55**: 597-599.

Johansen, S. and Hytteborn, H. 2001. A contribution to the discussion of biota dispersal with drift ice and driftwood in the North Atlantic. *Journal of Biogeography*105-115.

Johnson, G.L. 1990. Morphology and plate tectonics: the modern polar oceans. In: *Geological History of the Polar Oceans: Arctic versus Antarctic* (Eds U. Bleil and J. Thiede), **308**, pp. 11-28. NATO ASI series C.

Johnson, G.L., Pogrebitsky, J. and Macnab, R. 1994. Arctic structural evolution: relationship to paleoceanography. In: *The Polar Oceans and Their Role in Shaping the Global Environment* (Eds O.M. Johannessen, R.D. Muench and J.E. Overland), **85**, pp. 285-294. AGU Geophys. Monograph.

Johnson, M.E. 2002. Paleoislands in the stream: paleogeography and expected circulation patterns. *Geobios*, **35**: 96-106.

Jokat, W. 2003. Seismic investigations along the western sector of Alpha Ridge, Central Arctic Ocean. *Geophys. J. Int.*, **152**: 185-201.

Jordan, R.W. and Priddle, J. 1991. Fossil members of the diatom genus *Proboscia*. *Diatom Research*, **6**: 55-61.

Jousé, A.P. 1948. "Pre-Tertiary diatom algae". *Botanicheskii Zhurnal SSSR*, **33**: 345-356.

Jousé, A.P. 1949. Algae diatomaceae aetatis supernecretaceae ex arenis argillaceis systematis fluminis Bolschoy Aktay in declivitate orientali Ural Borealis. *Botanicheskie Materialy, Otdela Sporovykh Rastenii, Botanicheskii Institut, Akademia Nauk SSSR*, **6**: 65-78.

Jousé, A.P. 1951. Diatomeae et silicoflagellatae aetatis cretcae superne e Montibus Uralensis Septentrionalibus. *Botanicheskie Materialy, Otdela Sporovykh Rastenii, Botanicheskii Institut, Akademia Nauk SSSR*, **7**: 42-65.

Jousé, A.P. 1955. Species novae generis *Gladius* Schulz in stratura aetatis cretaceae superioris. *Botanicheskie Materialy, Otdela Sporovykh Rastenii, Botanicheskii Institut, Akademia Nauk SSSR*, **10**: 72-76.

Kane, R.P. 1992. Relationship between QBOs of stratospheric winds, ENSO variability and other atmospheric parameters. *International Journal of Climatology*, **12**: 435-447.

Kang, S., Mayewski, P.A. and Yan, Y. 2005. A 290-a record of atmospheric circulation over the North Pacific from a Mt. Logan ice core, Yukon Territory. *Acta Oceanologica Sinica*, **24**: 81-90.

Kemp, A.E.S. 1990. Sedimentary fabrics and variation in lamination style in Peru continental margin upwelling sediments. In: *Proceedings of ODP Scientific Results*, **112**, pp. 43-58. Ocean Drilling Program, College Station, TX.

Kemp, A.E.S. 1995. Laminated sediments from coastal and open ocean upwelling systems: what variability do they record? In: *Upwelling in the Ocean: Modern Processes and Ancient Records.* (Eds C.P. Summerhayes, K.-C. Emeis, M.V. Angel, R.L. Smith and B. Zeitzschel), pp. 239-257. Dahlem Workshop Report, ES18, Wiley, Chichester.

Kemp, A.E.S. 1996. *Palaeoclimatology and Palaeoceanography from Laminated Sediments.*, **116**. Geological Society of London Special Publications, 258 pp.

Kemp, A.E.S. 2003. Evidence for abrupt climate changes in annually laminated marine sediments. *Philosophical Transaction of the Royal Society of London A*, **361**: 1851-1870.

Kemp, A.E.S., Pearce, R.B., Koizumi, I., Pike, J. and Rance, S.J. 1999. The role of mat-forming diatoms in the formation of Mediterranean sapropels. *Nature*, **398**: 57-61.

Kemp, A.E.S., Pearce, R.B., Pike, J. and Marshall, J.E.A. 1998. Microfabric and microcompositional studies of Pliocene and Quaternary sapropels from the eastern Mediterranean. In: *Proceedings of the Ocean Drilling Program, Scientific Results* (Eds A.H.F. Robertson, K.-C. Emeis, C. Richter and A. Camerlenghi), **160**, pp. 333-348. College Station, TX.

Kemp, A.E.S., Pike, J., Pearce, R.B. and Lange, C. 2000. The "Fall dump" — a new perspective on the role of a "shade flora" in the annual cycle of diatom production and export flux. *Deep-Sea Research II*, **47**: 2129-2154.

Kim, K.H. and Burnett, W.C. 1988. Accumulation and biological mixing of Peru margin sediments. *Marine Geology*, **80**: 181-194.

Kirschvink, J.L. 1980. The least squares line and plane and the analysis of palaeomagnetic data. *Geophys. J. R. Astron. Soc.*, **62**: 699-718.

Kitchell, J.A. and Clark, D.L. 1982. Late Cretaceous-Paleogene paleogeography and paleocirculation: evidence of north polar upwelling. *Palaeogeography, Palaeoclimatology, Palaeoecology*, **40**: 135-165.

Kitchell, J.A., Clark, D.L. and Gombos, A.M. 1986. Biological selectivity of extinction: A link between background and mass extinction. *Palaios*, **1**: 504-511.

Kodama, K.P. and Ward, P.D. 2001. Compaction-corrected palaeomagnetic palaeolatitudes for Late Cretaceous rudists along the Cretaceous California margin: Evidence for less than 1500 km of post-Late Cretaceous offset for Baja British Columbia. *Geological Society of America Bulletin*, **113**: 1171-1178.

Koning, E., van Iperen, J.M., van Raaphorst, W., Helder, W., Brummer, G.-J.A. and van Weering, T.C.E. 2001. Selective preservation of upwelling-indicating diatoms in sediments off Somalia, NW Indian Ocean. *Deep-Sea Research Part I*, **48**: 2473-2495.

Koutsoukos, E.A.M. and Hart, M.B. 1991. Radiolarians and diatoms from the mid-Cretaceous successions of the Sergipe Basin, northeastern Brazil: palaeoceanographic assessment. *Journal of Micropalaeontology*, **9**: 45-64.

Krotov, A.I. 1957a. "Diatomaceous algae from the Upper Cretaceous and Paleogene deposits on the eastern slopes of the Urals and Transurals. In: *Proceedings of the Interdepartmental Conference on the developments in Stratigraphy*, pp. 298-302, Leningrad, Gostoptekhizdat.

Krotov, A.I. 1957b. The stratigraphy of the Upper Cretaceous and the Paleogene deposits on the eastern slope of the North and Middle Urals based on the diatom algae data. *Trudy Gorno-geologischeskogo, Inst. Uralisk., Akad. Nauk SSSR*, **28**: 17-38.

Krotov, A.I. 1959. Species novae diatomacearum e sedimentis cretae superioris in montibus Uralensibus. *Botanicheskie Materialy, Otdela Sporovykh Rastenii, Botanicheskii Institut, Akademia Nauk SSSR*, **12**: 106-112.

Kuypers, M.M.M., van Breugel, Y., Schouten, S., Erba, E. and Sinninghe Damsté, J.S. 2004. N_2-fixing cyanobacteria supplied nutrient N for Cretaceous oceanic anoxic events *Geology*, **32**: 853-856.

Labitzke, K. 2005. On the solar cycle-QBO relationship: a summary. *Journal of Atmospheric and Solar-Terrestrial Physics*, **67**: 45-54.

Labitzke, K. and van Loon, H. 1990. Associations between the 11 year solar cycle, the quasi-biennial oscillation and the atmosphere: a summary of recent work. *Philosophical Transaction of the Royal Society of London A*, **330**: 577-589.

Labitzke, K. and van Loon, H. 1999. *The stratosphere phenomena history and relevance*. Springer, Berlin, Heidelberg, New York, 179 pp.

Lagoe, M.B. and McDougall, K. 1986. Paleoenvironmental control of benthic foraminiferal ranges across a middle Miocene basin-margin, Central California. *Journal of Foraminiferal Research*, **16**: 232-243.

Lampitt, R.S. 1990. What happens to zooplankton faecal pellets? Implications for material flux. *Marine Biology*, **104**: 15-23.

Lane, L.S. 1997. Canada Basin, Arctic Ocean: Evidence against a rotational origin. *Tectonics*, **16**: 363-387.

Lange, C.B. 1987. El Niño in Santa Barbara Basin: diatom, radiolarian and foraminiferan responses to the "1983 El Niño" event. *Marine Geology*, **78**: 153-160.

Lange, C.B. and Berger, W.H. 1993. Diatom productivity and preservation in the western equatorial Pacific: the Quaternary record. In: *Proceedings of the Ocean Drilling Program, Scientific Results*, pp. 509-523.

Lange, C.B., Burke, S.K. and Berger, W.H. 1990. Biological production off southern California is linked to climate change. *Climatic Change*, **16**: 319-329.

Lange, C.B., Romero, O.E., Wefer, G. and Gagric, A.J. 1998. Offshore influence of coastal upwelling off Mauritania, NW Africa, as recorded by diatoms in sediment traps at 2195 m water depth. *Deep Sea Research Part I*, **45**: 985-1013.

Lange, C.B., Weinheimer, A.L., Reid, F.M.H., Tappa, E. and Thunell, R.C. 2000a. Response of the siliceous microplankton from the Santa Barbara Basin to the 1997-98 El Niño event. *Reports of California Cooperative Oceanic Fisheries Investigations*, **Rep. 41**.

Lange, C.B., Weinheimer, A.L., Reid, F.M.H. and Thunell, R.C. 1997. Sedimentation patterns of diatoms, radiolarians, and silicoflagellates in Santa Barbara Basin, California. *Reports of California Cooperative Oceanic Fisheries Investigations*, **38**: 161-170.

Lange, C.B., Weinheimer, A.L., Reid, F.M.H. and Thunell, R.C. 2000b. Temporal sedimentation patterns of diatoms, radiolarians and silicoflagellates in Santa Barbara Basin, California. *CalCOfi rep*, **38**: 161-170.

Lawver, L.A. and Mûller, R.D. 1994. Iceland hotspot track. *Geology*, **22**: 311-314.

Lean, J.L., White, O.R. and Skumanich, A. 1995. On the solar ultraviolet spectral irradiance during the Maunder Minimum. *Global Biogeochemical Cycles*, **9**: 171-182.

Lee, E.H., Ahn, Y.S., Yang, H.J. and Chen, K.Y. 2005. The sunspot and auroral activity cycle derived from Korean historical records of the 11th-18th century. *Solar Physics*, **224**: 373-386.

Li, L. and Keller, G. 1998. Maastrichtian climate, productivity and faunal turnovers in planktic foraminifera in south Atlantic DSDP Sites 525 NS 21. *Marine Micropaleontology*, **33**: 55-86.

Li, L. and Keller, G. 1999. Variability in Late Cretaceous climate and deep waters: evidence from stable isotopes. *Marine Geology*, **161**: 171-190.

Lindsley-Griffin, N., Kemp, A.E.S. and Swartz, J.F. 1990. Vein structures of the Peru margin, Leg 112. In: *Proceedings of the Ocean Drilling Program, Scientific Results* (Eds E. Suess and R. von Huene), **112**, pp. 3-11, College Station, TX.

Ling, H.Y., McPherson, L.M. and Clark, D.L. 1973. Late Cretaceous (Maestrichtian?) silicoflagellates from the Alpha Cordillera of the Arctic Ocean. *Science*, **180**: 1360-1361.

Liu, J., Curry, J.A. and Hu, Y. 2004. Recent Arctic Sea Ice Variability: Connections to the Arctic Oscillation and the ENSO. *Geophysical Research Letters*, **31**: L09211, doi:10.1029/2004GL019858.

Loeblich, A.R.J. 1958. Danian stage of Paleocene in California. *American Association of Petroleum Geologists Bulletin*, **42**: 2260-2261.

Lomb, N.R. 1976. Least-squares frequency analysis of unequally spaced data. *Astrophysics and Space Sciences*, **39**: 447-462.

Long, J.A., Fuge, D.P. and Smith, J. 1946. Diatoms of the Moreno Shale. *Journal of Paleontology*, **20**: 89-118.

Lonsdale, P.J., Bischoff, J.L., Burns, V.M., Kastner, M. and Sweeny, R.E. 1980. A high temperature thermal deposit on the seabed at a Gulf of California spreading center. *Earth and Planetary Science Letters*, **49**: 4-20.

Ly, A. and Kuhnt, W. 1994. Late Cretaceous benthic foraminiferal assemblages of the Casamance Shelf (Senegal, NW Africa) indication of a Late Cretaceous Oxygen Minimum Zone. *Revue de Micopaléontologie*, **37**: 49-74.

Lynn, R.S. and Simpson, J.J. 1987. The California current system-the seasonal variability of its physical characteristics. *Journal of Geophysical Research*, **92**: 12947-12966.

Macdonald, R.W. 1996. Awakenings in the Arctic. *Nature*, **380**: 286-287.

Mann, D.G. and Park, J. 1993. Spatial correlations of interdecadal variation in global surface temperatures. *Geophysical Research Letters*, **20**: 1055-1058.

Mann, D.G. and Park, J. 1994. Global-scale modes of surface temperature variability on interannual to century timescales. *Journal of Geophysical Research*, **99**: 25819-25833.

Mann, M.E. and Lees, J.M. 1996. Robust estimation of background noise and signal detection in climatic time series. *Climatic Change*, **331**: 409-445.

Mann, M.E. and Park, J. 1996. Joint spatiotemporal modes of surface temperature and sea level pressure variability in the Northern Hemisphere during the last century. *Journal of Climate*, **9**: 2137-2162.

Mantua, N.J., Hare, S.R., Zhang, Y., Wallace, J.M. and Francis, R.C. 1997. A Pacific interdecadal climate oscillation with impacts on salmon production. *Bulletin of the American Meteorological Society*, **78**: 1069-1079.

Martinez-Machiavello, J.C. 1987. Bioestratigrafía diatómica de un perfil de cretácio superior de la Isla Vicecomodoro Marambio, Antartida. *Ameghiniana*, **24**: 277-288.

Masuda, F. and Watanabe, K. 1979. Eleven-year cycle in Cretaceous Xenoxylon growth rings (trees). *University of Tsukuba, Institute of Geoscience, Annual Report*, **5**: 51-54.

McGuire, D.J. 1988. Depositional Framework of the Upper Cretaceous-Lower Tertiary Moreno Formation, Central San Joaquin Basin, California. In: *Studies of the Geology of the San Joaquin Basin.* (Ed S.A. Graham), **60**, pp. 173-188. Pacific Section S.E.P.M.

McPhaden, M.J. and Yu, X. 1999. Equatorial waves and the 1997-98 El Niño. *Geophysical Research Letters,* **26**: 2961-2964.

McQuoid, M.R. and Hobson, L.A. 1996. Diatom resting stages. *Journal of Phycology*, **32**: 889-902.

McQuoid, M.R. and Hobson, L.A. 1998. Assessment of paleoenvironmental conditions on southern Vancouver Island, British Columbia, Canada, using the tychoplankter *Paralia sulcata*. *Diatom Research*, **13**: 311-321.

McQuoid, M.R. and Nordberg, K. 2003. The diatom *Paralia sulcata* as an environmental indicator species in coastal sediments. *Estuarine, Coastal and Shelf Science*, **56**: 339-354.

Michael, R. and Stolz, M.R. 1999. Possible solar influences on the dust profile of the GISP2 ice core from Central Greenland. *Geophysical Research Letters,* **26**: 1043-1046.

Miller, A.J., Cayan, D.R., Barnett, T.P., Graham, N.E. and Oberhuber, J.M. 1994. Interdecadal variability of the Pacific Ocean: Model response to observed heat flux and wind stress anomalies. *Climate Dynamics,* **9**: 287-302.

Mingram, J. 1998. Laminated Eocene maar-lake sediments from Eckfeld (Eifel region, Germany) and their short-term periodicities. *Palaeogeography, Palaeoclimatology, Palaeoecology,* **140**: 289-305.

Minobe, S. 1997. A 50-70 year climate oscillation over the North Pacific and North America. *Geophysical Research Letters,* **24**: 683-686.

Minobe, S. and Mantua, N.J. 1999. Interdecadal modulation of interannual atmospheric and oceanic variability over the North Pacific. *Progress in Oceanography*, **43**: 163-192.

Moberg, A., Sonechkin, D.M., Holmgren, K., Datsenko, N.M. and Karlen, W. 2005. Highly variable Northern Hemisphere temperatures reconstructed from low- and high-resolution proxy data. *Nature,* **433**: 613-617.

Molnar, P. and Cane, M.A. 2002. El Niño's tropical climate and teleconnections as a blueprint for pre-Ice Age climates. *Paleoceanography,* **17**: 1021, doi:10.1029/2001PA000663.

Moodley, L., Middelburg, J.J., Herman, P.M.J., Soetaert, K. and de Lange, G.J. 2005. Oxygenation and organic-matter preservation in marine sediments: Direct experimental evidence from ancient organic carbon-rich deposits. *Geology*, **33**: 889-892.

Mori, Y. 1981. Evidence of an 11-year periodicity in tree-ring series from Formosa related to the sunspot cycle. *Journal of Climatology*, **1**: 345-353.

Moshkovitz, E., Erlich, A. and Soudry, D. 1983. Siliceous microfossils of the Upper Cretaceous Mishash Formation, Central Negec, Israel. *Cretaceous Research,* **4**: 173-194.

Moxon, I.W. 1988. Sequence Stratigraphy of the Great Valley Basin in the Context of Convergent Margin Tectonics. In: *Studies of the Geology of the San Joaquin Basin.* (Ed S.A. Graham), **60**, pp. 3-28. Pacific Section S.E.P.M.

Mudelsee, M. 2002. TAUEST: a computer program for estimating persistence in unevenly spaced weather/climate time series. *Computers & Geosciences,* **28**: 69-72.

Mudie, P.J. 1985. Palynology of the CESAR cores, Alpha Ridge. In: *Initial Geological Report on CESAR - the Canadian Expedition to Study the Alpha Ridge, Arctic Ocean* (Eds H.R. Jackson, P.J. Mudie and S.M. Blasco), pp. 149-174. Geological Survey of Canada, Paper 84-22, report 11.

Mudie, P.J. and Blasco, S.M. 1985. Lithostratigraphy of the CESAR Cores. In: *Initial Geological Report on CESAR - the Canadian Expedition to Study the Alpha Ridge, Arctic Ocean* (Eds H.R. Jackson, P.J. Mudie and S.M. Blasco), pp. 59-99. Geological Survey of Canada, Paper 84-22, report 6.

Mudie, P.J., Stoffyn-Egli, P. and Van Wagoner, N.A. 1986. Geological constraints for tectonic models of the Alpha Ridge. *Journal of Geodynamics*, **6**: 215-236.

Muggli, D.L., Lecourt, M. and Harrison, P.J. 1996. Effects of iron and nitrogen source on the sinking rate, physiology and metal composition of an oceanic diatom from the subarctic Pacific. *Marine Ecology Progress Series*, **132**: 215-227.

Mûhe, R. and Jokat, W. 1999. Recovery of Volcanic Rocks from the Alpha Ridge, Artic Ocean: Preliminary Results. In: *EOS, Transactions of the American Geophysical Union*, **80**, San Francisco, F1000.

Müller, O. 1912. Diatomeenrest aus der Turonschichten der Kreide. *Berichte fur Deutsche Botanische Gessellschaft*, **29**: 661-668.

Munoz, A., Ojeda, J. and Sanchez-Valverde, B. 2002. Sunspot-like and ENSO/NAO-like periodicities in lacustrine laminated sediments of the Pliocene Villarroya Basin (La Rioja, Spain). *Journal of Paleolimnology*, **27**: 453-463.

Mysak, A. and Venegas, S.A. 1998. Decadal climate oscillations in the Arctic: A new feedback loop for atmosphere-ice-ocean interactions. *Geophysical Research Letters*, **25**: 3607-3610.

Mysak, L.A., Ingram, R.G., Wang, J. and van der Baaren, A. 1996. The anomalous sea-ice extent in Hudson Bay, Baffin Bay and the Labrador Sea during three simultaneous NAO and ENSO episodes. *Atmosphere-Ocean*, **34**: 313-343.

Nederbragt, A.J. and Thurow, J. 2005. Amplitude of ENSO cycles in the Santa Barbara Basin, off California, during the past 15 000 years. *Journal of Quaternary Science*, **20**: 447-456.

Neelin, J.D., Battisti, D.S., Hirst, A.C., Jin, F.-F., Wakata, Y., Yamagata, T. and Zebiak, S.E. 1998. ENSO theory. *Journal of Geophysical Research*, **103**: 14261-14290.

Nelson, D.M., Tréguer, P., Brzezinski, M.A., Leyaert, A. and Queguiner, B. 1995. Production and dissolution of biogenic silica in the ocean: revised global estimates, comparison with regional data and relationship to biogenic sedimentation. *Global Biogeochemical Cycle*, **9**: 359-372.

Niemitz, M.D. and Billups, K. 2005. Millennial-scale variability in western tropical Atlantic surface ocean hydrography during the early Pliocene. *Marine Micropaleontology*, **54**: 155-166.

Nikolaev, V.A. and Harwood, D.M. 2000. Diversity and system of classification of centric diatoms. In: *The Origin and Early Evolution of the Diatoms: Fossil, Molecular and Biogeographical Approaches* (Eds A. Witkowski and J. Sieminska), pp. 37-53. Szafer Institute of Botany, Polish Academy of Sciences, Krakow.

Nikolaev, V.A., Kociolek, J.P., Fourtanier, E., Barron, J.A. and Harwood, D.M. 2001. Late Cretaceous diatoms (Bacillariophyceae) from the Marca Shale member of the Moreno Formation, California. In: *Occasional Papers of the California Academy of Sciences*, pp. 1-119.

Nordt, L., Atchley, S. and Dworkin, S.I. 2002. Paleosol barometer indicates extreme fluctuations in atmospheric CO_2 across the Cretaceous-Tertiary boundary. *Geology*, **30**: 703-706.

Nordt, L., Atchley, S. and Dworkin, S.I. 2003. Terrestrial Evidence for Two Greenhouse Events in the Latest Cretaceous. *GSA Today*, **13**: 4-9.

Nürnberg, D., Wollenburg, I., Dethleff, D., Eicken, H., Kassens, H., Letzig, T., Reimnitz, E. and Thiede, J. 1994. Sediments in Arctic sea ice: implications for entrainment, transport and release. *Marine Geology*, **119**: 185-214.

Ogurtsov, M.G., Kocharov, G.E., Lindholm, M., Meriläinen, J., Eronen, M. and Nagovotsyn, Y.A. 2002. Evidence of solar variations in tree-ring-based climate reconstructions. *Solar Physics*, **205**: 403-417.

Olapido, E.O. 1988. Spectral analysis of climatological time series: On the performance of periodgram, non-integer and maximum entropy methods. *Theoretical and Applied Climatology*, **39**: 40-53.

Olsen, P.E. and Kent, D.V. 1996. Milankovitch climate forcing in the tropics of Pangea during the Late Triassic. *Palaeogeography, Palaeoclimatology, Palaeoecology*, **122**: 1-26.

Onodera, J. and Takahashi, K. 2005. Silicoflagellate fluxes and environmental variations in the northwestern North Pacific during December 1997-May 2000. *Deep Sea Research Part I*, **52**: 371-388.

Osawa, M., Takahashi, K. and Hay, B.J. 2005. Shell-bearing plankton fluxes in the central Black Sea, 1989-1991. *Deep Sea Research Part I*, **52**: 1677-1698.

Otto-Bliesner, B.L., Brady, E.C. and Shields, C. 2002. Late Cretaceous ocean: Coupled simulations with the National Center for Atmospheric Research Climate System Model. *Journal of Geophysical Research*, **107**: 10.1029/2001JD000821.

Ozalas, K., Savrda, C.E. and Fullerton Jr., R.R. 1994. Bioturbated oxygenation-event beds in siliceous facies: Monterey Formation (Miocene), California. *Palaeogeography, Palaeoclimatology, Palaeoecology*, **112**: 63-83.

Paillard, D., Labeyrie, L. and Yiou, P. 1996. Macintosh program performs time-series analysis. *Eos, Trans. American Geophysical Union*, **77**: 379.

Pantocsek, J. 1889. Beiträge zur Kenntnis der Fossilen Bacillarien Ungars. v II. Brackwasser Bacilarien und Achang. Analyse der Marinen Depôts von Borny, Bremia Nagy-Kurös in Ungarn, Ananino und Kusnetkz in Russland, pp. 123.

Park, J., Lindberg, C.R. and Vernon, F.L.I. 1987. Multitaper spectral analysis of high-frequency seismograms. *Journal of Geophysical Research*, **92**: 12675-12684.

Park, Y.-H., Roquet, F. and Vivier, F. 2004. Quasi-stationary ENSO wave signals versus the Antarctic Circumpolar Wave scenario. *Geophysical Research Letters*, **31**: L09315, doi:10.1029/2004GL019806.

Parker, J.R. 1967. The Jurassic and Cretaceous sequence in Spitsbergen. *Geological Magazine*, **104**: 487-505.

Parrish, J.T. and Curtis, R.L. 1982. Atmospheric circulation, upwelling and organic-rich rocks in the Mesozoic and Cenozoic eras. *Palaeogeography, Palaeoclimatology, Palaeoecology*, **40**: 31-66.

Passow, U., Alldredge, A.L. and Logan, B.E. 1994. The role of particulate carbohydrate exudates in the flocculation of diatom blooms. *Deep Sea Research Part I*, **41**: 335-357.

Patience, R.L., Clayton, C.J., Kearsley, A.T., Rowlands, S.J., Bishop, A.N., Rees, A.W.G., Bibby, K.G. and Hopper, A.C. 1990. An integrated biochemical, geochemical and sedimentological study of organic diagenesis in sediments from Leg 112. *Proceedings of the Ocean Drilling Program, Scientific Results*, **112**: 135-153.

Patterson, R.T., Prokoph, A. and Chang, A. 2004. Late Holocene sedimentary response to solar and cosmic ray influenced climate variability in the NE Pacific. *Sedimentary Geology*, **172**: 67-84.

Paulsen, D.E., Li, H.-C. and Ku, T.-L. 2003. Climate variability in central China over the last 1270 years revealed by high-resolution stalagmite records. *Quaternary Science Reviews*, **22**: 691-701.

Payne, M.B. 1951. Type Moreno Formation and overlying Eocene strata on the west side of the San Joaquin Valley, Fresno and Merced Counties, California. *California Division of Mines and Geology Special Report*, **9**: 29.

Pearce, R.B., Kemp, A.E.S., Koizumi, I., Pike, J., Cramp, A.J. and Rowalnd, S.J. 1998. A lamina-scale SEM-based study of a late Quaternary diatom-ooze sapropel from the Mediterranean Ridge, ODP Site 971. In: *Proceedings of the ODP Scientific Results* (Eds K.-C. Emeis, A.H.F. Robertson and e. al.), **160**, pp. 349-363. Ocean Drilling Program, College Station, TX.

Pearson, P.N., Ditchfield, P.W., Singano, J., Harcourt-Brown, K.G., Nicholas, C.J., Olsson, R.K., Shackleton, N.J. and Hall, M.A. 2001. Warm tropical sea surface temperatures in the Late Cretaceous and Eocene epochs. *Nature*, **413**: 481-487.

Pfirman, S., Wollenburg, I., Thiede, J. and Lange, M.A. 1989. Lithogenic sediment on Arctic pack ice: potential aeolian flux and contributions to deep sea sediment. In: *Paleoclimatology and Paleometeorology: Modern and Past Pattern of Global Atmospheric Transport* (Eds M. Sarnthein and M. Leinen), pp. 463-493. Kluwer, Dordrecht.

Philander, S.G. 1990. *El Niño, La Niña and the Southern Oscillation*. Academic Press, London, 293 pp.

Pike, J. 1996. *High Resolution Palaeoceanography and Palaeoclimatology from Late Pleistocene and Holocene Laminated Sediments, Gulf of California*, University of Southampton, 286 pp.

Pike, J., Bernhard, J.M., Moreton, S.G. and Butler, I.B. 2001. Microbioirrigation of marine sediments in dysoxic environments: Implications for early sediment fabric formation and diagenetic processes. *Geology*, **29**: 923-926.

Pike, J. and Kemp, A.E.S. 1996a. Preparation and analysis techniques for studies of laminated sediments. In: *Palaeoclimatology and Palaeoceanography from Laminated Sediments* (Ed A.E.S. Kemp), **116**, pp. 37-48. Geological Society of London Special Publications.

Pike, J. and Kemp, A.E.S. 1996b. Records of seasonal flux in Holocene laminated sediments, Gulf of California. In: *Palaeoclimatology and Palaeoceanography from Laminated Sediments* (Ed A.E.S. Kemp), **116**, pp. 157-169. Geological Society of London Special Publications.

Pike, J. and Kemp, A.E.S. 1996c. Silt aggregates in laminated marine sediment produced by agglutinated foraminifera. *Journal of Sedimentary Research*, **66**: 625-631.

Pike, J. and Kemp, A.E.S. 1997. Early Holocene decadal-scale ocean variability recorded in Gulf of California laminated sediments. *Paleoceanography*, **12**: 227-238.

Pitcher, G.C. 1986. Sedimentary flux and the formation of resting spores of selected *Chaetoceros* species at two sites in the southern Benguela system. *South African Journal of Marine Science*, **4**: 231-244.

Polat, S. and Isik, O. 2002. Phytoplankton distribution, diversity and nutrients at the North-eastern Mediterranean coast of Turkey (Karatas-Adana). *Turkish Journal of Botany*, **26**: 77-86.

Poole, I., Cantrill, D. and Utescher, T. 2005. A multi-proxy approach to determine Antarctic terrestrial palaeoclimate during the Late Cretaceous and Early Tertiary. *Palaeogeography, Palaeoclimatology, Palaeoecology*, **222**: 95-121.

Press, W.H., Teukolsky, S.A., Vetterling, W.T. and Flannery, B.P. 1992. *Numerical Recipes, the Art of Scientific Computing*. Cambridge University Press, Cambridge, 963 pp.

Pugh, D.T. 1987. *Tides, Surges and Mean Sea-Level*. Wiley, Chichester, 472 pp.

Ram, M. and Stolz, M.R. 1999. Possible solar influences on the dust profile of the GISP2 ice core from central Greenland. *Geophysical Research Letters*, **26**: 1043-1046.

Rasmusson, E.M., Wang, X. and Ropelewski, C.F. 1990. The biennial component of ENSO variability. *Journal of Marine Systems*, **1**: 71-96.

Raspopov, O.M., Dergachev, V.A. and Kolström, T. 2004. Periodicity of climate conditions and solar variability derived from dendrochronological and other palaeoclimatic data in high latitudes. *Palaeogeography, Palaeoclimatology, Palaeoecology*, **209**: 127-139.

Reed, R.J., Campbell, W.J., Rasmussen, L.A. and Rogers, D.G. 1961. Evidence of a downward-propagating annual wind reversal in the equatorial stratosphere. *Journal of Geophysical Research*, **66**: 813-818.

Reiegraf, W. 1995. Radiolarien, diatomeen, cephalopoden und stratigraphie im pelagischen Campanium Westfalens (Oberkreide, NW-Deutschland). *Neues Jahrbuch für Geologie und Paläontologie, Abhandlungen*, **197**: 129-200.

Retallack, G.J. 1994. A pedotype approach to latest Cretaceous and early Tertiary paleosols in eastern Montana. *Geological Society of America Bulletin*, **106**: 1377-1397.

Riaux-Bobin, C., Hargraves, P.E., Neveux, J., Oriol, L. and Vétion, G. 1997. Microphyte pigments and resting spores at the water-sediment interface in the Subantarctic deep sea (Indian sector of the Southern Ocean). *Deep Sea Research Part II*, **44**: 1033-1051.

Rigozo, N.R., Vieira, L.E.A., Echer, E. and Nordemann, D.J.R. 2003. Wavelet Analysis of Solar-ENSO Imprints in Tree Ring Data from Southern Brazil in the Last Century. *Climatic Change*, **60**: 329-340.

Rines, J.E.B. and Hargraves, P.E. 1988. The *Chaetoceros* Ehrenberg (Bacillariophyceae) flora of Narragansett Bay, Rhode Island, USA. *Bibliotheca Phycologica*, **79**: 1-196.

Ripepe, M., Roberts, L.T. and Fischer, A.G. 1991. ENSO and sunspot cycles in varved Eocene oil shales from image analysis. *Journal of Sedimentary Petrology*, **61**: 1155-1163.

Rittenour, T.M., Brigham-Grette, J. and Mann, M.E. 2000. El Niño-Like Climate Teleconnections in New England During the Late Pleistocene. *Science*, **288**: 1039-1042.

Robinson, R.S., Meyers, P.A. and Murray, R.W. 2002. Geochemical evidence for variations in delivery and deposition of sediment in Pleistocene light-dark color cycles under the Benguela Current Upwelling System. *Marine Geology*, **180**: 249-270.

Rodbell, D.T., Seltzer, G.O., Anderson, D.M., Abbott, M.B., Enfield, D.B. and Newman, J.H. 1999. An ~15,000-year record of El Niño-driven alluviation in southwestern Ecuador. *Science*, **283**: 516-520.

Romero, O., Boeckel, B., Donner, B., Lavik, G., Fischer, G. and Wefer, G. 2002. Seasonal productivity dynamics in the pelagic central Benguela System inferred from the flux of carbonate and silicate organisms. *Journal of Marine Systems*, **37**: 259-278.

Romero, O.E., Hebbeln, D. and Wefer, G. 2001. Temporal and spatial variability in export production in the SE Pacific Ocean: evidence from siliceous plankton fluxes and surface sediment assemblages. *Deep Sea Research Part I*, **48**: 2673-2697.

Round, F.E., Crawford, R.M. and Mann, D.G. 1990. *The Diatoms: biology and morphology of the genera.* Cambridge University Press, 747 pp.

Ryua, E., Yia, S. and Lee, S.-J. 2005. Late Pleistocene–Holocene paleoenvironmental changes inferred from the diatom record of the Ulleung Basin, East Sea (Sea of Japan). *Marine Micropaleontology*, **55**: 157-182.

Ryves, D.B., Juggins, S., Fritz, S.C. and Battarbee, R.W. 2001. Experimental diatom dissolution and the quantification of microfossil preservation in sediments. *Palaeogeography, Palaeoclimatology, Palaeoecology*, **172**: 99-113.

Sancetta, C. 1989a. Processes controlling the accumulation of diatoms in sediments: a model derived from British Columbian fjords. *Paleoceanography*, **4**: 235-251.

Sancetta, C. 1989b. Spatial and temporal trends of diatom flux in British Columbian fjords. *Journal of Plankton Research*, **11**: 503-520.

Sancetta, C. 1992. Comparison of phytoplankton in sediment trap time series and surface sediments along a productivity gradient. *Paleoceanography*, **7**: 183-194.

Sancetta, C. 1995. Diatoms in the Gulf of California: Seasonal flux patterns and the sedimentary record for the last 15, 000 years. *Paleoceanography*, **10**: 67-84.

Sancetta, C., Villareal, T.A. and Falkowski, P. 1991. Massive fluxes of rhizosolenid diatoms: a common occurrence? *Limnology and Oceanography*, **36**: 1452-1457.

Scargle, J.D. 1982. Studies in astronomical time series analysis II. Statistical aspects of spectral analysis of unevenly spaced data. *The Astrophysical Journal*, **263**: 835-853.

Scharek, R., Latasa, M., Karl, D.M. and Bidigare, R.R. 1999a. Temporal variations in diatom abundance and downward vertical flux in the oligotrophic North Pacific gyre. *Deep Sea Research Part I*, **46**: 1051-1075.

Scharek, R., Tupas, L.M. and Karl, D.M. 1999b. Diatom fluxes to the deep sea in the oligotrophic North Pacific gyre at Station ALOHA. *Marine Ecology Progress Series*, **182**: 55-67.

Scherer, R.P. 1994. A new method for the determination of absolute abundance of diatoms and other silt-sized sedimentary particles. *Journal of Paleolimnology*, **12**: 171-179.

Schibkova, K.G. 1961. "Some new data of Upper Cretaceous and Paleogene flora of the diatom algae of the Eastern slope of the Ural and Transural". In: *Decisions and Proceedings of the Intraregional meeting on working out a stratigraphic scheme for the West Siberian depression*, pp. 239-243, Gostoptekhizdat, Leningrad.

Schmidt, A., Schmidt, M., Fricke, F., Muller, O., Heiden, H. and Hustedt, F. 1875-1959. *Atlas der Diatomaceenkunde*, Leipzig, Berlin, 480 plates.

Schouten, S., Hopmans, E.C., Schefuss, E. and Sinninghe Damsté, J.S. 2002. Distributional variations in marine crenarchaeotal membrane lipids: A new tool for reconstructing ancient sea water temperatures? *Earth and Planetary Science Letters*, **204**: 265-274.

Schrader, H., Swanberg, N., Lycke, A., Paetzel, M. and Schrader, T. 1993. Diatom inferred productivity changes in the eastern equatorial Pacific. The Quaternary record of ODP Leg 111, Site 677. *Hydrobiologia*, **269/270**: 137-151.

Schultz, L.G. 1964. Quantitive interpretation of mineralogical composition from X-ray and chemical data for the Pierre Shale. *U.S. Geol. Survey Prof. Paper*, **391 C**: 1-31.

Schulz, M. and Mudelsee, M. 2002. REDFIT: estimating red-noise spectra directly from unevenly spaced paleoclimatic time series. *Computers & Geosciences*, **28**: 421-426.

Schulz, P. 1935. Diatomeen aus senonen Schwammgesteinen der Danziger Bucht. Zugleich ein Beitrag zur Entwicklungsgeschichte der Diatomeen. *Botanisches Archiv*, **37**: 383-413.

Shipboard Scientific Party 1989. Site 748. In: *Proceedings of the Deep Sea Drilling Project Initial Reports* (Eds R. Schlich and S.W.J. Wise), **120**, pp. 157-233.

Siever, R. 1983. Evolution of chert at active and passive continental margin. In: *Developments in Sedimentology* (Eds A. Iijima, J.R. Hein and R. Siever), **34**, pp. 7-24.

Sims, P.A. 1988. The fossil genus *Trochosira*, its morphology, taxonomy and systematics. *Diatom Research*, **3**: 245-257.

Sims, P.A. 1989. Some Cretaceous and Palaeocene species of *Coscinodiscus*: a micromorphilogical and systematic study. *Diatom Research*, **4**: 351-371.

Sims, P.A. 1994a. *Benetorus, Gladiopsis* and related genera from the Cretaceous. *Diatom Research*, **9**: 165-187.

Sims, P.A. 1994b. *Skeletonemopsis,* a new genus based on the fossil species *Skeletonema* Grev. *Diatom Research*, **9**: 387-410.

Sims, P.A. 1998. The early history of the Biddulphiales. I. the Genus *Medlinia* Gen. Nov. *Diatom Research*, **13**: 337-374.

Sims, P.A. 2000. The early history of the Biddulphiales II. The Genus *Euodiella* P. A. Sims Gen. Nov. *Diatom Research*, **15**: 383-407.

Sims, P.A. and Hasle, G.R. 1987. Two Cretaceous *Stellarima* species: *S. steinyi* and *S. distincta*; their morphology, palaeogeography and phylogeny. *Diatom Research*, **2**: 229-240.

Sims, P.A. and Ross, R. 1988. Some Cretaceous and Paleogene *Trinacria* (diatoms) species. *Bulletin of the British Museum (Natural History), Botany Series*, **13-8**: 275-322.

Slepian, D. 1978. Prolate spheroidal wave functions, Fourier analysis, and uncertainty. V - The discrete case. *Bell System Technical Journal*, **57**: 1371-1430.

Sliter, W.V. and Baker, R.A. 1972. Cretaceous bathymetric distribution of benthic foraminifers. *Journal of Foraminiferal Research*, **2**: 167-183.

Smetacek, V. 2000. The giant diatom dump. *Nature*, **406**: 574-575.

Sonett, C.P., Williams, C.R. and Mörner, N.-A. 1992. The Fourier spectrum of Swedish riverine varves: evidence of sub-arctic quasi-biennial (QBO) oscillations. *Palaeogeography, Palaeoclimatology, Palaeoecology*, **98**: 57-65.

Soukharev, B.E. 1997. The interannual variability of temperature in the polar stratosphere during the winter: the influence of the QBO phase and an 11-yr solar cycle. *Journal of Atmospheric and Solar-Terrestrial Physics*, **59**: 469-477.

Spicer, R.A. and Parrish, J.T. 1986. Palaeobotanical evidence for cool north polar climates in the middle Cretaceous (Albanian-Cenomanian) time. *Geology*, **14**: 703-706.

Spicer, R.A. and Parrish, J.T. 1990. Late Cretaceous-early Tertiary palaeoclimates of northern high latitudes: a quantitative view. *J. Geol. Soc. London*, **147**: 329-341.

Steuber, T., Rauch, M., Masse, J.-P., Graaf, J. and Malkoè, M. 2005. Low-latitude seasonality of Cretaceous temperatures in warm and cold episodes. *Nature*, **437**: 1341-1344.

Stickley, C.E., Brinkhuis, H., Schellenberg, S.A., Sluijs, A., Röhl, U., Fuller, M., Grauert, M., Huber, M., Wamaar, J. and Williams, G.L. 2004. Timing and nature if the deepening of the Tasmanian Gateway. *Paleoceanography*, **19**: PA4027, doi:10.1029/2004PA001022.

Stoffyn-Egli, P. 1987. Iron and manganese micro-precipitates within a Cretaceous biosiliceous ooze from the Arctic Ocean: possible hydrothermal source. *Geo-Marine Letters*, **7**: 223-231.

Strelnikova, N.I. 1964. "New species of diatom algae from the Upper Cretaceous deposits of the Syny River Basin (West Siberia)", **239**, pp. 229-232, Paleophytologii Sbornik, "Nedra", Trudy Vsesoyuznogo Neft, Nauchnois, Geol-razved. Inst. (VNIGRI).

Strelnikova, N.I. 1965. Diatom algae from the Upper Cretaceous deposits of the Northwest part of the Siberian depression.

Strelnikova, N.I. 1971. Species novae bacillariophytorum e sedimentis cretae posterioris in declivate orientali partis polaris ac praepolaris Montium Uralensium. *Novosti Systematiki Nizshikh Rastenii, Botanicheskii Institut, Akademia Nauk SSSR*, **8**: 41-51.

Strelnikova, N.I. 1974. *Late Cretaceous diatoms of western Siberia*. Academie Nauk, SSSR, Roy. 8, 202 pp.

Strelnikova, N.I. 1975. Diatoms of the Cretaceous Period. In: *Third symposium on Recent and Fossil Diatoms*, **53**, pp. 311-321. Nova Hedwigia, Beihefte, Kiel.

Strub, P.T. and James, C. 2000. Altimeter-derived variability of surface velocities in the California Current System: 2. Seasonal circulation and eddy statistics. *Deep Sea Research Part II*, **47**: 831-870.

Strub, P.T. and James, C. 2002. Altimeter-derived surface circulation in the large-scale NE Pacific Gyres. Part 1. seasonal variability. *Progress in Oceanography*, **53**: 163-183.

Stüben, D., Kramar, U., Berner, Z.A., Meudt, M., Keller, G., Abramovich, S., Adatte, T., Hambach, U. and Stinnesbeck, W. 2003. Late Maastrichtian paleoclimatic and paleocenographic changes from Sr/Ca ratio and stable isotopes. *Palaeogeography, Palaeoclimatology, Palaeoecology*, **199**: 107-127.

Stuiver, M. and Quay, P.D. 1980. Changes in atmospheric carbon-14 attributed to a variable sun. *Science*, **207**: 11-19.

Sweeny, J.F., Irving, E. and Geuer, J.W. 1978. Evolution of the Arctic Basin. In: *Arctic Geophysical Review*, **45**, pp. 4. 91 Earth Physics Branch, Ottawa.

Syvertsen, E.E. 1985. Resting spore formation in the Antarctic diatoms *Coscinodiscus furcatus* Karsten and *Thalassiosira australis* Pergallo. *Polar Biology*, **4**: 113-119.

Takahashi, K., Honjo, S. and Tabata, S. 1989. Siliceous phytoplankton flux: interannual variability and response to hydrographic changes in the northeastern Pacific. In: *Aspects of Climate Variability in the Pacific and the Western Americas* (Ed D.H. Peterson), **55**, pp. 151-160. American Geophysical Union, Geophysical Monograph.

Takahashi, O., Kimura, M., Ishii, A. and Mayama, S. 1999. Upper Cretaceous diatoms from Central Japan. In: *Proceedings of the Fourteenth International Diatom Symposium* (Eds S. Mayama, M. Idei and I. Koizumi), pp. 146-155. Koeltz Scientific Books, Koenigstein, Tokyo.

Talbot, M.M.B. and Bate, G.C. 1988. The relative quantities of live and detrital organic matter in a beach-surf ecosystem. *Journal of Experimental Marine Biology and Ecology*, **121**: 255-264.

Tapia, P.M. and Harwood, D.M. 2002. Upper Cretaceous diatom biostratigraphy of the Arctic archipelago and northern continental margin, Canada. *Micropaleontology*, **48**: 303-342.

Thompson, D.W.J., Baldwin, M.P. and Wallace, J.M. 2002. Stratospheric Connection to Northern Hemisphere Wintertime Weather: Implications for Prediction. *Journal of Climate*, **15**: 1421-1428.

Thompson, D.W.J. and Wallace, J.M. 1998. The Arctic Oscillation signature in the wintertime geopotential height and temperature fields. *Geophysical Research Letters*, **25**: 1297-1300.

Thomson, D.J. 1982. Spectrum estimation and harmonic analysis. *Proc. IEEE*, **70**: 1055-1096.

Thomson, D.J. 1990. Time series analysis of Holocene climate data. *Philosophical Transaction of the Royal Society of London A*, **332**: 539-597.

Thomson, D.J. 1995. The seasons, global temperature and precession. *Science*, **268**: 59-68.

Thresher, R.E. 2002. Solar correlates of Southern Hemisphere mid-latitude climate variability. *International Journal of Climatology*, **22**: 901-915.

Thunell, R., Pride, C., Tappa, E. and Muller-Karger, F. 1993. Varve formation in the Gulf of California: Insights from time series sediment trap sampling and remote sensing. *Quaternary Science Reviews*, **12**.

Thunell, R.C. 1998a. Particle fluxes in a coastal upwelling zone: sediment trap results from Santa Barbara Basin, California. *Deep-Sea Research II*, **45**: 1863-1884.

Thunell, R.C. 1998b. Seasonal and annual variability in particle fluxes in the Gulf of California: A response to climate forcing. *Deep Sea Research Part I*, **45**: 2059-2083.

Thunell, R.C., Pride, C.J., Tappa, E. and MullerKarger, F.E. 1994. Biogenic silica fluxes and accumulation rates in the Gulf of California. *Geology*, **22**: 303-306.

Tiffany, M.A. and Lange, C.B. 2002. Diatoms provide attachment sites for other diatoms: A natural history of epiphytism from southern California. *Phycologia*, **41**: 116-124.

Tiwari, R.K. and Rao, K.N.N. 2004. Signature of ENSO Signals in the Coral Growth Rate Record of Arabian Sea and Indian Monsoons. *Pure and Applied Geophysics*, **161**: 413-427.

Torrence, C. and Compo, G.P. 1998. A practical guide to wavelet analysis. *Bulletin of the American Meteorological Society*, **79**: 61-78.

Torrence, C. and Webster, P.J. 1999. Interdecadal changes in the ENSO-monsoon system. *Journal of Climate*, **12**: 2679-2690.

Trenberth, K.E. 1997. The definitions of El Niño. *Bulletin of the American Meteorological Society*, **78**: 2771-2777.

Treppke, U.F., Lange, C.B. and Wefer, G. 1996. Vertical fluxes of diatoms and silicoflagellates in the eastern equatorial Atlantic, and their contribution to the sedimentary record. *Marine Micropaleontology*, **28**: 73-96.

Tsonis, A.A., Elsner, A.G. and Jagger, T.H. 2005. Unfolding the relation between global temperature and ENSO. *Geophysical Research Letters*, **32**: L09701, doi:10.1029/2005GL022875.

Tudhope, A.W., Cilcott, C.P., McCulloch, M.T., Cook, E.R., Chappell, J., Ellam, R.M., Lea, D.W., Lough, J.M. and Shimmield, G.B. 2001. Variability in the El Niño-Southern Oscillation through a glacial-interglacial cycle. *Science*, **1511-1517**.

Turner, J.T. 2002. Zooplankton fecal pellets, marine snow and sinking phytoplankton blooms. *Aquatic Marine Ecology,* **27**: 57-102.

Turner, J.T. and Farrante, J.G. 1979. Zooplankton fecal pellets in aquatic ecosystems. *BioScience,* **29**: 670-677.

Ulrych, T.J. and Bishop, T.N. 1975. Maximum entropy spectral analysis and autoregressive decomposition. *Reviews of Geophysics and Space Physics,* **13**: 183-200.

Urban, F.E., Cole, J.E. and Overpeck, J.T. 2000. Influence of mean climate change on climate variability from a 155-year tropical Pacific coral record. *Nature,* **407**: 989-993.

Vaillancourt, R.D., Marra, J., Seki, M.P., Parsons, M.L. and Bidigare, R.R. 2003. Impact of a cyclonic eddy on phytoplankton community structure and photosynthetic competency in the subtropical North Pacific Ocean. *Deep Sea Research Part I,* **50**: 829-847.

Van Heurck, H. 1883. *Synopsis des diatomées de Belgique, Atlas*, Fasc. 6. Anvers.

Van Wagoner, N.A. and Robinson, P.T. 1985. Petrology and geochemistry of a CESAR bedrock sample: implications for the origin of the Alpha Ridge. In: *Initial Geological Report on CESAR - the Canadian Expedition to Study the Alpha Ridge, Arctic Ocean* (Eds H.R. Jackson, P.J. Mudie and S.M. Blasco), pp. 47-57. Geological Survey of Canada, Paper 84-22.

VanLandingham, S.L. 1967-1979. *Catalogue of the recent and fossil genera and species of diatoms and their synonyms,* **8 volumes**. J. Cramer, Vaduz, 4654 pp.

Vekschina, V.N. 1961. "The scheme of subdivision of the Cretaceous and Paleogene deposits of the West Siberian Depression based on the analysis of algae diatoms, silicoflagellates, ebridaceae and coccolithophorids. In: *Decisions and Proceedings of the Intraregional meeting on working out a stratigraphic scheme for the West Siberian depression*, pp. 223-237, Gostoptekhizdat, Leningrad.

Villareal, T.A. 1991. Nitrogen-fixation by the cyanobacterial symbiont of the diatom genus *Hemiaulus*. *Marine Ecology Progress Series,* **76**: 201-204.

Villareal, T.A., Altabet, M.A. and Culver-Rymsza, K. 1993. Nitrogen transport by vertically migrating diatom mats in the North Pacific Ocean. *Nature*, **363**: 709-712.

Villareal, T.A. and Carpenter, E.J. 1989. Nitrogen fixation, suspension characteristics and chemical composition of Rhizosolenia mats in the central North Pacific gyre. *Biological Oceanography,* **6**: 327-345.

Villareal, T.A., Woods, S., Moore, J.K. and Culver-Rymsza, K. 1996. Vertical migration of Rhizosolenia mats and their significance to NO_{3-} fluxes in the central North Pacific gyre. *Journal of Plankton Research*, **18**: 1103-1121.

Vogt, P.R., Perry, R.K. and Taylor, P.T. 1984. Amerasia Basin, Arctic Ocean: magnetic anomalies and their decipherment. In: *Arctic Geology, 27th International Geology Congress,* **4**, pp. 152-161, Geological Society of America, Boulder.

Waite, A., Bienfang, P.K. and Harrison, P.J. 1992. Spring bloom sedimentation in a subarctic ecosystem. I. Nutrient sensitivity. *Marine Biology,* **114**: 119-129.

Wall, J.H. 1975. Diatoms and radiolarian from the Cretaceous System of Alberta, a preliminary report. In: *The Cretaceous System in the Western Interior of North America* (Ed W.G.E. Caldwell), **13**, pp. 391-440. Geological Association of Canada, Special Paper.

Wang, J. and Ikeda, M. 2000. Arctic Oscillation and Arctic Sea-Ice Oscillation. *Geophysical Research Letters*, **27**: 1287-1290.

Wang, J., Ikeda, M., Zhang, S. and Gerdes, R. 2005. Linking the northern hemisphere sea-ice reduction trend and the quasi-decadal arctic sea-ice oscillation. *Climate Dynamics*, **24**: 115-130.

Waple, A.M., Mann, M.E. and Bradley, R.S. 2002. Long-term patterns of solar irradiance forcing in model experiments and proxy based surface temperature reconstructions. *Climate Dynamics*, **18**: 563-578.

Ware, D.M. 1995. A century and a half of change in the climate of the NE Pacific. *Fisheries Oceanography*, **4**: 267-277.

Warwick, R.M. 1973. Freeliving marine nematodes from the Indian Ocean. *British Museum Bulletin (Natural History, Zoology)*, **25**: 27-257.

Weaver, A.J. 1990. Ocean currents and climate. *Nature*, **347**: 432.

Weedon, G. 2003. *Time-Series Analysis and Cyclostratigraphy: Examining stratigraphic records of environmental cycles*. Cambridge University Press, 259 pp.

Weisner, H. 1936. Sur la découverte de diatomées et autres microfossiles peu connus dans Crétacé superieur de la Bohême. *Annales de Protistologie*, **5**: 151-155.

Wiedermann, M. 1964. Présence de diatomées dans le Flysch á Helminthoïdes. *Bulletin des Laboratoires de Géologie, Minéralogie, Géophysique et du Musée géologique de l'Université de Lausanne*, **145**: 1-5.

Williams, T. 1996. *History and Controls of Subsidence, Cretaceous Great Valley Group, Sacramento Basin, California.* Unpublished Ph.D. dissertation, Stanford University, California, 412 pp.

Wilson, P.A. and Opdyke, B.N. 1996. Equatorial sea surface temperatures for the Maastrichtian revealed through remarkable preservation of metastable carbonate. *Geology*, **24**: 555-558.

Witt, O. 1985. Ueder den Polierschiefer von Archangelsk-Kurojedowo in Gouv. Simbirsk. In: *Verhandlungen der Russisch-kaiserlichen mineralogischen Gesellschaft zu St. Petersburg*, **22**, pp. 137-177.

Wolfe, J.A. and Upchurch, G.R. 1987. North American nonmarine climates and vegetation during the Late Cretaceous. *Palaeogeography, Palaeoclimatology, Palaeoecology*, **61**: 33-77.

Wuchter, C., Schouten, S., Wakeham, S.G. and Sinninghe Damsté, J.S. 2005. Temporal and spatial variation in tetraether membrane lipids of marine Crenarchaeota in particulate organic matter: Implications for TEX_{86} paleothermometry. *Paleoceanography*, **20**: PA3013, doi:10.1029/2004PA001110.

Yin, J.H. 2005. A consistent poleward shift of the storm tracks in simulations of 21st century climate. *Geophysical Research Letters*, **32**: L18701, doi:10.1029/2005GL023684.

Zhang, Y., Wallace, J.M. and Battisti, D.S. 1997. ENSO-like Interdecadal Variability: 1900-93. *Journal of Climate*, **10**: 1004-1020.